Contrôle de la réactivité et de la sélectivité de réactions chimiques par utilisation de porphyrines métalées via intéractions supramoléculaire et catalyseurs bio-inspirés

Jonathan Trouvé

UNIVERSITÉ DE RENNES 1

THESE DE DOCTORAT DE

L'UNIVERSITE DE RENNES 1

ECOLE DOCTORALE N° 596
Matière, Molécules, Matériaux
Spécialité : *Chimie Moléculaire et Macromoléculaire*

Par
Jonathan TROUVE

Control of Chemical Reactivity with Metallated Porphyrins as Supramolecular and Bio-Inspired Catalysts

Thèse présentée et soutenue à Rennes, le 20 décembre 2022
Unité de recherche : Institut des Sciences Chimiques de Rennes UMR6226

Rapporteurs avant soutenance :

Audrey AUFFRANT	Directrice de Recherche CNRS, Ecole Polytechnique Palaiseau
Jean-Pierre DJUKIC	Directeur de Recherche CNRS, Université de Strasbourg

Composition du Jury :

Président :	Jeanne CRASSOUS	Directrice de Recherche CNRS, Université de Rennes 1
Examinateurs :	Jean-Pierre DJUKIC	Directeur de Recherche CNRS, Université de Strasbourg
	Audrey AUFFRANT	Directrice de Recherche CNRS, Ecole Polytechnique Palaiseau
	Thomas R. WARD	Professeur, Université de Bale
	Bernold HASENKNOPF	Professeur, Sorbonne Université
Dir. de thèse :	Rafael GRAMAGE-DORIA	Chargé de Recherche CNRS, Université de Rennes 1

Acknowledgments

Je tiens tout d'abord à remercier mon directeur de thèse, le Dr. Rafael Gramage-Doria pour m'avoir permis de découvrir et de travailler sur des sujets aussi palpitants, de m'avoir encadré du début à la fin de ces travaux et de m'avoir permis de m'émanciper dans le monde scientifique. Mais je le remercie surtout pour n'avoir jamais perdu de vue que derrière chaque doctorant ou étudiant, se tient une personne. Cette thèse aura abouti en énorme partie grâce au soutien constant et l'humanité dont il a fait preuve.

Merci aux membres du jury, Dr. Jeanne Crassous, Dr. Jean-Pierre Djukic, Dr. Audrey Auffrant, Pr. Thomas R. Ward et le Pr. Bernold Hasenknopf d'avoir accepté d'accorder leur précieux temps à l'étude de cette thèse.

Ensuite je remercie les membres permanents de l'équipe OMC pour leur gentillesse, leur générosité leur soutien et conseils. Je remercie tout particulièrement le Dr. Cedric Fischmeister et le Pr. Christophe Darcel.

Je remercie l'ensemble de l'équipe en charge de l'entretien du laboratoire, et de l'équipement spectroscopique. Merci à Clement Orione ainsi que Christine Deponge pour les analyses et les discussions RMN. Un grand merci à Philippe Jehan et Fabian Lambert pour toutes les analyses de HRMS, qui n'ont définitivement pas toujours été un cadeau et pour les discussions constructives qui en ont découlées.

Je remercie aussi Jérôme Ollivier, non seulement pour toute l'aide apportée durant ma thèse, que pour sa sympathie, sa présence et son écoute. Moi et tous les étudiants du laboratoire lui devont beaucoup.

Merci à tous les étudiants qui ont travaillé avant moi et avec moi sur ces projets. Merci au Dr Paolo Zardi et à Shaymaa Al-Shehimy d'avoir élaboré le début d'une si vaste thématique. Merci à Khalil Youssef, Antoine Perennes, Mathis Joly, Rajeshwaran Purushothaman, Fanny Guicheteau et Heloise Guignon. J'espère que le temps passé au laboratoire aura été aussi instructif qu'il l'aura été pour moi.

Je remercie évidemment tous les membres non permanents de l'équipe, tous ceux qui font vivre le laboratoire sans qui le temps passé serait bien trop long. Je ne citerai pas tout le monde, mais je tiens à remercier spécialement Raphaël pour l'aide apporté à mon arrivé, et pour 2 ans bien sympathique à vivre dans le même bureau. Merci à Alphonso pour avoir été un collègue de paillasse plein d'énergie et de bonne humeur, à Naba pour la gentilesse, la générosité et the wondeful tiramisu. Et merci à Marie pour sa formidable capacité à rassembler et d'avoir établi une si bonne ambiance entre nous tous.

Enfin je tiens à remercier mes amis et ma famille pour le soutien naturel dont ils font preuve chaque jour, d'avoir été un phare dans les multiples tempêtes que la vie nous fait traverser, et de rendre les éclaircies d'autant plus lumineuses. Je leur suis infiniment reconnaissant et cette thèse leur est dédiée.

****

Each chapter contains independent numbering of compounds and independent citation of references

****

General introduction

Homogeneous catalysis is an enabling technology for the sustainable synthesis of daily-relevant chemicals in our society.[1] Typically, small molecules, either organic ones for organocatalysis[2,3] or inorganic ones for metal catalysis,[4] have served to accelerate reactions and control the selectivity for those cases where multiple products can form. Consequently, different reactivities and different selectivities can be reached by fine-tuning of the catalysts, enhancing the stability of the catalytic system as well. In the last decades, the merger of supramolecular catalysis, that is the implementation of strategies based on supramolecular chemistry into chemical catalysis, has shown a tremendous impact in contemporary research.[5] The toolbox offered by supramolecular systems provides new possibilities to address challenges difficult or impossible to tackle with more classic catalysts. These tools are versatile and mainly inspired from the multiple action modes encountered in enzymes, which are Nature's catalysts. Enzymes enabled catalysis to occur under relatively mild reaction conditions with high robustness and activity mainly because the catalytically active site is well protected in hydrophobic pockets.[6] Such feature has inspired scientists to design and study chemical catalysis in confined spaces, generated by covalent chemistry, non-covalent chemistry or coordination chemistry.[7-8]

In addition, enzymes can access key transition states and intermediates by lowering specific energetic pathways which is at the origin of their exquisite selectivity.[9] In fact, multiple reversible interactions mainly based on non-covalent hydrogen bonding fix the substrate around the active site in a given geometrical conformation, thus lowering its degree of freedom and pre-organize it to reach a precise selectivity.[10] Another specificity of enzymes, is the high affinity they have for substrates with respect to the products, which translates into enhanced reaction rates as the products are straightforward released from the active site.[11] As such, kinetically labile interactions have been explored in the design of man-made catalysts for generating new ligands by self-assembly as well as for substrate pre-organization due to ligand-to-catalyst binding.[12-13] The most developed non-covalent interactions so far studied in these directions are hydrogen bonding[14] and ion-pairing,[15] respectively.

In supramolecular chemistry, metalloporphyrins are pivotal building blocks that lead to new dimensions and chemical space owing to their ability to apically bind to nitrogen-containing building blocks (**Figure 1**).[16] Such level of supramolecular engineering has been applied to different fields, being particular relevant for physics (energy or charge transfer, photovoltaics) and materials sciences (molecular tectonics, oligomerization, polymerization, etc.).[17-19] The most studied interaction in this context is likely the one involving the binding of pyridine derivatives to zinc(II)-porphyrins, in which the zinc cation evolves from (almost perfect) square planar geometry to (slight distorted) square pyramidal (**Figure 1**). This type of interaction which is *stricto sensu* a coordination bond, but shares with the previously-described non-covalent interactions the reversible nature of the bonding. Depending on the

stereoelectronic properties of the pyridine and the zinc(II)-porphyrin derivative, this Zn···N interaction can be weaker or stronger, which results in a panel of different association constants $K_{1.1}$ = 10^2-10^6 M^{-1} in general,[20-21] which are routinely measured with conventional NMR and/or UV-vis titration techniques.[22] These values are comparable to those observed for instance with those found in hydrogen bonding, which are used in chemical catalysis.

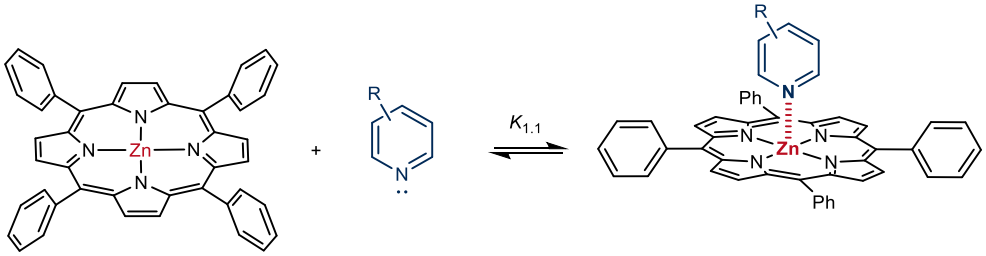

Figure 1. The binding of pyridine derivatives to zinc(II)-porphyrin derivatives is kinetically labile.

1. Organic reactions.

Consequently, the exploitation of Zn···N interactions for controlling the activity and the selectivity of chemical reactions appeared promising as it was shown in the 90's with the pioneering studies from the Sanders group (**Figure 2**).[23,24]

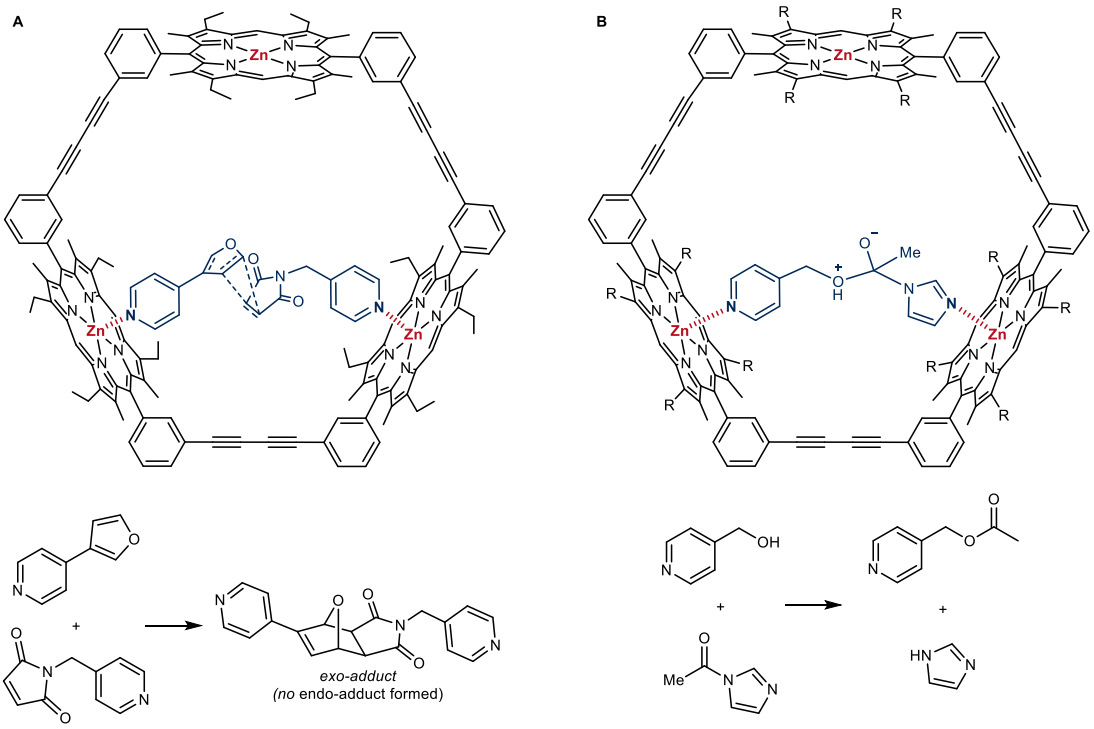

Figure 2. Sanders's pioneering zinc(II)-porphyrin-derived tricyclic Diels-Alderase (**A**) and its application in the acyl transfer reaction in a catalytic fashion (**B**) in which the pyridine-containing substrates react inside the cavity of the trimer.

They reported a number of trimeric zinc(II)-porphyrin macrocycles that served as Diels-Alderases for pyridinic substrates, with the overarching idea that the intermediates of the reaction will be accessible *via* simultaneous Zn···N interactions inside the macrocyclic structure. Because the systems were designed to fit better the transition state than the substrates and products, enhanced reaction rates and a switch in the stereoisomerism (*exo versus endo*) of the products were observed (**Figure 2A**).[25-28] A catalytic version was developed for acyl transfer reactions between nitrogen-containing reagents (**Figure 2B**).[29] These action modes mimic the tight binding of the transition state encountered in enzymes.[23,24] Later, Nguyen and co-workers reported related catalytic versions for the acyl transfer reactions but using a dimeric zinc(II)-porphyrin macrocycle that allosterically switches on/off between open and closed conformations, the former conformation exhibiting higher reactivity than the latter one (**Figure 3**).[30]

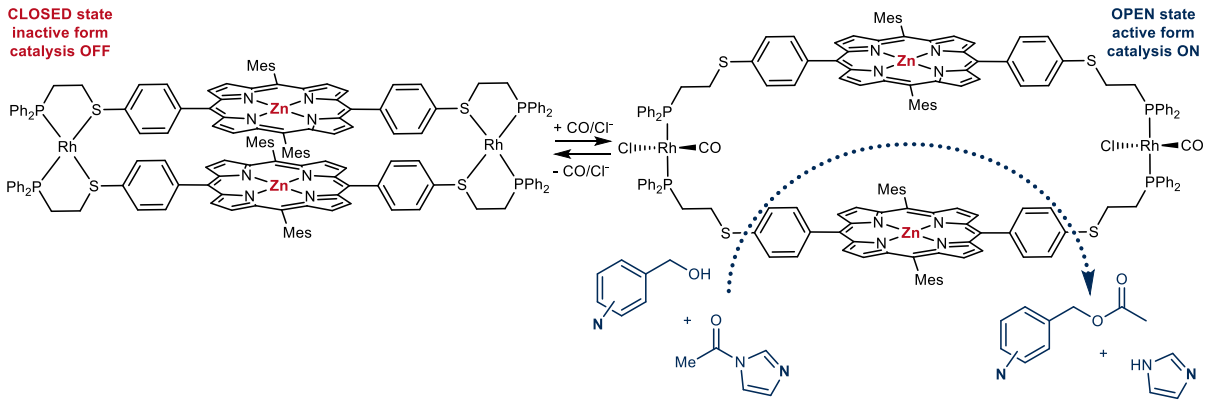

Figure 3. Nguyen's dimeric zinc(II)-porphyrin derivative displaying allosteric control of reactivity and substrate selectivity for acyl transfer reactions. Mes = mesitylene.

Interesting substrate selectivity was observed as the 2-substituted pyridine derivatives reacted poorly with respect to the 3- and 4- isomers. Analogous observations were found when using metal-organic frameworks built up from zinc(II)-porphyrin scaffolds[31] and cyclic tetramers for the methanolysis of phosphate triesters.[32]

2. Transition metal catalysis

Transition metal catalysis has enabled the streaming access to compounds impossible or difficult to obtain by other means.[33-34] Indeed the combination of transition metal ions (which display multiple coordination numbers, geometries and oxidation states) with fine-tuned ligands displaying unique stereoelectronic features, offers a myriad of possibilities to tackle unprecedented challenges in terms of chemical reactivity.[35] In this context, ligands equipped with zinc(II)-porphyrins as the substrate recognition site have been rarely developed for transition metal catalysis. In principle, this type of ligands would enable labile Zn···N interactions with nitrogen-containing substrates, thus inhibiting to some extent the undesired over-coordination of the substrates (or the products) to active metal catalysts, which is a major concern in homogeneous catalysis.

In this respect, Warnmark and co-workers developed a first approach to transition metal catalysts equipped with a substrate recognition site comprising a zinc(II)-porphyrin (**Figure 4**).[36]

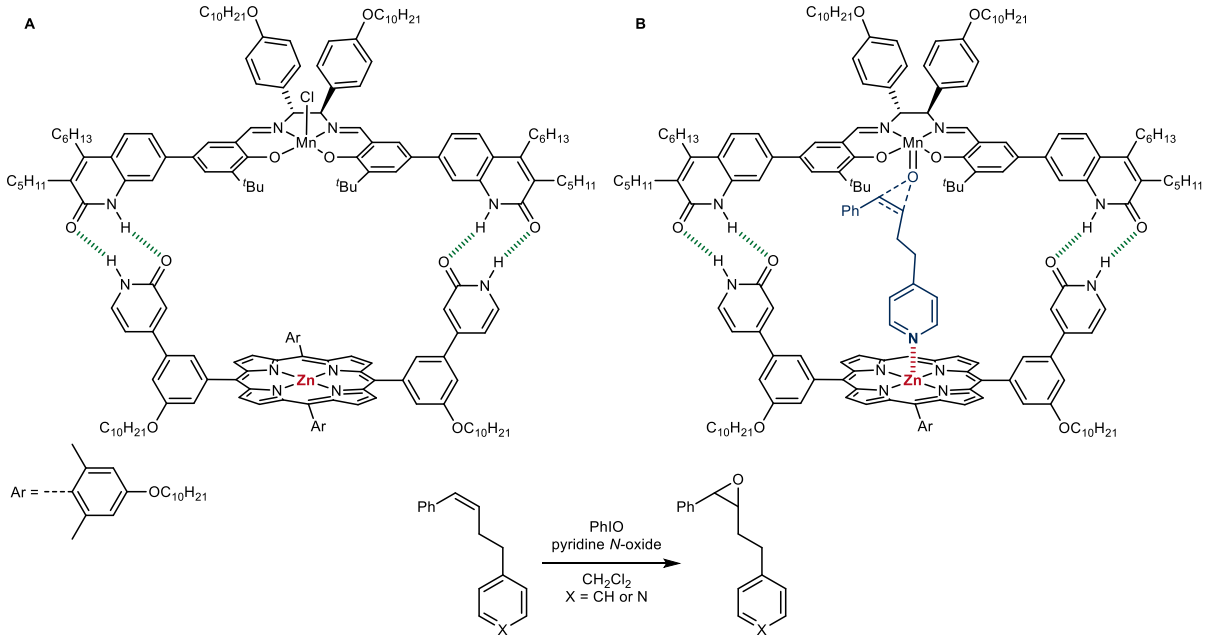

Figure 4. Warnmark's zinc(II)-porphyrin-based dynamic supramolecular manganese catalysts featuring substrate selectivity in epoxidation reactions *via* remote Zn···N interactions between the catalyst and the substrate (**A**) and the corresponding postulated transition state (**B**). Green dashed lines indicate intermolecular hydrogen bonding.

The overarching idea was to achieve substrate selective catalysis, a concept reminiscent of enzymes, but difficult to implement in abiological catalysis.[37] The design was based on the combination of a substrate-receptor unit and a catalytically active site *via* hydrogen bonding between amide groups. The receptor unit was constituted by a zinc(II)-porphyrin equipped with peripheral 2-pyridone units and the active transition metal catalyst site (i.e. Jacobsen-type manganese epoxidation catalyst) with 2-quinolone units (**Figure 4A**). This strategy gave rise to a dynamic supramolecular catalyst expected to form a heterodimer assembly that was applied in substrate selective epoxidation reactions, in which the nitrogen-containing substrates reacted preferentially over the other ones not containing nitrogen atoms. The nitrogen-containing substrates were claimed to bind inside the generated pocket of the catalyst *via* Zn···N interactions whilst the epoxidation occurred in the olefinic site, that is, in a remote fashion (**Figure 4B**). However, due to the reversible nature in the formation of this supramolecular catalyst, different assemblies could not be discarded, such as dimers, trimers, oligomers or even co-polymers.[38,39] This difficulty prompted the design of more rigid supramolecular catalysts by introducing straps in the recognition as well as in the catalytically active site with the aim to suppress to some extent unselective catalysis occurring outside of the cavity.[40]

In our laboratories, we have recently established a research line devoted to exploiting the substrate-recognition properties of porphyrins in transition metal catalysis with the aim to tackle issues difficult to address with traditional stereoelectronic ligand modification. In 2017, we showed that palladium-catalyzed cross-coupling reactions with halopyridine derivatives are controlled by the presence (or absence) of zinc(II)-containing scaffolds (**Figure 5**).[41]

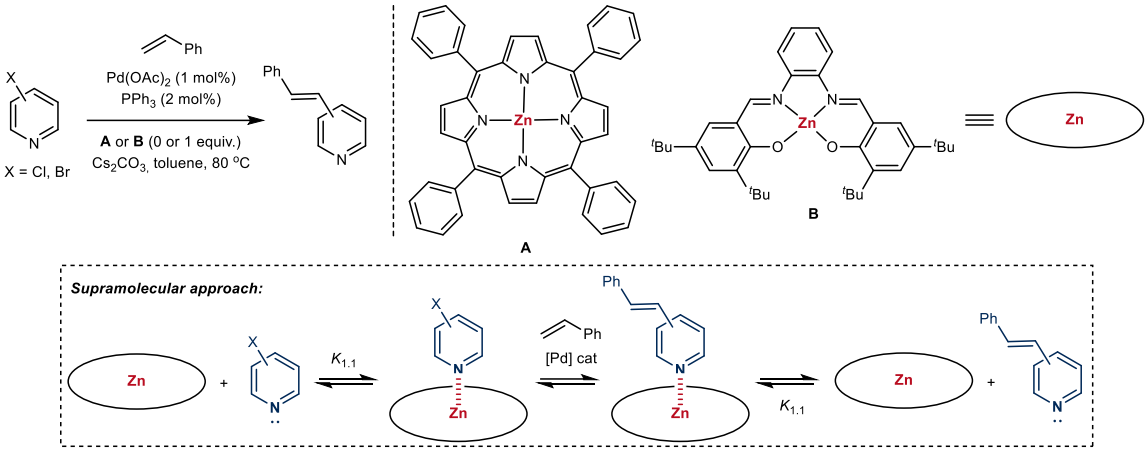

Figure 5. Palladium-catalyzed cross-coupling reactions with halopyridine derivatives controlled by remote Zn···N interactions.

Indeed, easily-accessible zinc(II)-porphyrin **A** and zinc(II)-salphen **B** were used, respectively, for Mizoroki-Heck reactions between chloro- and bromo-pyridines with styrene. In the presence of these zinc(II)-containing scaffolds higher yields and higher reaction rates were obtained in these cross-coupling reactions except for the combination of the 2-halopyridine derivatives and zinc(II)-porphyrin **A**, in which no binding event occurs due to steric shields. The yields and reaction rates were roughly correlated with the binding strength between the zinc(II)-containing scaffolds and the halopyridines, being higher with the zinc(II)-salphen **B** than with zinc(II)-porphyrin **A**. A less pronounced effect was found in Suzuki-Miyaura cross coupling reactions between the halopyridines and phenyl boronic acid in the presence of **A** (**B** was found unstable under the reaction conditions). Importantly, the active palladium catalyst was the same in all the cases, i.e. $Pd(OAc)_2/PPh_3$, which clearly shows that the reactivity of a trivial palladium catalyst can be indirectly controlled by this remote Zn···N interaction, even at high temperatures (80 °C). In other words, the zinc(II)-containing scaffolds inhibit to some extent the undesired pathway of over-coordination to palladium by the pyridine derivatives (substrates and/or products). Such observations were made possible only in the presence of one equivalent (at least) of the zinc(II)-containing scaffold using the non-coordinating toluene as the solvent.

In subsequent studies, we were attracted to the design of a truly catalytic system, that is, the incorporation of the active palladium site to a ligand comprising a substrate recognition site build around a zinc(II)-porphyrin (**Figure 6**).[42]

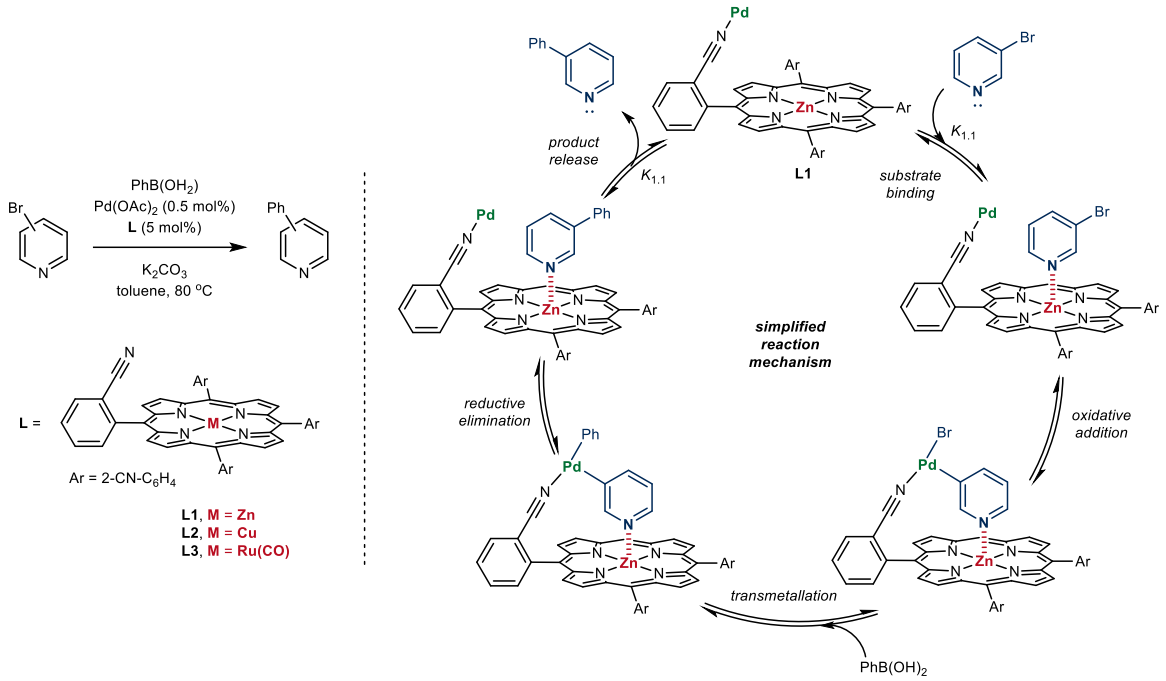

Figure 6. A supramolecular catalyst with a catalytically active palladium site and a substrate recognition site enabling Zn···N interactions between substrate and catalyst, together with the postulated catalytic cycle.

As such, we synthesized in a single-step operation porphyrin **L** that is appended with nitrile groups in the *ortho* position of the *meso* phenyl groups. In this way, different metal cations (Zn, Cu, Ru) can be embedded in the porphyrin core, thereby changing the binding ability towards pyridine derivatives as substrates; whereas the nitrile groups are available for binding catalytically active palladium cations. From the many metals incorporated inside of the porphyrin, zinc(II) revealed the most pertinent for representative Suzuki-Miyaura reactions. With this supramolecular ligand (**L1**), a unique substrate-selectivity was observed since 3-bromopyridine as the substrate reacted preferentially with phenyl boronic acid over the 2- or 4-bromopyridine ones. In addition, the catalytic system displayed remarkable substrate selectivity even in the presence of bromobenzene in competition experiments. This is a complete reversal of reactivity when compared to classical palladium catalysts that do exhibit higher reactivity for bromobenzene. A careful assessment of the origin of this unique reactivity revealed that the ideal substrate pre-organization provided by the porphyrin pocket as well as the distance and geometry between the active site and the substrate-recognition site were key parameters on stabilizing the different intermediates from the catalytic cycle. Furthermore, in depth NMR and X-ray diffraction studies indicated that the binding of palladium to the nitrile groups increased the binding strength of the substrate to the zinc(II)-porphyrin. This is not a mere allosteric effect, but it also shows that it is possible to fine-tune the strength of the Zn···N interaction in a remote fashion through coordination chemistry.

The last three decades have witnessed the birth and progress of the rational use of Zn···N interactions between substrates and catalysts in organic reactions as well as in transition metal catalysis. Although this type of interaction is rather unconventional compared to the ones more studied, i.e. hydrogen bonding, it has already shown that unique type of reactivities and selectivities can emerge. The interaction strength associated to Zn···N interaction is rather strong (when compared to a single

hydrogen bond for example) and kinetically labile with non-coordinating solvents, even at high temperatures. All these aspects are relevant for future implementations. At this stage, this interaction has been exploited between pyridine derivatives as substrates and ligands (or catalysts) derived from zinc(II)-porphyrin or zinc(II)-salphen derivatives. Owing to the chemical robustness and synthetic versatility of these and other zinc(II)-porphyrinoids, many of them will be readily accessible for the generation of new supramolecular catalysts featuring Zn···N interactions. For instance, many zinc(II)-porphyrins containing metal-appended fragments are known,[43-46] but their substrate recognition properties in catalysis remains to be addressed, not to mention the possibilities to design novel ones.

In this context, we report in this PhD thesis the synthesis of a new family of geometrically well-defined supramolecular zinc(II)-porphyrin ligands that display enhanced reactivity for iridium-catalyzed C-H borylations *via* subtle substrate pre-organization exploiting kinetically labile Zn···N (**chapter 2 and 3**) and Zn···O=C weak interactions (**chapter 4**) in the second coordination sphere of the catalyst. Unexpected reactivity for copper catalysis encountered during the course of the ligand synthesis is also disclosed (**chapter 5 and 6**). On another side, we showed that a bio-inspired iron porphyrin catalyst was able to yield excellent activity and selectivity in the sustainable Wacker-type oxidation reaction and we provide spectroscopic evidences of the so far elusive iron-hydride active intermediate (**chapter 7**).

The content of this PhD thesis manuscript is as it follows:

Chapter 1: This chapter is a literature review of the recent supramolecular strategies applied for transition metal catalysis using unconventional non-covalent interactions beyond the more common hydrogen bonding. In particular, we highlight how theses weak interactions can be rationally implemented to control the catalyst reactivity in a remote fashion, far away from the active site, as enzyme do. This survey covers the period of five years before stating this PhD, that is from 2015 to 2019/2020.

Chapter 2: This chapter is dedicated to the synthesis of a new supramolecular ligand possessing a zinc-porphyrin recognition site and a triazolo-pyridine peripherally appended coordinating arm. The application of such system towards the exceptionally *meta*-selective iridium catalyzed C-H borylation of pyridines and C-5 postion of *N*-alkylimidazoles was studied. It showed interesting enzyme-like properties according to mechanistic and kinetic investigations. Both a spatial and temporal control of the reaction was reported thanks to Zn···N dynamic weak interaction.

Chapter 3: In this chapter, the limitations encountered during the first optimization of the *meta*-selective C-H borylation of azines in chapter 2 were investigated. The understanding of the manifold deactivation pathways of the Zn···N interaction required for both the catalyst selectivity and activity led to the synthesis of an electron rich supramolecular ligand that outperforms state of the art iridium catalysts in C-H borylations of azines.

Chapter 4: This 4th chapter is devoted to the develomnet and the mechanistic investigation of the *ortho*-selective iridium-catalyzed C-H borylation of tertiary benzamides by the supramolecular and non supramolecular ligand families reported in previous chapters. It does represent a unique case which the selectivity encountered is controlled by the 1st coordination sphere of the catalyst, and the activity

enhanced by its 2nd coordination sphere *via* a single Zn···O=C weak interaction. On the other hand, the careful examination of the products distribution enabled the optimization of the experimental procedure in order to trap undesired side-products. This example represents the first use of simple triazolo-pyridines as a new *N*,*N*-chelating ligands for *ortho*-selective undirected C-H borylation of arenes.

Chapter 5: Chapter 5 describes the efforts devoted to establish a new route to access supramolecular ligands similar to those described in chapters 2 and 3. The strategy relies on the access to sulfonyl triazole intermediates by copper-catalyzed click chemistry that, unexpectedly, do not form due to the presence of the zinc-porphyrin scaffold near to the active copper species. Indeed, the copper catalyst undergoes a different chemo-selective reaction pathway reacting with traces of alcohols or water from the media as nucleophiles and leading to sulfonyl imidates or sulfonyl amides covalently-connected to zinc-porphyrins. We demonstrate that copper-catalyzed click reactions can undergo different reaction mechanisms when the catalytic events occur at close proximity of a zinc-porphyrin that acts as a Lewis acid to stabilize otherwise inaccessible reaction intermediates.

Chapter 6: This chapter describes the serendipitous formation of a by-product formed during the synthesis of the supramolecular ligands described in chapters 2 and 3. It results from the dimerization of a zinc-porphyrin containing an alkyne fragment in the *ortho* position of one of the *meso* phenyl rings. This species is highly sterically hindered since the two porphyrin platforms are connected through a relatively small and highly uni-directional 1,3-butadiyne motif. Alternatively, this species was prepared in high yields by copper catalysis using reaction conditions derived from the Glaser-Hay coupling. Although this dimeric zinc-porphyrin appears as highly encumbered, there is a free chemical bond rotation around the diacetylene backbone. As a result, this poorly pre-organized dimer behaves as a host by rearranging in the presence of 1,4-diazabicyclo[2.2.2]octane (DABCO), to form a pseudo-capsular supramolecular complex in which one molecule of DABCO is trapped between the two zinc-porphyrin units *via* Zn···N non-covalent interactions. As such, the requirements to take benefit from supramolecular encapsulation can be reduced to a minimal covalent linkage between zinc-porphyrins.

Chapter 7: The last chapter of this PhD thesis shows the use of a bio-inspired iron-porphyrin for the Wacker-type oxidation of both aromatic as well as aliphatic olefins using stoichiometric amounts of hydrosilane as the reductant with very high activity. The tetracarboxylic-tetraphenyl-iron-porphyrin synthesized was found to be an effective catalyst that unexpectedly deactivate itself *via* an aerobic pathway towards the formation of a μ-oxo bridged diiron, which is a catalytically unproductive form. Mechanism investigations enabled precise fine-tuning of experimental conditions by using more active hydrosilane derivative to boost catalyst reactivity. Furthermore, ^{1}H NMR studies showed formation of the so far elusive Fe-H postulated active intermediate. Simple recyclability of the catalyst as well as ON/OFF oxidation by chemical stimuli are also featured.

References

[1] *Catalysis: from principles to applications*, Eds: M. Beller, A. Renken, R. A. van Santen, Wiley-VCH, **2012**.

[2] *Organocatalysis*, Eds: M. Reetz, B. List, S. Jaroch, H. Weinmann, Springer, **2008**.

[3] *Comprehensive Enantioselective Organocatalysis: Catalysts, Reactions, and Applications*, Ed: P. I. Dalko, Wiley-VCH, **2013**.

[4] *Organotransition metal chemistry. From bonding to catalysis*, Ed: J. F. Hartwig, University Science Books, **2010**.

[5] *Supramolecular catalysis*, Ed: P. W. N. M. van Leeuwen, Wiley-VCH, **2008**.

[6] D. Ringe, G. A. Petsko, *Science* **2008**, *320*, 1428–1429.

[7] M. Raynal, P. Ballester, A. Vidal-Ferran, P. W. N. M. van Leeuwen, *Chem. Soc. Rev.* **2014**, *43*, 1734–1787.

[8] S. H. A. M. Leenders, R. Gramage-Doria, B. de Bruin, J. N. H. Reek, *Chem. Soc. Rev.* **2015**, *44*, 433–448.

[9] G. G. Hammes, S. J. Benkovic, S. Hammes-Schiffer, *Biochemistry* **2011**, *50*, 10422–10430.

[10] X. Zhang, K. N. Houk, *Acc. Chem. Res.* **2005**, *38*, 379–385.

[11] K. N. Houk, A. G. Leach, S. P. Kim, X. Zhang, *Angew. Chem. Int. Ed.* **2003**, *42*, 4872–4897.

[12] P. Dydio, J. N. H. Reek, *Chem. Sci.* **2014**, *5*, 2135–2145.

[13] M. Raynal, P. Ballester, A. Vidal-Ferran, P. W. N. M. van Leeuwen, *Chem. Soc. Rev.* **2014**, *43*, 1660–1733.

[14] A. G. Doyle, E. N. Jacobsen, *Chem. Rev.* **2007**, *107*, 5713–5743.

[15] A. Warshel, P. K. Sharma, M. Kato, Y. Xiang, H. Liu, M. H. M. Olsson, *Chem. Rev.* **2006**, *106*, 3210–3235.

[16] I. Beletskaya, V. S. Tyurin, A. Y. Tsivadze, R. Guilard, C. Stern, *Chem. Rev*. **2009**, *109*, 1659–1713.

[17] Y. Nakamura, N. Aratani, A. Osuka, *Chem. Soc. Rev.* **2007**, *36*, 831–845.

[18] M. W. Hosseini, *Acc. Chem. Res.* **2005**, *38*, 313–323.

[19] P. S. Bols, H. L. Anderson, *Acc. Chem. Res.* **2018**, *51*, 2083–2092.

[20] A. W. Kleij, J. N. H. Reek, *Chem. Eur. J.* **2006**, *12*, 4218–4227.

[21] K. S. Suslick, N. A. Rakow, M. E. Kosal, J.-H. Chou, *J. Porph. Phthalo.* **2000**, *4*, 407–413.

[22] P. Thodarson, *Chem. Soc. Rev.* **2011**, *40*, 1305–1323.

[23] R. P. Bonar-Law, L. G. Mackay, C. J. Walter, V. Marvaud, J. K. M. Sanders, *Pure Appl. Chem.* **1994**, *66*, 803–810.

[24] J. K. M. Sanders, *Pure Appl. Chem.* **2000**, *72*, 2265–2274.

[25] C. J. Waiter, H. L. Anderson, J. K. M. Sanders, *J. Chem. Soc., Chem. Commun.* **1993**, 458–460.

[26] R. S. Wylie, J. K. M. Sanders, *Tetrahedron* **1995**, *51*, 513–526.

[27] M. Marty, Z. Clyde-Watson, L. J. Twyman, M. Nakash, J. K. M. Sanders, *Chem. Commun.* **1998**, 2265–2266.

[28] M. Nakash, Z. Clyde-Watson, N. Feeder, J. E. Davies, S. J. Teat, J. K. M. Sanders, *J. Am. Chem. Soc.* **2000,** *122*, 5286–5293.

[29] L. G. Mackay, R. S. Wylie, J. K. M. Sanders, *J. Am. Chem. Soc.* **1994,** *116*, 3141–3142.

[30] C. G. Oliveri, N. C. Gianneschi, S. T. Nguyen, C. A. Mirkin, C. L. Stern, Z. Wawrzak, M. Pink, *J. Am. Chem. Soc.* **2006**, *128*, 16286–16296.
[31] A. M. Shultz, O. K. Farha, J. T. Hupp, S. T. Nguyen, *J. Am. Chem. Soc.* **2009**, *131*, 4204–4205.
[32] B. Kang, J. W. Kurutz, K.-T. Youm, R. K. Totten, J. T. Hupp, S. T. Nguyen, *Chem. Sci.* **2012**, *3*, 1938–1944.
[33] M. Beller, C. Bolm, *Transition Metals for Organic Synthesis*, Wiley-VCH, Weinheim, **2004**.
[34] A. de Meijere, S. Braese, M. Oestreich, *Metal-Catalyzed Cross-Coupling Reactions and More*, Wiley-VCH, Weinheim, **2014**.
[35] P. W. N. M. van Leeuwen, *Homogeneous Catalysis: Understanding the Art*, Kluwer, Dordrecht, **2004**.
[36] S. Jonsson, F. G. J. Odille, P.-O. Norrby, K. Warnmark, *Chem. Commun.* **2005**, 549–551.
[37] E. Lindback, S. Dawaigher, K. Warnmark, *Chem. Eur. J.* **2014**, *20*, 13432–13481.
[38] S. Jonsson, F. G. J. Odille, P.-O. Norrby, K. Warnmark, *Org. Biomol. Chem.* **2006**, *4*, 1927–1948.
[39] F. G. J. Odille, S. Jonsson, S. Stjernqvist, T. Ryden, K. Warnmark, *Chem. Eur. J.* **2007**, *13*, 9617– 9636.
[40] E. Lindback, S. Cherraben, J.-P. Francoia, Es. Sheibani, B. Lukowski, A. Pron, H. Norouzi-Arasi, K. Mansson, P. Bujalowski, A. Cederbalk, T. H. Pham, T. Wixe, S. Dawaigher, K. Warnmark, *ChemCatChem* **2015**, *7*, 333–348.
[41] M. Kadri, J. Hou, V. Dorcet, T. Roisnel, L. Bechki, A. Miloudi, C. Bruneau, R. Gramage-Doria, *Chem. Eur. J.* **2017**, *23*, 5033–5043.
[42] P. Zardi, T. Roisnel, R. Gramage-Doria, *Chem. Eur. J.* **2019**, *25*, 627–634.
[43] M. Saito, Y. Nishibayashi, S. Uemura, *Organometallics* **2004**, *23*, 4012–4017.
[44] P. D. Harvey, S. Tasan, C. P. Gros, C. H. Devillers, P. Richard, P. Le Gendre, E. Bodio, *Organometallics* **2015**, *34*, 1218−1227.
[45] B. M. J. M. Suijkerbuijk, R. J. M. Klein Gebbink, *Angew. Chem. Int. Ed.* **2008**, *47*, 7396–7421.
[46] J.-F. Longevial, S. Clément, J. A. Wytko, R. Ruppert, J. Weiss, S. Richeter, *Chem. Eur. J.* **2018**, *24*, 15442–15460.

Chapter 1. Beyond hydrogen bonding: recent trends in outer sphere interactions in transition metal catalysis

1.1. Introduction.

The fundamental understanding of transition metal reactivity is at the core of the design of efficient homogeneous catalysts with relevance for small molecule synthesis.[1] Consequently, new chemical reactions that are useful from drug discovery at the small scale to implementation in large industrial plants have been disclosed.[2] Furthermore, the last few decades have witnessed tremendous advancements that have established the importance of ligand design for controlling the reactivity outcome in homogeneous catalysis.[3]

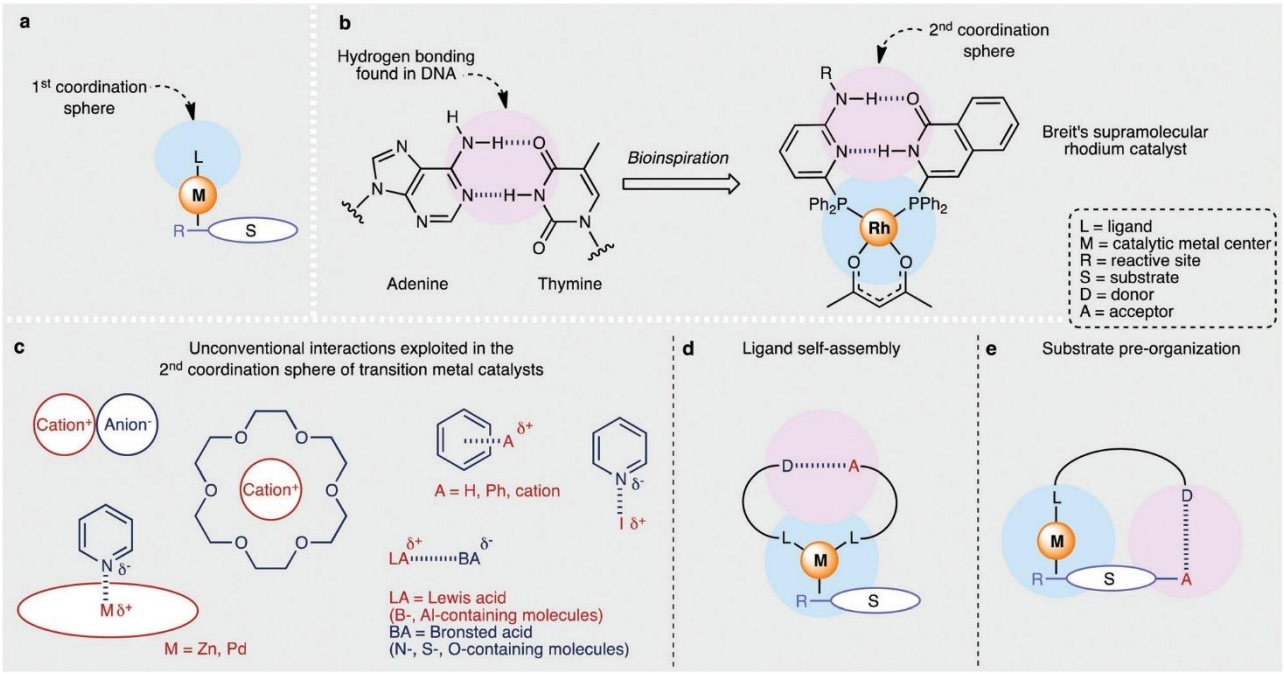

Figure 1. The relevance of first and second coordination sphere effects in transition metal catalysis. **(a)** Schematic representation of the first coordination sphere in a transition metal catalyst. **(b)** DNA-inspired hydrogen bonding features in the second coordination sphere of a transition metal catalyst to exert control on the reactivity. **(c)** Several examples of unconventional interactions that control the activity and selectivity in transition metal catalysts through the second coordination sphere. This type of interactions can be used for ligand self-assembly **(d)** or substrate pre-organization **(e)**.

As such, the careful fine-tuning of the stereoelectronic parameters of the ligand, that is, the first coordination sphere, has direct consequences on the catalyst performance (**Fig. 1a**).[4] For example, the P–M–P bite angle in diphosphane-ligated rhodium catalysts is an important parameter to control the linear:branched ratio of aldehydes formed in the hydroformylation of terminal olefins. Analogously, the rate of reductive elimination in phosphane-ligated palladium catalysts is largely determined by the electronic nature of the phosphorus center.[5]

On the other hand, nature's catalysts (enzymes) exploit a number of different strategies to control the activity and selectivity. Most of them are based on dynamic and reversible events occurring in locations remote from the active site to adapt their spatial conformation to the substrate with the aim of precisely pre-organizing it for reaching a given selectivity or to protect the active site in a hydrophobic pocket inside the whole protein.[6] Chemists have forever been fascinated to mimic these features in homo- geneous catalysis as it may lead to new reactivities in abiological systems.[7,8] Initially, catalyst encapsulation via covalent chemistry or hydrophobic effects,[9–13] and later, by means of supramolecular coordination chemistry,[14–16] led to catalytic systems featuring enhanced catalyst stability together with new chemical trajectories. These strategies laid the foundation of supramolecular catalysis, which is based on second coordination sphere effects, aiming to overcome the limitations and span the scope of traditional ligands.[17–20]

Alternatively, and much inspired from the hydrogen bonding in DNA base pairs, transition metal catalysts have incorporated hydrogen bonding recognition sites in the second coordination sphere (**Fig. 1b**). Thereafter, the use of hydrogen bonding for the formation of self-assembled ligands as well as the positioning of substrates around the active site in a restricted conformation has been extensively explored with remarkable reactivity patterns.[21–26] In order to surpass this existing knowledge and tackle the issues that cannot be addressed by the current approaches, it is important to rationally design catalytic systems with original action modes.[27] In this context, exploiting interactions other than hydrogen bonding occurring far from the first coordination sphere of the transition metal catalyst is an attractive concept that has received increasing attention (**Fig. 1c**). The most developed and studied interactions include dipole/dipole (those involving π aromatic systems, halogen bonding), electro- static (ion pairing, cation···crown ethers), and dative covalent bonds (Lewis pairing, metal···nitrogen bonding). The energy associated with these interactions, which can be as small as 1 kcal mol^{-1}, is enough to stabilize unique intermediates in transition metal catalysis, which allows access to otherwise unfavorable reaction pathways, thereby opening a new chemical space (**Fig. 1d and e**).

In this survey, particular focus has been devoted to those interactions taking place significantly far away from the first coordination sphere of the metal catalyst and those that do not impart any stereoelectronic effect to the active site. However, their manifolds provide interesting new ways of substrate pre-organization and customizing new self-assembled ligands. The present review covers the major advances accomplished in the last five years since starting this PhD thesis (from 2015 to 2019/2020),[24] in which the benefits of harnessing such uncommon interactions in transition metal

catalysis in a remote fashion have been undoubtedly validated by means of extensive control experiments and/or substantial computational modelling. Examples involving secondary sphere interactions for promoting the catalysis of small molecules (H_2, CO_2, O_2, N_2H_4, etc.), typically via electrocatalysis, are beyond the scope of this review and have been surveyed elsewhere.[28–34]

1.2. Ion-pairing.

1.2.1. Ion-pairing for substrate pre-organization.

Electrostatic interactions, a sub-class of non-covalent interactions, between cationic and anionic amino acid residues, cofactors, and/or substrates are prevalent in enzymes for accessing unique reaction pathways due to their reversibility.[35,36] However, the implementation of such type of non-covalent interactions in transition metal catalysis requires mastering them carefully at the molecular level, especially in order to prevent undesired aggregated species. One strategy is based on the use of electrostatic interactions to pre-organize substrates in a precise conformation around the catalytically active metal site.[37] In this context, the Ooi group showcased the unique potential of phosphine ligands covalently appended with chiral quaternary ammonium motifs for the palladium-catalyzed construction of contiguous all-carbon quaternary stereocenters.[38] The asymmetric reactions studied were designed in a way that the remote chiral ammonium moiety from the ligand was ion-paired with the in situ generated carbanion from the substrate in the intermediate species prior to the cycloaddition to the palladium-coordinated π-allyl fragment (**Scheme 1**).

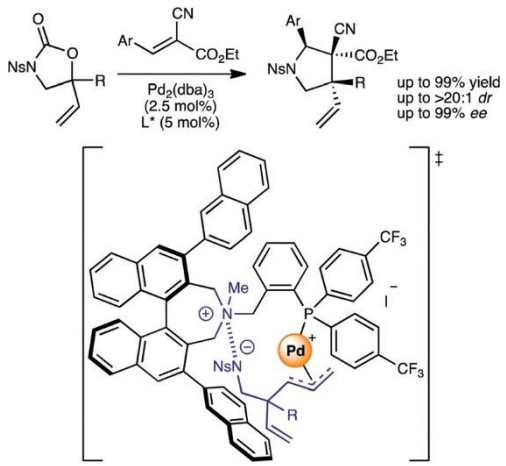

Scheme 1. An ammonium-containing phosphine ligand pre-organizes a substrate in a chiral pocket for highly asymmetric palladium-catalyzed reactions.

In particular, this was applied to the highly enantio- and diastereo-selective asymmetric [3+2] annulation of 5-vinyloxazolidinones and activated trisubstituted alkenes. The fine-tuning of the chiral ammonium-phosphine substituents in the ligands enabled a similar palladium-catalyzed reaction but

using N-protected primary imines instead of alkenes.[39] Ligands lacking the ammonium group led to poor reactivity and almost no selectivity.

The ammonium···anion pair interaction was utilized by Zhang's group for substrate pre-organization in the asymmetricrhodium-catalyzed hydrogenation of 1,1-disubstituted terminal olefins containing carboxylic acids.[40,41] Planar- and P-chiral ferrocene-derived ligands comprising both a rhodium-coordinating phosphane fragment and a tertiary amine unit were developed. The former served as an internal base for the deprotonation of the carboxylic acid group from the substrate and further as a non- covalent binding site to the latter (**Scheme 2**).

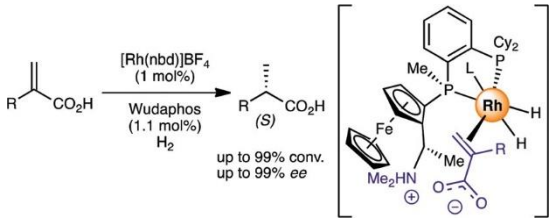

Scheme 2. The secondary ammonium···carboxylate interaction controls the asymmetric rhodium-catalyzed hydrogenation of carboxylic acid olefins.

A broad scope was demonstrated and impressive turnover numbers (up to 20 000) were reached with >99% enantioselectivity. An extension to substrates containing phosphoric acids in place of carboxylic acids led to high enantioselectivities thanks to the ammonium···phosphate anion pair interaction in this case.[42] The same group also reported ferrocene-derived phosphane ligands featuring a thiourea moiety that can undergo protonation under acidic conditions (i.e., HCl). In combination with rhodium or iridium, a variety of asymmetric hydrogenations were reported with chloride-assisted ion pairing with cationic substrates or cationic intermediates.[43–46]

The reversed possibility, which is the incorporation of cationic ammonium groups into substrates and anionic moieties in the ligand scaffold, was pioneered by the Phipps group. In order to tackle the very difficult regio-selective iridium-catalyzed C-H bond borylation of arenes, a bipyridine derivative ligand containing a peripheral sulfonate motif was successfully applied with quaternized benzylamines and anilines as the substrates, respectively.[47] In this scenario, the cationic ammonium group from the substrate underwent ion-pairing with the sulfonate group from the ligand, enforcing the iridium-catalyzed C-H bond borylation to selectively occur at the *meta* position of the arene ring (**Scheme 3**).

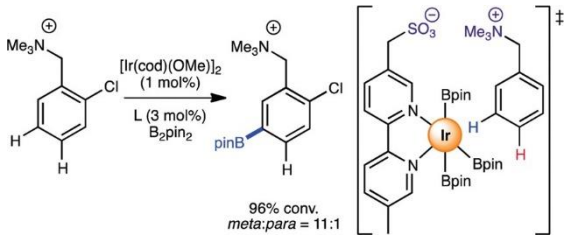

Scheme 3. The *meta*-selectivity in iridium-catalyzed C–H bond borylation is achieved due to secondary sulfonate···ammonium interactions between the ligand and the substrate.

The same ligand under comparable reaction conditions led to similar levels of *meta*-selectivity with substrates containing the ammonium group two or three bonds away from the arene ring.[48] Similar observations were reported with substrates containing cationic phoshonium groups.[49] In the absence of this outer sphere interaction, the selectivity drops to the expected statistical 1 : 1 mixture of *meta* and *para*-borylated products.

The same group devised a complementary strategy for *para*-selective C-H bond borylations employing sulfonated substrates containing cationic tetrabutylammonium counterions and a simple bipyridine ligand.[50] The perfect match between the sulfonate site and the bulky ammonium cation, both within the substrate, leaves exclusively the aromatic *para*-C-H bond accessible for functionalization (**Scheme 4**).

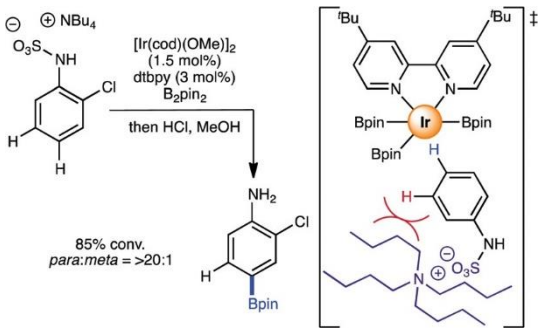

Scheme 4. The *para*-selectivity in iridium-catalyzed C–H bond borylation is achieved owing to secondary sulfonate···ammonium interactions between the substrate and an external ammonium salt.

Moreover, the regioselectivity outcome was fine-tuned by the size of the ammonium group. For instance, with a small tetramethylammonium anion, a *para* : *meta* ratio of 3.5 : 1 was obtained, whereas a larger tetrahexylammonium anion led to an exceptional 13 : 1 ratio. This is a unique case in which remote ion-pairing controls the regio-selectivity due to steric effects, although it cannot be strictly considered as an example of substrate-to-catalyst pre-organization as the previous examples. It is relevant to note that Smith, Malezcka, and co-workers described a very similar reaction design by remote ammonium···sulfonate anion pairing applied to alcohol-derived sulfates and amine-derived sulfamates, respectively.[51]

An increasing level of complexity was conceived by combining a threefold ion pairing as shown by the Phipps group. The design brings together both the anionic catalyst and substrate with the help of an alkali metal cation.[52] A Buchwald's type sulfonate-containing phosphine ligand enabled remote ion-pair interaction with the in situ deprotonated *N*-triflate-containing substrates via additional K^+ ion pairing, the latter originating from the base (**Scheme 5**).

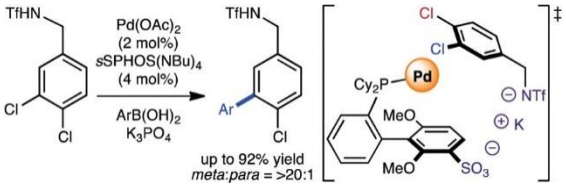

Scheme 5. The palladium-catalyzed *meta*-selective arylation of 1,2-dichlorobenzene derivatives was possible by exploiting a threefold ionic network.

This strategy was successfully utilized in site-selective palladium-catalyzed cross-couplings of 3,4-dichloroarenes, in which the differentiation of reactivity for both the chlorides is impossible with classical systems. Excellent levels of site-selectivity in favor of the reactivity at the *meta* chloride position were achieved due to the high pre-organization encountered between the substrate and the catalyst. Consequently, the remaining chloride substituent can readily undergo post-functionalization, thereby highlighting excellent orthogonal reactivity. The same type of dichlorinated substrates were also studied in palladium-catalyzed C-H bond arylation with fluorinated pyridine derivatives, in which this threefold ion pairing was responsible for the observed *meta* site-selectivity.[53] In subsequent studies, second coordination sphere electrostatic interactions involving potassium cations were exploited by the group of Chattopadhyay in regioselective iridium-catalyzed C-H bond borylations using a bipyridine ligand containing a quinolone moiety.[54] This functional group underwent tautomerization and deprotonation under catalytic conditions in order to recognize ester substrates *via* electrostatic interaction with the cationic alkali metals. Indeed, in the presence of catalytic amounts of a potassium source, the iridium-catalyzed C-H bond borylation was found to be *para*-selective (**Scheme 6**).

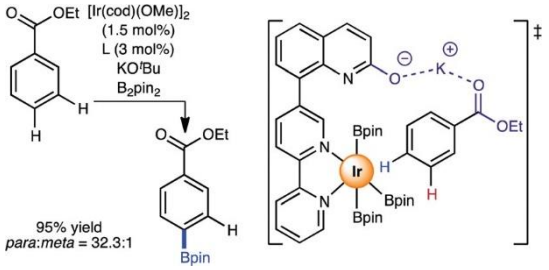

Scheme 6. An anionic ligand interacts with a neutral arene substrate via K^+···oxygen lone pair interactions, thus controlling the regioselectivity in iridium-catalyzed C-H bond borylation.

The same strategy applied to aromatic amides led to *meta*-selective borylated products, which was rationalized due to distorted K^+···O=C non-covalent interactions or through K^+··· π amide non-covalent interactions.[55] It is relevant to note that electrostatic interactions involving alkali cations (Li^+, Na^+, K^+, Cs^+) from (in)organic bases and anionic sites of substrates are known to decrease the key transition states' energy to some extent, according to theoretical calculations. Most of these types of interactions occur near to the first coordination sphere of the catalyst or they directly change the reactivity of the substrate; as such, they are typically postulated *a posteriori* due to the difficulty in anticipating the directionality of these interactions.[56–66]

1.2.2. Ion pairing for catalyst (and substrate) self-assembly.

Besides the use of ion pairing for substrate pre-organization, it is also possible to exploit it for the self-assembly of catalysts. Following their pioneering contribution regarding ion-pair self-assembled ligands for asymmetric palladium catalysis,[67] the Ooi group reported the further applications of this design by combining achiral phosphine ligands appended with cationic ammonium groups and deprotonated chiral phosphoric acids.[68] By these means, the control of the *E*/*Z* selectivity and the enantioselectivity was achieved for the palladium-catalyzed allylation of benzo- furanones with 1,2-disubstituted allylic carbonates (**Scheme 7**).

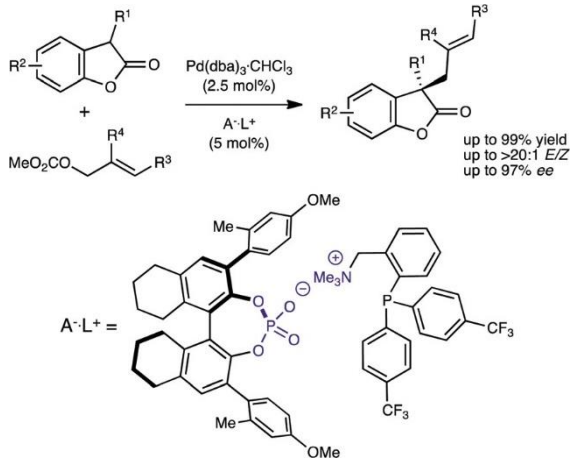

Scheme 7. A self-assembled ligand by secondary ammonium···phosphate interaction leads to highly asymmetric palladium-catalyzed transformation.

A clear advantage of this strategy is that there is no requirement to covalently introduce chiral elements in the phosphine ligand. In addition, owing to the straightforward in situ preparation of these supramolecular ligands, they were smartly used in a deconvolution strategy in which mixtures of ligands were employed for the rapid searching of the optimal catalytic system.[69] This was shown for the palladium-catalyzed asymmetric allylation of 3-benzylbenzothiophenone derivatives, in which 12 chiral acids and 12 achiral phosphine ligands were used. Compared to the 144 experiments that would have been conducted individually, the best conditions (*ee* up to 94%) were found with only 16 experiments by applying this combinatorial screening. Further applications to palladium-catalyzed branched-selective decarboxylative allylations were also addressed using achiral anions.[70]

Recently, the Phipps group assessed a similar ion pair strategy applied to the very challenging asymmetric iridium-catalyzed C-H bond borylation.[71] They employed an anionic sulfonated bipyridine ligand combined with a chiral cation derived from dihydroquinine (**Scheme 8**).

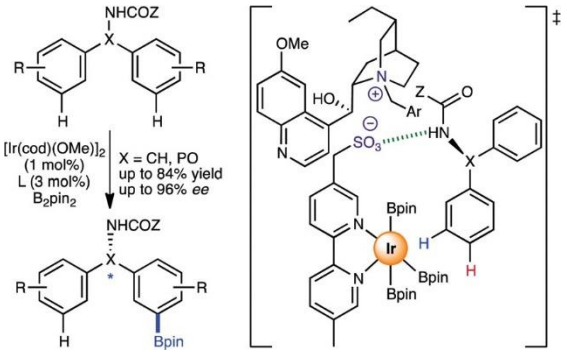

Scheme 8. A chiral cation self-assembles with an anionic catalyst, resulting in iridium-catalyzed C-H bond borylations with excellent enantioselectivity (green dashed lines indicate hydrogen bonding).

In addition, the sulfonate group in the ligand served for hydrogen bonding as well with the substrate to control the regioselectivity within the arene ring.[72] In this manner, a large number of chiral-at-carbon and chiral-at-phosphorus compounds were obtained with excellent enantioselectivities. The association constant for this type of assemblies was estimated to be 24 M^{-1}. This rather low value explains that small differences in the structure of both the ligands and the substrates lead to dramatic differences in the reactivity.

An interesting electrostatic interaction was rationalized for the outcome of the ruthenium-catalyzed cross-dehydrogenative coupling of arene carboxylic acids by Baidya and co-workers.[73] The role of DBU (1,8-diazabicyclo[5.4.0]undec-7-ene) as the base was not to directly participate in the C-H activation event but rather to handle the carboxylate anion *via* ion-pairing prior to the concerted metalation deprotonation step (**Scheme 9**).

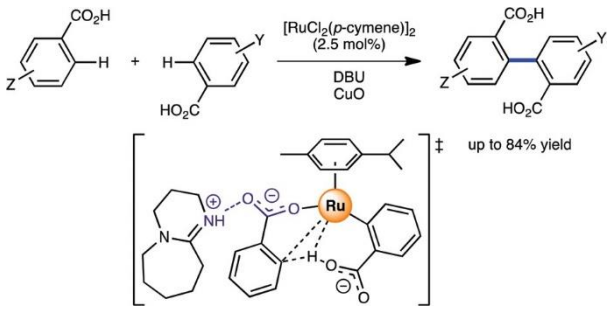

Scheme 9. Ruthenium-catalyzed cross-dehydrogenative coupling of arene carboxylicacids enabled by remote ion-pairing in the base-assisted C-H bond activation step.

Consequently, the energy required to access the key transition state was significantly reduced by 450 kcal mol^{-1} with respect to that required without the DBU remote ion pairing effect. With other bases, the reactivity of the catalyst was suppressed.

A very original case for the simultaneous pre-organization of both substrates and catalysts was shown by the Reek group thanks to multiple ion pairings inside the coordination-driven spheres.[74] Up

to 24 cationic guanidinium binding sites were endohedrically oriented and served as a platform to interact with both anionic sulfonate-containing gold catalysts and carboxylate-containing substrates (**Scheme 10**).

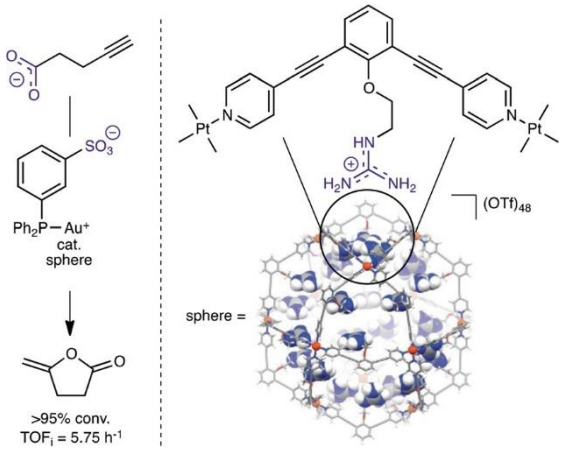

Scheme 10. Coordination-driven spheres self-assemble both sulfonated gold catalysts and anionic substrates, providing enhanced reactivities when compared to the bulk catalyst in solution. Adapted with permission from Springer Nature Limited.

The binding was two orders of magnitude higher for sulfonates than for carboxylates inside these spheres. As a result, the gold catalysts were well-fixed, whereas the carboxylate substrates were more dynamic, thus enabling their entrance and release, which is important for successful turnovers in catalysis. An on/off catalyst switch was showcased by using a more competitive sulfonate binder as well as a preliminary application to substrate-selective catalysis. This strategy also enabled to increase the gold concentration in the spheres at 41 M, which was used to study the effect of local gold concentrations in several gold-catalyzed cycloisomerization reactions.[75] The same type of guanidinium-containing spheres were used to encapsulate up to 12 sulfonate-containing copper catalysts via ion pairing.[76] This supramolecular design favored an unexpected dinuclear catalytic pathway that translated into reactions with increased rates and turnover numbers compared to the reactions in the bulk.

1.3. Cation···crown ether interactions.

1.3.1. Cation···crown ether interactions as cofactors or regulating agents.

One of the major breakthroughs of supramolecular chemistry was the discovery by Nobel-laureate Pedersen regarding the ability of crown ethers to bind to alkali metal cations via multiple electrostatic interactions between the cation and the crown ether oxygen lone pairs.[77,78] The association constants for this type of non-covalent interactions depend on the nature of the crown ether, i.e., the number of oxygen atoms available for binding and the spatial conformation, or the presence of additional heteroatoms.[79] In this context, the merger of these non-covalent interactions with transition metal catalysis has been reviewed in depth.[80–82]

Aiming to highlight herein only those recent examples in which a clear control by the second coordination sphere is evident, the contributions from Fan and Vidal-Ferran, independently, are remarkable (**Fig. 2**).

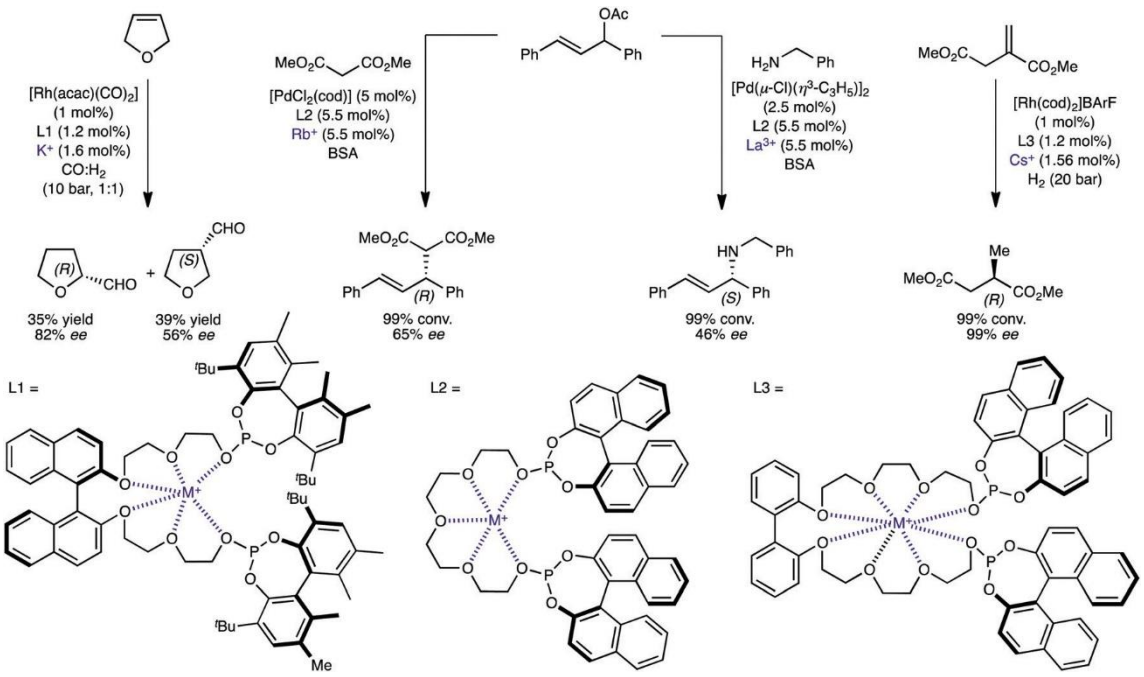

Figure 2. Chiral bisphosphite ligands appended with a crown ether self-fold in the presence of different cations (K^+, Rb^+, $La3^+$, or Cs^+), leading to highly asymmetric transformations under rhodium catalysis (hydroformylation, hydrogenation) or palladium catalysis (allylic alkylation).

They reported a number of chiral bis-phosphite ligands containing distal oligo(ethyleneglycol) backbones of different lengths and shapes. The overarching concept is that the flexible crown ether chain will fold in the presence of group 1 alkali metal cations, bringing the two nearby donor phosphorus atoms (P) for coordination to the transition metal center (M). Moreover, the geometry adopted in the remote binding of the alkali cation to the crown ether translates into a different coordination mode within the active site, for instance, providing different P–M–P bite angles that affect the activity and selectivity of catalysis. In particular, this strategy was successfully illustrated in asymmetric rhodium-catalyzed transformations (hydroformylation, hydrogenation)[83–86] and asymmetric palladium-catalyzed allylic substitutions.[87] Related versions for copper and gold catalysis, respectively, have been identified recently.[88,89] Overall, these alkali cations might be considered as regulating agents analogous to the cofactors that appear in enzymes as they modify the catalyst reactivity far from the active site (allosteric effect).[90] A similar supramolecular design based on a chelating diphosphane and a pyridine-containing crown ether has been successfully applied in asymmetric rhodium-and iridium-catalyzed hydrogenations.[91]

This supramolecular strategy was demonstrated to be also viable for asymmetric Henry reactions

between nitromethane and benzaldehydes when using Jacobsen-type chromium(III) salen complexes as the catalytically active sites.[92] As the mechanism is strongly supported to be dinuclear,[93] the presence of catalytic amounts of K^+ brings closer the two chromium centers, leading to a 13-fold enhancement in the reactivity (**Scheme 11**).

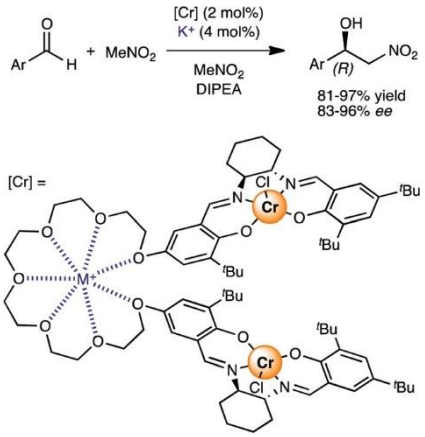

Scheme 11. The chromium-catalyzed asymmetric Henry reaction is feasible due to remote interactions between K+ and a crown ether moiety in the dinuclear catalyst.

Interestingly, this type of interaction was used for switching ON/OFF the catalytic activity. The Fan group developed (*S*)-aza-crownPhos supramolecular ligand consisting of a phosphoramidite backbone, which is known to be a suitable ligand for metal-catalyzed asymmetric hydrogenations, appended with a crown ether including a nitrogen heteroatom.[94] They showed that the coordination geometry around the phosphorus bis-ligated rhodium center was controlled by the presence or absence of sodium cations (**Scheme 12**).

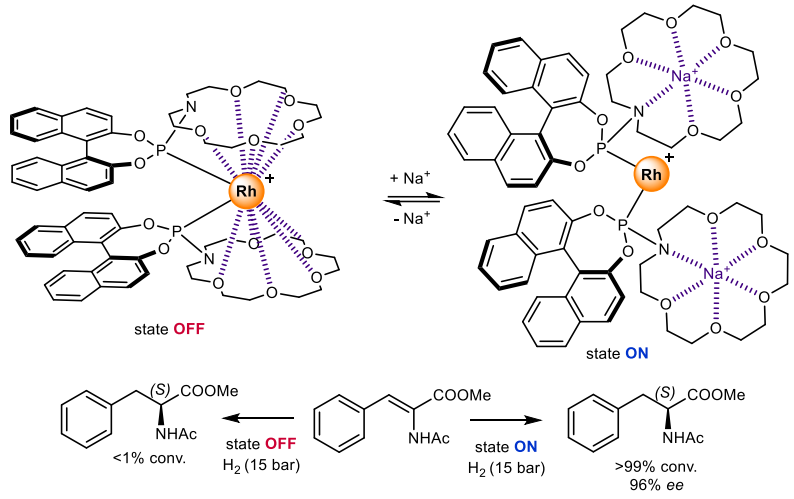

Scheme 12. The addition and removal of Na^+ alternatively leads to an in situ control of the activity (ON/OFF) of a rhodium catalyst.

When Na^+ cations were present in the reaction media, they were bound by the heterocyclic

crown ether, leaving the rhodium center free for engaging in the asymmetric hydrogenation of dehydroamino acid esters (ON state). On the other hand, in the absence of Na^+ cations, the phosphorus bis-ligated rhodium center was simultaneously interacting with both heterocyclic crown ethers, thereby inhibiting its catalytic activity (OFF state). The power of this strategy was further demonstrated by an *in situ* switch of the reactivity following the sequential addition of Na^+ (ON state) and [2.2.2]cryptand as the Na^+ scavenger (OFF state) in a couple of cycles.

1.3.2. Cation···crown ether interactions for substrate pre-organization.

Following the foundational work in palladium catalysis using crown ether functionalized ligands by Ito and Sawamura for substrate pre-organization,[95] in 2017, Costas and co-workers built up the first supramolecular metal catalyst exhibiting control of the site-selectivity via substrate pre-organization by means of cation···crown ether interactions.[96] A bispyridine-bipyrrolidine-coordinated manganese complex was covalently equipped with two remote crown ether receptors featuring a site selectivity (>50%) for the C8 and C9 oxidation of aliphatic ammonium salts, which is outstanding considering that the reactivity of all the aliphatic C-H bonds is energetically very similar. This unusual reactivity was a direct consequence of the suitable size and shape complementarity between the ammonium···crown ether recognition site and the catalytically active manganese site (**Scheme 13**).

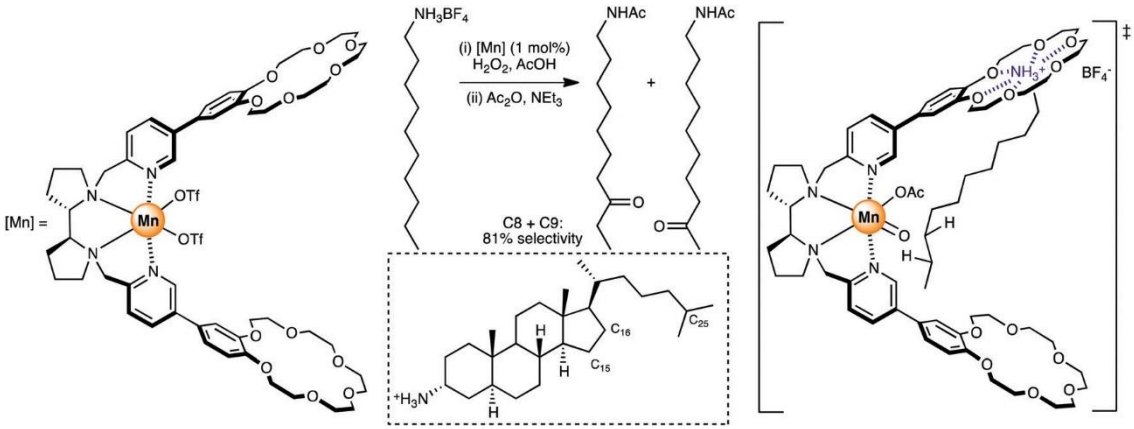

Scheme 13. Substrate-preorganization via ammonium···crown ether interactions within a manganese catalyst is responsible for the remote selectivity observed in the oxidation of alkanes.

The transition state for this system may adopt a very large 20-membered cycle, showing that even if the substrate recognition and the catalytically active sites are significantly wide apart, selective catalysis can take place. Application towards substrate-selectivity employing mixtures of substrates was disclosed.[97] Related iron and manganese catalysts were employed in the highly predictive oxidation of steroids at the challenging C15 and C16 positions (**Scheme 13**, framed).[98] Conventional catalysts will oxidize the most reactive C25 position or they will rather form a statistical mixture of products in other cases; thus, these supramolecular catalysts serve to reverse the classical selectivities.

1.4. π interactions.

1.4.1. CH···π interactions.

Reactions controlled by aromatic π interactions have witnessed a tremendous impact in organic synthesis and in asymmetric organocatalysis in particular.[99] The rational influence of such subtle interactions (typically <3 kcal mol^{-1} for the simplest case) in homogeneous transition metal catalysis is still under-exploited and it is usually detected *a posteriori*. This was the case for the seminal contribution from Noyori, unraveling the unexpected role of CH···π interactions for stabilizing the enantio-determining transition state in the ruthenium-catalyzed transfer hydrogenation of aromatic ketones that boosted further research in similar directions.[100] Examples of metal-catalyzed reactions controlled by non-covalent π-interactions in the first coordination sphere are known[101–105] but are beyond the scope of this review.

In 2018, the group of Mezzetti described a thorough computer-guided rational design of P-stereogenic iron pincer catalysts for the asymmetric hydrogenation of acetophenone, taking benefit of the CH···π interactions occurring in the second coordination sphere.[106] A modest enantiomeric excess was observed for one of the iron catalysts, which was rationalized by the presence of a single of these non-covalent interactions between a CH bond from the ligand and the aromatic ring from the substrate compatible with the well-accepted Noyori's bifunctional mechanism (**Scheme 14**, left).

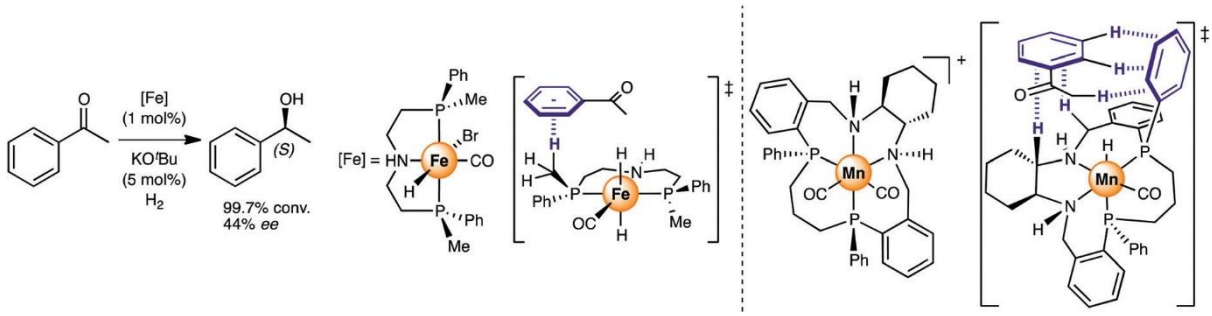

Scheme 14. The CH···π interactions stabilize the transition states in iron- and manganese-catalyzed asymmetric hydrogenation.

Similar findings were identified by replacing Fe(II) with Mn(I), although the system was less active.[107] In a very recent contribution, the same group developed an elegant Mn(I) catalyst derived from a $(NH)_2P_2$ macrocyclic ligand (**Scheme 14**, right) to access the *R* enantiomer with excellent enantioselectivity (>99% *ee*) and a broad functional group tolerance.[108] This time, multiple CH···π non-covalent interactions between the substrate and the ligand were at play (**Scheme 14**, right).

Analogously, Korenaga and co-workers reported the rhodium-catalyzed asymmetric 1,4-addition of arylboronic acids to coumarin, in which a fluorinated MeO-BIPHEP ligand was computationally identified on the basis of exclusive CH···π interactions between the ligand and the coumarin substrate (**Scheme 15**).[109]

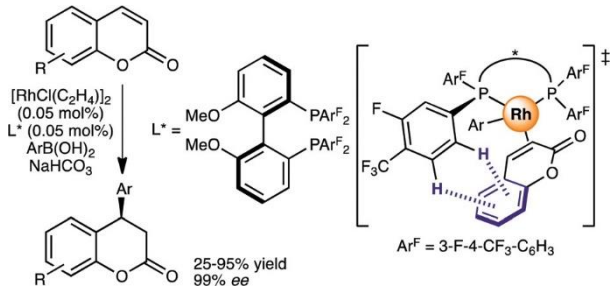

Scheme 15. A rhodium-catalyzed asymmetric 1,4-addition was controlled by remote CH···π interactions.

Although CH···π interactions are rather weak non-covalent interactions, they turn out to be significantly relevant when associated with other non-covalent interactions, typically, hydrogen bonding. For instance, this was demonstrated by Sigman and co-workers in the palladium-catalyzed enantioselective 1,1-diarylation of benzyl acrylates (**Scheme 16**),[110] and by Toste, Sunoj, and co-workers in the palladium-catalyzed enantioselective Heck–Matsuda arylation of a spyrocyclic pentene (**Scheme 17**).[111]

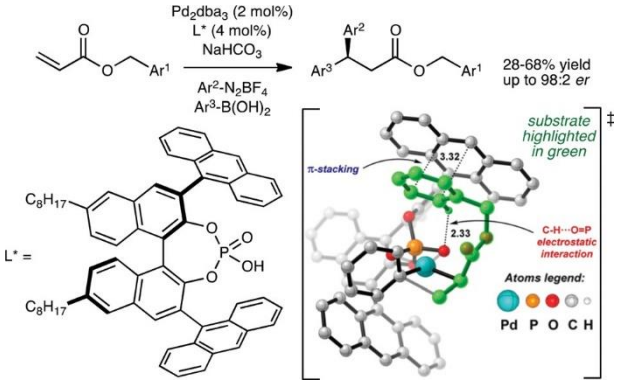

Scheme 16. The palladium-catalyzed enantioselective 1,1-diarylation of benzyl acrylates is assisted by a combination of remote CH···π interactions and hydrogen bonding. Adapted with permission from the American Chemical Society.

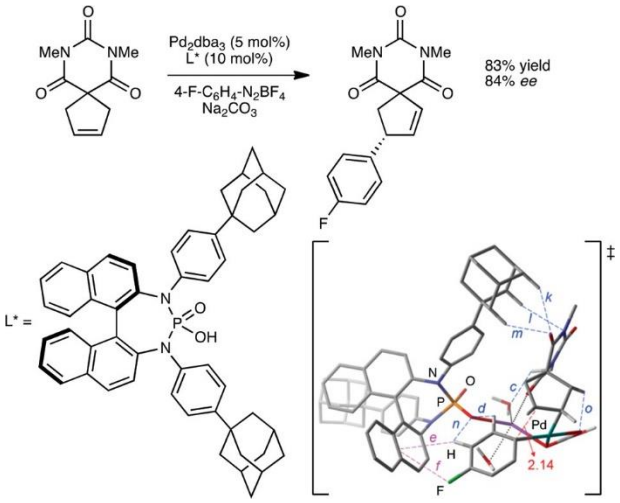

Scheme 17. Multiple weak interactions, some involving CH···π interactions, lead to highly asymmetric palladium-catalyzed Heck–Matsuda arylation. Adapted with permission from the American Chemical Society.

Sunoj and co-workers also identified similar features *a posteriori* in the asymmetric amination of alcohols by means of *in situ* dual catalysis, utilizing a phosphoric acid organocatalyst and a Cp*Ir(diamine) as the transition metal catalyst.[112] Similarly, Baudoin, Clot, and co-workers found that CH···π interactions played a key role in intramolecular asymmetric Pd-catalyzed functionalization of C(sp^3)-H bonds.[113]

1.4.2. π···π interactions.

Regarding transition metal catalysis exclusively directed by secondary π···π interactions, the group of Schomaker and Berry reported an interesting silver-catalyzed nitrene transfer highlighting such a feature.[114] The highly regio- and diasteroselective intramolecular C-H bond amination was largely driven by π···π stacking between the aromatic benzylic group from the substrate and one of the pyridine rings attached to the catalytically relevant cationic silver center (**Scheme 18**).

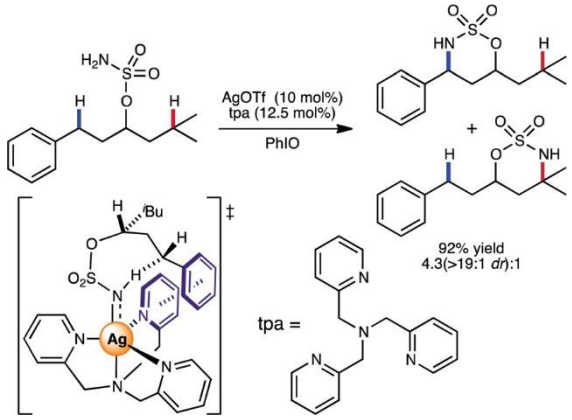

Scheme 18. The site- and diastereo-selectivity in silver-catalyzed C-H bond aminations is guided by remote π···π interactions.

Such a level of understanding enabled the successful utilization of this catalyst with challenging substrates to discriminate between energetically comparable C-H bonds.

In a subsequent study, a similar strategy was implemented by Chang and co-workers in a site-selective ruthenium-catalyzed C-H bond functionalization.[115] The mechanism-assisted design allowed the identification of a ruthenium-coordinated phenanthroline derivative as an unprecedented ligand for selective intramolecular C-H bond amidation in the benzylic position over a tertiary one in the same substrate (**Scheme 19**).

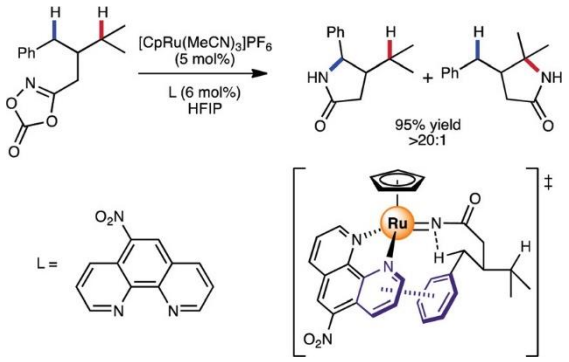

Scheme 19. The π···π interactions between the aromatic fragments in the ligand and the substrate dictate the site-selectivity in ruthenium-catalyzed C–H bond amidations.

The relevance of remote π···π stacking in the second coordination sphere of the catalyst between the substrate and the ligand was evidenced by the in-depth mechanistic studies and theoretical calculations. Very recently, Sawamura and co-workers reported a remote C(sp^3)-H borylation at the γ position of aliphatic amides and esters.[116] In the presence of a chiral phosphite and a urea-functionalized ligand, the iridium-catalyzed C-H borylation circumvented the classical reactivity patterns at the α and β positions due to a combination of secondary π···π interactions and hydrogen bonding (**Scheme 20**).

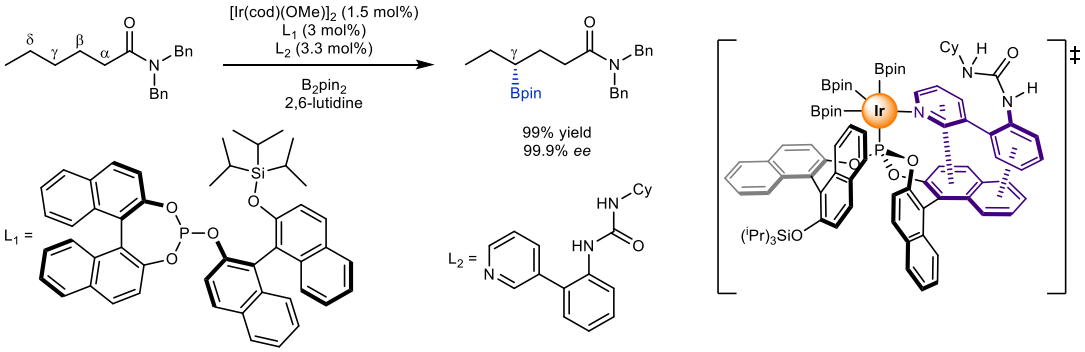

Scheme 20. Remote enantio-selectivity in the iridium-catalyzed C-H bond borylation with a ligand self-assembling by π···π interactions.

A previous design comprised π···π interactions between the ligand and a pyridine- containing substrate also for asymmetric iridium-catalyzed borylation.[117]

1.4.3. Cation···π interactions.

In the last decades, cation···π interactions have been studied by many research groups interested in organocatalysis, fine chemicals, and organometallics.[118–120] Unfortunately, little benefit is known from this type of interaction in transition metal homogeneous catalysis. The group of Walsh reported an appealing palladium-catalyzed benzylic arylation of toluene derivatives controlled by remote K^+···π non-covalent interactions.[121] The palladium-coordinated NIXANTPHOS ligand was responsible for this unique action mode thanks to the remote binding of nitrogen to potassium in such

a way that the aromatic toluene ring binds to the latter (**Scheme 21**).

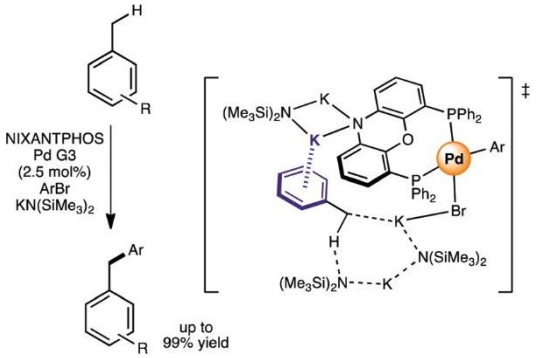

Scheme 21. The palladium-catalyzed benzylic arylation was possible due to remote $K^+\cdots\pi$ interactions.

This translates into a unique transition state, including a network of multiple interactions to access the key benzylic C-H bond activation/deprotonation step prior to the cross-coupling palladium events with the aryl bromide coupling partner. An expansion of this methodology towards aryl chlorides was shown by the same group using nickel catalysis and Na^+ for the remote cation π interaction.[122]

Analogously, *a posteriori* computational studies have revealed that $Cs^+\cdots\pi$ non-covalent interactions were involved in key intermediates for several palladium-catalyzed C-H bond functionalizations [123–126] and nickel-catalyzed C-O bond functionalizations,[127] although it remains difficult to categorize them as secondary interactions. The Miller group also postulated that distal $Cs^+\cdots\pi$ non-covalent interactions may explain the high enantioselectivity observed in some copper-catalyzed reactions using peptide-based ligands (**Scheme 22**).[128,129]

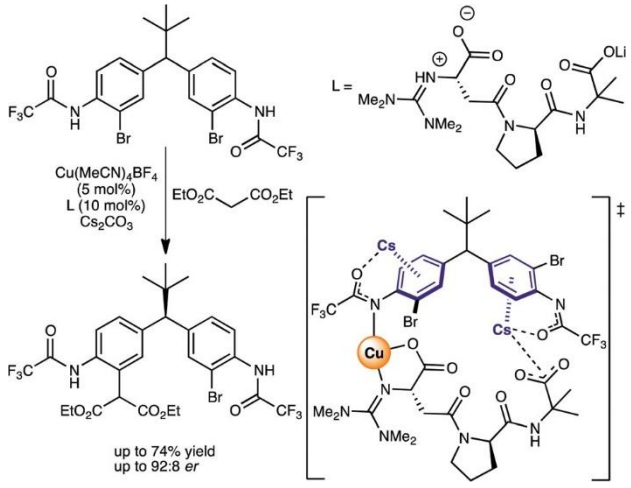

Scheme 22. The copper-catalyzed enantioselective desymmetrization of diarylmethane-based aryl bromides via secondary $Cs^+\cdots\pi$ interactions.

A more complex threefold cation···π···π interaction was evoked in a silver-catalyzed cycloisomerization.[130]

1.5. Halogen bonding.

In the last decade, organic transformations mediated by halogen bonding have received increasing attention.[131,132] However, their use in transition metal catalysis remains extremely rare to date since the pioneering discoveries from Charette's group in 2009, demonstrating that chiral Davies' rhodium cyclopropanation catalysts undergo an intramolecular halogen bonding network responsible for the all-up conformation that accounts for the excellent enantioselectivity observed employing this type of catalysts.[133,134] It was not until 2018 that Vidal-Ferran and co-workers reported the first example of a rationally-designed supramolecular rhodium catalyst, taking benefit of the unidirectional intermolecular halogen bonding.[135,136] Iodo-containing phosphanes and 2-pyridylphosphane self-assemble in the presence of a rhodium complex, leading to heteroleptic rhodium-carbonyl complexes featuring N···I halogen bonding. The iodine atom was additionally involved in coordination to the square-planar Rh(I) atom. These cationic rhodium complexes were remarkably stable in solution and in the solid state. Application to hydroboration of alkynes demonstrated that these systems are similarly reactive as $Rh(CO)(PPh_3)_3]^+$, although a different regio-selectivity (linear/branched) was observed (**Scheme 23**).

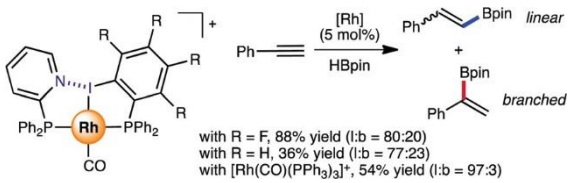

Scheme 23. N···I halogen bonding is used to self-assemble a rhodium catalyst that leads to high activity and branched-selectivity in the hydroboration of alkynes.

Halogen bonding can be rationally utilized for fixing a substrate in a precise conformation, as shown by Chevalier and co-workers. They reported a highly selective ruthenium- catalyzed 1 : 1 macrocyclization enabled by a halogen-bonded template comprising a tetra(iodoperfluorophenyl)ether scaffold.[137] The template was previously developed by Metrangolo and Resnati and was known for giving rise to a highly pre-organized conformation because of the π···π stacking as well.[138] In the catalytic system, the tetra(iodoperfluorophenyl)ether scaffold was bound to the bis-allyl-functionalized *N*-heterocycle substrate via N···I halogen bonding in a 1 : 2 stoichiometry, thereby locating the terminal alkene fragments at a sufficiently close proximity for the ruthenium catalyst to selectively perform the 1 : 1 olefin metathesis reaction, followed by *in situ* hydrogenation with $NaBH_4$ (**Scheme 24**).

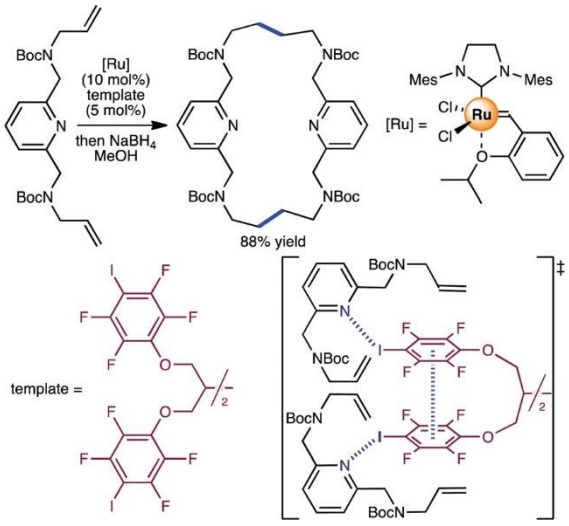

Scheme 24. A tetra(iodoperfluorophenyl)ether template pre-organizes two substrates via N···I halogen bonding prior to the ruthenium-catalyzed olefin metathesis macrocyclization.

Interestingly, the reaction required only catalytic amounts of the template and the catalytic outcome was correlated with the strength of the N···X halogen bonding utilizing other tetra(haloperfluorophenyl)ether scaffolds. Excellent isolated yields in the range of 90% were obtained for this challenging dimerization, which, under classical reaction conditions, should have formed substantial amounts of oligomeric side-products.

The groups of Arai and Yamanaka demonstrated the relevance of halogen bonding for the zinc-catalyzed asymmetric iodolactonization.[139] By means of control experiments and thorough theoretical calculations, a key halogen bonding between I_2 and both the reagents, the carboxylate-containing alkene substrate and *N*-iodosuccinimide (NIS), was proved (**Scheme 25**).

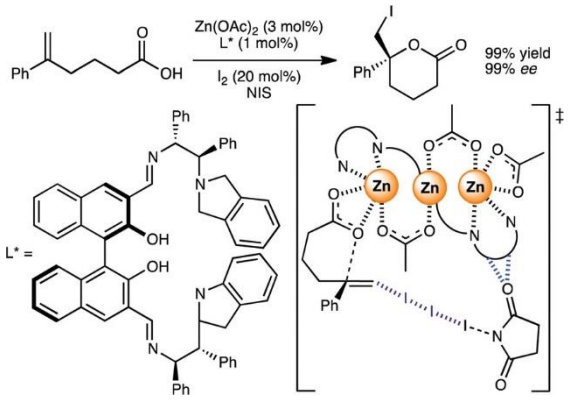

Scheme 25. The zinc-catalyzed asymmetric iodolactonization is dictated via a unique I···I···I···N halogen bonding network (blue dashed lines indicate hydrogen bonding).

This revealed that the true iodinating agent was I_2 and not the expected NIS with a catalytic cycle that regenerates I_2 at every turnover. As such, catalytic amounts of I_2 were enough to reach high levels of activity and asymmetric induction for this zinc-catalyzed transformation. Importantly, the key transition state of the reaction was accessible with a decrease of 410 kcal mol^{-1} owing to the secondary halogen bonding.

Very recently, Kitamura and co-workers reported a highly enantioselective ruthenium-catalyzed intramolecular cyclization of *N*-tethered pyrroles facilitated by secondary halogen bonding between a chloride substituent from the ligand and the aromatic cloud of the pyrrole unit (**Scheme 6**).[140]

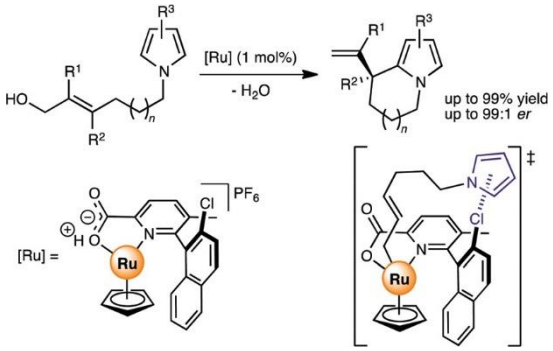

Scheme 26. The ruthenium-catalyzed allylative cyclization of pyrroles tethered at N(1) with allylic alcohols exploiting the secondary halogen bonding.

1.6. Lewis adducts.

1.6.1. Lewis adducts for substrate pre-organization.

In contrast to the previously described array of non-covalent interactions, the next ones cannot be categorized as non-covalent but dative; however, they share the reversible nature of interaction, which makes them suitable for reaching turnovers in catalysis. For instance, organocatalysis exploiting Lewis acid base adduct formation is well recognized in organic synthesis;[141] however, their rational use in transition metal catalysis is poorly developed.[142] Thereby, their successful application in transition metal catalysis is exemplified by the major breakthroughs reported by the groups of Kanai and Nakao. They designed different bipyridine derivative ligands appended with a remote Lewis acid site, enabling transient interaction with substrates comprising Lewis base functionalities.[143,144] After substantial ligand optimization, well-defined boron-containing acidic sites turned out to be suitable for interacting with sulfide fragments from thioanisole substrates and nitrogen atoms from 2-substituted pyridine substrates, respectively. When applied in iridium-catalyzed aromatic C-H bond borylations, *ortho*-borylated thioanisoles (**Scheme 27**, left) and *meta*-borylated 2-substituted pyridines (**Scheme 27**, right) were selectively formed due to the ideal pre-organization of the substrate around the catalyst to reach this regioselectivity.

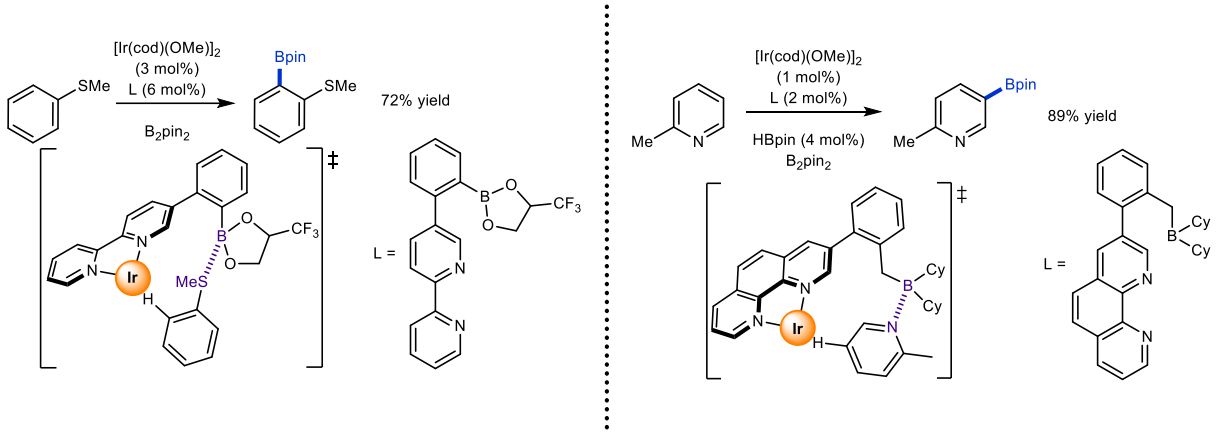

Scheme 27. Bipyridine ligands appended with boron sites control the regioselectivity of iridium-catalyzed aromatic C-H bond borylations via secondary B···S and B···N interactions.

This corresponds to the completely reversed regioselectivity that is obtained with a system lacking remote Lewis acid functionality.

In the same vein, Nakao and co-workers also showed the aptitude of aluminium-containing fragments to act as Lewis acidic sites for this type of catalysis.[144] In particular, benzamide derivatives gave rise to meta-selective borylated products due to the unique interaction between the carbonyl from the amide group and the aluminium center within the highly pre-organized ligand-to-substrate key intermediate (**Scheme 28**).

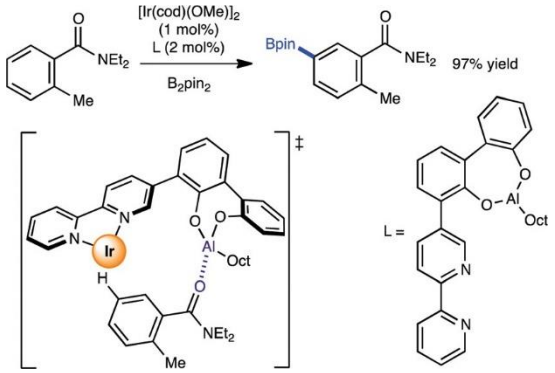

Scheme 28. A bipyridine ligand substituted with an aluminium site guides the meta-selectivity of iridium-catalyzed aromatic C-H bond borylations via secondary Al···O=C interactions.

1.6.2. Lewis adducts beyond ligand design.

Interestingly, in some cases, the Lewis acid functionality does not need to be covalently attached to the ligand but just present in catalytic amounts in the reaction mixture. In this way, the Nakao group showed that benzamide and pyridine derivatives were able to reversibly interact with aluminium-based Lewis acids (i.e., methylaluminium bis(2,6-di-tert-butyl-4-methylphen-oxide) = MAD), leaving the remote *para*-C-H bond exclusively available for borylation with an iridium

catalyst.[145] In this case, the formation of the Lewis adduct between the acid and the substrate sterically protects the C-H bonds in the *ortho* and *meta* position (**Scheme 29**).

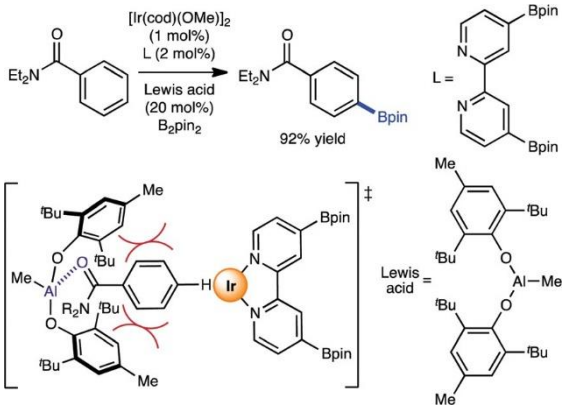

Scheme 29. The *para*-selectivity of the iridium-catalyzed C-H bond borylation of aromatic esters is achieved thanks to secondary Al···O=C interactions.

A complementary approach revealed *a posteriori* by the group of Chattopadhyay relied on B···N secondary interactions.[146] Benzaldehyde derivatives in situ formed the corresponding imines with over-stoichiometric amounts of primary amines that were further engaged in iridium-catalyzed C-H bond borylation using 3,4,7,8-tetramethyl-1,10-phenanthroline (TMP) as the ligand (**Scheme 30**).

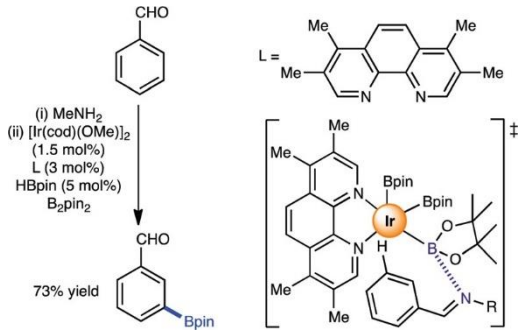

Scheme 30. The secondary B···N interactions are exploited for the iridium-catalyzed *meta*-C-H bond borylation of aromatic imines.

Control experiments suggested that the *meta*-selectivity outcome originated from secondary interactions between the Lewis base nitrogen atom from the substrate and the Lewis acid boron center belonging to an equatorial iridium-ligated pinacolato boron moiety. A similar reaction design was conceived through remote B···S interactions with aromatic substrates bearing a X-CH_2-SMe (X = O or NAc) pendant fragment.[147] This methodology allowed access to *ortho*-C-H borylated phenol and anilines after the deprotection of the sulfide-containing moiety.

1.7. M···N coordination.

1.7.1. Zn···N coordination for catalyst assembly.

Zn···N coordination between zinc(II)-porphyrins and nitrogen scaffolds have been largely utilized in supramolecular chemistry, material sciences, and physical processes (i.e., charge transfer).[148,149] Interestingly, in 2001, the Reek group showed that this type of interaction can be exploited for encapsulating a rhodium catalyst within a trispyridylphosphine *via* Zn···N coordination, leading to branched selectivity and high turnover frequencies (up to 400) in the hydroformylation of terminal olefins.[150] Since then, this type of secondary interaction has been utilized for the construction of effective metal catalysts, which have been reviewed.[151] Typically, the association constants for the binding between nitrogen scaffolds and Zn-porphyrinoids (or related zinc derivatives) lie in the range 10^3-10^5 M^{-1}, depending on the stereoelectronic parameters. In order to provide a recent overview here, it is worthy to mention the design of new zinc scaffolds to tune the second coordination sphere around the rhodium active site and its application in hydroformylation catalysis. For instance, zinc-porpholactones bind to the nitrogen atoms of tris(*meta*-pyridyl)phosphine one order of magnitude higher than their corresponding tetraphenylporphyrin version.[152] This resulted in an increase in the catalyst stability (even in the presence of polar and coordinating solvents) and higher branched-selectivity for the industrially relevant rhodium-catalyzed hydroformylation of propene (**Scheme 31**).

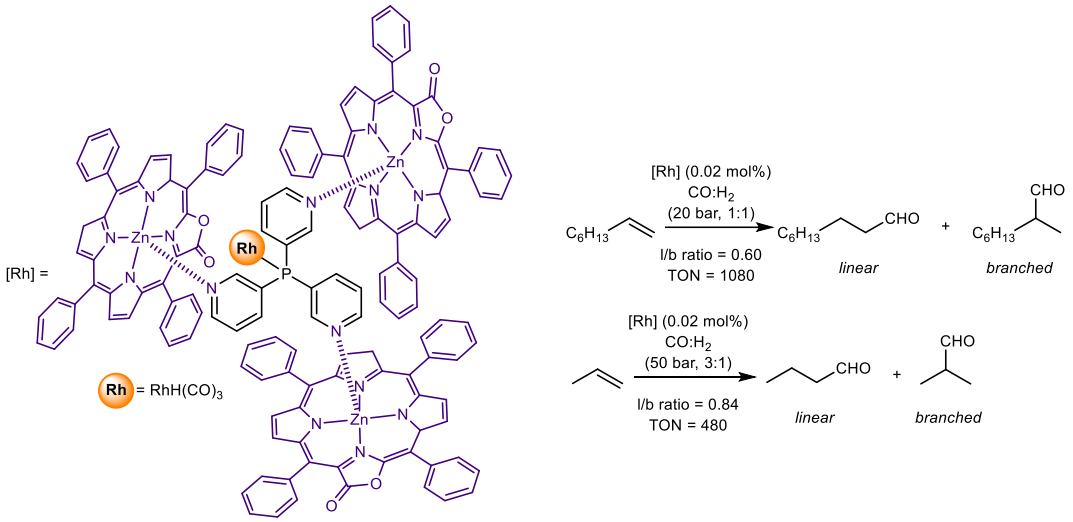

Scheme 31. The tris(*meta*-pyridyl)phosphine-ligated rhodium catalyst displays high branched selectivity and activity in the hydroformylation of olefins upon peripheral binding to zinc(II) porpholactone *via* Zn···N interactions.

Zinc-porphyrins bearing peripheral C-chiral moieties were used to create a secondary chiral environment around the active rhodium center; however, the level of enantio induction in the obtained chiral aldehydes was modest (up to 33% ee).[153]

The same tris(*meta*-pyridyl)phosphine ligand was able to interact with three Nolte's zinc-

porphyrin clips only in the presence of methylviologen derivatives as the co-factors (**Scheme 32**).[154]

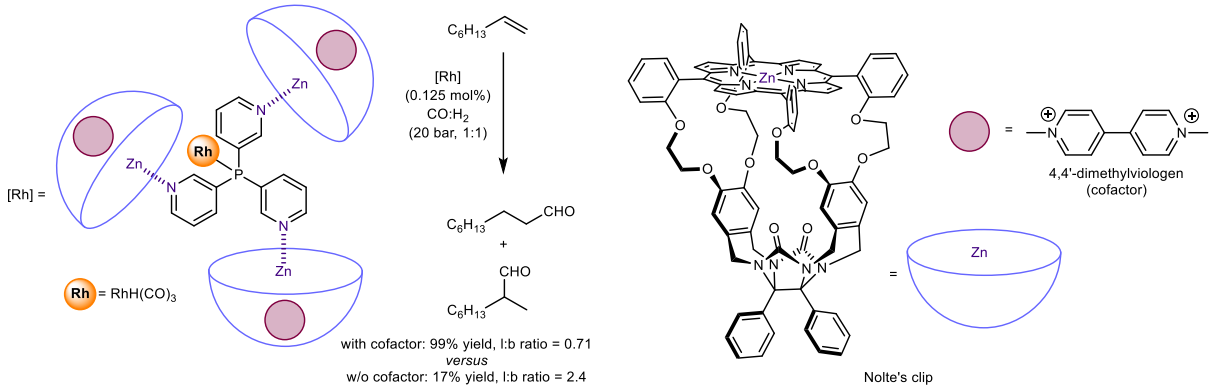

Scheme 32. The association of a cofactor (4,4'-dimethylviologen) within Nolte's zinc(II) porphyrin clip enables remote Zn···N interactions with the tris(*meta*-pyridyl)phosphine-ligated rhodium catalyst, leading to high activity and selectivity in the hydroformylation of olefins.

The former led to a charge-transfer complex within the clip, leaving the zinc center available for a strong *exo*-coordination to the nitrogen atoms of the phosphine ligand.[155] In the presence of rhodium, a confined active catalyst is formed, which displays high activity and selectivity for branched aldehydes in the hydroformylation of terminal olefins. In other words, the active catalyst forms only in the presence of the co-factor, which is rather novel for abiological catalysis.

Tris(*meta*-pyridyl)phosphine ligand was also identified as a suitable ditopic ligand to bind to a [FeFe] hdyrogenase mimic, leaving the nitrogen atoms free for interacting with a tetrahedral cage comprising zinc-porphyrin derivatives *via* Zn···N coordination (**Scheme 33**).[156]

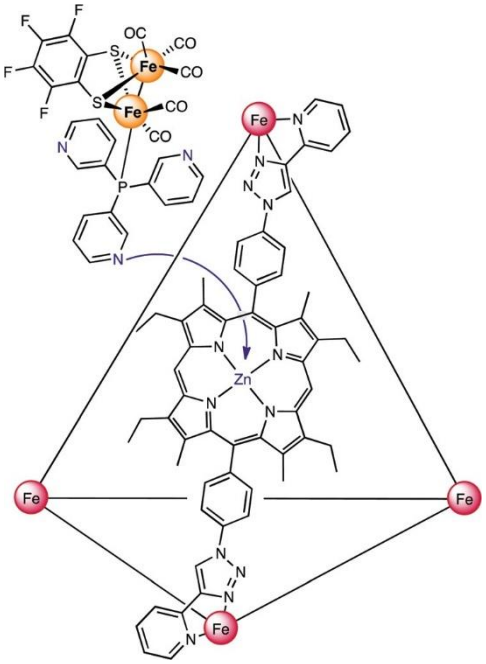

Scheme 33. An iron-based hydrogenase mimic (for proton reduction) featuring a tris(*meta*-pyridyl)phosphine ligand is encapsulated inside a zinc(II) porphyrin-based tetrahedral cage *via* Zn···N interactions.

The system was applied in the electrocatalytic proton reduction (H_2 evolution reaction), which is the half reaction of water splitting and is a relevant catalytic process for green and clean energies. Besides high stability, this system significantly decreased the overpotential of catalysis by 150 mV when compared to the non-confined one, which is an important step towards the design of artificial catalysts that compete with natural enzymes.

Other types of ditopic ligands other than tris(*meta*-pyridyl)-phosphine have been developed. For instance, tris(*para*-pyridyl)-phosphine was revealed to be appropriate due to its twofold encapsulation inside Nitschke's tetrahedral self-assembly made up from zinc-porphyrin derivatives *via* Zn···N coordination.[157] The design enables the *in situ* formation of a hydroformylation rhodium catalyst that features substrate selectivity, in which even-numbered olefins were more reactive than odd-numbered ones (**Scheme 34**).

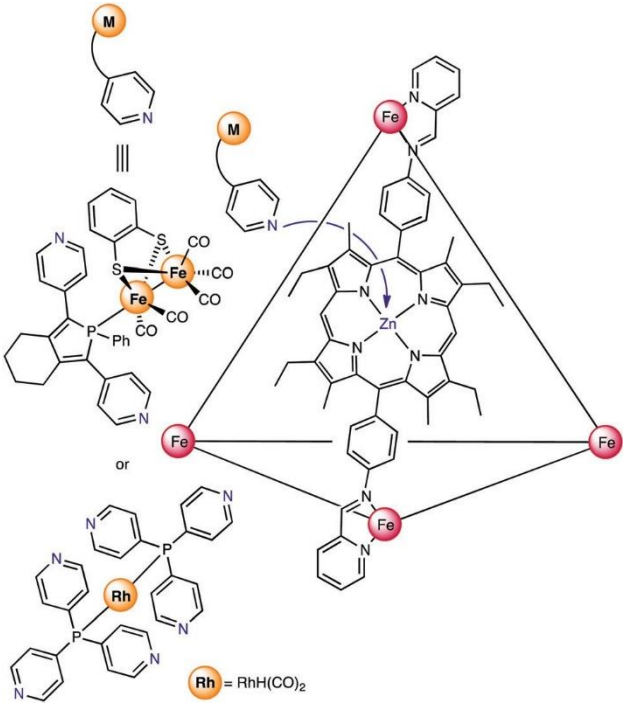

Scheme 34. An iron based hydrogenase mimic (for proton reduction) featuring a bis(para-pyridyl)phosphole ligand and a tris(para-pyridyl)phosphine-ligated rhodium catalyst (for hydroformylation) are confined in a zinc(II) porphyrin-based tetrahedral cage via Zn···N interactions.

The same tetrahedral assembly was used to encapsulate an [FeFe] hydrogenase mimic containing a pyridyl-phosphole moiety *via* Zn···N coordination.[158] The system was applied in the light-harvesting hydrogen evolution reaction, in which the zinc-porphyrins served as photosensitizers, allowing electron transfer to the encapsulated iron catalyst upon excitation (**Scheme 34**).

Secondary Zn···N coordination also drives the encapsulation of a chiral rhodium-coordinated phosphoramidite ligand inside Ribas's tetrahedral cage comprising zinc- porphyrins (**Scheme 35**).[159]

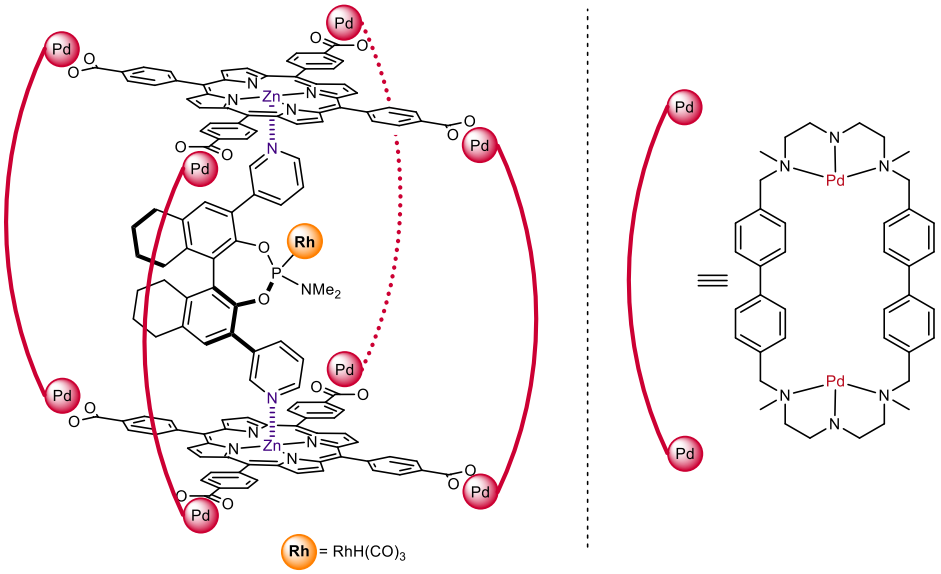

Scheme 35. A bis(*meta*-pyridyl)phosphoramidite-ligated rhodium catalyst (for hydroformylation) is confined in a zinc(II) porphyrin-based cage *via* Zn···N interactions.

The corresponding catalyst exhibited one of the highest activities (up to 1600 TOF) and enantioselectivities (up to 79% *ee*) for the mono-ligated rhodium species in the hydroformylation of styrene derivatives. Overall, the above-described examples show the impact of the second coordination sphere in the catalysis as the substrate can access only very selected geometrical conformations during the catalytic events.

1.7.2. Zn···N coordination for substrate pre-organization.

Alternatively to the previous approach, seminal contributions from the Sanders group have revealed the reversible nature of Zn···N coordination within dimers and trimers of zinc- porphyrins for accelerating and controlling the product selectivity in organic Diels-Alder transformations.[160,161] It was not until 2017 that this property was successfully utilized in transition metal catalysis. It was shown that the reactivity of chloro-and bromo-pyridines in palladium-catalyzed Suzuki and Heck reactions was strongly affected by the presence of zinc-containing scaffolds in the reaction mixture.[162] Increased reaction rates and reactivity were observed for those substrates able to interact with the zinc-containing scaffolds because they were involved in secondary Zn···N coordination whilst the palladium catalyst was operating. On the other hand, the substrates that did not interact with zinc-scaffolds led to catalyst deactivation by the over-coordination of the substrate (or product) to the palladium center. The catalytic activity of palladium was roughly correlated with the strength of the secondary Zn···N coordination, being higher with zinc-salphen than with zinc-tetraphenylporphyrin (**Scheme 36**, left).

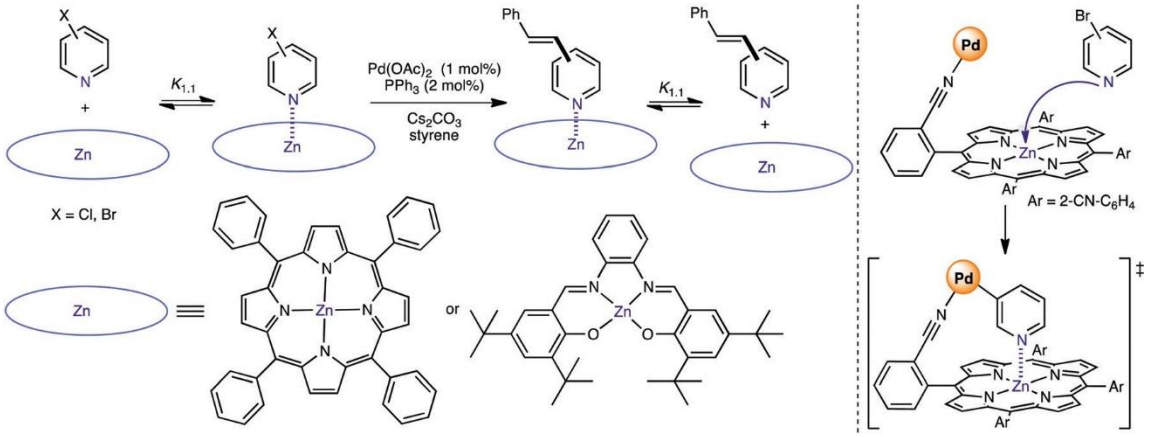

Scheme 36. Zn···N coordination between the zinc(II)-porphyrin or zinc(II)-salphen with halopyridine substrates indirectly increases the lifetime of the palladium catalyst to perform a Heck reaction (left) and a supramolecular palladium catalyst featuring a zinc(II) porphyrin as a substrate recognition site for halopyridine substrates (right).

Such an effect required, at least, one equivalent of zinc scaffold. A catalytic version was further developed customizing a zinc-tetraphenylporphyrin with four rigid nitrile groups in the periphery pointing to the porphyrin core. In this supramolecular ligand, there was space enough for pyridine derivatives to bind to the zinc center *via* Zn···N coordination, whereas the peripheral nitrile groups coordinate to the catalytically active palladium center.[163] In this manner, it was possible to perform substrate-selective catalysis for differentiating the reactivity between *ortho*-, *meta*-, and *para*-bromopyridine in Suzuki–Miyaura coupling reactions. The supramolecular catalyst fits perfectly for *meta*-bromopyridine (**Scheme 36**, right), a feature that was highlighted in competition experiments. Consequently, these studies established that the reversibility and dynamic nature of secondary Zn···N coordination are useful to design supramolecular catalysts in order to address reactivity issues arising from nitrogen-containing chemicals.

1.7.3. Pd···N coordination for substrate pre-organization.

The group of Yu has pioneered the use of highly sophisticated and covalently-linked directing groups to position a palladium active catalyst far beyond the classical *ortho*-selectivity for aromatic C-H bond functionalizations.[164] It is relevant to note that transition metal-catalyzed distal C-H bond activations are typically ensured by the directing groups, which impose issues associated to the introduction and removal of the directing group, besides the extensive efforts devoted to trial-and-error screening to search for an optimal catalytic system.[165,166] In 2017, the Yu group disclosed an approach based on so-called supramolecular templates that do not require the use of covalently-linked directing groups. These templates feature (1) a substrate recognition site based on a palladium-chelating unit and (2) a coordinating group based on nitriles or heterocyclic motifs to bind the active palladium catalyst. This design is particular useful for addressing difficult regio-selective C-H bond

functionalizations of nitrogen-containing heterocycles. The substrate interacts with the recognition site via secondary Pd···N coordination, thus pre-disposing a remote C-H bond at close proximity to the active palladium site. The distance and the geometry between both the binding and catalytic sites are the key parameters for the success of the catalysis (**Scheme 37**).

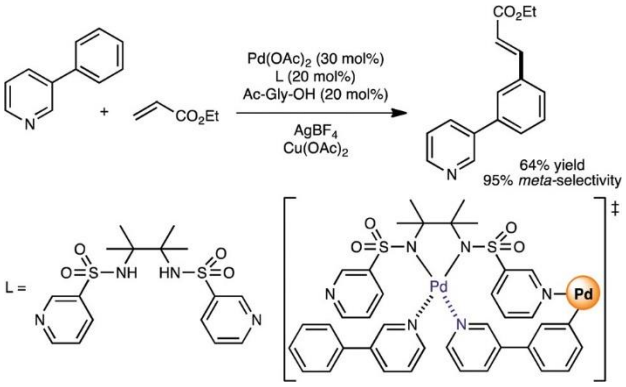

Scheme 37. The remote palladium-catalyzed C-H bond olefination of 3-phenylpyridines is possible owing to a supramolecular ligand containing a palladium fragment serving for substrate recognition *via* reversible Pd···N coordination.

For instance, this strategy was applied to palladium-catalyzed olefinations of C-H bonds located at the *meta*-position of the phenyl group belonging to 3-phenylpyridine derivatives under catalytic conditions.[167] C-H bond olefination at the C-5 position of quinoline derivatives was also demonstrated at the expense of using stoichiometric amounts of the palladium template (**Scheme 38**).[167]

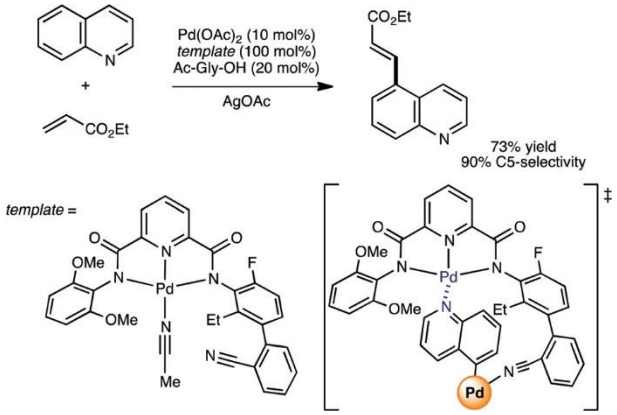

Scheme 38. Stoichiometric amounts of a C1-symmetric palladium template enabled the palladium-catalyzed C-H bond olefination of quinolines at the C5 position.

Such a methodology was corroborated by Maiti's group using C2-symmetric templates[168] and further expanded to thiazole substrates (**Scheme 39**).[169]

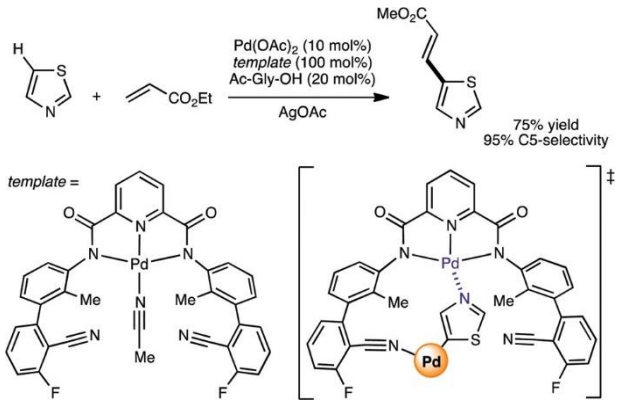

Scheme 39. A C2-symmetric palladium template displayed C5-selectivity for the palladium-catalyzed C–H bond olefination of thiazoles.

The same group employed allylic alcohols as coupling partners for the palladium-catalyzed C-H bond alkylation at the C-5 position of quinoline and thiazole derivatives, and at the C-7 position for benzothiazole and benzoxazole. This time, the reaction was enabled by a C1-symmetric template (**Scheme 40**).[170]

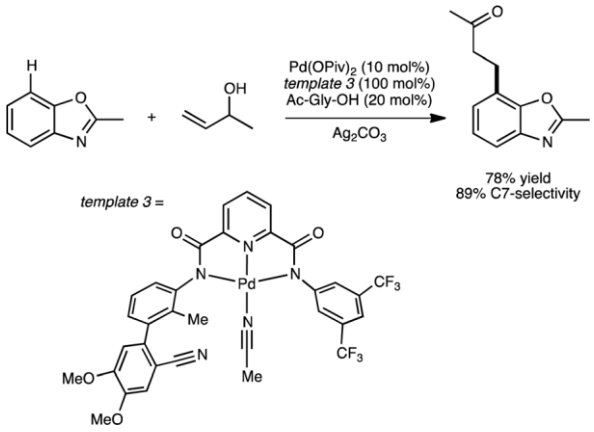

Scheme 40. A C1-symmetric palladium template enabling distal C-H bond selectivity for different heterocycles.

All these regio-selectivities cannot be achieved with ligands or templates lacking the well-designed recognition site within the second coordination sphere.

Such level of sophistication was upgraded by merging this template strategy with the Catellani reaction, which consists in employing a Pd/norbornene catalytic system to functionalize one C-H bond away from the first C-H bond activation.[171] As a consequence, remote C-H bond arylations of quinoline derivatives at the C-6 position were reached (**Scheme 41**). The exquisite control of regio-selectivity is astonishing as there are very little stereoelectronic differences between the C-6 and C-7

position within the quinoline skeleton.

Scheme 41. The C-H bond arylation at the C6 position of quinolines was addressed using a palladium template and a mediator (NBE-CO_2Me) exploiting secondary Pd···N coordination.

Due to the almost irreversible nature of the Pd···N interaction, this approach requires the use of significant amounts of expensive and scarce palladium (>100 mol% considering the template and the catalyst). Nevertheless, it provides access to regio-selectivities impossible to get with any other catalytic system to date. Furthermore, it is possible to recycle and recover the template by treatment with 4-dimethylaminopyridine, which coordinates more strongly to the palladium template than the substrates and the products, followed by a mild acidification.[167–171] It is relevant to note that the success of these strategies relies also on the non-negligible roles of mono-protected amino acids co-ligands, silver salts, and hexafluoroisopropanol as the solvent.

1.8. Conclusions and perspectives.

In summary, the above-described range of secondary interactions smartly combined with transition metal catalysts are efficient tools to provide unprecedented possibilities for controlling the activity and selectivity in organic transformations. These interactions are rather versatile. Indeed, they can be weak enough for substrate pre-organization in a reversible manner or much stronger, which make them relevant for the self-assembly of new ligand systems. The above-surveyed catalytic systems complement the traditional ones by increasing or reversing the selectivities (i.e., site, regio, stereo, enantio, diastereo) as well as by accessing otherwise unfavored products. New concepts, similar to those occurring in nature, emerge from these systems. For example, some catalysts display size-, shape-, or substrate-selectivity, which are difficult features to disclose with more classical homogeneous catalysts. In addition, several cases showcased high catalyst lifetime with notable turnover numbers and others displayed an *in situ* on/off control of reactivity, which are truly relevant for application purposes. Unfortunately, many examples still suffer from the lack of a detailed understanding of the strength of such interactions under catalytic conditions as well as kinetic studies that should help further rational developments. This knowledge might be useful for devising appropriate reaction conditions in which solvent properties and temperature are likely the most practical aspects for accessing the compatibility of the different components during catalysis.

A majority of the supramolecular catalysts discussed herein are based on scarce second and third

row late transition metals (Pd, Rh, Ir, Ru, etc.). Therefore, it will be also convenient to turn the attention to more abundant and affordable first row transition metals that have recently shown interesting catalytic performances,[172,173] in particular those derived from Fe, Cu, Co, Mn, and Ni. On the other hand, it remains difficult to fully predict the action mode of these new catalysts, which translates usually in significant efforts still devoted to trial-and-error screening to search for the optimal ones. In order to overcome this undesired consequence, the incorporation of deconvolution strategies,[174,175] high-throughput experimentation,[176,177] or exploiting dynamic combinatorial chemistry,[178] which are already well-established strategies in molecular catalysis, may play an important role in the future for this type of supramolecular catalysis.

Furthermore, it will be interesting to disclose the first examples of homogeneous transition metal catalysis controlled by well-defined secondary anion···π interactions,[179] which are so far elusive to date although known for organocatalysis.[180] Additional interactions such as London, dispersion interactions, or inductive effects, which could be considered more subtle and/or exotic interactions than the ones described in this review, may account for future developments,[181–183] although they appear to remain extremely difficult to apply for the prediction of catalytic outcomes.[184] Taking into account the entire discussion above, one can only expect a bright future for transition metal catalysts controlled by secondary interactions beyond hydrogen bonding and span the future possibilities of supramolecular catalysis.

1.9. References.

[1] *Homogeneous catalysis. Understanding the art*, ed. P. W. N. M. van Leeuwen, Springer, **2004**.

[2] *Catalysis: from principles to applications*, ed. M. Beller, A. Renken and R. A. van Santen, Wiley-VCH, **2012**.

[3] *Ligand design in metal chemistry: reactivity and catalysis*, ed. M. Stradiotto, R. J. Lundgren, Wiley-VCH, **2016**.

[4] *Organotransition metal chemistry. From bonding to catalysis*, ed. J. F. Hartwig, University Science Books, **2010**.

[5] *Phosphorus(III) ligands in homogeneous catalysis: design and synthesis*, ed. P. C. J. Kamer, P. W. N. M. van Leeuwen, Wiley-VCH, **2012**.

[6] D. Ringe, G. A. Petsko, *Science* **2008**, *320*, 1428-1429.

[7] *From enzyme models to model enzymes*, ed. A. J. Kirby, F. Hollfelder, RSC, **2009**.

[8] *Supramolecular catalysis*, ed. P. W. N. M. van Leeuwen, Wiley-VCH, **2008**.

[9] T. S. Koblenz, J. Wassenaar, J. N. H. Reek, Chem. Soc. Rev. **2008**, *37*, 247-262.

[10] D. M. Vriezema, M. Comellas Aragones, J. A. A. W. Elemans, J. L. M. Cornelissen, A. E. Rowand, R. J. M. Nolte, *Chem. Rev.* **2005**, *105*, 1445-1489.

[11] H. Amouri, C. Desmarets, J. Moussa, *Chem. Rev.* **2012**, *112*, 2015-2041.

[12] M. Yoshizawa, J. K. Klosterman, M. Fujita, *Angew. Chem. Int. Ed.* **2009**, *48*, 3418-3438.

[13] D. Fiedler, D. H. Leung, R. G. Bergman, K. N. Raymond, *Acc. Chem. Res.* **2005**, *38*, 349-358.

[14] M. J. Wiester, P. A. Ulmann, C. A. Mirkin, *Angew. Chem. Int. Ed.* **2011**, *50*, 114-137.

[15] I. Nath, J. Chakraborty, F. Verpoort, *Chem. Soc. Rev.* **2016**, *45*, 4127-4170.

[16] T. R. Cook, Y.-R. Zheng, P. J. Stang, *Chem. Rev.* **2013**, *113*, 734-777.

[17] M. Raynal, P. Ballester, A. Vidal-Ferran, P. W. N. M. van Leeuwen, *Chem. Soc. Rev.* **2014**, *43*, 1734-1787.

[18] Z. Dong, Q. Luo, J. Liu, *Chem. Soc. Rev.* **2012**, *41*, 7890-7908.

[19] J. Meeuwissen, J. N. H. Reek, *Nat. Chem.* **2010**, *2*, 615-621.

[20] K. T. Mahmudov, A. V. Gurbanov, F. I. Guseinov, M. F. C. Guedes da Silva, *Coord. Chem. Rev.* **2019**, *387*, 32-46.

[21] B. Breit, *Angew. Chem. Int. Ed.* **2005**, *44*, 6816-6825.

[22] S. Carboni, C. Gennari, L. Pignataro, U. Piarulli, *Dalton Trans.* **2011**, *40*, 4355-4373.

[23] P. Dydio, J. N. H. Reek, *Chem. Sci.* **2014**, *5*, 2135-2145.

[24] M. Raynal, P. Ballester, A. Vidal-Ferran, P. W. N. M. van Leeuwen, *Chem. Soc. Rev.* **2014**, *43*, 1660-1733.

[25] H. J. Davis, R. J. Phipps, *Chem. Sci.* **2017**, *8*, 864-877.

[26] M. R. Mote, S. H. Chikkali, *Chem. Asian J.* **2018**, *13*, 3623-3646.

[27] R. Noyori, *Nat. Chem.* **2009**, *1*, 5-6.

[28] A. J. Esswein, D. G. Nocera, *Chem. Rev.* **2007**, *107*, 4022-4047.

[29] R. L. Shook, A. S. Borovik, *Inorg. Chem.* **2010**, *49*, 3646-3660.

[30] M. Zhao, H.-B. Wang, L.-N. Ji, Z.-W. Mao, *Chem. Soc. Rev.* **2013**, *42*, 8360-8375.

[31] S. A. Cook, A. S. Borovik, *Acc. Chem. Res.* **2015**, *48*, 2407-2414.
[32] S. E. Creutz, J. C. Peters, *Chem. Sci.* **2017**, *8*, 2321-2328.
[33] M. L. Pegis, C. F. Wise, D. J. Martin, J. N. Mayer, *Chem. Rev.* **2018**, *118*, 2340-2391.
[34] M. A. Ehudin, A. W. Schaefer, S. M. Adam, D. A. Quist, D. E. Diaz, J. A. Tang, E. I. Solomon, K. D. Karlin, *Chem. Sci.* **2019**, *10*, 2893-2905.
[35] A.Warshel, P. K. Sharma, M. Kato, Y. Xiang, H. Liu, M. H. M. Olsson, *Chem. Rev.* **2006**, *106*, 3210-3235.
[36] G. G. Hammes, S. J. Benkovic, S. Hammes-Schiffer, *Biochemistry*, **2011**, *50*, 10422-10430.
[37] K. Ohmatsu, T. Ooi, *Top. Curr. Chem.* **2019**, *377*, 31.
[38] K. Ohmatsu, N. Imagawa, T. Ooi, *Nat. Chem.* **2014**, *6*, 47-51.
[39] K. Ohmatsu, S. Kawai, N. Imagawa, T. Ooi, *ACS Catal.* **2014**, *4*, 4304-4306.
[40] C. Chen, H. Wang, Z. Zhang, S. Jin, S. Wen, J. Ji, L. W. Chung, X.-Q. Dong, X. Zhang, *Chem. Sci.* **2016**, *7*, 6669-6673.
[41] S. Wen, C. Chen, S. Du, Z. Zhang, Y. Huang, Z. Han,X.-Q. Dong, X. Zhang, *Org. Lett.* **2017**, *19*, 6474-6477.
[42] X. Yin, C. Chen, X. Li, X.-Q. Dong, X. Zhang, *Org. Lett.* **2017**, *19*, 4375-4378.
[43] Q. Zhao, J. Wen, R. Tan, K. Huang, P. Metola, R. Wang, E. V. Anslyn, X. Zhang, *Angew. Chem. Int. Ed.* **2014**, *53*, 8467-8470.
[44] J. Wen, R. Tan, S. Liu, Q. Zhao, X. Zhang, *Chem. Sci.* **2016**, *7*, 3047-3051.
[44] J. Wen, X. Fan, R. Tan, H.-C. Chien, Q. Zhou, L. W. Chung, X. Zhang, *Org. Lett.* **2018**, *20*, 2143-2147.
[46] T. Yang, Y. Sun, H. Wang, Z. Lin, J. Wen, X. Zhang, *Angew. Chem. Int. Ed.* **2020**, *59*, 6108-6114.
[47] H. J. Davis, M. T. Mihai, R. J. Phipps, *J. Am. Chem. Soc.* **2016**, *138*, 12759-12762.
[48] M. T. Mihai, H. J. Davis, G. R. Genov, R. J. Phipps, *ACSCatal.* **2018**, *8*, 3764-3769.
[49] B. Lee, M. T. Mihai, V. Stojalnikova, R. J. Phipps, *J. Org. Chem.* **2019**, *84*, 13124-13134.
[50] M. T. Mihai, B. D. Williams, R. J. Phipps, *J. Am. Chem. Soc.* **2019**, *141*, 15477-15482.
[51] J. R. Montero Bastidas, T. J. Oleskey, S. L. Miller, M. R. Smith III, R. E. Maleczka Jr, *J. Am. Chem. Soc.* **2019**, *141*, 15483-15487.
[51] W. A. Golding, R. Pearce-Higgins, R. J. Phipps, *J. Am. Chem. Soc.* **2018**, *140*, 13570-13574.
[53] W. A. Golding, R. J. Phipps, *Chem. Sci.* **2020**, *11*, 3022-3027.
[54] M. E. Hoque, R. Bisht, C. Haldar, B. Chattopadhyay, *J. Am. Chem. Soc.* **2017**, *139*, 7745-7748.
[55] R. Bisht, M. E. Hoque, B. Chattopadhyay, *Angew. Chem. Int. Ed.* **2018**, *57*, 15762-15766.
[56] Q. Lu, H. Yu, Y. Fu, *J. Am. Chem. Soc.* **2014**, *136*, 8252-8260.
[57] H. Xu, K. Muto, J. Yamaguchi, C. Zhao, K. Itami, D. G. Musaev, *J. Am. Chem. Soc.* **2014**, *136*, 14834-14844.
[58] B. E. Haines, D. G. Musaev, *ACS Catal.* **2015**, *5*, 830-840.
[59] K. Muto, K. Yamaguchi, D. G. Musaev, K. Itami, *Nat. Commun.* **2015**, *6*, 7508.
[60] J. Jiang, J.-Q. Yu, K. Morokuma, *ACS Catal.* **2015**, *5*, 3648-3661.
[61] Y. Zhou, X. Bao, *Org. Lett.* **2016**, *18*, 4506-4509.

[62] B. E. Haines, J. F. Berry, J.-Q. Yu, D. G. Musaev, *ACSCatal.* **2016**, *6*, 829-839.
[63] M. Anand, R. B. Sunoj, H. F. Schaefer III, *ACS Catal.* **2016**, *6*, 696-708.
[64] A. L. Dewyer, P. M. Zimmerman, *ACS Catal.* **2017**, *7*,5466-5477.
[65] M. C. D'Alterio, Y.-C. Yuan, C. Bruneau, G. Talarico, R. Gramage-Doria and A. Poater, *Catal. Sci. Technol.* **2020**, *10*, 180-186.
[66] X. Jin, H. Xu, N. Zhao, R. Li, Y. Dang, *Org. Lett.* **2020**, *22*, 1464-1468.
[67] K. Ohmatsu, M. Ito, T. Kunieda, T. Ooi, *Nat. Chem.* **2012**, *4*, 473-477.
[68] K. Ohmatsu, M. Ito, T. Ooi, *Chem. Commun.* **2014**, *50*,4554-4557.
[69] K. Ohmatsu, Y. Hara, T. Ooi, *Chem. Sci.* **2014**, *5*, 3645-3650.
[70] Y. Hara, Y. Kusano, K. Ohmatsu, T. Ooi, *Chem. Lett.* **2016**, *45*, 552-554.
[71] G. R. Genov, J. L. Douthwaite, A. S. K. Lahdenperä, D. C. Gibson, R. J. Phipps, *Science*, **2020**, *367*, 1246-1251.
[72] H. J. Davis, G. R. Genov, R. J. Phipps, *Angew. Chem. Int.Ed.* **2017**, *56*, 13351-13355.
[73] S. Dana, D. Chowdhury, A. Mandal, F. A. S. Chipem, M. Baidya, *ACS Catal.* **2018**, *8*, 10173-10179.
[74] Q.-Q. Wang, S. Gonell, S. H. A. M. Leenders, M. Dürr, I. Ivanovic-Burmazovic, J. N. H. Reek, *Nat. Chem.* **2016**, *8*, 225-230.
[75] S. Gonell, J. N. H. Reek, *ChemCatChem*, **2019**, *11*, 1458-1464.
[76] S. Gonell, X. Caumes, N. Orth, I. Ivanovic-Burmazovic, J. N. H. Reek, *Chem. Sci.* **2019**, *10*, 1316-1321.
[77] C. J. Pedersen, *J. Am. Chem. Soc.* **1967**, *89*, 2495-2496.
[78] C. J. Pedersen, *J. Am. Chem. Soc.* **1967**, *89*, 7017-7036.
[79] G. W. Gokel, D. M. Goli, C. Minganti, L. Echegoyen, *J. Am. Chem. Soc.* **1983**, *105*, 6786-6788.
[80] M. Vaquero, L. Rovira, A. Vidal-Ferran, *Chem. Commun.* **2016**, *52*, 11038-11051.
[81] J. M. Miller, *Dalton Trans.* **2017**, *46*, 11987-12000.
[82] Yoo, H. M. Dodge, A. J. M. Miller, *Chem. Commun.* **2019**, *55*, 5047-5059.
[83] Y. Li, B. Ma, Y. He, F. Zhang, Q.-H. Fan, *Chem. Asian J.* **2010**, *5*, 2454-2458.
[84] Mon, D. A. Jose, A. Vidal-Ferran, *Chem. Eur. J.* **2013**, *19*, 2720-2725.
[85] Vidal-Ferran, I. Mon, A. Bauzá, A. Frontera, L. Rovira, *Chem. Eur. J.* **2015**, *21*, 11417-11426.
[86] L. Rovira, M. Vaquero, A. Vidal-Ferran, *J. Org. Chem.* **2015**, *80*, 10397-10403.
[87] L. Rovira, H. Fernández-Pérez, A. Vidal-Ferran, *Organometallics,* **2016**, *35*, 528-533.
[88] E. Iniesta, A. Vidal-Ferran, *Chem. Commun.* **2020**, *56*, 6364-6367.
[89] L. Carreras, A. Franconetti, A. Grabulosa, A. Frontera, A. Vidal-Ferran, *Org. Chem. Front.* **2020**, *7*, 1626-1634.
[90] L. Kovbasyuk, R. Krämer, *Chem. Rev.* **2004**, *104*, 3161-3188.
[91] X.-C. Zhang, Y.-H. Hu, C.-F. Chen, Q. Fang, L.-Y. Yang, Y.-B. Lu, L.-J. Xie, J. Wu, S. Li, W. Fang, *Chem. Sci.* **2016**, *7*, 4594-4599.
[92] G.-H. Ouyang, Y.-M. He, Q.-H. Fan, *Chem. Eur. J.* **2014**, *20*, 16454-16457.
[93] E. N. Jacobsen, *Acc. Chem. Res.* **2000**, *33*, 421-431.
[94] G.-H. Ouyang, Y.-M. He, Y. Li, J.-F. Xiang, Q.-H. Fan, *Angew. Chem. Int. Ed.* **2015**, *54*, 4334-4337.

[95] M. Sawamura, Y. Ito, *Chem. Rev.* **1992**, *92*, 857-871.
[96] G. Olivo, G. Farinelli, A. Barbieri, O. Lanzalunga, S. Di Stefano, M. Costas, *Angew. Chem. Int. Ed.* **2017**, *56*, 16347-16351.
[97] G. Olivo, G. Capocasa, O. Lanzalunga, S. Di Stefano, M. Costas, *Chem. Commun.* **2019**, *55*, 917-920.
[98] G. Olivo, G. Capocasa, B. Ticconi, O. Lanzalunga, S. Di Stefano, M. Costas, *Angew. Chem. Int. Ed.* **2020**, *59*, 12703-12708.
[99] J. Neel, M. J. Hilton, M. S. Sigman, F. D. Toste, *Nature* **2017**, *543*, 637-646.
[100] M. Yamakawa, I. Yamada, R. Noyori, *Angew. Chem. Int. Ed.* **2001**, *40*, 2818-2821.
[101] Sakakura, M. Hori, M. Fushimi, K. Ishihara, *J. Am. Chem. Soc.* **2010**, *132*, 15550-15552.
[102] W. Xie, J. Heo, D. Kim, S. Chang, *J. Am. Chem. Soc.* **2020**, *142*, 7487-7496.
[103] H.-Y. Luo, J.-W. Dong, Y.-Y. Xie, X.-F. Song, D. Zhu, T. Ding, Y. Liu, Z.-M. Chen, *Chem. Eur. J.* **2019**, *25*, 15411-15418.
[104] Z.-M. Chen, J. Liu, J.-Y. Guo, M. Loch, R. J. DeLuca, M. S. Sigman, *Chem. Sci.* **2019**, *10*, 7246-7250.
[105] M. A. B. Ferreira, J. De Jesus Silva, S. Grosslight, A. Fedorov, M. S. Sigman, C. Copéret, *J. Am. Chem. Soc.* **2019**, *141*, 10788-10800.
[106] R. Huber, A. Passera, E. Gubler, A. Mezzetti, *Adv. Synth. Catal.* **2018**, *360*, 2900-2913.
[107] Passera, A. Mezzetti *Adv. Synth. Catal.* **2019**, *361*, 4691-4706.
[108] Passera, A. Mezzetti, *Angew. Chem. Int. Ed.* **2020**, *59*, 187-191.
[109] T. Korenaga, R. Sasaki, T. Takemoto, T. Yasuda, M. Watanabe, *Adv. Synth. Catal.* **2018**, *360*, 322-333.
[110] M. Orlandi, M. J. Hilton, E. Yamamoto, F. D. Toste, M. S. Sigman, *J. Am. Chem. Soc.* **2017**, *139*, 12688-12695.
[111] Y. Reddi, C.-C. Tsai, C. M. Avila, F. D. Toste, R. B. Sunoj, *J. Am. Chem. Soc.* **2019**, *141*, 998-1009.
[112] S. Tribedi, C. M. Hadad,R. B. Sunoj, *Chem. Sci.* **2018**, *9*, 6126-6133.
[113] P. M. Holstein, M. Vogler, P. Larini, G.Pilet, E. Clot, O. Baudoin, *ACS Catal.* **2015**, *5*, 4300-4308.
[114] M. Huang, T. Yang, J. D. Paretsky, J. F. Berry,J. M. Schomaker, *J. Am. Chem. Soc.* **2017**, *139*, 17376-17386.
[115] H. Jung, M. Schrader, D. Kim, M.-H. Baik, Y. Park, S. Chang, *J. Am. Chem. Soc.* **2019**, *141*, 15356-15366.
[116] R. L. Reyes, M. Sato, T. Iwai, K. Suzuki, S. Maeda, M. Sawamura, *Science* **2020**, *369*, 970-974.
[117] R. L. Reyes, T. Iwai, S. Maeda, M. Sawamura, *J. Am. Chem. Soc.* **2019**, *141*, 6817-6821.
[118] R. Kennedy, S. Lin, E. N. Jacobsen, *Angew. Chem. Int. Ed.* **2016**, *55*, 12596-12624.
[119] S. Yamada, *Chem. Rev.* **2018**, *118*, 11353-11432.
[120] A. Dougherty, *Acc. Chem. Res.* **2013**, *4*6, 885-893.
[121] S.-C. Sha, S. Tcyrulnikov, M. Li, B. Hu, Y. Fu, M. C. Kozlowski, P. J. Walsh, *J. Am. Chem. Soc.* **2018**, *140*, 12415-12423.
[122] H. Jiang, S.-C. Sha, S. A. Jeong, B. C. Manor, P. J. Walsh, *Org. Lett.* **2019**, *21*, 1735-1739.
[123] G. Musaev, T. M. Figg, A. L. Kaledin, *Chem. Soc. Rev.* **2014**, *43*, 5009-5031.

[124] T. M. Figg, M. Wasa, J.-Q. Yu, D. G. Musaev, *J. Am. Chem. Soc.* **2013**, *135*, 14206-14214.
[125] H.-R. Tong, S. Zheng, X. Li, Z. Deng, H. Wang, G. He, Q. Peng, G. Chen, *ACS Catal.* **2018**, *8*, 11502-11512.
[126] E. Haines, X. Xu, P. Verma, X.-C. Wang, J.-Q. Yu, D. G. Musaev, *J. Am. Chem. Soc.* **2015**, *137*, 9022-9031.
[127] M. C. Schwarzer, R. Konno, T. Hojo, A. Ohtsuki, K. Nakamura, A. Yasutome, H. Takahashi, T. Shimasaki, M. Tobisu, N. Chatani, S. Mori, *J. Am. Chem. Soc.* **2017**, *139*, 10347-10358.
[128] B. Kim, A. J. Chinn, D. R. Fandrick, C. H. Senanayake, R. A. Singer, S. J. Miller, *J. Am. Chem. Soc.* **2016**, *138*, 7939-7945.
[129] J. Chinn, B. Kim, Y. Kwon, S. J. Miller, *J. Am. Chem. Soc.* **2017**, *139*, 18107-18114.
[130] G. Lian, Y. Ji, H. Liu, Y. Pang, B. Zhou, M. Cheng, Y. Liu, B. Lin, Y. Liu, *Adv. Synth. Catal.* **2020**, *362*, 192-205.
[131] Bulfield, S. M. Huber, *Chem. Eur. J.* **2016**, *22*, 14434-14450.
[132] R. L. Sutar, S. M. Huber, *ACS Catal.* **2019**, *9*, 9622-9639.
[133] V. N. G. Lindsay, W. Lin, A. B. Charette, *J. Am. Chem. Soc.* **2009**, *131*, 16383-16385.
[134] V. N. G. Lindsay, A. B. Charette, *ACS Catal.* **2012**, *2*, 1221-1225.
[135] L. Carreras, M. Serrano-Torne, P. W. N. M. van Leeuwen, A. Vidal-Ferran, *Chem. Sci.* **2018**, *9*, 3644-3648.
[136] L. Carreras, J. Benet-Buchholz, A. Franconetti, A. Frontera, P. W. N. M. van Leeuwen, A. Vidal-Ferran, *Chem. Commun.* **2019**, *55*, 2380-2383.
[137] K. Guillier, E. Caytan, V. Dorcet, F. Mongin, E. Dumont, F. Chevallier, *Angew. Chem. Int. Ed.* **2019**, *58*, 14940-14943.
[138] T. Caronna, R. Liantonio, T. A. Logothetis, P. Metrangolo, T. Pilati, G. Resnati, *J. Am. Chem. Soc.* **2004**, *126*, 4500-4501.
[139] T. Arai, K. Horigane, O. Watanabe, J. Kakino, N. Sugiyama, H. Makino, Y. Kamei, S. Yabe, M. Yamanaka, *iScience,* **2019**, *12*, 280-292.
[140] S. Iwase, Y. Suzuki, S. Tanaka, M. Kitamura, *Org. Lett.* **2020**, *22*, 1929-1933.
[141] S. E. Denmark, G. L. Beutner, *Angew. Chem. Int. Ed.* **2008**, *47*, 1560-1638.
[142] J. Becica, G. E. Dobereiner, *Org. Biomol. Chem.* **2019**, *17*, 2055-2069.
[143] H. L. Li, Y. Kuninobu, M. Kanai, *Angew. Chem. Int. Ed.* **2017**, *56*, 1495-1499.
[144] L. Yang, N. Uemura, Y. Nakao, *J. Am. Chem. Soc.* **2019**, *141*, 7972-7979.
[145] L. Yang, K. Semba, Y. Nakao, *Angew. Chem. Int. Ed.* **2017**, *56*, 4853-4857.
[146] R. Bisht, B. Chattopadhyay, *J. Am. Chem. Soc.* **2016**, *138*, 84-87.
[147] H.-L. Li, M. Kanai, Y. Kuninobu, *Org. Lett.* **2017**, *19*, 5944-5947.
[148] Beletskaya, V. S. Tyurin, A. Y. Tsivadze, R. Guilard, C. Stern, *Chem. Rev.* **2009**, *109*, 1659-1713.
[149] Y. Nakamura, N. Aratani, A. Osuka, *Chem. Soc. Rev.* **2007**, *36*, 831-845.
[150] V. F. Slagt, J. N. H. Reek, P. C. J. Kamer, P. W. N. M. van Leeuwen, *Angew. Chem. Int. Ed.* **2001**, *40*, 4271-4274.
[151] L. J. Jongkind, X. Caumes, A. P. T. Hartendorp, J. N. H. Reek, *Acc. Chem. Res.* **2018**, *51*, 2115-2128.

[152] X. Wang, S. S. Nurttila, W. I. Dzik, R. Becker, J. Rodgers, J. N. H. Reek, *Chem. Eur. J.* **2017**, *23*, 14769-14777.
[153] L. J. Jongkind, J. N. H. Reek, *Chem. Asian. J.* **2020**, *15*, 867-875.
[154] L. J. Jongkind, J. A. A. W. Elemans, J. N. H. Reek, *Angew. Chem. Int. Ed.* **2019**, *58*, 2696-2699.
[155] J. A. A. W. Elemans, M. B. Claase, P. P. M. Aarts, A. E. Rowan, A. P. H. J. Schenning, R. J. M. Nolte, *J. Org. Chem.* **1999**, *64*, 7009-7016.
[156] S. S. Nurttila, R. Zaffaroni, S. Mathew, J. N. H. Reek, *Chem. Commun.* **2019**, *55*, 3081-3084.
[157] S. S. Nurttila, W. Brenner, J. Mosquera, K. M. van Vliet, J. R. Nitschke, J. N. H. Reek, *Chem. Eur. J.* **2019**, *25*, 609-620.
[158] S. S. Nurttila, R. Becker, J. Hessels, S. Woutersen, J. N. H. Reek, *Chem. Eur. J.* **2018**, *24*, 16395-16406.
[159] C. García-Simón, R. Gramage-Doria, S. Raoufmoghaddam, T. Parella, M. Costas, X. Ribas, J. N. H. Reek, *J. Am. Chem. Soc.* **2015**, *137*, 2680-2687.
[160] M. Marty, Z. Clyde-Watson, L. J. Twyman, M. Nakash, J. K. M. Sanders, *Chem. Commun.* **1998**, 2265-2266.
[161] M. Nakash, Z. Clyde-Watson, N. Feeder, J. E. Davies, S. J. Teat, J. K. M. Sanders, *J. Am. Chem. Soc.* **2000**, *122*, 5286-5293.
[162] M. Kadri, J. Hou, V. Dorcet, T. Roisnel, L. Bechki, A. Miloudi, C. Bruneau, R. Gramage-Doria, *Chem. Eur. J.* **2017**, *23*, 5033-5043.
[163] P. Zardi, T. Roisnel, R. Gramage-Doria, *Chem. Eur. J.* **2019**, *25*, 627-634.
[164] G. Meng, N. Y. S. Lam, E. L. Lucas, T. G. Saint-Denis, P. Verma, N. Chekshin, J.-Q. Yu, *J. Am. Chem. Soc.* **2020**, *142*, 10571-10591.
[165] F. Khan, S. K. Sinha, G. K. Lahiri, D. Maiti, *Chem. Asian J.* **2018**, *13*, 2243-2256.
[166] C. Sambiagio, D. Schonbauer, R. Blieck, T. Dao-Huy, G. Pototschnig, P. Schaaf, T. Wiesinger, M. F. Zia, J. Wencel-Delord, T. Besset, B. U. W. Maes, M. Schnurch, *Chem. Soc. Rev.* **2018**, *47*, 6603-6743.
[167] Z. Zhang, K. Tanaka, J.-Q. Yu, *Nature* **2017**, *543*, 538-542.
[168] T. K. Achar, K. Ramakrishna, T. Pal, S. Porey, P. Dolui, J. P. Biswas, D. Maiti, *Chem. Eur. J.* **2018**, *24*, 17906-17910.
[169] T. K. Achar, J. P. Biswas, S. Porey, T. Pal, K. Ramakrishna, S. Maiti, D. Maiti, *J. Org. Chem.* **2019**, *84*, 8315-8321.
[170] Ramakrishna, J. P. Biswas, S. Jana, T. K. Achar, S. Porey, D. Maiti, *Angew. Chem. Int. Ed.* **2019**, *58*, 13808-13812.
[171] H. Shi, Y. Lu, J. Weng, K. L. Bay, X. Chen, K. Tanaka, P. Verna, K. N. Houk, J.-Q. Yu, *Nat. Chem.* **2020**, *12*, 399-404.
[172] M. Beller, *Chem. Rev.* **2019**, *119*, 2089.
[173] P. Chirik, R. Morris, *Acc. Chem. Res.* **2015**, *48*, 2495.
[174] J. Wieland, B. Breit, *Nat. Chem.* **2010**, *2*, 832-837.
[175] K. D. Collins, T. Gensch, F. Glorius, *Nat. Chem.* **2014**, *6*, 859-871.
[176] W. Robbins, J. F. Hartwig, *Science,* **2011**, *333*, 1423-1427.
[177] K. Troshin, J. F. Hartwig, *Science,* **2017**, *357*, 175-181.

[178] P. T. Corbett, J. Leclaire, L. Vial, K. R. West, J.-L. Wietor, J. K. M. Sanders, S. Otto, *Chem. Rev.* **2006**, *106*, 3652-3711.
[179] Giese, M. Albrecht, K. Rissanen, *Chem. Rev.* **2015**, *115*, 8867-8895.
[180] Y. Zhao, Y. Cotelle, L. Liu, J. López-Andarias, A.-B. Bornhof, M. Akamatsu, N. Sakai, S. Matile, *Acc. Chem. Res.* **2018**, *51*, 2255-2263.
[181] A. Thomas, K. Speck, I. Kevlishvili, Z. Lu, P. Liu, S. L. Buchwald, *J. Am. Chem. Soc.* **2018**, *140*, 13976-13984.
[182] P. Petrovic, J.-P. Djukic, A. Hansen, C. Bannwarth, S. Grimme, *Non-covalent Interactions in the Synthesis and Design of New Compounds* (ed. A. M. Maharramov, K. T. Mahmudov, M. N. Kopylovich and A. J. L. Pombeiro) 115–143 (Wiley-VCH, **2016**).
[183] L. Deng, Y. Fu, S. Y. Lee, C. Wang, P. Liu, G. Dong, *J. Am. Chem. Soc.* **2019**, *141*, 16260-16265.
[184] Foscato, V. R. Jensen, *ACS Catal.* **2020**, *10*, 2354-2377.

Chapter 2. Enzyme-like supramolecular iridium catalysis enabling C-H bond borylation of pyridines with meta-selectivity

2.1. Introduction.

In the last three decades, C-H bond functionalizations enabled by transition metal catalysts have shown a remarkable impact in the advancement of chemical synthesis due to high atom- and step-economy it represents.[1] Besides substrates with a biased reactivity[2] or controlled by metal-directing groups,[3] the reactivity at inherently unreactive sites is of paramount importance to access new chemical dimensions. To meet this challenge, a standard approach deals with extensive fine-tuning of the catalyst first coordination sphere with different stereo-electronic modifications [4] or to introduce multiple catalytic cycles.[5] Although useful, substantial costs and efforts need to be undertaken to trial-and-error studies to search for the optimal catalytic system.

On the other hand, enzymes, Nature's catalysts, exploit alternative approaches to control chemical reactivity.[6] Importantly, they incorporate a number of kinetically reversible interactions in the second coordination sphere of the active site to stabilize key transition states.[7] For chemists, this has been a source of inspiration to mimic in abiological catalysis.[8] As such, different strategies have been developed to design transition metal catalysts incorporating remote functionalities to pre-organize substrates in a specific geometry to access unprecedented C-H bond functionalizations.[9] In this context, the incorporation of hydrogen bonding,[10] ion-pairing[11] or Lewis-adducts formation,[12] respectively, to transition metal catalysts has emerged as promising approaches to control the regio-selectivity in iridium-catalyzed C-H bond borylation reactions (**Figure 1A**).[13]

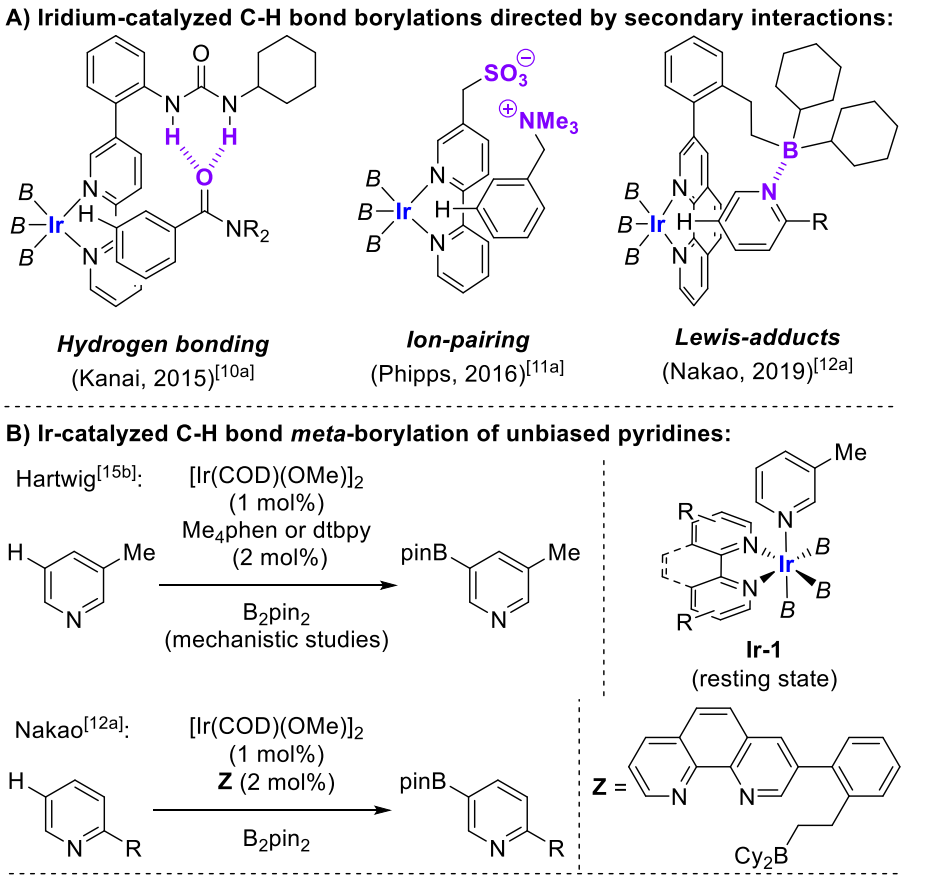

Figure 1. Overview of regio-selective iridium-catalyzed C-H bond borylation reactions guided by secondary interactions and issues encountered in pyridine *meta*-C-H bond reactivity (state-of-the art *vs* present work). *B* = (pinacolato)boron. B_2pin_2 = bis(pinacolato)diboron. COD = 1,5-cyclooctadiene.

Borylated products are relevant as they can straightforward be engaged in state-of-the-art carbon-carbon and carbon-heteroatom bond forming process.[14] Unfortunately, the predictability of these catalytic systems is still poor rationalized, basically due to the low association constants between the substrate and the catalyst, generally with $K < 10^2$ M^{-1}.[10-12] Consequently, small modifications in the commonly-used bipyridine-derived ligand and/or the substrate can lead to a complete lack of reactivity or absence of selectivity.[10-12] Precisely, we aimed at circumventing the poor reactivity of pyridine

derivatives at *meta* position.[15a] Iridium-catalyzed C-H bond borylations typically occur at the *meta* position of pyridine derivatives when bulky substituents are present in the *ortho* site in order to prevent the undesired coordination of the pyridine nitrogen lone pair to the iridium catalyst, which gives unproductive and unselective catalysis (**Figure 1B**).[12a,15b]

To overcome these challenges, we anticipated that a geometrically-constrained iridium catalyst featuring a relatively strong pyridine-to-catalyst interaction may increase the activity and selectivity for C-H bond borylation reactions. Herein, we present a rationally-designed supramolecular iridium catalyst exhibiting strong affinity for pyridine derivatives (K > 10^4 M^{-1}) by means of kinetically labile Zn···N coordination (**Figure 1C**).[16] Due to the perfect geometry and ideal atom-precise distance between the active site and the substrate-recognition site, only *meta*-borylated pyridines were obtained (**Figure 1C**). In addition, the catalytic system displayed enzyme-like features such as Michaelis-Menten kinetics and substrate selectivity. Applications to five-membered nitrogen-containing heterocycles and dormant reactivity are also disclosed.

2.2. Results and discussion.

Semi-empirical molecular modelling (PM3-level) showed that the geometry of ligand **L** (**Scheme 1** and **Figure 1C**) as well as the distance between the zinc(II)-porphyrin fragment (*the substrate binding site*) and the iridium *N*,*N*-chelating motif (*the potentially catalytically active site*) in the periphery is suitable to accommodate pyridine substrates with selective activation at the *meta*-C-H bond site.[17] In addition, the restricted motion between the *N*,*N*-chelating motif and the zinc(II)-porphyrin backbone will increase the rigidity of the system by keeping the peripheral iridium active site just above the zinc(II)-porphyrin plane. With this in mind, the targeted supramolecular ligand **L** was readily synthesized in a four-step reaction sequence starting from commercially available chemicals (see **Scheme S1**).[18] As expected, ligand **L** is in keeping with a C_s-symmetrical molecule according to NMR spectroscopy studies.[18] ^{1}H NMR and UV-vis binding studies established the ability of **L** to interact with pyridine as the model substrate with an association constant of $K_{1.1}$ = 5.7 x 10^4 ± 1.5 M^{-1} at room temperature (**Scheme 1**, see **Figures S1-S3**).[18,19] Notably, this substrate-to-catalyst binding is as tight as it can be found in some enzymes.[20] The binding of pyridine to **L** was also evidenced by ^{1}H NMR studies at temperatures up to 90 °C and by DOSY experiments that showed that the up-field shifted proton signals belonging to the pyridine diffused together with those corresponding to **L** (see **Figures S4-S7**).[18]

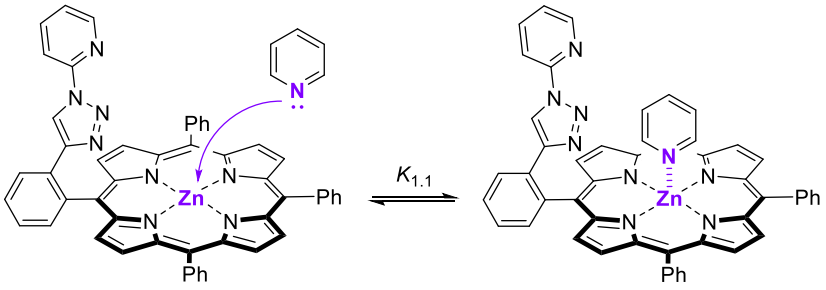

Scheme 1. Binding of pyridine to **L** *via* kinetically labile Zn···N coordination.

Moreover, single crystals suitable for X-ray diffraction studies were obtained from a solution containing **L** and pyridine in an equimolar ratio (**Figure 2**, left).[21] As anticipated, the nitrogen atom from pyridine binds to the zinc(II) center of **L**. Gratifyingly, the coordinating arm of **L** stands in the same face as the substrate with a volumetric space between both motifs enough to accommodate a catalytically active iridium center. Analogously, single crystals with a potential substrate, *N*-methylimidazole, were also obtained and analyzed by X-ray diffraction studies (**Figure 2**, right). As expected, the non-methylated nitrogen atom (N1) from the substrate was bound to the zinc(II) center from **L**. The binding of *N*-methylimidazole to **L** *via* Zn···N interaction was also corroborated in solution by ^{1}H NMR spectroscopy studies (see **Figure S13**).[18]

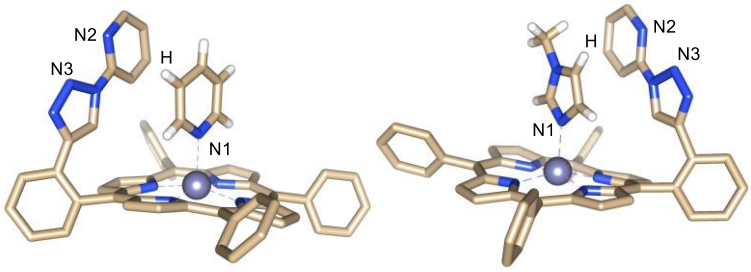

Figure 2. X-ray structures of the supramolecular assemblies between ligand **L** and pyridine (left) as well as *N*-methylimidazole (right) [capped sticks representation except the zinc atom that is ball representation, hydrogen atoms have been omitted except those from the nitrogen-containing substrates]. Color code: carbon (brown), nitrogen (blue), hydrogen (white). Selected distances [Å]: Zn···N1 2.14, H···N2 3.54, H···N3 3.92 (left) and Zn···N1 2.09, H···N2 3.79, H···N3.

In parallel, coordination chemistry studies by ^{1}H NMR and HRMS (*m/z* = 1121.2599) showed that the reaction between **L** and 0.5 equivalents of $[Ir(COD)(Cl)]_2$ afforded the corresponding cationic iridium complex **L1** (**Scheme 2**, see **Figures S8-S10**).[18] Subsequent ^{1}H NMR studies by treatment of the iridium complex **L1** with increasing amounts of pyridine showed a single set of up-field shifted protons belonging to pyridine (**Scheme 2**) in a similar way as it was observed with the titration studies between **L** and pyridine (see **Figures S11-S12**).[18]

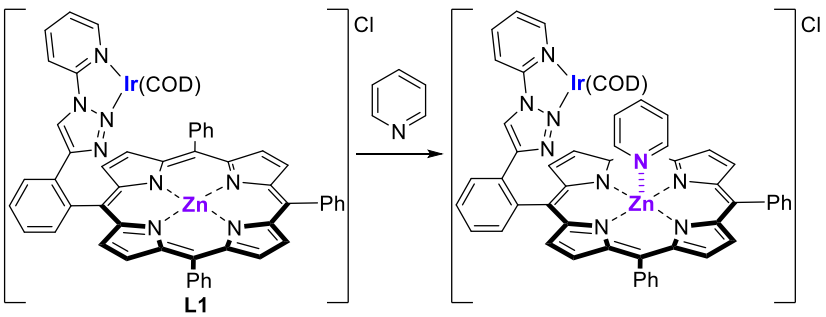

Scheme 2. Simultaneous coordination of both iridium and pyridine to **L**.

Having established that **L** enables the binding of pyridine inside the zinc(II)-porphyrin pocket simultaneously to the coordination of the *N*,*N*-chelating unit towards the potentially, catalytically active iridium center, we embarked in the catalytic assessment of **L** as a supramolecular ligand in iridium-catalyzed C-H bond borylations between unfunctionalized pyridine and bis(pinacolato)diboron (B_2pin_2) as a model reaction (**Table 1**). This reaction is well-known to give a mixture of *meta*- and *para*-borylated products with classical bipyridine ligands[15a] and it represents a benchmark test for evaluating the activity and the regio-selectivity outcome.[13] Initially, we screened solvents that were known to be used in iridium catalyzed C-H bond borylation of (hetero)arenes such as heptane and ethers at temperatures near to their boiling point.[10-15,22] Although poor conversions were observed, an exquisite *meta* selectivity was evidenced as only the products resulting from *mono*- and *bis*-borylation **1** and **2** formed without any detectable *para* or *ortho* regioisomers **3** or **4** (**Table 1**, entries 1-4). The reaction in toluene as solvent at 70 °C revealed as the optimal one for obtaining the *mono*-functionalized product with *meta* selectivity in an isolated yield of 54% (**Table 1**, entry 5, GC-yield 90%).[23] This is rather unexpected because non-functionalized arenes (i.e. toluene) are typically more reactive than pyridine using bipyridine- or phenantroline-derived ligands for iridium-catalyzed C-H bond borylation reactions.[13,22,24] In our case, we only detected trace amounts of borylated toluene and up to 15% (based on B_2pin_2) in the case of the reaction performed at higher 80 °C, that again exhibited excellent *meta*-selectivity for the C-H bond borylation of pyridine (**Table 1**, entry 6). For instance, with 58 times more toluene than pyridine in the reaction mixture, our supramolecular catalyst exhibits a high preference for the pyridine substrate than for the aromatic toluene one with an overall selectivity *S* estimated at 380 for the most unfavorable scenario.[25] Decreasing the temperature to 60 °C completely inhibited the catalysis (**Table 1**, entry 7). This suggests that the substrate-catalyst or product-catalyst binding *via* Zn···N coordination is strong and it only becomes reversible to enable turnovers in catalysis at higher temperatures.[26] Switching the toluene solvent for a more bulky *p*-xylene led to no borylation at the solvent and high reactivity towards *meta*-selectivity in only 12 hours (**Table 1**, entry 8). Doubling the amounts of both B_2pin_2 and the iridium catalyst led to the bis-borylated, *meta*-selective product **2** in an isolated yield of 70% (**Table 1**, entry 9), which represents the best result so far obtained for bis-functionalization to date.[27] The fact that aromatic apolar solvents such as toluene or *p*-xylene are crucial for the activity and selectivity of the catalysis, indirectly indicates that the polar ones (i.e. ethers) significantly disturb the binding of the substrate to the ligand **L**.[28] A similar reasoning may explain the higher reactivity encountered when using $[Ir(COD)(Cl)]_2$ instead of the typically more reactive $[Ir(COD)(OMe)]_2$[9-13,15,17,22-24] as the released methoxide anion from the former could bind to the zinc(II) center in **L** (**Table 1**, entry 2). The reactions performed in the absence of iridium or in the absence of ligand **L**, respectively, led to no conversion of pyridine substrate (see Table S1).[18]

Table 1. Reaction optimization for the iridium-catalyzed C-H bond borylation of pyridine.[a]

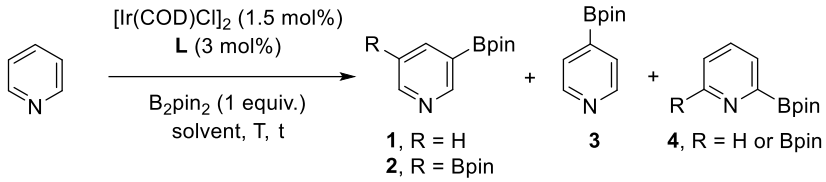

Entry	Solvent	T (°C)	t (h)	Conv. (%)[b]	(1+2):3:4[c]	1:2[d]
1	heptane	80	48	30	100:0:0	90:10
2[e]	heptane	80	48	21	100:0:0	100:0
2	THF	50	48	0	-	-
3	MTBE	80	48	33	100:0:0	89:11
4	2-MeTHF	80	24	17	100:0:0	100:0
5	toluene	70	24	>99 (54)[f]	100:0:0	90:10
6	toluene	80	24	>99	100:0:0	25:75
7	toluene	60	24	<5	-	-
8	*p*-xylene	80	12	>99	100:0:0	40:60
9[g]	*p*-xylene	80	48	>99 (70)[f]	100:0:0	13:87

[a] Reaction conditions: pyridine (0.162 mmol), B_2pin_2 (0.162 mmol), $[Ir(COD)(Cl)]_2$ (1.5 mol%), **L** (3 mol%), solvent (1 mL). [b] Conversion determined as pyridine consumption. [c] Ratio *meta*/*para*/*ortho* functionalization of pyridine determined by ^{1}H NMR and GC using *n*-dodecane as internal standard. [d] Ratio *mono*/*bis*-functionalization of the *meta*-borylated product determined by ^{1}H NMR and GC-MS using *n*-dodecane as internal standard. [d] Reaction performed with $[Ir(COD)(OMe)]_2$ instead of $[Ir(COD)(Cl)]_2$. [f] Isolated yield of the main product displayed in brackets. [g] Reaction performed with 3 equivalents of B_2pin_2, 3 mol% of $[Ir(COD)(Cl)]_2$ and 6 mol% of **L**.

To further rationalize the origin of this high *meta*-selectivity for the iridium-catalyzed C-H bond borylation reaction, a number of control experiments were performed (**Scheme 3**). First, the catalysis was attempted replacing the supramolecular ligand **L** for the individual components forming it, that is, zinc(II)-tetraphenylporphyrin (**ZnTPP**) and the *N*,*N*-chelating ligand **L*** (**Scheme 3A**). Under the standard reaction conditions, the starting material pyridine was fully recovered unreacted, highlighting the relevance of covalently-linking the substrate recognition site to the catalytically active site as it is the case in the supramolecular ligand **L**. For comparison purposes, the reaction performed using 4,4'-di-*tert*-butyl-2,2'-dipyridyl (**dtbpy**) as ligand with or without the presence of **ZnTPP** led to an almost statistical mixture of *meta*- and *para*-borylated products (**Scheme 3B**).[15a] The relevance of the substrate binding to the zinc(II)-porphyrin pocket was further evidenced by the lack of reactivity observed for pyridines having no lone pair available for binding (i.e. pyridinium derivatives, **Scheme 3C**) as well as for pyridines

unable to bind to the zinc atom due to steric shields (i.e. 2-methylpyridine, **Scheme 3C**).[28,29] A last experiment was performed adding to the standard reaction conditions zinc(II)-salphen (**ZS**) as a substrate competitive inhibitor (**Scheme 4**) since it is known that zinc(II)-salphen derivatives bind to pyridine derivatives typically two orders of magnitude higher than zinc(II)-porphyrins.[28a,30] In this scenario, an almost complete inhibition of catalysis took place with one equivalent of **ZS**. These observations show that the substrate is significantly bound to the zinc(II)-salphen **ZS** in which no catalysis takes place and that the catalysis do occur only if the substrate binds to the supramolecular ligand **L**.

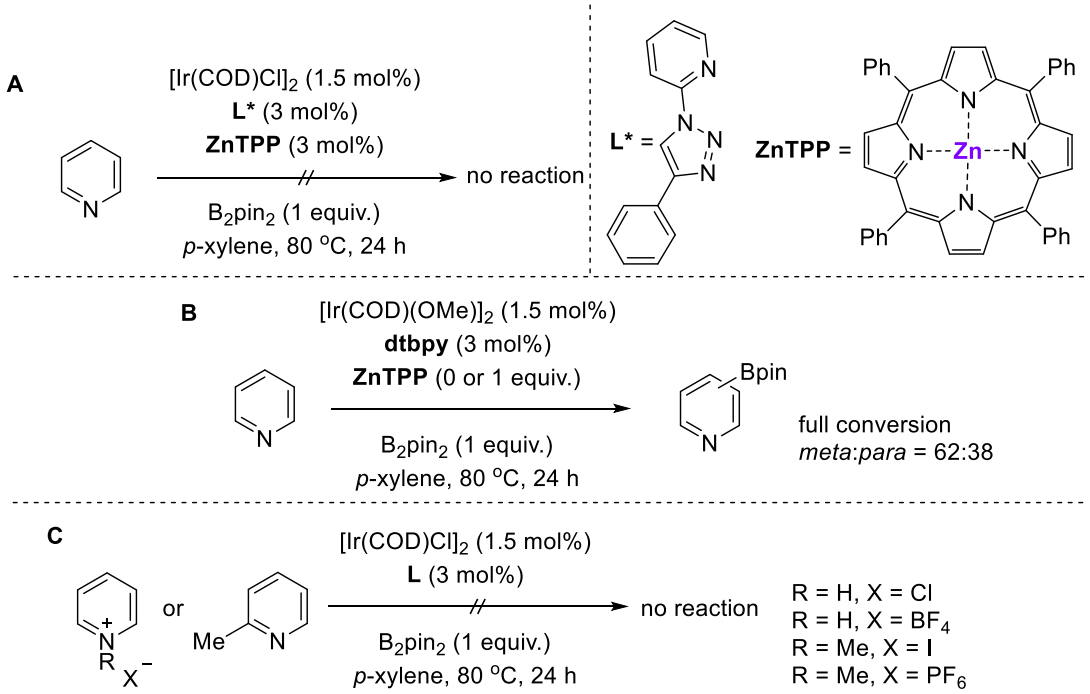

Scheme 3. Control experiments.

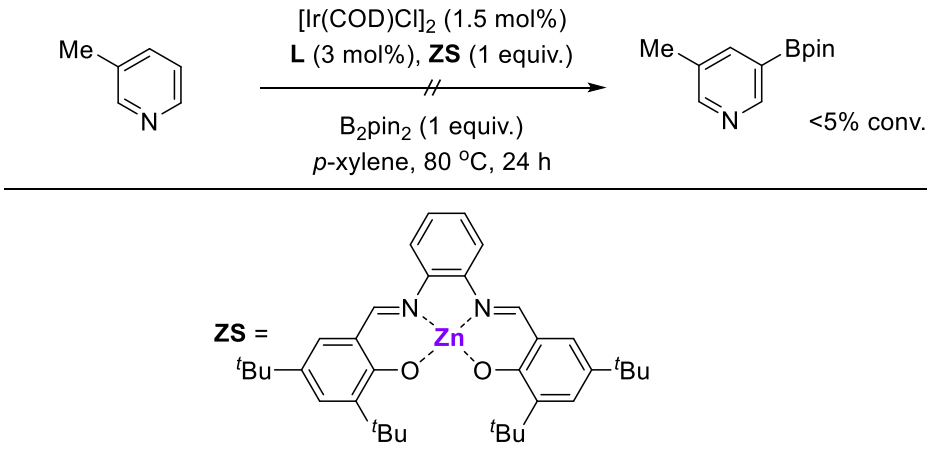

Scheme 4. Control experiments with zinc-slaphen (**ZS**).

Next, a substrate scope was evaluated. The supramolecular catalytic system was found compatible with 3-substituted pyridine derivatives giving the respective *meta*-borylated products in yields up to 99% (**Table 2**). For instance, alkyl, aryl, ether, ester, and halogen (F, Cl, Br, CF_3, except iodide) functionalities were tolerated (**5a**-**5h**, **Table 2**). On the other hand, no reactivity was observed for carboxylic acid or amide groups (**Table 2**). 5-membered ring heterocycles such as *N*-protected imidazoles delivered the *β*-substituted borylated products in virtually quantitative yields (**6a**-**6c**), which appears promising with respect to literature precedents.[31] Additionally, semi-empirical molecular modelling (PM3-level) showed that the supramolecular iridium catalyst fits well also for the *β*-C-H bond selectivity observed for 5-membered ring heterocycles (see **Figure S15**). Interestingly, the 2-methylimidazole substrate which is known to bind to zinc(II)-porphyrinoids derivatives[32] did afford the corresponding *β*-C-H bond borylated derivative **6c** in 97% isolated yield. This strikingly contrast with the lack of reactivity found for 2-methylpyridine (**Scheme 3C**) and it clearly shows that the geometry of the substrate is a key parameter for the reactivity observed within this supramolecular catalyst. Limitations of the catalytic system appeared when considering 4-substituted pyiridines and pyrimidines which did not react due to steric effects as it was noted elsewhere (**Table 2**).[33]

Table 2. Substrate evaluation for the supramolecular iridium-catalyzed C-H bond *meta*-borylation controlled by remote Zn···N interactions.

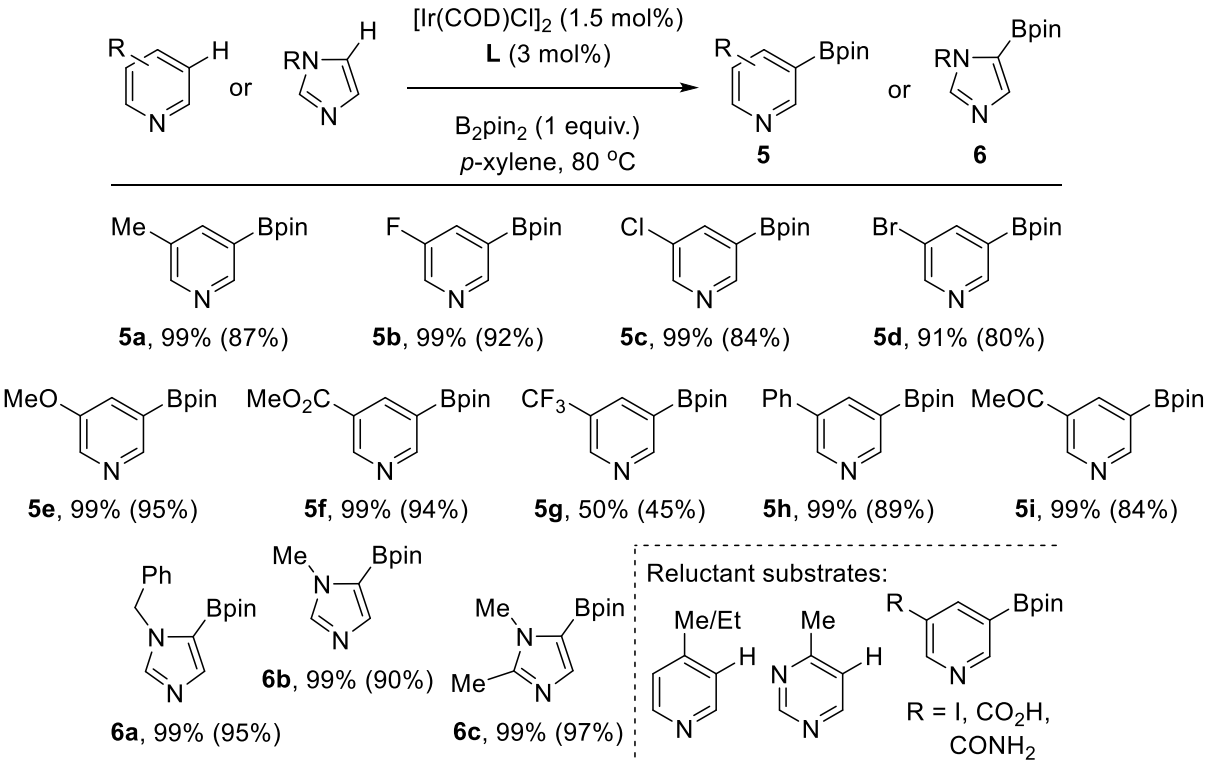

[a] Yields estimated by GC analysis and isolated yields shown in brackets, the slight difference in these values is due to loss and/or partial protodeboration of the products during purification.

We then embarked on the kinetic evaluation of this supramolecular catalysis with a model reaction using 3-methylpyridine as the substrate.[18] For this purpose, preliminar reaction progress kinetic analysis (RPKA) were carried out at same and different excess concentrations.[34] As it was found before,[17b] the reaction features an incubation period that depends on the catalyst loading, being shorter at higher catalyst loadings (**Figure 3**, left). In addition, we noted that at lower concentrations of B_2pin_2, its consumption was not directly correlated to the formation of the product as it is the case when considering the 3-methylpyridine substrate consumption (**Figure 3**, middle). Higher reaction rates have been observed with B_2pin_2 instead of HBpin for a certain types of substrates.[15b] This suggests, that a second catalytic cycle is operating to some extent involving a degradation side-product from B_2pin_2, probably HBpin because H_2 (another side-product)[35,36] is detected by ^{1}H NMR spectroscopy studies.[18] Besides these observations, the RPKA analysis showed that the catalysis is first order in iridium and pseudo-zero-order in B_2pin_2, as it could be expected.[15b,17a] On the other hand, the order in substrate did not match to zero as shown by Hartwig with a non-supramolecular catalyst,[15b] but it rather fitted to a pseudo-first order as it has been seen with non-heteroaromatic substrates.[17a] This strongly supports that the resting state in this supramolecular catalysis does not involve an iridium complex coordinated to the *N*-containing substrate *via* Ir-N bonding such as **Ir-1** (**Figure 1B**),[15b] but rather a tris-boryl iridium species formed later in the catalytic cycle likely upon substrate binding to the zinc(II)-porphyrin site such as **A** (**Scheme 5**). Although the overlay was not fully precise by RPKA analysis due to the limitations previously described, unambiguous catalyst deactivation was evidenced that we ascribed to catalyst degradation [37] as no product inhibition was observed by RPKA analysis.[18] This indicates that the catalyst immediately releases the product after formation in a similar way as enzymes do. We anticipate that the bulkiness of the product might be at the origin for the absence of product inhibition, thus indirectly enhancing substrate binding under catalytic conditions. Consequently, such catalytic system may follow an enzymatic Michaelis-Menten kinetic behavior in which the whole catalytic events occur upon binding of the substrate in the zinc(II)-porphyrin pocket (**Figure 3**, bottom). In fact, a decent fitting (R^2 = 0.994) was found for the plot of rate *versus* concentration of 3-methylpyridine substrate with V_{max} = 0.104 (±0.02) M h^{-1} and K_{mm} = 0.107 (±0.04) M.

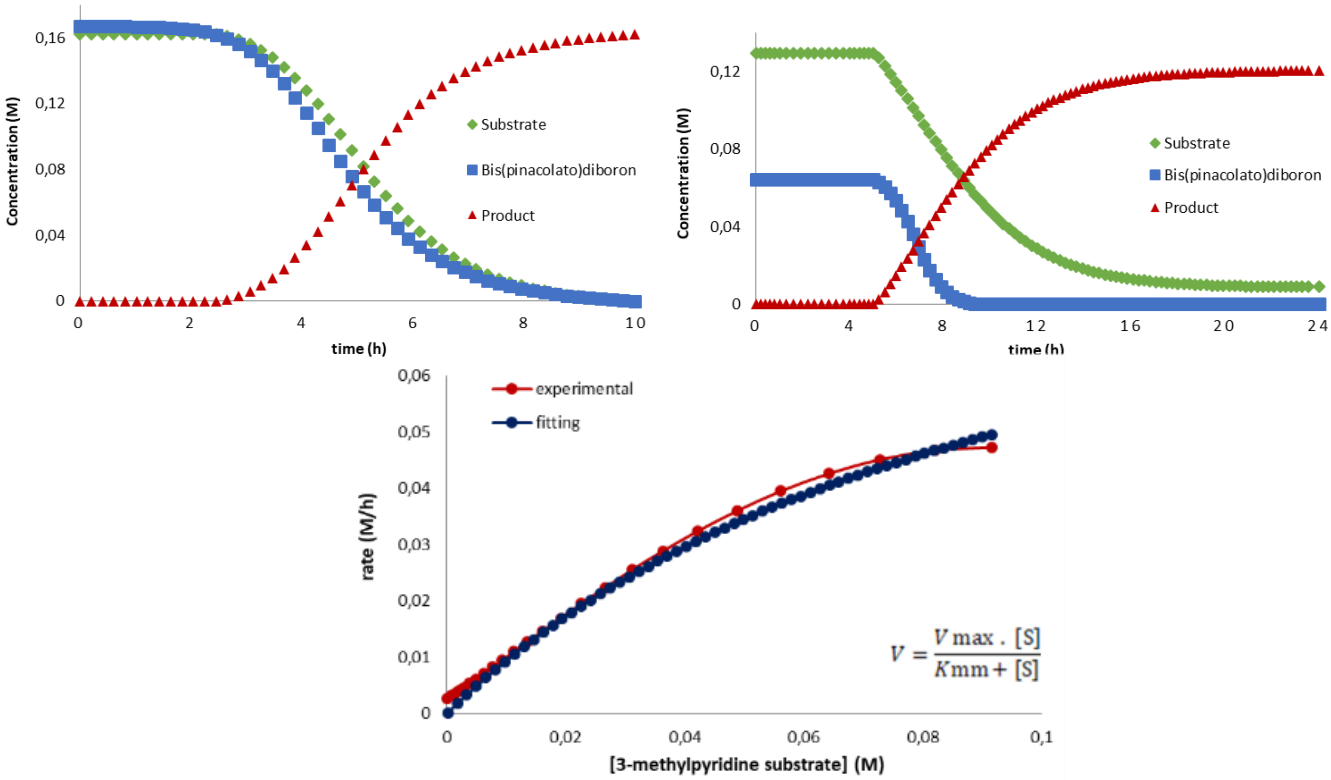

Figure 3. Graphical representation of the kinetic profiles under standard (stoichiometric) reaction conditions (left, [3-methylpyridine] = 0.162 M, [B_2pin_2] = 0.162 M) and under half concentration of B_2pin_2 with respect to the substrate (right; [3-methylpyridine] = 0.130 M, [B_2pin_2] = 0.065 M); and graphical representation of the reaction rate *versus* substrate concentration plots together with the fitting to the Michaelis-Menten rate equation (bottom).

Aiming at identifying potential catalytically active species, the *meta*-C-H bond borylation reaction was followed on time under catalytic conditions using mulitnuclei NMR spectroscopy (**Scheme 5**).

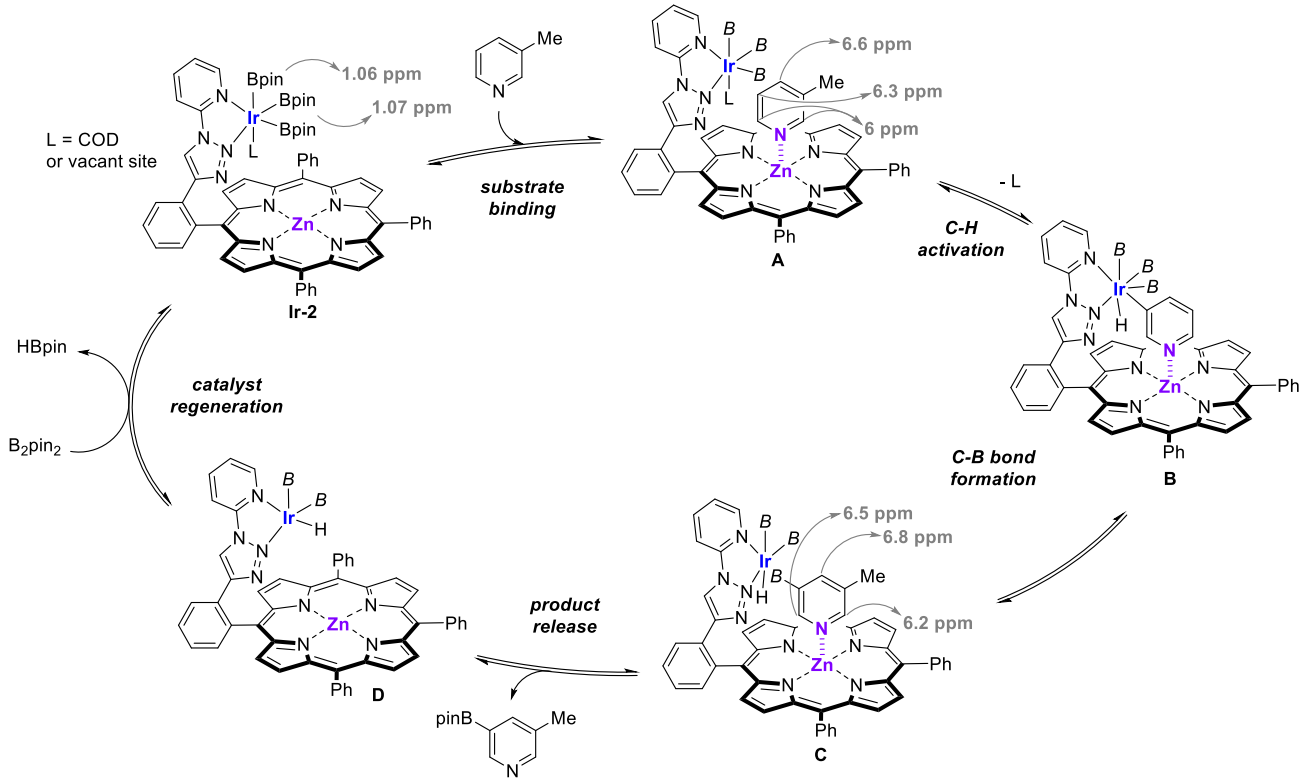

Scheme 5. Postulated reaction mechanism for the supramolecular iridium-catalyzed C-H bond *meta*-borylation of pyridines using **L**. *B* = (pinacolato)boron. The ppm values refer to the proton signals from the pyridine C-H bonds pointed out by the gray arrows that were determined by ^{1}H NMR spectroscopy at 80 °C under catalytic conditions.

First, the pre-active iridium catalyst **Ir-2** involving tris-boryl species was identified at catalytically-relevant temperatures.[18] The ^{1}H NMR studies of **Ir-2** showed two set of signals at δ = 1.07 and 1.06 ppm corresponding to two different set of Bpin groups in a 1:2 ratio (one Bpin fragment was in axial position and the other two Bpin fragments were in equatorial position; *note that they are not equivalent at high temperatures due to the low symmetry of the species*).[17a] Similar observations were evidenced by ^{11}B NMR studies (δ = 22 and 23 ppm in a 1:2 ratio).[18] Next, the reaction between 3-methylpyridine and B_2pin_2 with the *in situ* formed **Ir-2** was followed on time.[18] The 3-methylpyridine substrate was bound to the supramolecular ligand **L** *via* Zn···N interaction under catalytic conditions as regards of the up-field shifted pyridine proton signals strongly supporting the formation of species **A** (**Scheme 5**). Although the transient iridium-hydride species **B** (as well as **D**) was not detected, the product-to-catalyst species **C** was formed according to the disappearance of the pyridine signals belonging to **A** and the merger of a set of three new up-field shifted pyridine proton signals (**Scheme 5**). Further GC analysis and ^{1}H NMR spectroscopy studies indicated quantitative formation of *meta*-borylated product, indicating that the product is easily released from the catalyst pocket under the catalytic conditions. The

overall combination of above-described results together with previous data from the literature,[38] enabled us to propose a catalytic cycle in which all the reaction steps occur after substrate binding to the porphyrin pocket of **L** with final release of the product after selective *meta*-C-H bond borylation (**Scheme 5**).

To further show the enzyme-like behavior of this supramolecular iridium catalyst, we wondered whether it would be possible to perform substrate-selective catalysis with a reaction comprising a mixture of all three possible regioisomers derived from 3-methylpyridine as the substrates.[39] Indeed, the supramolecular catalyst formed upon combination of the iridium precursor and **L** gave a selective system towards the exclusive *meta*-selective borylation of the *meta* isomer with no reactivity observed at the other substrates even upon 24 hours reaction time (**Scheme 6**). A single product formed out of the 10 possible ones considering the different regio- and site-selectivities. Thus, the system leads to substrate-selectivity maintaining an exquisite level of regio-selectivity as well.

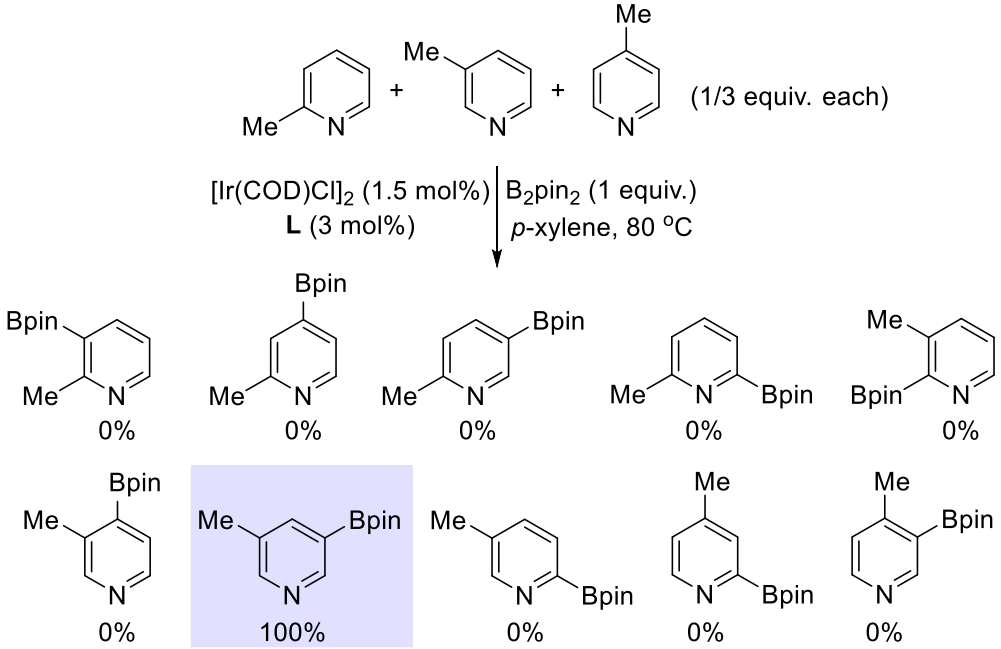

Scheme 6. Substrate-selectivity targeted using the supramolecular iridium catalyst featuring secondary Zn···N interactions.

Finally, we studied the ability of this supramolecular iridium catalyst to display dormant reactivity in a way that the borylation only occurs when an external stimuli is applied to the system. More precisely, and considering the lack of reactivity of pyridinium salts (*vide supra*), we decided to introduce after 3 hours of reaction time one equivalent of *N*,*N*-diisopropylethylamine base (DIPEA) as an external chemical stimuli with the hope that an *in situ* deprotonation of the substrate will bring the pyridine to bind the zinc pocket of the supramolecular ligand **L** following iridium-catalyzed remote borylation. Indeed, we were pleased to detect 90% conversion of pyridine after 16 h according to the above described reaction design (**Figure 4**).

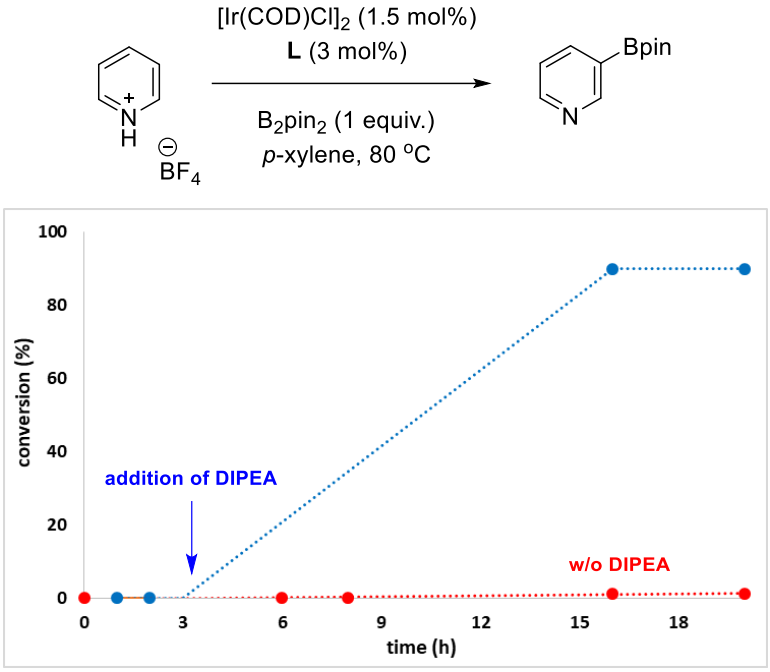

Figure 4. Dormant reactivity featured by the supramolecular iridium catalyst using a base (DIPEA) as an external chemical stimuli.

2.3. Conclusion.

In summary, we have reported a rationally-designed supramolecular borylating iridium catalyst displaying C-H bond *meta*-selectivity for challenging pyridine-like derivatives *via* reversible and dynamic Zn···N binding.[16] The predictability of the selectivity was made possible considering the relatively strong association constant between the substrates and the catalyst and the precise distance between the active site and the recognition site supported by a straightforward combination of experimental and theoretical (semi-empirical) studies. The catalytic system displayed unique enzymatic features as regards of the kinetics, mechanism and substrate-selectivity herein presented. The incorporation of substrate-recognition sites based on zinc(II)-porphyrin scaffolds in the second coordination sphere of *a priori* inactive or unselective catalytic moieties clearly constitutes an alternative to the more classical fine-tuning at the first coordination sphere. In addition, we showed that *N*,*N*-chelating ligands beyond bipyridine or phenantroline derivatives are suitable for iridium-catalyzed C-H bond borylations.[40] Because this presented approach is readily tunable at the active site and the substrate-recognition site, other types of transition metal-catalyzed transformations towards unbiased substrates could be envisioned as well as exploiting them for temporal control of reactivity considering the preliminary dormant reactivity studies.

2.4. Experimental section.

Solvents were purified with an MB SPS-800 purification system. Pyrrole was dried with CaH_2 and distilled prior to use. $CDCl_3$ was filtered through alumina and stored under argon over molecular sieves. All the other employed chemicals were purchased from commercial sources and used as received. Unless otherwise specified, reactions were carried out under argon atmosphere by employing standard Schlenk and vacuum-line techniques. ^1H and ^{13}C NMR spectra were recorded with a Bruker GPX (400 MHz) spectrometer. ^1H NMR spectra were referenced to residual protiated solvent (δ = 7.26 ppm for $CDCl_3$). ^{13}C NMR spectra were referenced to $CDCl_3$ δ = 77.16 ppm). Abbreviations for signal couplings are: br, broad; s, singlet; d, doublet; t, triplet; m, multiplet; dd, doublet of doublets; dt, triplet of doublets; td, doublet of triplets; tt, triplet of triplets; tdd, doublet of doublet of triplets. Coupling constants, *J*, were reported in hertz unit (Hz). The reactions were monitored by using a Shimadzu 2014 gas chromatograph equipped with an EquityTM-1 Fused Silica capillary column (30 m x 0.25 mm x 0.25 □m) and an FID detector; conversion and selectivity were determined by using dodecane as internal standard. UV/Vis absorption spectra were recorded with a Specord 205 UV/Vis/NIR spectrophotometer and quartz cuvettes of 1 cm path length. Mass spectroscopy and microanalysis were performed in the laboratories of the Centre Regional de Mesures Physiques de l'Ouest (CRMPO, Université de Rennes 1, Rennes, France). Molecular modeling calculations were performed with the PM3-Spartan molecular modeling program.

2.4.1. Synthesis and characterization of the molecules employed in this study.

The supramolecular ligand **L** was synthesized according to the **Scheme S1** shown below:

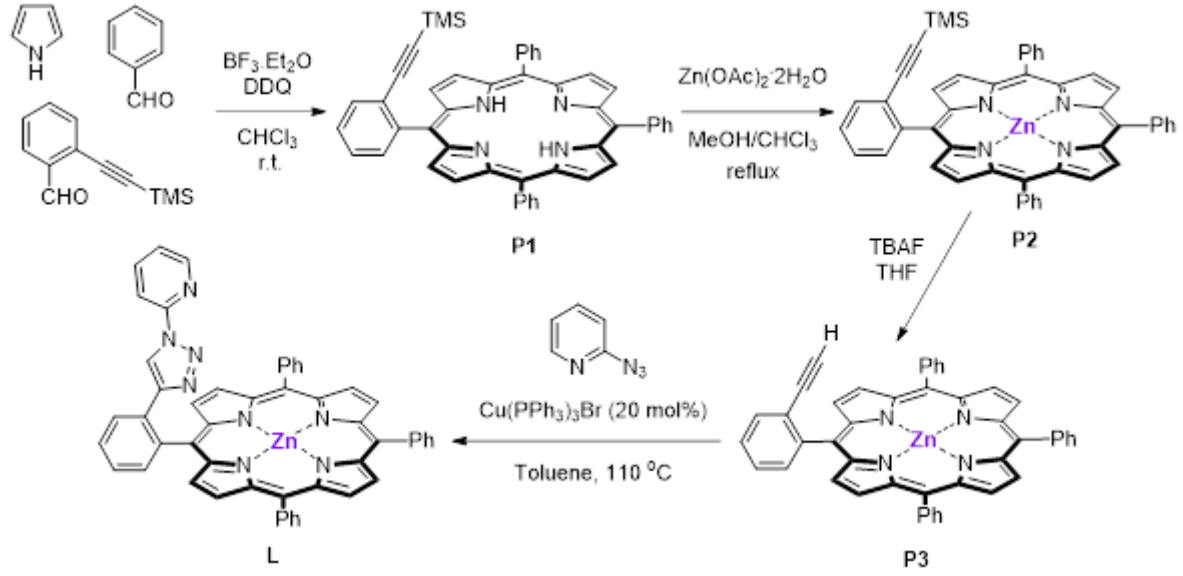

Scheme S1. Synthetic pathway towards the supramolecular ligand **L**.

Synthesis and characterization of 2-((trimethylsilyl)ethynyl)benzaldehyde: 2-Bromobenzaldehyde (1.57 mL, 2.49 mg, 13.5 mmol, 1 equiv.) was introduced into a dried Schlenk tube equipped with a stirring bar along with $Pd(OAc)_2$ (0.037 mg, 0.14 mmol, 0,01 equiv.), CuI (0.0626 mg, 0.33 mmol, 0,025 equiv.) and PPh_3 (0.0909 mg, 0.29 mmol, 0,021 equiv.). Dry triethylamine (20 mL) was added to the reaction mixture and ethynyltrimethylsilane (2.2 mL, 1.56 mg, 16 mmol, 1,189 equiv.) was added slowly to the reaction mixture. The mixture was heated at 50 °C over 18 hours after which GC-MS analysis showed full conversion of the starting materials. The crude mixture was filtered over celite with dichloromethane and the solvents evaporated under reduced pressure. The titled compound was further purified by column chromatography (SiO_2, *n*-heptane:EtOAc 1:0 to 0:1) and isolated in 95% yield (2.6 g). ^{1}H NMR (400 MHz, $CDCl_3$): δ = 10.56 (1H, s), 7.91 (1H, d, J = 8.3 Hz), 7.59-7.52 (2H, m), 7.44 (1H, t, J = 7.8 Hz), 0.28 (9H, s) ppm. The spectral data match those found in literature.[41]

Synthesis and characterization of P1: Distilled chloroform (650 mL), distilled pyrrole (1.4 mL, 20.2 mmol, 4 equiv.), benzaldehyde (1.53 mL, 15 mmol, 3 equiv.) and 2-(trimethylsilyl)ethynyl)benzaldehyde (1.01 g, 5.0 mmol, 1 equiv.) were introduced into a 1 L round bottom flask equipped with a stirring bar. At room temperature and under light protection, $BF_3{\cdot}Et_2O$ (288 mg, 0.25 mL, 2.0 mmol, 0,4 equiv.) was added and the reaction was stirred for 3 hours. Then, DDQ (2.3 g, 10.0 mmol, 2 equiv.) was introduced and the reaction mixture was stirred for 1 hour before being quenched with Et_3N (0.282 µL). The solvent was evaporated and the crude mixture was purified by column chromatography (SiO_2, *n*-heptane:DCM 9:1 to 6:4) affording **P1** as a purple powder (577 mg, 16% yield). ^{1}H NMR (400 MHz, $CDCl_3$): δ = 8.87-8.77 (8H, m, H_β), 8.23-8.13 (7H, m, $H_{meso\text{-}aryl}$), 7.9 (1H, dd, J = 7.6, 1.5 Hz, $H_{meso\text{-}aryl}$), 7.8-7.68 (11H, m, $H_{meso\text{-}aryl}$), -1.07 (9H, s), -2.73 (2H, s, $H_{pyrrole}$) ppm. $^{13}C\{^1H\}$ NMR (101 MHz, $CDCl_3$): δ = 144.88 (C_α), 142.32 (C_α), 134.84 ($C_{meso\text{-}aryl}$), 134.62 ($C_{meso\text{-}aryl}$), 134.52 ($C_{meso\text{-}aryl}$), 131.48 ($C_{meso\text{-}aryl}$), 128.06 (CH_β), 127.77 (CH_β), 127.75 (CH_β), 127.73 (CH_β),, 127.30 ($C_{meso\text{-}aryl}$), 126.89 ($C_{meso\text{-}aryl}$), 126.74 ($C_{meso\text{-}aryl}$), 126.72 ($C_{meso\text{-}aryl}$),

120.42 ($C_{meso\text{-}aryl}$), 120.22 ($C_{meso\text{-}aryl}$), 120.04 ($C_{meso\text{-}aryl}$), 118.21 ($C_{meso\text{-}aryl}$), 105.15 (CH_{alkyne}), 99.46(CH_{alkyne}), -1.23 (C_{TMS}) ppm. HRMS (ESI): *m/z* calcd for $C_{49}H_{39}N_4Si$ 711.2938 $[M+H]^+$; found: 711.2932 (1 ppm).

Synthesis and characterization of P2: Porphyrin **P1** (607 mg, 0.853 mmol, 1 equiv.) was introduced into a 250 mL round bottom flask equipped with a stirring bar and MeOH:$CHCl_3$ (100 mL, *v*/*v* = 1:4). $Zn(OAc)_2{\cdot}2H_2O$ (0.603 mg, 2.75 mmol, 3.2 equiv.) was added and the reaction mixture was heated at reflux for 1 hour. Back at room temperature, the solvents were removed under reduced pressure and the crude mixture was purified over Alumina with DCM affording **P2** as a purple powder (660 mg, quantitative). ^{1}H NMR (400 MHz, $CDCl_3$): δ = 8.95-8.86 (8H, m, H_β), 8.23-8.18 (7H, m, $H_{meso\text{-}aryl}$), 7.80-7.71 (11H, m, $H_{meso\text{-}aryl}$), 7.89 (1H, dd, *J* = 6.4, 2.7, $H_{meso\text{-}aryl}$), -1.14 (9H, s) ppm. $^{13}C\{^1H\}$ NMR (101 MHz, $CDCl_3$): δ = 150.69 (C_α), 150.38 (C_α), 150.36 (C_α), 150.07 (C_α), 145.67 ($C_{meso\text{-}aryl}$), 143.03 ($C_{meso\text{-}aryl}$), 143.01 ($C_{meso\text{-}aryl}$), 134.67 ($C_{meso\text{-}aryl}$), 134.55 ($C_{meso\text{-}aryl}$), 134.53 ($C_{meso\text{-}aryl}$), 134.50 ($C_{meso\text{-}aryl}$), 134.46 ($C_{meso\text{-}aryl}$), 132.30 (CH_β), 132.22 (CH_β), 132.18 (CH_β), 132.06 (CH_β), 132.03 (CH_β), 131.94 (CH_β), 131.42 (CH_β), 127.93 ($CH_{meso\text{-}aryl}$), 127.61 ($CH_{meso\text{-}aryl}$), 127.59 ($CH_{meso\text{-}aryl}$), 127.38 ($CH_{meso\text{-}aryl}$), 126.88 ($CH_{meso\text{-}aryl}$), 126.65 ($CH_{meso\text{-}aryl}$), 121.54 (C_{meso}), 121.16 (C_{meso}), 119.29 (C_{meso}), 105.52 (C_{alkyne}), 99.16 (C_{alkyne}), -1.11 (C_{TMS}) ppm. HRMS (ESI): *m/z* calcd for $C_{49}\ H_{36}\ N_4\ Si^{64}Zn$ 772.1995 $[M]^+$; found: 772.1993 (0 ppm).

Synthesis and characterization of P3: Porphyrin **P2** (500 mg, 0.56 mmol, 1 equiv.) was introduced in a dried Schlenk tube charged with a stirring bar and dry THF (20 mL). At room temperature, a solution of 1M TBAF in THF/water: 95/5 (0.56 mL, 1.94 mmol, 3 equiv.) was added dropwise and the mixture was stirred for 4 hours. Then, the mixture was evaporated to dryness and purified over neutral alumina using *n*-heptane:DCM (1:1) and afforded the analytically pure title porphyrin **P3** (431 mg, 95% yield). ^{1}H NMR (400 MHz, $CDCl_3$): δ = 8.95-8.82 (8H, m, H_β), 8.27-8.15 (7H, m, $H_{meso\text{-}aryl}$), 7.95 (1H, d, *J* = 8 Hz, $H_{meso\text{-}aryl}$), 7.76 (11H, m, $H_{meso\text{-}aryl}$), 2.12 (1H, s) ppm. $^{13}C\{^1H\}$ NMR (101 MHz, $CDCl_3$): δ = 150.29 (C_α), 150.21 (C_α), 150.18(C_α), 150.05 (C_α), 145.50 ($C_{meso\text{-}aryl}$), 142.83 ($C_{meso\text{-}aryl}$), 142.78 ($C_{meso\text{-}aryl}$), 134.48 ($CH_{meso\text{-}aryl}$), 134.45 ($CH_{meso\text{-}aryl}$), 134.37 ($CH_{meso\text{-}aryl}$), 134.23 ($CH_{meso\text{-}aryl}$),132.33 (CH_β), 131.99 (CH_β), 131.90 (CH_β), 131.47 (CH_β), 127.97 ($CH_{meso\text{-}aryl}$), 127.51 ($CH_{meso\text{-}aryl}$), 127.49 ($CH_{meso\text{-}aryl}$), 126.94 ($CH_{meso\text{-}aryl}$), 126.54 ($CH_{meso\text{-}aryl}$), 125.79 ($C_{meso\text{-}aryl}$), 121.44 (C_{meso}), 121.10 (C_{meso}), 118.63 (C_{meso}), 83.24 (C_{alkyne}), 80.95 (CH_{alkyne}) ppm. HRMS (ESI): *m/z* calcd for $C_{46}\ H_{28}\ N_4{}^{64}Zn$ 700.1599 $[M]^+$; found: 700.1600 (0 ppm).

Synthesis and characterization of 2-azidopyridine: In a two-necked dried round bottom flask, 2-bromopyridine (1.23 mL, 2.06 mg, 13 mmol, 1 equiv.), sodium azide (1.6962 g, 26 mmol, 2 equiv.), CuI (0.2472 g, 1.3 mmol, 0,1 equiv.), sodium ascorbate (0.1472 g, 0.7 mmol, 0,05 equiv) and dimethylethyldiamine (0.21 mL, 0.172 mg, 1.95 mmol, 0,15 equiv.) were dissolved in a mixture of EtOH:H_2O (60 mL, *v*/*v* 7:3). Then, the reaction mixture was degassed by Argon followed by stirring during 2 hours at reflux. Back at room temperature, DCM:H_2O (200 mL, *v*/*v* 1:1) were added and the crude reaction mixture was transferred into a separatory funnel and 3 spoons of ethylene diamine tetraacetic acid disodium salt were added. The aqueous layer was extracted with DCM (3 x 20 mL) and the combined organic layers were washed water (2 x 50 mL). After drying over $MgSO_4$ and filtration, the solvents were evaporated under reduced pressure. The product was further purified by filtration over Alumina using DCM as eluent affording 2-azidopyridine as a white powder (1.1 g, 70% yield). ^{1}H NMR (400 MHz, $CDCl_3$): δ = 8.84 (1H, d, *J* = 6.9 Hz, H_o), 8.07 (1H, d, *J* = 9Hz, H_m), 7.71-7.66 (1H, ddd, *J* = 9.0, 6.8, 1.0 Hz, H_p), 7.25 (1H, dt, *J* = 9.0, 6.9 Hz, H_m) ppm. The spectral data match those found in literature.[42]

Synthesis and characterization of L: Into a dried Schlenk tube charged with a stirring bar, **P3** (220 mg, 0.31 mmol, 1 equiv.), 2-azidopyridine (0,070 mg, 0.58 mmol, 1.9 equiv.), $Cu(PPh_3)_3Br$ (69 mg, 0.074 mmol, 0.2 equiv.) and dry toluene (15 mL) were added and the reaction mixture was stirred for 72 hours at 110 °C. Back at room temperature, the solvents were evaporated and the crude mixture was purified by column chromatography (SiO_2, *n*-heptane:DCM, 1:1 to 0:1). The fraction containing the product were further purified by column chromatography (neutral Al_2O_3, n-heptane:DCM: 1:1 to 0:1) affording **L1** as a purple powder (147 mg, 57% yield). ^{1}H NMR (400 MHz, $CDCl_3$): δ = 8.92-8.80 (8H, m, H_β), 8.74 (1H, d, J = 7.6 Hz, $H_{meso\text{-}aryl}$), 8.26-8.14 (7H, m, $H_{meso\text{-}aryl}$), 7.94 (1H, t, J = 8.3 Hz, $H_{meso\text{-}aryl}$), 7.77-7.67 (10H, m, Hmeso aryl), 7.59 (1H, d, J = 8.3 Hz, $H_{meso\text{-}aryl}$), 7.36 (1H, td, J = 8.1, 1.7 Hz, $H_{meso\text{-}aryl}$), 6.82 (1H, d, J = 5.0 Hz, $H_{meso\text{-}aryl}$), 6.58 (1H, m, $H_{meso\text{-}aryl}$), 5.41 (1H, s) ppm. $^{13}C\{^1H\}$ NMR (101 MHz, $CDCl_3$): δ = 150.51 (C_α), 150.47 (C_α), 150.26 (C_α), 148.23 (C_{pyr}), 147.52 (CH_{pyr}), 147.43 (C_{triaz}), 142.95 ($C_{meso\text{-}aryl}$), 142.83 ($C_{meso\text{-}aryl}$), 140.43 ($C_{meso\text{-}aryl}$), 138.28 (CH_{pyr}), 135.38 ($CH_{meso\text{-}aryl}$), 134.65 ($CH_{meso\text{-}aryl}$), 134.58 ($CH_{meso\text{-}aryl}$), 134.52 ($CH_{meso\text{-}aryl}$), 132.85 (CH_β), 132.72 ($C_{meso\text{-}aryl}$), 132.16 (CH_β), 131.54 (CH_β), 128.80 ($CH_{meso\text{-}aryl}$), 127.91 ($CH_{meso\text{-}aryl}$), 127.69 ($CH_{meso\text{-}aryl}$), 127.66 ($CH_{meso\text{-}aryl}$), 126.83-125.99 (m, $CH_{meso\text{-}aryl}$), 122.60 (CH_{pyr}), 121.56 (C_{meso}), 121.37 (C_{meso}), 119.03 (C_{meso}), 118.66 (CH_{triaz}), 113.38 (CH_{pyr}) ppm. HRMS (ESI): *m/z* calcd for $C_{51}H_{32}N_8{}^{64}Zn$ 820.2036 $[M]^+$; found: 820.2035 (0 ppm).

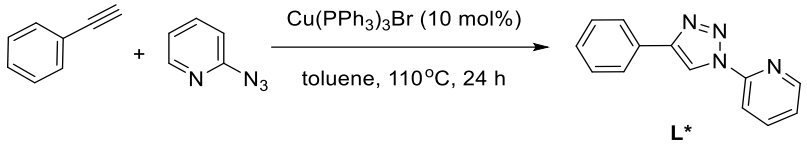

Synthesis and characterization of 2-(4-phenyl-1*H*-1,2,3-triazol-1-yl)pyridine (L*): 2-azidopyridine (204.2 mg, 1.7 mmol, 1 equiv.) and $Cu(PPh_3)_3Br$ (158.2 mg, 0.17 mmol, 0.1 equiv.) were suspended in dry toluene (12 mL) in a dry Schlenk tube. Then, ethynylbenzene (208.3 mg, 2 mmol, 1.18 equiv.) was introduced and the reaction mixture was stirred at 120 °C immediately for 24 hours. Back at room temperature, the solvent was evaporated under reduced pressure and the crude mixture was purified by column chromatography (SiO_2, *n*-heptane:EtOAc, 8:2 to 7:3) to afford **L*** (378 mg, 32% yield). ^{1}H NMR (400 MHz, $CDCl_3$): δ = 8.82 (1H, s, H_{triaz}), 8.54 (1H, d, J = 3.9 Hz, H_{pyr}), 8.26 (1H, d, J = 8.2 Hz, H_{pyr}), 7.94 (3H, m, H_{aryl}), 7.47 (2H, t, J = 7.5 Hz, H_{aryl}), 7.4-7.35 (2H, m, H_{pyr}) ppm. The spectral data match those found in literature.[43]

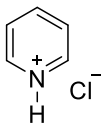

Synthesis of pyridinium derivatives: Pyridinium chloride: Dioxane (6 mL), pyridine (1 g, 1.02 mL, 1.3 mmol, 1 equiv.) and HCl (4 N in dioxane, 6.32 mL, 2.6 mmol, 2 equiv.) were added to an oven dried Schlenk flask. The reaction mixture was stirred overnight at room temperature. Then, the solvent was evaporated under reduced pressure yielding the pure product as a solid (1.4 g, 96% yield). ^{1}H NMR (400 MHz, D2O): δ = 8.73 (d, J = 5.8 Hz, 2H), 8.57 (t, J = 7.9 Hz, 1H), 8.02 (t, J = 7.0 Hz, 2H) ppm. The spectral data match those found in literature.[44]

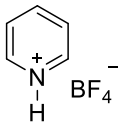

Pyridinium tetrafluoroborate: Dioxane (6 mL), pyridine (1 g, 1.02 mL, 1.3 mmol, 1 equiv.) and HBF4- (48% in diethyl ether, 2.28 mg, 4.6 mL, 2.6 mmol, 2 equiv.) were added to an oven dried Schlenk flask. The reaction mixture was stirred overnight at room temperature. Then, the solvent was evaporated under reduced pressure yielding the pure product as a solid (1.63 g, 75% yield). ^{1}H NMR (400 MHz, D2O): δ = 9.02 (d, J = 6.0 Hz 2H), 8.79 (td, J = 7.5, 1.6 Hz, 1H), 8.25 (t, J = 7.5 Hz, 2H) ppm. ^{11}B {1H} NMR (128 MHz, D2O): δ = -1.19 ppm. ^{19}F {^{1}H} NMR (376 MHz, D2O): δ = -151.46 ppm. The spectral data match those found in literature.[45]

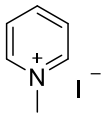

***N*-methylpyridinium iodide:** THF (50 mL), pyridine (1 g, 1.02 mL, 13 mmol, 1 equiv.) and methyl iodide (2.15 g, 0.94 mL, 15 mmol, 1.2 equiv.) were added to an oven dried round bottom flask. The reaction mixture was stirred overnight at 70°C. Back at room temperature, the precipitate was filtered off and washed with cold THF yielding the pure product as a solid (1.5 g, 54% yield). ^{1}H NMR (400 MHz, D2O): δ = 8.73 (d, *J* = 6.0 Hz, 2H), 8.47 (td, *J* = 7.1, 6.0 Hz, 1H), 7.99 (t, *J* = 7.1 Hz, 2H), 4.34 (s, 3H) ppm. The spectral data matchthose found in literature.[46]

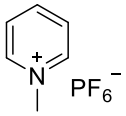

***N*-methylpyridinium hexafluorophosphate:** Water (25 mL), *N*-methylpyridinium iodide (0.5 g, 2.3 mmol, 1 equiv.) and potassium hexafluorophosphate (0.417 g, 2.3 mmol, 1 equiv.) were added to an oven dried round bottom flask. The reaction mixture was stirred overnight at 100°C. Back at room temperature, the precipate was filtered off and washed with cold water yielding the pure product as a solid (0.239 g, 47% yield). ^{1}H NMR (400 MHz, D2O): δ = 8.72 (d, *J* = 6.1 Hz, 2H), 8.47 (t, *J* = 8.0 Hz, 1H), 7.99 (t, *J* = 6.4 Hz, 2H), 4.33 (d, *J* = 2.2 Hz, 3H) ppm. ^{19}F {^{1}H} NMR (376 MHz, D2O): δ = -72.13 (d, *J* = 706.5 Hz) ppm. ^{31}P {^{1}H} NMR (162 MHz, D2O): δ = 145,02 (hept, *J* = 706.5 Hz) ppm. The spectral data match those found in literature.[47]

2.4.2. Coordination chemistry and substrate binding studies.

UV-vis titration between L and pyridine (binding experiment): 20 mL solution (A) of **L** (2.4 × 10^{-4} M) in dry dichloromethane was prepared first. 8.3 mL of (A) were diluted to 100 mL using dry DCM to give the stock solution (B) of **L** (2 x 10^{-5} M, 100 mL) that will be employed as solvent to prepare solution (C) (for pyridine: 4 x 10^{-2} M, 5 mL). Next, solution (D) of pyridine (2.0 x 10^{-3},10 mL) was prepared by dilution of (B) using stock solution (A). Different aliquots of solution D were withdrawn and diluted with solution B to give a volume of 2 mL. UV-vis spectra of each sample were recorded by using 3 mL quartz cuvettes with 10 mm path length (**Figure S1**). The binding constant was evaluated by considering a 1:1 stoichiometry and using the software BindFit with Nelder-Mead method[48] giving a value of $K_{1.1}$ = 5.7 x 10^{4} ± 1.5 M^{-1} (**Figure S2**).

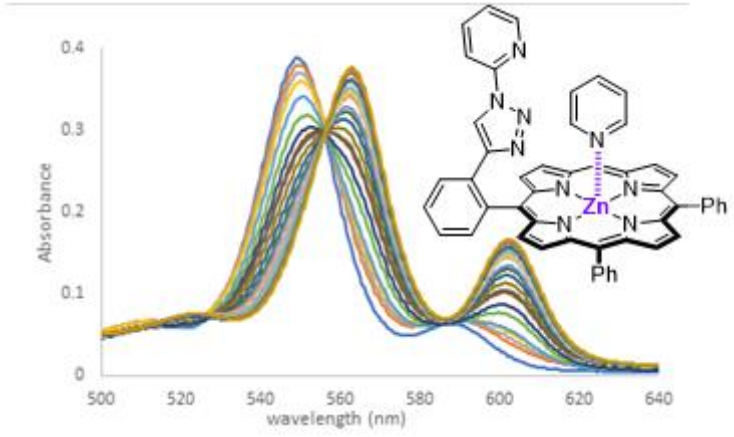

Figure S1. UV-vis spectra for **L** with pyridine to determine the binding constant.

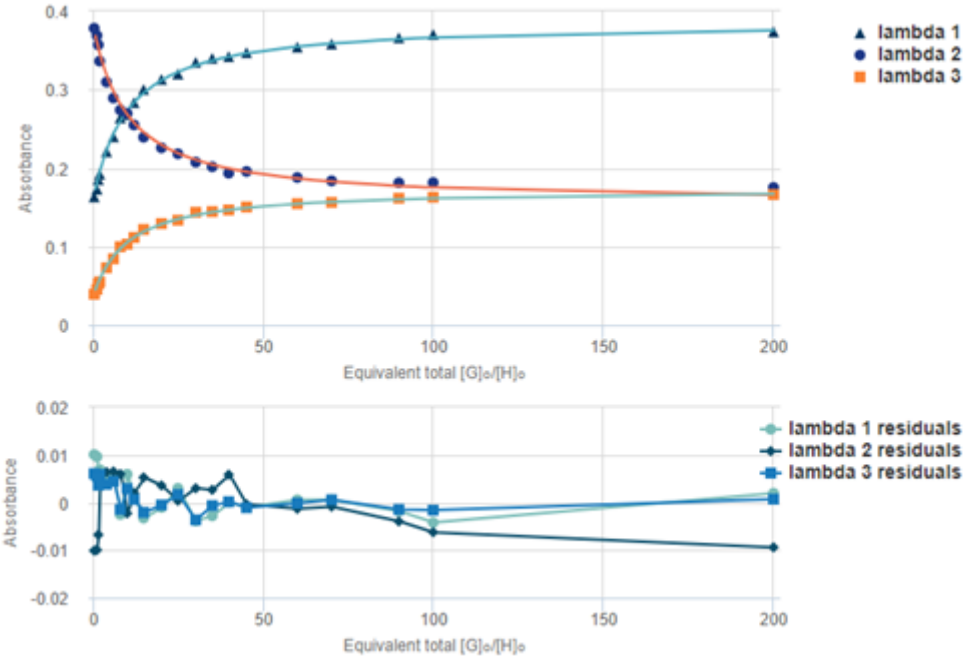

Figure S2. Curve fitting titration to determine the binding constant.

NMR binding experiment between L and pyridine (1:1 ratio): L (3.25 mg, 3.95 x 10^{-3} mmol) was placed in an NMR tube and dried under vacuum for few minutes. Then, dry $CDCl_3$ (0.75 mL) was added and the corresponding ^{1}H NMR spectrum was recorded. A previously dried Schlenk tube was charged with dry pyridine (12.8 µL, 0.158 mmol) and $CDCl_3$ (1 mL): named stock solution A. Then, 1 equiv. of pyridine (25 µL of the stock solution A) were added to the NMR tube containing the ligand **L** and the corresponding ^{1}H NMR spectrum was recorded showing strong up-field shifts for the pyridine proton signals (Figure S3). ^{1}H NMR (400 MHz, $CDCl_3$): δ = 8.86-8.80 (8H, m, H_β), 8.59 (1H, d, $H_{meso\text{-}aryl}$), 8.20-8.15 (6H, m, $H_{meso\text{-}aryl}$), 8.04 (1H, d, J = 6.8 Hz, $H_{meso\text{-}aryl}$), 7.91 (1H, t, J = 7.1 Hz, $H_{meso\text{-}aryl}$), 7.75-7.56 (10H, m, $H_{meso\text{-}aryl}$), 7.44 (1H, d, J = 8.2 Hz, $H_{meso\text{-}aryl}$), 7.32 (1H, t, 8.2 Hz, $H_{meso\text{-}aryl}$), 7.21 (1H, d, J = 6.0 Hz, $H_{meso\text{-}aryl}$), 6.65-6.62 (1H, m, $H_{meso\text{-}aryl}$), 6.51 (1H, bs, $H_{p\text{-}pyr}$), 6.16 (1H, s, H_{triaz}), 5.86 (2H, bs, $H_{m\text{-}pyr}$), 4.16 (2H, bs, $H_{o\text{-}pyr)}$ ppm.

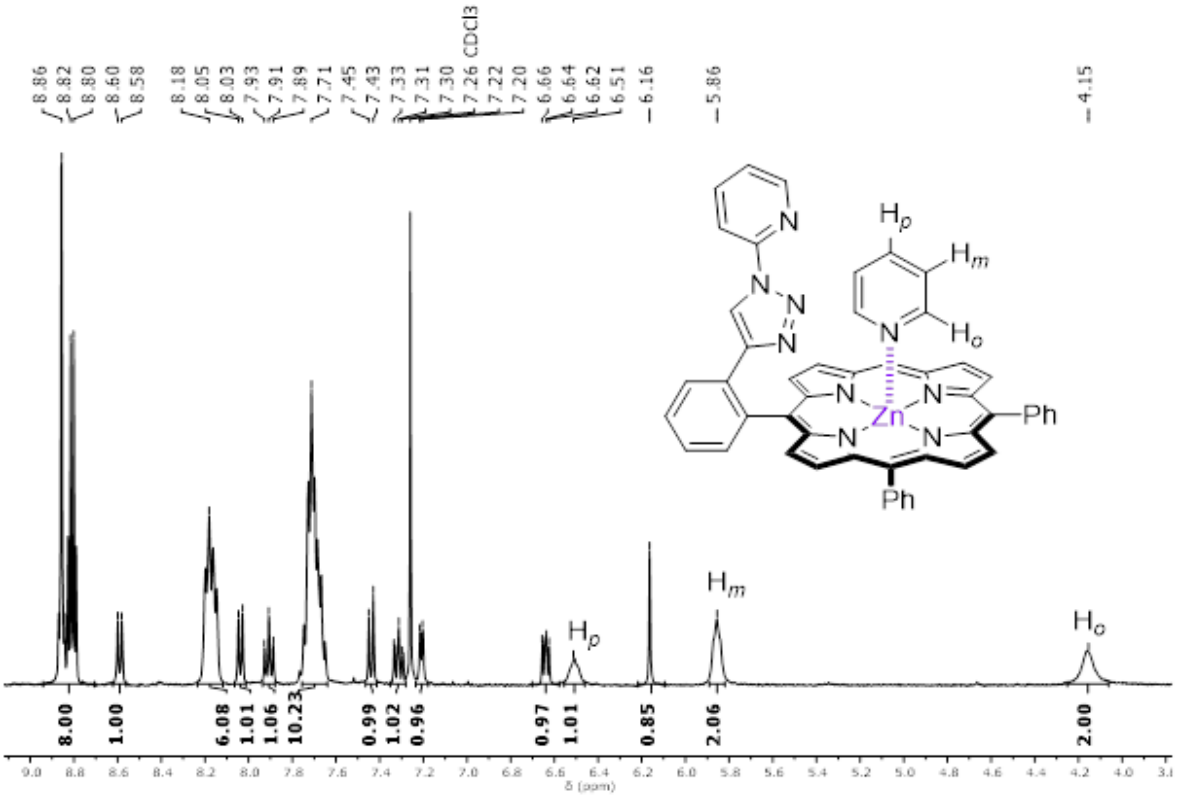

Figure S3. ^{1}H NMR spectrum ($CDCl_3$) of the self-assembly [**L**·pyridine] in an equimolar ratio.

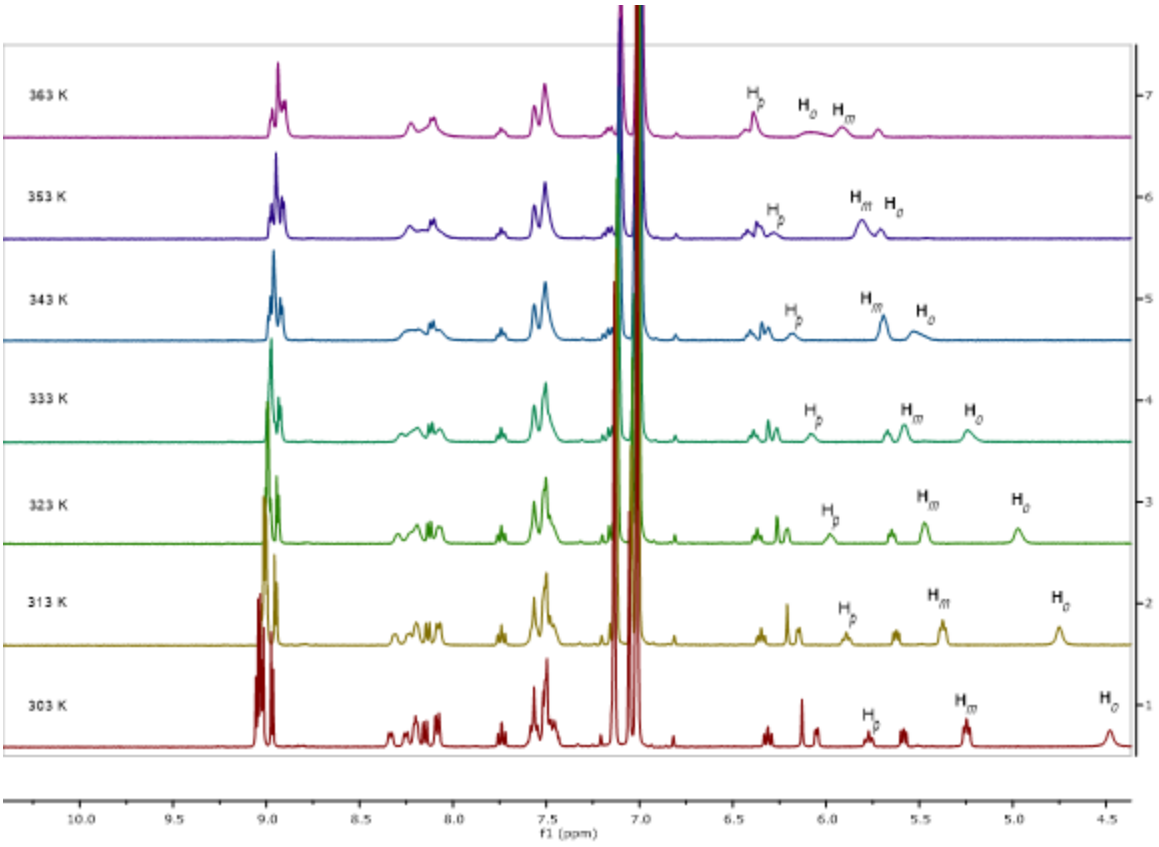

Figure S4. Variable high-temperature ^{1}H NMR (toluene-d^{8}) spectra of pyridine and **L** in an equimolar ratio. It shows that the binding of pyridine to **L** is in fast exchange at the NMR time scale and it is kinetically labile in the range 25-90 °C (bottom to top).

DOSY experiments:

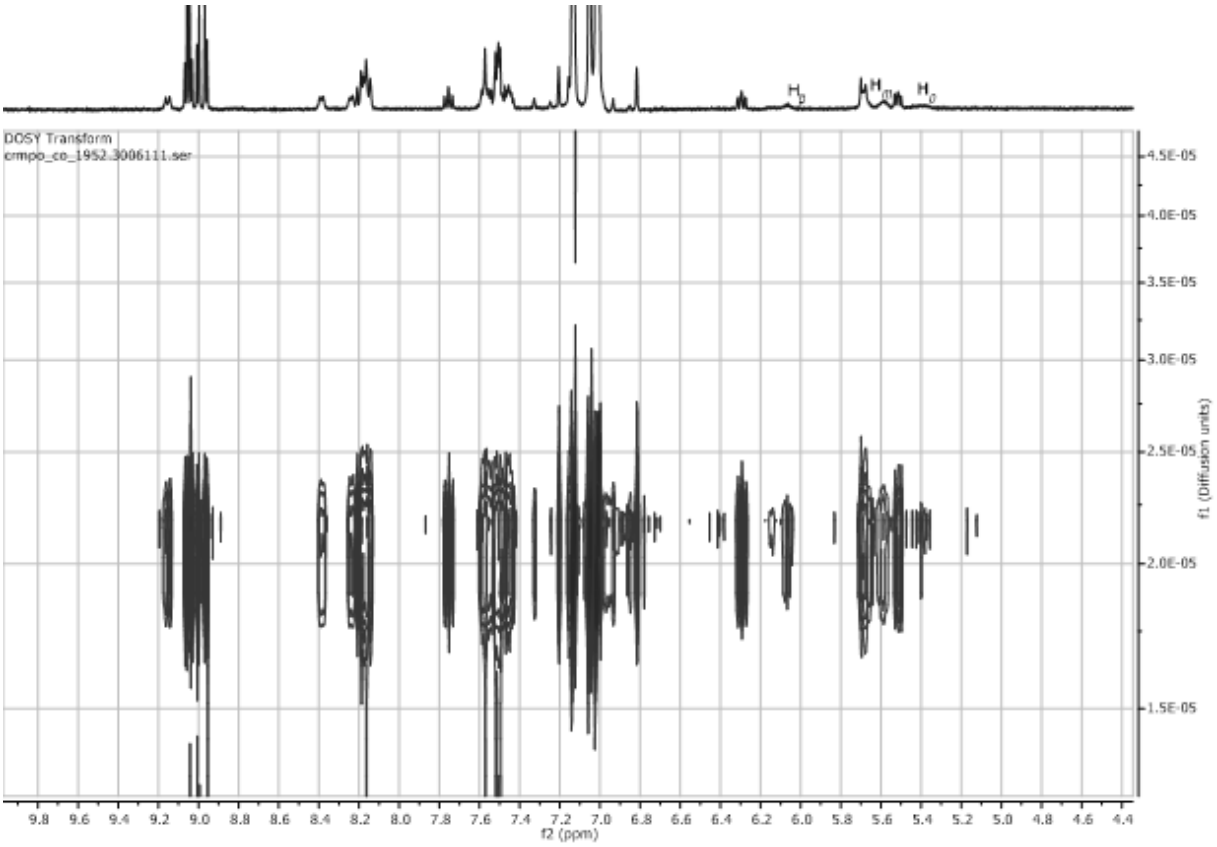

Figure S5. DOSY experiment of pyridine and **L** in equimolar ratio (toluene-d^8).

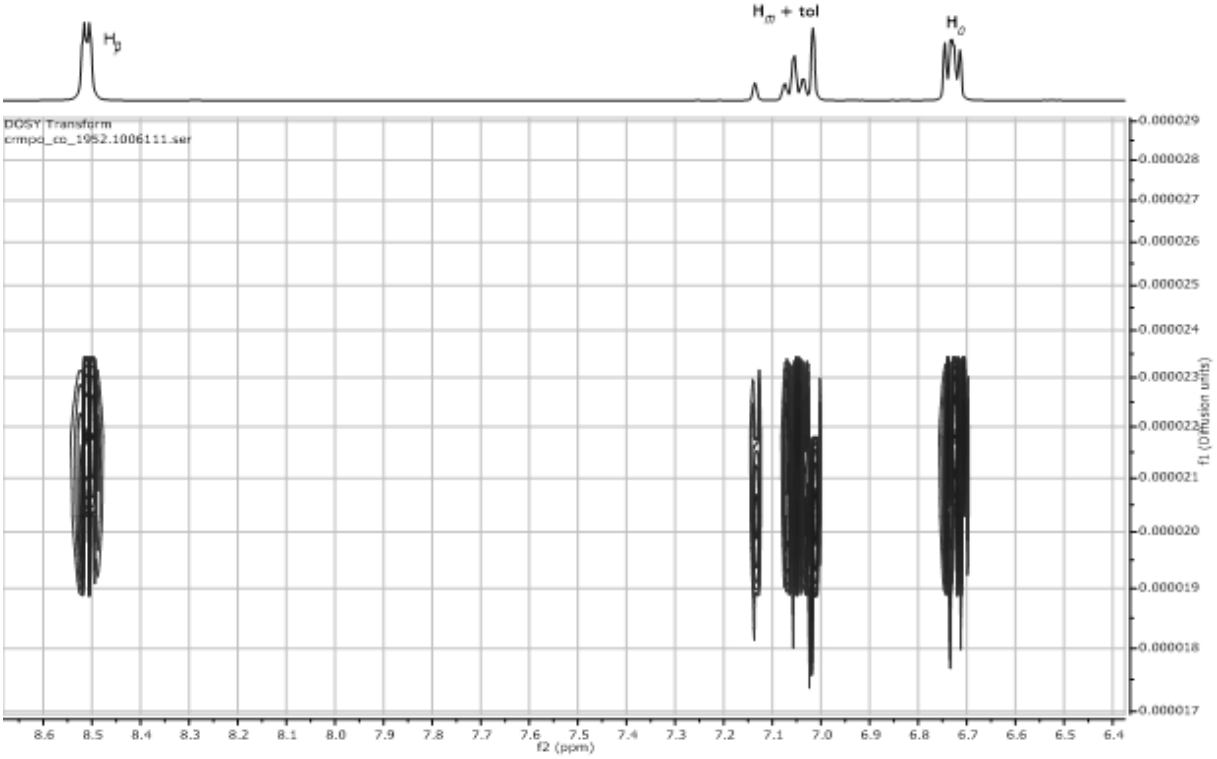

Figure S6. DOSY experiment of pure pyridine (toluene-d^8).

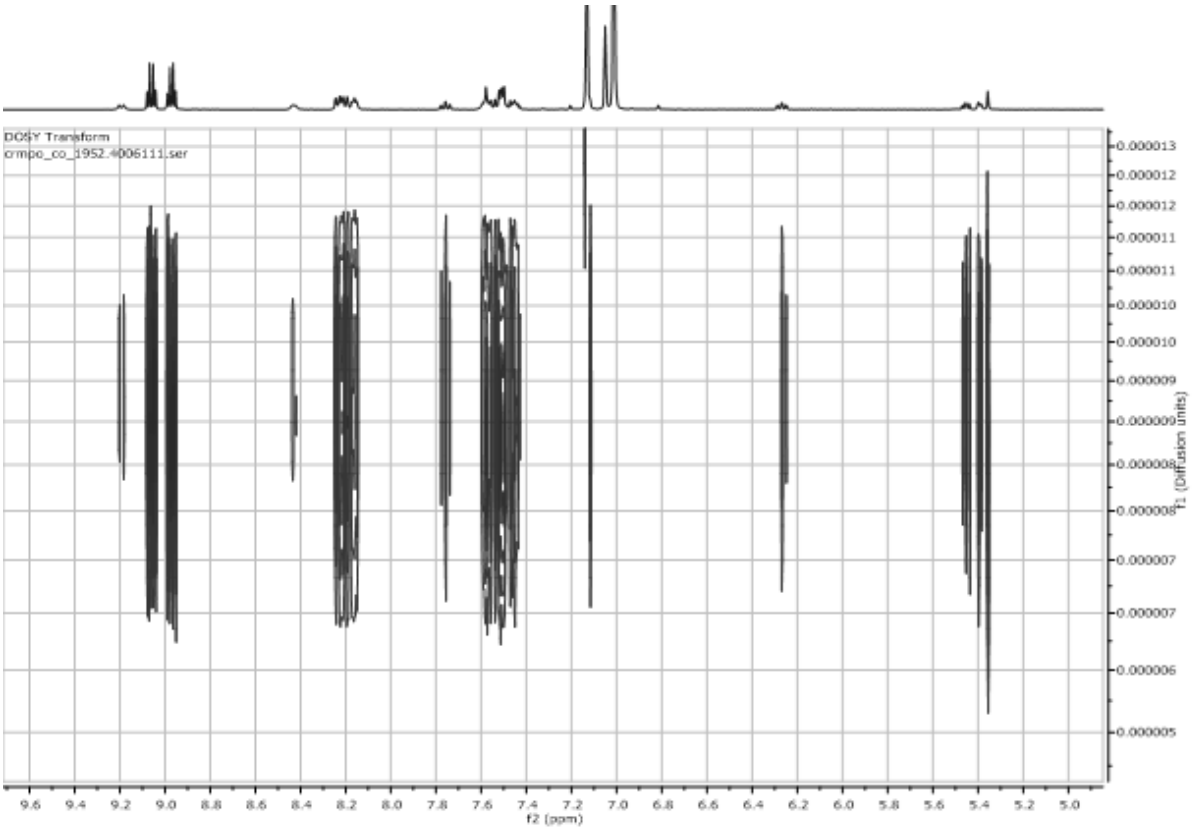

Figure S7. DOSY experiment of pure **L** (toluene-d^8).

The above-presented experiments indicate that the pyridine diffuses together with the supramolecular ligand **L** when both are together in solution. Qualitatively, the log D for the self-assembly [**L**·pyridine] is different than the ones derived from the individual partners.

Coordination chemistry studies for the iridium complex L1: Into a dry Schlenk tube equipped with a stirring bar, **L** (4 mg, 4.86 x 10^{-3} mmol) and $[Ir(COD)(\mu\text{-}Cl)]_2$ (1.7 mg, 2.43 x 10^{-3} mmol) were introduced. After drying the reagents under vacuum for 30 minutes, dry DCM (1 mL) was added and the reaction mixture was stirred for 30 minutes at 60 °C. Back at room temperature, the solvents were removed under reduced pressure and the product was dried and characterized by NMR and HRMS. ^{1}H NMR (400 MHz, $CDCl_3$): δ = 8.95-8.84 (8H, m, H_β), 8.63 (1H, d, J = 7.8 Hz, $H_{meso\text{-}aryl}$), 8.23-8.14 (7H, m, $H_{meso\text{-}aryl}$), 7.95 (1H, t, J = 7.8 Hz, $H_{meso\text{-}aryl}$), 7.79-7.72 (10H, m, $H_{meso\text{-}aryl}$), 7.52 (1H, d, J = 8.3 Hz, $H_{meso\text{-}aryl}$), 7.34 (1H, d, J = 7.9 Hz,$H_{meso\text{-}aryl}$), 7.02 (1H, d, J = 4.9 Hz, $H_{meso\text{-}aryl}$), 6.60 (1H, t, J = 6.2 Hz, $H_{meso\text{-}aryl}$), 5.77 (1H, s, H_{triaz}), the proton singals from the COD ligand could not be detected due to broadness. HRMS (ESI): *m/z* calcd for $C_{59}H_{44}N_8{}^{64}Zn^{193}Ir$ 1121.2604 $[M]^+$; found: 1121.2599 (0 ppm). Note: Although minor changes were observed between the NMR signals of **L** and **L1** (**Figure S8**), the HRMS spectrum displayed a single peak unambiguously corresponding to the [Ir(COD)] fragment coordinated to the supramolecular ligand **L** resulting in a cationic species (**Figure S9**). A low temperature NMR experiment also supported the formation of a single species (**Figure S10**).

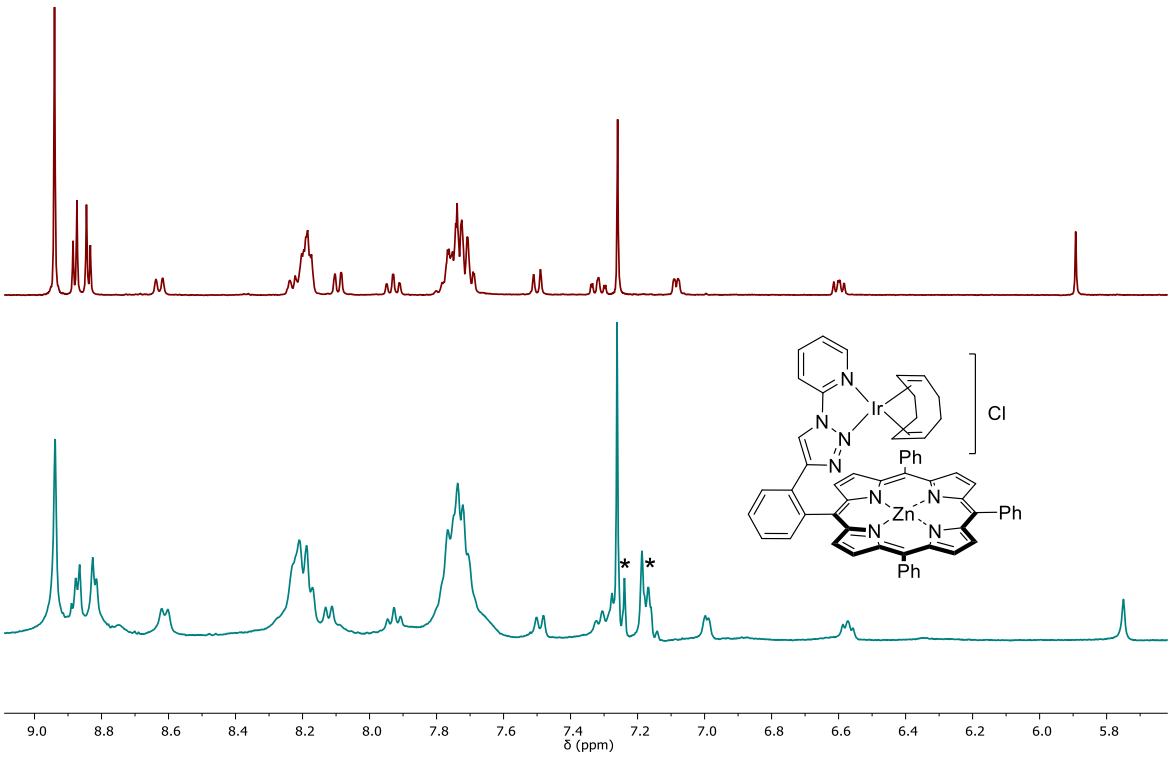

Figure S8. ^{1}H NMR ($CDCl_3$) spectra of **L** (top) and the iridium complex **L1** (bottom). *denotes traces of residual toluene solvent.

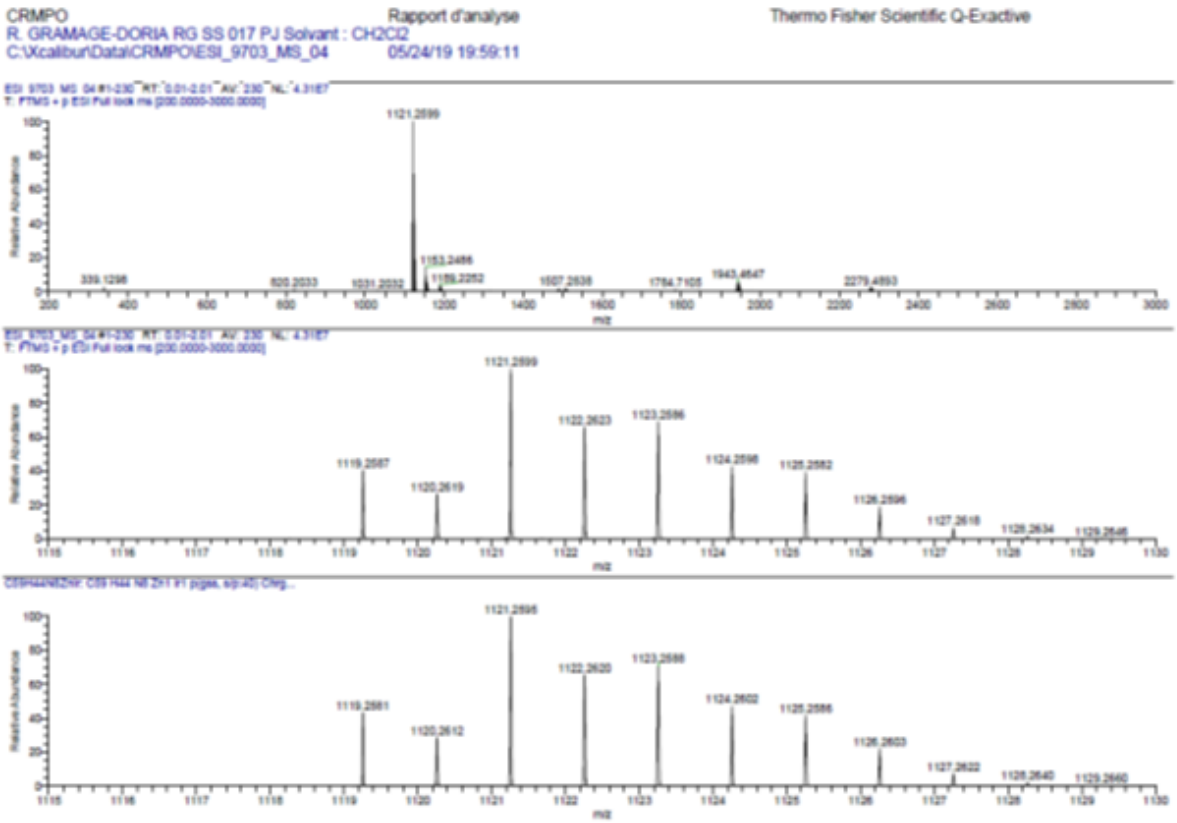

Figure S9. HRMS spectrum of the cationic iridium complex **L1**.

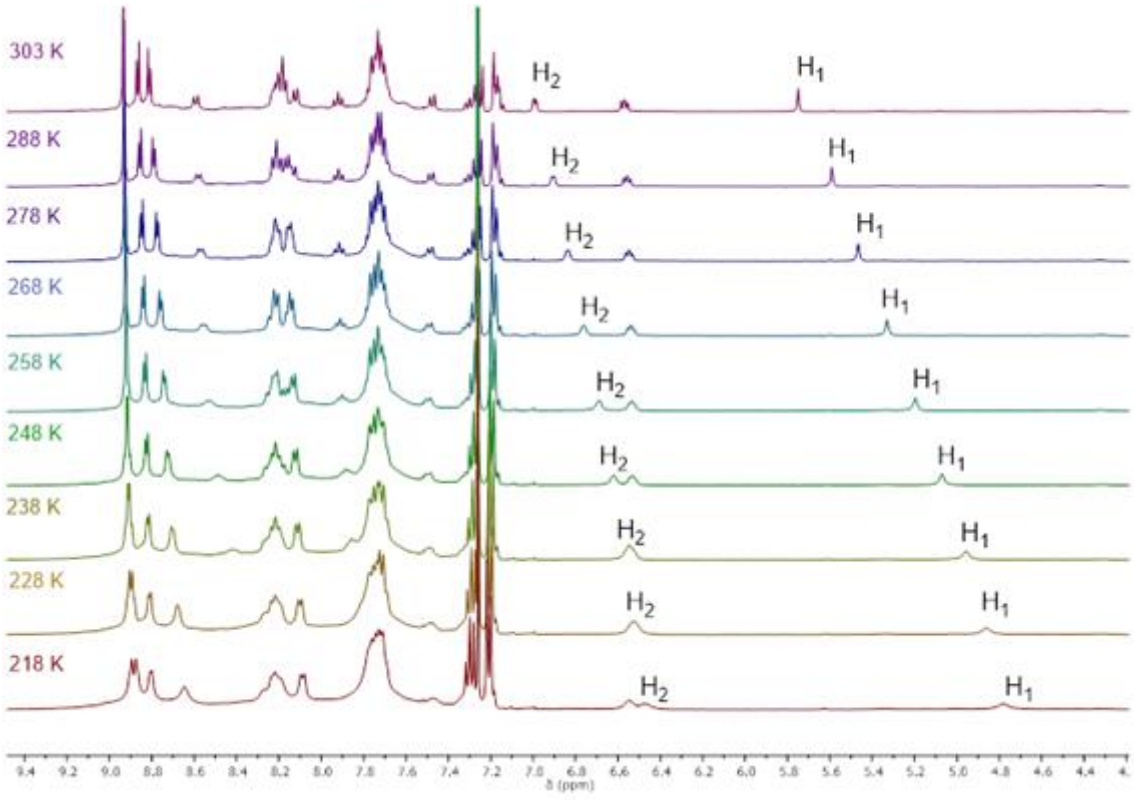

Figure S10. Variable low-temperature ^{1}H NMR ($CDCl_3$) spectra of the cationic iridium complex **L1**.

Competition experiments between L, pyridine and [Ir(COD)(μ-Cl)]$_2$ precursor: Into a dry Schlenk tube equipped with a stirring bar, **L** (4 mg, 4.86 x 10^{-3} mmol) and [Ir(COD)(μ-Cl)]$_2$ (1.7 mg, 2.43 x 10^{-3} mmol) were introduced. After drying the reagents under vacuum for 30 minutes, dry DCM (1 mL) was added and the reaction mixture was stirred for 30 minutes at 60 ^{o}C. Back at room temperature, the solvents were removed under reduced pressure and the product was dried and analyzed by ^{1}H NMR confirming formation of the cationic iridium **L1** complex. Next, aliquots of pyridine in $CDCl_3$ (1 equiv., 2 equiv., and 3 equiv.) were subsequently added to the NMR tube and analyzed by ^{1}H NMR spectroscopy studies (**Figure S11**). In the present of excess pyridine under the highly concentrated conditions required for NMR studies, pyridine preferentially binds to the zinc cation than to the iridium unit, as the proton signals from pyridine remain up-field shifted and they are not participating in any other equilibria than the one involving the zinc cation from the porphyrin **L**. This supports that pyridine binding to the zinc-porphyrin pocket is compatible with the iridium coordinating to the triazolopyridine chelating arm in the ligand **L**. This observation is corroborated in the case of the catalysis since they are performed in a more diluted media than in the experiments performed in the ^{1}H NMR studies. It seems plausible to evoke a top-bottom equilibria in which the coordination of pyridine occurs from a given side of the porphyrin plane at each time. If this likely occurs, this equilibria is fast at the NMR time scale because only one set of pyridine signals are observed even in the presence of an excess of pyridine (**Scheme S2**). No NOE cross-peaks were observed between the COD moiety and the pyridine. This was ascribed to the broadness of the COD proton signals and, also, to the fast equilibria shown in **Scheme S2**.

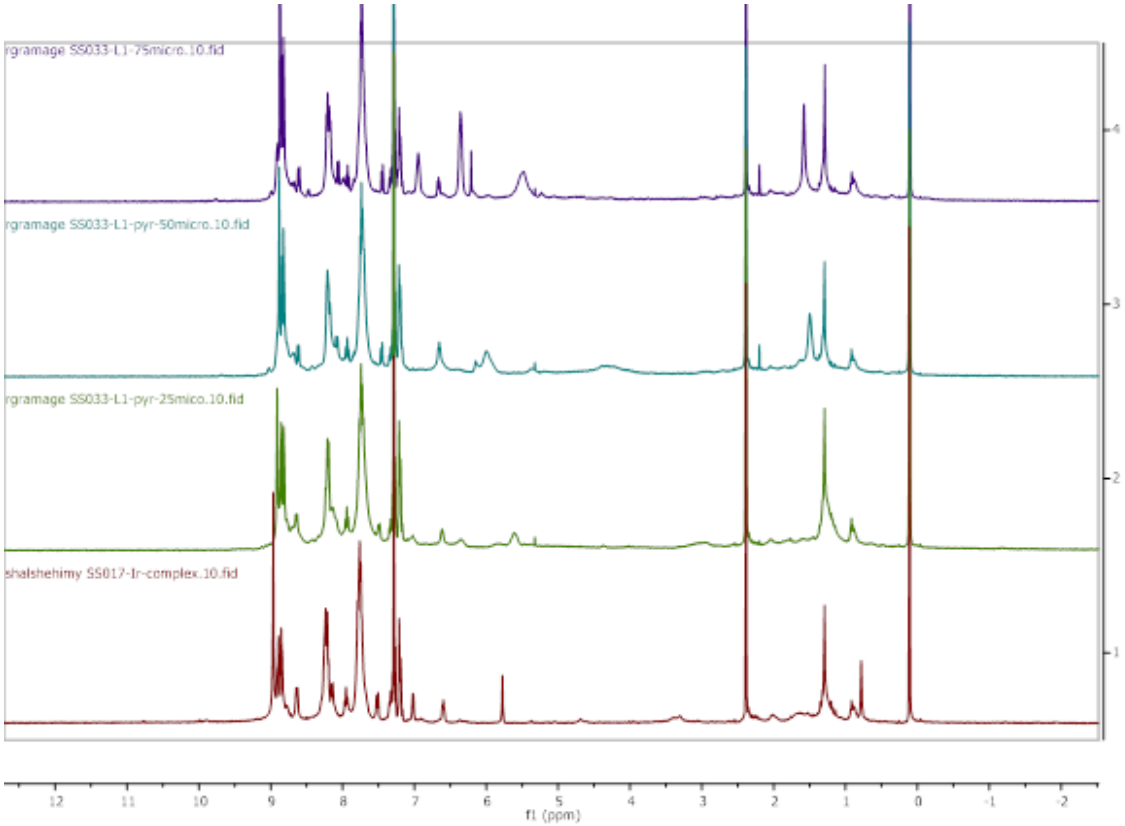

Figure S11. ^{1}H NMR ($CDCl_3$) spectra of the cationic iridium complex **L1** in the presence of increasing amounts of pyridine (0 to 3 equiv., bottom to top).

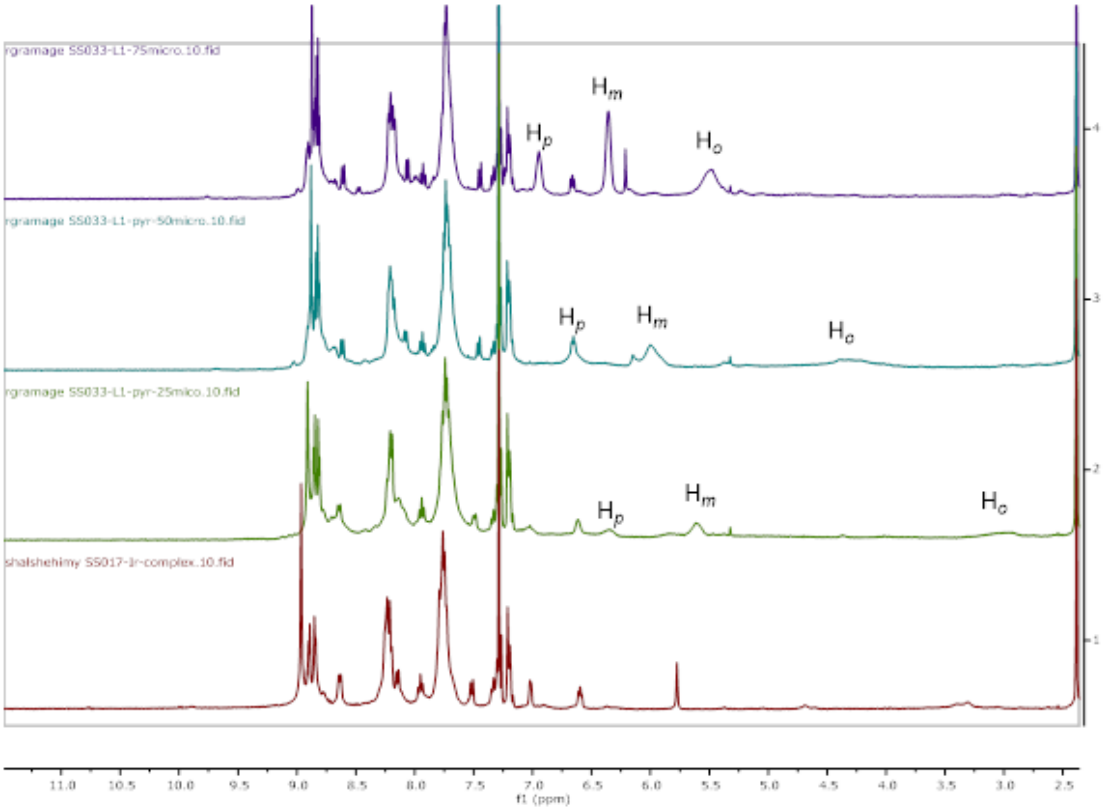

Figure S12. Zoom of the ^{1}H NMR ($CDCl_3$) spectra of the cationic iridium complex **L1** in the presence of increasing amounts of pyridine (0 to 3 equiv., bottom to top).

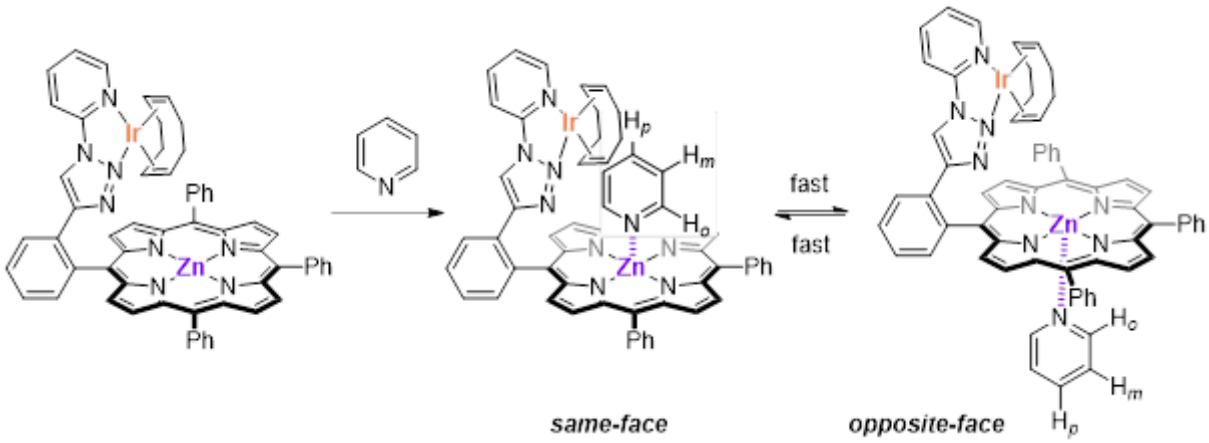

Scheme S2. Binding of pyridine to cationic iridium complex **L1** and postulated, fast top-bottom side equilibria.

NMR binding experiment between L and *N*-methylimidazole (1:1 ratio): L (3.25 mg, 3.95 x 10^{-3} mmol) was placed in an NMR tube and dried under vacuum for few minutes. Then, dry $CDCl_3$ (0.75 mL) was added and the corresponding ^1H NMR spectrum was recorded. A previously dried Schlenk tube was charged with dry *N*-methylimidazole (10.4 µL, 130 mmol) and $CDCl_3$ (1 mL): named stock solution A. Then, 1 equiv of *N*-methylimidazole (30 µL of the stock solution A) were added to the NMR tube containing the ligand **L** and the corresponding ^1H NMR spectrum was recorded showing strong up-field shifts for the *N*-methylimidazole proton signals in accordance to Zn···N coordination (see below).

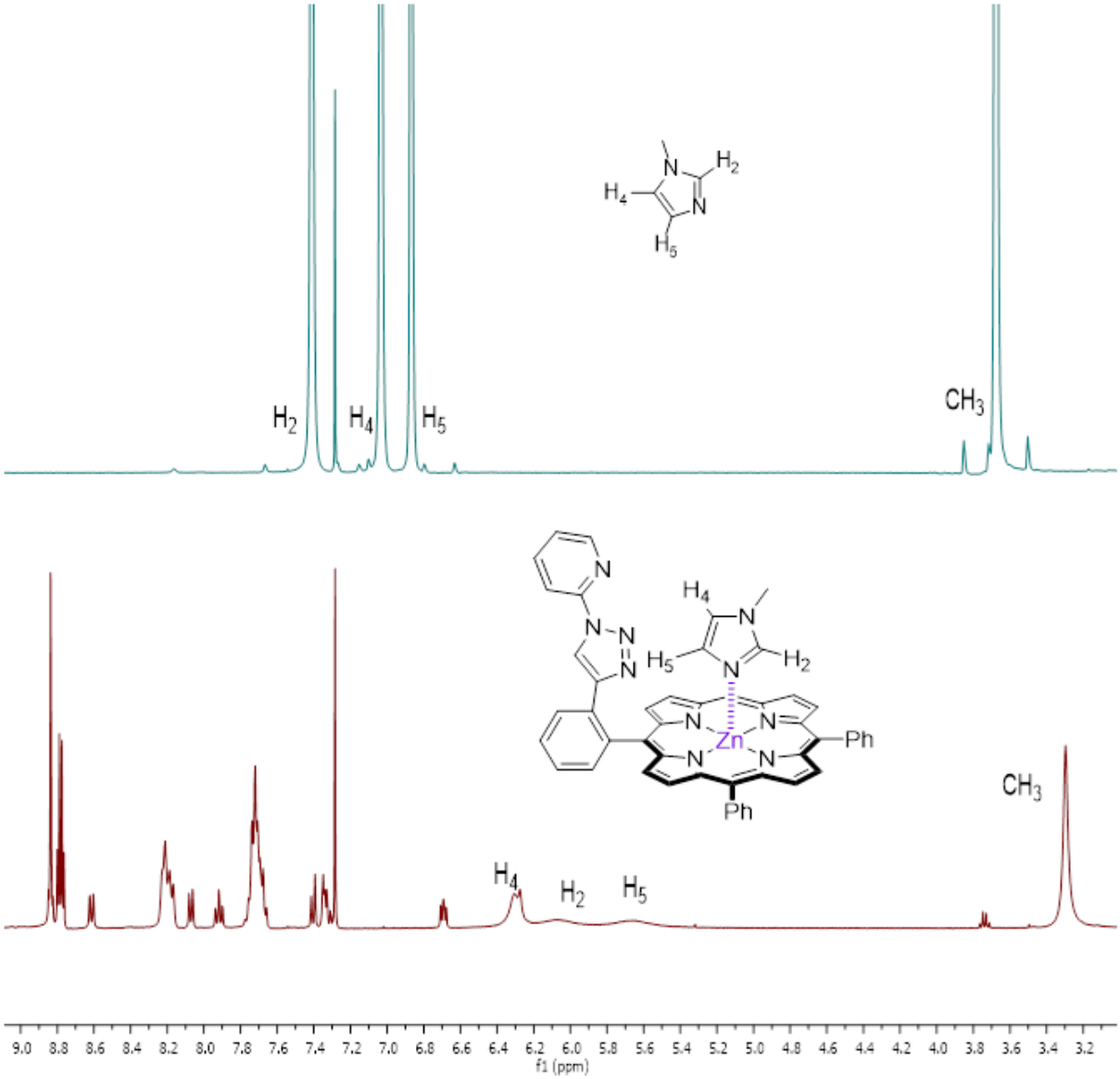

Figure S13. ^{1}H NMR ($CDCl_3$) spectra of *N*-methylimidazole (top) and of the assembly between *N*-methylimidazole and **L** (bottom) showcasing the up-field shifted protons from the substrate, thus indicating Zn···N coordination in solution.

2.4.3. Modelled structures (PM3 calculations-Spartan).

The postulated species responsible for the regio-selectivity observed, namely the Ir(Bpin)$_3$(**L**)(pyridine) complex, was modelled with Spartan at the PM3-level of semi-empirical calculations (**Figure S14**). It shows that *meta*-C-H bond functionalization in the pyridine substrate is feasible. On the other hand, the protons in *ortho* and *para* from the pyridine are two far away from the iridium active site to be activated.

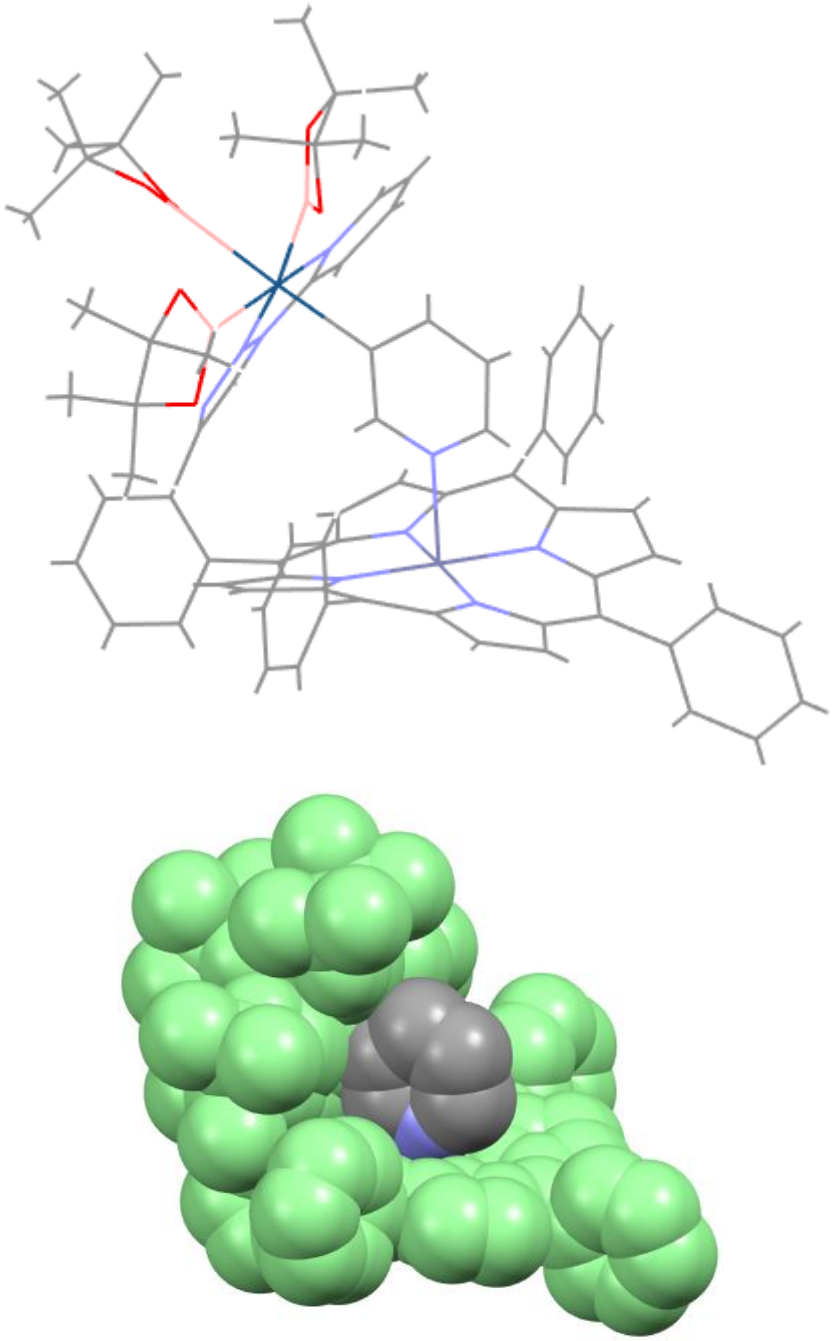

Figure S14. Molecular modelling (semi-empirical calculations) of the targeted supramolecular approach for pyridine functionalization. Top: wireframe representation, gray = carbon, blue = nitrogen, pink = boron, red = oxygen, green = iridium, dark blue = zinc. Bottom: van der Waals representation (hydrogen atoms omitted), green = catalyst, blue/gray = pyridine substrate.

The postulated species responsible for the regio-selectivity observed for five-membered heterocycles have been modelled for imidazole. The namely the Ir(Bpin)$_3$(**L**)(imidazole) complex, was modelled with Spartan at the PM3-level of semi-empirical calculations (**Figure S15**). It shows that *beta*-C-H bond functionalization in the imidazole substrate is feasible. Importantly, the other heterocyclic protons are too far away from the iridium active site to be activated.

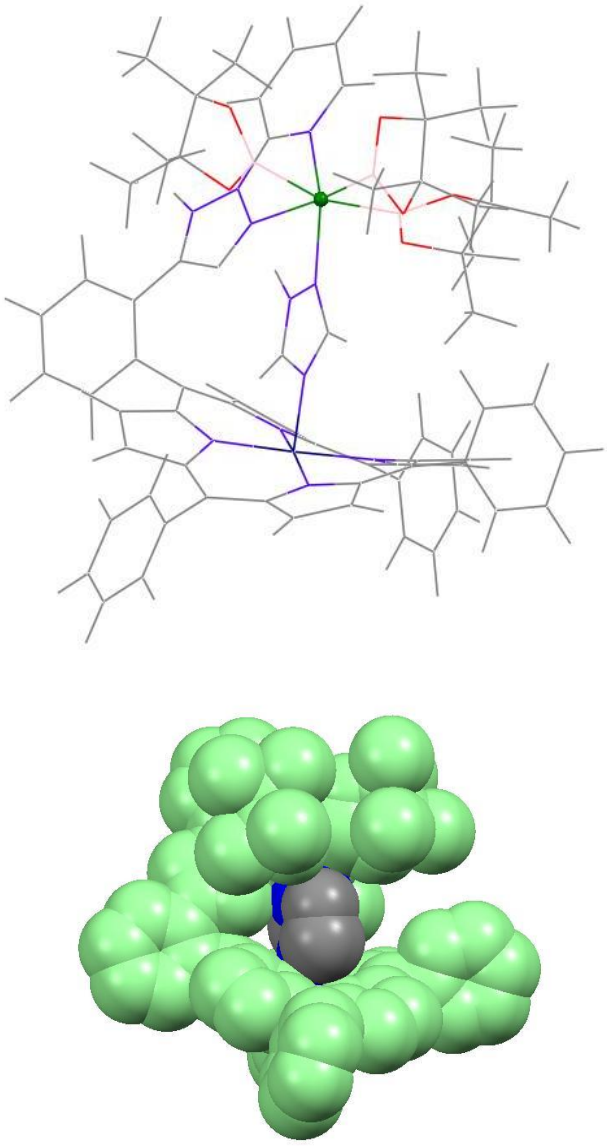

Figure S15. Molecular modelling (semi-empirical calculations) of the targeted supramolecular approach for pyridine functionalization. Top: wireframe representation, gray = carbon, blue = nitrogen, pink = boron, red = oxygen, green = iridium, dark blue = zinc. Bottom: van der Waals representation (hydrogen atoms omitted), green = catalyst, blue/gray = imidazole substrate.

2.4.4. Catalysis experiments.

2.4.4.1. Optimization general procedure: Iridium catalyst precursor, B_2pin_2, ligand **L**, and dodecane (4.05 x 10^{-5} mol, 0.25 equiv.) as the internal standard were introduced in an oven dried Schlenk flask. Solvent (1 mL) was added and the reaction mixture was stirred at room temperature for 30 minutes. Next, pyridine (1.62 x 10^{-4} mol, 1 equiv.) was added and the reaction was stirred at a given temperature during a given time. Back at room temperature, the reactions were analyzed by GC-MS. The optimization study is provided in the **Table S1** below:

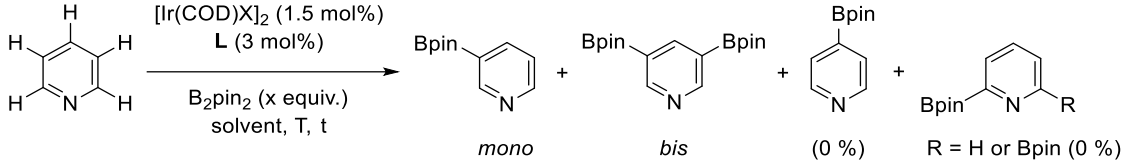

Entry	$[Ir(COD)X]_2$	x	solvent	T (°C)	t (h)	conv. (%)[a]	yield (%)[b]	*mono*:*bis*[c]
1	X = Cl	1	heptane	80	48	<50	26	90:10
2	X = OMe	1	heptane	80	48	<25	16	100:0
3	X = OMe	1	heptane	80	72	<25	18	88:12
4	X = OMe	1	heptane	80	24	<25	10	100:0
5	X = Cl	1	DCE	70	48	<5	<5	-
6	X = Cl	1	THF	50	48	0	0	-
7	X = Cl	1	MTBE	80	48	<50	26	89:11
8	X = Cl	1	2-Me-THF	80	24	<25	12	100:0
9	X = Cl	1	2-Me-THF	80	72	<50	26	100:0
10	X = Cl	1	toluene	r.t.	24	0	0	-
11	X = OMe	1	toluene	r.t.	24	0	0	-
12	X = Cl	1	toluene	40	24	0	0	-
13	X = Cl	1	toluene	60	24	0	0	-
14	X = Cl	1	toluene	70	24	>99	60	90:10
15	X = Cl	1	toluene	80	24	>99	>99	25:75
16	X = Cl	1	*p*-xylene	80	24	>99	>99	40:60
17	X = OMe	1	*p*-xylene	80	24	>75	73	75:25
18	X = Cl	1	*p*-xylene	50	48	0	0	-
19	X = Cl	1.5	*p*-xylene	80	24	>99	84	25:75
20	X = Cl	0.5	*p*-xylene	80	24	<50	35	90:10
21	X = Cl	1	neat	80	24	<5	<5	-
22	X = Cl	1	*p*-xylene	90	24	>99	87	50:50
23	X = Cl	2	*p*-xylene	110	24	>99	63	50:50
24	X = Cl	1.5	toluene	70	24	>99	52	60:40
25	X = Cl	1	*p*-xylene	70	24	<50	45	83:17
26	X = Cl	2	*p*-xylene	100	24	>99	>99	33:67
27[d]	X = Cl	1	*p*-xylene	80	24	>99	75	33:67
28	X = Cl	3	*p*-xylene	80	24	>99	75	33:67
29[d]	X = Cl	3	*p*-xylene	80	48	>99	94	13:87

[a]conversion of pyridine.[b]yield of products. [c]ratio of mono/bis-borylated products.[d]Ir precursor (3 mol%) and **L** (6 mol%).

2.4.4.2. Control experiments.

Control experiment without any iridium precursor: B_2pin_2 (41.1 mg, 1.62 x 10^{-4} mol, 1 equiv.) Ligand **L** (4.1 mg, 4.9 x 10^{-6} mol, 0.03 equiv.) and dodecane (6.9 mg, 9.2 µL, 4.05 x 10^{-5} mol, 0.25 equiv.) were introduced in an oven dried Schlenk flask. *p*-xylene (1 mL) was added and the reaction mixture was stirred at room temperature for 30 minutes. Then, pyridine (13 mg, 13 µL, 1.62 x 10^{-4} mol, 1 equiv.) was added. The reaction mixture was stirred during 24 h at 80 °C. The reaction was cooled down to room temperature and analyzed by GC-MS analysis showing no conversion of starting materials nor product formation.

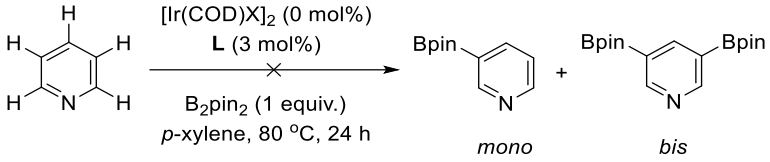

Control experiment without L: [Ir(COD)(Cl)]$_2$ (1.7 mg, 2.4 x 10^{-6}, 0.015 equiv.), B_2pin_2 (41.1 mg, 1.62 x 10^{-4} mol, 1 equiv.) and dodecane (6.9 mg, 9.2 µL, 4.05 x 10^{-5} mol, 0.25 equiv.) were introduced in an oven dried Schlenk flask. *p*-xylene (1 mL) was added and the reaction mixture was stirred at room temperature for 30 minutes. Then pyridine (13 mg, 13 µL, 1.62 x 10^{-4} mol, 1 equiv.) was added. The reaction mixture was stirred during 24 h at 80°C. The reaction was cooled down to room temperature and analyzed by GC-MS analysis showing no conversion of starting materials nor product formation.

Control experiment using ligand L* + ZnTPP: [Ir(COD)(Cl)]$_2$ (1.7 mg, 2.4 x 10^{-6} mol, 0.015 eq.), B_2pin_2 (41.1 mg, 1.62 x 10^{-4} mol, 1 equiv.), ligand **L*** (1.1 mg, 4.9 x 10^{-6} mol, 0.03 equiv.), ZnTPP (3.3 mg, 4.9 x 10^{-6} mol, 0.03 equiv.), and dodecane (6.9 mg, 9.2 µL, 4.05 x 10^{-5} mol, 0.25 equiv.) were introduced in an oven dried Schlenk flask. *p*-xylene (1 mL) was added and the reaction mixture was stirred at room temperature for 30 minutes. Then pyridine (13 mg, 13 µL, 1.62 x 10^{-4} mol, 1 equiv.) was added. The reaction mixture was stirred during 24 h at 80°C. The reaction was cooled down to room temperature and analyzed by GC-MS analysis showing no conversion of starting materials nor product formation.

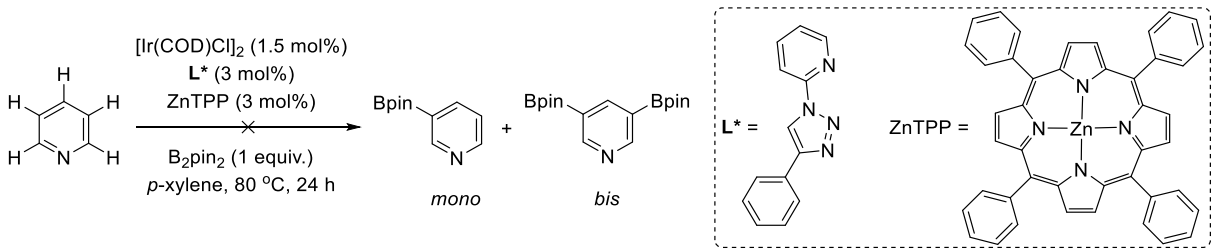

Control experiment for N-methyl imidazole borylation using ligand L* + ZnTPP: [Ir(COD)(Cl)]$_2$ (1.7 mg, 2.4 x 10^{-6} mol, 0.015 eq.), B_2pin_2 (41.1 mg, 1.62 x 10^{-4} mol, 1 equiv.), ligand **L*** (1.1 mg, 4.9 x 10^{-6} mol, 0.03 equiv.), ZnTPP (3.3 mg, 4.9 x 10^{-6} mol, 0.03 equiv.), and dodecane (6.9 mg, 9.2 µL, 4.05 x 10^{-5} mol, 0.25 equiv.) were introduced in an oven dried Schlenk flask. *p*-xylene (1 mL) was added and the reaction

mixture was stirred at room temperature for 30 minutes. Then N-methylimidazole (13,5 mg, 13 µL, 1.62 x 10^{-4} mol, 1 equiv.) was added. The reaction mixture was stirred during 24 h at 80°C. The reaction was cooled down to room temperature and analyzed by GC-MS analysis showing no conversion of starting materials nor product formation

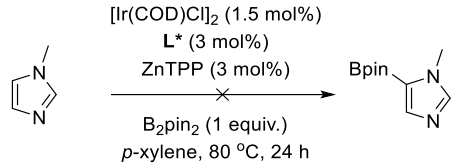

Using ZnTPP as a hindered lewis acid:

Standard reaction using [Ir(dtbpy)] complex as the catalyst: $[Ir(COD)(OMe)]_2$ (1.6 mg, 2.4 x 10^{-6} mol, 0.015 eq.), B_2pin_2 (41.1 mg, 1.62 x 10^{-4} mol, 1 equiv.), dtbpy (1.3 mg, 4.9 x 10^{-6} mol, 0.03 equiv.), and dodecane (6.9 mg, 9.2 µL, 4.05 x 10^{-5} mol, 0.25 equiv.) were introduced in an oven dried Schlenk flask. *p*-xylene (1 mL) was added and the reaction mixture was stirred at room temperature for 30 minutes. Then pyridine (13 mg, 13 µL, 1.62 x 10^{-4} mol, 1 equiv.) was added. The reaction mixture was stirred during 24 h at 80°C. The reaction was cooled down to room temperature and analyzed by GC-MS analysis showing a quantitative conversion and a mixture of product *meta* (27% mono borylated and 9% bis borylated) and *para* (26%) substituted.

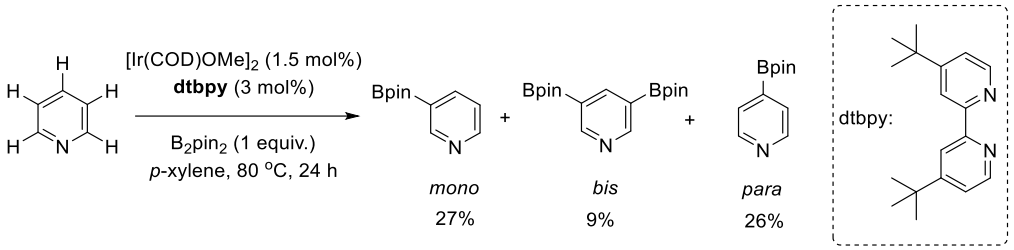

Borylation using ZnTPP as an hindered lewis acid: $[Ir(COD)(OMe)]_2$ (1.6 mg, 2.4 x 10^{-6} mol, 0.015 eq.), B_2pin_2 (41.1 mg, 1.62 x 10^{-4} mol, 1 equiv.), dtbpy (1.3 mg, 4.9 x 10^{-6} mol, 0.03 equiv.), ZnTPP (55.5 mg, 1.62 x 10^{-4} mol, 1 equiv.), and dodecane (6.9 mg, 9.2 µL, 4.05 x 10^{-5} mol, 0.25 equiv.) were introduced in an oven dried Schlenk flask. *p*-xylene (1 mL) was added and the reaction mixture was stirred at room temperature for 30 minutes. Then pyridine (13 mg, 13 µL, 1.62 x 10^{-4} mol, 1 equiv.) was added. The reaction mixture was stirred during 24 h at 80°C. The reaction was cooled down to room temperature and analyzed by GC-MS analysis showing a quantitative conversion and a mixture of product *meta* (30% mono borylated and 10% bis borylated) and *para* (25%) substitued.

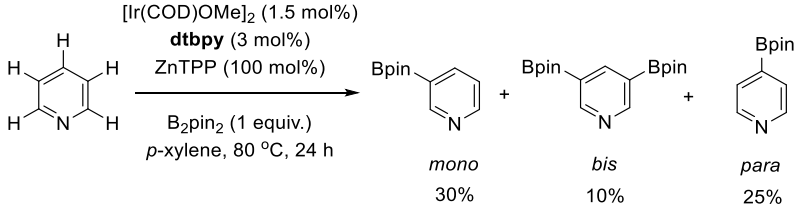

These results clearly show that ZnTPP is not bulky enough to induce a regioselective *para*-borylation of pyridine using our reaction conditions.

Control experiment using pyridinium chloride instead of pyridine as the substrate: $[Ir(COD)(Cl)]_2$ (1.7 mg, 2.4 x 10^{-6} mol, 0.015 eq.), B_2pin_2 (41.1 mg, 1.62 x 10^{-4} mol, 1 equiv.), ligand **L** (4.1 mg, 4.9 x 10^{-6} mol, 0.03 equiv.), and dodecane (6.9 mg, 9.2 µL, 4.05 x 10^{-5} mol, 0.25 equiv.) were introduced in an oven dried Schlenk flask. *p*-xylene (1 mL) was added and the reaction mixture was stirred at room temperature for 30 minutes. Then pyridinium chloride (19 mg, 1.62 x 10^{-4} mol, 1 equiv.) was added and the reaction mixture was stirred during 24 h at 80°C. The reaction was cooled down to room temperature and analyzed by GC-MS analysis showing no conversion of starting materials nor product formation.

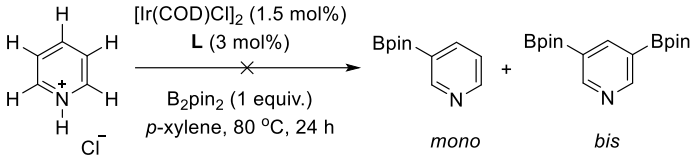

Control experiment using pyridinium tetrafluoroborate instead of pyridine as the substrate: $[Ir(COD)(Cl)]_2$ (1.7 mg, 2.4 x 10^{-6} mol, 0.015 eq.), B_2pin_2 (41.1 mg, 1.62 x 10^{-4} mol, 1 eq.), ligand **L** (4.1 mg, 4.9 x 10^{-6} mol, 0.03 eq.), pyridinium tetrafluoroborate (27 mg, 1,62 x 10^{-4} mol, 1eq.) and dodecane (6.9 mg, 9.2 µL, 4.05 x 10^{-5} mol, 0.25 eq.) were introduced in an oven dried Schlenk flask. *p*-xylene (1 mL) was added and the reaction mixture was stirred at room temperature for 30 minutes and at 80°C for 24 hours. The reaction was cooled down to room temperature and analyzed by GC-MS analysis showing no conversion of starting materials nor product formation.

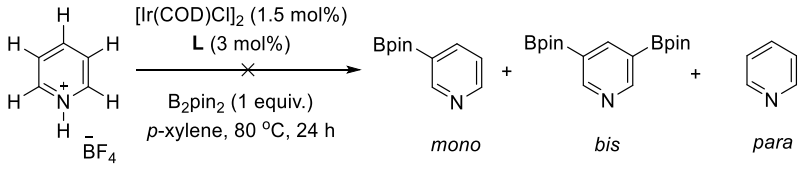

Control experiment using *N*-methylpyridinium iodide instead of pyridine as the substrate: $[Ir(COD)(Cl)]_2$ (1.7 mg, 2.4 x 10^{-6} mol, 0.015 eq.), B_2pin_2 (41.1 mg, 1.62 x 10^{-4} mol, 1 equiv.), ligand **L** (4.1 mg, 4.9 x 10^{-6} mol, 0.03 equiv.), and dodecane (6.9 mg, 9.2 µL, 4.05 x 10^{-5} mol, 0.25 equiv.) were introduced in an oven dried Schlenk flask. *p*-xylene (1 mL) was added and the reaction mixture was stirred at room temperature for 30 minutes. Then *N*-methylpyridinium iodide (36 mg, 1.62 x 10^{-4} mol, 1 equiv.) was added and the reaction mixture was stirred during 24 h at 80°C. The reaction was cooled down to room temperature and analyzed by GC-MS analysis showing no conversion of starting materials nor product formation.

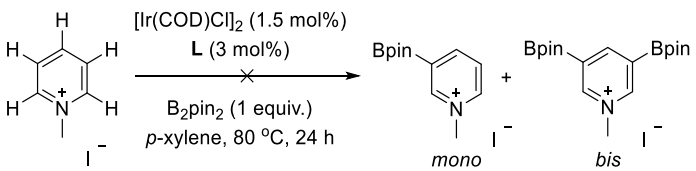

Control experiment using *N*-methylpyridinium hexafluorophosphate instead of pyridine as the substrate: $[Ir(COD)(Cl)]_2$ (1.7 mg, 2.4 x 10^{-6} mol, 0.015 eq.), B_2pin_2 (41.1 mg, 1.62 x 10^{-4} mol, 1 equiv.), ligand **L** (4.1 mg, 4.9 x 10^{-6} mol, 0.03 equiv.), and dodecane (6.9 mg, 9.2 µL, 4.05 x 10^{-5} mol, 0.25 equiv.)

were introduced in an oven dried Schlenk flask. *p*-xylene (1 mL) was added and the reaction mixture was stirred at room temperature for 30 minutes. Then *N*-methylpyridinium hexafluorophosphate (39 mg, 1.62 x 10^{-4} mol, 1 equiv.) was added and the reaction mixture was stirred during 24 h at 80°C. The reaction was cooled down to room temperature and analyzed by GC-MS analysis showing no conversion of starting materials nor product formation.

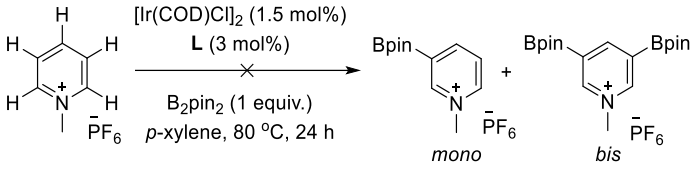

Control experiment using 2-methylpyridine as the substrate: $[Ir(COD)(Cl)]_2$ (1.7 mg, 2.4 x 10^{-6} mol, 0.015 eq.), B_2pin_2 (41.1 mg, 1.62 x 10^{-4} mol, 1 equiv.), ligand **L** (4.1 mg, 4.9 x 10^{-6} mol, 0.03 equiv.), and dodecane (6.9 mg, 9.2 µL, 4.05 x 10^{-5} mol, 0.25 equiv.) were introduced in an oven dried Schlenk flask. *p*-xylene (1 mL) was added and the reaction mixture was stirred at room temperature for 30 minutes. Then 2-Me-pyridine (15 mg, 16 µL, 1.62 x 10^{-4} mol, 1 equiv.) was added and the reaction mixture was stirred during 24 h at 80°C. The reaction was cooled down to room temperature and analyzed by GC-MS analysis showing no conversion of starting materials nor product formation.

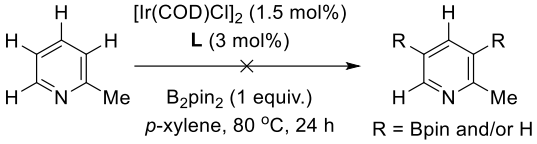

Competition between ligand L and zinc(II)-salphen using pyridine type substrate: $[Ir(COD)(Cl)]_2$ (1.7 mg, 2.4 x 10^{-6} mol, 0.015 eq.), B_2pin_2 (41.1 mg, 1.62 x 10^{-4} mol, 1 equiv.), ligand **L** (4.1 mg, 4.9 x 10^{-6} mol, 0.03 equiv.) and Zn(II)-salphen (2.9 mg, 4.9 x 10^{-6} mol, 0.03 equiv.) were introduced in an oven dried Schlenk flask. *p*-xylene (1 mL) was added and the reaction mixture was stirred at room temperature for 30 minutes. Then 3-methylpyridine (15 mg, 16 µL, 1.62 x 10^{-4} mol, 1 equiv.) was added and the reaction mixture was stirred during 24 h at 80°C. The reaction was cooled down to room temperature and analyzed by GC-MS analysis showing 53% conversion and an estimated GC-yield of 47%. *This indicates that the zinc(II)-salphen competes with the ligand to bind to the substrate, thus leading to a decrease in the catalytic activity.*

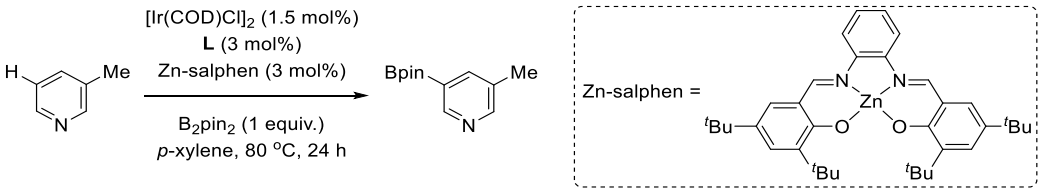

$[Ir(COD)(Cl)]_2$ (1.7 mg, 2.4 x 10^{-6} mol, 0.015 eq.), B_2pin_2 (41.1 mg, 1.62 x 10^{-4} mol, 1 equiv.), ligand **L** (4.1 mg, 4.9 x 10^{-6} mol, 0.03 equiv.) and Zn(II)-salphen (97.9 mg, 1.62 x 10^{-4} mol, 1 equiv.) were introduced in an oven dried Schlenk flask. *p*-xylene (1 mL) was added and the reaction mixture was stirred at room temperature for 30 minutes. Then pyridine (13 mg, 13 µL, 1.62 x 10^{-4} mol, 1 equiv.) was added and the reaction mixture was stirred during 24 h at 80°C. The reaction was cooled down to room temperature and analyzed by GC-MS analysis showing conversion <5% and traces amount of product. *This indicates*

that the zinc(II)-salphen likely binds quantitatively to the substrate in a equimolar ratio thus leading to almost no catalytic activity.

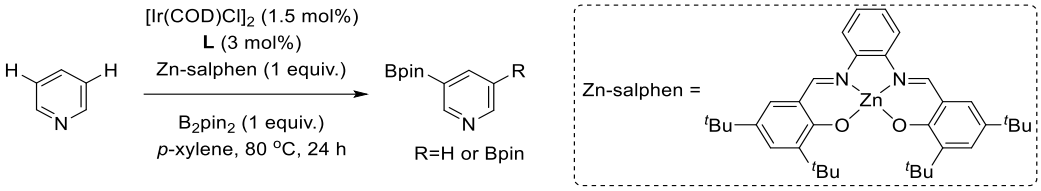

Competition between different pyridine substrate: $[Ir(COD)(Cl)]_2$ (1.7 mg, 2.4 x 10^{-6} mol, 0.015 eq.), B_2pin_2 (41.1 mg, 1.62 x 10^{-4} mol, 1 equiv.), ligand **L** (4.1 mg, 4.9 x 10^{-6} mol, 0.03 equiv.), and dodecane (6.9 mg, 9.2 µL, 4.05 x 10^{-5} mol, 0.25 equiv.) were introduced in an oven dried Schlenk flask. *p*-xylene (1 mL) was added and the reaction mixture was stirred at room temperature for 30 minutes. Then 2-Me-pyridine (5 mg, 5.3 µL, 0.53 x 10^{-5} mol, 1 equiv.), 3-Me-pyridine (5 mg, 5.3 µL, 0.53 x 10^{-5} mol, 1 equiv.) and 4-Me-pyridine (5 mg, 5.3 µL, 0.53 x 10^{-5} mol, 1 equiv.) were added and the reaction mixture was stirred during 24 h at 80°C. The reaction was cooled down to room temperature and analyzed by GC-MS analysis showing full conversion of 3-Me-pyridine as well as an estimated yield of 30% of borylated product and no conversion of 2-Me-pyridine or 4-Me-pyridine.

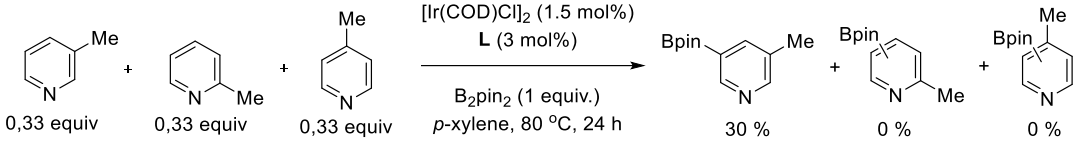

2.4.4.3. Characterization of the products formed in the reaction optimization.

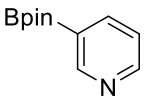

3-(4,4,5,5-Tetramethyl-1,3,2-dioxaborolan-2-yl)-pyridine (1): Following the optimized conditions (Table 1, entry 14), full conversion and 54% yield was estimated by GC-MS analysis. Purification by Kugelrorh distillation afforded the analytically pure product (16 mg, 50% yield). ^{1}H NMR (400 MHz, $CDCl_3$): δ = 8.95 (s, 1H), 8.67 (d, *J* = 2 Hz, 1H), 8.07 (dt, *J* = 7.6, 2 Hz, 1H), 7.26-7.32 (m, 1H), 1.38 (s, 12H) ppm. $^{13}C\{^1H\}$ NMR (101 MHz, $CDCl_3$): δ = 155.44, 151.94, 142.22, 123.06, 84.23, 24.86 ppm. $^{11}B\{^1H\}$ NMR (128 MHz, $CDCl_3$): δ = 30.86 (s) ppm. The spectral data match those found in literature.[49]

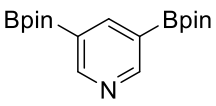

3-5-bis(4,4,5,5-Tetramethyl-1,3,2-dioxaborolan-2-yl)-pyridine (2): Following the optimized conditions (Table 1, entry 29), full conversion and 81% yield was estimated by GC-MS analysis. Purification by Kugelrorh distillation afforded the analytically pure product (37mg, 70% yield). ^{1}H NMR (400 MHz, $CDCl_3$): δ = 9.00 (d, *J* = 1.9 Hz, 1H), 8.48 (t, *J* = 1.9 Hz, 1H), 1.35 (s, 12H) ppm. $^{13}C\{^1H\}$ NMR (101 MHz, Chloroform-*d*) δ = 157.50, 148.78, 84.18, 24.85.ppm. $^{11}B\{^1H\}$ NMR (128 MHz, $CDCl_3$): δ = 31.15 (s) ppm. The spectral data match those found in literature.[50]

2.4.4.4. Kinetic study following reaction progress kinetic analysis.[51]

General procedure: $[Ir(COD)(Cl)]_2$, ligand **L**, B_2pin_2 , and dodecane (0.25 eq.) were introduced in an oven dried Schlenk flask. *p*-xylene was added and the reaction mixture was stirred at room temperature for 30 minutes. Then 3-methylpyridine was added and the mixture was stirred at 80°C. Small aliquots were taken from the flask under argon flow every hour using a dry needle. Conversion and yield were estimated by GC-MS using dodecane as the internal standard. Fitting of the experimental data was done using sigmoidal Boltzmann function.

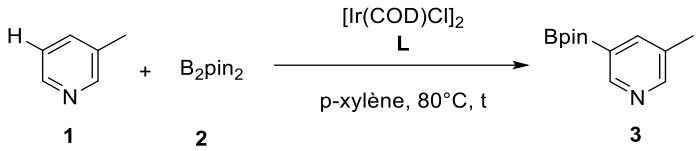

Reaction at standard conditions.

Following the general procedure, $[Ir(COD)(Cl)]_2$ (16.5 mg, 2.43 x 10^{-5} mol, 0.015 eq.), ligand **L** (41 mg, 4.86 x 10^{-5} mol, 0.03 eq.), B_2pin_2 (411 mg, 1.62 x 10^{-3} mol, 1 eq.) and 3-methylpyridine (160 µL, 1.62 x 10^{-3} mol, 1 eq.) were dissolved in *p*-xylene (10 mL). The reaction mixture was stirred at 80°C for 12 hours. Formation of *meta*-borylated product product [3] versus time (h) is plotted below (fitted values are shown in bleu, and experimental values are shown in orange dots):

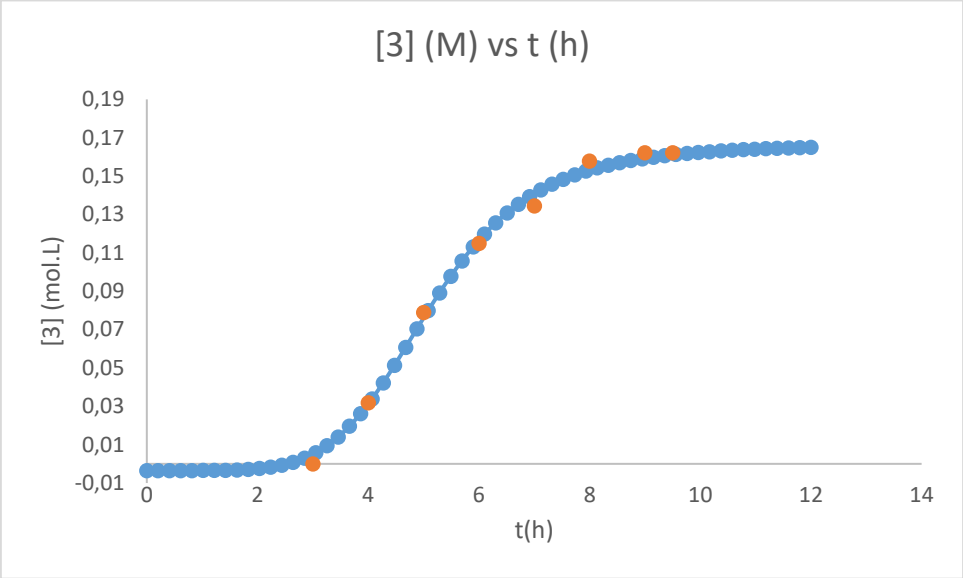

Reaction at different catalyst loading: determination of the catalyst kinetic order.

Following the general procedure, $[Ir(COD)(Cl)]_2$ (25 mg, 3.65 x 10^{-5} mol, 0.0225 eq.), ligand **L** (61.5 mg, 7.29 x 10^{-5} mol, 0.045 eq.), B_2pin_2 (411 mg, 1.62 x 10^{-3} mol, 1 eq.) and 3-methylpyridine (160 µL, 1.62 x 10^{-3} mol, 1 eq.) were dissolved in *p*-xylene (10 mL). The reaction mixture was stirred at 80°C for 7 hours. Formation of *meta*-borylated product product [3] versus time (h) is plotted below (fitted values are shown in bleu, and experimental values are shown in orange dots):

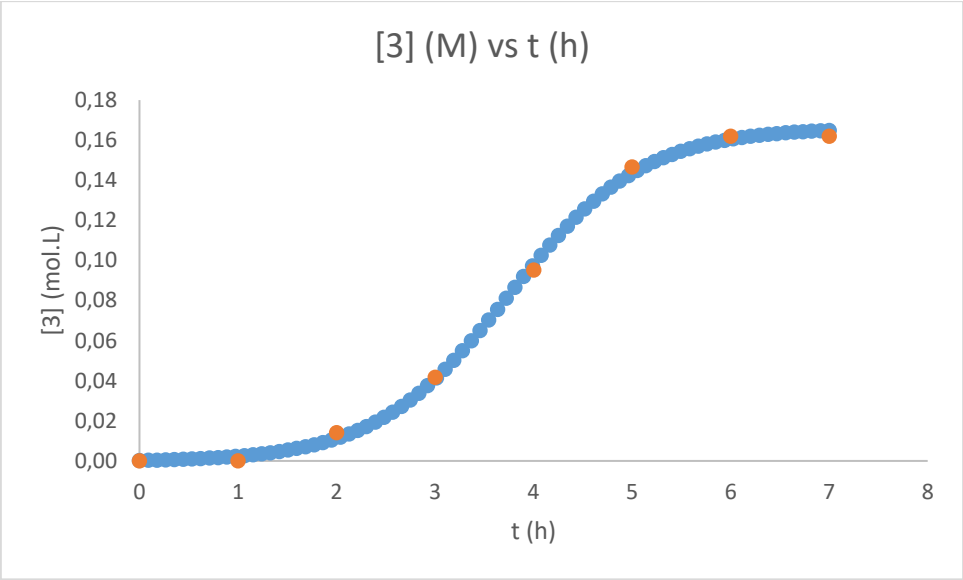

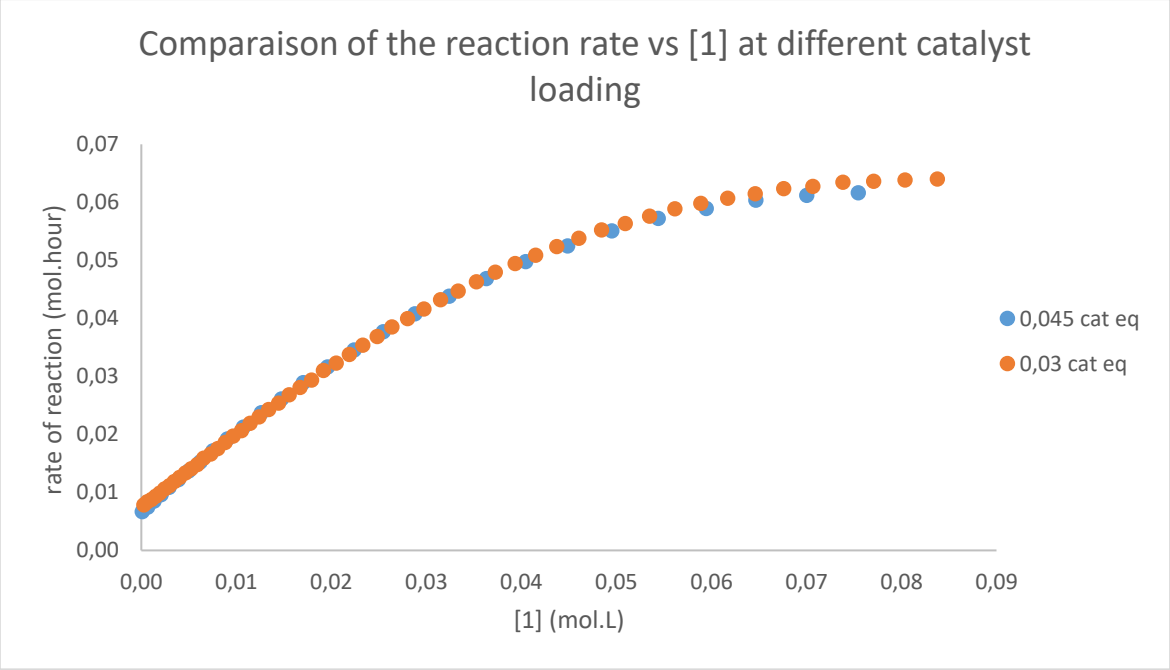

If the reaction is first order in catalyst, then the rate is directly related to the catalyst concentration following this formula:

Rate = k x [catalyst]

Then: Rate(reaction1) = Rate(reaction2) x (catalyst excess]

Overlapping of the two curves upon multiplication of the brown curve reaction rate by the catalyst excess (1.5) indicate a first order in catalyst.[6]

Reaction at same excess: determination of the substrates kinetic order.

A/1 equivalent of (1) and 0.6 equivalent of (2).

Following the general procedure, $[Ir(COD)(Cl)]_2$ (16.5 mg, 2.43 x 10^{-5} mol, 0.015 eq.), ligand **L** (41 mg, 4.86 x 10^{-5} mol, 0.03 eq.), B_2pin_2 (247 mg, 0.972 x 10^{-4} mol, 0.6 eq.) and 3-methylpyridine (160 µL, 1.62 x 10^{-3} mol, 1 eq.) were dissolved in *p*-xylene (10 mL). The reaction mixture was stirred at 80°C and followed on time. Formation of *meta*-borylated product product [3] versus time (h) is plotted below (fitted values are shown in bleu, and experimental values are shown in orange dots):

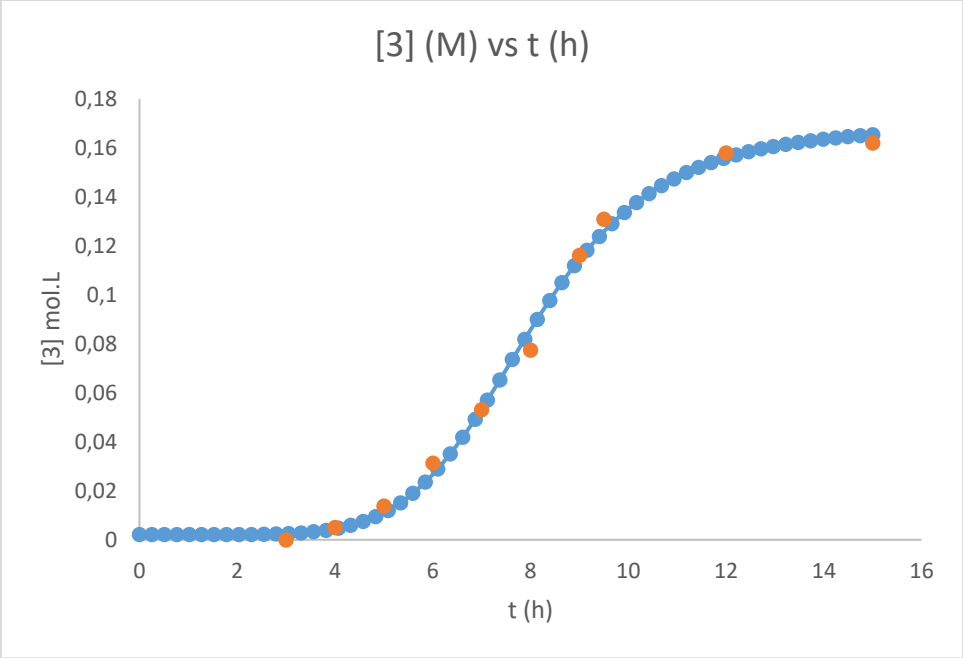

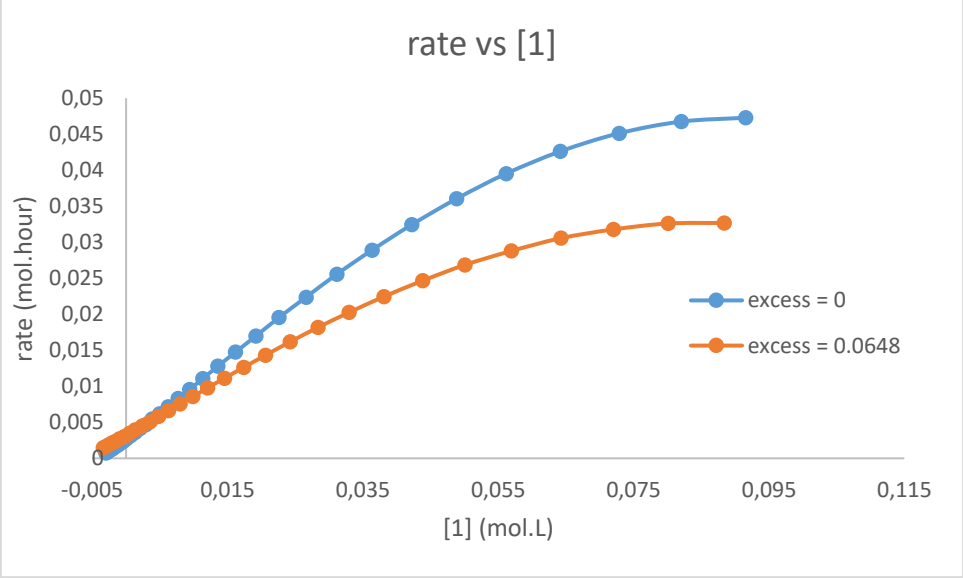

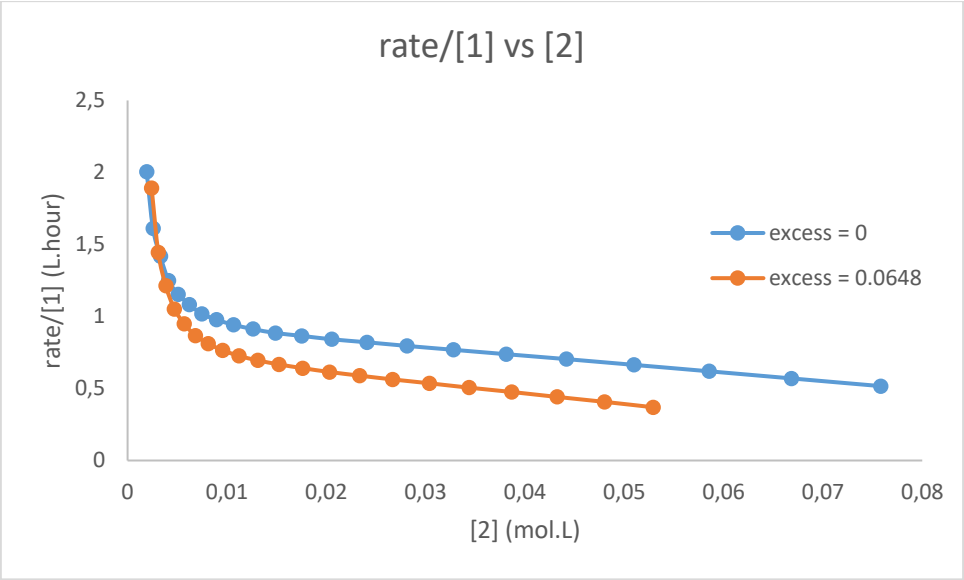

Following Blackmond's rules,[45] graphical data above suggests a pseudo-zero-order in B_2pin_2 as the curves are almost overlapping in the former case and very non-overlapping was observed for a pseudo-first order.

B/0.8 equivalent of (1) and 0.4 equivalent of (2).

Following the general procedure, $[Ir(COD)(Cl)]_2$ (16.5 mg, 2.43 x 10^{-5} mol, 0.015 eq.), ligand **L** (41 mg, 4.86 x 10^{-5} mol, 0.03 eq.), B_2pin_2 (164 mg, 0.648 x 10^{-4} mol, 0.4 eq.) and 3-methylpyridine (128 µL, 1.3 x 10^{-3} mol, 0.8 eq.) were dissolved in *p*-xylene (10 mL). The reaction mixture was stirred at 80°C for 24 hours. Formation of *meta*-borylated product product [3] versus time (h) is plotted below (fitted values are shown in bleu, and experimental values are shown in orange dots):

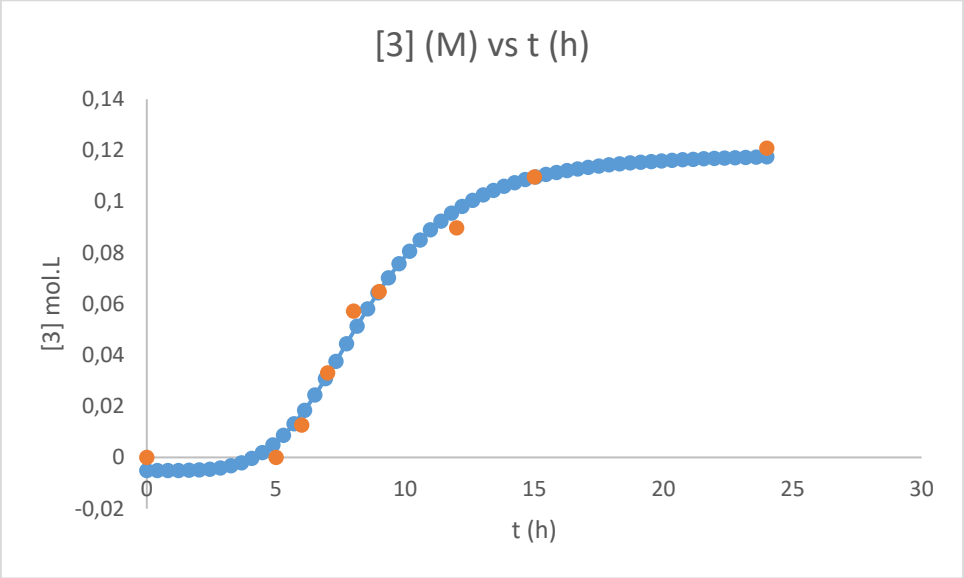

Note: a side-product of B_2pin_2 reaction with 3-mepyridine is also a borylating agent as almost 2 equivalents of product relative to B_2pin_2 are generated. However, the kinetic data suggest that this side-product is less active than the starting reagent B_2pin_2 as the reaction appears to be slower upon total consumption of B_2pin_2.

Reaction with added product: determination of product inhibition or catalyst deactivation.

Following the general procedure, $[Ir(COD)(Cl)]_2$ (16.5 mg, 2.43 x 10^{-5} mol, 0.015 eq.), ligand **L** (41 mg, 4.86 x 10^{-5} mol, 0.03 eq.), B_2pin_2 (205.5 mg, 0.81 x 10^{-3} mol, 0.5 eq.), 3-methylpyridine (80 µL, 0.81 x 10^{-3} mol, 0.5 eq.), and 3-(4,4,5,5-Tetramethyl-1,3,2-dioxaborolan-2-yl)-5-methylpyridine (175 mg, 0.81 x 10^{-3} mol, 0.5 eq.) were dissolved in *p*-xylene (10 mL). The reaction mixture was stirred at 80°C for 6 hours. Formation of newly *meta*-borylated product product [3] versus time (h) is plotted below (fitted values are shown in bleu, and experimental values are shown in orange dots):

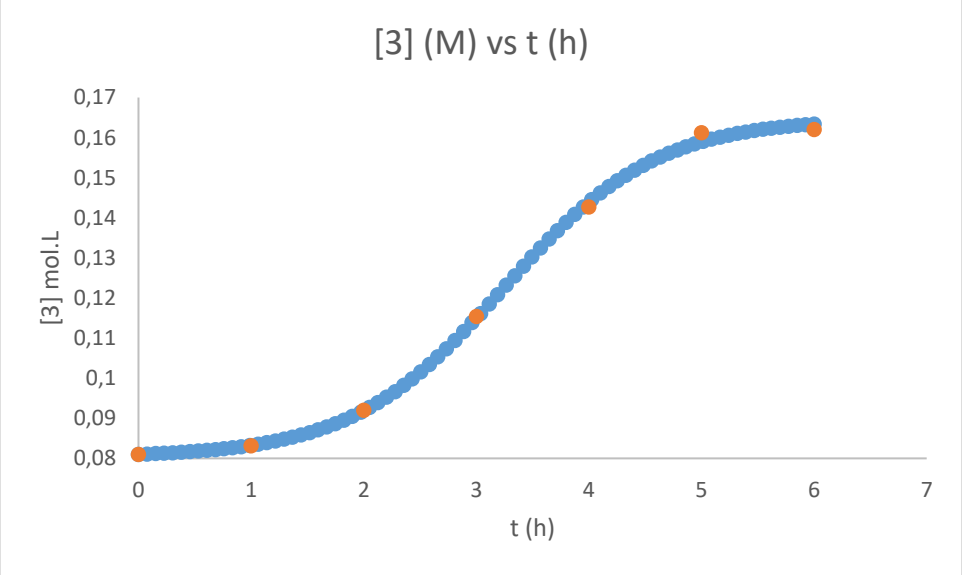

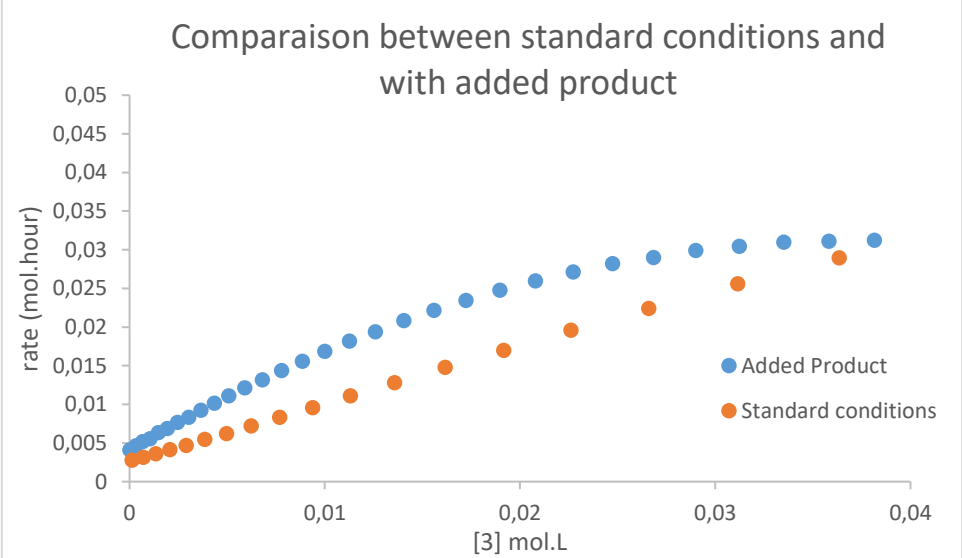

Because there is no overlapping, product inhibition is very unlikely in the present case. Indeed, the reaction with added product (blue dots) is faster than the reaction under standard conditions (orange dots) which indicate that the catalyst is deactivated during the course of the reaction. We assume catalyst deactivation due to (multiple) borylation on the ligand or other type of chemical degradation/modification.

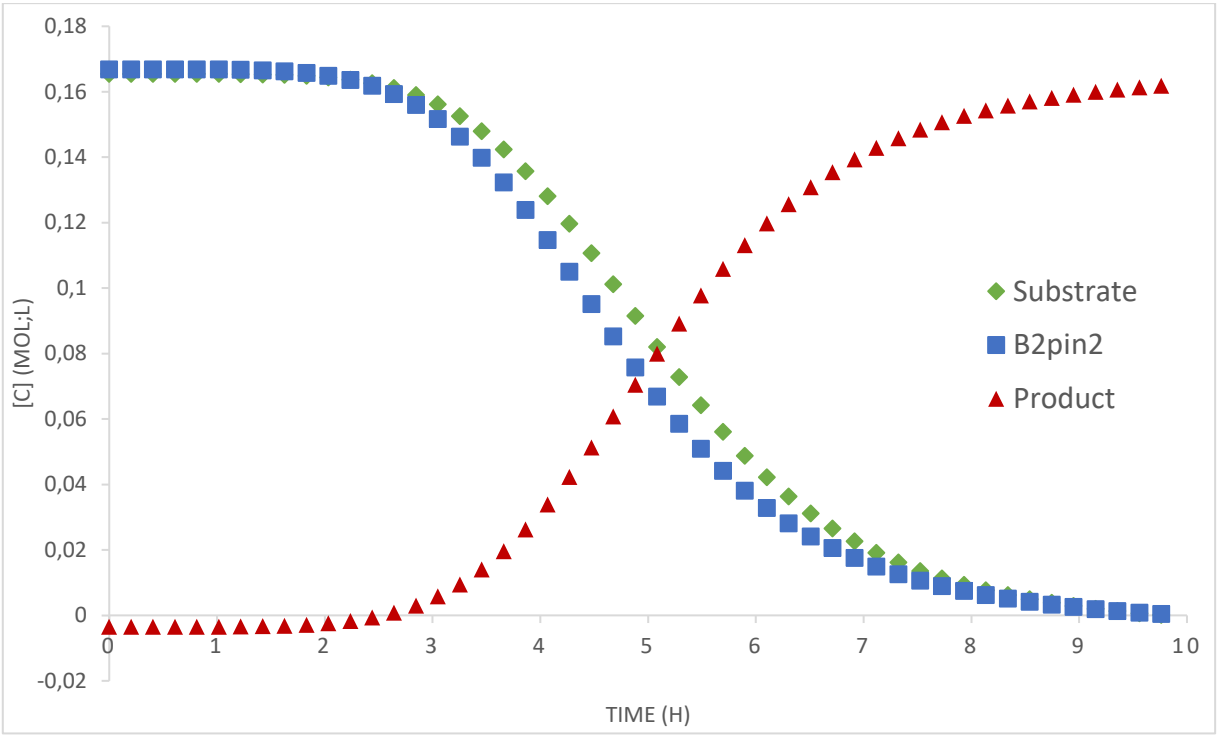

Kinetic profile for the C-H bond *meta*-borylation of 3-methylpyridine under standard conditions.

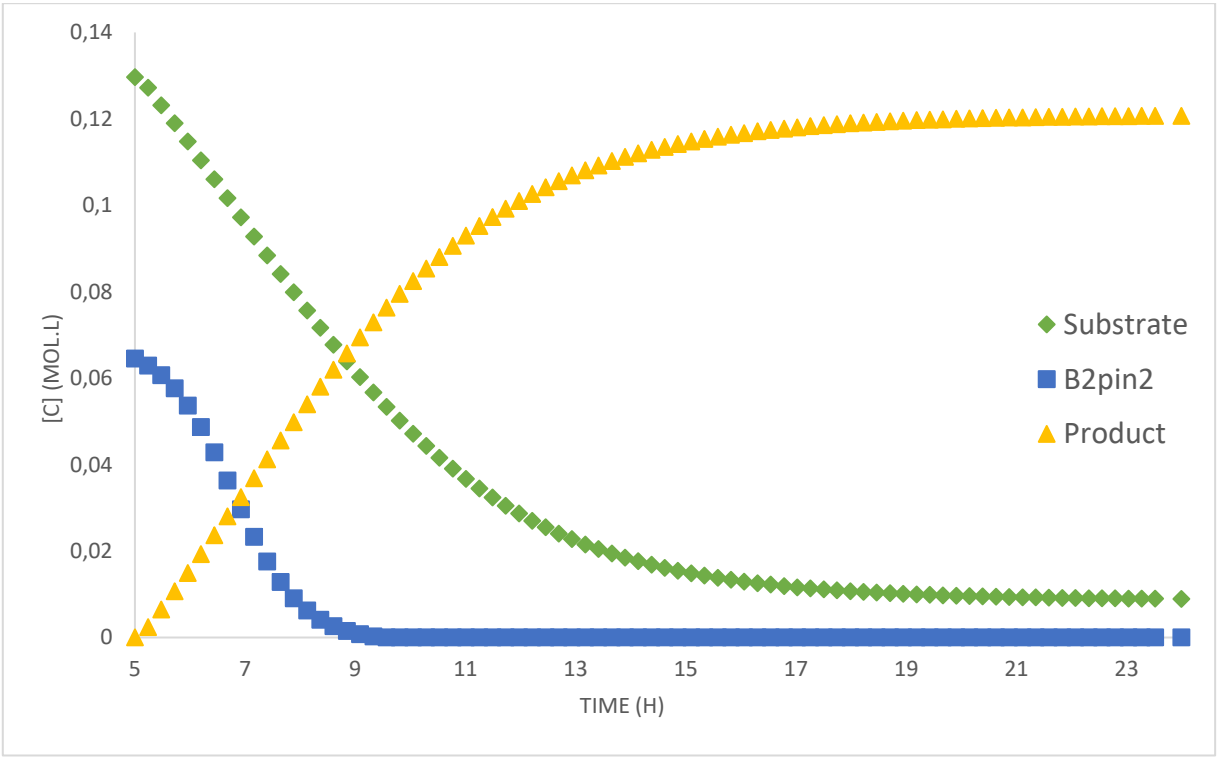

Kinetic profile for the C-H bond *meta*-borylation of 3-methylpyridine under conditions **B**.

2.4.5. Identification of reaction intermediates.

High temperature ^{1}H and ^{11}B NMR study of the active catalyst formation: [Ir(Bpin)$_3$].L:

Procedure for ^{1}H NMR follow-up of the borylation reaction: [Ir(COD)(Cl)]$_2$ (2 mg, 3.0 x 10^{-6} mol, 0.5 eq.), B_2pin_2 (4.63 mg, 1.83 x 10^{-5} mol, 3 eq.), and ligand **L** (5 mg, 6.1 x 10^{-6} mol, 1 eq) were introduced in an oven dried NMR tube. Deuterated toluene (1 mL) was added inside the NMR tube under argon atmosphere. The reaction mixture was analyzed every five minutes for 24 hours by ^{1}H NMR at 80°C. The below-presented ^{1}H NMR spectrum from bottom to top: r.t to 80°C (1 to 6) then every 2.4 hours at 80°C (6 to 16):

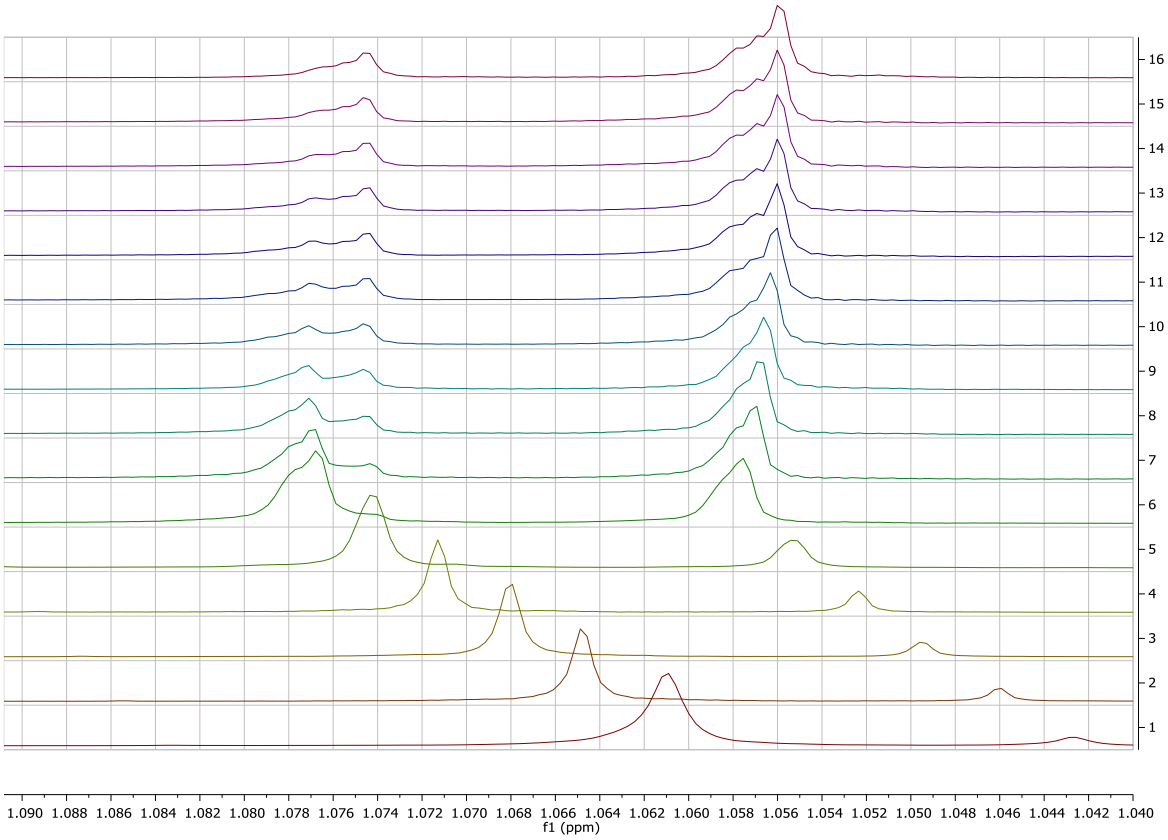

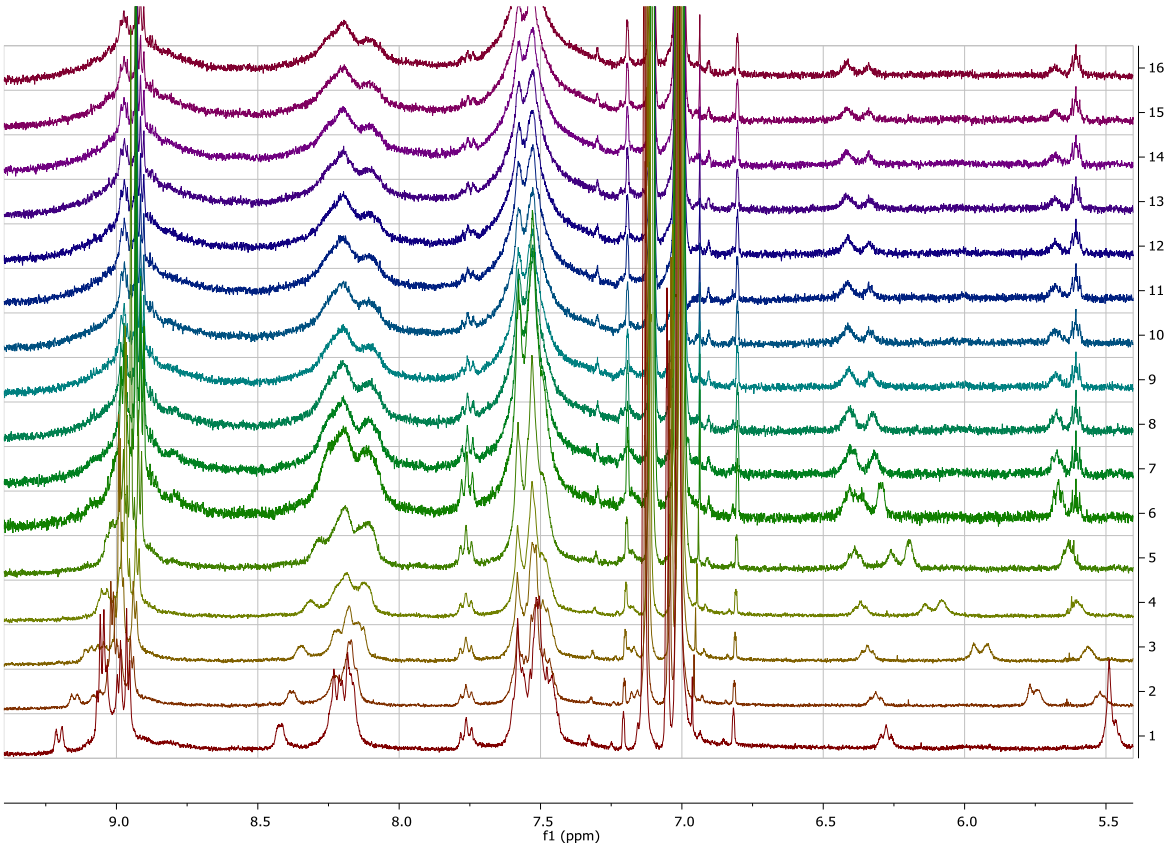
16
15
14
13
12
11
10
9
8
7
6
5
4
3
2
1
9.0
8.5
8.0
7.5
7.0
6.5
6.0
5.5
f1 (ppm)

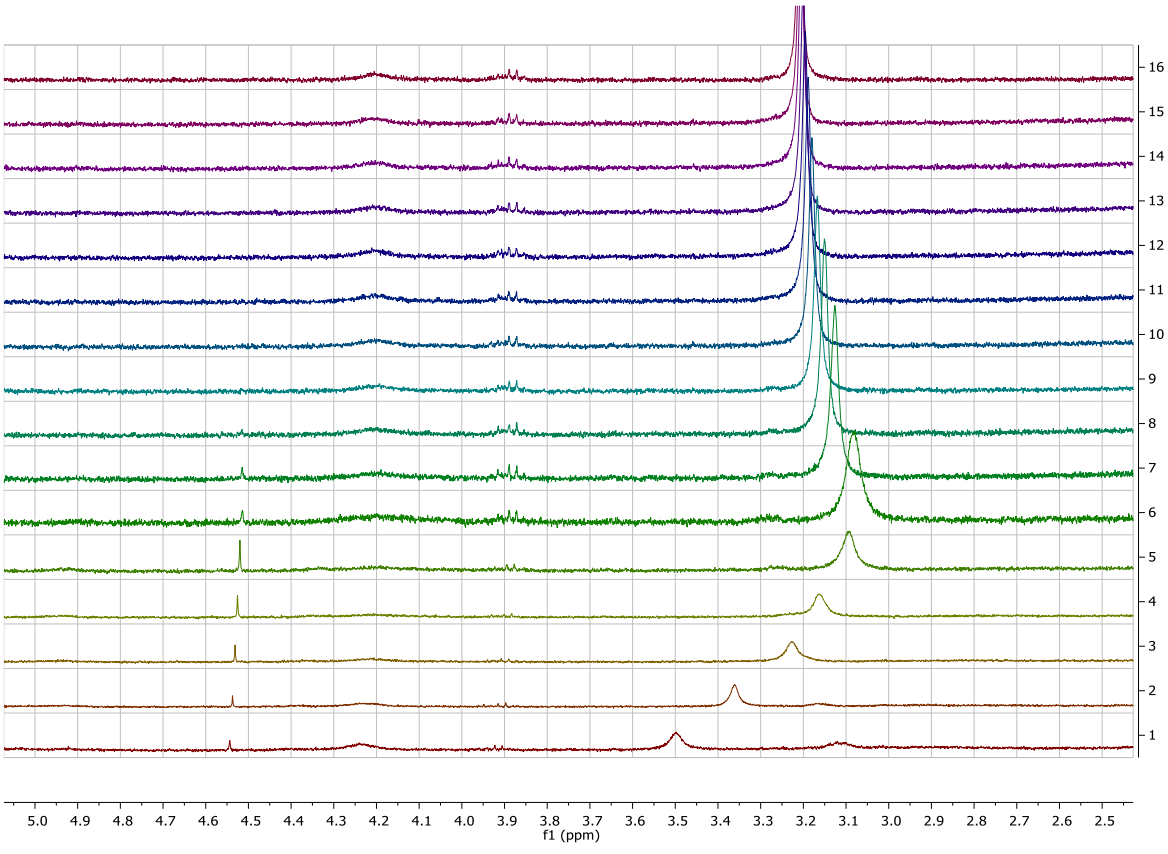
16
15
14
13
12
11
10
9
8
7
6
5
4
3
2
1
5.0
4.9
4.8
4.7
4.6
4.5
4.4
4.3
4.2
4.1
4.0
3.9
3.8
3.7
3.6
3.5
3.4
3.3
3.2
3.1
3.0
2.9
2.8
2.7
2.6
2.5
f1 (ppm)

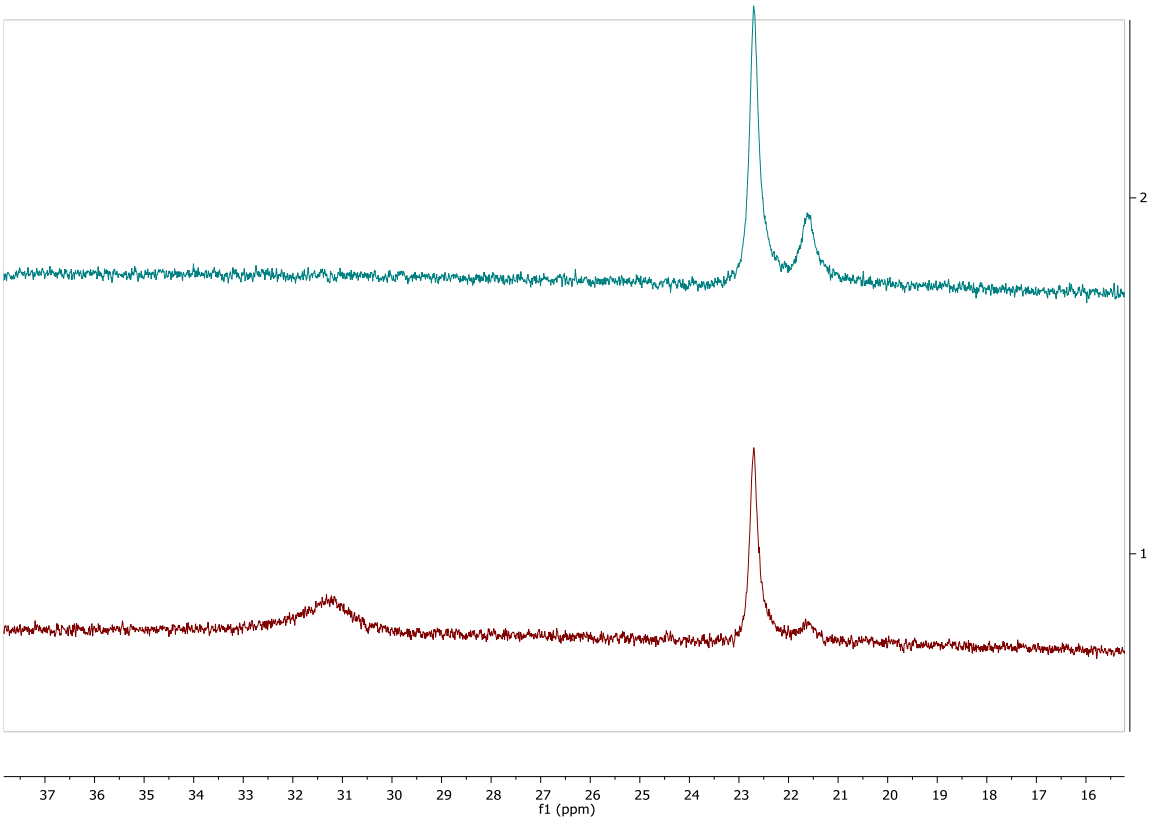

^{11}B NMR experiment: from 80°C at t_{0h} to 80°C at t_{24h} (bottom to top).

The above experiments indicate formation of the catalytically active L·$(Bpin)_3$ species at 80 °C with two set of peaks in the ^{1}H and ^{11}B NMR spectra while the COD ligand seems to de-coordinate the iridium center (a chemical shift in ^{1}H NMR from 3.5 to 3.15 ppm at 80 °C).

High temperature ^{1}H NMR study for the *meta*-C-H bond borylation of 3-methylpyridine.

Procedure for ^{1}H NMR follow-up of the borylation reaction: $[Ir(COD)(Cl)]_2$ (2 mg, 3.0 x 10^{-6} mol, 0.5 eq.), B_2pin_2 (4.63 mg, 1.83 x 10^{-5} mol, 3 eq.), and ligand **L** (5 mg, 6.1 x 10^{-6} mol, 1 eq) were introduced in an oven dried NMR tube. Deuterated toluene (1 mL) and 3-methylpyridine (0.6 µL, 6.1 x 10^{-6} mol, 1 eq.) were added inside the NMR tube under argon atmosphere. The reaction mixture was analyzed every five minutes for 24 hours by ^{1}H NMR at 80°C. GC-MS analysis of the resulting mixture showed full conversion of the starting material towards the *meta*-C-H bond borylated product. The below-presented NMR spectra from top to bottom: r.t., then 80°C then every 2.4 hours at 80°C:

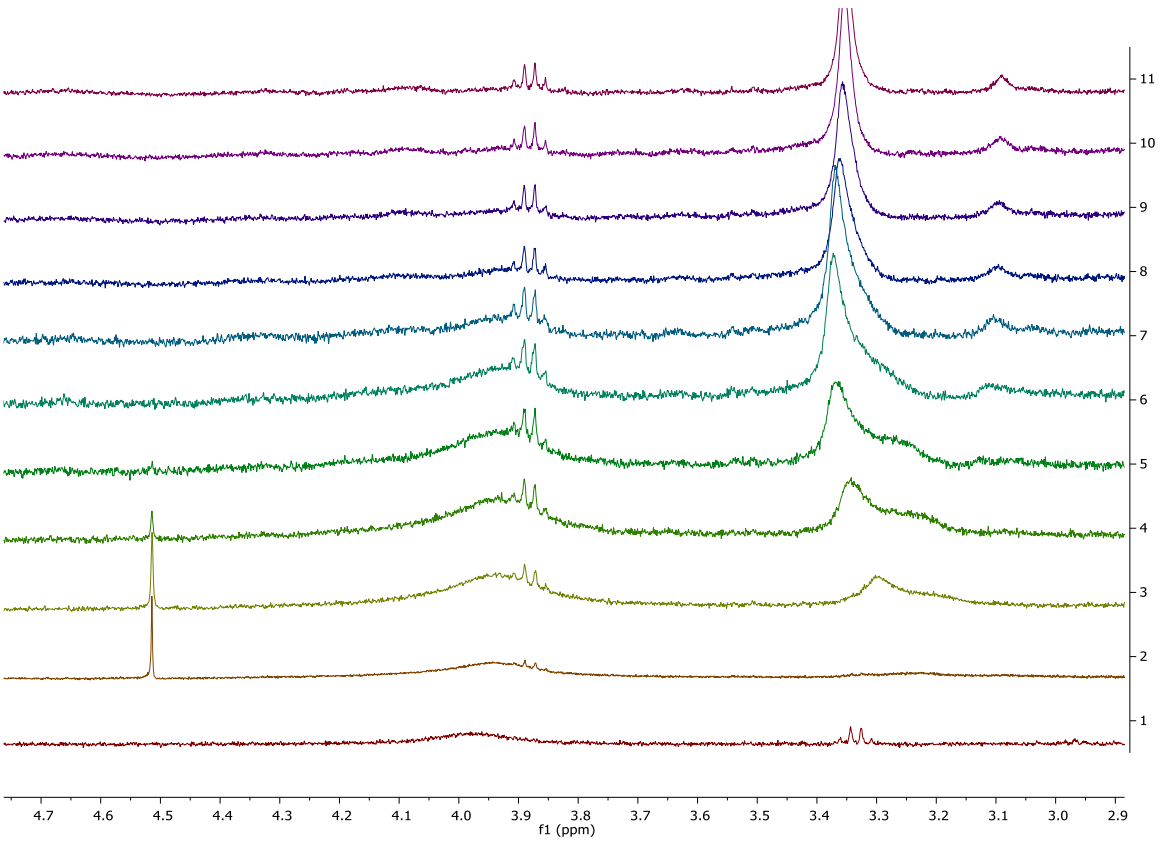

From the above-presented NMR spectra, there is a clear formation of H_2 (*ca.* 4.5 ppm) and a chemical shift in the proton singlet belonging to the COD ligand from a broad singlet (*ca.* 4 ppm) to an up-field shifted 3.35 ppm (as seen it is seen above in the formation of $L^{\cdot}(Bpin)_3$ species)

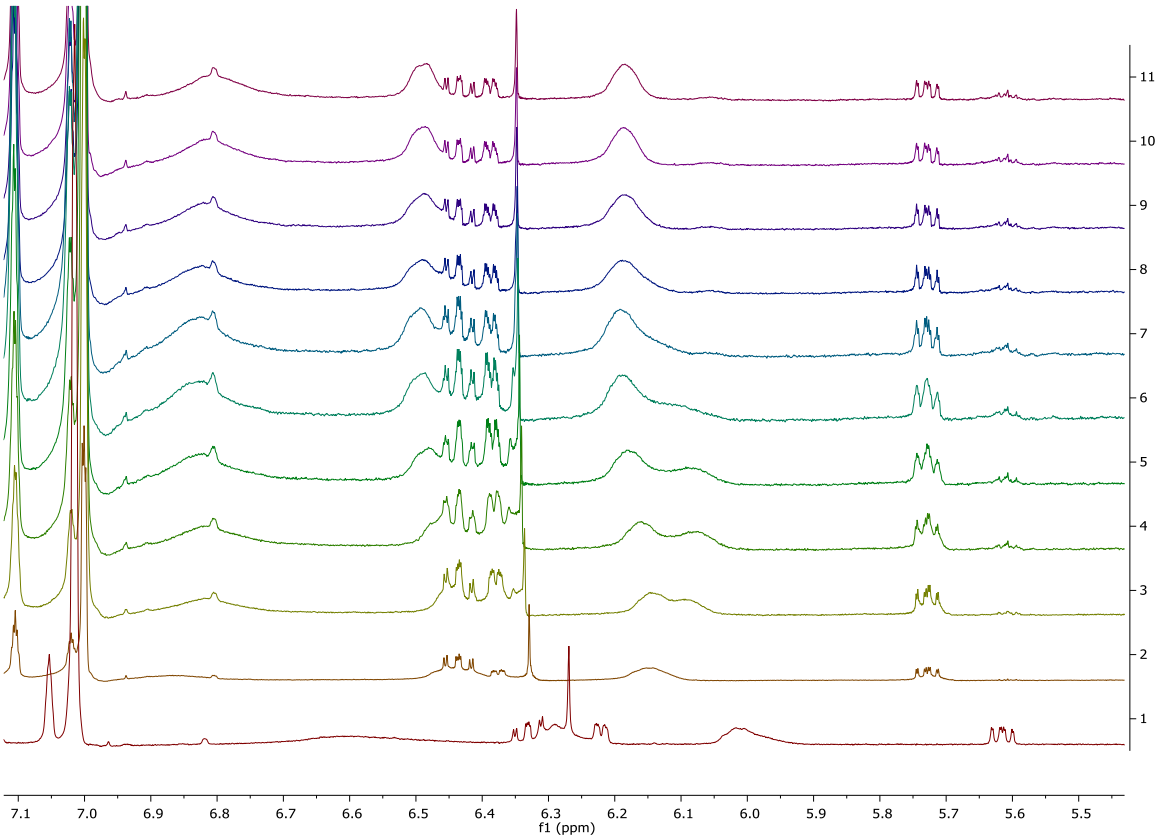

The above-presented NMR spectra for the aromatic area shows the dissappearance of the protons belonging to the bound substrate and emergence of new proton signals belonging to the bound product. Qualitatively, the proton peaks from the product are less up-field shifted, thus less coordinating to the zinc(II) center when compared to the substrate. This likely indicates that the substrate is more coordinating to the recogntion site than the borylated product. We ascribe this difference to the high bulkiness encountered in the product with respect to the substrate.

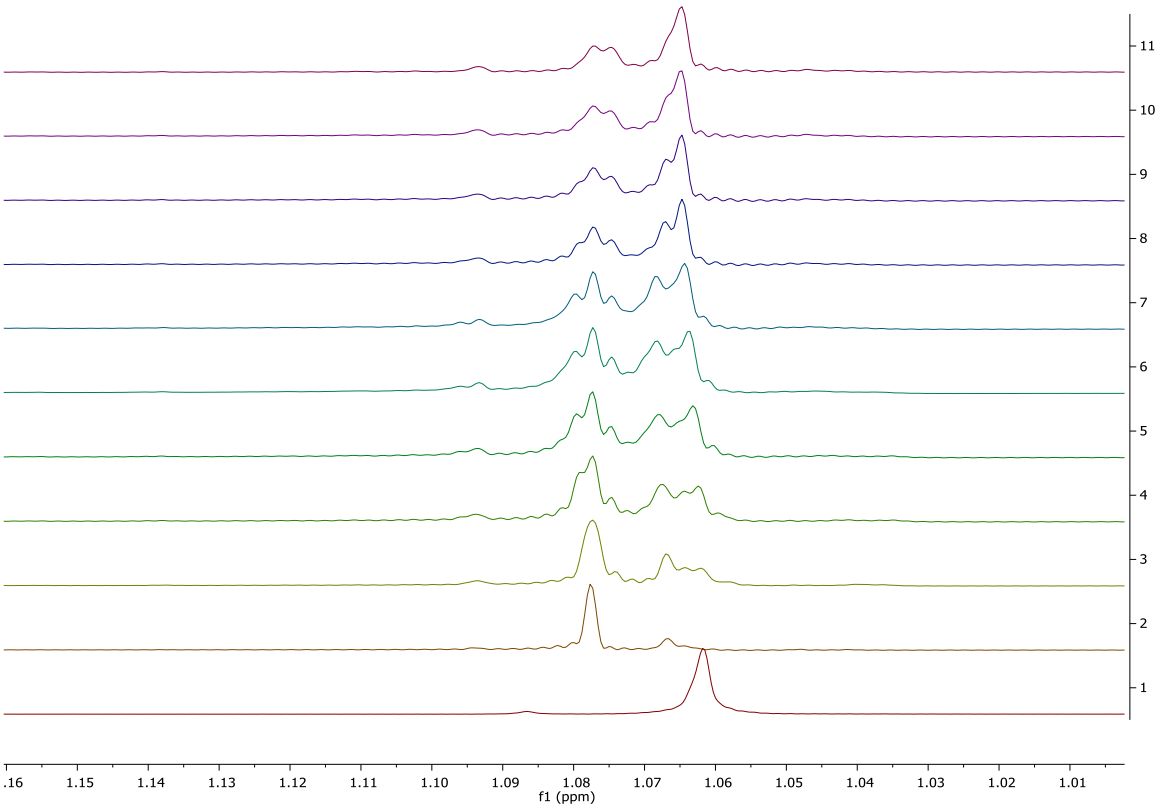

The above-presented NMR spectra for the aliphatic area shows the fast dissappearance of B_2pin_2 into the catalytically active species. However, due to overlapping, it is not clear to differentiate which protong signals correspond to the catalytically active species or the potential intermediates or the boryalted product.

2.4.6. Dormant reactivity using pyridinium tetrafluoroborate as the substrate.

Dormant reactivity procedure: $[Ir(COD)(Cl)]_2$ (1.7 mg, 2.4 x 10^{-6} mol, 0.015 eq.), B_2pin_2 (41.1 mg, 1.62 x 10^{-4} mol, 1 eq.), ligand **L** (4.1 mg, 4.9 x 10^{-6} mol, 0.03 eq.), pyridinium tetrafluoroborate (27 mg, 1,62 x 10^{-4} mol, 1eq.) and dodecane (6.9 mg, 9.2 µL, 4.05 x 10^{-5} mol, 0.25 eq.) were introduced in an oven dried Schlenk flask. *p*-xylene (1 mL) was added and the reaction mixture was stirred at room temperature for 30 minutes. The reaction mixture was heated up to 80°C for 3 hours, and DIPEA (21 mg, 1,62 x 10^{-4} mol, 28 µL, 1eq.) was added. After 13 hours, the crude mixture was allowed to cool down to room temperature. A conversion of 90% and a yield of 49 % mono *meta*-borylated, 5% bis *meta*-borylated and 8% *para*-borylated product were estimated by GC-MS analysis.

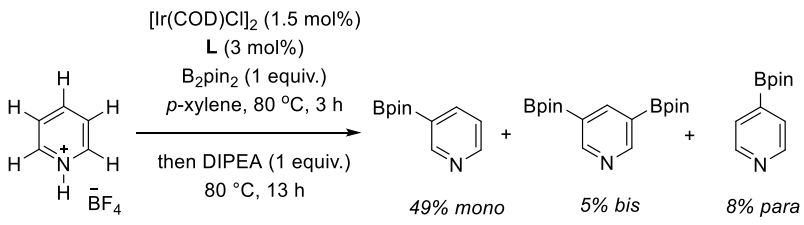

2.4.7. Characterization of products resulting from the catalytic experiments.

General procedure: $[Ir(COD)(Cl)]_2$ (1.7 mg, 2.4 x 10^{-6} mol, 0.015 eq.), B_2pin_2 (41.1 mg, 1.62 x 10^{-4} mol, 1 eq.), ligand **L** (4.1 mg, 4.9 x 10^{-6} mol, 0.03 eq.), and dodecane (6.9 mg, 9.2 µL, 4.05 x 10^{-5} mol, 0.25 eq.) were introduced in an oven dried Schlenk flask. *p*-xylene (1 mL) was added and the reaction mixture was stirred at room temperature for 30 minutes. Then, the substrate (1.62 x 10^{-4} mol, 1 eq.) was added. Upon completion monitored by GC-MS analysis, conversion and yield were estimated using dodecane as the internal standard. The solvent was then evaporated and the residue was purified using Kugelrohr distillation apparatus yielding the analytically pure product.

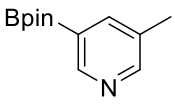

3-(4,4,5,5-Tetramethyl-1,3,2-dioxaborolan-2-yl)-5-methylpyridine (5a): Following the general procedure **A**, the reaction mixture was stirred at 80°C for 9 hours. Quantitative conversion and yield were estimated by GC-MS analysis. Purification by Kugelrorh distillation afforded the analytically pure product (31 mg, 87% yield). ^{1}H NMR (400 MHz, $CDCl_3$): δ = 8.72 (s, 1H), 8.47 (s, 1H), 7.87 (s, 1H), 2.32 (s, 3H), 1.35 (s, 12H) ppm. $^{13}C\{^1H\}$ NMR (101 MHz, $CDCl_3$): δ = 152.55, 152.40, 142.68, 132.29, 84.16, 24.86, 18.30 ppm. $^{11}B\{^1H\}$ NMR (128 MHz, $CDCl_3$): δ = 31.06 (s) ppm. GC: t_R = 16.5 min; MS (EI): *m/z* = 219 (M^+, 25), 204 (50), 162 (25), 120 (100). HRMS (ESI): *m/z* calcd for ($C_{12}H_{19}NO_2{}^{11}B$) $[M+H]^+$ 220.15033; found: 220.1503 (0 ppm).

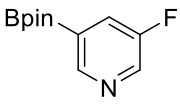

3-(4,4,5,5-Tetramethyl-1,3,2-dioxaborolan-2-yl)-5-Fluoropyridine (5b): Following the general procedure **A**, the reaction mixture was stirred at 80°C for 20 hours. Quantitative conversion and yield were estimated by GC-MS analysis. Purification by Kugelrorh distillation afforded the analytically pure product (33 mg, 92% yield.). ^{1}H NMR (400 MHz, $CDCl_3$): δ = 8.74 (s, 1H), 8.52 (s, 1H), 7.74 (dd, *J* = 8.6, 2.2 Hz, 1H), 1.35 (s, 12H) ppm. $^{13}C\{^1H\}$ NMR (101 MHz, $CDCl_3$): δ = 151.12 (d, *J* = 5.1 Hz), 140.40 (d, *J* = 23.7 Hz), 128.18 (d, *J* = 16.3 Hz), 84.58, 24.84 ppm. $^{11}B\{^1H\}$ NMR (128 MHz, $CDCl_3$): δ = 30.27 (s) ppm. $^{19}F\{^1H\}$ NMR (376 MHz, $CDCl_3$): δ = -127.44 (s) ppm. GC: t_R = 13.9 min; MS (EI): *m/z* = 223 (M^+, 30), 208 (100), 166 (50), 137 (40), 124 (85), 58 (45). HRMS (ESI): *m/z* calcd for ($C_{11}H_{16}NO_2F{}^{11}B$) $[M+H]^+$ 224.12526; 224.1254 (1 ppm).

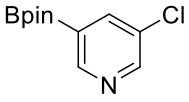

3-(4,4,5,5-Tetramethyl-1,3,2-dioxaborolan-2-yl)-5-chloropyridine (5c): Following the general procedure **A**, the reaction mixture was stirred at 80°C for 24 hours. Quantitative conversion and yield were estimated by GC-MS analysis. Purification by Kugelrorh distillation afforded the analytically pure product (32 mg, 84% yield). ^{1}H NMR (400 MHz, $CDCl_3$): δ = 8.79 (d, *J* = 1.0 Hz, 1H), 8.62 (d, *J* = 2.5 Hz, 1H), 8.03 (t, *J* = 2.5, 1.0 Hz, 1H), 1.35 (s, 12H) ppm. $^{13}C\{^1H\}$ NMR (101 MHz, $CDCl_3$): δ = 152.92, 150.84, 141.66, 132.03, 84.61, 24.84 ppm. $^{11}B\{^1H\}$ NMR (128 MHz, $CDCl_3$): δ = 30.64 (s) ppm. GC: t_R = 16.4 min; MS (EI): *m/z* = 239 (M^+, 45), 226 (35), 224 (100), 182 (45), 153 (50), 140 (80), 139 (20), 85 (30), 58 (50). HRMS (ESI): *m/z* calcd for ($C_{11}H_{16}NO_2{}^{35}Cl{}^{11}B$) $[M+H]^+$ 240.09571; 240.0957 (0 ppm).

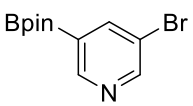

3-(4,4,5,5-Tetramethyl-1,3,2-dioxaborolan-2-yl)-5-bromopyridine (5d): Following the general procedure **A**, the reaction mixture was stirred at 80°C for 24 hours. 91% conversion and a yield of 80% were estimated by GC-MS analysis. Purification by Kugelrorh distillation afforded the analytically pure product (34 mg, 75% yield). ^{1}H NMR (400 MHz, $CDCl_3$): δ = 8.83 (d, *J* = 1.2 Hz, 1H), 8.72 (d, *J* = 2.4 Hz, 1H), 8.18 (dd, *J* = 2.4, 1.2 Hz, 1H), 1.35 (s, 12H) ppm. $^{13}C\{^1H\}$ NMR (101 MHz, $CDCl_3$): δ = 153.24, 152.98, 144.53, 120.95, 84.62, 24.85 ppm. $^{11}B\{^1H\}$ NMR (128 MHz, $CDCl_3$): δ = 30.70 (s) ppm. GC: t_R = 17.7 min; MS (EI): *m/z* = 283 (M^+, 30), 285 (30), 270

(95), 268 (100), 226 (30), 186 (50), 184 (50), 85 (30), 58 (70). The spectral data match those found in literature.[52]

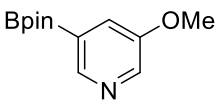

3-(4,4,5,5-Tetramethyl-1,3,2-dioxaborolan-2-yl)-5-methoxypyridine (5e): Following the general procedure **A**, the reaction mixture was stirred at 80°C for 24 hours. Quantitative conversion and yield were estimated by GC-MS analysis. Purification by Kugelrorh distillation afforded the analytically pure product (36 mg, 95 % yield). ^{1}H NMR (400 MHz, $CDCl_3$): δ = 8.53 (d, *J* = 1.5 Hz, 1H), 8.35 (d, *J* = 3.1 Hz, 1H), 7.53 (t, *J* = 3.1, 1.5 Hz, 1H), 3.85 (s, 3H), 1.34 (s, 12H) ppm. $^{13}C\{^{1}H\}$ NMR (101 MHz, $CDCl_3$): δ = 155.23, 147.54, 140.58, 125.20, 84.25, 55.47, 24.83 ppm. $^{11}B\{^{1}H\}$ NMR (128 MHz, $CDCl_3$): δ = 30.78 (s) ppm. GC: t_R = 17.9 min; MS (EI): *m/z* = 235 (M^+, 80), 220 (50), 178 (30), 149 (80), 135 (100). The spectral data match those found in literature.[53]

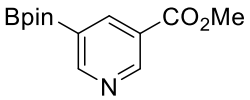

3-Pyridinecarboxylic acid, 5-(4,4,5,5-tetramethyl-1,3,2-dioxaborolan-2-yl)-, methyl ester (5f): Following the general procedure **A**, the reaction mixture was stirred at 80°C for 18 hours. Quantitative conversion and yield were estimated by GC-MS analysis. Purification by Kugelrorh distillation afforded the analytically pure product (40 mg, 94% yield). ^{1}H NMR (400 MHz, $CDCl_3$): δ = 9.27 (d, *J* = 2.3 Hz, 1H), 9.08 (d, *J* = 1.6 Hz, 1H), 8.67 (dd, *J* = 2.3, 1.6 Hz 1H), 3.95 (s, 3H), 1.37 (s, 12H) ppm. $^{13}C\{^{1}H\}$ NMR (101 MHz, $CDCl_3$): δ = 165.78, 158.75, 152.84, 143.34, 125.44, 84.60, 52.36, 24.86 ppm. $^{11}B\{^{1}H\}$ NMR (128 MHz, $CDCl_3$): δ = 31.07 (s) ppm. GC: t_R = 19.6 min; MS (EI): *m/z* = 263 (M^+, 10), 248 (35), 220 (100), 164 (85). The spectral data match those found in literature.[54]

3-(4,4,5,5-Tetramethyl-1,3,2-dioxaborolan-2-yl)-5-trifluoromethylpyridine (5g): Following the general procedure **A**, the reaction mixture was stirred at 80°C for 20 hours. 50% conversion and a yield of 45 % were estimated by GC-MS analysis. Purification by Kugelrorh distillation afforded the product containing traces of Bpin impurities. ^{1}H NMR (400 MHz, Chloroform-*d*) δ = 9.13 (s, 1H), 8.96 (d, *J* = 1.7 Hz, 1H), 8.32 (s, 1H), 1.39 (s, 12H). $^{13}C\{^{1}H\}$ NMR (101 MHz, Chloroform-*d*) δ = 158.24, 148.53 (q, *J* = 4.2 Hz), 139.27 (q, *J* = 3.8 Hz), 84.81, 25.02. $^{11}B\{^{1}H\}$ NMR (128 MHz, $CDCl_3$): δ = 30.56 (s) ppm. $^{19}F\{^{1}H\}$ NMR (376 MHz, $CDCl_3$): δ = -62.64 (s) ppm. GC: t_R = 13.4 min; MS (EI): *m/z* = 273 (M^+, 10), 258 (100), 216 (40), 174 (25), 58 (35). The spectral data match those found in literature.[55]

3-(4,4,5,5-Tetramethyl-1,3,2-dioxaborolan-2-yl)-5-phenylpyridine (5h): Following the general procedure **A**, the reaction mixture was stirred at 80°C for 17 hours. Quantitative conversion and yield were estimated by GC-MS analysis. Purification by Kugelrorh distillation afforded the analytically pure product (41 mg, 89% yield). ^{1}H NMR (400 MHz, $CDCl_3$): δ = 8.92 (d, *J* = 1.6 Hz, 1H), 8.91 (d, *J* = 2.5 Hz, 1H), 8.27 (m, 1H), 7.64-7.58 (m, 2H), 7.51-7.44 (m, 2H), 7.42-7.35 (m, 1H), 1.37 (s, 12H) ppm. $^{13}C\{^{1}H\}$ NMR (101 MHz, $CDCl_3$): δ = 154.07, 150.41, 140.62, 137.82, 135.87, 128.98, 128.01, 127.20, 84.32, 24.89 ppm. $^{11}B\{^{1}H\}$ NMR (128 MHz, $CDCl_3$): δ = 30.94 (s) ppm. GC: t_R = 23.4 min; MS (EI): *m/z* = 281 (M^+, 100), 266 (65), 224 (35), 195 (50), 181 (80). HRMS (ESI): *m/z* calcd for ($C_{17}H_{21}NO_2{}^{11}B$) $[M+H]^+$ 282.16598; 282.1664 (2 ppm).

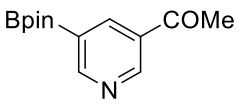

3-acetyl-5-(4,4,5,5-tetramethyl-1,3,2-dioxaborolan-2-yl)pyridine (5i): Following the general procedure, the reaction mixture was stirred at 80 °C for 18 hours. Quantitative conversion and yield were estimated by GC-MS analysis. Purification by Kugelrorh distillation afforded the analytically pure product (33 mg, 84% yield). ^{1}H NMR (400 MHz,

$CDCl_3$): δ = 9.21 (d, *J* = 1.9 Hz, 1H), 9.08 (d, *J* = 1.9 Hz, 1H), 8.56 (t, *J* = 1.9 Hz, 1H), 2.64 (s, 3H), 1.37 (s, 12H) ppm. $^{13}C\{^1H\}$ NMR (101 MHz, $CDCl_3$): δ = 206.89, 158.86, 151.78, 141.84, 84.62, 30.88, 24.85 ppm. $^{11}B\{^1H\}$ NMR (128 MHz, $CDCl_3$): δ = 30.69 (s) ppm. HRMS (ESI, MeOH/DCM: 95/5): *m/z* calcd for $C_{13}H_{18}NO_3{}^{11}B$ $[M+Na]^+$: 270.12719; found: 270.1273 (0 ppm).

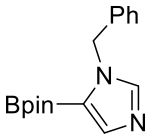

1-Benzyl-5-(4,4,5,5-tetramethyl-1,3,2-dioxaborolan-2-yl)-1H-imidazole (6a): Following the general procedure **A**, the reaction mixture was stirred at 80°C for 24 hours. Quantitative conversion and yield were estimated by GC-MS analysis. Purification by Kugelrorh distillation afforded the analytically pure product (44 mg, 95% yield.). ^1H NMR (400 MHz, $CDCl_3$): δ = 7.65 (d, *J* = 11.6 Hz, 2H), 7.36-7.24 (m, 3H), 7.14 (d, *J* = 6.7 Hz, 2H), 5.37 (s, 2H), 1.25 (s, 12H) ppm. $^{13}C\{^1H\}$ NMR (101 MHz, $CDCl_3$): δ = 142.21, 141.72, 137.62, 128.58, 127.67, 127.11, 83.71, 50.46, 24.63 ppm. $^{111}B\{^1H\}$ NMR (128 MHz, $CDCl_3$): δ = 28.01 (s) ppm. GC: t_R = 22.7 min; MS (EI): *m/z* = 284 (M^+, 40), 184 (95), 168 (20), 91 (100). The spectral data match those found in literature.[56]

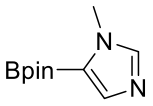

1-Methyl-5-(4,4,5,5-tetramethyl-1,3,2-dioxaborolan-2-yl)-1*H*-imidazole (6b): Following the general procedure **A**, the reaction mixture was stirred at 80°C for 24 hours. Quantitative conversion and yield were estimated by GC-MS analysis. Purification by Kugelrorh distillation afforded the analytically pure product (30 mg, 90% yield). ^1H NMR (400 MHz, $CDCl_3$): δ = 7.56 (s, 1H), 7.54 (s, 1H), 3.79 (s, 3H), 1.31 (s, 12H) ppm. $^{13}C\{^1H\}$ NMR (101 MHz, $CDCl_3$): δ = 141.98, 141.50, 83.62, 33.96, 24.80 ppm. $^{11}B\{^1H\}$ NMR (128 MHz, $CDCl_3$): δ = 28.59 (s) ppm. GC: t_R = 16.6 min; MS (EI): *m/z* = 208 (M^+, 60), 193 (25), 165 (40), 123 (30), 108 (100), 83 (25), 81 (25). The spectral data match those found in literature.[56]

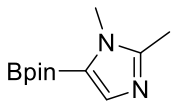

1,2-dimethyl-5-(4,4,5,5-tetramethyl-1,3,2-dioxaborolan-2-yl)-1H-imidazole (6c): Following the general procedure **A**, the reaction mixture was stirred at 80°C for 24 hours. Quantitative conversion and yield were estimated by GC-MS analysis. Purification by Kugelrorh distillation afforded the analytically pure product (35 mg, 97% yield). ^1H NMR (400 MHz, Chloroform-*d*) δ = 7.41 (s, 1H), 3.66 (s, 3H), 2.35 (s, 3H), 1.27 (s, 12H).$^{11}B\{^1H\}$ (128 MHz, Chloroform-*d*) δ = 28.06. $^{13}C\{^1H\}$ NMR (101 MHz, Chloroform-*d*) δ = 149.52, 140.27, 83.39, 32.59, 24.73, 13.11. GC: t_R = 17.5 min; MS (EI): *m/z* = 222 (M^+, 95), 122 (100), 179 (50), 137 (35), 56 (20), 81 (15), 207 (15). The spectral data match those found in literature.[56]

2.4.8. References.

[1] (a) *C-H Activation in Topics in Current Chemistry* (Eds.: J.-Q. Yu, Z. Shi), Springer-Verlag, Berlin-Heidelberg, **2010**; (b) R. Shang, L. Ilies, E. Nakamura, *Chem. Rev.* **2017**, *117*, 9086-9139; (c) Y. Yang, J. Lan, J. You, *Chem. Rev.* **2017**, *117*, 8787-8863; (d) L. McMurray, F. O'Hara, M. J. Gaunt, *Chem. Soc. Rev.* **2011**, *40*, 1885-1898; (e) R. R. Karimov, J. F. Hartwig, *Angew. Chem. Int. Ed.* **2018**, *57*, 4234-4241; (f) J. Yamaguchi, A. D. Yamaguchi, K. Itami, *Angew. Chem. Int. Ed.* **2012**, *51*, 8960-9009.

[2] (a) K. M. Engle, T.-S. Mei, M. Wasa, J.-Q. Yu, *Acc. Chem. Res.* **2012**, *45*, 788-802; (b) X.-S. Xue, P. Ji, B. Zhou, J.-P. Cheng, *Chem. Rev.* **2017**, *117*, 8622-8648.

[3] (a) C. Sambiagio, D. Schönbauer, R. Blieck, T. Dao-Huy, G. Pototschnig, P. Schaaf, T. Wiesinger, M. F. Zia, J. Wencel-Delord, T. Besset, B. U. W. Maes, M. Schnürch, C*hem. Soc. Rev.* **2018**, *47*, 6603-6743; (b) S. Rej, Y. Ano, N. Chatani, *Chem. Rev.* **2020**, *120*, 1788-1887; (c) G. Meng, N. Y. S. Lam, E. L. Lucas, T. G. Saint-Denis, P. Verma, N. Chekshin, J.-Q. Yu, *J. Am. Chem. Soc.* **2020**, *142*, 10571-10591; (d) R.-Y. Zhu, M. E. Farmer, Y.-Q. Chen, J.-Q. Yu, *Angew. Chem. Int. Ed.* **2016**, *55*, 10578-10599.

[4] (a) D. L. Davies, S. A. Macgregor, C. L. McMullin, *Chem. Rev.* **2017**, *117*, 8649-8709; (b) L. Ackermann, *Chem. Rev.* **2011**, *111*, 1315-1345.

[5] (a) N. Della Ca', M. Fontana, E. Motti, M. Catellani, *Acc. Chem. Res.* **2016**, *49*, 1389-1400; (b) D. Lichosyt, Y. Zhang, K. Hurej, P. Dydio, *Nat. Catal.* **2019**, *2*, 114-122.

[6] (a) D. Ringe, G. A. Petsko, *Science* **2008**, *320*, 1428-1429; b) *From enzyme models to model enzymes* (Eds.: A. J. Kirby, F. Hollfelder), RSC, London, **2009**.

[7] (a) A. Warshel, P. K. Sharma, M. Kato, Y. Xiang, H. Liu, M. H. M. Olsson, *Chem. Rev.* **2006**, *106*, 3210-3235; (b), G. G. Hammes, S. J. Benkovic, S. Hammes-Schiffer, *Biochemistry* **2011**, *50*, 10422-10430.

[8] (a) *Supramolecular Catalysis* (Ed.: P. W. N. M. van Leeuwen), Wiley-VCH, Weinheim, **2008**; (b) M. J. Wiester, P. A. Ulmann, C. A. Mirkin, *Angew. Chem. Int. Ed.* **2011**, *50*, 114-137; (c) M. Raynal, P. Ballester, A. Vidal-Ferran, P. W. N. M. van Leeuwen, *Chem. Soc. Rev.* **2014**, *43*, 1660-1733; (d) M. Raynal, P. Ballester, A. Vidal-Ferran, P. W. N. M. van Leeuwen, *Chem. Soc. Rev.* **2014**, *43*, 1734-1787; (e) J. Meeuwissen, J. N. H. Reek, *Nat. Chem.* **2010**, *2*, 615-621; (f) P. Dydio, J. N. H. Reek, *Chem. Sci.* **2014**, *5*, 2135-2145; (g) H. J. Davis, R. J. Phipps, *Chem. Sci.* **2017**, *8*, 864-877.

[9] Y. Kuninobu, T. Torigoe, *Org. Biomol. Chem.* **2020**, *18*, 4126-4134.

[10] (a) Y. Kuninobu, H. Ida, M. Nishi, M. Kanai, *Nat. Chem.* **2015**, *7*, 712-717; (b) J. Zeng, M. Naito, T. Torigoe, M. Yamanaka, Y. Kuninobu, *Org. Lett.* **2020**, *22*, 3485-3489; (c) S.-T. Bai, C. B. Bheeter, J. N. H. Reek, *Angew. Chem. Int. Ed.* **2019**, 58, 13039-13043; (d) J. Wang, T. Torigoe, Y. Kuninobu, *Org. Lett.* **2019**, 21, 1342-1346; (e) X. Lu, Y. Yoshigoe, H. Ida, M. Nishi, M. Kanai, Y. Kuninobu, *ACS Catal.* **2019**, *9*, 1705-1709.

[11] (a) H. J. Davis, M. T. Mihai, R. J. Phipps, *J. Am. Chem. Soc.* **2016**, *138*, 12759-12762; (b) G. R. Genov, J. L. Douthwaite, A. S. K. Lahdenpera, D. C. Gibson, R. J. Phipps, *Science* **2020**, *367*, 1246-1251; (c) J. R. Montero Bastidas, T. J. Oleskey, S. L. Miller, M. R. Smith, R. E. Maleczka, *J. Am. Chem. Soc.* **2019**, *141*, 15483-15487; (d) M. T. Mihai, B. D. Williams, R. J. Phipps, *J. Am. Chem. Soc.* **2019**, *141*, 15477-15482; (e) B. Lee, Bernadette, M. T. Mihai, V. Stojalnikova, R. J. Phipps, *J. Org. Chem.* **2019**, *84*, 13124-13134; (f) M. T. Mihai, H. J. Davis, G. R. Genov, R. J. Phipps, *ACS Catal.* **2018**, *8*, 3764-3769;

(g) M. E. Hoque, R. Bisht, C. Haldar, B. Chattopadhyay, *J. Am. Chem. Soc.* **2017**, *139*, 7745-7748; (h) W. A. Golding, R. J. Phipps, *Chem. Sci.* **2020**, *11*, 3022-3027; (i) R. Bisht, M. E. Hoque, B. Chattopadhyay, *Angew. Chem. Int. Ed.* **2018**, *57*, 15762-15766; (j) B. Chattopadhyay, J. E. Dannatt, I. L. Andujar-De Sanctis, K. A. Gore, R. E. Maleczka, D. A. Singleton, M. R. Smith, *J. Am. Chem. Soc.* **2017**, *139*, 7864-7871.

[12] (a) L. Yang, N. Uemura, Y. Nakao, *J. Am. Chem. Soc.* **2019**, *141*, 7972-7979; (b) L. Yang, K. Semba, Y. Nakao, *Angew. Chem. Int. Ed.* **2017**, *56*, 4853-4857.

[13] (a) Y. Kuroda, Y. Nakao, *Chem. Lett.* **2019**, *48*, 1092-1100; (b) C. Haldar, M. E. Hoque, R. Bisht, B. Chattopadhyay, *Tetrahedron Lett.* **2018**, *59*, 1269-1277; (c) K. Murakami, S. Yamada, T. Kaneda, K. Itami, *Chem. Rev.* **2017**, 117, 9302-9332.

[14] (a) A. Ros, R. Fernández, J. M. Lassaletta, *Chem. Soc. Rev.* **2014**, *43*, 3229-3243; (b) *Boronic Acids. Preparation, Applications in Organic Synthesis*, (Ed.: D. G. Hall), Wiley-VCH, Weinheim, **2011**; (c) E. C. Neeve, S. J. Geier, I. A. I. Mkhalid, S. A. Westcott, T. B. Marder, *Chem. Rev.* **2016**, *116*, 9091-9161; (d) M. Wang, Z. Shi, *Chem. Rev.* **2020**, *120*, 7348-7398.

[15] (a) J. Takagi, K. Sato, J. F. Hartwig, T. Ishiyama, N. Miyaura, *Tetrahedron Lett.* **2002**, *43*, 5649-5651; (b) M. A. Larsen, J. F. Hartwig, *J. Am. Chem. Soc.* **2014**, *136*, 4287-4299.

[16] For pioneering findings on kinetically labile Zn···N interactions for purely organic reactions, see: (a) R. P. Bonar-Law, L. G. Mackay, C. J. Walter, V. Marvaud, J. K. M. Sanders, *Pure Appl. Chem.* **1994**, *66*, 803-810; (b) J. K. M. Sanders, *Pure Appl. Chem.* **2000**, *72*, 2265-2274. The uniqueness of Zn^{2+} over other cations for metal catalysis have been studied in reference 28.

[17] The active catalytic species in iridium-catalyzed C-H bond borylation is postulated to be a *N*,*N*-chelated iridium trisboryl complex, for seminal works see: (a) T. M. Boller, J. M. Murphy, M. Hapke, T. Ishiyama, N. Miyaura, J. F. Hartwig, *J. Am. Chem. Soc.* **2005**, *127,* 14263-14278; (b) T. Ishiyama, J. Takagi, K. Ishida, N. Miyaura, N. R. Anastasi, J. F. Hartwig, *J. Am. Chem. Soc.* **2002**, *124*, 390-391; (c) C. W. Liskey, C. S. Wei, D. R. Pahls, J. F. Hartwig, *Chem. Commun.* **2009**, 5603-5605.

[18] For details, see the experimental section.

[19] P. Thordarson, *Chem. Soc. Rev.* **2011**, *40*, 1305-1323.

[20] (a) X. Zhang, K. N. Houk, *Acc. Chem. Res.* **2005**, *38*, 379-385; (b) K. N. Houk, A. G. Leach, S. P. Kim, X. Zhang, *Angew. Chem. Int. Ed.* **2003**, *42*, 4872-4897.

[21] CCDC 2061921-2061922 contain the supplementary crystallographic data for this paper. These data are provided free of charge by The Cambridge Crystallographic Data Centre.

[22] (a) T. Ishiyama, Y. Nobuta, J. F. Hartwig, N. Miyaura, *Chem. Commun.* **2003**, 2924-2925; (b) R. J. Oeschger, M. A. Larsen, A. Bismuto, J. F. Hartwig, *J. Am. Chem. Soc.* **2019**, *141*, 16479-16485; see reference 15b.

[23] A similar conversion and yield was obtained under extensive ligand optimization in dioxane at room temperature, see reference 12a.

[24] (a) T. Ishiyama, J. Takagi, J. F. Hartwig, N. Miyaura, *Angew. Chem. Int. Ed.* **2002**, *41*, 3056-3058; (b) T. Ishiyama, J. Takagi, Y. Yonekawa, J. F. Hartwig, N. Miyaura, *Adv. Synth. Catal.* **2003**, *345*, 1103-1106.

[25] (a) A. F. Schmidt, A. A. Kurokhtina, E. V. Larina, *Catal. Sci. Technol.* **2014**, *4*, 3439-3457; (b) 1 mL of toluene as solvent corresponds to 9.4 mmol, as such, in the case of 15% borylation of toluene, the

following formula for the overall selectivity is applied according to reference 24a: S = $(n_{1+2}/n_{pyridine})/(n_{borylated\ toluene}/n_{toluene})$= [(0.162x0.99)/0.162]/[(0.162x0.15)/9.4] = 381.

[26] ^{1}H NMR studies at room temperature show that both pyridine derivatives (substrates) and borylated ones (products) bind to **L** alternatively in a fast exchange at the NMR time scale. For details, see the experimental section. However, it cannot be ruled out that other inactive pathways are operating at 60 ^{o}C.

[27] 16% of isolated bis-borylated product **2** was obtained according to reference 12a.

[28] *O*-containing polar solvents (DMF, DMSO, acetone, THF, etc.) completely cleave the Zn···N interaction between zinc(II)-porphyrinoids and pyridine derivatives, for examples see references: (a) M. Kadri, J. Hou, V. Dorcet, T. Roisnel, L. Bechki, A. Miloudi, C. Bruneau, R. Gramage-Doria, *Chem. Eur. J.* **2017**, *23*, 5033-5043; (b) P. Zardi, T. Roisnel, R. Gramage-Doria, *Chem. Eur. J.* **2019**, *25*, 627-634.

[29] For selected examples of negligible binding between 2-substituted pyridines and zinc(II)-porphyrinioids, see: (a) M.Morisue, T. Morita,Y. Kuroda, *Org. Biomol. Chem.* **2010**, *8*, 3457-3463; (b) J. S. Summers, A. M. Stolzenberg, *J. Am. Chem. Soc.* **1993**, *115*, 10559-10567; (c) C. H. Kirksey, P. Hambright, C. B. Storm, *Inorg. Chem.* **1969**, *8*, 2141-2144; and reference 27.

[30] (a) A. L. Singer, D. A. Atwood, *Inorg. Chim. Acta.* **1998**, *277*, 157-162; (b) G. A. Morris, H. Zhou, C. L. Stern, S. T. Nguyen, *Inorg. Chem.* **2001**, *40,* 3222-3227; (c) A. W. Kleij, M. Lutz, A. L. Spek, P. W. N. M. van Leeuwen, J. N. H. Reek, *Chem. Commun.* **2005**, 3661-3663; (d) A. W. Kleij, M. Kuil, D. M. Tooke, M. Lutz, A. L. Spek, J. N. H. Reek, *Chem. Eur. J.* **2005**, *11*, 4743-4750.

[31] M. R. Smith III, R. E. Maleczka, Jr., A. K. Venkata, E. Onyeozili, Process for Producing Oxazole, Imidazole, Pyrazole Boryl Compounds, US Pat. 7,709,654B2, **2008**.

[32] For selected examples of binding between 2-methylimidazole and zinc(II)-porphyrinoids, see: (a) M. Nappa, J. S. Valentine, *J. Am. Chem. Soc.* **1978**, *100*, 5075-5080; (b) K. M. Kadish, L. R. Shiue, R. K. Rhodes, L. A. Bottomley, *Inorg. Chem.* **1981**, *20*, 1274-1277.

[33] S. A. Sadler, H. Tajuddin, I. A. I. Mkhalid, A. S. Batsanov, D. Albesa-Jove, M. S. Cheung, A. C. Maxwell, L. Shukla, B. Roberts, D. C. Blakemore, Z. Lin, T. B. Marder, P. G. Steel, *Org. Biomol. Chem.* **2014**, *12*, 7318-7327.

[34] D. G. Blackmond, *Angew. Chem. Int. Ed.* **2005**, *44*, 4302-4320.

[35] The stoichiometric reaction between 3-methylpyridine and HBpin under our standard conditions led to 79% of borylated product and 15% of unreacted HBpin, indicating that B_2pin_2 is a better borylating reagent than HBpin under our standard reaction conditions.

[36] Although we do not have any spectroscopical evidence for the formation of HBpin or any other borylated species derived from B_2pin_2, previous reports from the literature indicate that HBpin is indeed a borylating reagent with side-formation of H_2, but less reactive than B_2pin_2, for details see: J. S. Wright, P. J. H. Scott, P. G. Steel, *Angew. Chem. Int. Ed.* **2021**, *60*, 2796-2821.

[37] Attempts to isolate **L** after the catalysis indicate substantial degradation according to TLC analysis.

[38] (a) I. A. I. Mkhalid, J. H. Barnard, T. B. Marder, J. M. Murphy, J. F. Hartwig, *Chem. Rev.* **2010**, 110, 890-931; (b) J. F. Hartwig, *Chem. Soc. Rev.* **2011**, *40*, 1992-2002; (c) J. F. Hartwig, *Acc. Chem. Res.* **2012**, *45*, 864-873; (d) L. Xu, G. Wang, S. Zhang, H. Wang, L. Wang, L. Liu, J. Jiao, P. Li, *Tetrahedron* **2017**, *73*, 7123-7157.

[39] E. Lindback, S. Dawaigher, K. Warnmark, *Chem. Eur. J.* **2014**, *20*, 13432-13481.

[40] R. L. Reyes, M. Sato, T. Iwai, K. Suzuki, S. Maeda, M. Sawamura, *Science* **2020**, *369*, 970-974.

[41] (a) J. He, Y. Shi, W. Cheng, Z. Man, D. Yang, C.-Y. Li, *Angew. Chem. Int. Ed.* **2016**, *55*, 4557-4561; (b) M. Mishra, D. Twardy, C. Ellstrom, K. A. Wheeler, R. Dembinski, B. Török, *Green Chem.* **2019**, *21*, 99-108.

[42] (a) E. P. McCarney, C, S. Hawes, S. Blasco, T. Gunnlaugsson, *Dalton Trans.* **2016**, *45*, 10209-10221; (b) I. Stengel, A. Mishra, N. Pootrakulchote, S.-J. Moon, S. Zakeeruddin, M. Grätzel, P. Bäuerle, *J. Mater. Chem.* **2011**, *21*, 3726-3734.

[43] B. Chattopadhyay, C. I. Rivera Vera, S. Chuprakov, V. Gevorgyan, *Org. Lett.* **2010**, *12*, 2166-2169.

[44] S. Hu, Z. Zhang, Y. Zhou, B. Han, H. Fan, W. Li, J. Song, Y. Xiea, *Green Chem.* **2008**, 10, 1280-1283.

[45] R. Guo, X. Qi, H. Xiang, P. Geaneotes, R. Wang, P. Liu, Y.-M. Wang, *Angew. Chem. Int. Ed.* **2020**, *59*, 16651-16660.

[46] D. Jun, M. Paar, J. Binder, J. Marek, M. Pohanka, P. Stodulka, K. Kuca, Lett. Org. Chem. **2009**, *6*, 500-503.

[47] P. Bolduc, A. Jacques, S. K. Collins, *J. Am. Chem. Soc.* **2010**, *132*, 12790-12791

[48] (a) http://app.supramolecular.org/bindfit/; (b) P. Thordarson, *Chem. Soc. Rev.* **2011**, *40*, 1305-1323.

[49] N. Kishi, Z. Li, K. Yoza, M. Akita, M. Yoshizawa, *J. Am. Chem. Soc.* **2011**, *30*, 11438-11441.

[50] P. B. Fidelibus, G. F. Silbestri, M. T. Lockhart, S. D. Mandolesi, A. B. Chopa, J. C. Podesta, *Appl. Organometal. Chem.* **2007**, *21*, 682-687.

[51] D. G. Blackmond, *Angew. Chem. Int. Ed.* **2005**, *44*, 4302-4320.

[52] M. Peters, M. Trobe, R. Breinbauer, *Chem. Eur. J.* **2013**, *19*, 2450-2456.

[53] N. Kishi, Z. Li, K. Hasegawa, K. Yoza, M. Akita, M. Yoshizawa, *Chem. Commun.* **2011**, *47*, 8605-8607.

[54] J. Gràcia, M. A. Buil, J. Castro, P. Eichhorn, M. Ferrer, A. Gavaldà, B. Hernández, V. Segarra, M. D. Lehner, I. Moreno, L. Pagès, R. S. Roberts, J. Serrat, S. Sevilla, J. Taltavull, M. Andrés, J. Cabedo, D. Vilella, E. Calama, C. Carcasona, M. Miralpeix, *J. Med. Chem.* **2016**, *23*, 10479-10497.

[55] H. Li, B. Ma, Q-S. Liu, M-L. Wang, Z-Y. Wang, H. Xu, L-J. Li, X. Wang, H-X. Dai, *Angew. Chem. Int. Ed.* **2020**, *59*, 14388-14393.

[56] M. R. Smith III, R. E. Maleczka Jr, V. A. Kallepalli, E. Onyeozili. United states patent US7709654B2. **2007**.

Chapter 3. Understanding deactivation pathways in a supramolecular iridium catalyst leads to the outperformance of a meta-C-H borylation of pyridines

3.1. Introduction.

The efficient production of chemicals at will in a sustainable manner is of high interest for industrial and academic laboratories.[1] As such, the last century has witnessed tremendous efforts devoted to the development of catalytic technologies for such purposes.[2] In this context, homogeneous transition metal-catalyzed processes occupy a central place since the ease of ligand fine-tuning is advantageous to disclose new reactivity patterns.[3] Most of these transformations require the use of pre-activated coupling partners to selectively form new carbon-carbon or carbon-heteroatom bonds at specific positions at the expenses of generating substantial amounts of side-products including those from the pre-activation reactions as well.[4] In this regard, transition metal-catalyzed C-H bond functionalizations have revolutionized in the last decades the way to conceive organic synthesis by providing unprecedented chemical disconnections and novel bond-forming processes.[5] Currently, a myriad of methodologies exist for C-H bond functionalizations by means of transition metal catalysts.[6] However, most of them rely on the intrinsic reactivity of substrates to reach a precise C-H bond activation or by exploiting directing groups introduced in previous steps to the molecule of interest to bring the metal catalyst at close proximity to the C-H bond to be functionalized.[7] It is clear from a sustainable point of view, that the avoidance of directing groups for C-H bond functionalizations in unbiased substrates needs to be circumvented.[8]

From the many transition metal-catalyzed C-H functionalization strategies, metal-catalyzed C-H borylations are extremely appealing.[9] Indeed, the newly created C-B bond is a readily transformable moiety towards the formation of carbon-carbon and carbon-heteroatom bonds by using well-established methodologies.[10] Besides the use of rhodium,[11] platinum,[12] cobalt,[13] nickel[14] or lanthanide catalysts,[15] the iridium catalysts are exceptionally active enough to tackle the functionalization of C-H bonds belonging to highly inert aliphatic and aromatic fragments without the requirements to introduce directing groups in the substrates.[16] Consequently, the site-, regio- and enantio-selectivity of such reactions have been an important focus of research because the bond dissociation energies associated for discriminating those C-H bonds lie on a narrow range.[17] As pioneered by Hartwig and Ishiyama, the iridium-coordinated *N*,*N*-bipyridine frameworks appear to be the most powerful family of ligands for iridium-catalyzed C-H borylation reactions.[18] For instance, 4,4'-di-*tert*-butyl-2,2'-bipyridine (**dtbpy**) is considered the most suitable ligand for enabling the iridium-catalyzed borylation of aromatic as well as heteroaromatic C-H bonds using bis(pinacolato)diboron (B_2pin_2) as the borylating agent (**Figure 1A**).[19]

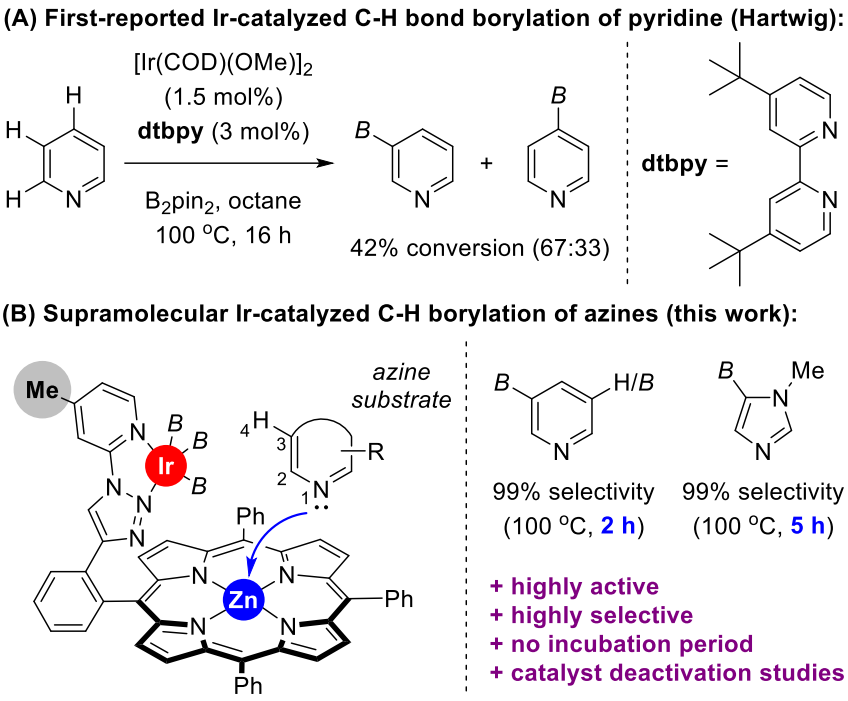

Figure 1. First-reported iridium-catalyzed C-H borylation of pyridine **(A)** and the supramolecular iridium-catalyzed borylation developed in this study **(B)**. *B* = (pinacolato)boron.

Recently, modified versions from the **dtbpy** ligand have been disclosed in order to reach unprecedented, remote regio- and site-selectivities by introducing in the secondary coordination sphere of the catalyst a variety of functional groups that enable molecular recognition with functional groups from the aromatic substrate *via* hydrogen bonding or ion pairing.[20]

In the case of nitrogen-containing heterocyclic substrates, the challenge is upgraded substantially since the nitrogen lone pair from these compounds can over-coordinate to the iridium catalyst, thus preventing productive borylation to occur.[21] Although powerful and selective C-H bond borylation of azines, typically pyridines, have been reported by the groups of Hartwig and Ishiyama,[22] Nakao,[23] Maleczka and Smith,[24] Marder and Steel,[25] ourselves,[26] and others,[27] extensive long reaction times are required (i.e. 12 to 72 hours). This is due to (1) the significant incubation period that the pre-catalyst needs in order to form the active iridium tris-boryl catalytic species[28] and (2) the mild reaction conditions (i.e. low temperature) that are required to avoid unselective transformations that would result in a mixture of borylated compounds or other side-products resulting from product decomposition.[29] Overall, increasing catalyst performance by reducing reaction time while keeping exquisite levels of selectivity remains a major breakthrough to be addressed in iridium-catalyzed C-H borylation of unbiased substrates. In the following, we present a supramolecular iridium catalyst that circumvents these above-stated limitations resulting in a highly productive and selective system for the C-H bond borylation of pyridines in unprecedented, short reaction times up to 2 hours (**Figure 1B**). The catalyst features a zinc-porphyrin molecular recognition site in the secondary coordination sphere and

it was selected after thorough experimentation to identify, and further avoidance of, catalyst deactivation pathways. In particular, we demonstrate that the pyridine substrates compete with (i) water, (ii) the methoxide ligand from the iridium precursor and (iii) the triazolopyridine fragment from the first coordination sphere of the catalyst, for binding to the molecular recognition pocket. By ligand fine-tuning and precise control of reaction conditions (presence of HBpin in catalytic amounts), we found that a 4-methyl-substituted pattern in the first coordination sphere of the catalyst outperforms existing state-of-the-art iridium catalysts for the selective C-H bond borylation of nitrogen-containing heterocycles (**Scheme 1B**). In addition, the catalyst design enables the C-H bond borylation at a precise distance of four chemical bonds apart from the molecular recognition site for the pyridine derivatives including an example of imidazole substrate.

3.2. Results and discussion.

3.2.1. Synthesis, characterization and supramolecular coordination chemistry studies of supramolecular ligands L1-L6.

Since the C-H bond activation event appears to be the rate-determining step for this type of catalysis according to computational calculations,[30] we anticipated that the fine-tuning at the first-coordination sphere around the iridium center could be beneficial in terms of reactivity. As such, we synthesized the supramolecular ligands **L1**-**L6** according to our preliminary findings,[26] in which a key alkylnyl-substituted zinc-porphyrin **1** is engaged in a copper-catalyzed click reaction with a 2-azido-substituted pyridine derivative (**Scheme 1**). In this manner, the supramolecular catalysts **L1**-**L6** featuring different electronic and steric patterns (H, 4-^{t}Bu, 4-Me, 6-Me, 4-OMe, 4-CF_3) in the pyridine ring that will be involved in the coordination to iridium were obtained and characterized by NMR spectroscopy as well as HRMS studies.[31]

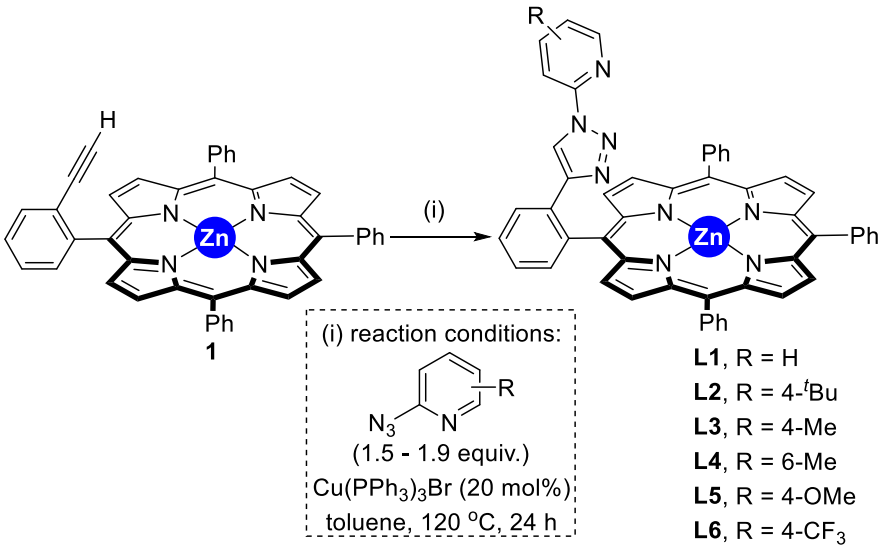

Scheme 1. Synthesis of the supramolecular ligands **L1**-**L6**.

Next, we evaluated the ability of these ligands to interact with pyridine derivatives *via* kinetically labile Zn···N non-covalent interactions.[32] ^{1}H NMR spectroscopy studies were performed combining equimolar amounts of unfunctionalized pyridine (**1a**) with each ligand **L1**-**L6**, respectively, in a $CDCl_3$ solution at room temperature (**Table 1**).[31]

Table 1. Chemical shifts (δ in ppm) corresponding to pyridine (**1a**) upon equimolar binding to the supramolecular ligands **L1**-**L6**.[a]

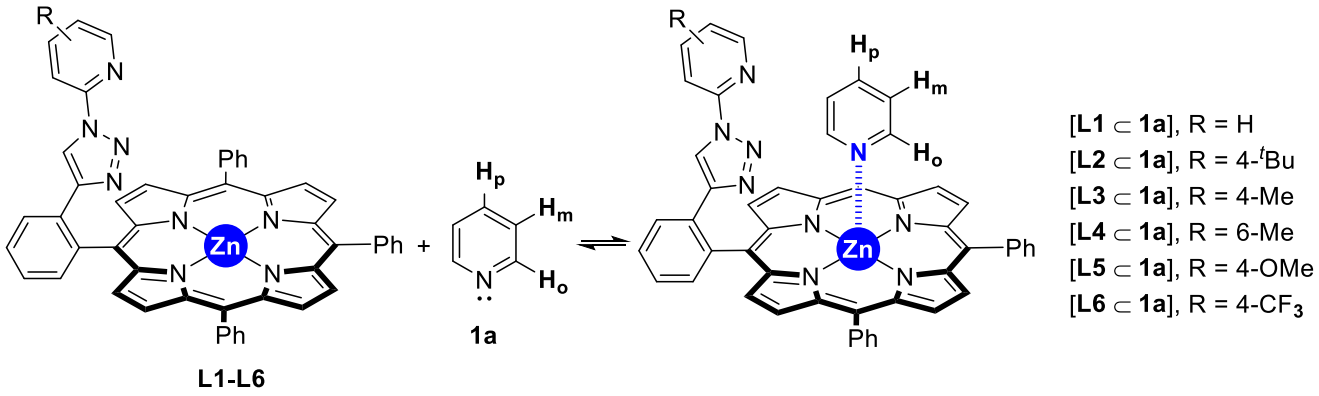

Compound	H_o (δ, ppm)	H_m (δ, ppm)	H_p (δ, ppm)
pyridine **(1a)**	8.56	7.60	7.22
[**L1** ⊂ **1a**]	4.15	5.86	6.51
[**L2** ⊂ **1a**]	4.3	5.93	6.58
[**L3** ⊂ **1a**]	4.8	6.08	6.71
[**L4** ⊂ **1a**]	4.6	6	6.63
[**L5** ⊂ **1a**]	4.79	6.1	6.75
[**L6** ⊂ **1a**]	4.82	6.11	6.74

[a] ^{1}H NMR spectroscopy experiments performed in $CDCl_3$ (400 MHz, 298 K).

A representative case is shown in **Figure 2** for the self-assembly of the bulkiest ligand (**L4**) with pyridine ([**L4** ⊂ **1a**]). In all cases, the three pyridine proton signals underwent remarkable up-filed shifts as shown in **Table 1**, indicating an interaction to the zinc-porphyrin core *via* apical Zn···N coordination (Experimental section, **Figures S1**-**S6**).

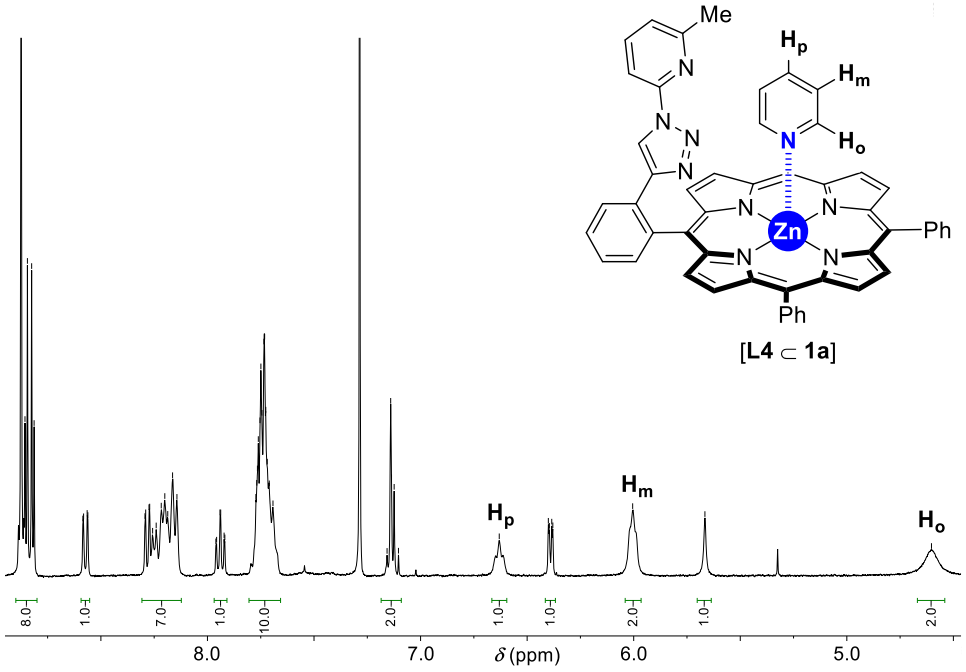

Figure 2. ^{1}H NMR spectrum ($CDCl_3$, 400 MHz) of the self-assembly [**L4** ⊂ **1a**] in an equimolar ratio.

The formation of a single species in solution points out that the binding of the pyridine is fast at the NMR timescale and it is in exchange between a coordination at the same face where the triazolopyridine ring lies and a coordination at the opposite face (top-bottom equilibria, **Scheme 2**).

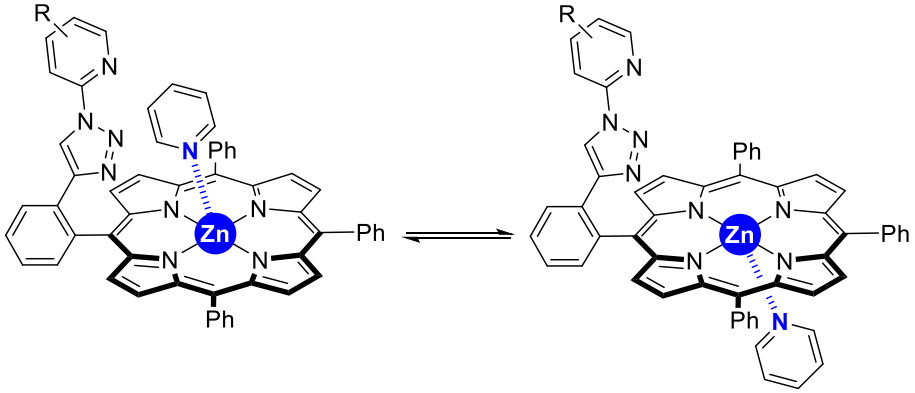

Scheme 2. Top-bottom side equilibria for the binding of pyridine to the supramolecular ligands.

According to previous observations by us and others,[26,32] the binding constant between these supramolecular ligands and pyridine is estimated in the rage of $K_{1.1}$ *ca.* 10^3-10^4 M^{-1}. In addition DOSY studies carried out with all supramolecular ligands **L1**-**L6**, respectively, in the presence of equimolar amounts of pyridine also strongly support the presence of supramolecular interaction as the diffusion coefficient of pyridine is greatly reduced in the presence of supramolecular ligand (Experimental section, **Figures S7**-**S13**).[31]

The molecular structure of **L1** was further confirmed by X-ray diffraction studies performed in single crystals obtained from a concentrated solution in undistilled 1,2-dichloroethane. The compound **L1** crystallizes with one water molecule binding to the zinc atom (**Figure 3**) which is further involved in an intramolecular hydrogen bonding with the nitrogen atom (N1) from the pyridine ring ($d_{O\text{-}H\cdots N1}$ = 2.006 Å) and in an intermolecular hydrogen bonding with a nitrogen atom (N4) from the triazole motif ($d_{O\text{-}H\cdots N4}$ = 2.155 Å). As such, it is clear that traces of water need to be avoided to further enhance the binding of pyridine to the zinc-porphyrin site, especially during the catalytic experiments that operate at high temperature (*vide infra*), thereby identifying the water binding to the molecular recognition site as an undesired deactivation pathway.[33]

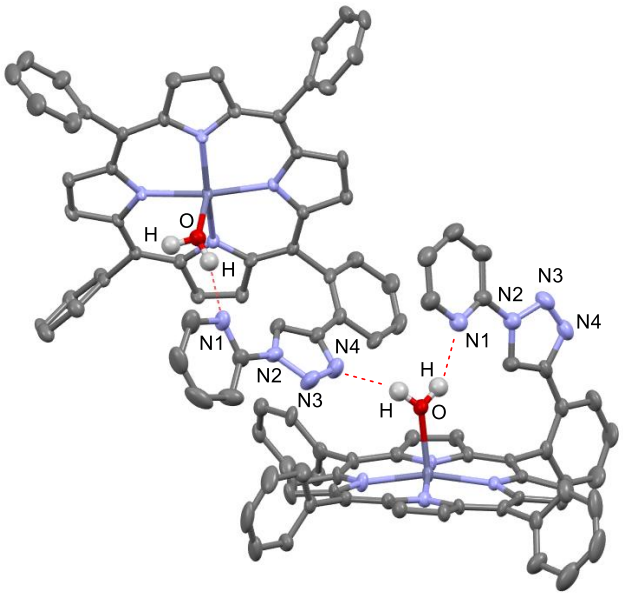

Figure 3. ORTEP of assembly [**L1** ⊂ **H_2O**] determined by single-crystal X-ray diffraction studies with thermal ellipsoids at 50% probability indicating hydrogen bonding in dashed lines (red). All hydrogen atoms except of those of water and 1,2-dichloroethane solvent molecules are omitted for clarity.

3.2.2. Assessment of the iridium precursor for the supramolecular meta-selective C-H borylation of pyridine.

A vast number of studies regarding iridium-catalyzed C-H borylation of unbiased and directing-group-free substrates have demonstrated the superior reactivity encountered when using $[Ir(COD)(OMe)]_2$ (COD = 1,5-cyclooctadiene) over $[Ir(COD)(Cl)]_2$ as the precursor for generating the active cationic iridium(I) species with *N*,*N*-chelating ligands derived from the 2,2'-bipyridine family.[18-25,27,28] The main reasons were ascribed to (1) the increased lability of the Ir-OMe bond with respect to the more thermodynamically stable Ir-Cl bond and (2) the formation of catalytically active iridium tris-boryl species in the presence of B_2pin_2 by release of MeO-Bpin side-product which is energetically more favorable than the corresponding Cl-Bpin countepart.[34] Alternatively, Colacot and co-workers demonstrated that $[Ir(COD)(Cl)]_2$ might be a suitable precursor in THF solvent as it generates a catalytically active iridium species that compare well with those derived from using $[Ir(COD)(OMe)]_2$.[35]

In our case, the catalysis was only effective in the presence of aromatic solvents (i.e. *p*-xylene or toluene) that solubilize well the supramolecular ligand.[26] Surprisingly, we noted that $[Ir(COD)(Cl)]_2$ precursor was more appropriate than $[Ir(COD)(OMe)]_2$ with our supramolecular ligands (**Table 2**). For instance, using the supramolecular ligand **L1** at **80** °C, the C-H borylation of pyridine (**1a**) was finished in 12 hours with a boost in reactivity that leads mainly to the bis-borylated product **2aa** with the $[Ir(COD)(Cl)]_2$ precursor (**Table 2**, entry 1), whereas the reaction with $[Ir(COD)(OMe)]_2$ precursor did not reach completion even after 24 hours affording a modest 73% conversion with major formation of the mono-borylated product **2a** (**Table 2**, entry 2). In both cases, the regio-selectivity was directed towards the *meta*-borylated products **2a** and **2aa** with undetectable formation of *para*- or *ortho*-isomers **3a** and **4a**, respectively (**Table 2**, entries 1-2). Clearly, in our case, the reactivity found in the presence of the supramolecular ligand **L1** for the $[Ir(COD)(Cl)]_2$ precursor is remarkable compared to the$[Ir(COD)(OMe)]_2$ precursor.

Table 2. Influence of the iridium precursor in the supramolecular *meta*-selective C-H borylation of pyridine.[a]

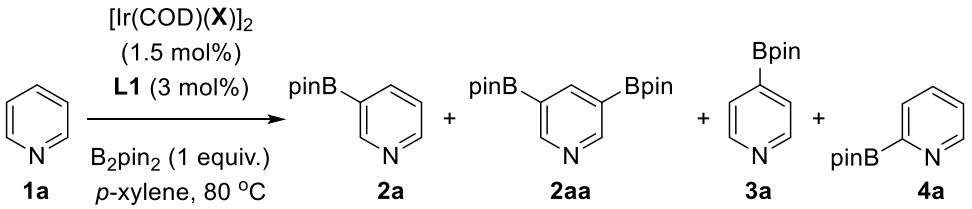

Entry	X	Time	Conv.[b]	2a : 2aa : 3a : 4a (%)[c]
1	Cl	12 h	>99 %	40 : 60 : 0 : 0
2	OMe	24 h	73 %	75 : 25 : 0: 0

[a] Reaction conditions: pyridine (0.162 mmol), B_2pin_2 (0.162 mmol), $[Ir(COD)(Cl)]_2$ (1.5 mol%), **L1** (3 mol%), *p*-xylene (1 mL), 80 °C. [b] Conversion determined as pyridine consumption. [c] Ratio of borylated products determined by ^{1}HNMR and GC using *n*-dodecane as internal standard.

In order to further understand such unexpected, reversed behavior when compared to literature precedents,[18-25,27,28,34,35] we designed a series of experiments to verify whether the anionic methoxide ligand from the iridium precursor $[Ir(COD)(OMe)]_2$ could bind to the zinc-porphyrin molecular recognition site via *via* Zn···O-Me interaction considering the known oxophilicity displayed by zinc-porphyrin derivatives,[36] thereby competing eventually with the pyridine substrate for the same binding site. The supramolecular ligand **L1** was treated with 0.5 equivalents of $[Ir(COD)(OMe)]_2$ at room temperature in a toluene-d_8 solution (similar solvent as used for the catalytic experiments) and the resulting ^{1}H NMR spectrum displayed a methoxide signal at δ = 2.14 ppm, which is up-field shifted when compared to the methoxide signal from the starting iridium precursor that resonates at δ = 3.12 ppm (Experimental section, Figures S14-S19).[31] In addition, whereas the carbon signal belonging to the methoxide ligand in the $[Ir(COD)(OMe)]_2$ precursor appears as a well-resolved singlet at δ = 56 ppm in its $^{13}C\{^1H\}$ NMR spectrum, in the case of combining $[Ir(COD)(OMe)]_2$ precursor with **L1**, the signal

belonging to the methoxide ligand was not detectable likely due to broadening (Experimental section, Figure S20).[31] Such methoxide effect was not observed when performing NMR experimentation with **dtbpy** and 0.5 equivalents of $[Ir(COD)(OMe)]_2$ (Experimental section, **Figure S21**).[31] For comparison purposes, **L1** was mixed with 1 equivalent of potassium *tert*-butoxide (sodium methoxide and potassium methoxide were poorly soluble in toluene solution) and its ^1H NMR spectrum displayed a similar trend as observed for the methoxide ligand: the singlet belonging to *tert*-butyl group was slightly up-field shifted ($\Delta\delta$ = 0.03 ppm) in the presence of **L1** (Experimental section, **Figures S22-S25**).[31] These observations indicate that the methoxide ligand is oxophilic enough for binding in a reversible manner to the zinc-porphyrin site from the supramolecular ligand **L1** *via* Zn···O-Me interaction (**Scheme 3**), thereby establishing the suitability of the, typically less employed, $[Ir(COD)(Cl)]_2$ as the ideal precursor for this particular supramolecular catalysis.[37]

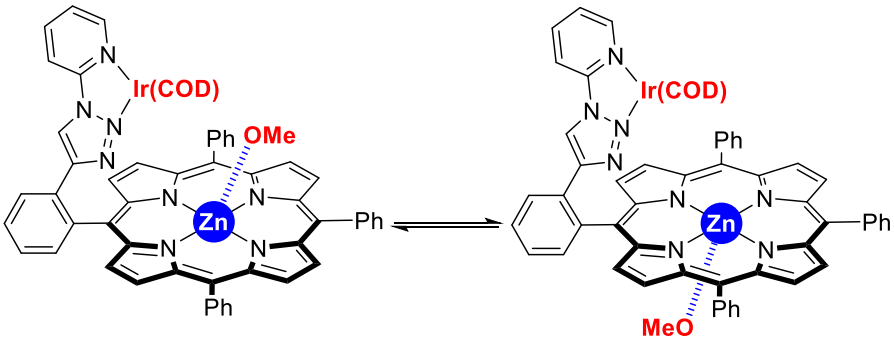

Scheme 3. Catalyst deactivation pathway *via* methoxide binding to the zinc-porphyrin site from supramolecular ligand **L1** in the presence of 0.5 equivalents of $[Ir(COD)(OMe)]_2$ precursor according to NMR spectroscopy studies.

3.2.3. Evidences for the involvement of the triazolopyridine fragment in a deactivation pathway.

As above-discussed in the introductory section of this contribution, **dtbpy** and their derivatives are prominently used as superior ligands for iridium-catalyzed borylations.[18-25,27,28] Consequently, the parent supramolecular version, namely **L2** (**Scheme 1**), which contains a *tert*-butyl group in *para* position of the triazolopyridine ring, was employed as a prospective ligand in the iridium-catalyzed C-H bond borylation of pyridine **1a** (**Table 3**). Unexpectedly, the catalysis was inefficient with a conversion of **1a** not exceeding 5% at 80 °C when employing **L2** (**Table 3**, entry 2), whereas the supramolecular ligand **L1** afforded full conversion (**Table 3**, entry 1). Even at high temperatures of 100 °C and 120 °C (**Table 3**, entries 3-4), the conversions of **1a** by using **L2** did not surpass 15% with a same *meta*-selectivity as observed for **L1**. There was no catalysis at room temperature with **L1** or **L2** (**Table 3**, entries 5-6). In addition, no C-H borylation occurs if the triazolopyridine fragment is not covalently-linked to the zinc-porphyrin scaffold.[26]

Table 3. Initial ligand assessment of the supramolecular iridium-catalyzed *meta*-selective C-H borylation of pyridine.[a]

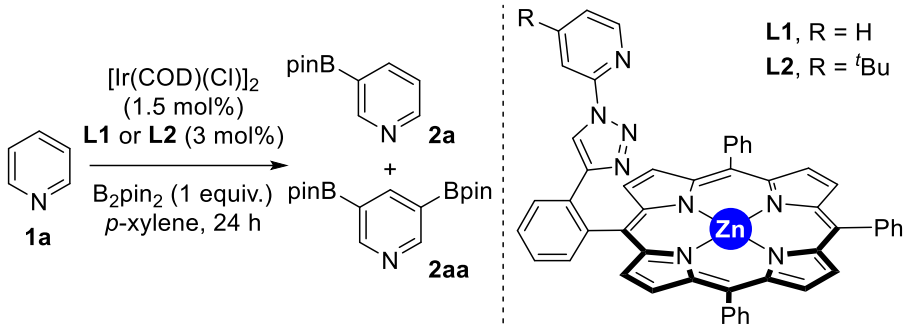

Entry	L	T (°C)	Conv.[b]	2a : 2aa (%)[c]
1	**L1**	80	>99 %	40 : 60
2	**L2**	80	5 %	100 : 0
3	**L2**	100	10 %	100 : 0
4	**L2**	120	15 %	100 : 0
5	**L1**	20	0 %	-
6	**L2**	20	0 %	-

[a] Reaction conditions: pyridine (0.162 mmol), B_2pin_2 (0.162 mmol), $[Ir(COD)(Cl)]_2$ (1.5 mol%), **L** (3 mol%), *p*-xylene (1 mL), 24 h. [b] Conversion determined as pyridine consumption. [c] Ratio of borylated products determined by ^{1}HNMR and GC using *n*-dodecane as internal standard.

Considering such contra-intuitive reactivity of **L1** and **L2**, together with the relatively short distance existing between the triazolopyridine fragment and the zinc-porpyrin site in the X-ray structure of [**L1** ⊂ **H_2O**] (*vide infra*), we decided to investigate the potential coordination of the triazolopyridine fragment to the zinc-porphyrin site as a catalyst deactivation pathway in this supramolecular catalysis. Such plausible event might be enhanced by the presence of a strong electro-donating substituent as it is the case for **L2**, which presents a *tert*-butyl group in *para* position of the iridium-coordinating pyridine ring. To this aim, ^{1}H NMR spectroscopy studies were performed in $CDCl_3$ at room temperature by combining equimolar amounts of zinc-tetraphenylporphyrin (**ZnTPP**) with triazolopyridine **L1*** and **L2*** (**Scheme 4**), respectively, which are the corresponding molecular components of the supramolecular ligands **L1** and **L2**.[31] In both cases, albeit small, significant up-field shifts were observed (0.04 ppm > Δ δ > 0.01 ppm) for the signals belonging to the triazole C-H proton (H_{tr}) and the *ortho*-pyridinic proton (H_{op}) from **L1*** and **L2***, respectively, upon interaction with **ZnTPP** (Experimental section, **Figures S26-S32**).[31] It is worthy to mention at this stage that five-membered ring azines are well-known to bind to zinc-porphyrins[26,38] whilst *ortho*-substituted pyridine derivatives exhibit negligible binding to zinc-porphyrins.[26,32,39] As such, it is reasonable to assume that the triazole unit is engaged in a kinetically labile Zn···N non-covalent interaction with **ZnTPP** (**Scheme 4**). In principle, both nitrogen atoms N3 and N4, (see atom numbering in **Figure 3**) can be involved in the reversible coordination to zinc (**Scheme 4**).

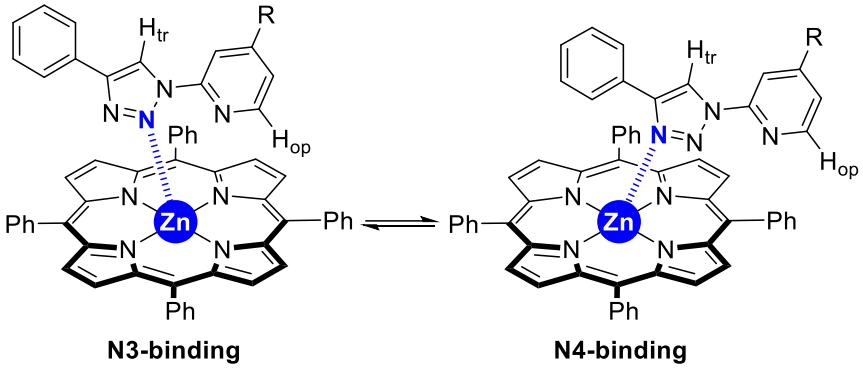

Scheme 4. Binding of triazolopyridine derivatives **L1*** (R = H) and **L2*** (R = ^{t}Bu) to unfunctionalized **ZnTPP** according to ^{1}H NMR spectroscopy studies.

The above-stated observations are in agreement with the triazolopyridine motif belonging to the supramolecular ligand binding to the zinc-porphyrin site *via* kinetically labile Zn···N non-covalent interaction, which is enhanced by the presence of an electron-donating group such as 4-*tert*-butyl in the supramolecular ligand **L2** (**Scheme 5**). CPK modelling and previous literature on zinc-porphyrins appended with triazole fragments in the *ortho*-position of the *meso*-substituted phenyl rings[40] further indicate that the triazolopyridine fragment from the supramolecular ligands is highly rigid and hardly flexible to enable intramolecular binding to zinc. This leads only to intermolecular binding as feasible with an equilibria involving four chemical species depending on the nitrogen atom that is involved in the binding to zinc as well as the top/bottom side-coordination (**Scheme 5**). The formation of higher oligomers or aggregates beyond dimers cannot be ruled out, but should be significantly less favored during the C-H bond borylation catalysis considering the low concentration of the catalyst in solution and the bulkiness of the substitution pattern in the triazolopyridine fragment (i.e. 4-*tert*-butyl group in **L2**). Moreover, it should be noted that the triazole protons (H_{tr}) from the supramolecular ligands resonate at high up-field shifts (δ = 5.28 ppm for **L2**) compared to the parent triazolopyiridine lacking a zinc-porphyrin ($\Delta\ \delta$ = 8.80 ppm for **L2***). Whether this is due to the zinc porphyrin current effect [40] or due to intermolecular binding as shown in **Scheme 5** or both effects simultaneously remains to be addressed and it is beyond the scope of the current contribution.

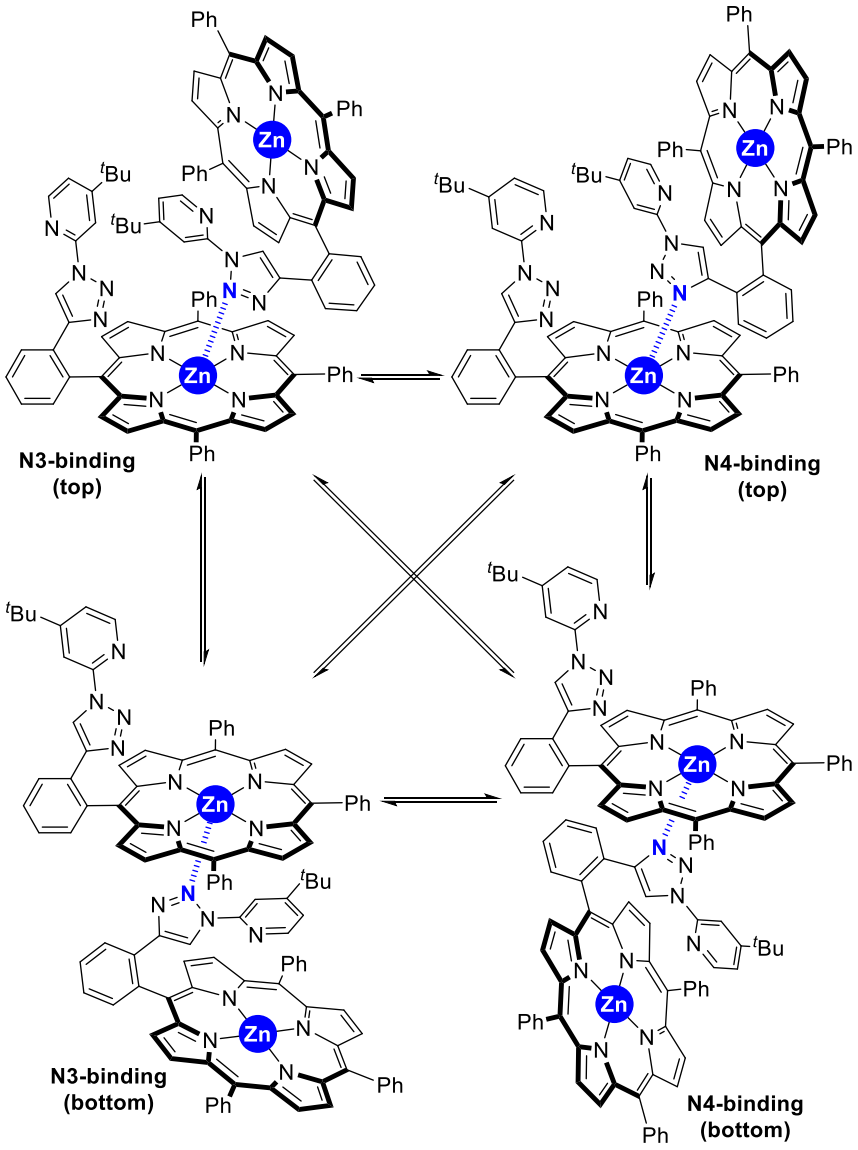

Scheme 5. Catalyst deactivation pathway *via* intermolecular binding of the triazolopyridine fragment to the zinc-porphyrin site from the supramolecular ligand **L2**.

3.2.4. Identification of the most reactive supramolecular catalyst and substrate evaluation.

Having established several experimentally-assessed deactivation pathways that need to be circumvented in order to reach a reactive system for this supramolecular catalysis, we evaluated the supramolecular ligands **L3**-**L6** in the iridium-catalyzed C-H borylation of pyridine (**1a**) with B_2pin_2 (**Table 4**). At 80 ^oC and using 3 mol% of the *in situ* formed supramolecular iridium catalyst during 24 hours, the *para*- and *ortho*-methyl-substituted supramolecular ligands **L3** and **L4** performed equally well (**Table 4**, entries 1-2) as the unfunctionalized supramolecular ligand **L1** (**Table 3**, entry 1) with full conversion of starting material and similar ratios of mono- and bis-borylated products resulting from *meta*-C-H bond selectivity. On the other hand, and as it could be expected for electron-donating groups placed in the triazolopyridine fragment such as **L2** (*vide supra*), **L5**, which contains 4-methoxy substituent in *para*-

position of the pyridine ring, enabled a modest 55% conversion of **1a** (**Table 4**, entry 3). The strong electron withdrawing trifluoromethoxy-substituted supramolecular ligand **L6** only converted 36% of the starting material (**Table 4**, entry 4). This is in agreement with the fact that the rate determining step of the iridium-catalyzed (hetero)aromatic C-H borylation with *N*,*N*-chelating type ligands is the oxidative addition of the C-H bond, largely favored by electron density enhancement on the iridium-coordinated ligand backbone.[17-19,30] Along these lines, raising the reaction temperature to 100 °C when employing the supramolecular ligands **L5** and **L6** led to full conversion of **1a** (**Table 4**, entries 5-6). The reactivity of the supramolecular ligands **L5** and **L6** is in stark contrast with that observed with the supramolecular ligand **L2** that does not lead to full conversion even at such high temperatures and beyond (*vide supra*). At full conversion, the ratio of mono- *versus* bis-borylation **2a**: **2aa** varied little (in the range 40 : 60 to 60 : 40) to establish any relevant trend between the supramolecular ligands **L1** (**Table 3**, entry 1) and **L3**-**L6** (**Table 4**, entries 1-2 and 5-6).

Table 4. Evaluation of the supramolecular ligands in the iridium-catalyzed *meta*-selective C-H borylation of pyridine.[a]

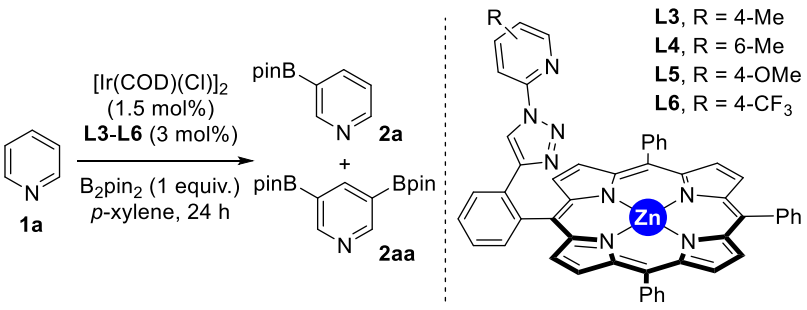

Entry	L	T (°C)	Conv.[b]	2a : 2aa (%)[c]
1	**L3**	80	>99 %	50 : 50
2	**L4**	80	>99 %	60 : 40
3	**L5**	80	55 %	84 : 16
4	**L6**	80	36 %	89 : 11
5	**L5**	100	>99 %	56 : 44
6	**L6**	100	>99 %	44 : 56

[a] Reaction conditions: pyridine (0.162 mmol), B_2pin_2 (0.162 mmol), $[Ir(COD)(Cl)]_2$ (1.5 mol%), **L** (3 mol%), *p*-xylene (1 mL), 24 h. [b] Conversion determined as pyridine consumption. [c] Ratio of borylated products determined by ^{1}HNMR and GC using *n*-dodecane as internal standard.

Remarkably, the regio-selectivity observed for the supramolecular iridium-catalyzed C-H bond borylation of the unfunctionalized pyridine **1a** was the same for any supramolecular ligand being tested. An excellent *meta*-selectivity (>99%) was obtained with no presence of the *ortho*- or *para*-borylated products. Consequently, the selectivity is determined exclusively by the high level of substrate pre-

organization taking place within the secondary coordination sphere in which the *meta*-C-H bond from pyridine is brought at very close proximity of iridium to undergo C-H bond cleavage regardless of the nature of the iridium-coordinated triazolopyridine fragment. However, the reactivity is clearly controlled by the first coordination sphere at iridium as observed by kinetic studies using the most promising supramolecular ligands **L1**, **L3** and **L4**. For this kinetic evaluation, 3-methylpyridine (**1b**) was selected as substrate of choice since it only provides a single product resulting from *meta*-C-H borylation, namely **2b** (**Figure 4**). The main difference between these supramolecular ligands is the length of the incubation period in order to form the catalytically active iridium species. At 80 °C, the unfunctionalized supramolecular ligand **L1** leads to a system in which the catalysis begins after 3 hours (red dashed line, **Figure 4**). This incubation period is reduced by more than half when using the methyl-substituted supramolecular ligands **L3** (1 hour incubation time, blue dashed line - **Figure 4**) and **L4** (1.5 hours incubation time, yellow dashed line - **Figure 4**). A superior reaction rate was found for the supramolecular ligand **L3** with almost full conversion reached in less than 6 hours (blue dashed line - **Figure 4**). The lower reaction rate found for the supramolecular ligand **L4** that contains an *ortho*-substituted methyl group in the triazolopyridine fragment indicates that the reactivity of the supramolecular catalyst is sensitive to steric effects at the first coordination sphere of the active iridium site.

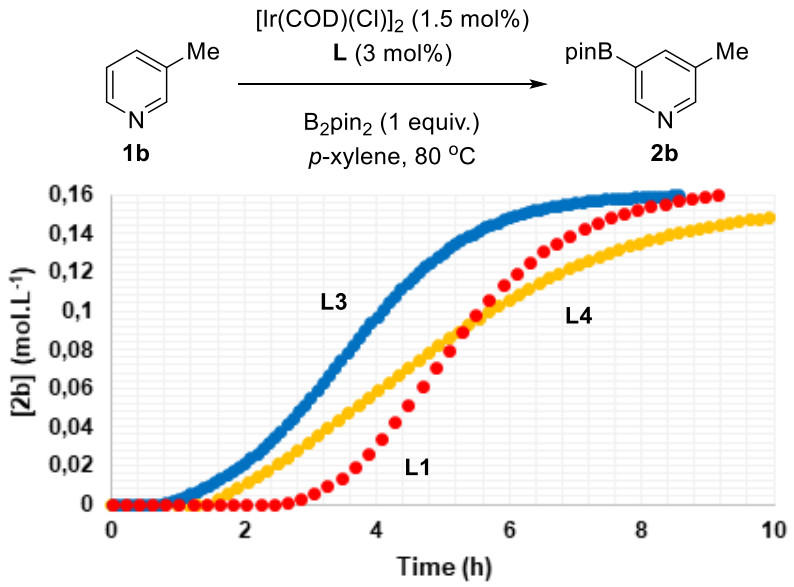

Figure 4. Kinetic evaluation (formation of product **2b** *versus* time) of the supramolecular ligands **L1** (red dashed line), **L3** (blue dashed line) and **L4** (yellow dashed line) in the iridium-catalyzed C-H borylation of 3-methylpyridine (**1b**).

Next, we envisioned the use of catalytic amounts of additives such as 2,6-lutidine and HBpin, respectively, because they are known to promote the formation of the catalytically active iridium tris-boryl species in some cases.[21a] The supramolecular ligand **L3**, which features a 4-methyl substitution pattern, was selected considering its higher performance over the other ligands and the iridium-

catalyzed C-H borylation of **1b** was monitored over time in the presence of catalytic amounts of each additive (**Figure 5**). Whereas the reaction in the presence of 2,6-lutidine (4 mol%) slowed down the reaction (red dashed line, **Figure 5**) compared to the catalysis performed in the absence of any additive (blue dashed line, **Figure 5**), the experiment in the presence of of HBpin (4 mol%) led to an almost negligible incubation period at 80 °C (green dashed line, **Figure 5**), which is so far unprecedented for iridium-catalyzed C-H borylation reactions. [17-28]

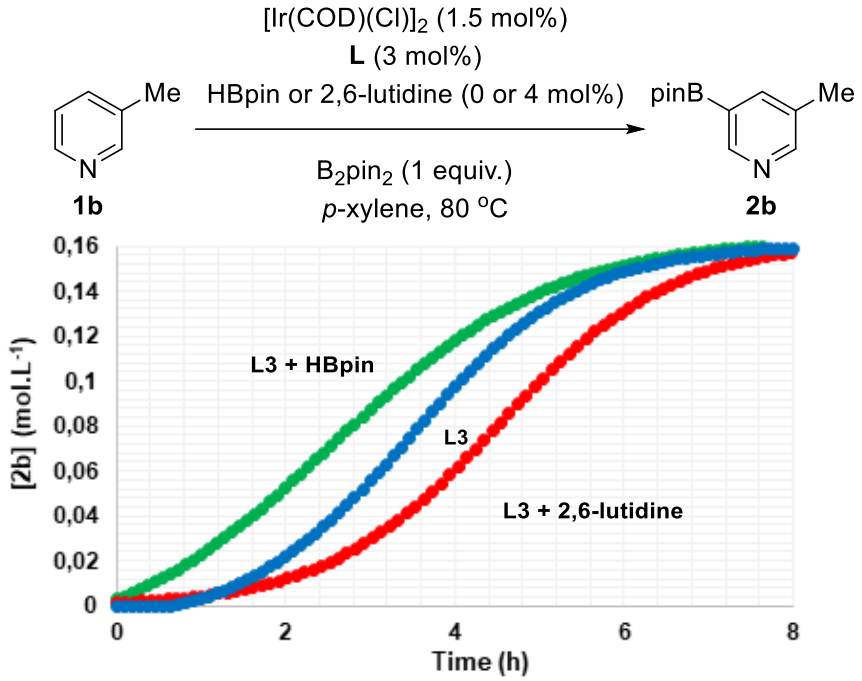

Figure 5. Kinetic evaluation (formation of product **2b** *versus* time) of the supramolecular ligand **L3** in the presence (HBpin -green dashed line-, 2,6-lutidine -red dashed line-) or absence of additive (blue dashed line) for the iridium-catalyzed C-H borylation of 3-methylpyridine (**1b**).

Importantly, it was possible to reduce the reaction time to only 2 hours with 99% formation of the *meta*-borylated product **2b** by increasing the reaction temperature to 100 °C in the presence of 4 mol% of HBpin and 3 mol% of the supramolecular iridium catalyst (**Scheme 6**).

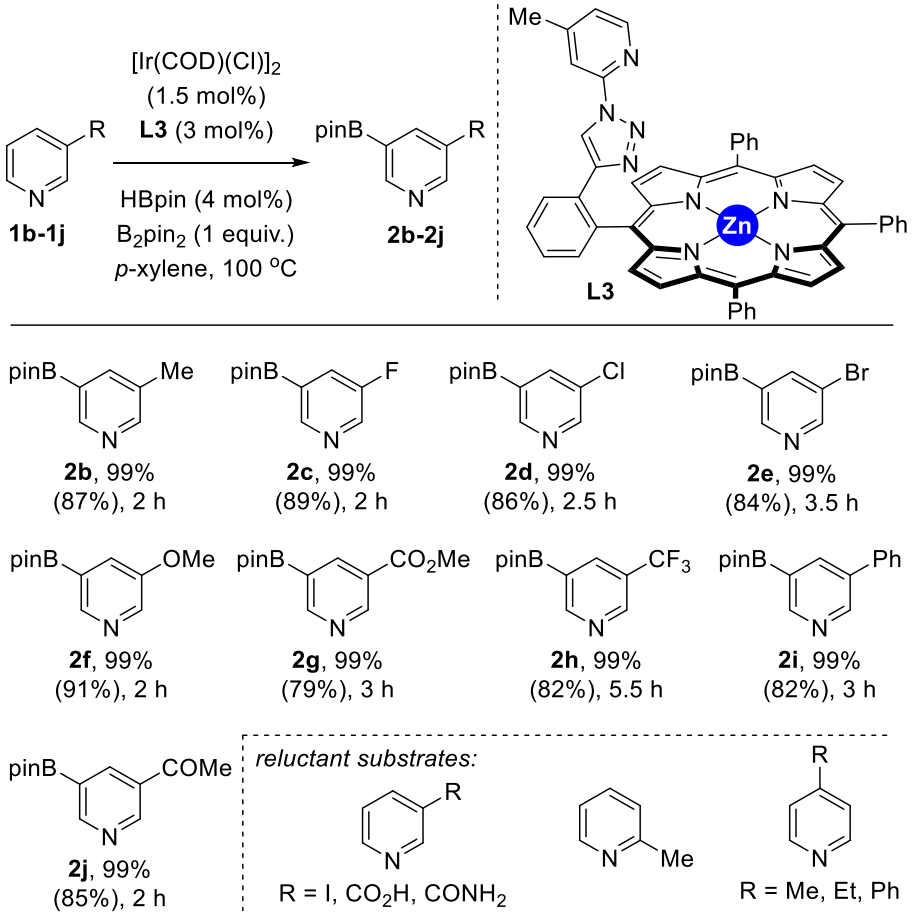

Scheme 6. Substrate evaluation for the supramolecular iridium-catalyzed C-H bond *meta*-borylation of pyridine derivatives using ligand **L3** (yields are determined by GC analysis and isolated yields are shown in brackets).[41]

Compared to our previously reported methodology,[26] the reaction time was notably reduced from 9 to 2 hours in the present case. Such observation was a general trend as regards of the substrate scope evaluation reported in **Scheme 6** with carefully optimized reaction time for each starting material. By using the optimal reaction conditions with **L3**, a variety of *meta*-substituted pyridine derivatives (**1b**-**1j**) with different steric and electronic properties selectively underwent iridium-catalyzed C-H bond borylation in very short reaction times (from 2 to 5.5 hours) affording the corresponding *meta*-borylated products **2b**-**2j** in excellent yields. For instance, the superb reactivity encountered for this supramolecular iridium catalyst was exemplified with the borylation of the methoxy-containing pyridine substrate **1f**. Whereas the previous methodology required 24 hours to get full conversion,[26] the present one affords the same selective product in only 2 hours. An even much clearer example concerns the fluorinated compound **2h**, which was obtained previously in a modest 50% yield in 24 hours,[26] whilst the current methodology affords it in 99% yield in less than 6 hours. Importantly, 3-phenylpyridine **1i** was selectively borylated at the heteroaromatic pyridine ring and not in the aromatic phenyl ring,

additionally supporting the fact that Zn···N non-covalent interactions are at play for controlling not only the regio-selectivity but also the site-selectivity of the supramolecular iridium-catalyzed C-H bond borylation. The highly selective formation of carbonyl-containing *meta*-borylated products **2g** and **2j** further indicates that the supramolecular catalysis is compatible with even potentially competing *ortho*-directing groups such as ketone and esters.[5-7] Limitations in the catalysis were encountered by using iodide, carboxylic acid and primary amide functional groups (**Scheme 6**). As shown previously for the supramolecular ligand **L1**,[26] the catalysis was sensitive to steric shields with a lack of reactivity found for *ortho*- and *para*-substituted pyridines (**Scheme 6**). At 120 °C, we noted that the iridium catalyst started to borylate the *p*-xylene solvent and the B_2pin_2 decomposed significantly under our reaction conditions. Other borylating reagents such as HBpin, bis(catecholato)diboron and bis(neopentyl glycolato)diboron were evaluated although leading to low levels of activity and selectivity when compared to B_2pin_2.[42]

In view to address the reactivity for other nitrogen-containing heterocycles, we turned our attention to imidazoles (**Scheme 7**).[43] The supramolecular iridium-catalyzed C-H borylation using ligand **L3** in the presence of B_2pin_2 and catalytic amounts of HBpin enabled the functionalization of *N*-methylimidazole (**1k**) in 5 hours at 100 °C leading selectively to **2k** in 99% selectivity and 90% isolated yield (**Scheme 7**).[31] Such reactivity strikingly contrasts with the previously reported methodology that required 24 hours of reaction time.[26] As it is the case for pyridine derivatives, the borylation in the imidazole backbone takes place in the C-H bond located at a distance of four chemical bonds from the substrate-recognition site of the catalyst. In addition, attempts to perform iridium-catalyzed C-H borylation with **1k** employing **dtbpy** ligand with or without **ZnTPP** instead of **L3** revealed unsuccessful under our reaction conditions (<10% conversion of **1k**).[31] Such observations indicate that the substrate pre-organization between the active site and the binding of the substrate to the molecular recognition site *via* kinetically labile Zn···N non-covalent interactions is mandatory to reach the observed activity and selectivity for the imidazole backbone. Note that functionalized *N*-H imidazole was unreactive for the supramolecular iridium-catalyzed C-H borylation.

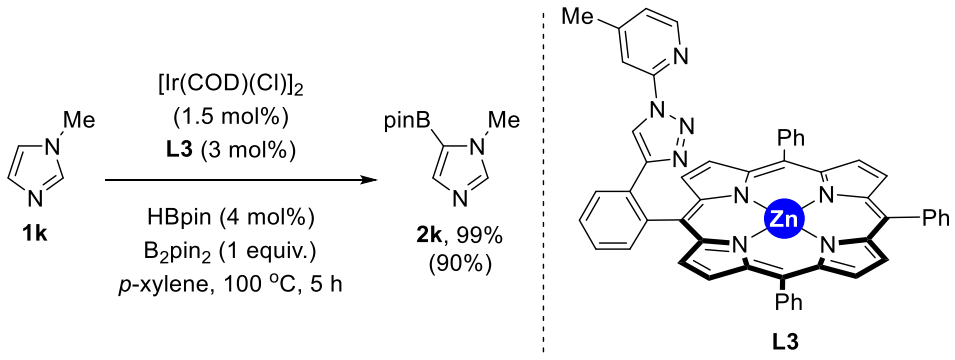

Scheme 7. Selective supramolecular iridium-catalyzed C-H bond borylation of *N*-methylimidazole **1k** using ligand **L3** (yield is determined by GC analysis and isolated yield is shown in brackets).[41]

3.3. Conclusion.

In summary, the overall reported data indicate that the supramolecular iridium catalyst formed when using ligand **L3** offers a suitable balance of steric and electronic effects in order to reach selective C-H bond borylations with pyridine derivatives, including an example of imidazole, while avoiding, to some extent, several catalyst deactivation pathways experimentally identified. Interestingly, in this supramolecular approach, the selectivity is well compatible with the reactivity at high temperatures and short reaction times.[44] The main reason is due to the identification of the distance between the active site and the substrate recognition site in the second coordination sphere of the catalyst as the exclusive parameter that determines the selectivity of the borylation reactions. On the other hand, the activity of the catalyst is strongly dependent by the first coordination sphere around iridium, which is upgraded by the use of catalytic amounts of HBpin as additive at 100 ^{o}C that further enables almost negligible incubation period for catalyst activation, which is so far unprecedented in iridium-catalyzed C-H bond borylation reactions. The supramolecular catalysis herein disclosed represents a unique example of extremely fast and selective C-H bond functionalizations by exploiting remote non-covalent interactions.[20] The benefits of exploiting kinetically labile non-covalent interactions between Lewis base-containing substrates and metalloporphyrins containing peripherally located active sites may give rise to new tools to control activity and selectivity in challenging transformations.[45] This contribution demonstrates the power of supramolecular catalysts featuring rationally-designed substrate-recognitions sites for the development of extremely active and selective catalytic systems.[46]

3.4. Experimental section.

3.4.1. General methods.

Solvents were purified with an MB SPS-800 purification system. Pyrrole was dried with CaH_2 and distilled prior to use. $CDCl_3$ was filtered through alumina and stored under argon over molecular sieves. All the other employed chemicals were purchased from commercial sources and used as received. Unless otherwise specified, all reactions were carried out under argon atmosphere by employing standard Schlenk and vacuum-line techniques. ^1H and ^{13}C NMR spectra were recorded with a Bruker GPX (400 MHz) spectrometer. ^1H NMR spectra were referenced to residual protiated solvent (δ = 7.26 ppm for $CDCl_3$). ^{13}C NMR spectra were referenced to $CDCl_3$ δ = 77.16 ppm). Abbreviations for signal couplings are: br, broad; s, singlet; d, doublet; t, triplet; m, multiplet; dd, doublet of doublets; dt, triplet of doublets; td, doublet of triplets; tt, triplet of triplets; tdd, doublet of doublet of triplets. Coupling constants, *J*, were reported in hertz unit (Hz). The reactions were monitored by using a Shimadzu 2014 gas chromatograph equipped with an EquityTM-1 Fused Silica capillary column (30 m x 0.25 mm x 0.25 □m) and an FID detector; conversion and selectivity were determined by using dodecane as internal standard. UV/Vis absorption spectra were recorded with a Specord 205 UV/Vis/NIR spectrophotometer and quartz cuvettes of 1 cm path length. Mass spectroscopy and microanalysis were performed in the laboratories of the Centre Regional de Mesures Physiques de l'Ouest (CRMPO, Université de Rennes 1, Rennes, France).

3.4.2. Synthesis and characterization of the ligands employed in this study.

The supramolecular ligands **L1-L6** were synthesized according to the **Scheme S1** shown below:

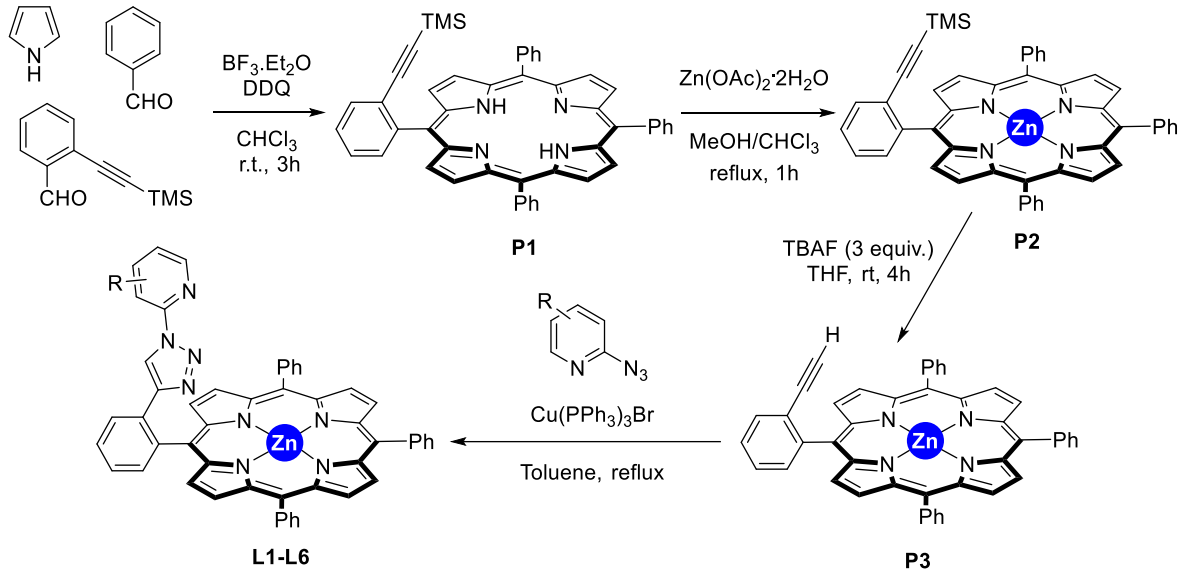

Scheme S1. Synthetic pathway towards supramolecular ligands **L1-L6**.

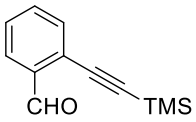

Synthesis and characterization of 2-((trimethylsilyl)ethynyl)benzaldehyde: 2-Bromobenzaldehyde (1.57 mL, 2.49 mg, 13.5 mmol, 1 equiv.) was introduced into a dried Schlenk tube equipped with a stirring bar along with $Pd(OAc)_2$ (0.037 mg, 0.14 mmol, 0,01 equiv.), CuI (0.0626 mg, 0.33 mmol, 0,025 equiv.) and PPh_3 (0.0909 mg, 0.29 mmol, 0,021 equiv.). Dry triethylamine (20 mL) was added to the reaction mixture and ethynyltrimethylsilane (2.2 mL, 1.56 mg, 16 mmol, 1,189 equiv.) was added slowly to the reaction mixture. The mixture was heated at 50 °C over 18 hours after which GC-MS analysis showed full conversion of the starting materials. The crude mixture was filtered over celite with dichloromethane and the solvents evaporated under reduced pressure. The titled compound was further purified by column chromatography (SiO_2, *n*-heptane:EtOAc, v/v 1:0 to 0:1) and isolated in 95% yield (2.6 g). ^{1}H NMR (400 MHz, $CDCl_3$): δ = 10.56 (1H, s), 7.91 (1H, d, *J* = 8.3 Hz), 7.59-7.52 (2H, m), 7.44 (1H, t, *J* = 7.8 Hz), 0.28 (9H, s) ppm. The spectral data match those found in literature.[47]

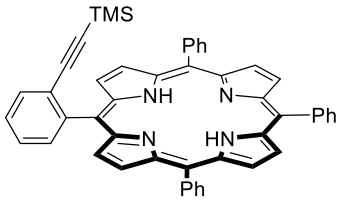

Synthesis and characterization of P1: Distilled chloroform (650 mL), distilled pyrrole (1.4 mL, 20.2 mmol, 4 equiv.), benzaldehyde (1.53 mL, 15 mmol, 3 equiv.) and 2-(trimethylsilyl)ethynyl)benzaldehyde (1.01 g, 5.0 mmol, 1 equiv.) were introduced into a 1 L round bottom flask equipped with a stirring bar under argon atmosphere. At room temperature and under light protection, $BF_3{\cdot}Et_2O$ (288 mg, 0.25 mL, 2.0 mmol, 0,4 equiv.) was added and the reaction was stirred for 3 hours. Then, DDQ (2.3 g, 10.0 mmol, 2 equiv.) was introduced and the reaction mixture was stirred for 1 hour before being quenched with Et_3N (0.282 µL). The solvent was evaporated and the crude mixture was purified by column chromatography (SiO_2, *n*-heptane:DCM,

v/v 9:1 to 6:4) affording **P1** as a purple powder (577 mg, 16% yield). ^{1}H NMR (400 MHz, $CDCl_3$): δ = 8.87-8.77 (8H, m, H_β), 8.23-8.13 (7H, m, $H_{meso\text{-}aryl}$), 7.9 (1H, dd, J = 7.6, 1.5 Hz, $H_{meso\text{-}aryl}$), 7.8-7.68 (11H, m, $H_{meso\text{-}aryl}$), -1.07 (9H, s), -2.73 (2H, s, $H_{pyrrole}$) ppm. $^{13}C\{^{1}H\}$ NMR (101 MHz, $CDCl_3$): δ = 144.88 (C_α), 142.32 (C_α), 134.84 ($C_{meso\text{-}aryl}$), 134.62 ($C_{meso\text{-}aryl}$), 134.52 ($C_{meso\text{-}aryl}$), 131.48 ($C_{meso\text{-}aryl}$), 128.06 (CH_β), 127.77 (CH_β), 127.75 (CH_β), 127.73 (CH_β),, 127.30 ($C_{meso\text{-}aryl}$), 126.89 ($C_{meso\text{-}aryl}$), 126.74 ($C_{meso\text{-}aryl}$), 126.72 ($C_{meso\text{-}aryl}$), 120.42 ($C_{meso\text{-}aryl}$), 120.22 ($C_{meso\text{-}aryl}$), 120.04 ($C_{meso\text{-}aryl}$), 118.21 ($C_{meso\text{-}aryl}$), 105.15 (CH_{alkyne}), 99.46(CH_{alkyne}), -1.23 (C_{TMS}) ppm. HRMS (ESI): *m/z* calcd for $C_{49}H_{39}N_4Si$ 711.2938 $[M+H]^+$; found: 711.2932 (1 ppm). The spectral data match those found in literature.[47]

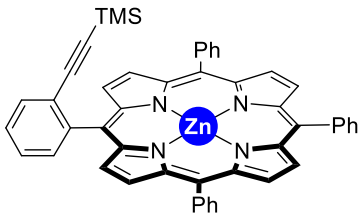

Synthesis and characterization of P2: Porphyrin **P1** (607 mg, 0.853 mmol, 1 equiv.) was introduced into a 250 mL round bottom flask equipped with a stirring bar and MeOH:$CHCl_3$ (100 mL, v/v 1:4). $Zn(OAc)_2{\cdot}2H_2O$ (0.603 mg, 2.75 mmol, 3.2 equiv.) was added and the reaction mixture was heated at reflux for 1 hour under air atmosphere. Back at room temperature, the solvents were removed under reduced pressure and the crude mixture was purified over alumina with DCM affording **P2** as a purple powder (660 mg, 99% yield). ^{1}H NMR (400 MHz, $CDCl_3$): δ = 8.95-8.86 (8H, m, H_β), 8.23-8.18 (7H, m, $H_{meso\text{-}aryl}$), 7.80-7.71 (11H, m, $H_{meso\text{-}aryl}$), 7.89 (1H, dd, J = 6.4, 2.7, $H_{meso\text{-}aryl}$), -1.14 (9H, s) ppm. $^{13}C\{^{1}H\}$ NMR (101 MHz, $CDCl_3$): δ = 150.69 (C_α), 150.38 (C_α), 150.36 (C_α), 150.07 (C_α), 145.67 ($C_{meso\text{-}aryl}$), 143.03 ($C_{meso\text{-}aryl}$), 143.01 ($C_{meso\text{-}aryl}$), 134.67 ($C_{meso\text{-}aryl}$), 134.55 ($C_{meso\text{-}aryl}$), 134.53 ($C_{meso\text{-}aryl}$), 134.50 ($C_{meso\text{-}aryl}$), 134.46 ($C_{meso\text{-}aryl}$), 132.30 (CH_β), 132.22 (CH_β), 132.18 (CH_β), 132.06 (CH_β), 132.03 (CH_β), 131.94 (CH_β), 131.42 (CH_β), 127.93 ($CH_{meso\text{-}aryl}$), 127.61 ($CH_{meso\text{-}aryl}$), 127.59 ($CH_{meso\text{-}aryl}$), 127.38 ($CH_{meso\text{-}aryl}$), 126.88 ($CH_{meso\text{-}aryl}$), 126.65 ($CH_{meso\text{-}aryl}$), 121.54 (C_{meso}), 121.16 (C_{meso}), 119.29 (C_{meso}), 105.52 (C_{alkyne}), 99.16 (C_{alkyne}), -1.11 (C_{TMS}) ppm. HRMS (ESI): *m/z* calcd for $C_{49}H_{36}N_4Si^{64}Zn$ 772.1995 $[M]^+$; found: 772.1993 (0 ppm). The spectral data match those found in literature.[47]

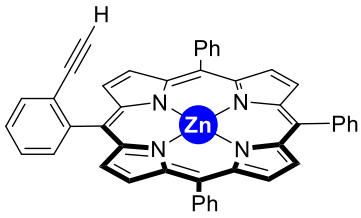

Synthesis and characterization of P3: Porphyrin **P2** (500 mg, 0.56 mmol, 1 equiv.) was introduced in a dried Schlenk tube charged with a stirring bar and dry THF (20 mL). At room temperature, a solution of 1M TBAF (0.56 mL, 1.94 mmol, 3 equiv.) in THF/water (v/v 95:5) was added dropwise and the mixture was stirred for 4 hours at rt under air atmosphere. Then, the mixture was evaporated to dryness and purified over neutral alumina using *n*-heptane:DCM (v/v 1:1) and afforded the analytically pure title porphyrin **P3** (431 mg, 95% yield). ^{1}H NMR (400 MHz, $CDCl_3$): δ = 8.95-8.82 (8H, m, H_β), 8.27-8.15 (7H, m, $H_{meso\text{-}aryl}$), 7.95 (1H, d, J = 8 Hz, $H_{meso\text{-}aryl}$), 7.76 (11H, m, $H_{meso\text{-}aryl}$), 2.12 (1H, s) ppm. $^{13}C\{^{1}H\}$ NMR (101 MHz, $CDCl_3$): δ = 150.29 (C_α), 150.21 (C_α), 150.18(C_α), 150.05 (C_α), 145.50 ($C_{meso\text{-}aryl}$), 142.83 ($C_{meso\text{-}aryl}$), 142.78 ($C_{meso\text{-}aryl}$), 134.48 ($CH_{meso\text{-}aryl}$), 134.45 ($CH_{meso\text{-}aryl}$), 134.37 ($CH_{meso\text{-}aryl}$), 134.23 ($CH_{meso\text{-}aryl}$),132.33 (CH_β), 131.99 (CH_β), 131.90 (CH_β), 131.47 (CH_β), 127.97 ($CH_{meso\text{-}aryl}$), 127.51 ($CH_{meso\text{-}aryl}$), 127.49 ($CH_{meso\text{-}aryl}$), 126.94 ($CH_{meso\text{-}aryl}$), 126.54 ($CH_{meso\text{-}aryl}$), 125.79 ($C_{meso\text{-}aryl}$), 121.44 (C_{meso}), 121.10 (C_{meso}), 118.63 (C_{meso}), 83.24 (C_{alkyne}), 80.95 (CH_{alkyne}) ppm. HRMS (ESI): *m/z* calcd for $C_{46}H_{28}N_4{}^{64}Zn$ 700.1599 $[M]^+$; found: 700.1600 (0 ppm). The spectral data match those found in literature.[47]

Synthesis and characterization of azidopyridines AP:

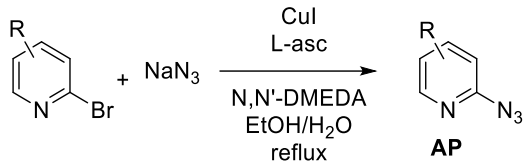

General procedure for the synthesis of 2-azidopyridine AP: In a two-necked dried round bottom flask, 2-bromopyridine derivative (1 equiv.), sodium azide (2 equiv.), CuI (0.1 equiv.), sodium ascorbate (0.05 equiv) and N,N'-dimethylethylenediamine (0.15 equiv.) were dissolved in a mixture of EtOH:H_2O (v/v 7:3). The reaction mixture was stirred for 2 hours at reflux under air atmosphere. Then, the mixture was evaporated to dryness. A mixture of EtOAc and H_2O were added and the aqueous layer was extracted with EtOAc three times. Then the combined organic layers were washed with water two times and once with brine solution. After drying over $MgSO_4$ and filtration, the solvents were evaporated under reduced pressure. If needed, the product was further purified by column chromatography (SiO_2, *n*-heptane:EtOAc).

Important Note: Azide are sensitive compound that are prone to explosion or decomposition under harsh conditions (high temperature, low pressure…). Careful attention should be taken to prevent any unwanted reactivity as well as safety incident. In the same regard, quenching the remaining aqueous sodium azide at the end of reaction should be carried out for safety and toxicity reason.

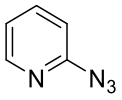

Synthesis and characterization of 2-azidopyridine (AP1): According to the general procedure, 2-bromopyridine (1.23 mL, 2.06 g, 13 mmol, 1 equiv.), sodium azide (1.696 g, 26 mmol, 2 equiv.), CuI (0.247 g, 1.3 mmol, 0,1 equiv.), sodium ascorbate (0.147 g, 0.7 mmol, 0,05 equiv.) and N,N'-dimethylethylenediamine (0.21 mL, 0.172 g, 1.95 mmol, 0.15 equiv.) were dissolved in a mixture of EtOH:H_2O (60 mL, v/v 7:3). The final product was isolated as an analytically pure white powder (1.1 g, 70% yield). ^{1}H NMR (400 MHz, $CDCl_3$): δ = 8.84 (1H, d, *J* = 6.9 Hz, H_o), 8.07 (1H, d, *J* = 9Hz, H_m), 7.71-7.66 (1H, ddd, *J* = 9.0, 6.8, 1.0 Hz, H_p), 7.25 (1H, dt, *J* = 9.0, 6.9 Hz, H_m) ppm. The spectral data matchthose found in literature.[48]

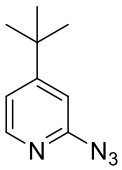

Synthesis and characterization of 2-azido-4-*tert*-butylpyridine (AP2): According to the general procedure, 2-bromo-4-*tert*-butylypyridine (0,417 mL, 0.539 g, 2.66 mmol, 1 equiv.), sodium azide (0.345 g, 5.32 mmol, 2 equiv.), CuI (0.050 g, 0.27 mmol, 0.1 equiv.), sodium ascorbate (0.026 g, 0.13 mmol, 0.05 equiv.) and N,N'-dimethylethylenediamine (0.04 mL, 0.033 g, 0.40 mmol, 0.15 equiv.) were dissolved in a mixture of EtOH:H_2O (12 mL, v/v 7:3). The final product was isolated as an analytically pure white powder (0.410 g, 90% yield). ^{1}H NMR (400 MHz, $CDCl_3$): δ = 8.72 (dd, *J* = 7.3, 1.0 Hz, 1H), 7.90 (dd, *J* = 1.8, 1.0 Hz, 1H), 7.27 (dd, *J* = 7.3, 1.8 Hz, 1H), 1.41 (s, 9H) ppm. $^{13}C\{^1H\}$ NMR (101 MHz, $CDCl_3$): δ = 156.67, 149.02, 124.34, 116.14, 110.19, 35.64, 30.27 ppm. HRMS (ESI, MeOH/DCM : 95/5): m/z calcd for $C_9H_{12}N_4$: 199.09542 $[M+Na]^+$; found: 199.0954 (0 ppm).

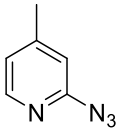

Synthesis and characterization of 2-azido-4-methylpyridine (AP3): According to the general procedure, 2-bromo-4-methylpyridine (0.314 mL, 0.485 g, 2.66 mmol, 1equiv.), sodium azide (0.345 g, 5.32 mmol, 2 equiv.), CuI (0.050 g, 0.27 mmol, 0.1 equiv.), sodium ascorbate (0.026 g, 0.13 mmol, 0.05 equiv.) and N,N'-dimethylethylenediamine (0.04 mL, 0.033 g, 0.40 mmol, 0.15 equiv.) were dissolved in a mixture of EtOH:H_2O (12 mL, v/v 7:3). The final product was isolated as an analytically pure white powder (0.362 g, 85% yield). ^{1}H NMR (400 MHz, $CDCl_3$): δ = 8.69 (d, *J* = 7.0 Hz,

1H), 7.77 (dd, *J* = 1.4, 1.1 Hz 1H), 7.03 (dd, *J* = 7.1, 1.4 Hz, 1H), 2.56 (d, *J* = 1.1 Hz, 3H) ppm. $^{13}C\{^{1}H\}$ NMR (101 MHz, $CDCl_3$): δ = 143.66, 135.50, 124.31, 119.21, 113.96, 21.68 ppm. HRMS (ESI, MeOH/DCM: 95/5): m/z calcd for $C_6H_6N_4$: 157.04847 $[M+Na]^+$; found: 157.0486 (1 ppm).

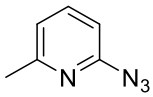

Synthesis and characterization of 2-azido-6-methylpyridine (AP4): According to the general procedure, 2-bromo-6-methylpyridine (0.321 mL, 0.485 g, 2.66 mmol, 1 equiv.), sodium azide (0.345 g, 5.32 mmol, 2 equiv.), CuI (0.050 g, 0.27 mmol, 0.1 equiv.), sodium ascorbate (0.026 g, 0.13 mmol, 0.05 equiv.) and N,N'-dimethylethylenediamine (0.04 mL, 0.033 g, 0.40 mmol, 0.15 equiv.) were dissolved in a mixture of EtOH:H_2O (12 mL, v/v 7:3). The final product was isolated as an analytically pure white powder (370 mg, 88% yield). ^{1}H NMR (400 MHz, $CDCl_3$): δ = 7.91 (dt, *J* = 9.1, 1.0 Hz, 1H), 7.60 (dd, *J* = 9.0, 6.8 Hz, 1H), 7.00 (dt, *J* = 6.8, 1.0 Hz, 1H), 2.95 (t, *J* = 1.0 Hz, 3H) ppm. $^{13}C\{^{1}H\}$ NMR (101 MHz, $CDCl_3$): δ = 152.65, 136.79, 131.74, 115.24, 113.11, 17.40 ppm. HRMS (ESI, DCM): m/z calcd for $C_6H_7N_4$: 135.06652 $[M+H]^+$; found: 135.0664 (1 ppm). The spectral data match those found in literature.[49]

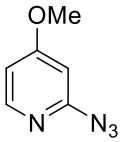

Synthesis and characterization of 2-azido-4-methoxylpyridine (AP5): According to the general procedure, 2-bromo-4-methoxypyridine (0.324 mL, 0.500 g, 2.66 mmol, 1 equiv.), sodium azide (0.345 g, 5.32 mmol, 2 equiv.), CuI (0.050 g, 0.27 mmol, 0.1 equiv.), sodium ascorbate (0.026 g, 0.13 mmol, 0.05 equiv.) and N,N'-dimethylethylenediamine (0.04 mL, 0.033 g, 0.40 mmol, 0.15 equiv.) were dissolved in a mixture of EtOH:H_2O (12 mL, v/v 7:3). The final product was isolated as an analytically pure white powder (0.390 g, 90% yield). ^{1}H NMR (400 MHz, $CDCl_3$): δ = 8.61 (dd, *J* = 7.5, 0.6 Hz, 1H), 7.16 (d, *J* = 2.4 Hz, 1H), 6.86 (dd, *J* = 7.5, 2.4 Hz, 1H), 3.97 (s, 3H) ppm. $^{13}C\{^{1}H\}$ NMR (101 MHz, $CDCl_3$): δ = 162.30, 150.44, 125.37, 111.95, 91.78, 56.38 ppm. HRMS (ESI, MeOH/DCM : 90/10): m/z calcd for $C_6H_6N_4O$: 173.04338 $[M+Na]^+$; found: 173.0435 (1 ppm).The spectral data match those found in literature.[50]

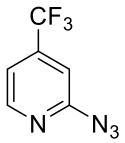

Synthesis and characterization of 2-azido-4-trifluoromethylpyridine (AP6): According to the general procedure, 2-bromo-4-trifluoromethylpyridine (0.255 mL, 0.465 g, 2.66 mmol, 1 equiv.), sodium azide (0.345 g, 5.32 mmol, 2 equiv.), CuI (0.050 g, 0.27 mmol, 0.1 equiv.), sodium ascorbate (0.026 g, 0.13 mmol, 0.05 equiv.) and N,N'-dimethylethylenediamine (0.04 mL, 0.033 g, 0.40 mmol, 0.15 equiv.) were dissolved in a mixture of EtOH:H_2O (12 mL, v/v 7:3). The reaction mixture was stirred at reflux for 45 minutes. It is important to note that longer reaction time induce partial to full decomposition of the expected product. The final product was isolated as an analytically pure white powder (0.320 mg, 56% yield). ^{1}H NMR (400 MHz, $CDCl_3$): δ = 9.00 (d, *J* = 7.2 Hz, 1H), 8.37 (d, *J* = 1.7 Hz, 1H), 7.43 (dd, *J* = 7.2, 1.7 Hz, 1H) ppm. $^{13}C\{^{1}H\}$ NMR (101 MHz, $CDCl_3$): δ = 147.84, 134.27 (q, *J* = 35.2 Hz), 126.85, 121.93 (d, *J* = 273.5 Hz), 114.42 (q, *J* = 4.8 Hz), 112.79 (q, *J* = 2.8 Hz) ppm. ^{19}F NMR (376 MHz, $CDCl_3$): δ = -64.30 (s) ppm. HRMS (ESI, DCM): m/z calcd for $C_6H_3N_4F_3$: 211.0202 $[M+Na]^+$; found: 211.0203 (0 ppm).

Synthesis and characterization of the triazolopyridine supramolecular ligands L1-L6:

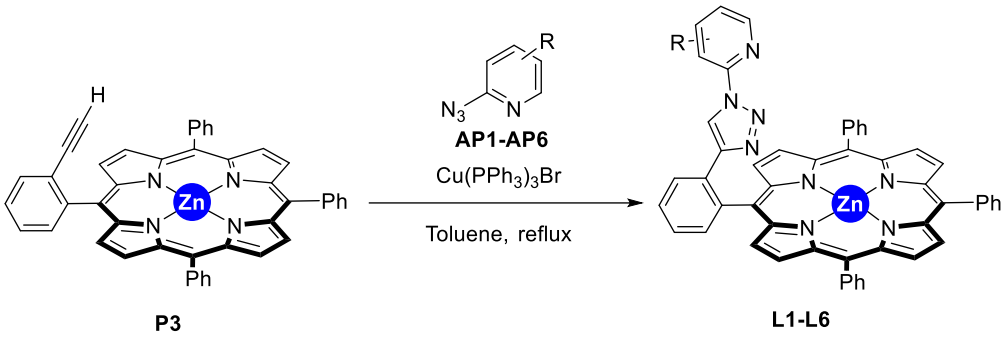

General procedure for the synthesis of the supramolecular ligands L1-L6: Into a dried Schlenk tube charged with a stirring bar, **P3** (1 equiv.), azidopyridine **AP1**-**AP6** (1.5 to 1.9 equiv.), $Cu(PPh_3)_3Br$ (0.2 equiv.) and dry toluene were added. The reaction mixture was stirred for 24 hours at 120 °C. Back at room temperature, the solvents were evaporated and the crude mixture was purified by column chromatography (SiO_2, *n*-heptane:DCM) affording the supramolecular Ligands **L1-L6** as a purple powder.

Important note: If azidopyridines **AP1**-**AP6** did co-eluate with the products **L1**-**L6** (identified by NMR), the supramolecular ligand was further purified by column chromatography (neutral Al_2O_3, n-heptane:DCM, v/v 1:0 to 0:1) affording the supramolecular ligand as a pure purple powder. Alternatively, Kuegelrorh distillation is also suitable to remove traces of contaminating azidopyridines **AP1**-**AP6**.

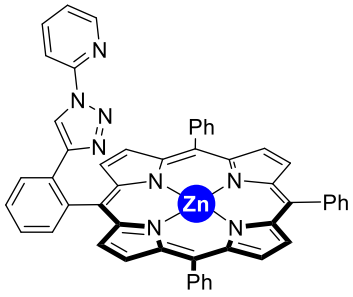

Synthesis and characterization of supramolecular ligand L1: According to the general procedure, **P3** (0.220 g, 0.31 mmol, 1 equiv.), 2-azidopyridine **AP1** (0,070 g, 0.58 mmol, 1.9 equiv.), $Cu(PPh_3)_3Br$ (0.069 g, 0.074 mmol, 0.2 equiv.) and dry toluene (15 mL) were added and the reaction mixture was stirred for 24 hours at 120 °C. Back at room temperature, the solvents were evaporated and the crude mixture was purified by column chromatography (SiO_2, *n*-heptane:DCM, v/v 1:0 to 0:1) affording analytically pure **L1** (0.254 g, 57% yield). ^1H NMR (400 MHz, $CDCl_3$): δ = 8.92-8.80 (8H, m, H_β), 8.74 (1H, d, J = 7.6 Hz, $H_{meso\text{-}aryl}$), 8.26-8.14 (7H, m, $H_{meso\text{-}aryl}$), 7.94 (1H, t, J = 8.3 Hz, $H_{meso\text{-}aryl}$), 7.77-7.67 (10H, m, Hmeso aryl), 7.59 (1H, d, J = 8.3 Hz, $H_{meso\text{-}aryl}$), 7.36 (1H, td, J = 8.1, 1.7 Hz, $H_{meso\text{-}aryl}$), 6.82 (1H, d, J = 5.0 Hz, $H_{meso\text{-}aryl}$), 6.58 (1H, m, $H_{meso\text{-}aryl}$), 5.41 (1H, s) ppm. $^{13}C\ \{^1H\}$ NMR (101 MHz, $CDCl_3$): δ = 150.51 (C_α), 150.47 (C_α), 150.26 (C_α), 148.23 (C_{pyr}), 147.52 (CH_{pyr}), 147.43 (C_{triaz}), 142.95 ($C_{meso\text{-}aryl}$), 142.83 ($C_{meso\text{-}aryl}$), 140.43 ($C_{meso\text{-}aryl}$), 138.28 (CH_{pyr}), 135.38 ($CH_{meso\text{-}aryl}$), 134.65 ($CH_{meso\text{-}aryl}$), 134.58 ($CH_{meso\text{-}aryl}$), 134.52 ($CH_{meso\text{-}aryl}$), 132.85 (CH_β), 132.72 ($C_{meso\text{-}aryl}$), 132.16 (CH_β), 131.54 (CH_β), 128.80 ($CH_{meso\text{-}aryl}$), 127.91 ($CH_{meso\text{-}aryl}$), 127.69 ($CH_{meso\text{-}aryl}$), 127.66 ($CH_{meso\text{-}aryl}$), 126.83-125.99 (m, $CH_{meso\text{-}aryl}$), 122.60 (CH_{pyr}), 121.56 (C_{meso}), 121.37 (C_{meso}), 119.03 (C_{meso}), 118.66 (CH_{triaz}), 113.38 (CH_{pyr}) ppm. HRMS (ESI): *m/z* calcd for $C_{51}H_{32}N_8{}^{64}Zn$ 820.2036 $[M]^+$; found: 820.2035 (0 ppm). The spectral data match those found in literature.[47]

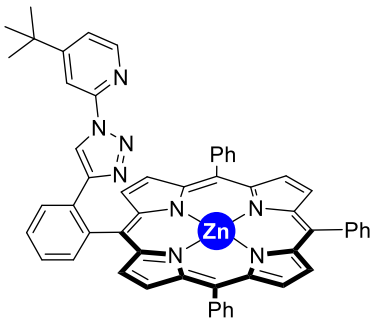

Synthesis and characterization of supramolecular ligand L2: According to the general procedure, **P3** (0.320 g, 0.5 mmol, 1equiv.) 2-azido-4-*tert*-butylpyridine **AP2** (0.140 g, 0.75 mmol, 1.5 equiv.), $Cu(PPh_3)_3Br$ (0.106 mg, 0.2 mmol, 0.2 equiv.) and dry toluene (20 mL) were added and the reaction mixture was stirred for 24 hours at 120 °C. Back at room temperature, the solvents were evaporated and the crude mixture was purified by column chromatography (SiO_2, *n*-heptane:DCM, v/v 1:0 to 2:8) affording analytically pure **L2** (0.203 g, 54% yield.). ^{1}H NMR (400 MHz, $CDCl_3$): δ = 8.94-8.89 (AB, 4H, *J* = 6.8 Hz, H_β), 8.85-8.77 (AB, 4H, *J* = 18.2 Hz, H_β), 8.70 (d, *J* = 8.1 Hz, 1H, $H_{meso\text{-}aryl}$), 8.27 (dd, *J* = 6.2, 2.3 Hz, 1H, $H_{meso\text{-}aryl}$), 8.24-8.19 (m, 4H, $H_{meso\text{-}aryl}$), 8.18-8.11 (m, 2H, $H_{meso\text{-}aryl}$), 7.94 (td, *J* = 7.7, 1.4 Hz, 1H, $H_{meso\text{-}aryl}$), 7.81-7.65 (m, 10H, $H_{meso\text{-}aryl}$), 7.54 (d, *J* = 1.7 Hz, 1H, $H_{pyridine}$), 6.64 (d, *J* = 5.5 Hz, 1H, $H_{pyridine}$), 6.53 (dd, *J* = 5.5, 1.7 Hz, 1H, $H_{pyridine}$), 5.28 (s, 1H, $H_{triazole}$), 0.97 (s, 9H H_{tBu}) ppm. $^{13}C\{^1H\}$ NMR (101 MHz, $CDCl_3$): δ = 163.74 ($C_{triazole}$), 150.26 (C_α), 150.08 (C_α), 149.82 (C_α), 148.00 (C_α), 147.43 ($C_{pyridine}$), 146.54 ($C_{pyridine}$), 143.07 ($C_{meso\text{-}aryl}$), 142.91 ($C_{meso\text{-}aryl}$), 140.51 ($CH_{pyridine}$), 134.68 ($C_{meso\text{-}aryl}$), 134.59 ($C_{meso\text{-}aryl}$), 134.55 ($C_{meso\text{-}aryl}$), 134.40 ($C_{meso\text{-}aryl}$), 134.37 ($C_{meso\text{-}aryl}$), 132.75 (CH_β), 132.51 (CH_β), 131.88 (CH_β), 131.85 (CH_β), 131.07 (CH_β), 128.59 ($C_{meso\text{-}aryl}$), 127.41 ($C_{meso\text{-}aryl}$), 127.36 ($C_{meso\text{-}aryl}$), 127.27 ($C_{meso\text{-}aryl}$), 126.54 ($C_{meso\text{-}aryl}$), 126.50 ($C_{meso\text{-}aryl}$), 126.42 ($C_{meso\text{-}aryl}$), 126.38 ($C_{meso\text{-}aryl}$), 121.23 (C_{meso}), 120.94(C_{meso}), 119.90 ($CH_{pyridine}$), 118.39($CH_{triazole}$), 110.72 ($CH_{pyridine}$), 30.04 ($C_{tBu\text{-}pyridine}$) ppm. HRMS (ESI, CH_2Cl_2): m/z calcd for $C_{55}H_{40}N_8{}^{64}Zn$: 876.26619 $[M]^+$; found: 876.2664 (0 ppm).

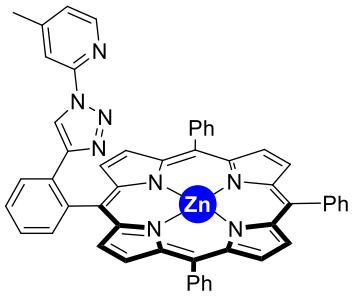

Synthesis and characterization of supramolecular ligand L3: According to the general procedure, **P3** (0.320 g, 0.5 mmol, 1equiv.), 2-azido-4-methylpyridine **AP3** (0.140 g, 0.75 mmol, 1.5 equiv.), Cu $(PPh_3)_3Br$ (0.106 mg, 0.2 mmol, 0.2 equiv.) and dry toluene (20 mL) were added and the reaction mixture was stirred for 24 hours at 120 °C. Back at room temperature, the solvents were evaporated and the crude mixture was purified by column chromatography (SiO2, *n*-heptane:DCM, v/v 1:0 to 3:7) affording analytically pure **L3** (0.254 g, 61% yield). ^{1}H NMR (400 MHz, $CDCl_3$): δ = 8.92 (AB, 4H, *J* = 5.6 Hz, H_β), 8.8 (AB, 4H, *J* = 20 Hz, H_β) 8.67 (d, *J* = 8.0 Hz, 1H, $H_{meso\text{-}aryl}$), 8.30–8.11 (m, 7H, $H_{meso\text{-}aryl}$), 7.93 (td, *J* = 7.8, 1.4 Hz, 1H, $H_{meso\text{-}aryl}$), 7.81–7.63 (m, 10H, $H_{meso\text{-}aryl}$), 7.35 (s, 1H, $H_{pyridine}$), 6.52 (d, *J* = 5.3 Hz, 1H, $H_{pyridine}$), 6.34 (d, *J* = 4.8 Hz, 1H, $H_{pyridine}$), 5.17 (s, 1H, $H_{triazole}$), 2.00 (s, 3H, CH_3) ppm. $^{13}C\{^1H\}$ NMR (101 MHz, $CDCl_3$): δ = 150.67 ($C_{triazole}$), 150.26 (C_α), 150.25 (C_α), 150.09 (C_α), 149.76 (C_α), 147.76 ($C_{pyridine}$), 147.37 ($C_{pyridine}$), 146.33 ($CH_{pyridine}$), 143.08 ($C_{meso\text{-}aryl}$), 142.92 ($C_{meso\text{-}aryl}$), 140.50 ($C_{meso\text{-}aryl}$), 134.66 ($C_{meso\text{-}aryl}$), 134.60 ($C_{meso\text{-}aryl}$), 134.57 ($C_{meso\text{-}aryl}$), 134.39 ($C_{meso\text{-}aryl}$), 132.65 (CH_β), 132.48(CH_β), 131.89 (CH_β), 131.85 (CH_β), 131.02 (CH_β), 128.58 ($C_{meso\text{-}aryl}$), 127.40 ($C_{meso\text{-}aryl}$), 127.36 ($C_{meso\text{-}aryl}$), 127.16 ($C_{meso\text{-}aryl}$), 126.54 ($C_{meso\text{-}aryl}$), 126.50 ($C_{meso\text{-}aryl}$), 126.41 ($C_{meso\text{-}aryl}$), 126.37 ($C_{meso\text{-}aryl}$), 123.59 ($CH_{pyridine}$), 121.22 (C_{meso}), 120.93 (C_{meso}), 118.33 (C_{meso}), 118.23 ($CH_{triazole}$), 114.13 ($CH_{pyridine}$), 20.81 ($C_{Me\text{-}pyridine}$) ppm. HRMS (MALDI, $CHCl_3$, DCTB matrix): m/z calcd for $C_{52}H_{34}N_8{}^{64}Zn$: 834.21924 [M]+; found: 834.223 (4 ppm).

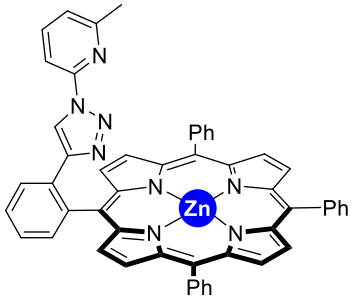

Synthesis and characterization of supramolecular ligand L4: According to the general procedure, **P3** (0.320 g, 0.5 mmol, 1equiv.), 2-azido-6-methylpyridine **AP4** (0.140 g, 0.75 mmol, 1.5 equiv.), $Cu(PPh_3)_3Br$ (0.106 mg, 0.2 mmol, 0.2 equiv.) and dry toluene (20 mL) were added and the reaction mixture was stirred for 24 hours at 120 °C. Back at room temperature, the solvents were evaporated and the crude mixture was purified by column chromatography (SiO_2, *n*-heptane:DCM, v/v 1:0 to 2:8) affording analytically pure **L4** (0.203 g, 54% yield). ^{1}H NMR (400 MHz, $CDCl_3$): δ = 8.93 (s, 4H, H_β), 8.88-8.76 (m, 4H, H_β), 8.48 (dd, *J* = 7.7, 1.4 Hz, 1H, $H_{meso\text{-}aryl}$), 8.37 (dd, *J* = 7.7, 1.4 Hz, 1H, $H_{meso\text{-}aryl}$), 8.26 (dd, *J* = 6.3, 2.8 Hz, 1H, $H_{meso\text{-}aryl}$), 8.22-8.11 (m, 5H, $H_{meso\text{-}aryl}$), 7.92 (td, *J* = 7.5, 1.4 Hz, 1H, $H_{meso\text{-}aryl}$), 7.84-7.59 (m, 10H, $H_{meso\text{-}aryl}$), 7.18-6.96 (m, 2H, $H_{pyridine}$), 6.33 (dd, *J* = 6.1, 2.3 Hz, 1H, $H_{pyridine}$), 5.11 (s, 1H, $H_{triazole}$), 0.66 (s, 3H, CH_3) ppm. $^{13}C\{^1H\}$ NMR (101 MHz, $CDCl_3$): δ = 156.65 ($C_{triazole}$), 150.28 (C_α), 150.15 (C_α), 150.05 (C_α), 147.05 ($C_{pyridine}$), 146.88 ($C_{pyridine}$), 142.93 ($C_{meso\text{-}aryl}$), 142.78 ($C_{meso\text{-}aryl}$), 140.26 ($C_{meso\text{-}aryl}$), 138.37 ($CH_{pyridine}$), 134.57 ($C_{meso\text{-}aryl}$), 134.51 ($C_{meso\text{-}aryl}$), 134.43 ($C_{meso\text{-}aryl}$), 133.94 ($C_{meso\text{-}aryl}$), 133.24 ($C_{meso\text{-}aryl}$), 132.60 (CH_β), 131.98 (CH_β), 131.92 (CH_β), 131.27 (CH_β), 128.66 ($C_{meso\text{-}aryl}$), 127.48 ($C_{meso\text{-}aryl}$), 127.45 ($C_{meso\text{-}aryl}$), 127.39 ($C_{meso\text{-}aryl}$), 126.59 ($C_{meso\text{-}aryl}$), 126.57 ($C_{meso\text{-}aryl}$), 126.48 ($C_{meso\text{-}aryl}$), 126.34 ($C_{meso\text{-}aryl}$), 121.96 ($CH_{pyridine}$), 121.31 (C_{meso}), 121.11 (C_{meso}), 118.58 (C_{meso}), 118.28 ($CH_{triazole}$), 109.85 ($CH_{pyridine}$), 22.02 ($C_{Me\text{-}pyridine}$) ppm. HRMS (ESI, CH_2Cl_2/MeOH 9/1): m/z calcd for $C_{52}H_{34}N_8{}^{64}Zn$: 834.21924 $[M]^+$; found: 834.2189 (0 ppm).

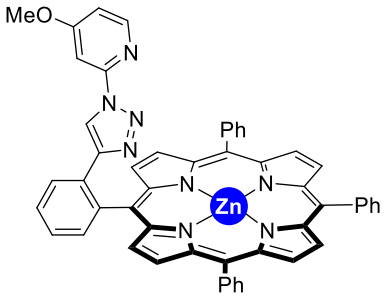

Synthesis and characterization of supramolecular ligand L5: According to the general procedure, **P3** (0.320 g, 0.5 mmol, 1equiv.) 2-azido-4-methoxypyridine **AP5** (0.162 g, 0.75 mmol, 1.5 equiv.), $Cu(PPh_3)_3Br$ (0.106 mg, 0.2 mmol, 0.2 equiv.) and dry toluene (20 mL) were added and the reaction mixture was stirred for 24 hours at 120 °C. Back at room temperature, the solvents were evaporated and the crude mixture was purified by column chromatography (SiO_2, *n*-heptane:DCM, v/v 1:0 to 2:8) affording analytically pure **L5** (0.245 g, 63% yield). ^{1}H NMR (400 MHz, $CDCl_3$): δ = 8.91 (AB, 4H, *J* = 7.7 Hz, H_β), 8.81 (AB, 4H, *J* = 29.5 Hz, H_β), 8.69 (d, *J* = 7.9 Hz, 1H, $H_{meso\text{-}aryl}$), 8.28-8.13 (m, 7H, $H_{meso\text{-}aryl}$), 7.92 (td, *J* = 7.9, 1.4 Hz, 1H, $H_{meso\text{-}aryl}$), 7.80-7.65 (m, 10H, $H_{meso\text{-}aryl}$), 7.05 (d, *J* = 2.3 Hz, 1H, $H_{pyridine}$), 6.52 (d, *J* = 6.0 Hz, 1H, $H_{pyridine}$), 6.05 (dd, *J* = 6.0, 2.3 Hz, 1H, $H_{pyridine}$), 5.28 (s, 1H, $H_{triazole}$), 3.55 (s, 3H, H_{OMe}) ppm. $^{13}C\{^1H\}$ NMR (101 MHz, $CDCl_3$): δ = 167.37 ($C_{triazole}$), 150.26 (C_α), 150.21 (C_α), 150.11 (C_α), 149.61 (C_α), 149.19 ($C_{pyridine}$), 147.43 ($C_{pyridine}$), 147.27 ($CH_{pyridine}$), 143.20 ($C_{meso\text{-}aryl}$), 143.02 ($C_{meso\text{-}aryl}$), 140.61 ($C_{meso\text{-}aryl}$), 134.65 ($C_{meso\text{-}aryl}$), 134.48 ($C_{meso\text{-}aryl}$, 134.40 ($C_{meso\text{-}aryl}$), 132.55 (CH_β), 132.41 (CH_β), 131.87 (CH_β), 131.82 (CH_β), 130.86 (CH_β), 128.91 ($C_{meso\text{-}aryl}$), 128.56 ($C_{meso\text{-}aryl}$), 127.35 ($C_{meso\text{-}aryl}$), 127.31 ($C_{meso\text{-}aryl}$), 126.94 ($C_{meso\text{-}aryl}$), 126.56 ($C_{meso\text{-}aryl}$), 126.52 ($C_{meso\text{-}aryl}$), 126.49 ($C_{meso\text{-}aryl}$), 126.38 ($C_{meso\text{-}aryl}$), 126.33 ($C_{meso\text{-}aryl}$), 121.18 (C_{meso}), 120.84 (C_{meso}), 118.22 (C_{meso}), 118.06 ($CH_{triazole}$), 110.12 ($CH_{pyridine}$), 98.39 ($CH_{pyridine}$), 55.51 ($C_{OMe\text{-}pyridine}$) ppm. HRMS (MALDI, $CHCl_3$, DCTB matrix): m/z calcd for $C_{52}H_{34}N_8O^{64}Zn$: 850.21415 $[M]^+$; found: 850.214 (0 ppm).

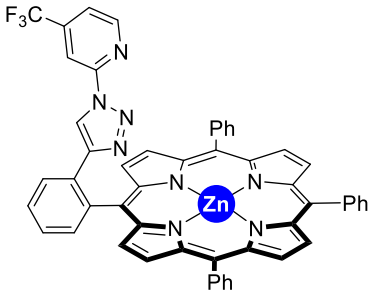

Synthesis and characterization of supramolecular ligand L6: According to the general procedure, **P3** (0.320 g, 0.5 mmol, 1equiv.) 2-azido-4-trifluoromethylpyridine **AP6** (0.153 g, 0.75 mmol, 1.5 equiv.), $Cu(PPh_3)_3Br$ (0.106 mg, 0.2 mmol, 0.2 equiv.) and dry toluene (20 mL) were added and the reaction mixture was stirred for 24 hours at 120 °C. Back at room temperature, the solvents were evaporated and the crude mixture was purified by column chromatography (SiO_2, *n*-heptane:DCM, v/v 1:0 to 2:8) affording analytically pure **L6** (0.115 g, 36% yield.). ^{1}H NMR (400 MHz, $CDCl_3$): δ = 8.95 (s, 4H, H_β), 8.80 (AB, 4H, J = 52.1 Hz, H_β), 8.38 (d, J = 7.8 Hz, 1H, $H_{meso\text{-}aryl}$), 8.26-8.10 (m, 7H, $H_{meso\text{-}aryl}$), 7.90 (t, J = 7.8 Hz, 1H, $H_{meso\text{-}aryl}$), 7.83-7.65 (m, 11H, $H_{meso\text{-}aryl}$), 7.02 (d, J = 5.2 Hz, 1H, $H_{pyridine}$), 6.76 (d, J = 5.2 Hz, 1H, $H_{pyridine}$), 5.49 (s, 1H, $H_{triazole}$) ppm. $^{13}C\{^1H\}$ NMR (101 MHz, $CDCl_3$): δ = 150.32 (C_α), 150.30 (C_α), 150.16 (C_α), 149.81 (C_α), 148.50 ($C_{pyridine}$), 148.36 ($CH_{pyridine}$), 147.63 ($C_{pyridine}$), 142.87 ($C_{meso\text{-}aryl}$), 142.73 ($C_{meso\text{-}aryl}$), 140.97 ($C_{meso\text{-}aryl}$), 140.62 ($C_{meso\text{-}aryl}$), 140.45 ($C_{meso\text{-}aryl}$), 134.99 ($C_{meso\text{-}aryl}$), 134.59 ($C_{meso\text{-}aryl}$), 134.50 ($C_{meso\text{-}aryl}$), 134.36 ($C_{meso\text{-}aryl}$), 132.69 (CH_β), 132.07 (CH_β), 132.01 (CH_β), 131.91 (CH_β), 131.08 (CH_β), 130.92 (CH_β), 128.90 ($C_{meso\text{-}aryl}$), 128.84 ($C_{meso\text{-}aryl}$), 128.63 ($C_{meso\text{-}aryl}$), 127.50 ($C_{meso\text{-}aryl}$), 127.43 ($C_{meso\text{-}aryl}$), 126.70 ($C_{meso\text{-}aryl}$), 126.60 ($C_{meso\text{-}aryl}$), 126.52 ($C_{meso\text{-}aryl}$), 126.49 ($C_{meso\text{-}aryl}$), 123.02 (C_{meso}), 121.44 (C_{meso}), 121.14 (C_{meso}), 120.29 (C_{meso}), 118.16($C_{pyridine}$), 118.03($CH_{triazole}$), 109.75 ($C_{meso\text{-}aryl}$ ppm. $^{19}F\{^1H\}$ NMR (376 MHz, $CDCl_3$): δ = -65.22 (s) ppm. HRMS (MALDI, $CHCl_3$, DCTB matrix): m/z calcd for $C_{52}H_{31}N_8F_3{}^{64}Zn$: 888.19097 $[M]^+$; found: 888.188 (3 ppm)**.**

Synthesis and characterization of triazolopyridine ligands L*:

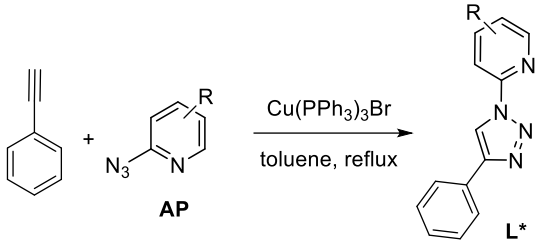

General procedure for the synthesis of ligands L*: Into a dried Schlenk tube charged with a stirring bar, azidopyridine **AP** (1 equiv.), $Cu(PPh_3)_3Br$ (0.1 equiv.) and dry toluene were added followed by phenylacetylene (1.2 equiv.) addition. The reaction mixture was stirred for 24 hours at 120 °C. Back at room temperature, the solvents were evaporated and the crude mixture was purified by column chromatography (SiO_2, *n*-heptane:EtOAc).

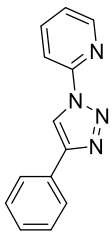

Synthesis and characterization of ligand L1*: According to the general procedure, 2-azidopyridine **AP1** (0.204 g, 1.7 mmol, 1 equiv.) and $Cu(PPh_3)_3Br$ (0.158 g, 0.17 mmol, 0.1 equiv.) were suspended in dry toluene (12 mL) in a dry Schlenk tube. Then, phenylacetylene (0.208 mg, 0.224 mL, 2 mmol, 1.2 equiv.) was introduced and the reaction mixture was stirred at 120 °C for 24 hours. Back at room temperature, the solvent was evaporated under reduced pressure and the crude mixture was purified by column chromatography (SiO_2, *n*-heptane:EtOAc, v/v 1:0 to 7:3) to afford analytically pure **L1*** (0.120 g, 32% yield). ^{1}H NMR (400 MHz, $CDCl_3$): δ = 8.82 (1H, s), 8.54 (1H, d, J = 3.9 Hz), 8.26 (1H, d, J = 8.2 Hz), 7.94 (3H, m), 7.47 (2H, t, J = 7.5 Hz), 7.4-7.35 (2H, m) ppm. The spectral data match those found in literature.[51]

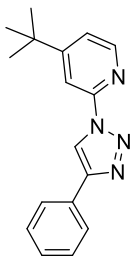

Synthesis and characterization of ligand L2*: According to the general procedure, 2-azido-4-tert-butylpyridine **AP2** (0.299 g, 1.7 mmol, 1 equiv.) and $Cu(PPh_3)_3Br$ (0.158 g, 0.17 mmol, 0.1 equiv.) were suspended in dry toluene (12 mL) in a dry Schlenk tube. Then, phenylacetylene (0.208 mg, 0.224 mL, 2 mmol, 1.2 equiv.) was introduced and the reaction mixture was stirred at 120°C for 24 hours. Back at room temperature, the solvent was evaporated under reduced pressure and the crude mixture was purified by column chromatography (SiO_2, *n*-heptane:EtOAc, v/v 1:0 to 7:3) to afford analytically pure **L2*** (0.142 g, 30% yield). ^1H NMR (400 MHz, $CDCl_3$): δ = 8.80 (s, 1H), 8.42 (d, J = 6.0 Hz, 1H), 8.25 (d, J = 1.2 Hz, 1H), 7.95 (dd, J = 6.0, 1.2 Hz, 2H), 7.57-7.30 (m, 5H), 1.41 (s, 9H) ppm. $^{13}C\{^1H\}$ NMR (101 MHz, $CDCl_3$): δ = 164.10, 149.48, 148.28, 147.98, 132.49, 130.37, 128.88, 128.42, 128.36, 125.91, 120.92, 116.97, 110.90, 35.39, 30.50 ppm. HRMS (ESI, DCM): m/z calcd for $C_{17}H_{18}N_4$: 301.14237 $[M+Na]^+$; found: 301.1424 (0 ppm).

3.4.3. Binding studies.

3.4.3.1. Binding studies between supramolecular ligands and pyridine.

General procedure for NMR binding experiment between supramolecular ligands L1-L6 and pyridine (1:1 ratio): Supramolecular ligand **L1**-**L6** (3.95×10^{-3} mmol) was placed in an NMR tube and dried under vacuum for few minutes. Then, dry $CDCl_3$ (0.75 mL) was added and the corresponding ^1H NMR spectrum was recorded. A previously dried Schlenk tube was charged with dry pyridine (12.8 µL, 0.158 mmol) and $CDCl_3$ (1 mL): named stock solution A. Then, 1 equiv. of pyridine (25 µL of the stock solution A) were added to the NMR tube containing the supramolecular ligand and the corresponding ^1H NMR spectrum (see **Figures S1-S6** below) and the DOSY spectrum (see **Figures S7-S12** below) were recorded showing strong up-field shifts for the pyridine proton signals. Note that for DOSY experiments due to the fast exchange between bound and unbound pyridine, the diffusion of the supramolecular ligands and the pyridine does not perfectly overlap in some cases, however, the observed diffusion is different than that observed for free pyridine (see **Figure S13**). This limitation of DOSY is a known phenomena that has been discussed in the literature.[52]

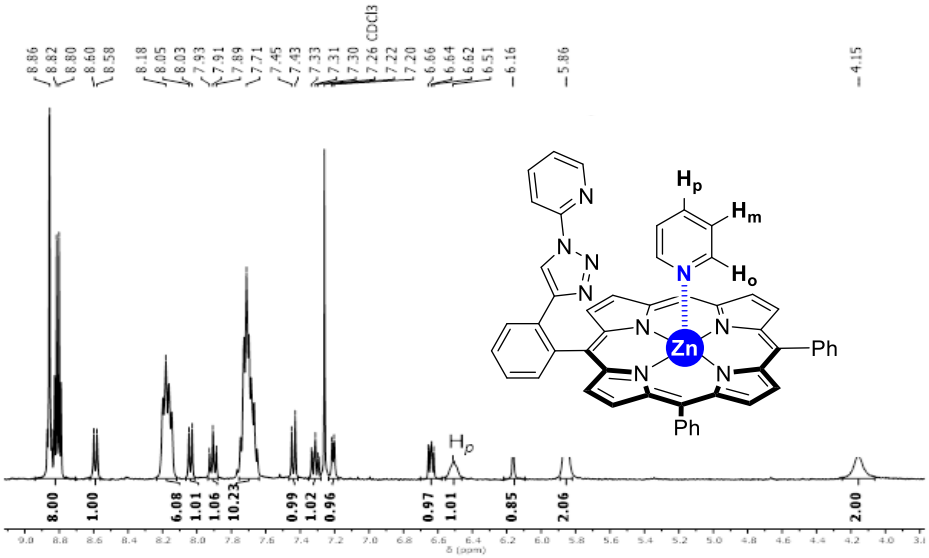

Figure S1. ^1H NMR spectrum ($CDCl_3$, 400 MHz) of the self-assembly [**L1** ⊂ pyridine] in an equimolar ratio.

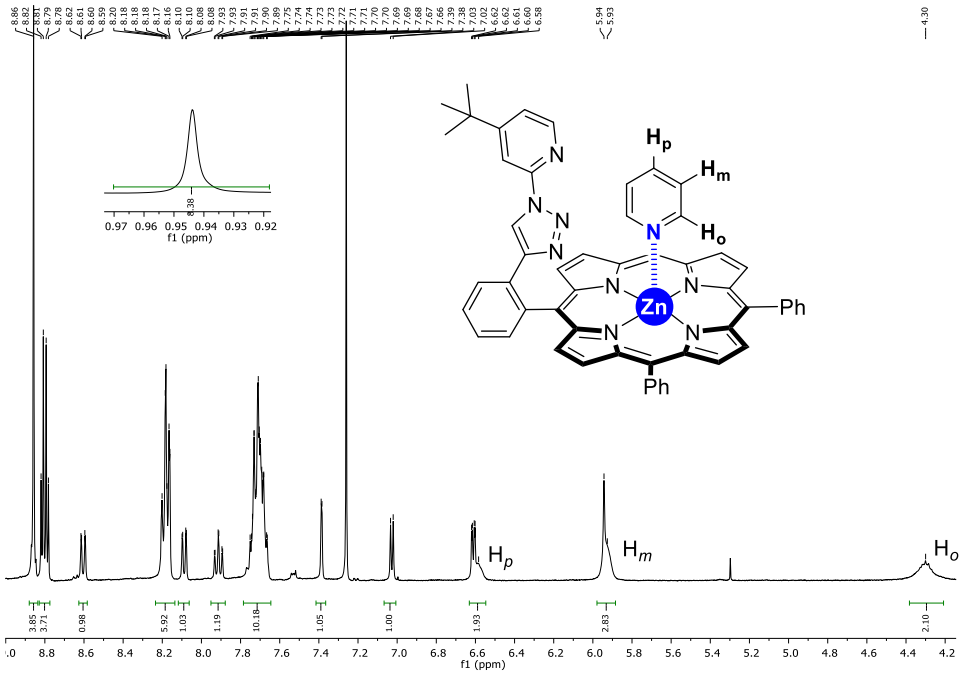

Figure S2. ^{1}H NMR spectrum ($CDCl_3$, 400 MHz) of the self-assembly [**L2** ⊂ pyridine] in an equimolar ratio.

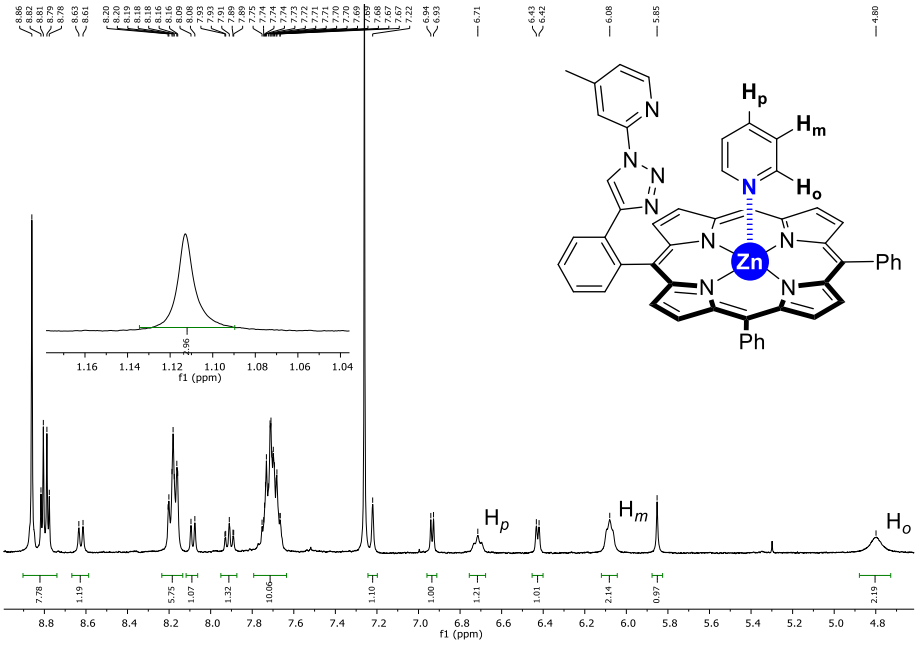

Figure S3. ^{1}H NMR spectrum ($CDCl_3$, 400 MHz) of the self-assembly [**L3** ⊂ pyridine] in an equimolar ratio.

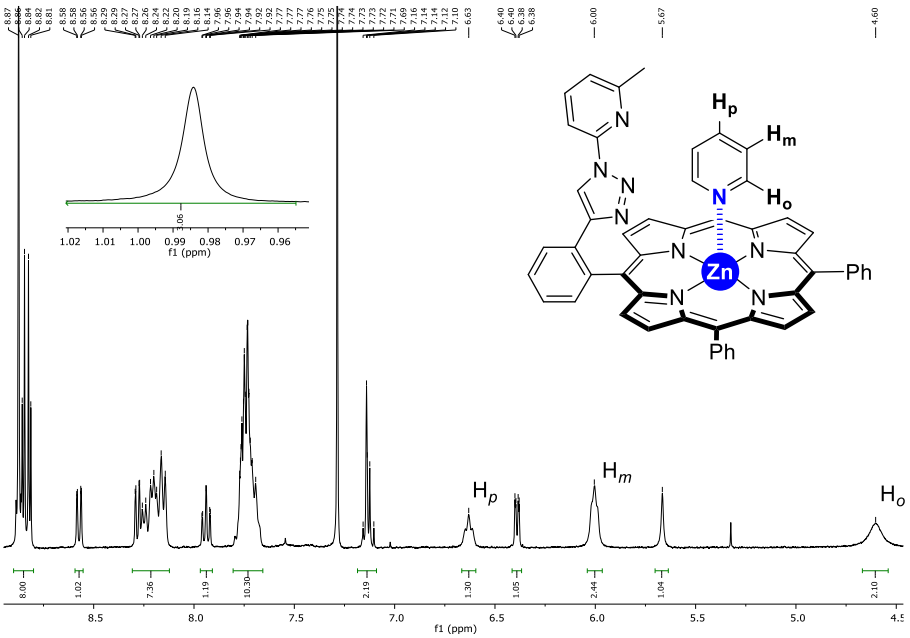

Figure S4. ^{1}H NMR spectrum ($CDCl_3$, 400 MHz) of the self-assembly [**L4** ⊂ pyridine] in an equimolar ratio.

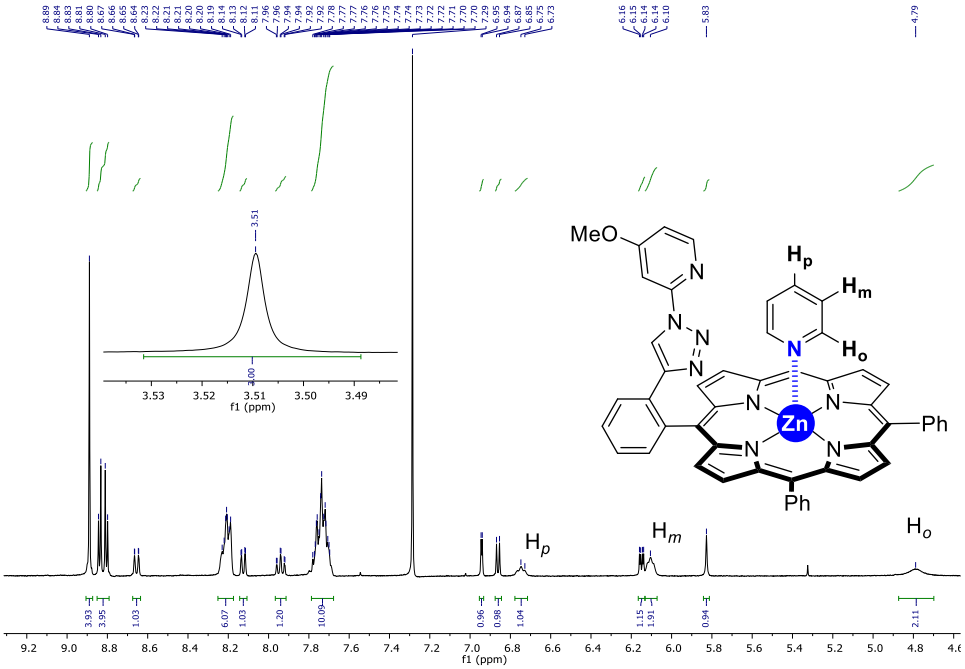

Figure S5. ^{1}H NMR spectrum ($CDCl_3$, 400 MHz) of the self-assembly [**L5** ⊂ pyridine] in an equimolar ratio.

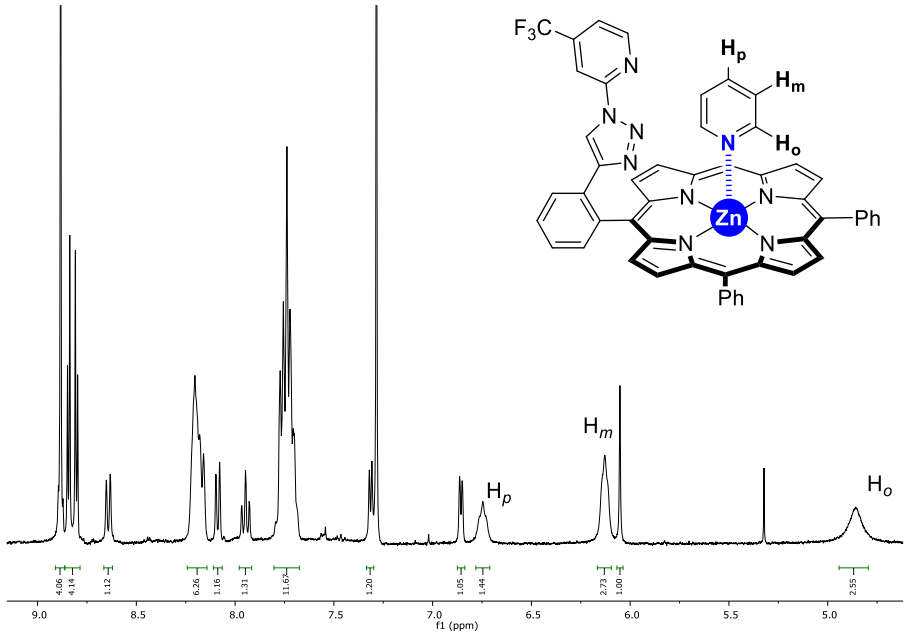

Figure S6. ^{1}H NMR spectrum ($CDCl_3$, 400 MHz) of the self-assembly [**L6** ⊂ pyridine] in an equimolar ratio.

Table S1. Summary of the ^{1}H NMR coordination experiments.

Entry	ligand + pyridine	H*o* (ppm)	H*m* (ppm)	H*p* (ppm)
1	pyridine only	8.56	7.60	7.22
2	L1 + pyridine	4.15	5.86	6.51
3	L2 + pyridine	4.3	5.93	6.58
4	L3 + pyridine	4.8	6.08	6.71
5	L4 + pyridine	4.6	6	6.63
6	L5 + pyridine	4.79	6.1	6.75
7	L6 + pyridine	4.82	6.11	6.74

Every supramolecular ligand **L1**-**L6** synthetized is found to be able to bind pyridine via Zn…N dynamic interaction as a strong upfield shifts were observed for all the pyridine proton signals. Stronger effects are observed for H_o than H_m and than H_p.

NOESY experiments did not reveal any NOE cross-peaks between the triazolopyridine fragment from the supramolecular ligands and the pyridine guest. This indicates that the pyridine substrate binds to the zinc from either site of the porphyrin plane at a time and this equilibrum is fast at the ^{1}H NMR spectroscopy time scale.

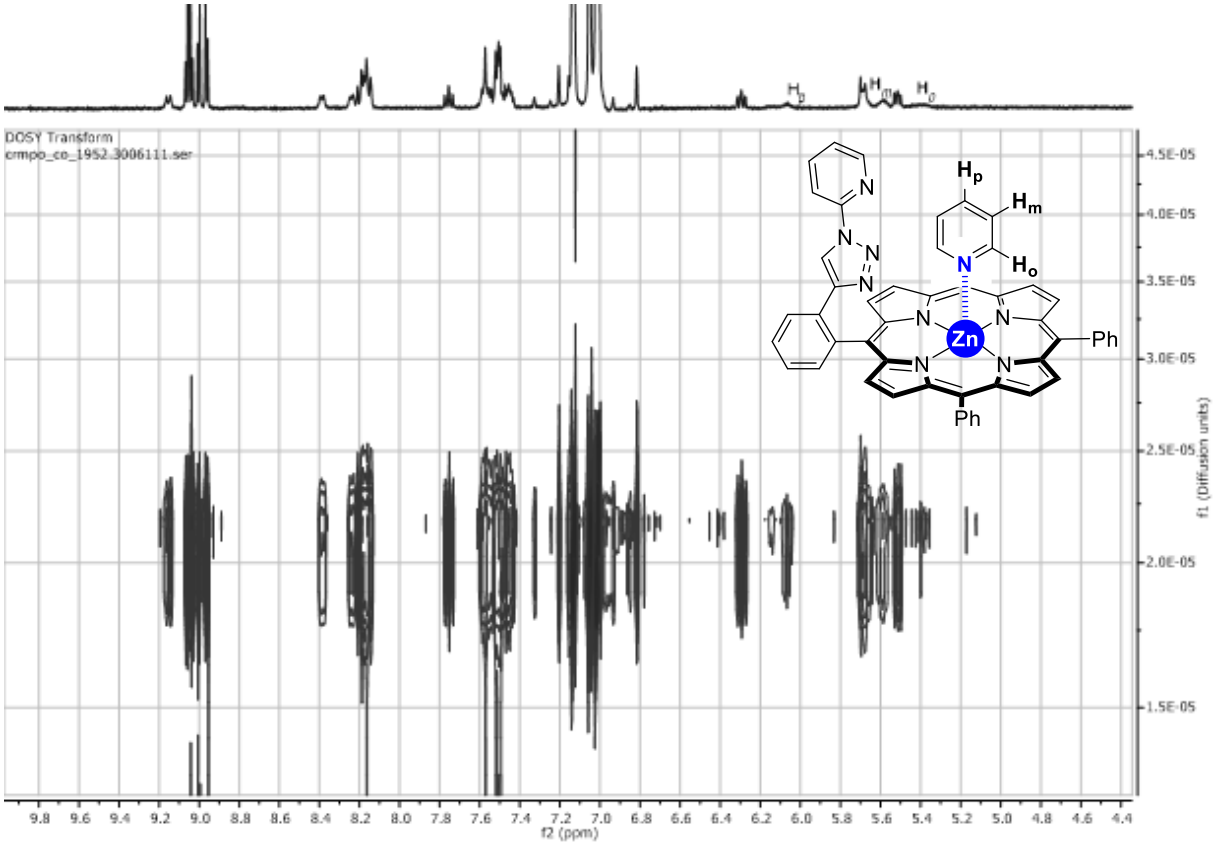

Figure S7. DOSY (toluene-d_8, 400 MHz) spectrum of **L** and pyridine in equimolar ratio.

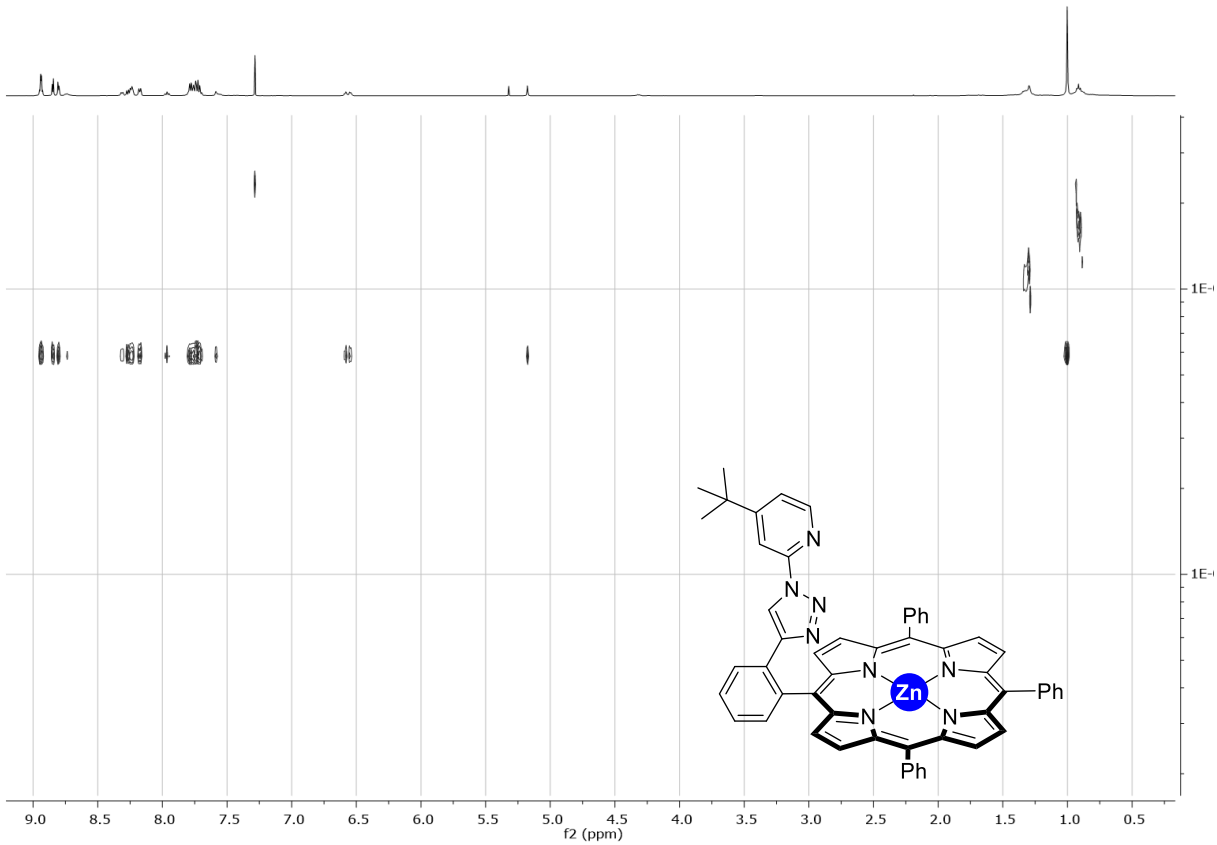

Figure S8.1. DOSY ($CDCl_3$, 400 MHz) spectrum of pure **L2**.

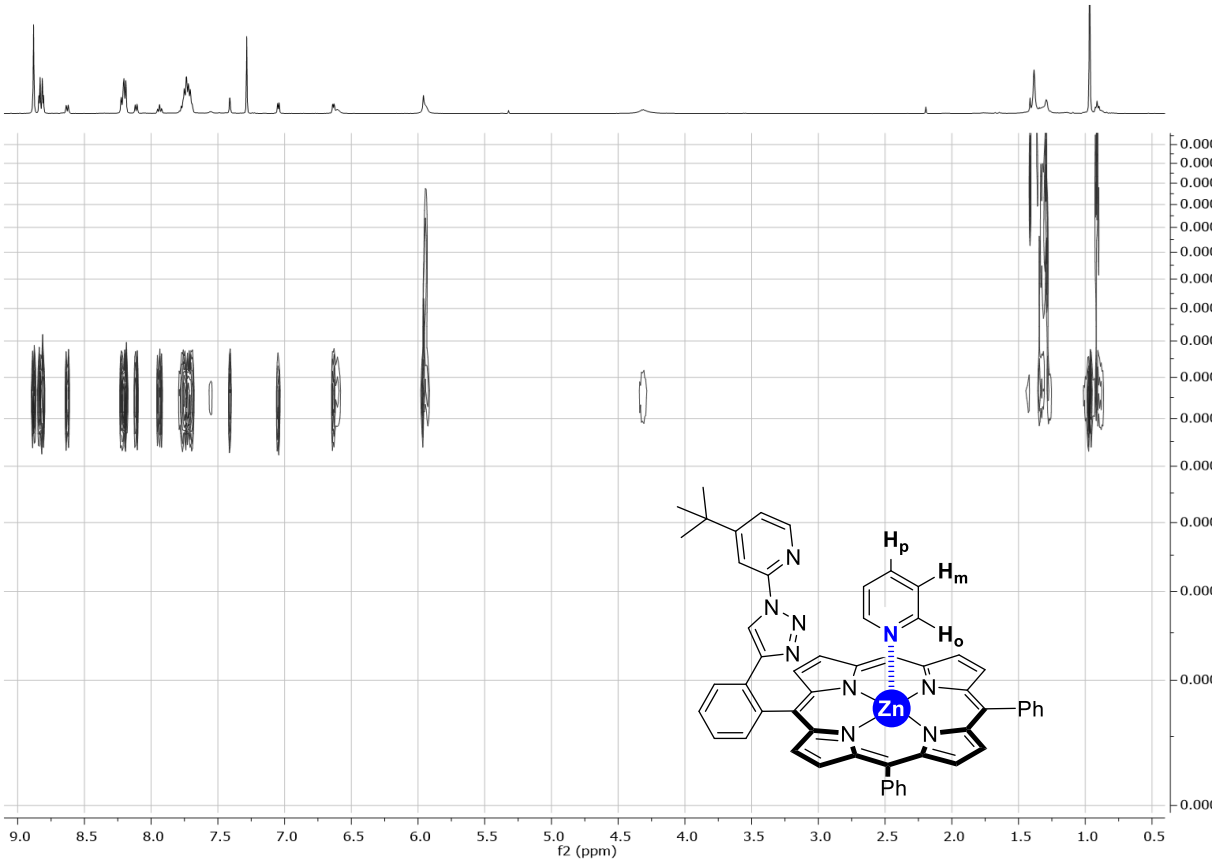

Figure S8.2. DOSY ($CDCl_3$, 400 MHz) spectrum of **L2** and pyridine in equimolar ratio.

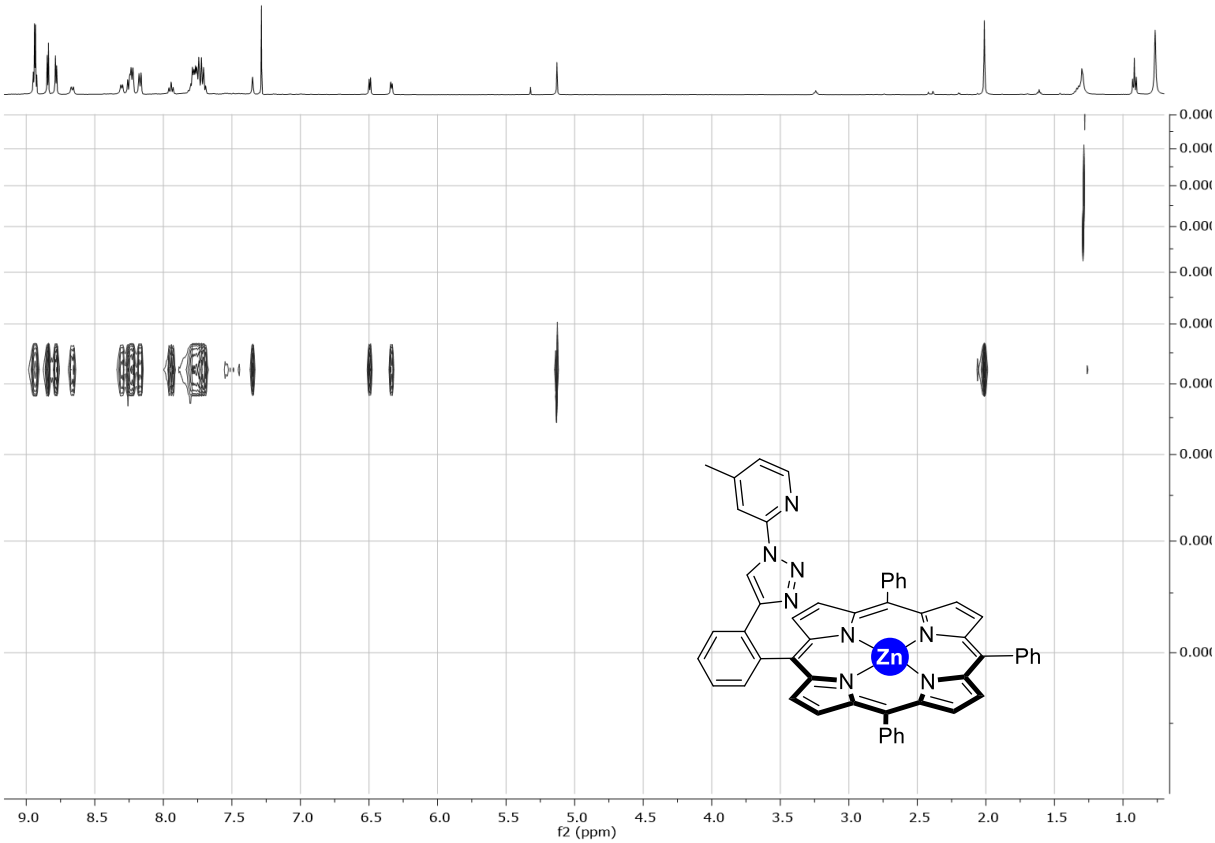

Figure S9.1. DOSY ($CDCl_3$, 400 MHz) spectrum of pure **L3**.

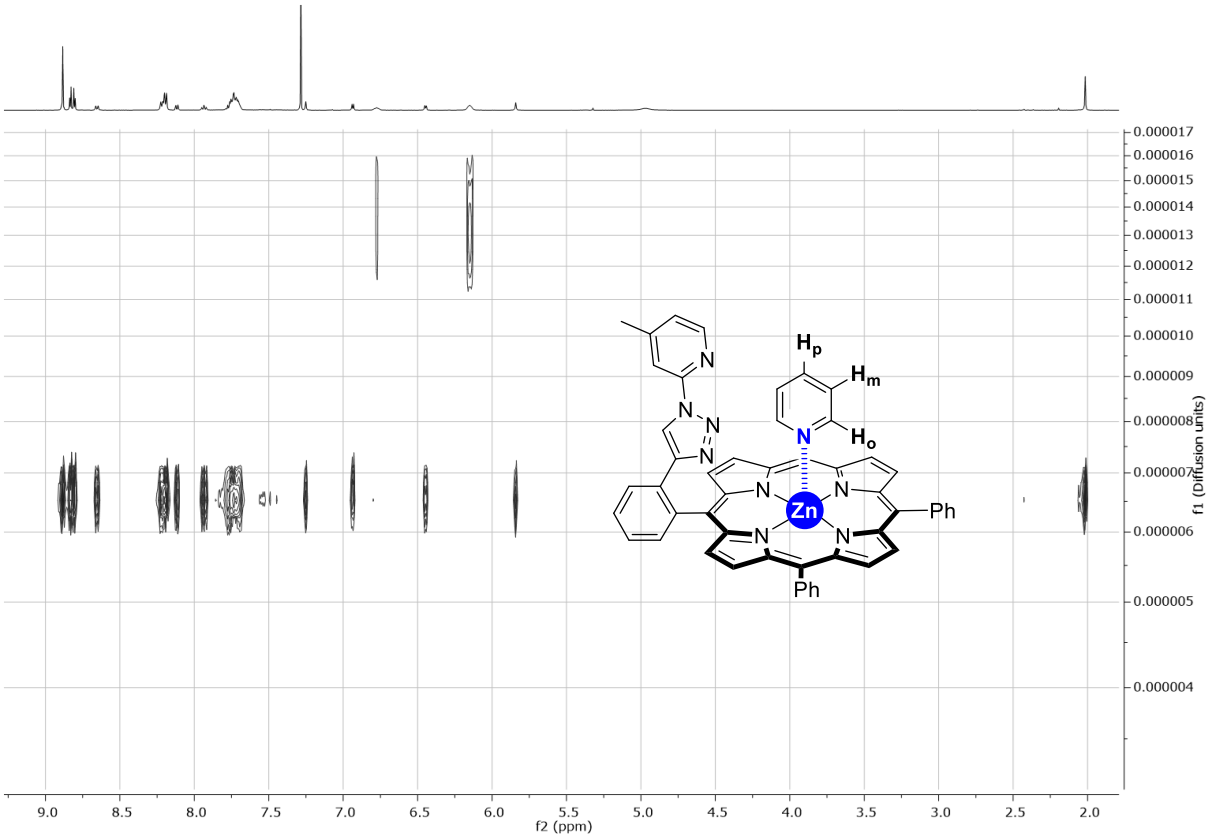

Figure S9.2. DOSY ($CDCl_3$, 400 MHz) spectrum of **L3** and pyridine in equimolar ratio.

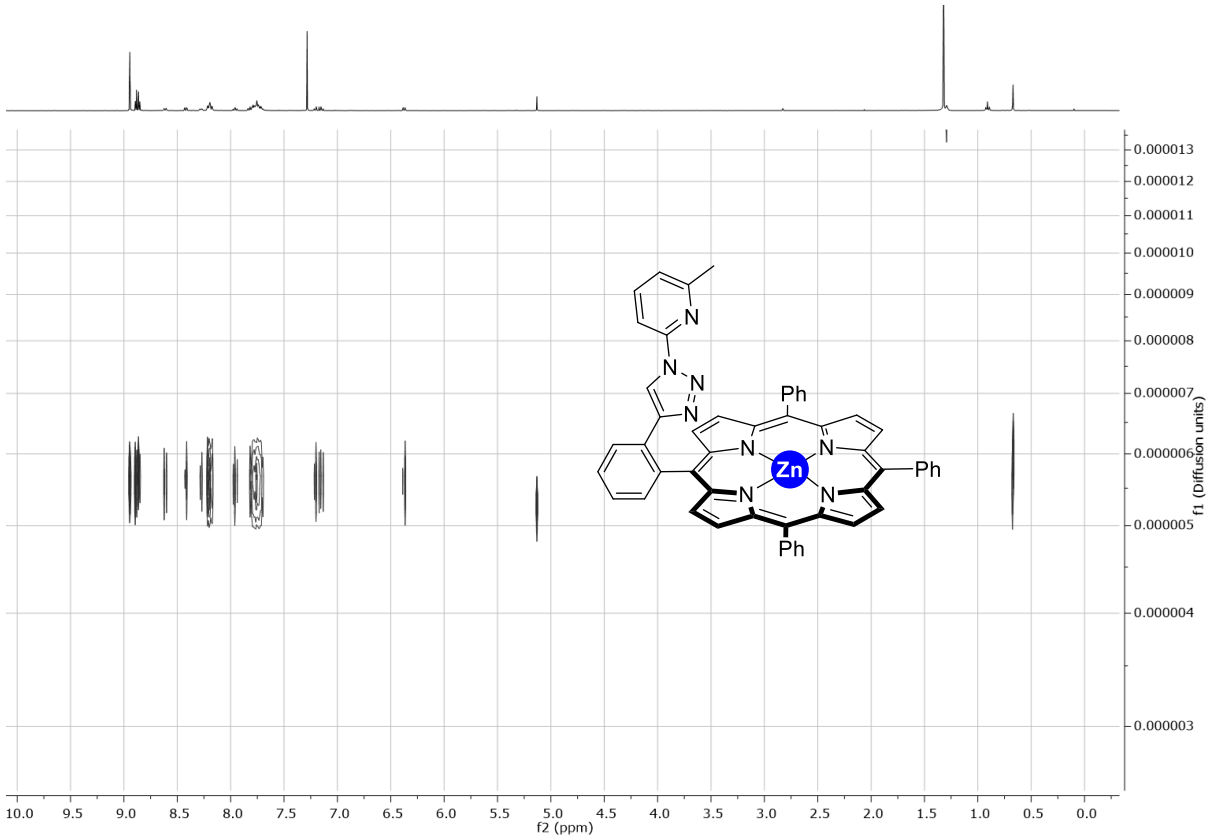

Figure S10.1. DOSY ($CDCl_3$, 400 MHz) spectrum of pure **L4**.

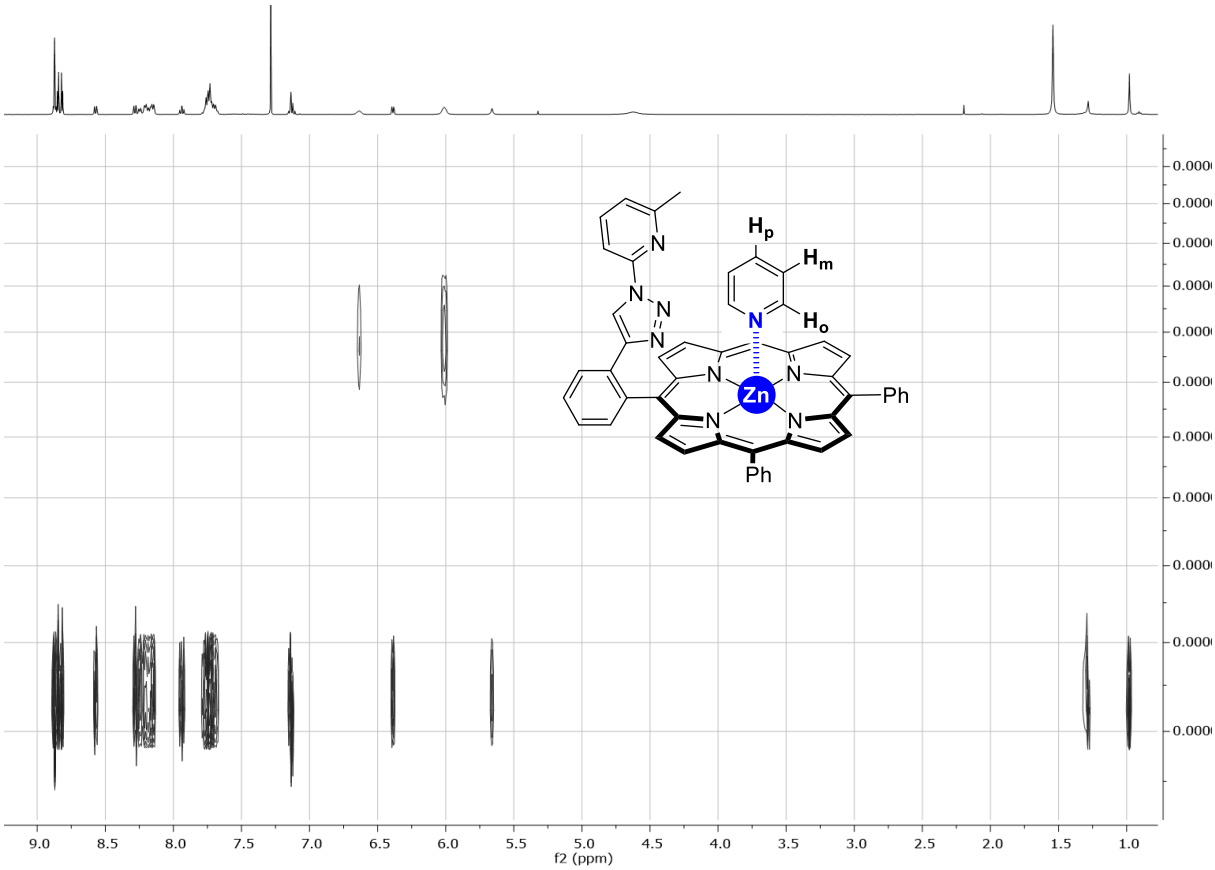

Figure S10.2. DOSY ($CDCl_3$, 400 MHz) spectrum of **L4** and pyridine in equimolar ratio.

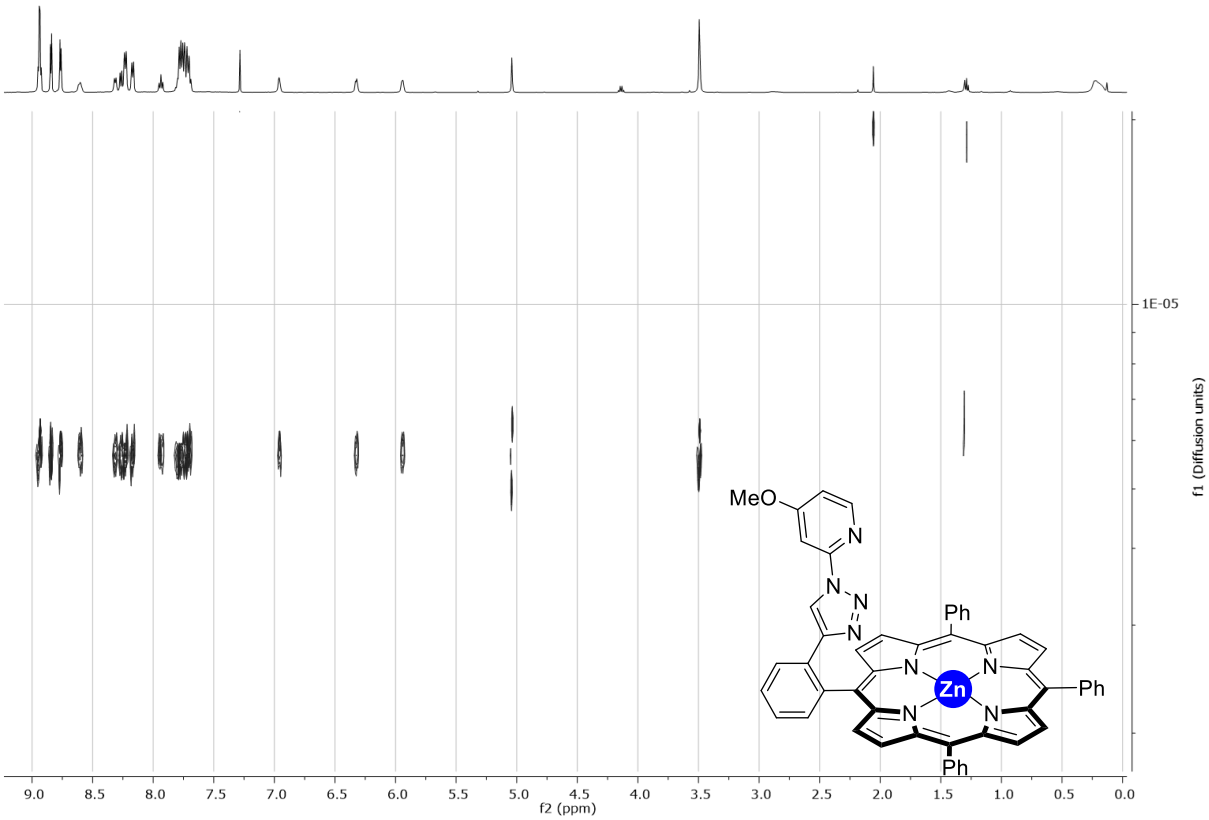

Figure S11.1. DOSY ($CDCl_3$, 400 MHz) spectrum of pure **L5**.

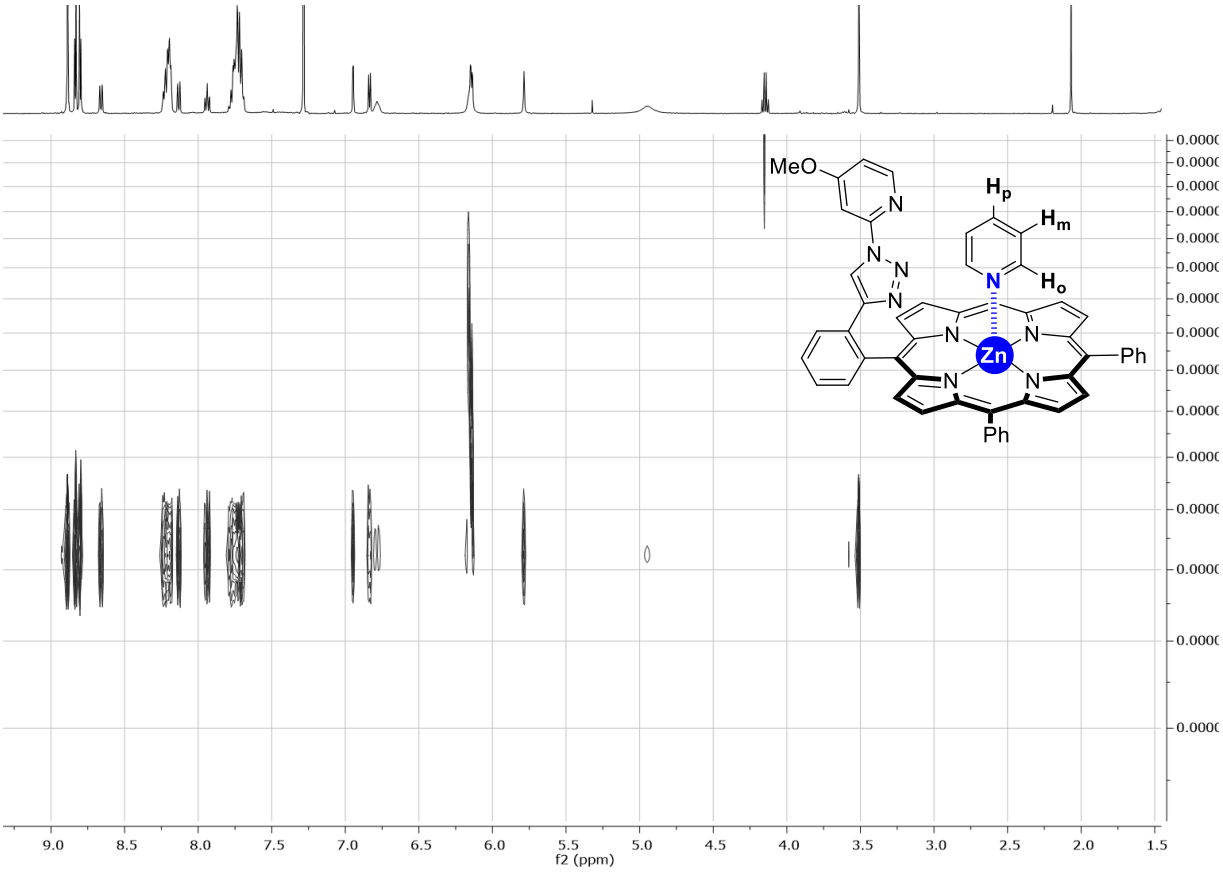

Figure S11.2. DOSY ($CDCl_3$, 400 MHz) spectrum of **L5** and pyridine in equimolar ratio.

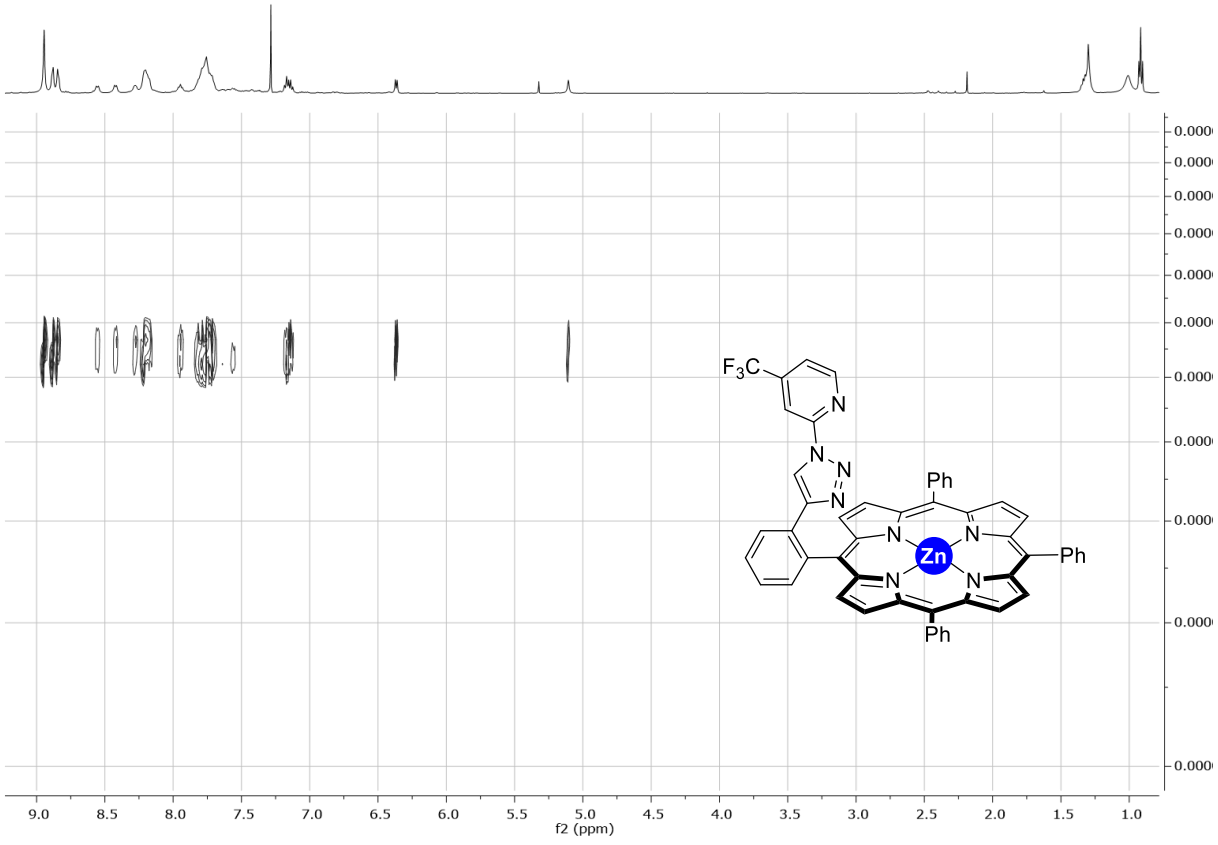

Figure S12.1. DOSY ($CDCl_3$, 400 MHz) spectrum of pure **L6**.

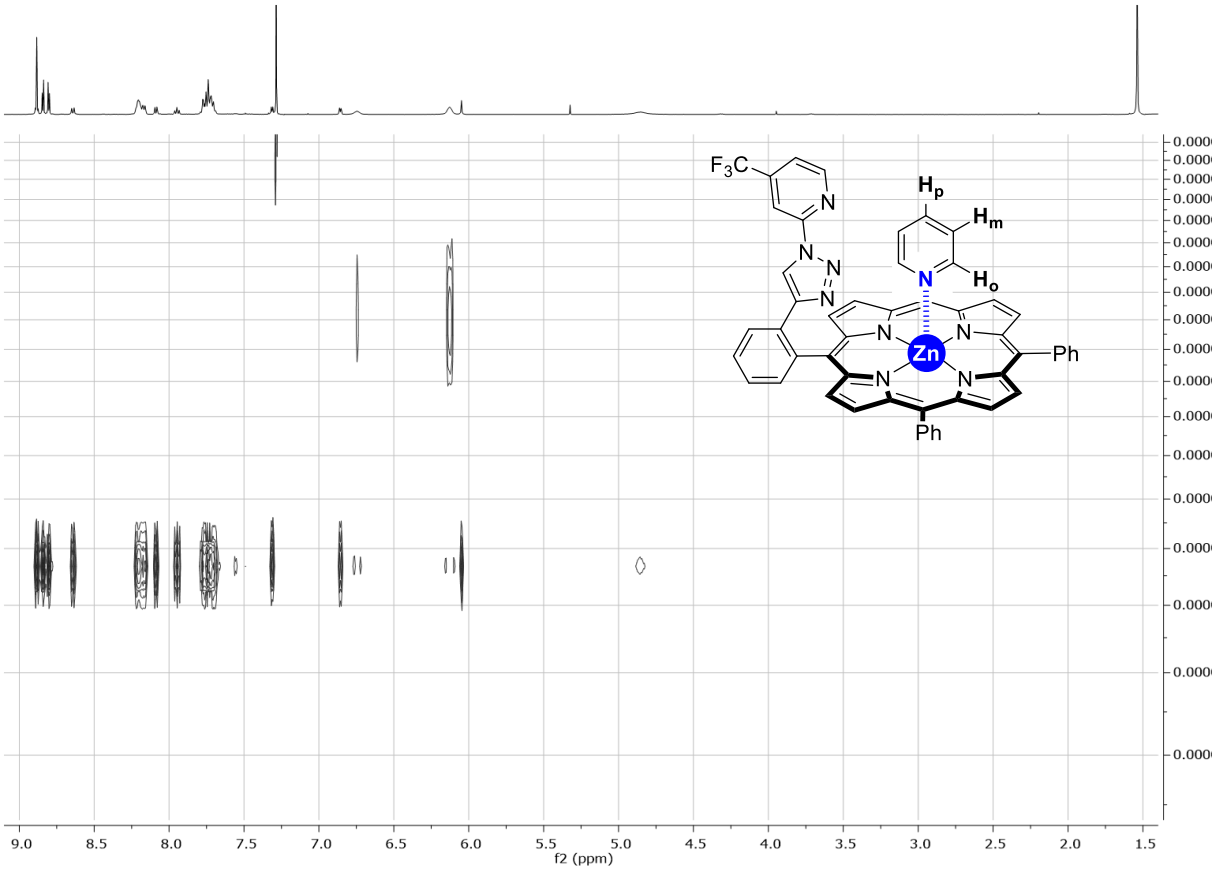

Figure S12.2. DOSY ($CDCl_3$, 400 MHz) spectrum of **L6** and pyridine in equimolar ratio.

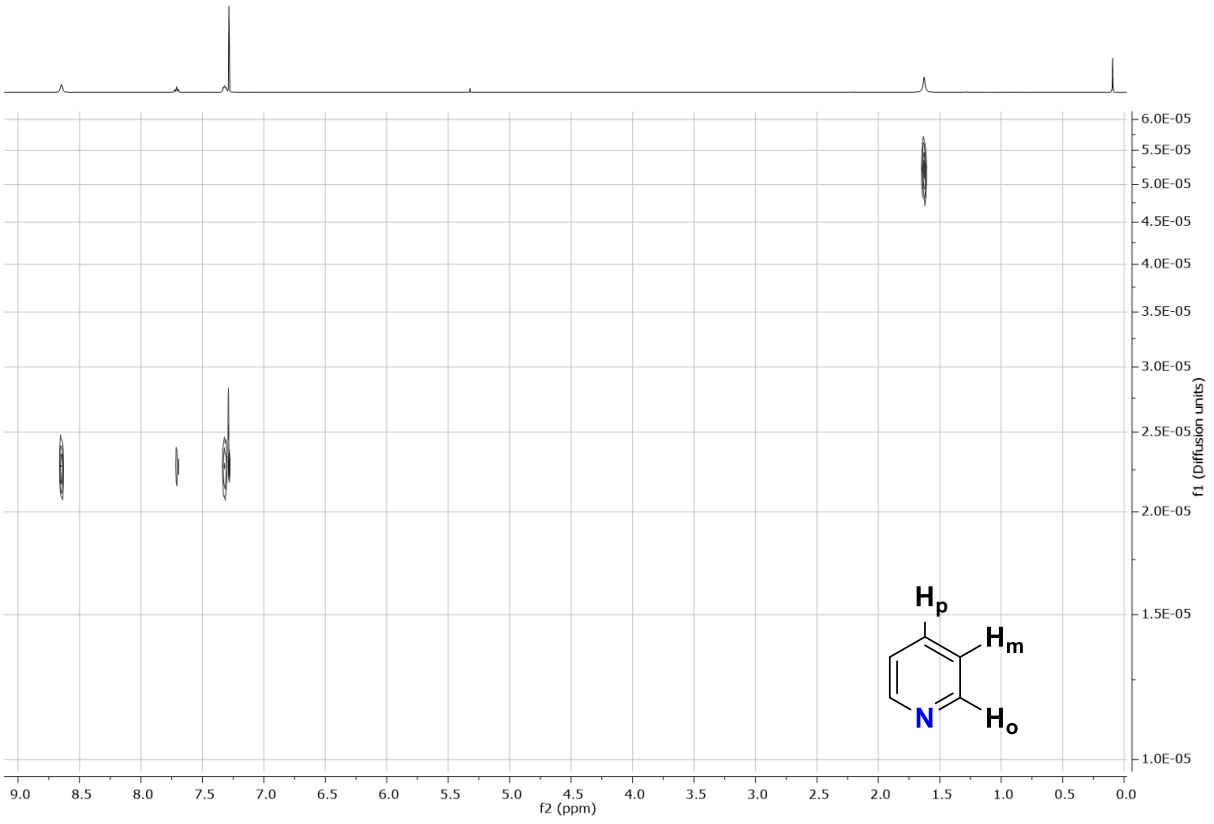

Figure S13. DOSY ($CDCl_3$, 400 MHz) spectrum of pure pyridine.

3.4.3.2. Binding studies to disclose Zn···O-Me binding between the supramolecular ligands and $[Ir(COD)(OMe)]_2$.

Characterization of $[Ir(COD)(OMe)]_2$: ^{1}H NMR (400 MHz, toluene-d_8): δ = 3.49 (d, J = 3.9 Hz, 8H), 3.13 (s, 6H), 2.16-2.09 (m, 8H), 1.33-1.23 (m, 8H) ppm. $^{13}C\{^1H\}$ NMR (101 MHz, toluene-d_8): δ = 55.89, 31.85 ppm.

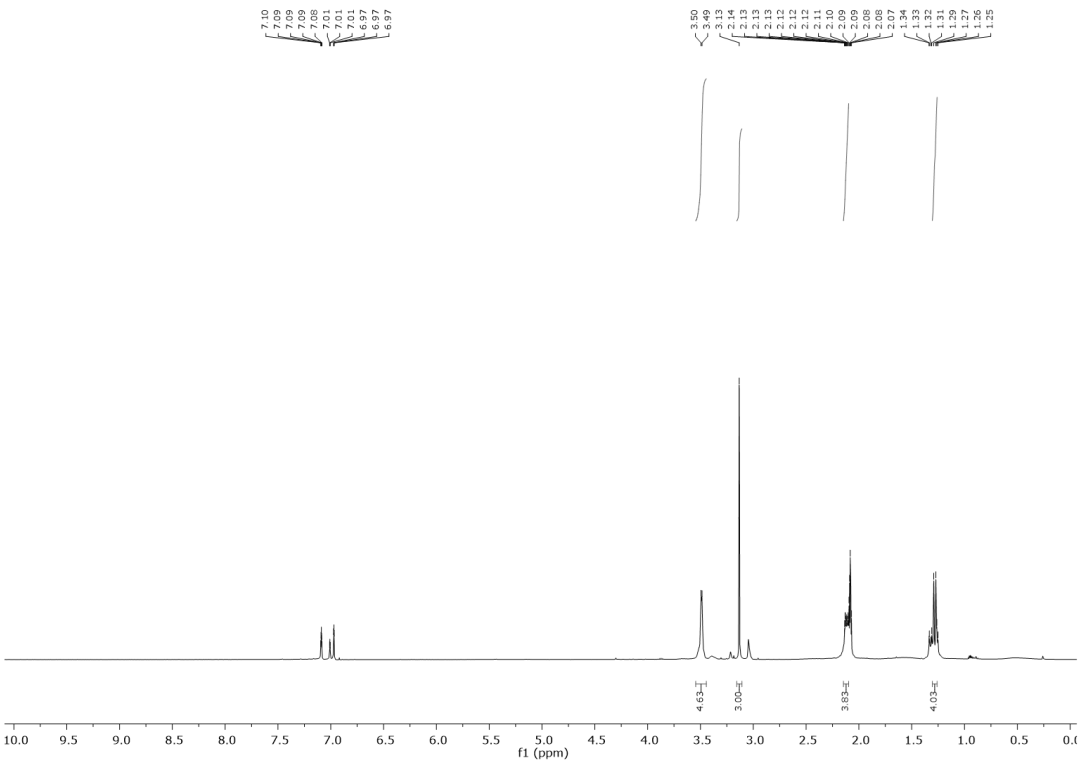

Figure S14. ^{1}H NMR (toluene-d_8, 400 MHz) spectrum of $[Ir(COD)(OMe)]_2$.

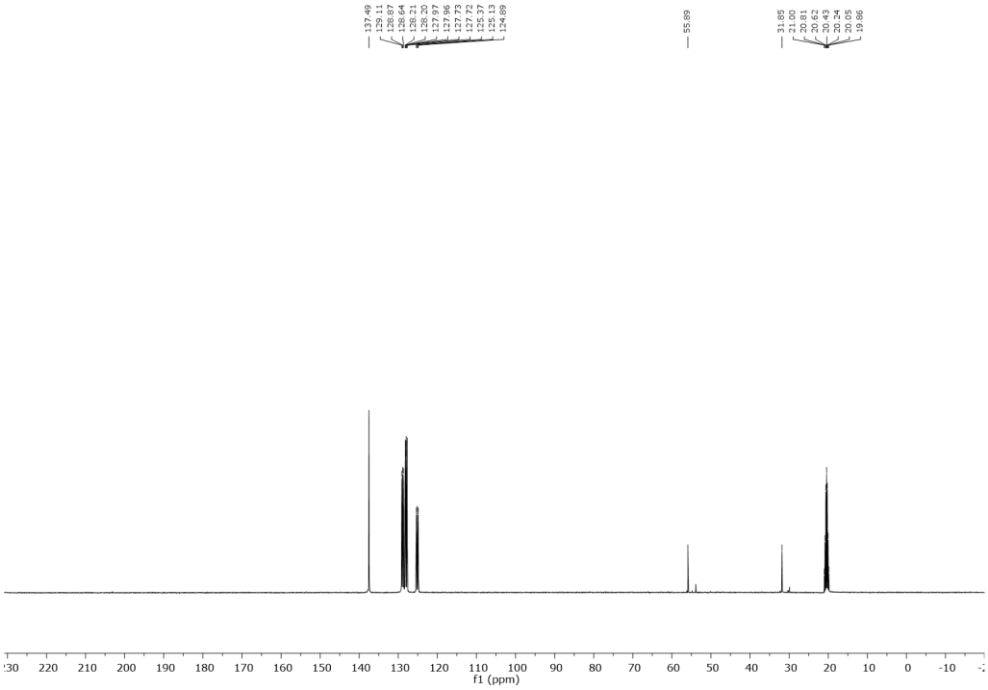

Figure S15. $^{13}C\{^1H\}$ NMR (toluene-d_8, 100 MHz) spectrum of $[Ir(COD)(OMe)]_2$.

NMR experiment combining the supramolecular ligand L with [Ir(COD)(OMe)]$_2$ (1:0.5 ratio): The supramolecular ligand **L** (5 mg, 6.1 x 10^{-6} mmol, 1 equiv.) and [Ir(COD)(OMe)]$_2$ (2 mg, 3.05 x 10^{-6} mmol, 0.5 equiv.) were placed in an J Young NMR tube and dried under vacuum for few minutes. Then, dry toluene-d_8 (0.75 mL) was added under a flow of Argon, the cap was sealed and the corresponding NMR spectra were recorded.

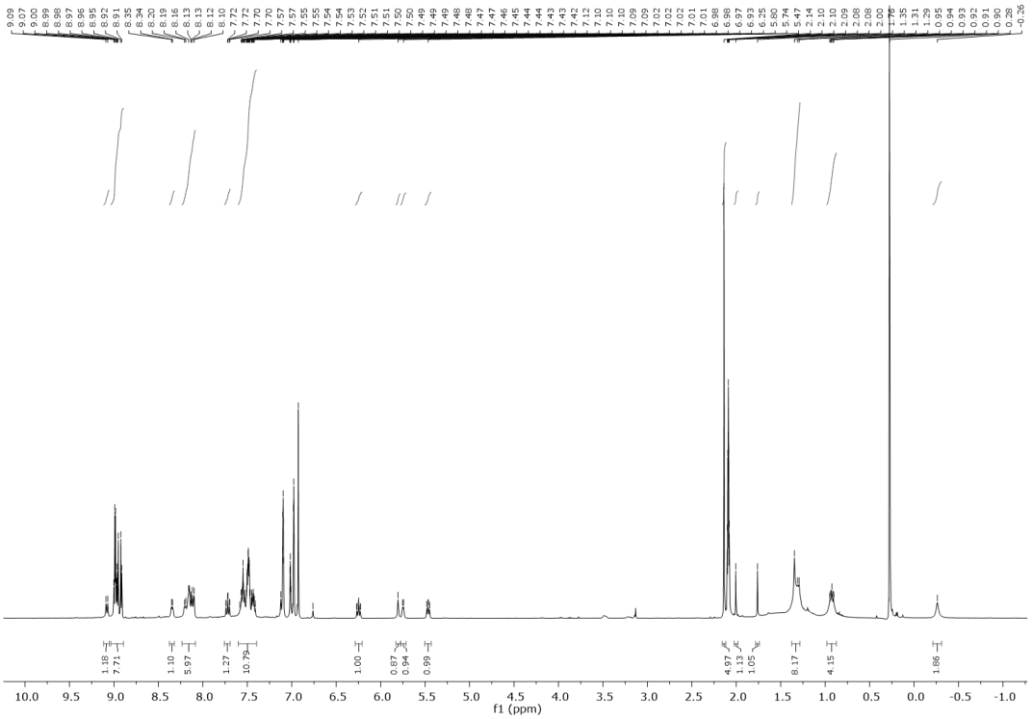

Figure S16. ^{1}H NMR (toluene-d_8, 400 MHz) spectrum of a combination of **L1** and [Ir(COD)(OMe)]$_2$ in a 1 : 0.5 ratio.

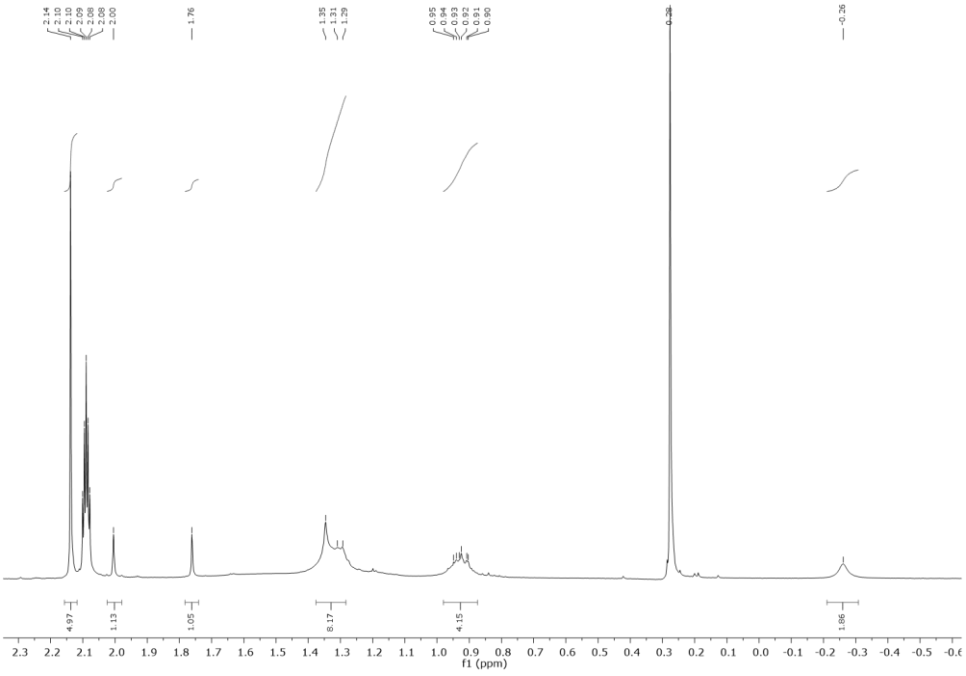

Figure S17. ^{1}H NMR (toluene-d_8, 400 MHz) spectrum of a combination of **L1** and [Ir(COD)(OMe)]$_2$ in a 1 : 0.5 ratio -zoom of the aliphatic area-.

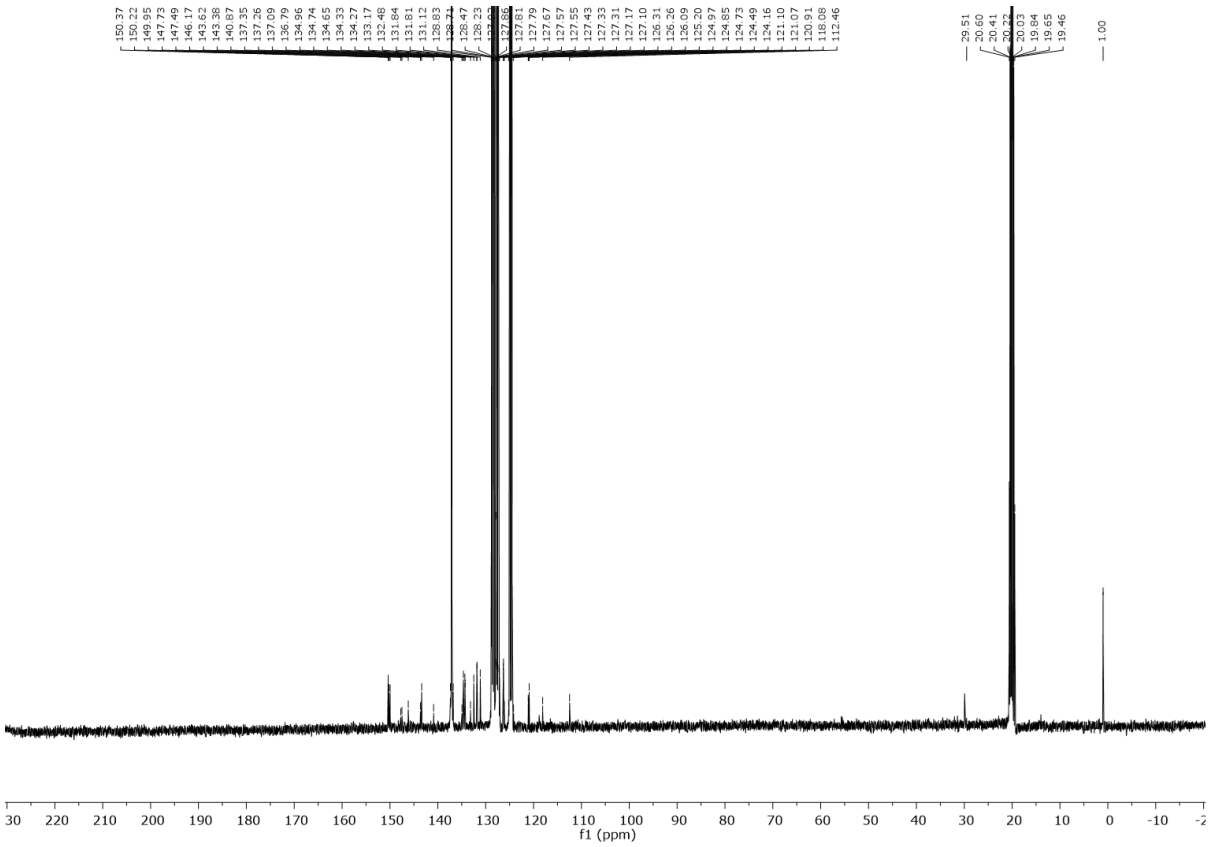

Figure S18. $^{13}C\{^{1}H\}$ NMR (toluene-d_8, 100 MHz) spectrum of a combination of **L1** and $[Ir(COD)(OMe)]_2$ in a 1 : 0.5 ratio.

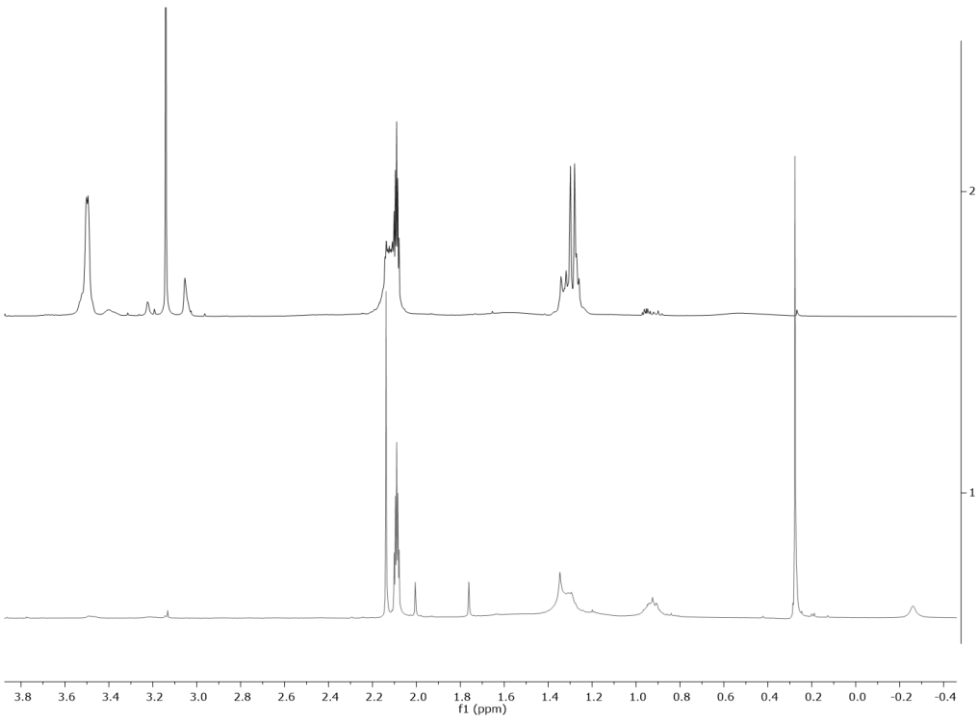

Figure S19. ^{1}H NMR (toluene-d_8, 400 MHz) spectra -aliphatic area zoom- of $[Ir(COD)(OMe)]_2$ (top) and a combination of **L1** and $[Ir(COD)(OMe)]_2$ in a 1 : 0.5 ratio (bottom).

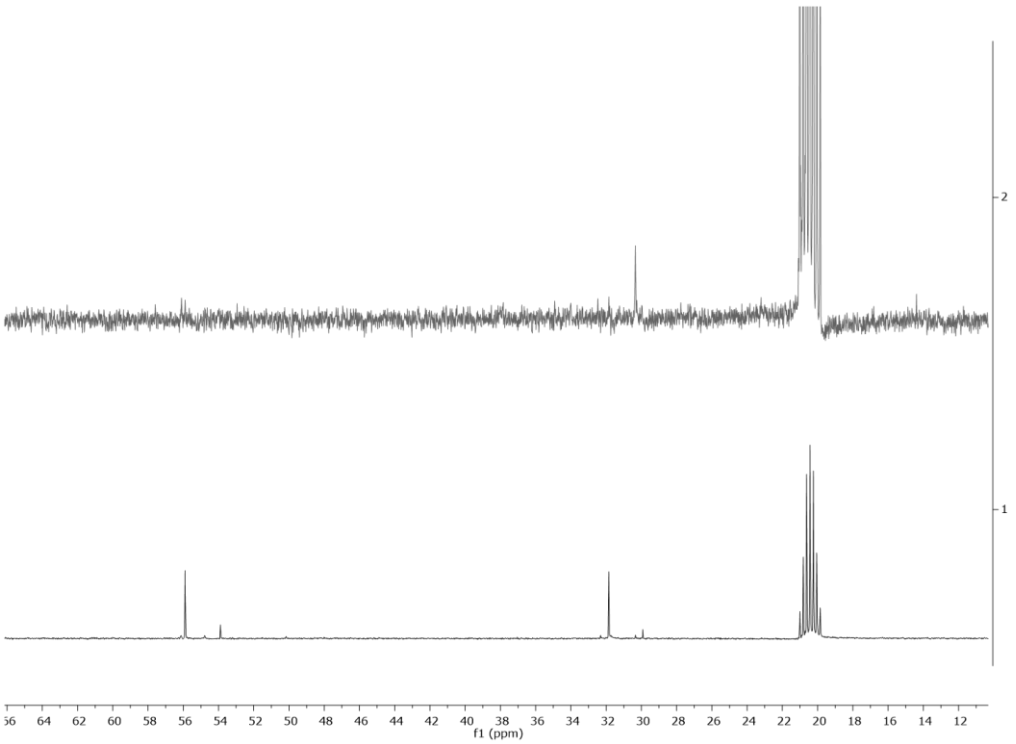

Figure S20. $^{13}C\{^{1}H\}$ NMR (toluene-d_8, 100 MHz) spectra -aliphatic area zoom- of $[Ir(COD)(OMe)]_2$ (top) and a combination of **L1** and $[Ir(COD)(OMe)]_2$ in a 1 : 0.5 ratio (bottom).

NMR experiment combining the dtbpy ligand with $[Ir(COD)(OMe)]_2$ (1:0.5 ratio): dtbpy (1.6 mg, 6.1 x 10^{-6} mmol, 1 equiv.) and $[Ir(COD)(OMe)]_2$ (2 mg, 3.05 x 10^{-6} mmol, 0.5 equiv.) were placed in an J Young NMR tube and dried under vacuum for few minutes. Then, dry toluene-d_8 (0.75 mL) was added under a flow of Argon, the cap was sealed and the corresponding ^{1}H NMR spectrum was recorded (**Figure S21**).

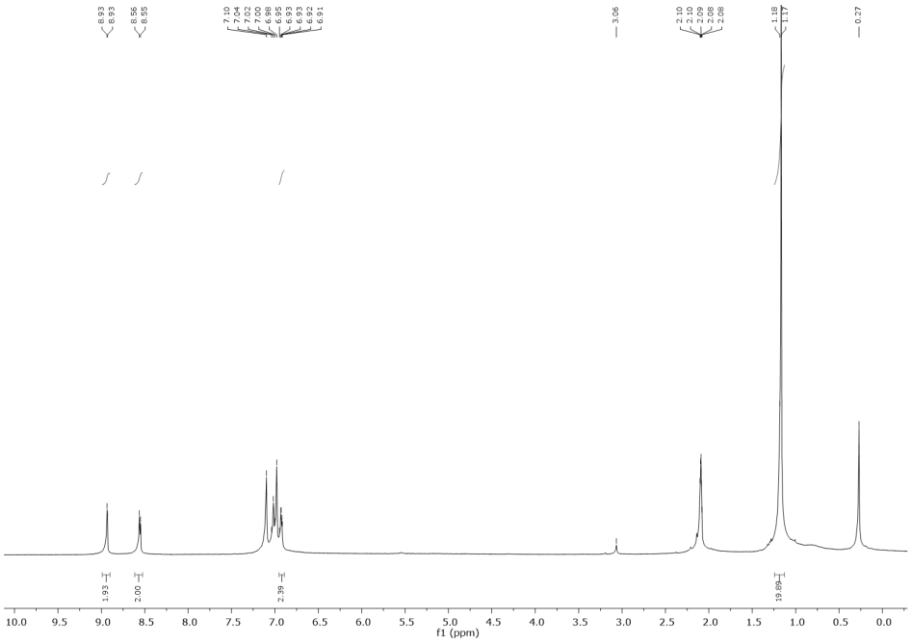

Figure S21. ^{1}H NMR (toluene-d_8, 400 MHz) spectrum of **dtbpy** and $[Ir(COD)(OMe)]_2$ in a 1 : 0.5 ratio.

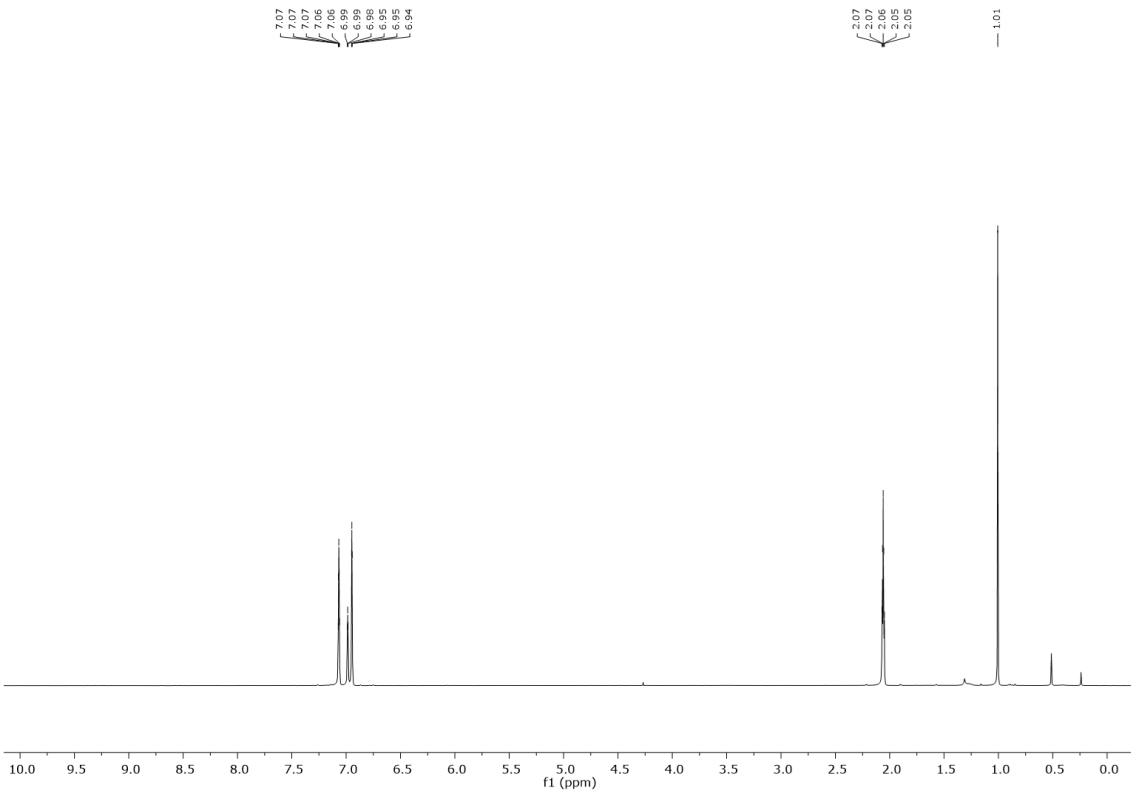

Figure S22. ^{1}H NMR (toluene-d_8, 400 MHz) spectrum of ^{t}BuOK.

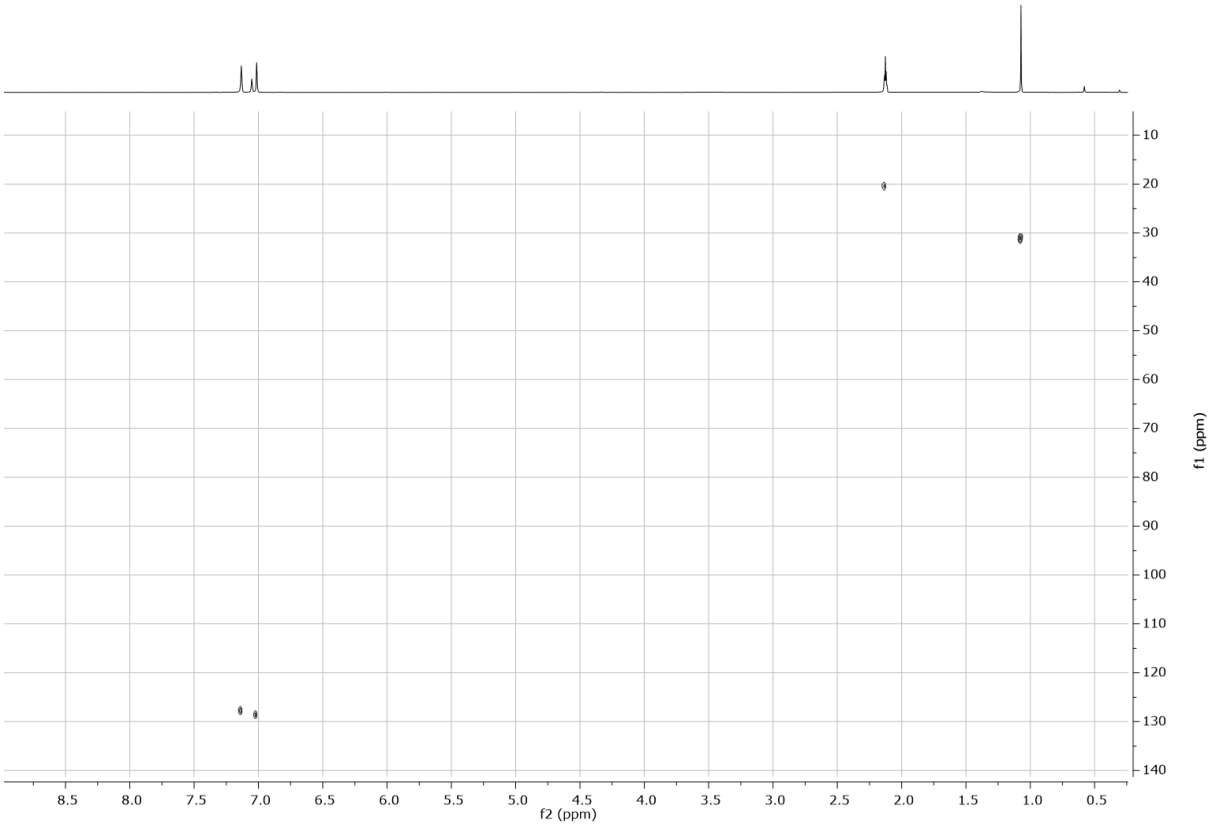

Figure S23. ^{1}H-^{13}C HSQC (toluene-d_8, 400 MHz) spectrum of ^{t}BuOK.

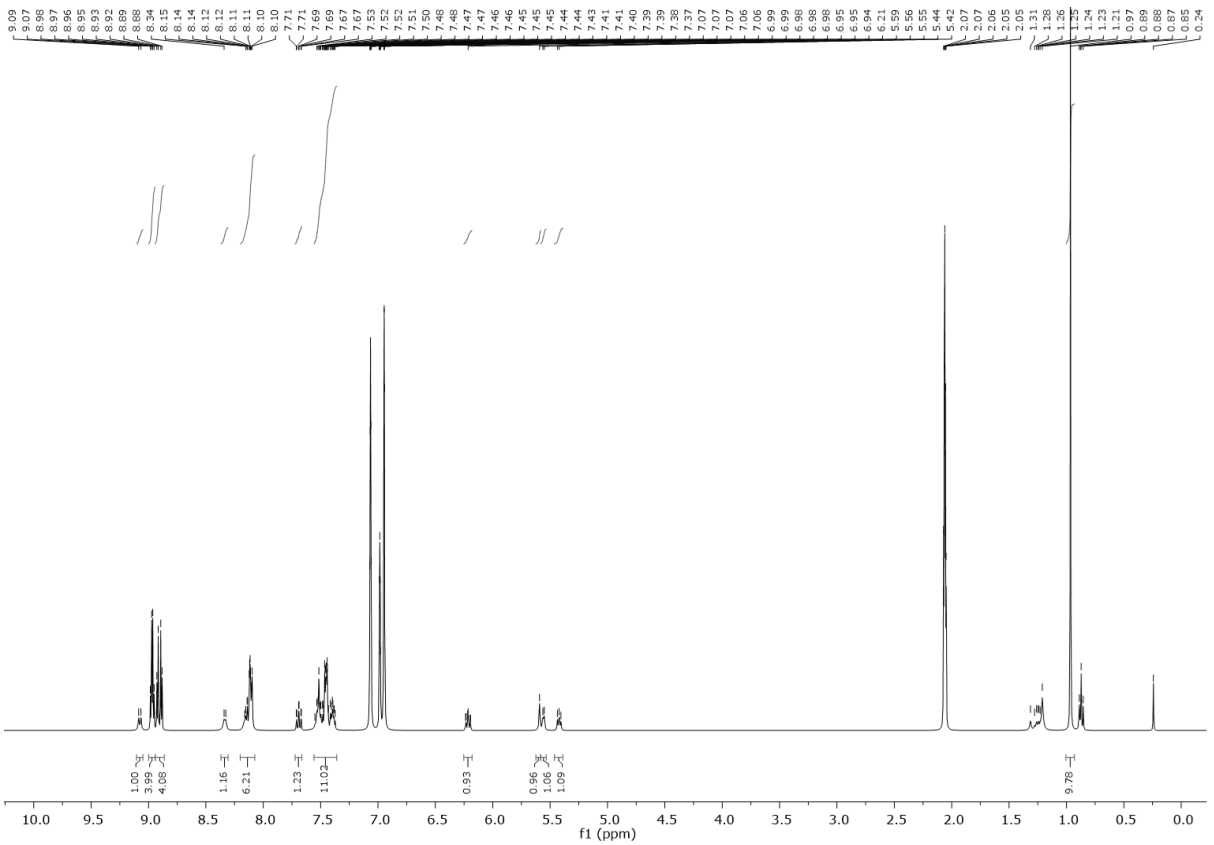

Figure S24. ^{1}H NMR (toluene-d_8, 400 MHz) spectrum of a combination of supramolecular ligand **L** with ^{t}BuOK in a 1 : 1 ratio. Characterization data for the self-assembly [**L1** ⊂ ^{t}BuOK]: ^{1}H NMR (400 MHz, toluene-d_8): δ = 9.08 (d, J = 8.0 Hz, 1H), 8.97 (q, J = 4.6 Hz, 4H), 8.90 (d, J = 14.2 Hz, 4H), 8.33 (d, J = 6.2 Hz, 1H), 8.19 – 8.07 (m, 6H), 7.69 (td, J = 7.8, 1.4 Hz, 1H), 7.58 – 7.34 (m, 11H), 6.21 (td, J = 7.9, 1.6 Hz, 1H), 5.59 (s, 1H), 5.56 (d, J = 5.0 Hz, 1H), 5.42 (t, J = 7.9 Hz, 1H), 0.97 (s, 9H) ppm.

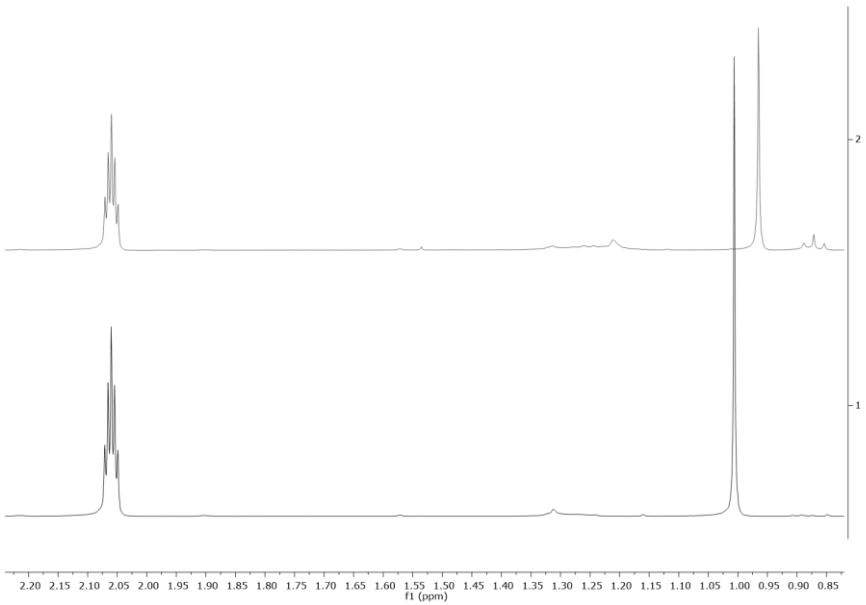

Figure S25. ^{1}H NMR (toluene-d_8, 400 MHz) spectra -aliphatic area zoom- of [**L1** ⊂ ^{t}BuOK] (top) and pure ^{t}BuOK (bottom).

3.4.3.3. Binding studies to disclose Zn···N binding between triazolopyridine motifs and zinc-teraphenylporphyrin (ZnTPP).

NMR binding experiment between L1* and ZnTPP (1:1 ratio): L* (1.6 mg, 7.4 x 10^{-6} mmol, 1equiv.) and **ZnTPP** (5 mg, x 10^{-6} mmol, 1 equiv.) were placed in an NMR tube and dried under vacuum for few minutes. Then, dry $CDCl_3$ (0.75 mL) was added and the corresponding ^1H NMR spectrum was recorded. ^1H NMR of **ZnTPP** and **L*** were also recorded independently for comparison purposes.

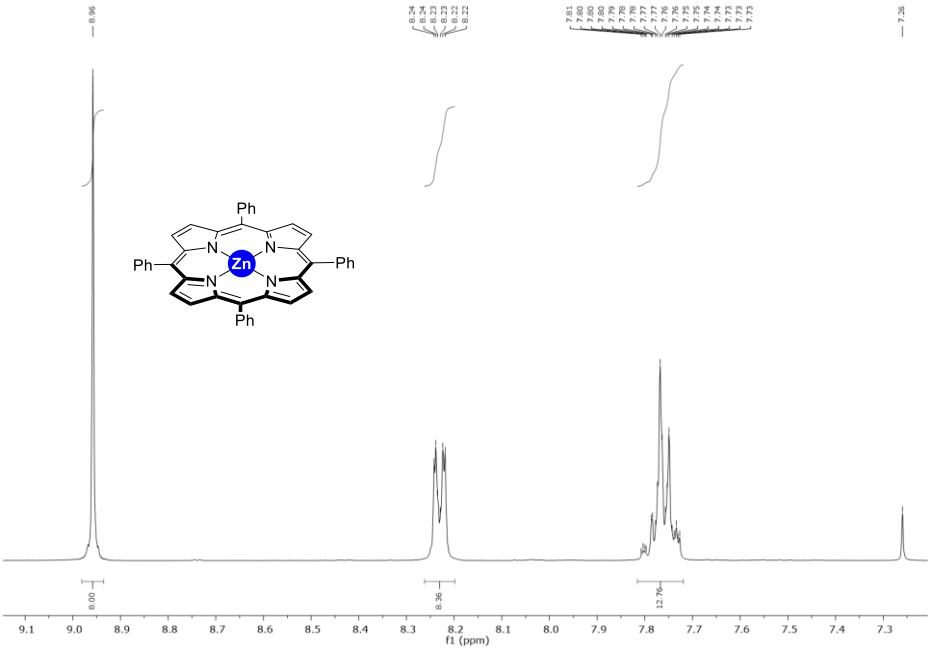

Figure S26. ^1H NMR ($CDCl_3$, 400 MHz) spectrum of **ZnTPP** (aromatic area zoom).

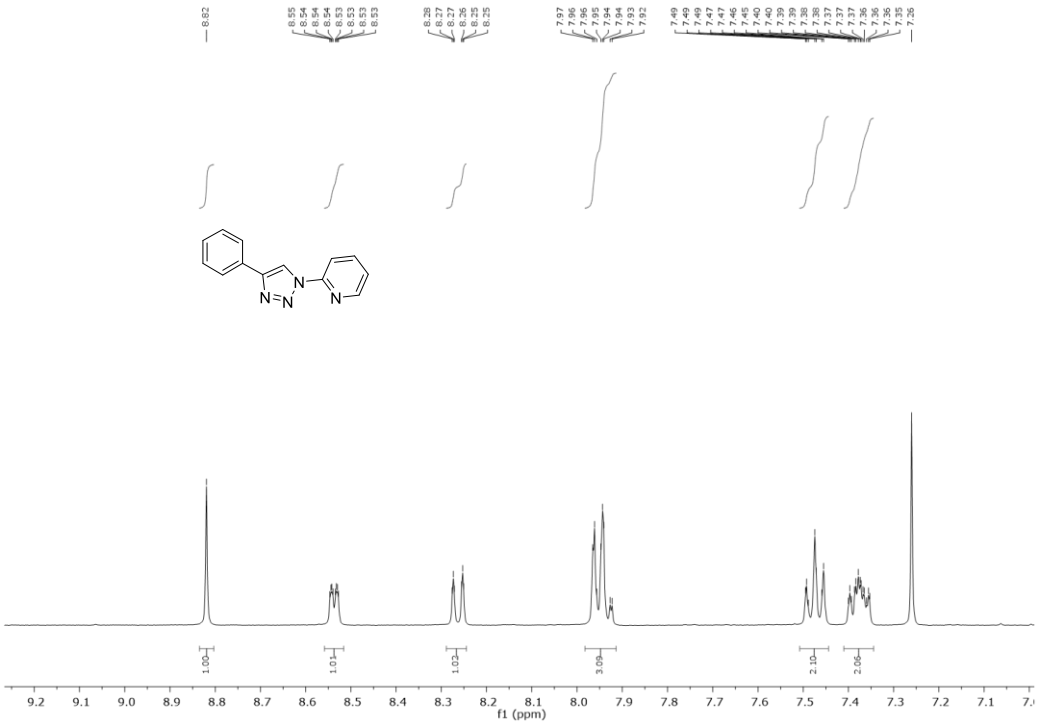

Figure S27. ^1H NMR ($CDCl_3$, 400 MHz) spectrum of **L1*** (aromatic area zoom).

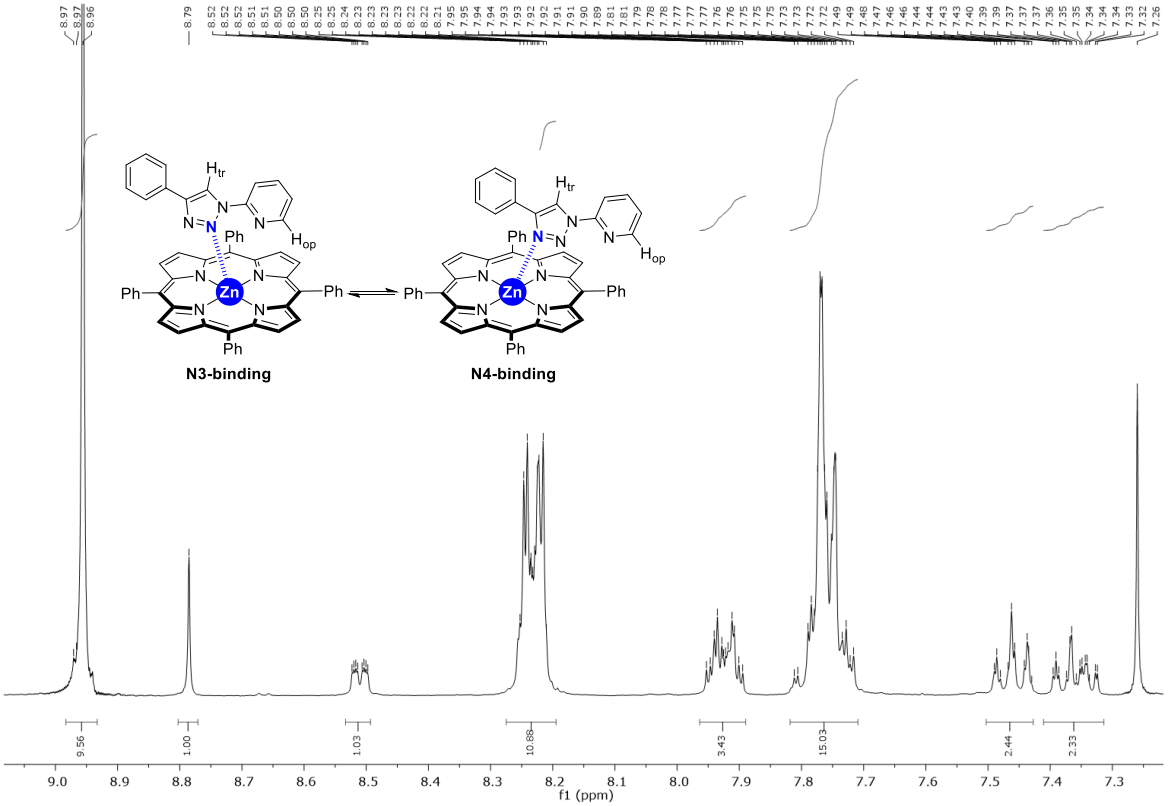

Figure S28. ^{1}H NMR ($CDCl_3$, 400 MHz) spectrum of an equimolar combination of **L1*** and **ZnTPP** (aromatic area zoom).

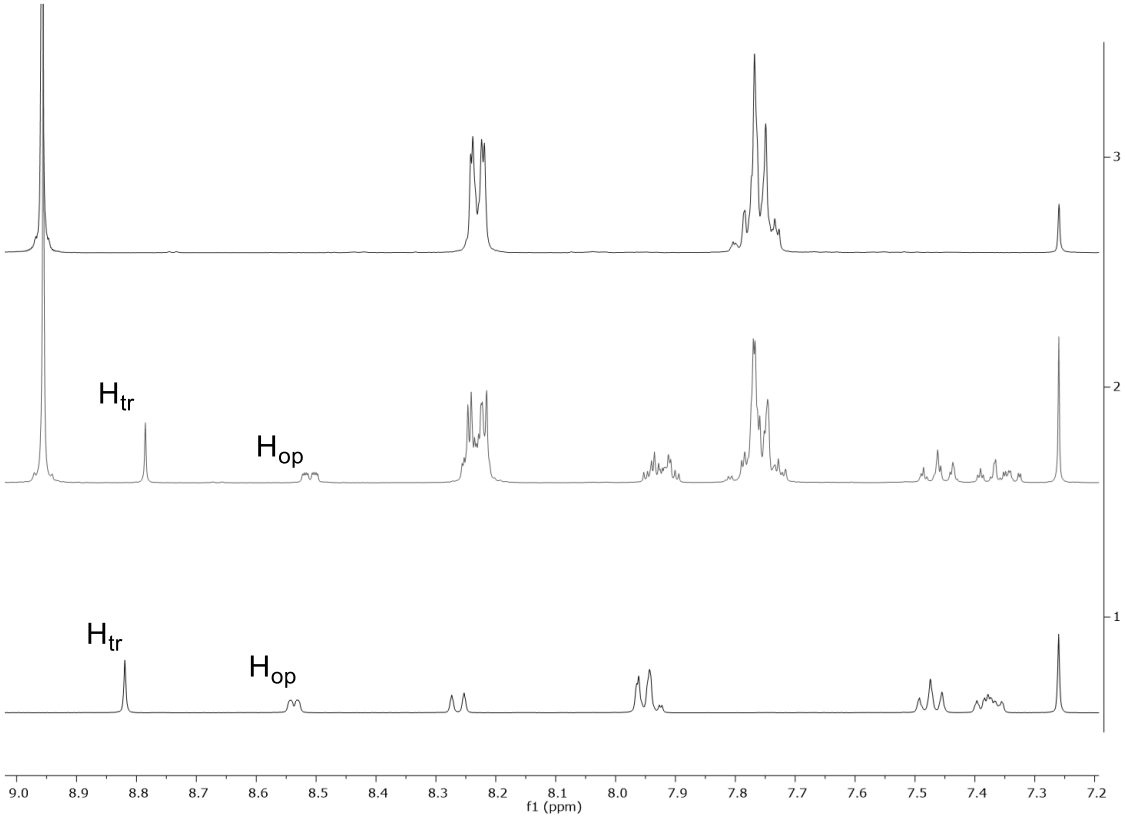

Figure S29. ^{1}H NMR ($CDCl_3$, 400 MHz) spectra -aromatic area zoom- of **ZnTPP** (top), an equimolar combination of **L1*** and **ZnTPP** (middle), and **L1*** (bottom).

NMR binding experiment between L2* and ZnTPP (1:1 ratio): L2* (2.1 mg, 7.4 x 10^{-6} mmol, 1 equiv.) and **ZnTPP** (5 mg, 7.4 x 10^{-6} mmol, 1 equiv.) were placed in an NMR tube and dried under vacuum for few minutes. Then, dry $CDCl_3$ (0.75 mL) was added and the corresponding ^1H NMR spectrum was recorded. ^1H NMR of **L2*** were also recorded independently for comparison purposes.

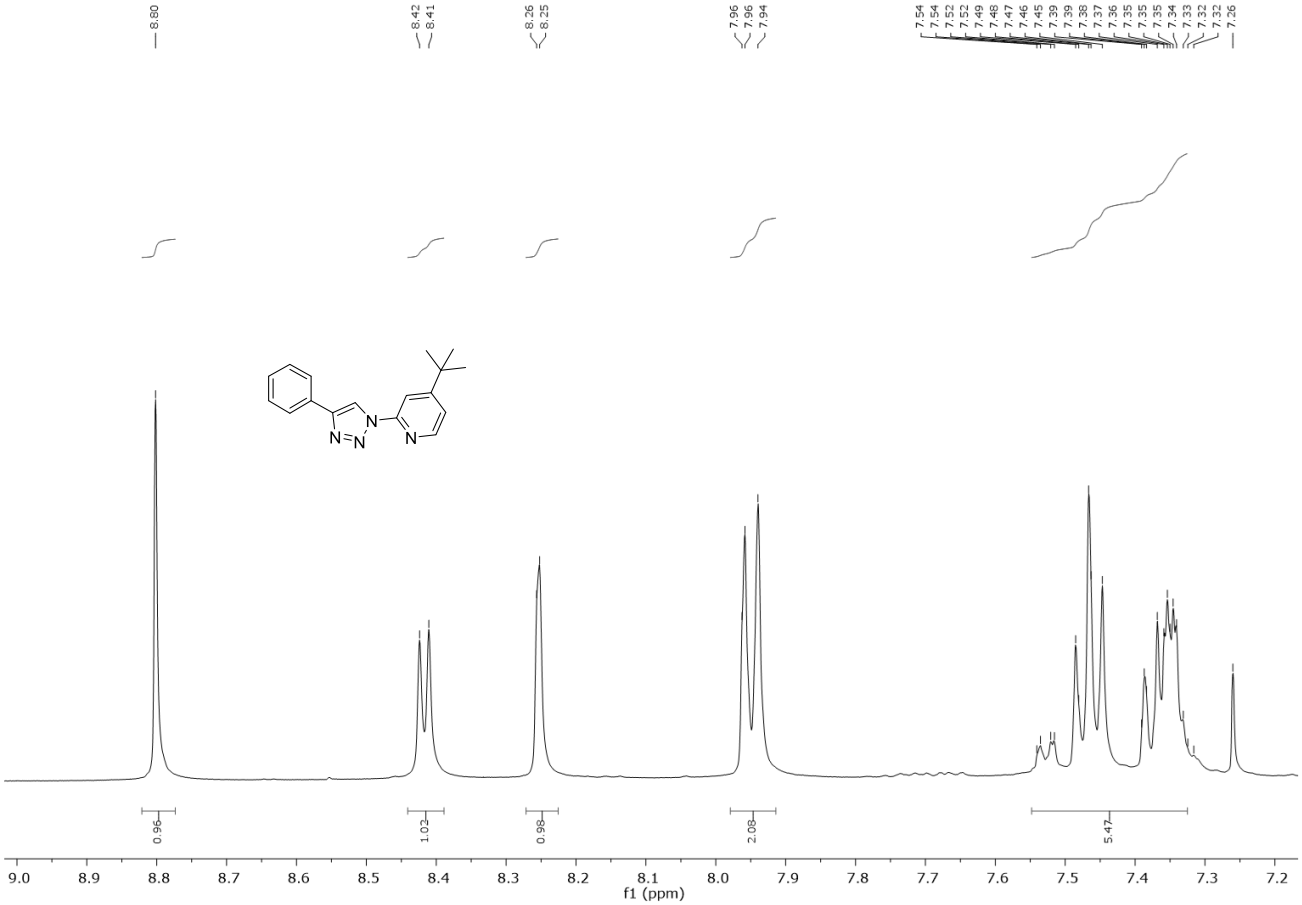

Figure S30. ^1H NMR ($CDCl_3$, 400 MHz) spectrum of **L2*** (aromatic area zoom).

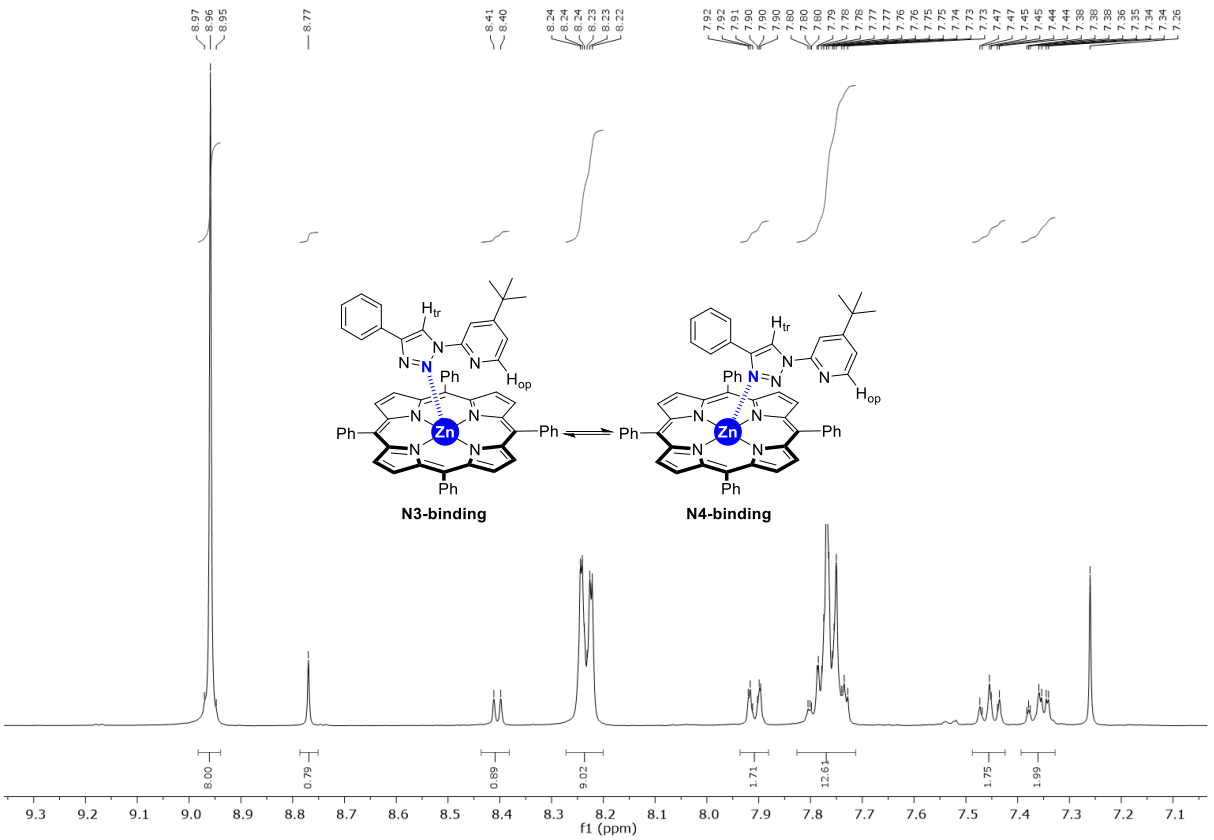

Figure S31. ^{1}H NMR ($CDCl_3$, 400 MHz) spectrum of an equimolar combination of **L2*** and **ZnTPP** (aromatic area zoom).

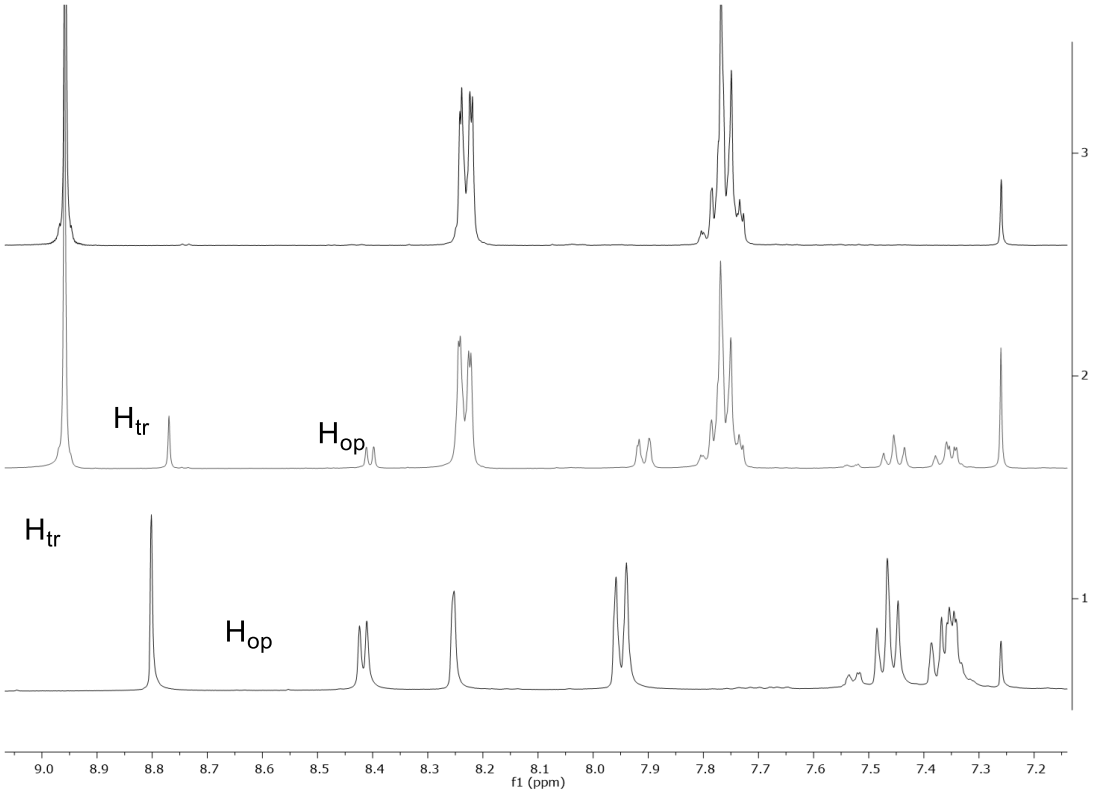

Figure S32. ^{1}H NMR ($CDCl_3$, 400 MHz) spectra -aromatic area zoom- of **ZnTPP** (top), an equimolar combination of **L2*** and **ZnTPP** (middle), and **L2*** (bottom).

3.4.4. Catalytic experiments.

3.4.4.1. Evaluation of catalysts.

General procedure: $[Ir(COD)(Cl)]_2$, ligand **L**, B_2pin_2 , and dodecane (0.25 eq.) were introduced in an oven dried Schlenk flask. *p*-xylene was added and the reaction mixture was stirred at room temperature for 5 minutes. Then pyridine was added and the mixture was stirred at a given temperature. Small aliquots were taken from the flask under argon flow after a 16 h using a dry pipette. Conversion and yield were estimated by GC-MS/GC-FID using dodecane as the internal standard. All experiment were done al least 2 times, the results of conversion and yield given are the average value.

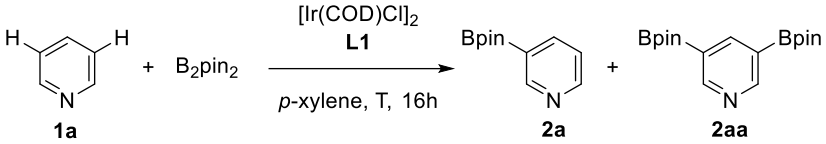

1) Following the general procedure, $[Ir(COD)(Cl)]_2$ (1.7 mg, 2.43 x 10^{-6} mol, 0.015 eq.), ligand **L1** (4.1 mg, 4.86 x 10^{-6} mol, 0.03 eq.), B_2pin_2 (41.1 mg, 1.62 x 10^{-4} mol, 1 eq.) and pyridine (13 mg, 13 µL, 1.62 x 10^{-4} mol, 1 eq.) were dissolved in *p*-xylene (1 mL). The reaction mixture was stirred at 80°C for 16 hours. Full conversion and an estimated yield of 40% for **2a** and 60% for **2aa** was determined by GC-FID analysis.

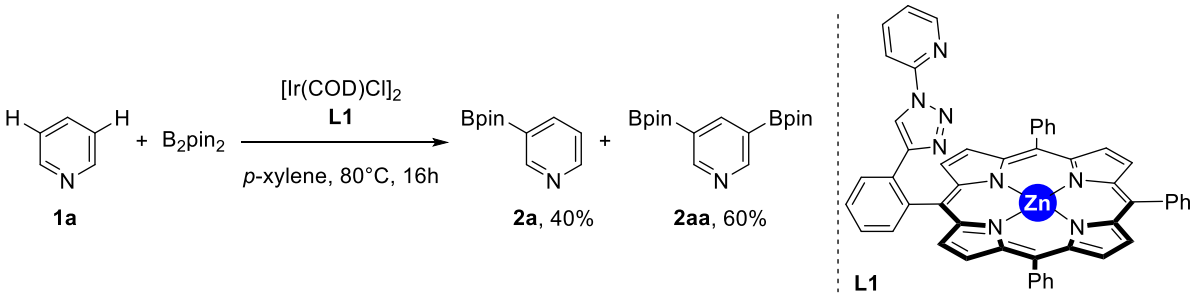

2) Following the general procedure, $[Ir(COD)(Cl)]_2$ (1.7 mg, 2.43 x 10^{-6} mol, 0.015 eq.), ligand **L3** (4.1 mg, 4.86 x 10^{-6} mol, 0.03 eq.), B_2pin_2 (41.1 mg, 1.62 x 10^{-4} mol, 1 eq.) and pyridine (13 mg, 13 µL, 1.62 x 10^{-4}

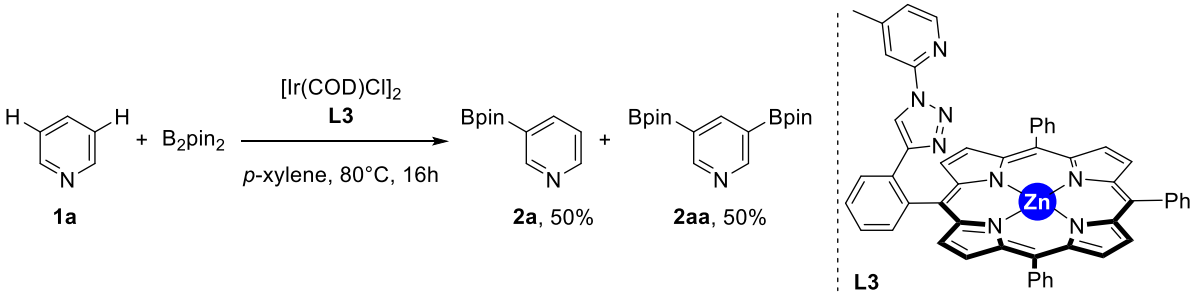

mol, 1 eq.) were dissolved in *p*-xylene (1 mL). The reaction mixture was stirred at 80°C for 16 hours. Full conversion and an estimated yield of 50% for **2a** and 50% for **2aa** was determined by GC-FID analysis.

3) Following the general procedure, $[Ir(COD)(Cl)]_2$ (1.7 mg, 2.43 x 10^{-6} mol, 0.015 eq.), ligand **L4** (4.1 mg, 4.86 x 10^{-6} mol, 0.03 eq.), B_2pin_2 (41.1 mg, 1.62 x 10^{-4} mol, 1 eq.) and pyridine (13 mg, 13 µL, 1.62 x 10^{-4} mol, 1 eq.) were dissolved in *p*-xylene (1 mL). The reaction mixture was stirred at 80°C for 16 hours. Full conversion and an estimated yield of 60% for **2a** and 40% for **2aa** was determined by GC-FID analysis.

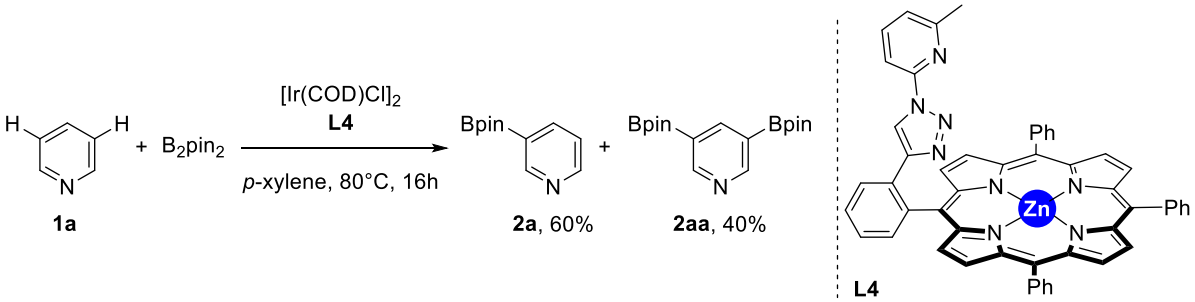

4) Following the general procedure, $[Ir(COD)(Cl)]_2$ (1.7 mg, 2.43 x 10^{-6} mol, 0.015 eq.), ligand **L5** (4.1 mg, 4.86 x 10^{-6} mol, 0.03 eq.), B_2pin_2 (41.1 mg, 1.62 x 10^{-4} mol, 1 eq.) and pyridine (13 mg, 13 µL, 1.62 x 10^{-4} mol, 1 eq.) were dissolved in *p*-xylene (1 mL). The reaction mixture was stirred at two different temperatures for 16 hours.

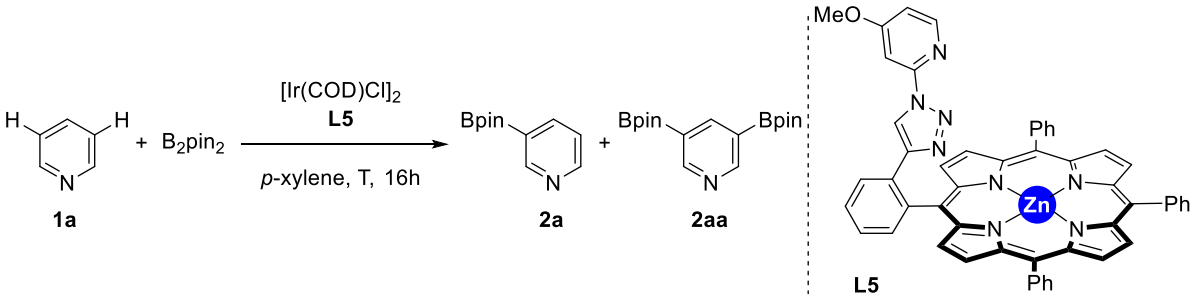

Conversion as well as estimated yield are given in the table below:

Entry	Temperature (°C)	Conversion (%)	**2a** (%)	**2aa** (%)
1	80	55	46	9
2	100	>99	56	44

5) Following the general procedure, $[Ir(COD)(Cl)]_2$ (1.7 mg, 2.43 x 10^{-6} mol, 0.015 eq.), ligand **L6** (4.3 mg, 4.86 x 10^{-6} mol, 0.03 eq.), B_2pin_2 (41.1 mg, 1.62 x 10^{-4} mol, 1 eq.) and pyridine (13 mg, 13 µL, 1.62 x 10^{-4} mol, 1 eq.) were dissolved in *p*-xylene (1 mL). The reaction mixture was stirred at two different temperatures for 16 hours.

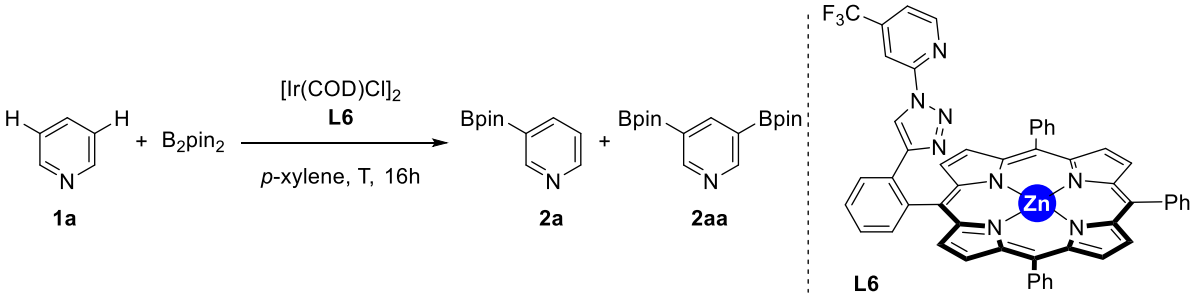

Conversion as well as estimated yield are given in the table below:

Entry	Temperature (°C)	Conversion (%)	**2a** (%)	**2aa** (%)
1	80	36	32	4
2	100	>99	44	56

6) Following the general procedure, $[Ir(COD)(Cl)]_2$ (1.7 mg, 2.43 x 10^{-6} mol, 0.015 eq.), ligand **L4** (4.3 mg, 4.86 x 10^{-6} mol, 0.03 eq.), B_2pin_2 (41.1 mg, 1.62 x 10^{-4} mol, 1 eq.) and pyridine (13 mg, 13 µL, 1.62 x 10^{-4} mol, 1 eq.) were dissolved in *p*-xylene (1 mL). The reaction mixture was stirred at four different temperatures for 16 hours.

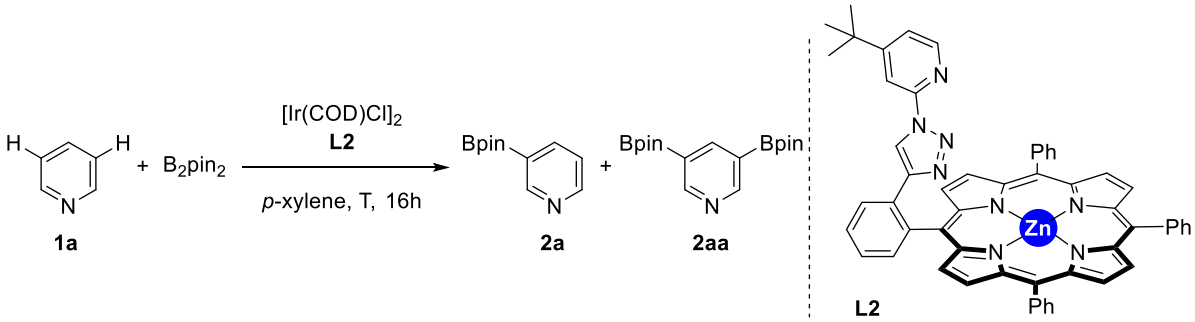

Conversion as well as estimated yield are given in the table below:

Entry	Temperature (°C)	Conversion (%)	3 (%)	4 (%)
1	20	0	0	0
2	80	5	5	0
3	100	11	10	0
4	120	15	15	traces

Summary of the catalytic performance using the supramolecular ligands L1-L6 at 80°C: mono-borylation 2a (blue color) versus bis-borylation 2aa (red color).

.

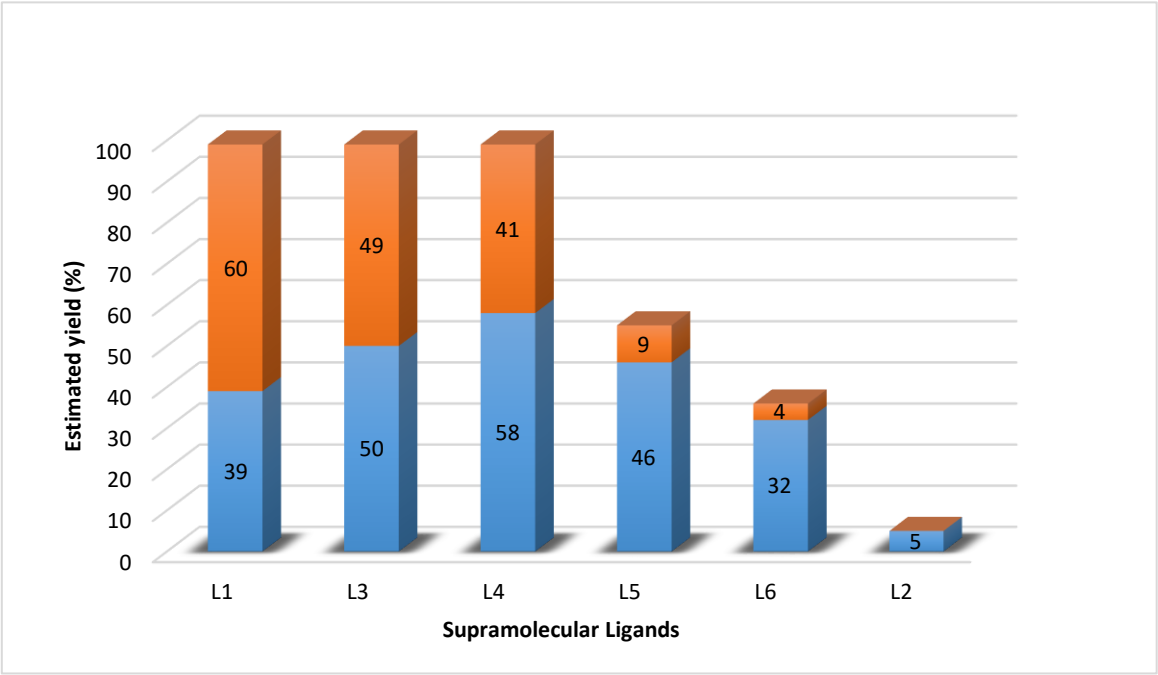

Plot of the evaluation of the least active supramolecular ligands (L2, L5 and L6) at different temperatures

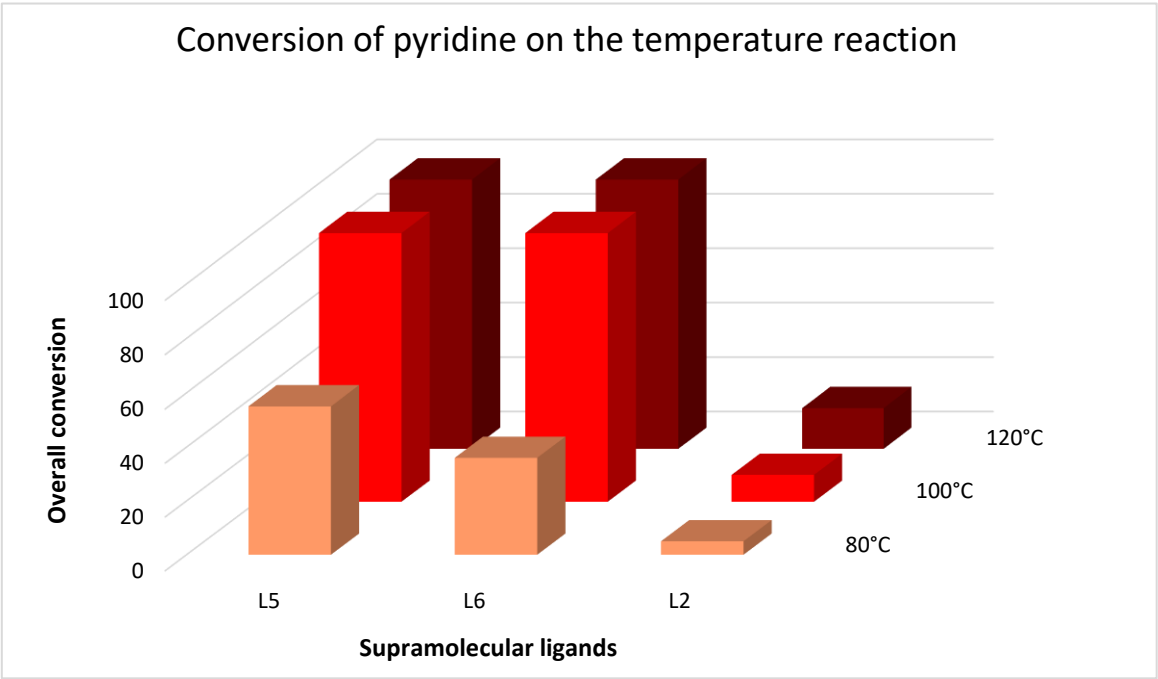

3.4.4.2. Kinetic studies on pyridine borylation using the most effective supramolecular ligands.

General procedure: $[Ir(COD)(Cl)]_2$, ligand **L**, B_2pin_2, and dodecane (0.25 eq.) were introduced in an oven dried Schlenk flask. *p*-xylene was added and the reaction mixture was stirred at room temperature for 5 minutes. Then 3-methylpyridine was added and the mixture was stirred at a 80 °C. Small aliquots were taken from the flask under argon flow every 1 hour using a dry pipette. Conversion and yield were estimated by GC-MS/GC-FID using dodecane as the internal standard. Fitting of the experimental data was done using sigmoidal Boltzmann function.

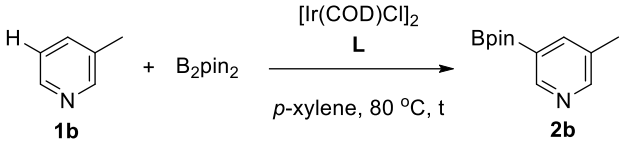

Reaction at standard conditions with ligand L1: Following the general procedure, $[Ir(COD)(Cl)]_2$ (16.5 mg, 2.43 x 10-5 mol, 0.015 eq.), ligand **L1** (41 mg, 4.86 x 10-5 mol, 0.03 eq.), B_2pin_2 (411 mg, 1.62 x 10-3 mol, 1 eq.) and 3 methylpyridine (160 µL, 1.62 x 10-3 mol, 1 eq.) were dissolved in *p*-xylene (10 mL). The reaction mixture was stirred at 80°C for 10 hours. Formation of *meta*-borylated product [**2b**] versus time (h) is plotted below (fitted values are shown in yellow, and experimental values are shown in orange dots):

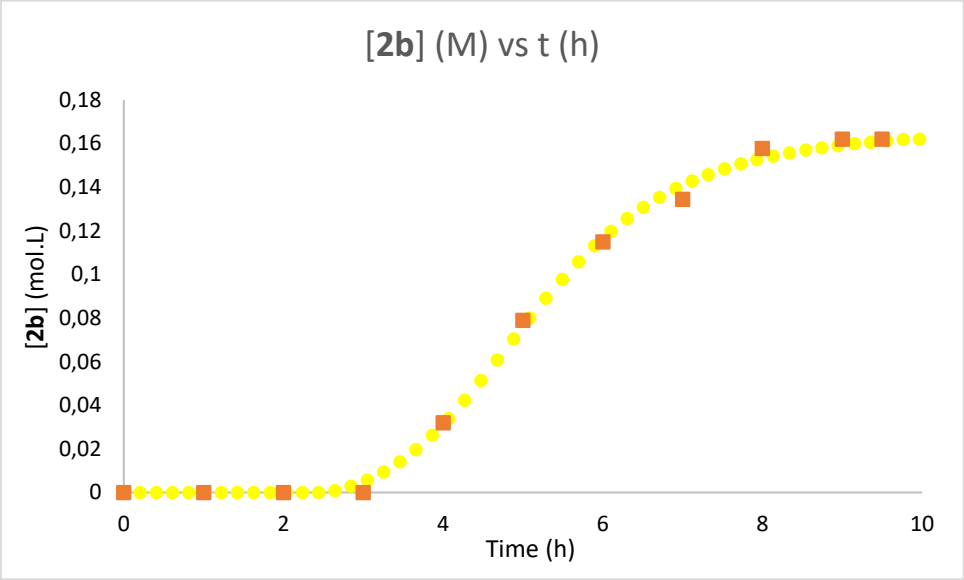

Reaction at standard conditions with ligand L3:

Following the general procedure, $[Ir(COD)(Cl)]_2$ (16.5 mg, 2.43 x 10-5 mol, 0.015 eq.), ligand **L3** (41 mg, 4.86 x 10-5 mol, 0.03 eq.), B_2pin_2 (411 mg, 1.62 x 10-3 mol, 1 eq.) and 3 methylpyridine (160 µL, 1.62 x 10-3 mol, 1 eq.) were dissolved in *p*-xylene (10 mL). The reaction mixture was stirred at 80°C for 9 hours. Formation of *meta*-borylated product [**2b**] versus time (h) is plotted below (fitted values are shown in red, and experimental values are shown in orange dots):

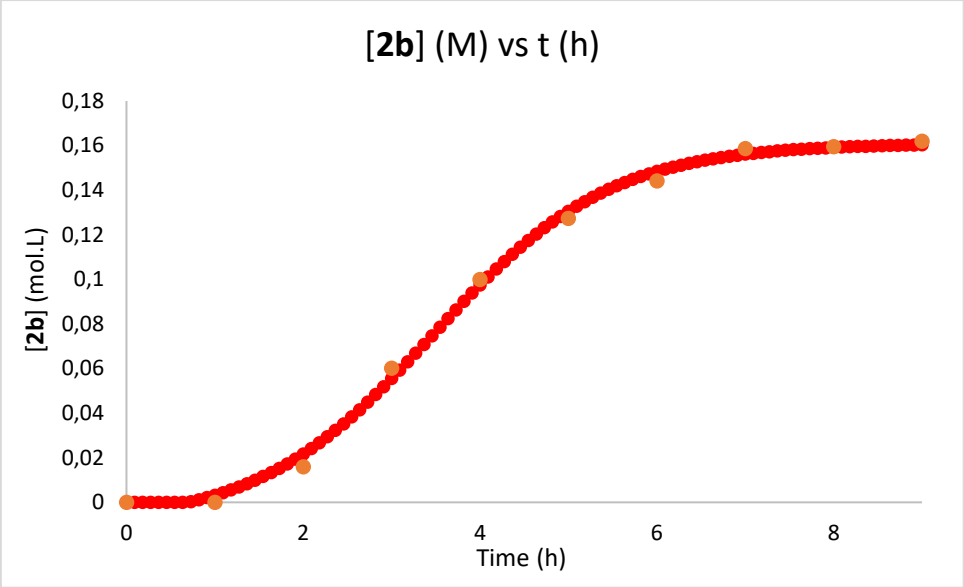

Reaction at standard conditions with ligand L4:

Following the general procedure, $[Ir(COD)(Cl)]_2$ (16.5 mg, 2.43 x 10-5 mol, 0.015 eq.), ligand **L4** (41 mg, 4.86 x 10-5 mol, 0.03 eq.), B_2pin_2 (411 mg, 1.62 x 10-3 mol, 1 eq.) and 3 methylpyridine (160 µL, 1.62 x 10-3 mol, 1 eq.) were dissolved in *p*-xylene (10 mL). The reaction mixture was stirred at 80°C for 16 hours. Formation of *meta*-borylated product [**2b**] versus time (h) is plotted below (fitted values are shown in blue, and experimental values are shown in orange dots):

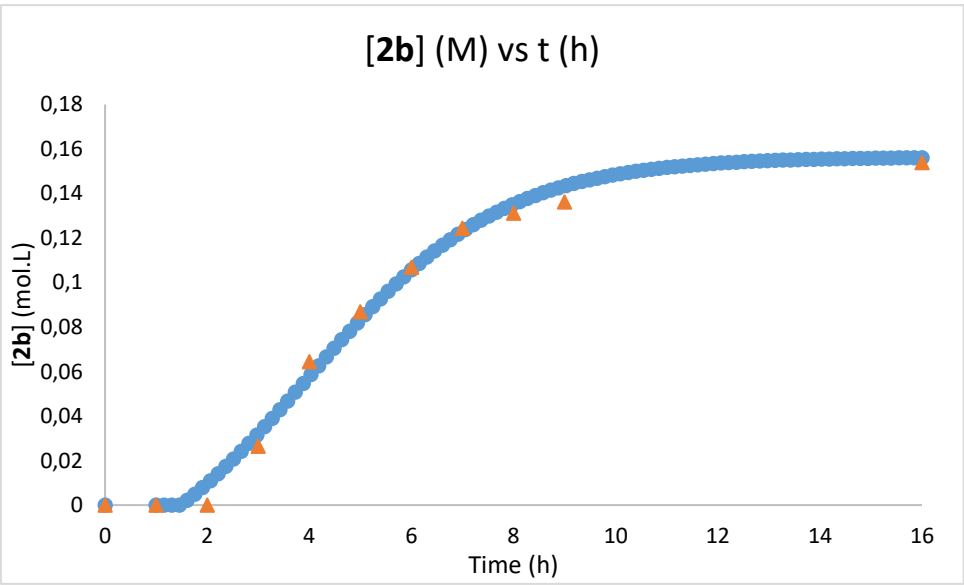

Summary of kinetic experiments

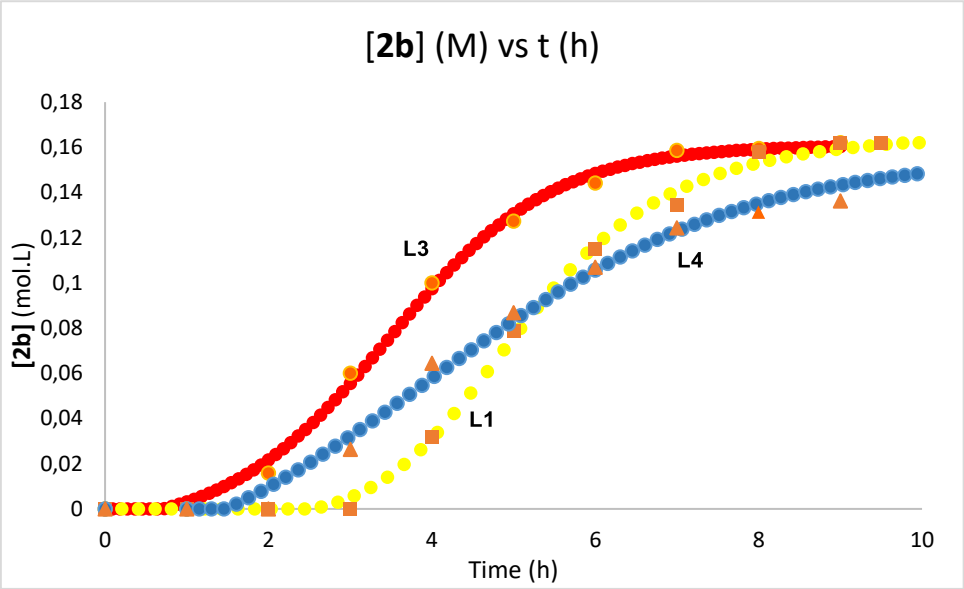

3.4.4.3. Evaluation of the catalytic performance of L2 in the presence of additives.

General procedure: $[Ir(COD)(Cl)]_2$, ligand **L2**, B_2pin_2, and dodecane (0.25 eq.) were introduced in an oven dried Schlenk flask. *p*-xylene was added and the reaction mixture was stirred at room temperature for 5 minutes. Then 3-methylpyridine and an additive were added and the mixture was stirred at 80°C. Small aliquots were taken from the flask under argon flow every 1 hour using a dry pipette. Conversion and yield were estimated by GC-MS/GC-FID using dodecane as the internal standard. Fitting of the experimental data was done using sigmoidal Boltzmann function.

Following the general procedure, $[Ir(COD)(Cl)]_2$ (16.5 mg, 2.43×10^{-5} mol, 0.015 eq.), ligand **L3** (41 mg, 4.86×10^{-5} mol, 0.03 eq.), B_2pin_2 (411 mg, 1.62×10^{-3} mol, 1 eq.), HBpin (18 µL, 6.48×10^{-5} mol, 0.04 eq.) and 3 methylpyridine (160 µL, 1.62×10^{-3} mol, 1 eq.) were dissolved in *p*-xylene (10 mL). The reaction mixture was stirred at 80°C for 9 hours. Formation of *meta*-borylated product [**2b**] versus time (h) is plotted below (fitted values are shown in yellow, and experimental values are shown in orange dots):

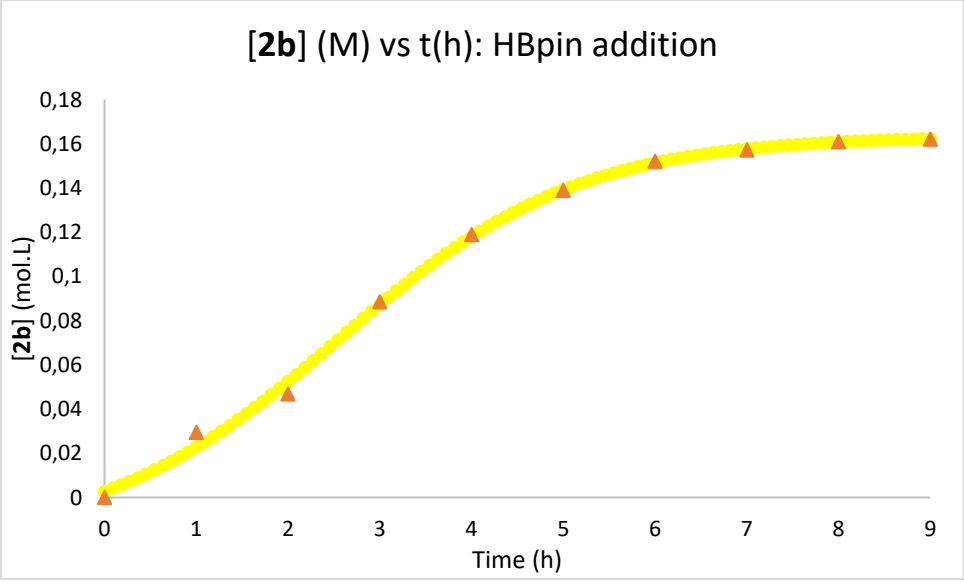

Following the general procedure, $[Ir(COD)(Cl)]_2$ (16.5 mg, 2.43 x 10^{-5} mol, 0.015 eq.), ligand **L2** (41 mg, 4.86 x 10^{-5} mol, 0.03 eq.), B_2pin_2 (411 mg, 1.62 x 10^{-3} mol, 1 eq.), 2,6-lutidine (8 µL, 6.48 x 10^{-5} mol, 0.04 eq.) and 3 methylpyridine (160 µL, 1.62 x 10^{-3} mol, 1 eq.) were dissolved in *p*-xylene (10 mL). The reaction mixture was stirred at 80°C for 9 hours. Formation of meta-borylated product [**2b**] versus time (h) is plotted below (fitted values are shown in blue, and experimental values are shown in orange dots):

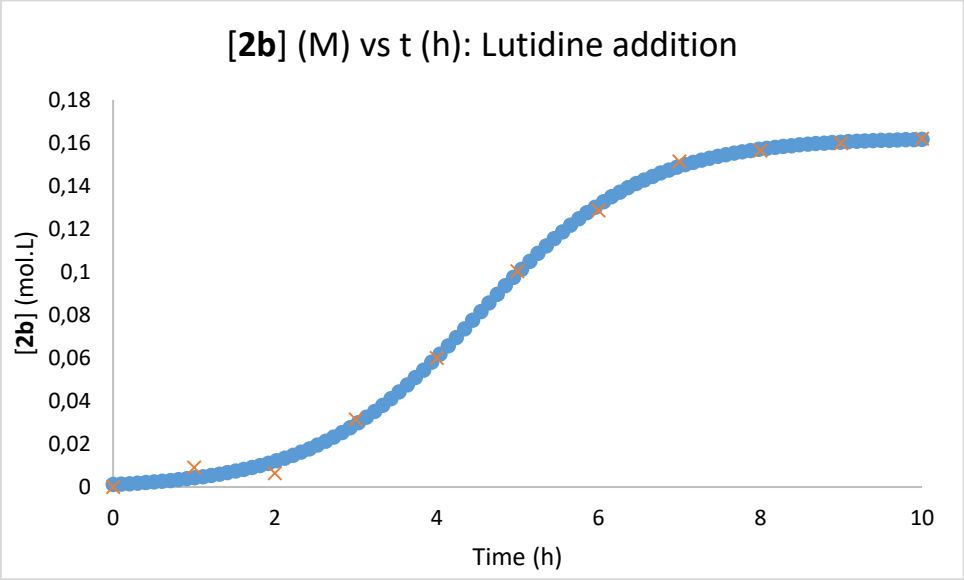

Summary of C-H borylation experiment using supramolecular ligand L-4-Me and additive

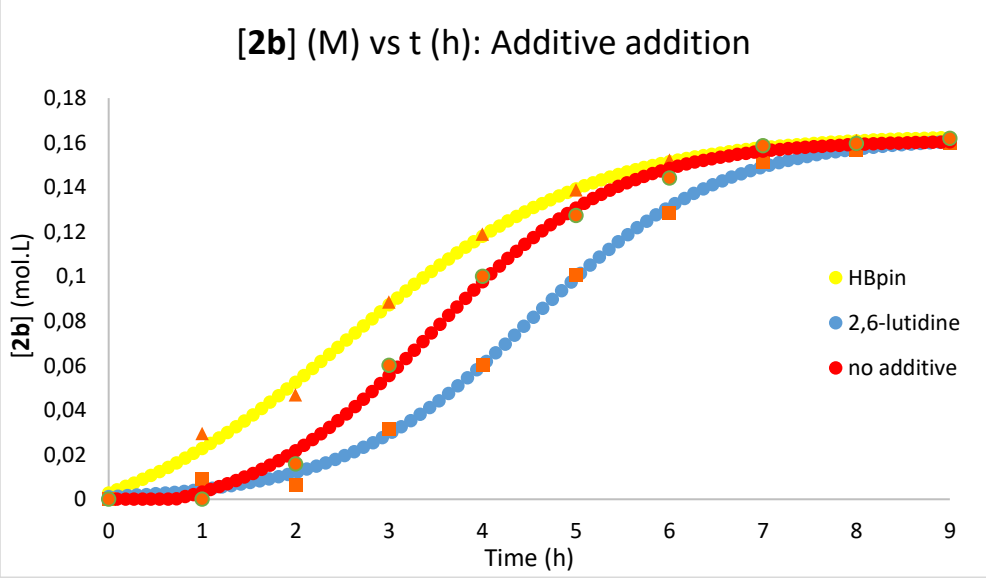

3.4.4.4. Final optimization of C-H borylation of pyridine at high temperature.

Following the general procedure, $[Ir(COD)(Cl)]_2$ (1.7 mg, 2.43 x 10^{-6} mol, 0.015 eq.), ligand **L3** (4.1 mg, 4.86 x 10^{-6} mol, 0.03 eq.), B_2pin_2 (41.1 mg, 1.62 x 10^{-4} mol, 1 eq.), HBpin (1 µL, 6.48 x 10^{-6} mol, 0.04 eq.) and 3 methylpyridine (16 µL, 1.62 x 10^{-4} mol, 1 eq.) were dissolved in *p*-xylene (10 mL). The reaction mixture was stirred at 100°C for 2 hours. Due to partial to total evaporation of 3-methylpyridine and of *p*-xylene solvent at 100°C when opening the Schlenk under a flow of argon, only two points at 1 and 2 hours were taken. More aliquots taken results in poor overall conversion, non reproducible values and a non-fitting kinetic plot using Boltzmann sigmoidal function.

Entry	Time (h)	Conversion (%)	Estimated yield (%)
1	0	0	0
2	1	58	57
3	2	100	99

As a note, increasing the temperature to 120°C results in almost no conversion of pyridine, and traces amount of borylated pyridine produced.

3.4.4.5. Control experiments.

- Control experiment without any iridium precursor: B_2pin_2 (41.1 mg, 1.62 x 10^{-4} mol, 1 equiv.) Ligand **L3** (4.1 mg, 4.9 x 10^{-6} mol, 0.03 equiv.) and dodecane (6.9 mg, 9.2 µL, 4.05 x 10^{-5} mol, 0.25 equiv.) were introduced in an oven dried Schlenk flask. *p*-xylene (1 mL) was added and the reaction mixture was stirred at room temperature for 30 minutes. Then, 3-methylpyridine (15 mg, 16 µL, 1.62 x 10^{-4} mol, 1 equiv.) and HBpin (1.5 mg, 1.8 µL, 6.5 x 10^{-6} mol, 0.04 equiv.) were added. The reaction mixture was stirred during 24 h at 100 °C. The reaction was cooled down to room temperature and analyzed by GC-MS analysis showing no conversion of starting materials nor product formation.

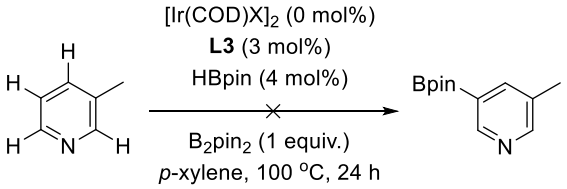

Control experiment without L3: $[Ir(COD)(Cl)]_2$ (1.7 mg, 2.4 x 10^{-6}, 0.015 equiv.), B_2pin_2 (41.1 mg, 1.62 x 10^{-4} mol, 1 equiv.) and dodecane (6.9 mg, 9.2 µL, 4.05 x 10^{-5} mol, 0.25 equiv.) were introduced in an oven dried Schlenk flask. *p*-xylene (1 mL) was added and the reaction mixture was stirred at room temperature for 30 minutes. Then 3-methylpyridine (15 mg, 16 µL, 1.62 x 10^{-4} mol, 1 equiv.) and HBpin (1.5 mg, 1.8 µL, 6.5 x 10^{-6} mol, 0.04 equiv.) were added. The reaction mixture was stirred during 24 h at 100°C. The reaction was cooled down to room temperature and analyzed by GC-MS analysis showing no conversion of starting materials nor product formation.

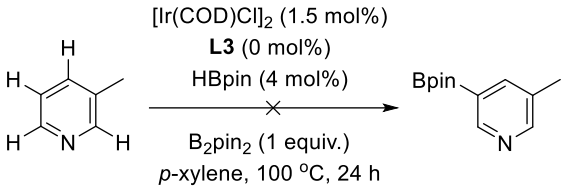

Control experiment using ligand L1* + ZnTPP: $[Ir(COD)(Cl)]_2$ (1.7 mg, 2.4 x 10^{-6} mol, 0.015 eq.), B_2pin_2 (41.1 mg, 1.62 x 10^{-4} mol, 1 equiv.), ligand **L1*** (1.1 mg, 4.9 x 10^{-6} mol, 0.03 equiv.), **ZnTPP** (3.3 mg, 4.9 x 10^{-6} mol, 0.03 equiv.) and dodecane (6.9 mg, 9.2 µL, 4.05 x 10^{-5} mol, 0.25 equiv.) were introduced in an oven dried Schlenk flask. *p*-xylene (1 mL) was added and the reaction mixture was stirred at room temperature for 30 minutes. Then 3-methylpyridine (15 mg, 16 µL, 1.62 x 10^{-4} mol, 1 equiv.) and HBpin (1.5 mg, 1.8 µL, 6.5 x 10^{-6} mol, 0.04 equiv.) were added. The reaction mixture was stirred during 24 h at 100°C. The reaction was cooled down to room temperature and analyzed by GC-MS analysis showing no conversion of starting materials nor product formation.

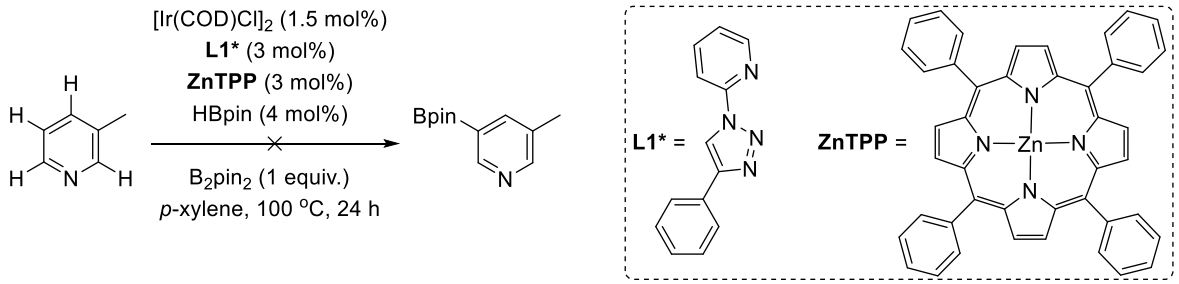

General procedure for pyridine borylation using different boron source: $[Ir(COD)(Cl)]_2$ (1.7 mg, 2.4 x 10^{-6} mol, 0.015 eq.), B_2X_2 (0 or 1 equiv.), ligand **L1** (4.1 mg, 4.9 x 10^{-6} mol, 0.03 equiv.) and dodecane (6.9 mg, 9.2 µL, 4.05 x 10^{-5} mol, 0.25 equiv.) were introduced in an oven dried Schlenk flask. *p*-xylene (1 mL) was added and the reaction mixture was stirred at room temperature for 30 minutes. Then the substrate (1.62 x 10^{-4} mol, 1 equiv.) and HBpin (0 or 1 equiv.) were added. The reaction mixture was stirred a given temperature and followed by GC-MS analysis. Purification by Kugelrorh distillation afforded the borylated product as a pure product (entry 1 and 2) or as a mixture of isomer (entry 4).

Entry	Boron source	Time (h)	T (°C)	Yield (%)	meta/others
1	B_2pin_2	12	80	>99	>99%
2	HBpin	16	80	79	>99%
3[a]	B_2cat_2	24	80	0	-

[a]Full decomposition of B_2cat_2.

3.4.5. Characterization of products from the catalysis.

Characterization of products resulting from the catalytic C-H borylation of 3-substitued -pyridines experiments at 100°C.

General procedure: $[Ir(COD)(Cl)]_2$ (1.7 mg, 2.4 x 10^{-6} mol, 0.015 eq.), B_2pin_2 (41.1 mg, 1.62 x 10^{-4} mol, 1 eq.), ligand **L** (4.1 mg, 4.9 x 10^{-6} mol, 0.03 eq.), and dodecane (6.9 mg, 9.2 µL, 4.05 x 10^{-5} mol, 0.25 eq.) were introduced in an oven dried Schlenk flask. *p*-xylene (1 mL) was added and the reaction mixture was stirred at room temperature for 5 minutes. Then, the substrate (1.62 x 10^{-4} mol, 1 eq.) and HBpin (0.9 µL, 6.48 x 10^{-6} mol, 0.04 eq) was added and the reaction was stirred at 100°C. Upon completion monitored by GC-MS analysis, conversion and yield were estimated using dodecane as the internal standard by GC-MS and GC-FID. The solvent was then evaporated and the residue was purified using Kugelrohr distillation apparatus yielding the analytically pure product.

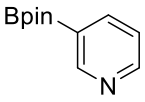

3-(4,4,5,5-Tetramethyl-1,3,2-dioxaborolan-2-yl)-pyridine (2a): Following the optimized conditions. Purification by Kugelrorh distillation afforded the analytically pure product. ^{1}H NMR (400 MHz, $CDCl_3$): δ = 8.95 (s, 1H), 8.67 (d, *J* = 2 Hz, 1H), 8.07 (dt, *J* = 7.6, 2 Hz, 1H), 7.26-7.32 (m, 1H), 1.38 (s, 12H) ppm. $^{13}C\{^1H\}$ NMR (101 MHz, $CDCl_3$): δ = 155.44, 151.94, 142.22, 123.06, 84.23, 24.86 ppm. $^{11}B\{^1H\}$ NMR (128 MHz, $CDCl_3$): δ = 30.86 (s) ppm. The spectral data match those found in literature.[7]

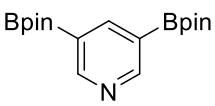

3-5-bis(4,4,5,5-Tetramethyl-1,3,2-dioxaborolan-2-yl)-pyridine (2aa): Following the optimized conditions. Purification by Kugelrorh distillation afforded the analytically pure product. ^{1}H NMR (400 MHz, $CDCl_3$): δ = 9.00 (d, *J* = 1.9 Hz, 1H), 8.48 (t, *J* = 1.9 Hz, 1H), 1.35 (s, 12H) ppm. $^{13}C\{^1H\}$ NMR (101 MHz, Chloroform-*d*) δ = 157.50, 148.78, 84.18, 24.85 ppm. $^{11}B\{^1H\}$ NMR (128 MHz, $CDCl_3$): δ = 31.15 (s) ppm. The spectral data match those found in literature.[8]

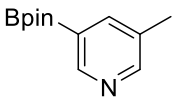

3-(4,4,5,5-Tetramethyl-1,3,2-dioxaborolan-2-yl)-5-methylpyridine (2b): Following the general procedure, the reaction mixture was stirred at 100 °C for 2 hours. Quantitative conversion and yield were estimated by GC-MS analysis. Purification by Kugelrorh distillation afforded the analytically pure product (31 mg, 87% yield). ^{1}H NMR (400 MHz, $CDCl_3$): δ = 8.72 (s, 1H), 8.47 (s, 1H), 7.87 (s, 1H), 2.32 (s, 3H), 1.35 (s, 12H) ppm. $^{13}C\{^1H\}$ NMR (101 MHz, $CDCl_3$): δ = 152.55, 152.40, 142.68, 132.29, 84.16, 24.86, 18.30 ppm. $^{11}B\{^1H\}$ NMR (128 MHz, $CDCl_3$): δ = 31.06 (s) ppm. GC: t_R = 16.5 min; MS (EI): *m/z* = 219 (M^+, 25), 204 (50), 162 (25), 120 (100). HRMS (ESI): *m/z* calcd for $C_{12}H_{19}NO_2{}^{11}B$ $[M+H]^+$ 220.15033; found: 220.1503 (0 ppm).

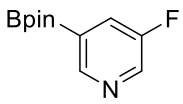

3-(4,4,5,5-Tetramethyl-1,3,2-dioxaborolan-2-yl)-5-Fluoropyridine (2c): Following the general procedure, the reaction mixture was stirred at 100 °C for 2 hours. Quantitative conversion and yield were estimated by GC-MS and GC-FID analysis. Purification by Kugelrorh distillation afforded the analytically pure product (31 mg, 89% yield.). ^{1}H NMR (400 MHz, $CDCl_3$): δ = 8.74 (s, 1H), 8.52 (s, 1H), 7.74 (dd, *J* = 8.6, 2.2 Hz, 1H), 1.35 (s, 12H) ppm. $^{13}C\{^1H\}$ NMR (101 MHz, $CDCl_3$): δ = 151.12 (d, *J* = 5.1 Hz), 140.40 (d, *J* = 23.7 Hz), 128.18 (d, *J* = 16.3 Hz), 84.58, 24.84 ppm. $^{11}B\{^1H\}$ NMR (128 MHz, $CDCl_3$): δ = 30.27 (s) ppm. $^{19}F\{^1H\}$ NMR (376 MHz, $CDCl_3$): δ = -127.44 (s) ppm. GC: t_R = 13.9 min; MS (EI): *m/z* = 223 (M^+, 30), 208 (100), 166 (50), 137 (40), 124 (85), 58 (45). HRMS (ESI): *m/z* calcd for $C_{11}H_{16}NO_2F{}^{11}B$ $[M+H]^+$ 224.12526; 224.1254 (1 ppm).

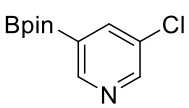

3-(4,4,5,5-Tetramethyl-1,3,2-dioxaborolan-2-yl)-5-chloropyridine (2d): Following the general procedure, the reaction mixture was stirred at 100 °C for 2.5 hours. Quantitative conversion and yield were estimated by GC-MS and GC-FID analysis. Purification by Kugelrorh distillation afforded the analytically pure product (33 mg, 86% yield). ^{1}H NMR (400 MHz, $CDCl_3$): δ = 8.79 (d, *J* = 1.0 Hz, 1H), 8.62 (d, *J* = 2.5 Hz, 1H), 8.03 (t, *J* = 2.5, 1.0 Hz, 1H), 1.35 (s,

12H) ppm. $^{13}C\{^1H\}$ NMR (101 MHz, $CDCl_3$): δ = 152.92, 150.84, 141.66, 132.03, 84.61, 24.84 ppm. $^{11}B\{^1H\}$ NMR (128 MHz, $CDCl_3$): δ = 30.64 (s) ppm. GC: t_R = 16.4 min; MS (EI): *m/z* = 239 (M^+, 45), 226 (35), 224 (100), 182 (45), 153 (50), 140 (80), 139 (20), 85 (30), 58 (50). HRMS (ESI): *m/z* calcd for $C_{11}H_{16}NO_2{}^{35}Cl^{11}B$ $[M+H]^+$ 240.09571; 240.0957 (0 ppm).

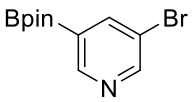

3-(4,4,5,5-Tetramethyl-1,3,2-dioxaborolan-2-yl)-5-bromopyridine (2e): Following the general procedure, the reaction mixture was stirred at 100 °C for 3.5 hours. Quantitative conversion and yield were estimated by GC-MS and GC-FID analysis. Purification by Kugelrorh distillation afforded the analytically pure product (38 mg, 84% yield). ^1H NMR (400 MHz, $CDCl_3$): δ = 8.83 (d, *J* = 1.2 Hz, 1H), 8.72 (d, *J* = 2.4 Hz, 1H), 8.18 (dd, *J* = 2.4, 1.2 Hz, 1H), 1.35 (s, 12H) ppm. $^{13}C\{^1H\}$ NMR (101 MHz, $CDCl_3$): δ = 153.24, 152.98, 144.53, 120.95, 84.62, 24.85 ppm. $^{11}B\{^1H\}$ NMR (128 MHz, $CDCl_3$): δ = 30.70 (s) ppm. GC: t_R = 17.7 min; MS (EI): *m/z* = 283 (M^+, 30), 285 (30), 270 (95), 268 (100), 226 (30), 186 (50), 184 (50), 85 (30), 58 (70). The spectral data match those found in literature.[9]

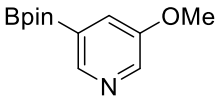

3-(4,4,5,5-Tetramethyl-1,3,2-dioxaborolan-2-yl)-5-methoxypyridine (2f): Following the general procedure, the reaction mixture was stirred at 100 °C for 2 hours. Quantitative conversion and yield were estimated by GC-MS and GC-FID analysis. Purification by Kugelrorh distillation afforded the analytically pure product (35 mg, 91 % yield). ^1H NMR (400 MHz, $CDCl_3$): δ = 8.53 (d, *J* = 1.5 Hz, 1H), 8.35 (d, *J* = 3.1 Hz, 1H), 7.53 (t, *J* = 3.1, 1.5 Hz, 1H), 3.85 (s, 3H), 1.34 (s, 12H) ppm. $^{13}C\{^1H\}$ NMR (101 MHz, $CDCl_3$): δ = 155.23, 147.54, 140.58, 125.20, 84.25, 55.47, 24.83 ppm. $^{11}B\{^1H\}$ NMR (128 MHz, $CDCl_3$): δ = 30.78 (s) ppm. GC: t_R = 17.9 min; MS (EI): *m/z* = 235 (M^+, 80), 220 (50), 178 (30), 149 (80), 135 (100). The spectral data match those found in literature.[10]

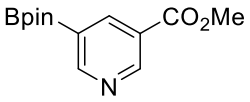

3-Pyridinecarboxylic acid, 5-(4,4,5,5-tetramethyl-1,3,2-dioxaborolan-2-yl)-, methyl ester (2g): Following the general procedure, the reaction mixture was stirred at 100 °C for 3 hours. Quantitative conversion and yield were estimated by GC-MS analysis. Purification by Kugelrorh distillation afforded the analytically pure product (35 mg, 79% yield). ^1H NMR (400 MHz, $CDCl_3$): δ = 9.27 (d, *J* = 2.3 Hz, 1H), 9.08 (d, *J* = 1.6 Hz, 1H), 8.67 (dd, *J* = 2.3, 1.6 Hz, 1H), 3.95 (s, 3H), 1.37 (s, 12H) ppm. $^{13}C\{^1H\}$ NMR (101 MHz, $CDCl_3$): δ = 165.78, 158.75, 152.84, 143.34, 125.44, 84.60, 52.36, 24.86 ppm. $^{11}B\{^1H\}$ NMR (128 MHz, $CDCl_3$): δ = 31.07 (s) ppm. GC: t_R = 19.6 min; MS (EI): *m/z* = 263 (M^+, 10), 248 (35), 220 (100), 164 (85). The spectral data match those found in literature.[11]

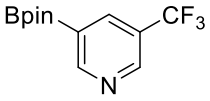

3-(4,4,5,5-Tetramethyl-1,3,2-dioxaborolan-2-yl)-5-trifluoromethylpyridine (2h): Following the general procedure, the reaction mixture was stirred at 100 °C for 5.5 hours. Quantitative conversion and yield were estimated by GC-MS analysis. Purification by Kugelrorh distillation afforded the analytically pure product (36 mg, 82% yield). ^1H NMR (400 MHz, $CDCl_3$): δ = 9.13 (s, 1H), 8.96 (d, *J* = 1.7 Hz, 1H), 8.32 (s, 1H), 1.39 (s, 12H) ppm. $^{13}C\{^1H\}$ NMR (101 MHz, $CDCl_3$): δ = 158.24, 148.53 (q, *J* = 4.2 Hz), 139.27 (q, *J* = 3.8 Hz), 84.81, 25.02 ppm. $^{11}B\{^1H\}$ NMR (128 MHz, $CDCl_3$): δ = 30.56 (s) ppm. $^{19}F\{^1H\}$ NMR (376 MHz, $CDCl_3$): δ = -62.64 (s) ppm. GC: t_R = 13.4 min; MS (EI): *m/z* = 273 (M^+, 10), 258 (100), 216 (40), 174 (25), 58 (35). The spectral data match those found in literature.[12]

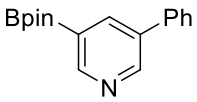

3-(4,4,5,5-Tetramethyl-1,3,2-dioxaborolan-2-yl)-5-phenylpyridine (2i): Following the general procedure, the reaction mixture was stirred at 100 °C for 3 hours. Quantitative conversion and yield were estimated by GC-MS analysis. Purification by Kugelrorh distillation afforded the analytically pure product (38 mg, 82% yield). ^{1}H NMR (400 MHz, $CDCl_3$): δ = 8.92 (d, *J* = 1.6 Hz, 1H), 8.91 (d, *J* = 2.5 Hz, 1H), 8.27 (m, 1H), 7.64-7.58 (m, 2H), 7.51-7.44 (m, 2H), 7.42-7.35 (m, 1H), 1.37 (s, 12H) ppm. $^{13}C\{^{1}H\}$ NMR (101 MHz, $CDCl_3$): δ = 154.07, 150.41, 140.62, 137.82, 135.87, 128.98, 128.01, 127.20, 84.32, 24.89 ppm. $^{11}B\{^{1}H\}$ NMR (128 MHz, $CDCl_3$): δ = 30.94 (s) ppm. GC: t_R = 23.4 min; MS (EI): *m/z* = 281 (M^+, 100), 266 (65), 224 (35), 195 (50), 181 (80). HRMS (ESI): *m/z* calcd for $C_{17}H_{21}NO_2{}^{11}B$ $[M+H]^+$ 282.16598; 282.1664 (2 ppm). The spectral data match those found in literature.[1]

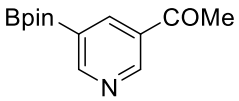

3-acetyl-5-(4,4,5,5-tetramethyl-1,3,2-dioxaborolan-2-yl)pyridine (2j): Following the general procedure, the reaction mixture was stirred at 100 °C for 3 hours. Quantitative conversion and yield were estimated by GC-MS analysis. Purification by Kugelrorh distillation afforded the analytically pure product (34 mg, 85% yield). ^{1}H NMR (400 MHz, $CDCl_3$): δ = 9.21 (d, *J* = 1.9 Hz, 1H), 9.08 (d, *J* = 1.9 Hz, 1H), 8.56 (t, *J* = 1.9 Hz, 1H), 2.64 (s, 3H), 1.37 (s, 12H) ppm. $^{13}C\{^{1}H\}$ NMR (101 MHz, $CDCl_3$): δ = 206.89, 158.86, 151.78, 141.84, 84.62, 30.88, 24.85 ppm. $^{11}B\{^{1}H\}$ NMR (128 MHz, $CDCl_3$): δ = 30.69 (s) ppm. HRMS (ESI, MeOH/DCM: 95/5): *m/z* calcd for $C_{13}H_{18}NO_3{}^{11}B$ $[M+Na]^+$: 270.12719; found: 270.1273 (0 ppm).

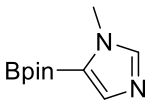

1-Methyl-5-(4,4,5,5-tetramethyl-1,3,2-dioxaborolan-2-yl)-1*H*-imidazole (2k): $[Ir(COD)(Cl)]_2$ (1.7 mg, 2.4 x 10^{-6} mol, 0.015 eq.), B_2pin_2 (41.1 mg, 1.62 x 10^{-4} mol, 1 eq.), ligand L (4.1 mg, 4.9 x 10^{-6} mol, 0.03 eq.), and dodecane (6.9 mg, 9.2 µL, 4.05 x 10^{-5} mol, 0.25 eq.) were introduced in an oven dried Schlenk flask. *p*-xylene (1 mL) was added and the reaction mixture was stirred at room temperature for 5 minutes. Then, the substrate (13 mg, 13 µL, 1.62 x 10^{-4} mol, 1 eq.) and HBpin (0.9 µL, 6.48 x 10^{-6} mol, 0.04 eq) was added and the reaction was stirred at 50°C. Upon completion monitored by GC-MS analysis, conversion and yield were estimated using dodecane as the internal standard by GC-MS and GC-FID. The solvent was then evaporated and the residue was purified using Kugelrohr distillation apparatus yielding the analytically pure product (30 mg, 90% yield). ^{1}H NMR (400 MHz, $CDCl_3$): δ = 7.56 (s, 1H), 7.54 (s, 1H), 3.79 (s, 3H), 1.31 (s, 12H) ppm. $^{13}C\{^{1}H\}$ NMR (101 MHz, $CDCl_3$): δ = 141.98, 141.50, 83.62, 33.96, 24.80 ppm. $^{11}B\{^{1}H\}$ NMR (128 MHz, $CDCl_3$): δ = 28.59 (s) ppm. GC: t_R = 16.6 min; MS (EI): *m/z* = 208 (M^+, 60), 193 (25), 165 (40), 123 (30), 108 (100), 83 (25), 81 (25). The spectral data match those found in literature.[13]

3.5 References

[1] (a) R. Noyori, *Nat. Chem.* **2009**, *1*, 5-6; (b) K. Sanderson, *Nature* **2011**, *469*, 18-20.

[2] R. A. Sheldon, *Chem. Soc. Rev.* **2012**, *41*, 1437-1451.

[3] (a) P. W. N. M. van Leeuwen, *Homogeneous Catalysis: Understanding the Art*, Kluwer, Dordrecht, **2004**; (b) P. C. J Kamer, P. W. N. M. van Leeuwen, *Phosphorus(III) Ligands in Homogeneous Catalysis: Design and Synthesis*, Wiley-VCH, Weinheim, **2012**

[4] (a) J. F. Hartwig, *Organotransition Metal Chemistry: From Bonding to Catalysis*, University Science Books, Sausalito, **2009**; (b) A. de Meijere, S. Braese, M. Oestreich, *Metal-Catalyzed Cross-Coupling Reactions and More*, Wiley-VCH, Weinheim, **2014**.

[5] (a) J.-Q. Yu, Z. Shi, *C-H Activation in Topics in Current Chemistry*, Springer, Berlin, **2010**; (b) R. Shang, L. Ilies, E. Nakamura, *Chem. Rev.* **2017**, *117*, 9086-9139; (c) Y. Yang, J. Lan, J. You, *Chem. Rev.* **2017**, *117*, 8787-8863; (d) L. McMurray, F. O'Hara, J. M. Gaunt, *Chem. Soc. Rev.* **2011**, *40*, 1885;1898; (e) R. R. Karimov, J. F. Hartwig, *Angew. Chem. Int. Ed.* **2018**, *57*, 4234-4241; (f) J. Yamaguchi, A. D. Yamaguchi, K. Itami, *Angew. Chem. Int. Ed.* **2012**, *51*, 8960-9009; (g) T. Dalton, T. Faber, F. Glorius, *ACS Cent. Sci.* **2021,** *7*, 245-261; (h) T. Rogge, N. Kaplaneris, N. Chatani, J. Kim, S. Chang, B. Punji, L. L Schafer, D. G. Musaev, J. Wencel-Delord, C. A. Roberts, R. Sarpong, Z. E. Wilson, M. A. Brimble, M. J. Johansson, L. Ackermann, *Nat. Rev. Methods Primers* **2021**, *1*, 43; (i) R. Jana, H. M. Begam, E. Dinda, *Chem. Commun.* **2021,** *57*, 10842-10866; (j) L. Guillemard, N. Kaplaneris, L. Ackermann, M. J. Johansson, *Nat. Rev. Chem.* **2021**, **5**, 522-545.

[6] (a) S. Rej, Y. Ano, N. Chatani, *Chem. Rev.* **2020**, *120*, 1788-1887; (b) G. Meng, N. Y. S. Lam, E. L. Lucas, T. G. Saint- Denis, P. Verma, N. Chekshin, J.-Q. Yu, *J. Am. Chem. Soc.* **2020**, *142*, 10571-10591; (c) R.-Y. Zhu, M. E. Farmer, Y.-Q. Chen, J.-Q. Yu, *Angew. Chem. Int. Ed.* **2016**, *55*, 10578-10599; (d) D. L. Davies, S. A. Macgregor, C. L. McMullin, *Chem. Rev.* **2017**, *117*, 8649-8709; (e) L. Ackermann, *Chem. Rev.* **2011**, *111*, 1315-1345; (f) T. Cernak, K. D. Dykstra, S. Tyagarajan, P. Vachalb, S. W. Krskab, *Chem. Soc. Rev.* **2016**, *45*, 546-576; (g) J. F. Hartwig, *J. Am. Chem. Soc.* **2016**, *138*, 2-24; (h) S. K. Sinha, S. Guin, S. Maiti, J. P. Biswas, S. Porey, D. Maiti, *Chem. Rev.* **2022**, *122*, 5682-5841.

[7] (a) C. Sambiagio, D. Schönbauer, R. Blieck, T. Dao-Huy, G. Pototschnig, P. Schaaf, T. Wiesinger, M. F. Zia, J. Wencel-Delord, T. Besset, B. U. W. Maes, M. Schnürch, *Chem. Soc. Rev.* **2018**, *47*, 6603-6743; (b) K. M. Engle, T.-S. Mei, M. Wasa, J.-Q. Yu, *Acc. Chem. Res.* **2012**, *45*, 788-802.

[8] (a) N. Kuhl, M. N. Hopkinson, J. Wencel-Delord, F. Glorius, *Angew. Chem. Int. Ed.* **2012**, *51*, 10236-10254; (b) N. Della Ca, M. Fontana, E. Motti, M. Catellani, *Acc. Chem. Res.* **2016**, *49*, 1389-1400; (c) D. Lichosyt, Y. Zhang, K. Hurej, P. Dydio, *Nat. Catal.* **2019**, *2*, 114-122; (d) J. F. Hartwig, M. A. Larsen, *ACS Cent. Sci.* **2016**, *2*, 281-292.

[9] R. Bisht, C. Haldar, M. M. M. Hassan, M. E. Hoque, J. Chaturvedi, B. Chattopadhyay, *Chem. Soc. Rev.* **2022,** *51*, 5042-5100.

[10] (a) J. F. Hartwig, *Acc. Chem. Res.* **2012,** *45*, 864-87; (b) A. Ros, R. Fernandez, J. M Lassaletta, *Chem. Soc. Rev.* **2014**, *43*, 3229-3243; (c) D. G. Hall, *Boronic Acids. Preparation, Applications in Organic Synthesis*, Wiley-VCH, Weinheim, **2011**; (d) E. C. Neeve, S. J. Geier, I. A. I. Mkhalid, S. A. Westcott, T. B. Marder, *Chem. Rev.* **2016**, *116*, 9091-9161; (e) M. Wang, Z. Shi, *Chem. Rev.* **2020**, *120*, 734-7398.

[11] (a) J. Wen, D. Wang, J. Qian, D. Wang, C. Zhu, Y. Zhao, Z. Shi, *Angew. Chem. Int. Ed.* **2019**, *58*, 2078-2082; (b) J. Tanaka, Y. Nagashima, A. J. A. Dias, K. Tanaka, *J. Am. Chem. Soc.* **2021**, *143*, 11325-11331.

[12] T. Furukawa, M. Tobisu, N. Chatani, *Bull. Chem. Soc. Jpn.* **2017,** *90*, 332-342.

[13] (a) J. V. Obligacion, S. P. Semproni, P. J. Chirik, *J. Am. Chem. Soc.* **2014**, *136*, 4133-4136 ; (b) J. V. Obligacion, S. P. Semproni, I. Pappas, P. J. Chirik, *J. Am. Chem. Soc.* **2016**, *138*, 10645-10653; (c) T. P. Pabst, P. J. Chirik, J. Am. Chem. Soc. **2022,** *144*, 6465-6474; (d) H. Ren, Y.-P. Zhou, Y. Bai, C. Cui, M. Driess, *Chem. Eur. J.* **2017,** *23*, 5663-5667.

[14] (a) T. Furukawa, M. Tobisu, N. Chatani, *Chem. Commun.* **2015**, *51*, 6508-6511; (b) Y.-M. Tian, X.-N. Guo, Z. Wu, A. Friedrich, S. A. Westcott, H. Braunschweig, U. Radius, T. B. Marder, *J. Am. Chem. Soc.* **2020**, *142*, 13136-13144.

[15] (a) Y. Luo, S. Jiang, X. Xu, *Angew. Chem. Int. Ed.* **2022**, *61*, e202117750; (b) J. O. Rothbaum, A. Motta, Y. Kratish, T. J. Marks, *J. Am. Chem. Soc.* **2022**, *144*, 17086-17096.

[16] (a) I. A. I. Mkhalid, J. H. Barnard, T. B. Marder, J. M. Murphy, J. F. Hartwig, *Chem. Rev.* **2010,** *110*, 890-931; (b) E. Fernandez, *Top. Organomet. Chem.* **2020**, *69*, 207-225; (c) O. Kuleshova, S. Asako, L. Ilies, *ACS Catal.* **2021**, *11*, 5968-5973; (d) M. E. Hoque, M. M. M. Hassan, B. Chattopadhyay, *J. Am. Chem. Soc.* **2021**, *143*, 5022-5037; (e) W. Chang, Y. Chen, S. Lu, H. Jiao, Y. Wang, T. Zheng, Z. Shi, Y. Han, Y. Lu, Y. Wang, Y. Pan, J.-Q. Yu, K. N. Houk, F. Liu, Y. Liang, *Chem* **2022,** *8*, 1775-1788.

[17] (a) B. Su, J. F. Hartwig, *Angew. Chem. Int. Ed.* **2022,** *61,* e202113343; (b) L. Xu, G. Wang, S. Zhang, H. Wang, L. Wang, L. Liu, J. Jiao, P. Li, *Tetrahedron* **2017**, *73*, 7123-7157; (c) X.-S. Xue, P. Ji, B. Zhou, J.-P. Cheng, *Chem. Rev.* **2017**, *117*, 8622-8648; (d) M. A. Larsen, R. J. Oeschger, J. F. Hartwig, *ACS Catal.* **2020**, *10*, 3415-3424; (e) M. A. Larsen, C. V. Wilson, J. F. Hartwig, *J. Am. Chem. Soc*. **2015**, *137*, 8633-8643; (f) R. Oeschger, B. Su, Y. Yu, C. Ehinger, E. Romero, S. He, J. F. Hartwig, *Science* **2020** *368*, 736-741.

[18] (a) T. Ishiyama, J. Takagi, K. Ishida, N. Miyaura, N. R. Anastasi, J. F. Hartwig, *J. Am. Chem. Soc.* **2002**, *124*, 390-391; (b) T. Ishiyama, J. Takagi, J. F. Hartwig, N. Miyaura, *Angew. Chem. Int. Ed.* **2002**, *41*, 3056-3058; (c) T. Ishiyama, Y. Nobuta, J. F. Hartwig, N. Miyaura, *Chem. Commun.* **2003**, 2924-2925.

[19] (a) C. W. Liskey, C. S. Wei, D. R. Pahlsa, J. F. Hartwig, *Chem. Commun.* **2009**, 5603-5605; (b) R. J. Oeschger, M. A. Larsen, A. Bismuto, J. F. Hartwig, *J. Am. Chem. Soc.* **2019**, *141*, 16479-16485

[20] (a) S. Pandit, S. Maiti, D. Maiti, *Org. Chem. Front.* **2021**, *8*, 4349-4358; (b) X. Zou, S. Xu, *Chin. J. Org. Chem.* **2021**, *41*, 2610-2620; (c) S.-T. Bai, C. B. Bheeter, J .N .H. Reek, *Angew. Chem. Int. Ed.* **2019**, *58*, 37, 13039-13043; (d) Y. Kuninobu, H. Ida, M. Nishi, M. Kanai, *Nat. Chem.* **2015**, *7*, 712-717; (e) J. Wang, T. Torigoe, Y. Kuninobu, Y. *Org. Lett.* **2019**, *21*, 1342-1346; (f) X. Lu, Y. Yoshigoe, H. Ida, M. Nishi, M. Kanai, Y. Kuninobu, *ACS Catal.* **2019**, *9*, 1705-1709; (g) H. J. Davis, M. T. Mihai, R. J. Phipps, *J. Am. Chem. Soc.* **2016**, *138*, 12759-12762; (h) B. Lee, M. T. Mihai, V. Stojalnikova, R. J. Phipps, *J. Org. Chem.* **2019**, *84*, 13124-13134; (j) M. T. Mihai, H. J. Davis, G. R. Genov, R. J. Phipps, *ACS Catal.* **2018**, *8*, 3764-3769; (i) M. E. Hoque, R. Bisht, C. Haldar, B. Chattopadhyay, *J. Am. Chem. Soc.* **2017**, *139*, 7745-7748; (j) R. Bisht, M. E. Hoque, B. Chattopadhyay, *Angew. Chem. Int. Ed.* **2018**, *57*, 15762-15766.

[21] (a) J. S. Wright, P. J. H. Scott, P. G. Steel, *Angew. Chem. Int. Ed.* **2021,** *60*, 2796-2821; (b) Y. Yang, Q. Gao, S. Xu, *Adv. Synth. Catal.* **2018**, *361*, 858-862; (c) K. Murakami, S. Yamada, T. Kaneda, K. Itami, *Chem. Rev.* **2017**, *117*, 9302-9332.

[22] (a) J. Takagi, K. Sato, J. F. Hartwig, T. Ishiyama, N. Miyaura, *Tetrahedron Lett.* **2002**, *43*, 5649-5651; (b) T. Ishiyama, J. Takagi, Y. Yonekawa, J. F. Hartwig, N. Miyaura, *Adv. Synth. Catal.* **2003**, *345*, 1103-1106; (c) M. A. Larsen, J. F. Hartwig, *J. Am. Chem. Soc.* **2014**, *136*, 4287-4299; (d) I. Sasaki, J. Taguchi, S. Hiraki, H. Ito, T. Ishiyama, *Chem. Eur. J.* **2015**, *21*, 9236-9241.

[23] (a) L. Yang, N. Uemura, Y. Nakao, Y. *J. Am. Chem. Soc.* **2019**, *141*, 7972-7979; (b) L. Yang, K. Semba, Y. Nakao, *Angew. Chem. Int. Ed.* **2017**, *56*, 4853-4857.

[24] (a) V. A. Kallepalli, F. Shi, S. Paul, E. N. Onyeozili, R. E. Maleczka, M. R. Smith, *J. Org. Chem.* **2009**, *74*, 9199-9201; (b) S. M. Preshlock, D. L. Plattner, P. E. Maligres, S. W. Krska, R. E. Maleczka, M. R. A. Smith, *Angew. Chem. Int. Ed.* **2013**, *52*, 12915-12919.

[25] (a) S. A. Sadler, H. Tajuddin, I. A. I. Mkhalid, A. S. Batsanov, D. Albesa-Jove, M. S. Cheung, A. C. Maxwell, L. Shukla, B. Roberts, D. C. Blakemore, Z. Lin, T. B. Marder, P. G. Steel, *Org. Biomol. Chem.* **2014,** *12*, 7318-7327; (b) H. Tajuddin, P. Harrisson, B. Bitterlich, J. C. Collings, N. Sim, A. S. Batsanov, M. S. Cheung, S. Kawamorita, A. C. Maxwell, L. Shukla, J. Morris, Z. Lin, T. B. Marder, P. G. Steel, *Chem. Sci.* **2012,** *3*, 3505-3515; (c) I. A. I. Mkhalid, D. N. Coventry, D. Albesa-Jove, A. S. Batsanov, J. A. K. Howard, R. N. Perutz, T. B. Marder, *Angew. Chem. Int. Ed.* **2006,** *45*, 489-491; (d) P. Harrisson, J. Morris, T. B. Marder, P. G. Steel, *Org. Lett.* **2009**, *11*, 3586-3589; (e) J. A. Reuven, O. A. Salih, S. A. Sadler, C. L. Thomas, P. G. Steel, *Tetrahedron* **2020**, *76*, 130836.

[26] J. Trouvé, P. Zardi, S. Al-Shehimy, T. Roisnel, R. Gramage-Doria, *Angew. Chem. Int. Ed.* **2021**, *60*, 18006-18013.

[27] (a) H. T. Shahzadi, S. Fatima, N. Akhter, M. Alazmi, A. Nawaf, K. B. Said, A. AlGhadhban, A. M. E. Sulieman, R. S. Z. Saleem, G. A. Chotana, *ACS Omega* **2022**, *7*, 11460-11472; (b) A. Hickey, J. Merz, H. H. Al Mamari, A. Friedrich, T. B. Marder, G. P. McGlacken, *J. Org. Chem.* **2022**, *87*, 9977-9987; (c) M. Klecka, R. Pohl, B. Klepetarova, M. Hocek, *Org. Biomol. Chem.* **2009**, *7*, 866-868; (d) L. Britton, M. Skrodzki, G. S. Nichol, A. P. Dominey, P. Pawluć, J. H. Docherty, S. P. Thomas, *ACS Catal.* **2021**, *11*, 6857-6864; (e) W.-C. Shih, O. V. Ozerov, *J. Am. Chem. Soc.* **2017**, *139*, 17297-17300; (f) Y. Pang, T. Ishiyama, L. Kubota, H. Ito, *Chem. Eur. J.* **2019,** *25*, 4654-4659; (g) M. Murai, N. Nishinaka, K. Takai, *Angew. Chem. Int. Ed.* **2018**, *57*, 5843-5847.

[28] (a) H. Tamura, H. Yamazaki, H. Sato, S. Sakaki, *J. Am. Chem. Soc.* **2003**, *125*, 16114-16126; (b) R.-L. Zhong, S. Sakaki, *J. Am. Chem. Soc.* **2019,** *141*, 9854-9866; (c) L. Zhu, X. Qi, Y. Li, M. Duan, L. Zou, R. Bai, Y. Lan, *Organometallics* **2017**, *36*, 2107-2115; (d) G. Wang, L. Xu, P. Li, *J. Am. Chem. Soc.* **2015**, *137*, 8058-806; (e) A. G. Green, P. Liu, C. A. Merlic, K. N. Houk, *J. Am. Chem. Soc.* **2014**, *136*, 4575-4583; (f) T. M. Boller, J. M. Murphy, M. Hapke, T. Ishiyama, N. Miyaura, J. F. Hartwig, *J. Am. Chem. Soc.* **2005,** *127*, 14263-14278; (g) L. Dang, Z. Lin, T. B. Marder, *Chem. Commun.* **2009**, 3987-3995.

[29] (a) P. A. Cox, A. G. Leach, A. D. Campbell, G. C. Lloyd-Jones, *J. Am. Chem. Soc.* **2016**, *138*, 9145- 9157; (b) H. L. D. Hayes, R. Wei, M. Assante, K. J. Geogheghan, N. Jin, S. Tomasi, G. Noonan, A. G. Leach, G. C. Lloyd-Jones, *J. Am. Chem. Soc.* **2021**, *143*, 14814-14826; (c) R. H. Crabtree, *Chem. Rev.* **2015,** *115*, 127-150.

[30] M. Tomasini, L. Caporaso, J. Trouvé, J. Poater, R. Gramage-Doria, A. Poater, *Chem. Eur. J.* **2022**, *28*, e202201970.

[31] See details in the Experimental section.

[32] (a) K. M. Kadish, L. R. Shiue, R. K. Rhodes, L. A. Bottomley, *Inorg. Chem.* **1981**, *20*, 1274-1277; (b) V. F. Slagt, J. N. H. Reek, P. C. J. Kamer, P. W. N. M van Leeuwen, *Angew. Chem. Int. Ed.* **2001**, *40*, 4271-4274; (c) M. Kadri, J. Hou, V. Dorcet, T. Roisnel, L. Bechki, A. Miloudi, C. Bruneau, R. Gramage-Doria, *Chem. Eur. J.* **2017**, *23*, 5033-5043; (d) P. Zardi, T. Roisnel, R. Gramage-Doria, *Chem. Eur. J.* **2019**, *25*, 627-634.

[33] For a unique case of iridium-catalyzed borylation tolerant to water, see: B. J. Foley, O. V. Ozerov, *Organometallics* **2020**, *39*, 2352-2355.

[34] T. Ishiyama, N. Miyaura, *Pure Appl. Chem.* **2006**, *78*, 1369-1375.

[35] (a) C. .C .C. Johansson Seechurn, V. Sivakumar, D. Satoskar, T. J. Colacot, *Organometallics* **2014**, *33*, 3514-3522; (b) E. D. Slack, T. J. Colacot, *Org. Lett.* **2021**, *23*, 1561-1565.

[36] (a) K. M. Kadish, K. M. Smith, R. Guillard, *Handbook of Porphyrin Science*, Vol. 1–44, World Scientific, Singapore, **2010**–**2016**; (b) I. Beletskaya, V. S. Tyurin, A. Y. Tsivadze, R. Guillard, C. Stern, *Chem. Rev.* **2009**, *109*, 1659-1713; (c) S. Olsson, C. Dahlstrand, A. Gogoll, *Dalton Trans.* **2018**, *47*, 11572-11585.

[37] For a rare and single case of chlorophilicity in zinc-porphyrins, see: Y. Yamamoto, Y. Hirata, M. Kodama, T. Yamaguchi, S. Matsukawa, K.-y. Akiba, D. Hashizume, F. Iwasaki, A. Muranaka, M. Uchiyama, P. Chen, K. M. Kadish, N. Kobayashi, *J. Am. Chem. Soc.* **2010**, *132*, 12627-12638.

[38] (a) J. Froidevaux, P. Ochsenbein, M. Bonin, K. Schenk, P. Maltese, J.-P Gisselbrecht, J. Weiss, *J. Am. Chem. Soc.* **1997**, *119*, 12362-12363; (b) D. Paul, F. Melin, C. Hirtz, J. Wytko, P. Ochsenbein, M. Bonin, K. Schenk, P. Maltese, J. Weiss, *Inorg. Chem.* **2003**, *42*, 3779-3787; (c) T. C. Berto, V. K. K. Praneeth, L. E. Goodrich, N. Lehnert, N, *J. Am. Chem. Soc.* **2009**, *131*, 17116-17126.

[39] (a) M. Morisue, T. Morita, Y. Kuroda, *Org. Biomol. Chem.* **2010**, *8*, 3457-3463; (b) J. S. Summers, A. M. Stolzenberg, *J. Am. Chem. Soc.* **1993**, *115*, 10559-10567; (c) C. H. Kirksey, P. Hambright, C. B. Storm, *Inorg. Chem.* **1969**, *8*, 2141–2144. (d) R. J. Abraham, G. R. Bedford, B. Wright, *Org. Magn. Reson.* **1982**, *18*, 45-52; (e) G. Szintay, A. Horvath, *Inorg. Chim. Acta* **2000**, *310*, 175-182.

[40] (a) H. Yoon, C.-H. Lee, Y.-H. Jeong, H.-C. Gee, W.-D. Jang, *Chem. Commun.* **2012**, *48*, 5109-5111; (b) C.-H. Lee, S. Lee, H. Yoon, W.-D. Jang, *Chem. Eur. J.* **2011**, *17*, 13898-13903.

[41] The slight difference in these values is due to loss and/or partial protodeboration of the products during purification.

[42] S. M. Preshlock, B. Ghaffari, P. E. Maligres, S. W. Krska, R. J. Maleczka Jr., M. R. Smith III, *J. Am. Chem. Soc.* **2013**, *135*, 7572-7582.

[43] M. R. Smith III, R. E. Maleczka Jr., A. K. Venkata, E. Onyeozili, US Pat. 7,709,654B2, **2008**.

[44] (a) H. Mayr, A. R. Ofial, Chemistry. *Angew. Chem. Int. Ed.* **2006**, *45*, 1844-1854; (b) H. Mayr, M. Breugst, A. R. Ofial, *Angew. Chem. Int. Ed.* **2011**, *50*, 6470-6505.

[45] (a) N. Abuhafez, A. Perennes, R. Gramage-Doria, *Synthesis* **2022**, *54*, 3473-3481; (b) J.-F. Longevial, S. Clément, J. A. Wytko, R. Ruppert, J. Weiss, S. Richeter, *Chem. Eur. J.* **2018**, *24*, 15442-15460.

[46] (a) P. Dydio, J. N. H. Reek, *Chem. Sci.* **2014**, *5*, 2135-2145; (b) H. J. Davis, R. J. Phipps, *Chem. Sci.* **2017**, *8*, 864-877; (c) J. Trouvé, R. Gramage-Doria, *Chem. Soc. Rev.* **2021**, *50*, 3565-3584; (d) G. Olivo, G. Capocasa, D. Del Giudice, O. Lanzalunga, S. Di Stefano, *Chem. Soc. Rev.* **2021**, *50*, 7681-7724; (e) Y. Jiao, X.-Y. Chen, J. F. Stoddart, *Chem* **2022**, *8*, 414-438; (f) P. W. N. M. van Leeuwen, M. Raynal, *Supramolecular Catalysis: New Directions and Developments*, Wiley-VCH, Weinheim, **2022**.

Chapter 4. Ortho-C-H borylation of tertiary aromatic amides directed by Zn···O=C non-covalent interactions.

4.1. Introduction.

The functionalization of C-H bonds by means of transition metal catalysis is one of the most powerful methodologies in chemical synthesis as it enables the access to highly elaborated molecules with step- and atom-economy in a predictive manner.[1] Consequently, compounds difficult or impossible to form otherwise are nowadays accessible,[2] which is relevant for drug discovery in the application of late-stage functionalization methodologies for upgrading the available chemical space[3] as well as in the area of material sciences to find chemical systems with unique photo-, electro- and physicochemical properties.[4] Usually, the presence of directing groups in the substrate of interest direct the selectivity *via* metal-coordination in C-H bond functionalizations.[5] Consequently, it is highly important to develop selective metal-catalyzed C-H bond functionalizations for unbiased substrates, thus reducing the costs devoted to the introduction and further removal of metal-coordinating directing groups.[6]

In this context, C-B bond-forming processes *via* C-H activation with iridium catalysts are particularly attractive since they take place without the need of covalently-linking directing groups to the substrate of interest[7] and well-known methodologies can be applied to further transform the boron functional group into carbon- or heteroatom-containing fragments.[8] Indeed, the reactivity and the selectivity at iridium is highly affected by the nature of the ligand attached to, with bipyridine-type ligands being of choice.[9] In the case of aromatic substrates the borylation typically occurs at the less sterically demanding *meta* and *para* positions.[10] This regio-selectivity is largely controlled by the rational design of catalysts enabling substrate-to-ligand interactions *via* hydrogen bonding or ion-pairing in view to place a specific C-H bond at close spatial proximity of the active *N*,*N*-chelated iridium site.[11] In the case of benzamides, which are important constituents in agrochemicals[12] and active pharmaceutical ingredients,[13] the selective *meta*- and *para*-borylation, respectively, has been accomplished with unique iridium catalysts developed, independently, by Nakao, Chattopadhyay, and Kuninobu and Kanai.[14] In the case of *ortho*-C-H bond borylations, Reek developed a bipyridine ligand featuring an hydrogen bonding site that works selectively for secondary benzamides (**Figure 1A**).[15] Alternatively, *ortho*-C-H bond borylations of tertiary benzamides have been disclosed utilizing hybrid chelating ligands as shown by Maleczka and R. Smith (*P*,*Si*- or *N*,*Si*-chelating ligands) and by Chattopadhyay (N,C_{thienyl}- or N,C_{furyl}-chelating ligands) using an $[Ir(COD)(OMe)]_2$ precursor (**Figure 1B**, right).[16a-c] A series of hybride *S*,*Si* and *N*,*B*-chelating ligands enabling *ortho*-C-H bond borylations of tertiary benzamides with modest activity have been reported by Li and co-workers.[16d,e] Herein, we report a supramolecular strategy that enables the selective *ortho*-C-H bond borylation of tertiary benzamides with a *N*,*N*-chelating ligand and an $[Ir(COD)Cl]_2$ metal precursor. The iridium catalyst is build up around a zinc-porphyrin backbone that enables weak Zn···O=C non-covalent interactions between

the amide group in the substrate and the catalyst favoring *ortho*-C-H bond functionalization for benzamide substrates (**Figure 1B**, left). By means of control experiments and catalyst screening, we demonstrate that the selectivity is exclusively controlled by the triazolopyridine-*N*,*N*-chelating site at iridium, whereas the activity is significantly enhanced by the substrate pre-organization within this supramolecular catalyst.

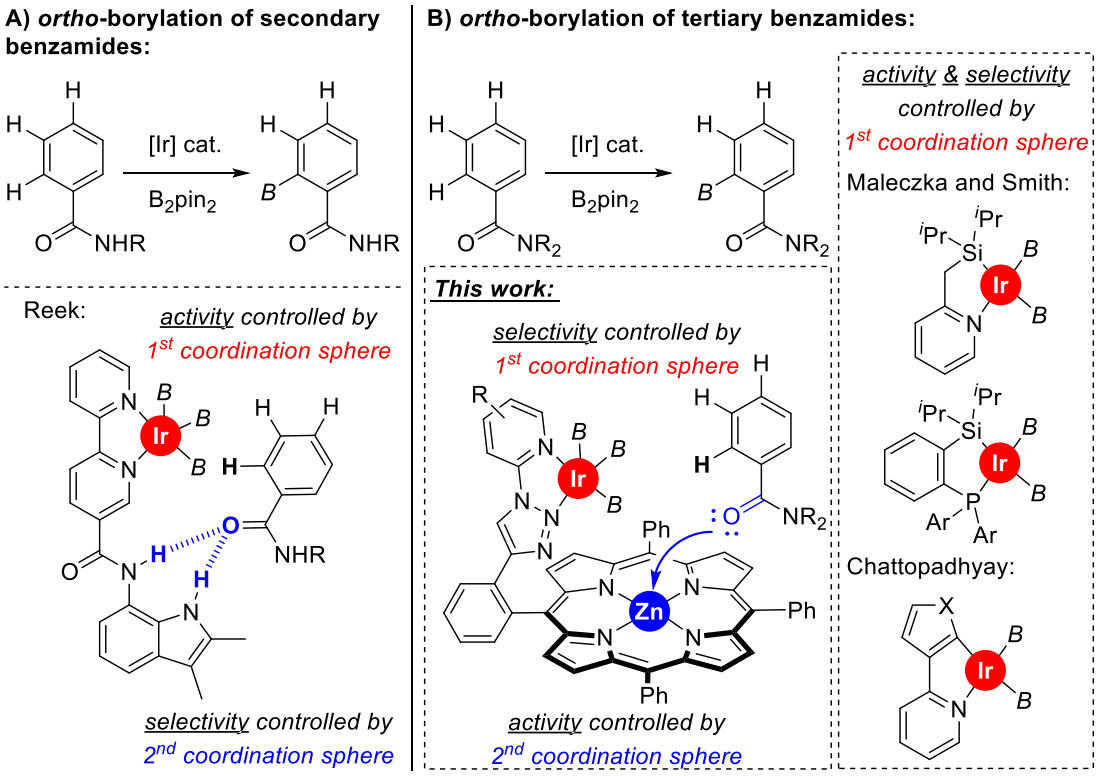

Figure 1. Previous catalysts enabling *ortho*-selective C-H borylation of benzamides (**A** and **B**, right) and our supramolecular approach (**B**, left). B_2pin_2 = bis(pinacolato)diboron, *B* = (pinacolato)boron, Ar = *para*-tolyl.

4.2. Results and discussion.

Recently, we reported on the *meta*-selective C-H bond borylation of pyridines using a well-defined supramolecular iridium catalyst equipped with a zinc-porphyrin unit that served for the specific molecular recognition of pyridine substrates (**Figure 2**, top, left).[17] We anticipated that other molecules different than pyridine could potentially bind in a reversible manner to the zinc center of the molecular recognition site, thereby placing potentially reactive C-H sites at close proximity of the catalytically active iridium site. During the course of our studies, we successfully obtained single crystals suitable for X-ray diffraction studies upon slow evaporation of a dichloromethane solution containing zinc-tetraphenylporpyrin (ZnTPP) and *N*,*N*-dimethylformamide (DMF).[18] Analogously to the binding of other tertiary amides to zinc-porphyrin derivatives,[19] the DMF molecule apically binds to the zinc center of ZnTPP *via* the oxygen atom (**Figure 2**, top, right). With these considerations, we build a semi-empirical preliminar molecular model combining our supramolecular iridium catalyst with a tertiary benzamide as the substrate (**Figure 2**, bottom). As a result, this prediction suggests that this supramolecular iridium

catalyst might be suitable for activating the aromatic C-H bond in *ortho* of the benzamide, which is located at a distance of four chemical bonds apart from the molecular recognition site (distance that is the same for the case of pyridine substrates).[17] In this case a single Zn···O=C non-covalent interaction between the substrate and the catalyst is at play.

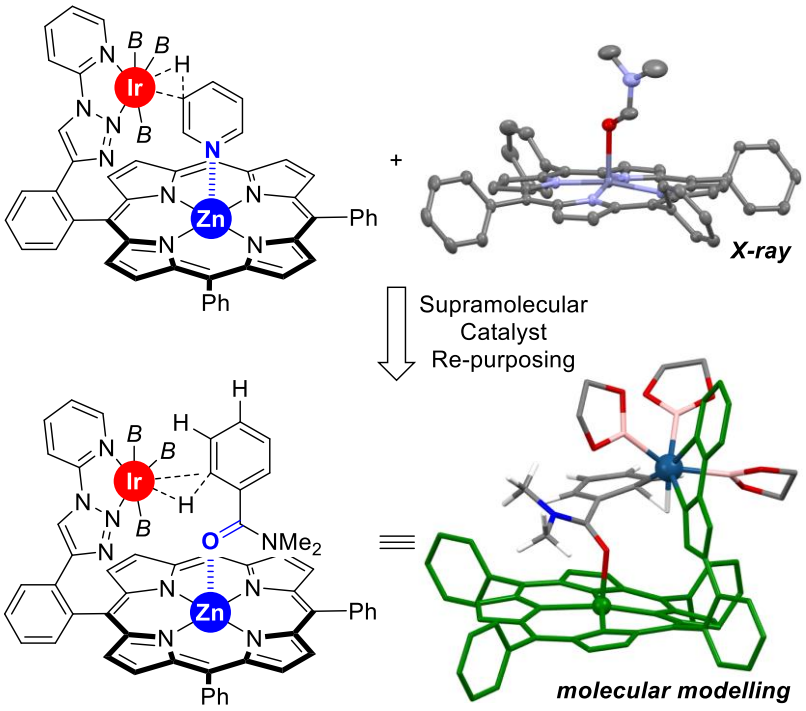

Figure 2. Previous supramolecular iridium catalyst displaying *meta*-selective C-H bond borylation of pyridines (top, left), ORTEP of assembly [ZnTPP ⊂ DMF] determined by single-crystal X-ray diffraction studies with thermal ellipsoids at 50% probability (all hydrogen atoms are omitted for clarity, top, right), re-purposed supramolecular iridium catalyst for the *ortho*-borylation of tertiary benzamides (bottom, left) and its PM3-minimized molecular modelling associated to a plausible intermediate (for clarity the methyl groups on the boryl ligand and all hydrogen atoms except those of the N,N-dimethylbenzamide substrate were omitted and the supramolecular ligand backbone is green color, bottom, right). *B* = (pinacolato)boron.

Next, we evaluated the supramolecular ligands **L1**-**L6** synthesized in chapter 3 as well as their corresponding ligands lacking the zinc-porphyrin substrate recognition site **L1***-**L6***, respectively, in the iridium-catalyzed C-H bond borylation of *N*,*N*-dimethylbenzamide (**1a**) as the model substrate (**Figures 3** and **4**). The results were compared with 4,4'-di-*tert*-butyl-2,2'-bipyridine (**dtbpy**) under identical reaction conditions (**Figures 3** and **4**). In terms of conversion of **1a**, the iridium-catalyzed borylation employing each supramolecular ligand **L** outperformed its non-supramolecular counterpart **L*** (**Figure 4**). On the other hand, the *ortho*-selectivity was comparable for all of them being in an excellent range of 89-97%, which compare well with previous precedents (**Figure 4**).[15] In contrast, and as it was expected, using the classical **dtbpy** ligand afforded a mixture of *meta*- and *para*-borylated products formed with negligible formation of *ortho* isomers (**Figure 4**). These observations clearly indicate that the selectivity of this transformation is exclusively controlled by the trivial iridium-coordinated

triazolopyridine ligand in the first coordination sphere and that the activity is enhanced by the presence of the molecular recognition zinc-porphyrin site. The best results in terms of selectivity (96-97% *ortho*-selectivity) and activity (83% conversion) were encountered for the supramolecular ligands **L1** and **L4**, most notably, without the need to employ the air and moisture sensitive $[Ir(COD)(OMe)]_2$ metal precursor in stark contrast with precedents in the literature.[7-16] The only difference between **L1** and **L4** was found in the ratio of mono- *versus* bis-borylation (**2a** : **2aa**, Figure 4). Using **L1** afforded a 81 : 19 ratio, whereas the bulkier **L4** containing a 6-methyl-substitution pattern in the iridium-coordinated pyridine moiety led to an increased mono-selectivity by 90 : 10 ratio. This was reasoned by the significant steric shields that should have to be overcome in order to get a second borylation in compound **2a** around the supramolecular iridium catalyst derived from **L4**. By increasing the reaction temperature from 80 °C to 100 °C and 120 °C, respectively, side-products derived from the hydroboration of the ketone group from the borylated products were observed in a range of 13-24%, thereby highlighting the challenges associated to get high reactivity while keeping excellent selectivity for iridium-catalyzed C-H borylations. Additional experiments demonstrate the lack of reactivity when the catalytic reactions were carried out in the absence of iridium precursor and/or ligand. Unfortunately, we did not succeed to provide direct evidences by NMR and UV-vis spectroscopy studies of the Zn···O=C non-covalent interaction between the supramolecular ligands and the benzamide substrate in solution likely due to the concentration and the time scale for this types of measurements.

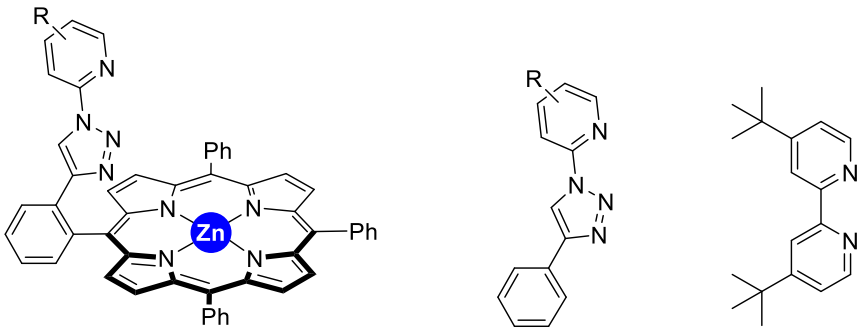

L1, R = H
L2, R = 4-^{t}Bu
L3, R = 4-Me
L4, R = 6-Me
L5, R = 4-OMe
L6, R = 4-CF_3

L1*, R = H
L2*, R = 4-^{t}Bu
L3*, R = 4-Me
L4*, R = 6-Me
L5*, R = 4-OMe
L6*, R = 4-CF_3

Figure 3. Ligands employed in this study: supramolecular ligands **L1**-**L6** (left), non-supramolecular counterparts **L1***-**L6*** (middle) and 4,4'-di-*tert*-butyl-2,2'-bipyridine (**dtbpy,** right).

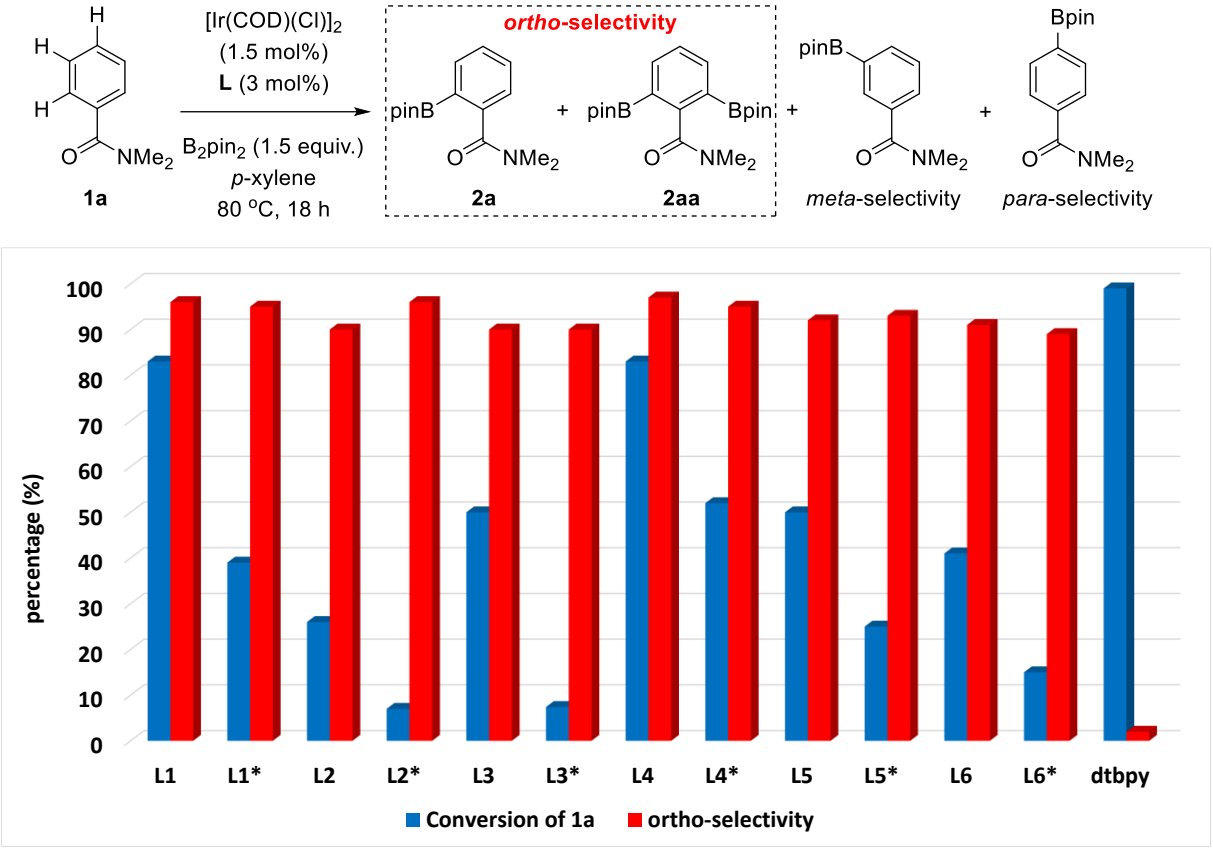

Figure 4. Assessment of ligands in the iridium-catalyzed C-H borylation of *N*,*N*-dimethylbenzamide **1a** [reaction conditions: **1a** (0.024 g, 0.162 mmol), $[Ir(COD)(Cl)]_2$ (1.7 mg, 2.43 x 10^{-3} mmol), ligand (4.86 x 10^{-3} mmol), B_2pin_2 (61.7 mg, 0.243 mmol), *p*-xylene (1 mL), 80 °C, 24 h; conversion and product selectivity were determined by GC analysis or ^1H NMR analysis].

Control experiments were further performed to further understand the unique behavior of the supramolecular ligands **L** in the selective *ortho*-C-H borylation of benzamide **1a**. First, a catalytic reaction was carried out using a mixture of **L1*** and **ZnTPP** at 3 mol% loading each (**Scheme 1**, top). In this case, full *ortho*-selectivity was obtained again showing the importance of the metal-coordinated ligand backbone. However, the conversion dropped to 65% when compared to the supramolecular version **L1**, thus demonstrating the requirement to covalently-linking the triazolopyridine fragment to the substrate recognition site. Interestingly, the amount of bis-functionalized borylated product significantly increased (**2a** : **2aa** = 71 : 29, **Scheme 1**, top) when compared to the supramolecular ligand **L1** (**2a** : **2aa** = 81 : 19, **Scheme 1**, bottom). This observation suggests that supramolecular ligands are rather bulky and disfavor to some extent the second borylation pathway towards **2aa**.

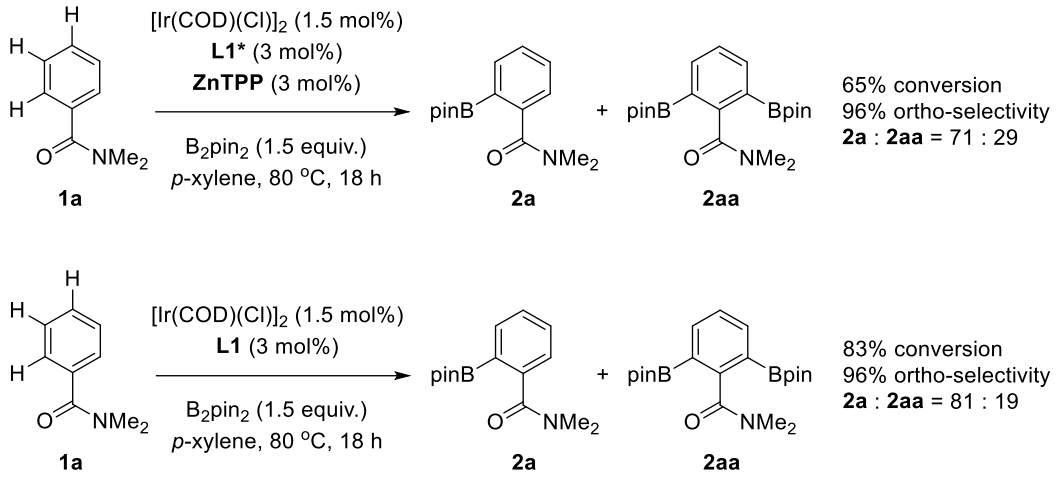

Scheme 1. Control experiment (top) *versus* the optimal reaction conditions (bottom).

The sensitivity to electronic and steric shields associated to this supramolecular iridium catalysis was additionally addressed by evaluating a number of benzamides bearing different substituents around the nitrogen atom (**Figure 5**). For this study, the reaction time was kept at 24 hours to ensure the maximum reactivity for each substrate. In line with previous observations, the supramolecular iridium catalysis was indeed affected by steric nature of the tertiary amide group with the conversion decreasing from 90% for **1a** to 18% for the bulkiest isopropyl substituent in **1d**. However, the *ortho*-selectivity was still remarkable ranging from 97% in the best case (**1a** and **1b**) to 87% for **1c** and 77% for the challenging **1d**. Secondary benzamides such as **1e** were not compatible with this supramolecular iridium catalysis. This could be attributed to (1) the poorer coordinating ability of the carbonyl group due to tautomerization[20] or (2) catalyst inhibition due to *N*-coordination to iridium with HBpin release.[21]

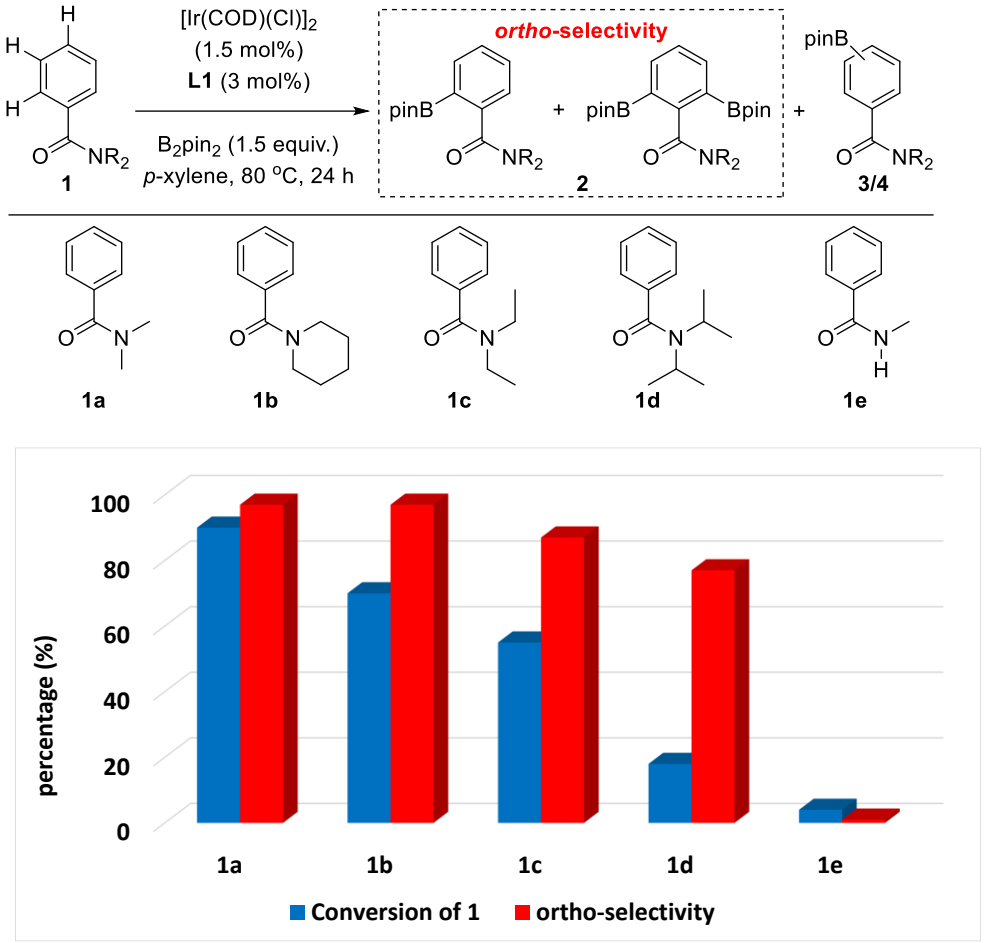

Figure 5. Relevance of the steric and electronic parameters of the amide group in **1** for the iridium-catalyzed C-H borylation [reaction conditions: **1** (0.162 mmol), $[Ir(COD)(Cl)]_2$ (1.7 mg, 2.43 x 10^{-3} mmol), ligand **L1** (4.1 mg, 4.86 x 10^{-3} mmol), B_2pin_2 (61.7 mg, 0.243 mmol), *p*-xylene (1 mL), 80 °C, 24 h; conversion and product selectivity were determined by GC analysis or ^{1}H NMR analysis].

As stated above, the catalytic reactions performed at a higher reaction temperature of 100 °C instead of 80 °C led to *ca.* 20% of deoxygenated borylated product of formula **5a** although the conversions of starting material **1a** were higher than at 80 °C and the *ortho*-selectivity was excellent too (**Table 1**, entry 1). We hypothesized, that this by-product may result from an iridium-catalyzed deoxygenative reduction of amides with pinacolborane (HBpin) that forms at each turnover during the major iridium-catalyzed borylation cycle.[22] To overcome this issue, we reasoned that cyclohexene additive could serve to trap the *in situ* formed HBpin.[23] As such, not only the by-product might be reduced but also the reactivity of the supramolecular catalyst could be increased by the precise acceleration of the HBpin release event that precedes catalyst regeneration.[24] In fact, the iridium-catalyzed C-H bond borylation of benzamide **1a** performed in the presence of one equivalent of cyclohexene led to a similar 92% conversion (**Table 1**, entry 2) as it was observed in the absence of cyclohexene (90%, **Table 1**, entry 1) with an almost perfect *ortho*-selectivity for both cases. Importantly, the side-product borylated amine **5a** was reduced to only trace amounts when the reaction was carried out in the presence of cyclohexene additive and the yield of mono-*ortho*-borylated benzamide **2a** raised

from a 60% to 85%. Leaving the catalysis for longer times (30 hours) in the presence of cyclohexene, led to full conversion of starting material and 97% *ortho*-selectivity with an 87% isolated yield of *ortho*-mono-borylated benzamide **2a** (**Table 1,** entry 3).

Table 1. Cylohexene as additive to suppress the formation of by-product **5a** at 100 °C by searching the optimal reaction conditions.[a]

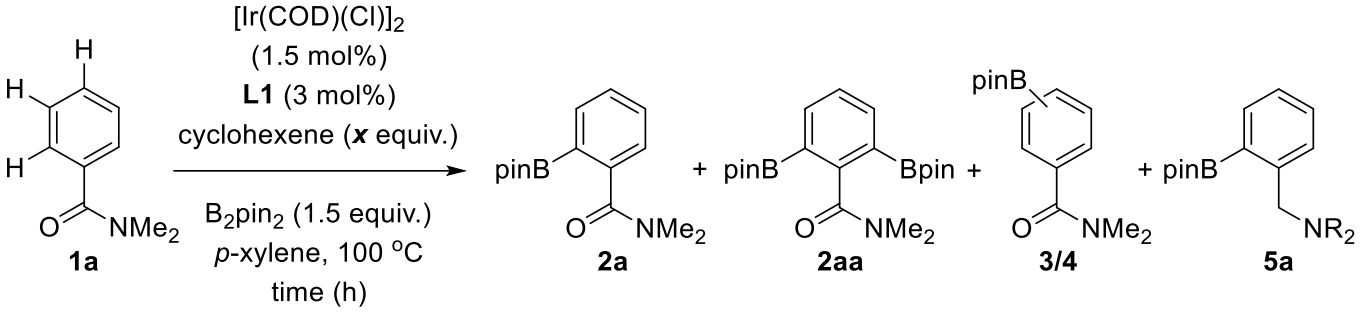

Entry	*x*	Time (h)	Conv. **1** (%)[b]	Yield **2a** (%)[b]	Yield **2aa** (%)[b]	Yield **3/4** (%)[b]	Yield **5a** (%)[b]
1	0	24	90	60	8	n.d.	22
2	1	24	94	85	4	n.d.	5
3	1	30	>99	91 (87)[c]	5	n.d.	5

[a] Reaction conditions: **1a** (0.024 g, 0.162 mmol, $[Ir(COD)(Cl)]_2$ (1.7 mg, 2.43 x 10^{-3} mmol), ligand **L1** (4.1 mg, 4.86 x 10^{-3} mmol), B_2pin_2 (61.7 mg, 0.243 mmol), cyclohexene (13 mg, 16 µL, 0.162 mmol), *p*-xylene (1 mL), 100 °C. [b] Conversion and product selectivity were determined by GC analysis or ^1H NMR analysis. [c] Isolated yield displayed in brackets after purification by column chromatography. The mono-borylated structure of **5a** was confirmed by GC-MS comparing with mono-borylation product of *N*,*N*-dimethylbenzylamine (see experimental section **5aa** synthesis).

With the optimal conditions in hand using cyclohexene as additive, we evaluated the substrate scope for this iridium-catalyzed *ortho*-C-H borylation of tertiary benzamides directed by Zn···O=C non-covalent interactions between the substrate and the catalyst (**Scheme 2**). Alhough slightly better results were obtained for ligand **L4**, ligand **L1** was employed for the substrate evaluation in order to provide a fair comparison about the activity and selectivity displayed by the different substitution patterns around the tertiary benzamide structure. Different steric patterns at the amide site (methyl, ethyl, iso-propyl) were tolerated including the case in which the amide is part of a piperidine fragment. The corresponding *ortho*-borylated products **2a**-**2d** were isolated in the range of 82-91% yields. As discussed above, the secondary benzamide **2e** formed but only in trace amounts. The catalysis tolerates halides such as fluoride, chloride and bromide in both *ortho* and *meta* position of the aromatic ring as well as alkyl, benzyl and aryl substituents. The reactions appeared sensitive for the case in which the halide substituents are in the other *ortho* position. For instance, the *ortho*-borylated product containing a fluoride atom in the other *ortho* position **2f** was obtained in a remarkable 91% isolated yield whereas the yield gradually decreased from chloride (70% for **2g**) to bromide (28% for **2h**). Alternatively, the *ortho*-borylated benzamide comprising *meta*-functionalized fluoride (**2i**), choride (**2j**) and bromide (**2k**) were isolated in 94%, 72% and 84% yields. In this cases, no C-H borylation took place in the *ortho* C-H bond between the amide and the halide groups. On the contrary, a methoxy group placed in *meta*

position of the benzamide ring led, besides the expected major borylated compound **2l** in 67% yield, to 13% of **2m** in which the borylation occurred also at the *ortho*-C-H bond located between the amide and the methoxy group, thus supporting some directing group character for the methoxy group.[25] Tertiary benzamides comprising electronically different methyl and ether groups in *para* position were compatible for the irdium-catalyzed C-H bond ortho-borylation affording the corresponding products **2n** and **2o** in 94% and 61% isolated yields, respectively. In the case of benzamide **1o** that comprises two aromatic groups, only the benzamide ring was prone to react by affording **2o**. A mixture of borylated products were obtained when the substrate contained a strongly withdrawing group such as nitro (**Scheme 2**, bottom). As it could be expected considering our previous contribution,[17] using a pyridine derivative containing a tertiary amide group in *meta* position afforded a mixture of borylated products as the nitrogen atom from pyridine and the carbonyl group from the amide are engaged in a non-covalent binding to the zinc-porphyrin molecular recognition site.

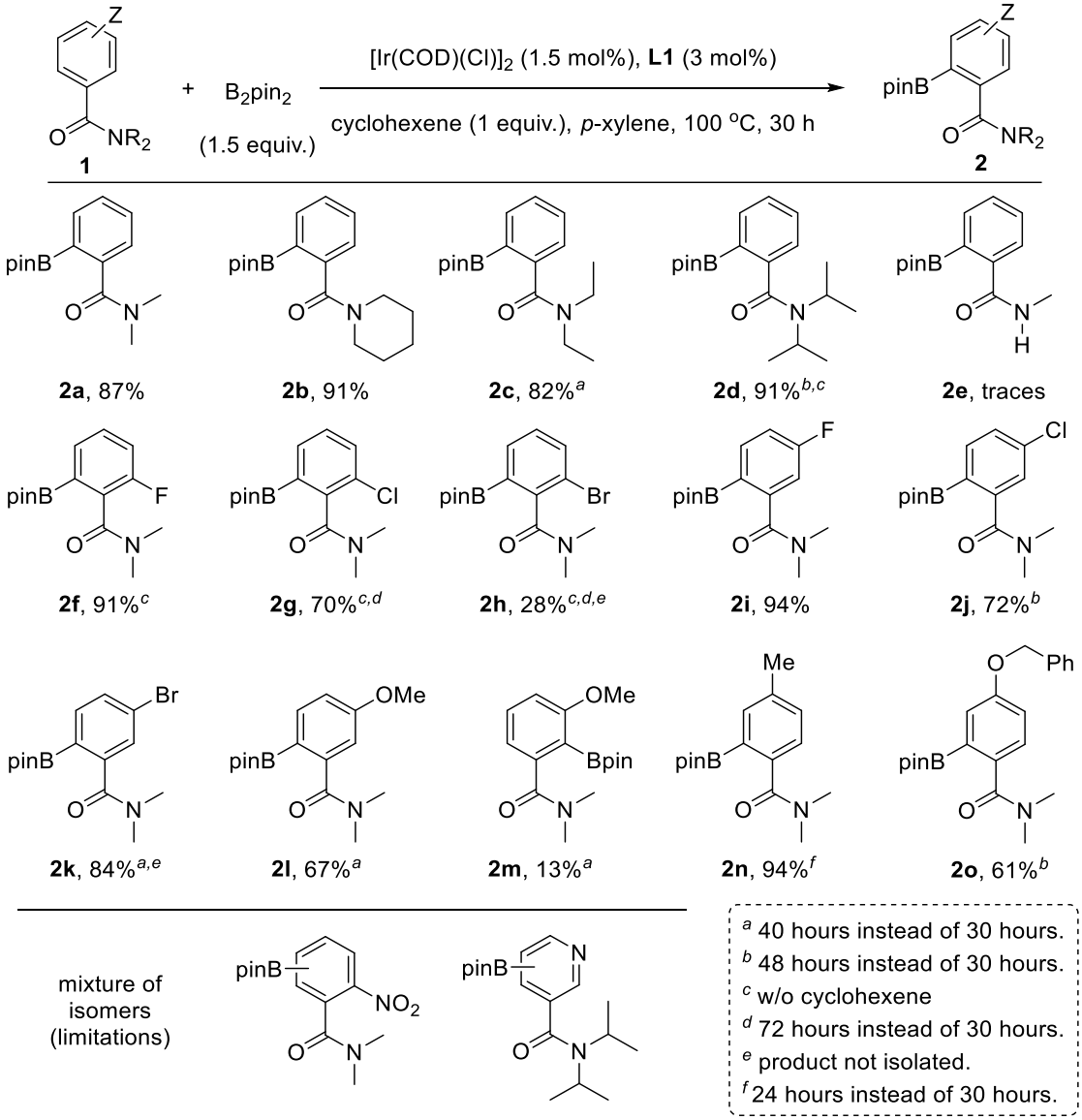

Scheme 2. Substrate scope of the iridium-catalyzed ortho-selective C-H borylation with benzamides [reaction conditions: **1** (0.162 mmol), $[Ir(COD)(Cl)]_2$ (1.7 mg, 2.43 x 10^{-3} mmol), ligand **L1** (4.1 mg, 4.86 x 10^{-3} mmol), B_2pin_2 (61.7 mg, 0.243 mmol), cyclohexene (13 mg, 16 µL, 0.162 mmol), *p*-xylene (1 mL), 100 °C, 30 h; isolated yields after purification by column chromatography are reported unless otherwise stated].

Finally, we aimed at exploring other carbonyl-containing substrates (**6**) different than amides **1** in the iridium-catalyzed *ortho*-C-H borylation using our supramolecular iridium catalyst (**Scheme 3**). The very sensitive benzaldehyde did not afforded any *ortho*-borylated product **7a**. On the other hand, acetophenone and methylbenzoate afforded the corresponding *ortho*-borylated products **7b** and **7c**, respectively, in promising 49% isolated yield in both cases. Replacing a carbonyl group in the substrate by a sulfone (i.e. methyphenylsulfone) provided a mono-borylated in a very modest 27% yield, being not possible to isolate it for further characterization.

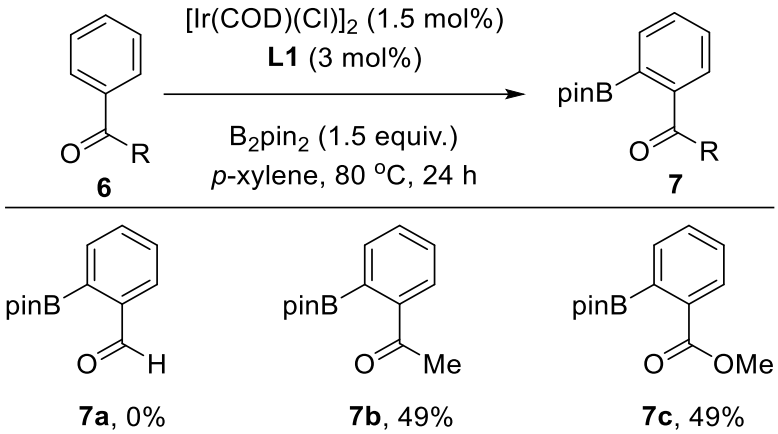

Scheme 3. Substrate scope of the iridium-catalyzed *ortho*-selective C-H borylation with carbonyl-containing substrates [reaction conditions: **6** (0.162 mmol), $[Ir(COD)(Cl)]_2$ (1.7 mg, 2.43 x 10^{-3} mmol), ligand **L1** (4.1 mg, 4.86 x 10^{-3} mmol), B_2pin_2 (61.7 mg, 0.243 mmol), cyclohexene (13 mg, 16 µL, 0.162 mmol), *p*-xylene (1 mL), 100 °C, 30 h; isolated yields after purification by column chromatography are reported unless otherwise stated].

Considering the many specificities presented by this supramolecular iridium catalysis and previous iridium-catalyzed C-H bond borylations,[7-17] we propose the reaction mechanism depicted in **Scheme 4**. Initially, species **A**, an iridium(COD)trisboryl species coordinated to the triazolopyridine site of **L**, formed and further reacted with the starting material liberating the COD to form the intermediate **B** in which the carbonyl group from the tertiary benzamide binds to the zinc centre of the porphyrin molecular recognition site. After selective *ortho*-C-H activation (**C**) and C-B bond formation at iridium (**D**), the catalyst was regenerated with B_2pin_2 generating one equivalent of HBpin. This catalyst regeneration likely takes place with the product is still bound to the molecular recognition site as it may stabilize some the transition state via additional Ir···π interactions.[24b] Final product release and substrate binding enables to pursue the catalytic cycle. The generated HBpin at each turnover in the catalyst regeneration step may partially serve to deoxygenated product **2** forming **5**. However, the presence of cyclohexene suppress such reaction pathway since the HBpin trapping event is faster than the deoxygenative reduction.

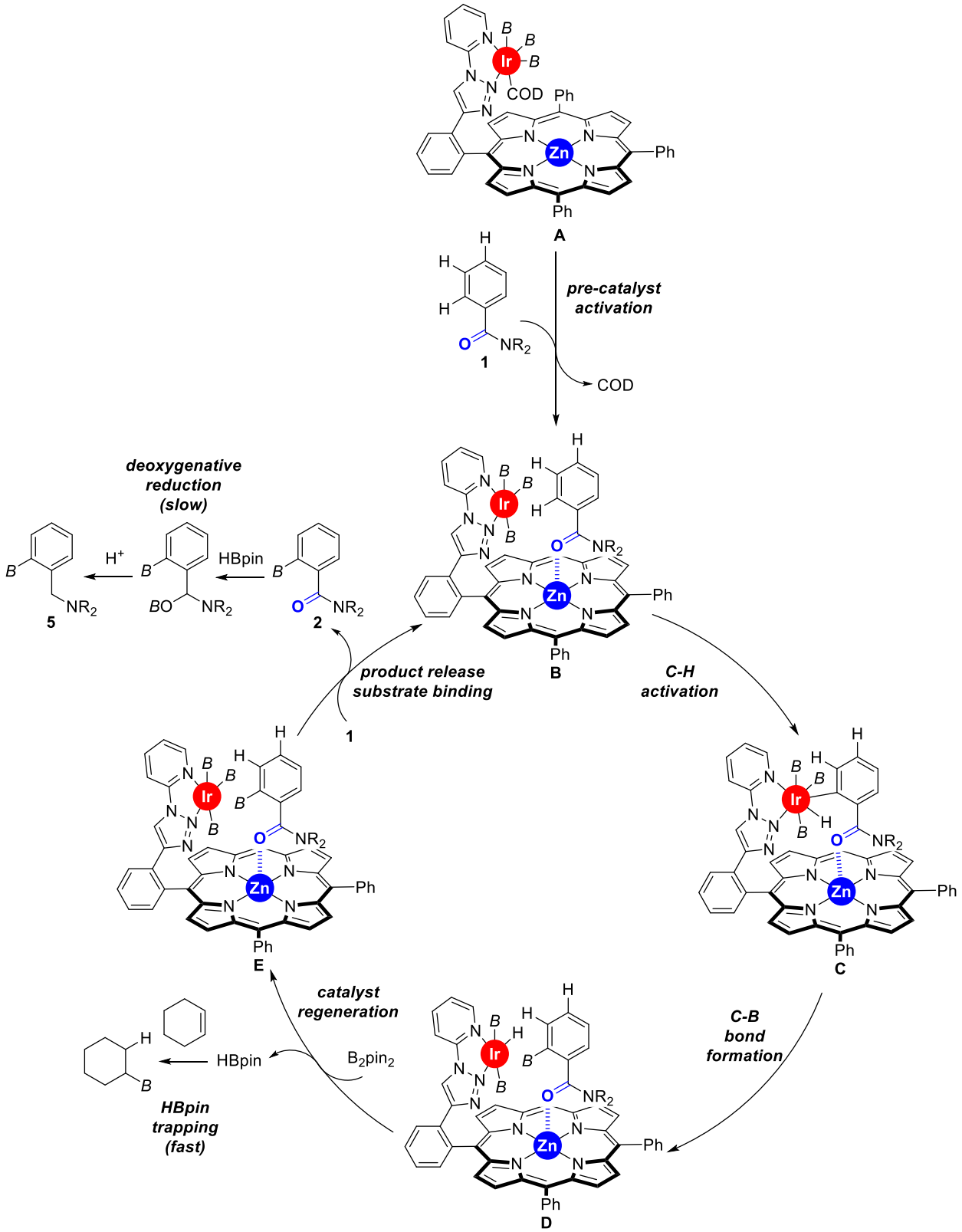

Scheme 4. Postulated reaction mechanism for the iridium-catalyzed *ortho*-selective C-H borylation of tertiary benzamides using **L1**. *B* = (pinacolato)boron.

4.3. Conclusion.

In summary, in this chapter we report the first use of Zn···O=C non-covalent interactions to exert control on the reactivity of metal catalysts. In particular, we have demonstrated that the iridium-catalyzed C-H bond borylations of tertiary benzamides occur in the *ortho* position with a triazolopyridine ligand equipped a zinc-porphyrin molecular recognition site. The selectivity is dominated by the first coordination sphere of the catalyst since tuning the triazolopyridine fragment results in minimal changes regarding the formation of the *ortho*-borylated products. Interestingly, the activity was controlled by the presence of the zinc-porphyrin backbone that brings the substrate close to the active site, reminiscent of the Michaelis complex formed between a substrate and an enzyme in biological catalysis.[26] The optimization of the reaction conditions enabled to identify $[Ir(COD)Cl]_2$ as a suitable precursor. This is somehow unprecedented for iridium-catalyzed C-H borylations as most of the studies employed the costly $[Ir(COD)(OMe)]_2$ that, in addition, is highly air- and moisture-sensitive.[27] Careful analysis of reaction conditions revealed the unexpected formation of a deoxygenated borylated side-product resulting from the reaction of HBpin formed during the catalyst regeneration with the borylated benzamide. This issue was circumvented by utilizing one equivalent of cyclohexene during the catalysis as HBpin scavenger. In this way, many *ortho*-borylated tertiary benzamides were obtained in excellent yields. Preliminary studies indicate that enlarging the substrate scope to other oxygen-containing substrates (ketone, ester, sulfone) is feasible.

4.4. Experimental section.

General methods.

Solvents were purified with an MB SPS-800 purification system. Pyrrole was dried with CaH_2 and distilled prior to use. $CDCl_3$ was filtered through alumina and stored under argon over molecular sieves. All the other employed chemicals were purchased from commercial sources and used as received. Unless otherwise specified, reactions were carried out under argon atmosphere by employing standard Schlenk and vacuum-line techniques. ^1H and ^{13}C NMR spectra were recorded with a Bruker GPX (400 MHz) spectrometer. ^1H NMR spectra were referenced to residual protiated solvent (δ = 7.26 ppm for $CDCl_3$). ^{13}C NMR spectra were referenced to $CDCl_3$ δ = 77.16 ppm). Abbreviations for signal couplings are: br, broad; s, singlet; d, doublet; t, triplet; m, multiplet; dd, doublet of doublets; dt, triplet of doublets; td, doublet of triplets; tt, triplet of triplets; tdd, doublet of doublet of triplets. Coupling constants, *J*, were reported in hertz unit (Hz). The reactions were monitored by using a Shimadzu 2014 gas chromatograph equipped with an EquityTM-1 Fused Silica capillary column (30 m x 0.25 mm x 0.25 µm) and an FID detector; conversion and selectivity were determined by using dodecane as internal standard. UV/Vis absorption spectra were recorded with a Specord 205 UV/Vis/NIR spectrophotometer and quartz cuvettes of 1 cm path length. Mass spectroscopy and microanalysis were performed in the laboratories of the Centre Regional de Mesures Physiques de l'Ouest (CRMPO, Université de Rennes 1, Rennes, France). Molecular modeling calculations were performed with the PM3-Spartan molecular modeling program.

The ligands **L1**-**L6** and **L1***-**L6*** were prepared as discussed in chapter 3.

General method for the synthesis of the tertiary benzamides: To an oven dried round bottom flask was added the corresponding benzoic acid (10 mmol, 1 equiv.) and DMF (10 mL). Then, freshly distillated $POCl_3$ (1.53 g, 0.930 mL, 10 mmol, 1 equiv.) was slowly added and the reaction mixture was heated to 120°C for 16h. Then the reaction mixture was quench by addition of a saturated solution of $NaHCO_3$ until no bubbling was noticed. The aqueous layer was extracted with EtOAc (3 x 20 mL). The combined organic layers were washed with a saturated solution of K_2CO_3 and then brine solution. After drying over $MgSO_4$ and filtration, the solvents were evaporated under reduced pressure. The crude mixture was further purified by column chromatography (SiO_2, *n*-heptane:EtOAc, v/v 1:0 to 2:8).

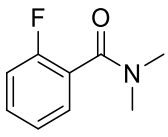

Synthesis and characterization of 2-fluoro-*N*,*N*'-dimethylbenzamide (1f): According to the general method, 2-fluoro-*N*,*N*'-dimethylbenzamide was isolated as a yellow oil (1.57 g, 94% yield). ^1H NMR (400 MHz, $CDCl_3$): δ = 7.40-7.32 (m, 2H), 7.21-7.13 (m, 1H), 7.10-7.03 (m, 1H), 3.11 (q, *J* = 1.3 Hz, 3H), 2.91 (q, *J* = 1.3 Hz, 3H) ppm. $^{13}C\{^1H\}$ NMR (101 MHz, $CDCl_3$) δ = 166.69, 158.15 (d, *J* = 247.5 Hz), 131.07 (d, *J* = 8.0 Hz), 128.98 (d, *J* = 3.9 Hz), 124.70, 124.52 (d, *J* = 3.4 Hz), 115.64 (d, *J* = 21.6 Hz), 38.23 (d, *J* = 2.8 Hz), 34.89. The data match those found in the literature.[28]

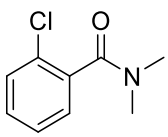

Synthesis and characterization of 2-chloro-*N*,*N*'-dimethylbenzamide (1g): According to the general method, 2-chloro-*N*,*N*'-dimethylbenzamide was isolated as a yellow oil (1.67 g, 91% yield). ^1H NMR (400 MHz, $CDCl_3$): δ = 7.37-7.31 (m, 1H), 7.31-7.22 (m, 3H), 3.09 (d, *J* = 0.9 Hz, 3H), 2.81 (d, *J* = 0.9 Hz, 3H) ppm. $^{13}C\{^1H\}$ NMR (101 MHz, $CDCl_3$): δ = 168.18, 136.16, 130.01, 129.85, 129.32, 127.52, 126.97, 37.83, 34.41 ppm. The data match those found in the literature.[29]

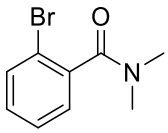

Synthesis and characterization of 2-bromo-*N,N*'-dimethylbenzamide (1h): According to the general method, 2-bromo-*N,N*'-dimethylbenzamide was isolated as a yellow oil (1.98 g, 87% yield). ^{1}H NMR (400 MHz, $CDCl_3$): δ = 7.56 (dd, *J* = 7.7, 1.0 Hz, 1H), 7.35 (dd, *J* = 7.7, 1.0 Hz, 1H), 7.29-7.20 (m, 2H), 3.13 (s, 3H), 2.85 (s, 3H) ppm. $^{13}C\{^{1}H\}$ NMR (101 MHz, $CDCl_3$): □ = 169.17, 138.56, 132.68, 130.13, 127.69, 127.68, 119.09, 38.15, 34.61 ppm. The data match those found in the literature.[30]

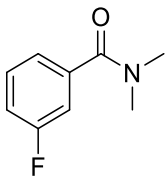

Synthesis and characterization of 3-fluoro-*N,N*'-dimethylbenzamide (1i): According to the general method, 3-methoxy-N,N'-dimethylbenzamide was isolated as a yellow oil (1.49 g, 89% yield). ^{1}H NMR (400 MHz, $CDCl_3$): □ = 7.36 (td, *J* = 7.7, 5.6 Hz, 1H), 7.17 (d, *J* = 7.7 Hz, 1H), 7.10 (ddt, *J* = 10.9, 8.4, 4.0 Hz, 2H), 3.09 (s, 3H), 2.96 (s, 3H) ppm. $^{13}C\{^{1}H\}$ NMR (101 MHz, $CDCl_3$): δ = 170.09 (d, *J* = 2.4 Hz), 163.68, 161.22, 138.40 (d, *J* = 6.9 Hz), 130.14 (d, *J* = 8.1 Hz), 122.70 (d, *J* = 3.2 Hz), 116.50 (d, *J* = 21.1 Hz), 114.31 (d, *J* = 22.8 Hz), 39.43, 35.34 ppm. $^{19}F\{^{1}H\}$ NMR (376 MHz, $CDCl_3$): δ = -112.12 (s) ppm. The data match those found in the literature.[28]

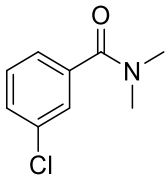

Synthesis and characterization of 3-chloro-*N,N*'-dimethylbenzamide (1j): According to the general method, 3-chloro-*N,N*'-dimethylbenzamide was isolated as a yellow oil (1.76 g, 96% yield).^{1}H NMR (400 MHz, $CDCl_3$): δ = 7.45-7.22 (m, 4H), 3.09 (s, 3H), 2.96 (s, 3H) ppm. $^{13}C\{^{1}H\}$ NMR (101 MHz, $CDCl_3$): δ = 170.00, 138.06, 134.42, 129.75, 129.63, 127.25, 125.13, 39.48, 35.35 ppm. The data match those found in the literature.[28]

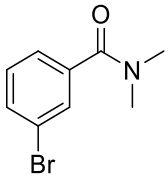

Synthesis and characterization of 3-bromo-*N,N*'-dimethylbenzamide (1k): According to the general method, 3-bromo-*N,N*'-dimethylbenzamide was isolated as a yellow oil (1.84 g, 81% yield). ^{1}H NMR (400 MHz, $CDCl_3$): δ = 7.60-7.48 (m, 2H), 7.36-7.23 (m, 2H), 3.09 (s, 3H), 2.96 (s, 3H) ppm. $^{13}C\{^{1}H\}$ NMR (101 MHz, $CDCl_3$): δ = 169.86, 138.29, 132.56, 130.10, 129.99, 125.58, 122.48, 39.49, 35.36 ppm. The data match those found in the literature.[28]

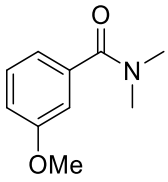

Synthesis and characterization of 3-methoxy-*N,N*'-dimethylbenzamide (1l): According to the general method, 3-methoxy-*N,N*'-dimethylbenzamide was isolated as a yellow oil (1.49 g, 83% yield). ^{1}H NMR (400 MHz, $CDCl_3$): δ = 7.30 (t, *J* = 7.7 Hz, 1H), 6.99-6.90 (m, 3H), 3.82 (s, 3H), 3.10 (s, 3H), 2.97 (s, 3H) ppm. $^{13}C\{^{1}H\}$ NMR (101 MHz, $CDCl_3$): δ = 171.39, 159.55, 137.65, 129.43, 119.16, 115.42, 112.38, 55.34, 39.52, 35.31 ppm. The data match those found in the literature.[28]

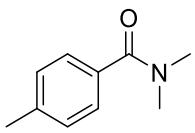

- Synthesis and characterization of 4-methyl-*N,N*'-dimethylbenzamide (1n): According to the general method, 4-methyl-*N,N*'-dimethylbenzamide was isolated as a white solid (1.50 g, 92% yield).^{1}H NMR (400 MHz, $CDCl_3$): δ = 7.34-7.15 (AB, J = 52 Hz, 4H), 3.08 (s, 3H), 2.98 (s, 3H), 2.36 (s, 3H) ppm. $^{13}C\{^{1}H\}$ NMR (101 MHz, $CDCl_3$): δ = 171.76, 139.55, 133.41, 128.89, 127.17, 39.61, 35.37, 21.35 ppm. The data match those found in the literature.[28]

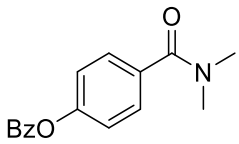

Synthesis and characterization of 4-(phenylmethyleneoxy)-*N,N*'-dimethylbenzamide (1o): According to the general method, 4-(phenylmethyleneoxy)-*N,N*'-dimethylbenzamide was isolated as a white solid (1.58 g, 62% yield). ^{1}H NMR (400 MHz, $CDCl_3$): δ = 7.45-7.29 (m, 7H), 7.00 – 6.94 (m, 2H),

5.09 (s, 2H), 3.05 (s, 6H) ppm. $^{13}C\{^1H\}$ NMR (101 MHz, $CDCl_3$): δ = 171.41, 159.74, 136.55, 129.09, 128.69, 128.59, 128.04, 127.40, 114.46, 70.02 ppm. The data match those found in the literature.[31]

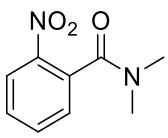

Synthesis and characterization of 2-nitro-*N*,*N*'-dimethylbenzamide: According to the general method, 2-nitro-*N*,*N*'-dimethylbenzamide was isolated as a yellow solid (0.99 g, 52% yield). ^1H NMR (400 MHz, $CDCl_3$): δ = 8.18 (dd, *J* = 8.3, 1.2 Hz, 1H), 7.70 (td, *J* = 7.5, 1.2 Hz, 1H), 7.55 (td, *J* = 8.3, 7.5, 1.5 Hz, 1H), 7.39 (dd, *J* = 7.5, 1.5 Hz, 1H), 3.16 (s, 3H), 2.83 (s, 3H) ppm. $^{13}C\{^1H\}$ NMR (101 MHz, $CDCl_3$): δ = 167.86, 145.10, 134.46, 133.34, 129.64, 128.09, 124.65, 38.19, 34.85 ppm. The data match those found in the literature.[32]

General method for catalysis experiments: To an oven dried round bottom flask was added $[Ir(COD)(Cl)]_2$ (1.7 mg, 2.43 x 10^{-6} mol, 0.015 equiv.), ligand **L1** (4.1 mg, 4.86 x 10^{-6} mol, 0.03 equiv.), B_2pin_2 (61.7 mg, 2.43 x 10^{-4} mol, 1.5 equiv.). Then, *p*-xylene (1 mL), the corresponding benzamide (0.162 mmol, 1 equiv.) and cyclohexene (13 mg, 16 µL, 1.62 x 10^{-4} mol, 1 equiv.) were introduced and the reaction mixture was heated at 100 °C during 24 hours. Back at room temperature, the crude mixture was analyzed by GC-MS and evaporated under vacuum until full evaporation of *p*-xylene. Heptane (1 mL) was added and the mixture was filtrated on celite. The solid was washed with heptane and the filtrate was further purified by column chromatography (SiO_2, *n*-heptane:EtOAc, v/v 1:0 to 1:1) to afford the analytically pure product.

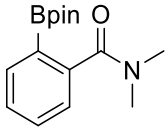

Synthesis and characterization of 2-(4,4,5,5-tetramethyl-1,3,2-dioxaborolan-2-yl)-N,N'-dimethylbenzamide (2a): Following the general procedure, *N*,*N*'-dimethylbenzamide (24 mg, 1.62 x 10^{-4} mol, 1 equiv.) was borylated at 100 °C during 30 hours using cyclohexene (13 mg, 16 µL, 1.62 x 10^{-4} mol, 1 equiv.) as a pinacolborane scavenger. A conversion of 99% and a selectivity of 97% toward the *ortho* derivative were detected by GC-MS and GC-FID. The *ortho*-C-H borylated product **2a** was isolated as a solid (39 mg, 87% yield). ^1H NMR (400 MHz, $CDCl_3$): δ = 7.81 (dd, *J* = 7.5, 1.4 Hz, 1H), 7.46 (td, *J* = 7.5, 1.2 Hz, 1H), 7.37 (td, *J* = 7.5, 1.2 Hz, 1H), 7.30 (dd, *J* = 7.5, 1.2 Hz, 1H), 2.98 (s, 6H), 1.33 (s, 12H) ppm. $^{13}C\{^1H\}$ NMR (101 MHz, $CDCl_3$): δ = 172.47, 142.67, 135.03, 130.90, 128.11, 125.53, 83.56, 24.94 ppm. $^{11}B\{^1H\}$ NMR (128 MHz, $CDCl_3$): δ = 29.56 (s) ppm. The data match those found in the literature.[33]

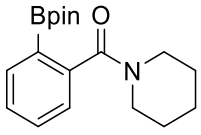

Synthesis and characterization of 2-(4,4,5,5-tetramethyl-1,3,2-dioxaborolan-2-yl)-benzoylpiperidine (2b): Following the general procedure, benzoylpiperidine (31 mg, 1.62 x 10^{-4} mol, 1 equiv.) was borylated at 100 °C during 30 hours using cyclohexene (13 mg, 16 µL, 1.62 x 10^{-4} mol, 1 equiv.) as a pinacolborane scavenger. A conversion of 99% and a selectivity of 98% toward the *ortho* derivative were detected by GC-MS and GC-FID. The *ortho*-C-H borylated product **2b** was isolated as a solid (46 mg, 91% yield). ^1H NMR (400 MHz, $CDCl_3$): δ = 7.82 (dd, *J* = 7.5, 1.3 Hz, 1H), 7.45 (td, *J* = 7.5, 1.3 Hz, 1H), 7.35 (td, *J* = 7.5, 1.3 Hz, 1H), 7.25 (dt, *J* = 7.5, 1.3 Hz, 1H), 3.73 (t, *J* = 5.4 Hz, 2H), 3.17 (t, *J* = 5.4 Hz, 2H), 1.74-1.62 (m, 4H), 1.53-1.46 (m, 2H), 1.34 (s, 12H) ppm. $^{13}C\{^1H\}$ NMR (101 MHz, $CDCl_3$): δ = 170.6, 143.1, 135.2, 130.8, 127.6, 125.2, 83.6, 48.1, 42.4, 25.6,

25.0, 24.7, 24.4. ppm. $^{11}B\{^1H\}$ NMR (128 MHz, $CDCl_3$): δ = 30.32 (s) ppm. The data match those found in the literature.[16c]

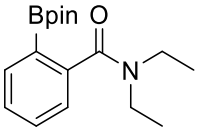

Synthesis and characterization of 2-(4,4,5,5-tetramethyl-1,3,2-dioxaborolan-2-yl)- *N,N*'-diethylbenzamide (2c): Following the general procedure, *N,N*'-diethylbenzamide (29 mg, 1.62 x 10^{-4} mol, 1 equiv.) was borylated at 100 °C during 40 hours using cyclohexene (13 mg, 16 µL, 1.62 x 10^{-4} mol, 1 equiv.) as a pinacolborane scavenger. A conversion of 92% and a selectivity of 86% toward the *ortho* derivative were detected by GC-MS and GC-FID. The *ortho*-C-H borylated product **2c** was isolated as a solid (40 mg, 82% yield). ^{1}H NMR (400 MHz, $CDCl_3$): δ = 7.80 (dd, *J* = 7.5, 1.5 Hz, 1H), 7.41 (td, *J* = 7.5, 1.3 Hz, 1H), 7.35 (td, *J* = 7.5, 1.3 Hz, 1H), 7.26 (dd, *J* = 7.5, 1.3 Hz, 1H), 3.57 (q, *J* = 7.1 Hz, 2H), 3.21 (q, *J* = 7.1 Hz, 2H), 1,31 (m, 3H), 1.30 (s, 12H), 1.06 (t, *J* = 7.1 Hz, 3H) ppm. $^{13}C\{^{1}H\}$ NMR (101 MHz, $CDCl_3$): δ = 171.69, 142.43, 135.05, 130.45, 128.16, 125.42, 83.44, 43.03, 39.76, 24.89, 13.69, 12.50 ppm. $^{11}B\{^{1}H\}$ NMR (128 MHz, $CDCl_3$): δ = 28.35 (s) ppm. The data match those found in the literature.[16c]

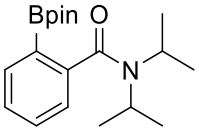

Synthesis and characterization of 2-(4,4,5,5-tetramethyl-1,3,2-dioxaborolan-2-yl)- N,N'-diisopropylbenzamide (2d): Following the general procedure without cyclohexene, *N,N*'-diisopropylbenzamide (33 mg, 1.62 x 10^{-4} mol, 1 equiv.) was borylated at 100 °C during 48 hours. A conversion of 99% and a selectivity of 77% toward the *ortho* derivative were detected by GC-MS and GC-FID. The mixture of C-H borylated isomer product **2d** was isolated as a solid (46 mg, 91% yield). ^{1}H NMR (400 MHz, $CDCl_3$): δ = 7.82 (dd, *J* = 7.5, 1.3 Hz, 1H), 7.42 (td, *J* = 7.5, 1.3 Hz, 1H), 7.34 (td, *J* = 7.5, 1.3 Hz, 1H), 7.18 (dt, *J* = 7.5, 0.8 Hz, 1H), 3.75 (dt, *J* = 13.0, 5.9 Hz, 1H), 3.53 (dt, *J* = 13.0, 5.9 Hz, 1H), 1.60 (d, *J* = 6.8 Hz, 6H), 1.33 (s, 12H), 1.14 (d, *J* = 6.8 Hz, 6H) ppm. $^{13}C\{^{1}H\}$ NMR (101 MHz, $CDCl_3$): δ = 171.29, 144.97, 135.53, 130.54, 127.34, 124.57, 83.77, 50.87, 45.73, 24.86, 20.42, 20.22 ppm. $^{11}B\{^{1}H\}$ NMR (128 MHz, $CDCl_3$): δ = 30.00 (s) ppm. The data match those found in the literature.[16c]

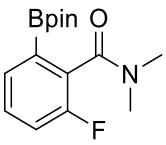

Synthesis and characterization of 2-(4,4,5,5-tetramethyl-1,3,2-dioxaborolan-2-yl)-6-fluoro-N,N'-dimethylbenzamide (2f): Following the general procedure without cyclohexene, 2-fluoro-N,N'-dimethylbenzamide (27 mg, 1.62 x 10^{-4} mol, 1 equiv.) was borylated at 100 °C during 30 hours. A conversion of 99% and a selectivity of 94% toward the *ortho* derivative were detected by GC-MS and GC-FID. The *ortho*-C-H borylated product **2f** was isolated as a solid (46 mg, 91% yield). ^{1}H NMR (400 MHz, $CDCl_3$): δ = 7.60 (dd, *J* = 7.4, 1.1 Hz, 1H), 7.39-7.32 (m, 1H), 7.18 (td, *J* = 8.2, 7.4, 1.1 Hz, 1H), 3.13 (s, 3H), 2.85 (s, 3H), 1.33 (s, 12H) ppm. $^{11}B\{^{1}H\}$ NMR (128 MHz, $CDCl_3$): δ = 30.61 (s) ppm.

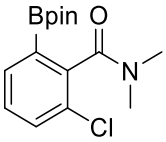

Synthesis and characterization of 2-(4,4,5,5-tetramethyl-1,3,2-dioxaborolan-2-yl)-6-chloro-N,N'-dimethylbenzamide (2g): Following the general procedure without cyclohexene, 2-chloro-N,N'-dimethylbenzamide (30 mg, 1.62 x 10^{-4} mol, 1 equiv.) was borylated at 100 °C during 72 hours. A conversion of 85% and a selectivity of 77% toward the *ortho* derivative were detected by GC-MS and GC-FID. The *ortho*-C-H borylated product **2g** was isolated as a solid (35 mg, 70% yield). ^{1}H NMR (400 MHz, $CDCl_3$): δ = 7.72 (dd, *J* = 7.4, 1.2 Hz, 1H), 7.47 (dd, *J* = 8.1, 1.2 Hz, 1H), 7.30 (t, *J* = 8.1, 7.4 Hz, 1H), 3.12 (s, 3H), 2.80 (s, 3H), 1.33 (s, 12H) ppm. $^{13}C\{^{1}H\}$NMR (101 MHz, $CDCl_3$): δ = 168.77, 142.00, 133.83, 131.98, 130.22, 128.91, 84.14, 38.05, 34.38, 24.85 ppm. $^{11}B\{^{1}H\}$ NMR (128 MHz, $CDCl_3$): δ = 30.51 (s) ppm.

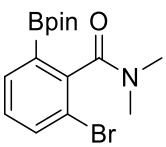

Synthesis and characterization of 2-(4,4,5,5-tetramethyl-1,3,2-dioxaborolan-2-yl)-6-bromo-*N,N*'-dimethylbenzamide (2h): Following the general procedure without cyclohene, 2-bromo-*N,N*'-dimethylbenzamide (37 mg, 1.62 x 10^{-4} mol, 1 equiv.) was borylated at 100

°C during 72h. A conversion of 30% and a yield of 28% of the *ortho*-C-H borylated product **2h** was determined by GC-MS and GC-FID. The compound could not be isolated.

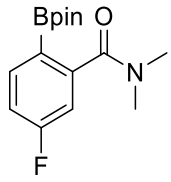

Synthesis and characterization of 2-(4,4,5,5-tetramethyl-1,3,2-dioxaborolan-2-yl)-5-fluoro-*N*,*N*'-dimethylbenzamide (2i): Following the general procedure, 3-fluoro-N,N'-dimethylbenzamide (27 mg, 1.62 x 10^{-4} mol, 1 equiv.) was borylated at 100 °C during 30h. A conversion of 99% and a selectivity of 98% toward the ortho derivative were detected by GC-MS and GC-FID. The *ortho*-C-H borylated product **2i** was isolated as a solid (48 mg, 94% yield). ^{1}H NMR (400 MHz, $CDCl_3$): δ = 7.56 (dd, *J* = 7.3, 1.1 Hz, 1H), 7.35-7.27 (m, 1H), 7.14 (td, *J* = 8.3, 7.3, 1.1 Hz, 1H), 3.08 (s, 3H), 2.80 (s, 3H), 1.29 (s, 12H) ppm. $^{11}B\{^{1}H\}$ NMR (128 MHz, $CDCl_3$): δ = 30.31 (s) ppm.

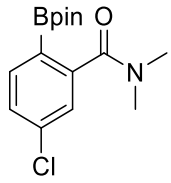

- Synthesis and characterization of 2-(4,4,5,5-tetramethyl-1,3,2-dioxaborolan-2-yl)-5-chloro-*N*,*N*'-dimethylbenzamide (2j): Following the general procedure, 3-chloro-*N*,*N*'-dimethylbenzamide (30 mg, 1.62 x 10^{-4} mol, 1 equiv.) was borylated at 100 °C during 48 hours. A conversion of 99% and a selectivity of 90% toward the *ortho* derivative were detected by GC-MS and GC-FID. The *ortho*-C-H borylated product **2j** was isolated as a solid (36 mg, 72% yield). ^{1}H NMR (400 MHz, $CDCl_3$): δ = 7.76 (d, *J* = 8.0 Hz, 1H), 7.36 (dd, *J* = 8.0, 2.0 Hz, 1H), 7.30-7.27 (m, 1H), 3.08 (s, 3H), 2.85 (s, 3H), 1.33 (s, 12H) ppm. $^{13}C\{^{1}H\}$ NMR (101 MHz, $CDCl_3$): δ = 170.89, 144.65, 137.42, 136.74, 128.17, 125.85, 83.94, 38.29, 34.68, 24.90 ppm. $^{11}B\{^{1}H\}$ NMR (128 MHz, $CDCl_3$): δ = 30.10 (s) ppm.

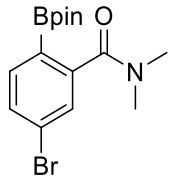

Synthesis and characterization of 2-(4,4,5,5-tetramethyl-1,3,2-dioxaborolan-2-yl)-5-bromo-*N*,*N*'-dimethylbenzamide (2k): Following the general procedure, 3-bromo-*N*,*N*'-dimethylbenzamide (37 mg, 1.62 x 10^{-4} mol, 1 equiv.) was borylated at 100 °C during 40 hours. A conversion of 95% and a selectivity of 87% toward the *ortho* derivative were detected by GC-MS and GC-FID. The compound could not be isolated.

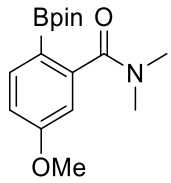

Synthesis and characterization of (4,4,5,5-tetramethyl-1,3,2-dioxaborolan-2-yl)-5-methoxy-*N*,*N*'-dimethylbenzamide (2l): Following the general procedure, 3-methoxy-*N*,*N*'-dimethylbenzamide (29 mg, 1.62 x 10^{-4} mol, 1 equiv.) was borylated at 100 °C during 40 hours. A conversion of 99% and a selectivity of 76% toward the *ortho* derivative were detected by GC-MS and GC-FID. The *ortho*-C-H borylated product **2l** was isolated as a solid (33 mg, 67% yield). ^{1}H NMR (400 MHz, $CDCl_3$): δ = 7.74 (d, *J* = 8.3 Hz, 1H), 6.86 (dd, *J* = 8.3, 2.5 Hz, 1H), 6.79 (d, *J* = 2.5 Hz, 1H), 3.81 (s, 3H), 3.06 (s, 3H), 2.78 (s, 3H), 1.29 (s, 12H) ppm. $^{11}B\{^{1}H\}$ NMR (128 MHz, $CDCl_3$): δ = 30.72 (s) ppm.

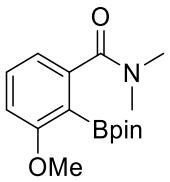

Characterization of 2-(4,4,5,5-tetramethyl-1,3,2-dioxaborolan-2-yl)-3-methoxy-*N*,*N*'-dimethylbenzamide (2m): This *ortho* isomer product was isolated as a solid (7 mg, 13% yield). ^{1}H NMR (400 MHz, $CDCl_3$): δ = 7.34 (t, *J* = 8.1 Hz, 1H), 6.99 (dd, *J* = 8.1, 0.8 Hz, 1H), 6.89 (d, *J* = 8.1 Hz, 1H), 3.83 (s, 3H), 3.10 (s, 6H), 1.37 (s, 12H) ppm. $^{11}B\{^{1}H\}$ NMR (128 MHz, $CDCl_3$): δ = 27.69 (s) ppm.

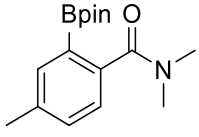

Synthesis and characterization of 2-(4,4,5,5-tetramethyl-1,3,2-dioxaborolan-2-yl)-4-methyl-*N*,*N*'-dimethylbenzamide (2n): Following the general procedure, 4-methyl-*N*,*N*'-dimethylbenzamide (26 mg, 1.62 x 10^{-4} mol, 1 equiv.) was borylated at 100 °C during 24 hours. A conversion of 99% and a selectivity of 97% toward the *ortho* derivative

were detected by GC-MS and GC-FID. The *ortho*-C-H borylated product **2n** was isolated as a solid (44 mg, 94% yield). ^{1}H NMR (400 MHz, $CDCl_3$): δ = 7.59 (s, 1H), 7.32-7.12 (m, 2H), 2.99 (s, 6H), 2.35 (s, 3H), 1.31 (s, 12H) ppm. $^{13}C\{^{1}H\}$ NMR (101 MHz, $CDCl_3$): δ = 172.68, 139.13, 138.29, 135.25, 131.31, 125.59, 83.26, 24.98, 21.18 ppm. $^{11}B\{^{1}H\}$ NMR (128 MHz, $CDCl_3$): δ = 28.46 (s) ppm.

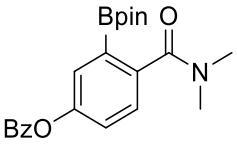

Synthesis and characterization of 2-(4,4,5,5-tetramethyl-1,3,2-dioxaborolan-2-yl)-4-(phenylmethoxy)-*N*,*N*'-dimethylbenzamide (2o): Following the general procedure, 4-(phenylmethoxy)-*N*,*N*'-dimethylbenzamide (41 mg, 1.62 x 10^{-4} mol, 1 equiv.) was borylated at 100 °C during 48 hours. A conversion of 82% and a selectivity of 97% toward the *ortho* derivative were detected by GC-MS and GC-FID. The *ortho*-C-H borylated product **2o** was isolated as a solid (39 mg, 61% yield). ^{1}H NMR (400 MHz, $CDCl_3$): δ = 7.49-7.32 (m, 7H), 6.97 (dd, *J* = 8.6, 2.6 Hz, 1H), 5.14 (s, 2H), 3.19 (s, 6H), 1.35 (s, 12H) ppm. $^{11}B\{^{1}H\}$ NMR (128 MHz, $CDCl_3$): δ = 22.45 (s) ppm.

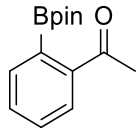

Synthesis and characterization of 2-(4,4,5,5-tetramethyl-1,3,2-dioxaborolan-2-yl)-acetophenone (7b): Following the general procedure, acetophenone (19 mg, 1.62 x 10^{-4} mol, 1 equiv.) was borylated at 80 °C during 24 hours without cyclohexene. A conversion of 55% and a selectivity of 93% toward the *ortho* derivative were detected by GC-MS and GC-FID. The *ortho*-C-H borylated product **7b** was isolated in 49% yield as a solid (20 mg). ^{1}H NMR (400 MHz, $CDCl_3$): δ = 7.82 (d, J = 7.7 Hz, 1H), 7.55-7.48 (m, 2H), 7.45-7.42 (m, 1H), 2.62 (s, 3H), 1.40 (s, 12H) ppm. The data match those found in the literature.[16c]

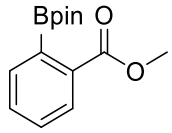

Synthesis and characterization of 2-(4,4,5,5-tetramethyl-1,3,2-dioxaborolan-2-yl)-methylbenzoate (7c): Following the general procedure, methylbenzoate (22 mg, 1.62 x 10^{-4} mol, 1 equiv.) was borylated at 80 °C for 24 hours without cyclohexene. A conversion of 55% and a selectivity of 93% toward the *ortho* derivative were detected by GC-MS and GC-FID. The *ortho*-C-H borylated product **7c** was isolated in 49% yield as a solid. ^{1}H NMR (400 MHz, $CDCl_3$): δ = 7.93 (dt, *J* = 7.8, 1.0 Hz, 1H), 7.53-7.48 (m, 2H), 7.45-7.38 (m, 1H), 3.91 (s, 3H), 1.42 (s, 12H) ppm. $^{11}B\{^{1}H\}$ NMR (128 MHz, $CDCl_3$): δ = 31.12 (s) ppm. The data match those found in the literature.[33]

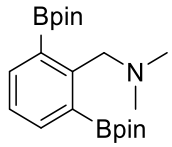

- **Synthesis and characterization of 2-(4,4,5,5-tetramethyl-1,3,2-dioxaborolan-2-yl)-methylphenylsulfone (5aa):** Following the general procedure **B**, 4-(phenylmethoxy)-N,N'-dimethylbenzamide (19 mg, 1.62 x 10^{-4} mol, 1 equiv.) was borylated at 100°C for 24h. A conversion of 95% and a selectivity of 97% toward the ortho derivative were detected by GC-MS and GC-FID. *Mono*/*bis* (%): 3/92. ^{1}H NMR (400 MHz, CDCl3) δ = 7.63 (d, *J* = 7.3 Hz, 2H), 7.20 (t, *J* = 7.3 Hz, 1H), 4.14 (s, 2H), 2.60 (s, 6H), 1.29 (s, 24H). $^{11}B\{^{1}H\}$ NMR (128 MHz, CDCl3) δ = 22.68. The data match those found in the literature.[34]

4.5. References.

[1] (a) M. C. White, *Science* **2012**, *335*, 807-809; (b) T. Gensch, M. N. Hopkinson, F. Glorius, J. Wencel-Delord, *Chem. Soc. Rev.* **2016**, *45*, 2900-2936; (c) S. K. Sinha, S. Guin, S. Maiti, J. P. Biswas, S. Porey, D. Maiti, *Chem. Rev.* **2022**, *122*, 5682-5841. (d) T. Dalton, T. Faber, F. Glorius, *ACS Cent. Sci.* **2021**, *7*, 245-261; (e) J. A. Labinger, *Chem. Rev.* **2017**, *117*, 8483-8496; (f) K. Godula, D. Sames, *Science* **2006**, *312*, 67-72; (g) M. M. Diaz-Requejo, P. J. Perez, *Chem. Rev.* **2008**, *108*, 3379-3394.

[2] (a) T. Cernak, K. D. Dykstra, S. Tyagarajan, P. Vachal, S. W. Krska, *Chem. Soc. Rev.* **2016**, *45*, 546-576; (b) P. S. Fier, J. F. Hartwig, *Science* **2013**, *342*, 956-960; (c) W. Liu, J. T. Groves, *Acc Chem. Res.* **2015**, *48*, 1727-1735; (d) M. Simonetti, D. M. Cannas, X. Just-Baringo, I. J. Vitorica-Yrezabal, I. Larrosa, *Nat. Chem.* **2018**, *10*, 724-731; (e) J. Wencel-Delord, F. Glorius, *Nat. Chem.* **2013**, *5*, 369-375; (f) Y. Yang, J. Lan, J. You, *Chem. Rev.* **2017**, *117*, 8787-8863; (f) J. F. Hartwig, *J. Am. Chem. Soc.* **2016**, *138*, 2-24; (g) Z. Dong, Z. Ren, S. J. Thompson, Y. Xu, G. Dong, *Chem. Rev.* **2017**, *117*, 9333-9403;

[3] (a) D. C. Blakemore, L. Castro, I. Churcher, D. C. Rees, A.W. Thomas, D. M. Wilson, A. Wood, *Nat. Chem.* **2018**, *10*, 383-394; (b) J. Yamaguchi, A.i D. Yamaguchi, K. Itami, *Angew. Chem. Int. Ed.* **2012**, *51*, 8960-9009; (c) L. Guillemard, N. Kaplaneris, L. Ackermann, M. J. Johansson, *Nat. Rev. Chem.* **2021**, *5*, 522-545; (d) R.; Jana, H. M.; Begam, E. Dinda, *Chem. Commun.* **2021**, *57*, 10842-10866; (e) R. R. Karimov, J. F. Hartwig, *Angew. Chem. Int. Ed.* **2018**, *57*, 4234-4241;(f) L. McMurray, F. O'Hara, M. J. Gaunt, *Chem. Soc. Rev.* **2011**, *40*, 1885-1898;

[4] (a) D. J. Schipper, K. Fagnou, *Chem. Mater.* **2011**, *23*, 1594-1600; (b) H. Bohra; M. Wang, *J. Mater. Chem. A* **2017**, *5*, 11550-11571; (c) L. G., Mercier, M. Leclerc, *Acc. Chem. Res.* **2013**, *46*, 1597-1605; (d) L. Xing, C. K. Luscombe, *J. Mater. Chem. C* **2021**, *9*, 16391-16409; (e) Y. Segawa, T. Maekawa, K. Itami, *Angew. Chem. Int. Ed.* **2015**, *54*, 66-81; (f) I. A. Stepek, K. Itami, *ACS Materials Lett.* **2020**, *2*, 951-974;

[5] (a) D. A. Colby, R. G. Bergman, J. A. Ellman, Chem. Rev. **2010**, 110, 624-655; (b) G. Rouquet, N. Chatani, *Angew. Chem. Int. Ed.* **2013**, *52*, 11726-11743; (c) T. W. Lyons, M. S. Sanford, *Chem. Rev.* **2010**, *110*, 1147-1169; (d) K. M. Engle, T.-S. Mei, M. Wasa, J.-Q. Yu, *Acc. Chem. Res.* **2012**, 45, 788-802; (e) C. Sambiagio, D. Schönbauer, R. Blieck, T. Dao-Huy, G. Pototschnig, P. Schaaf, T. Wiesinger, M. F. Zia, J. Wencel-Delord, T. Besset, B. U. W. Maes, M. Schnürch, *Chem. Soc. Rev.* **2018**, *47*, 6603−6743; (f) S. De Sarkar, W. Liu, S. I. Kozhushkov, L. Ackermann, *Adv. Synth. Catal.* **2014**, *356*, 1461-1479; (g) P. B. Arockiam, C. Bruneau, P. H. Dixneuf, *Chem. Rev.* **2012**, *112*, 5879-5918; (h) L. Ackermann, *Chem. Rev.* **2011**, *111*, 1315-1345; (i) G. Meng, N. Y. S. Lam, E. L. Lucas, T. G. Saint-Denis, P. Verma, N. Chekshin, J. Q. Yu, *J. Am. Chem. Soc.* **2020**, *142*, 10571-10591; (j) R. Shang, L. Ilies, E. Nakamura, *Chem. Rev.* **2017**, *117*, 9086-9139; (k) S. Rej, Y. Ano, N. Chatani, *Chem. Rev.* **2020**, *120*, 1788-1887; (l) R.-Y. Zhu, M. E. Farmer, Y.-Q. Chen, J.-Q. Yu, *Angew. Chem. Int. Ed.* **2016**, *55*, 10578-10599; (m) N. Kuhl, M. N. Hopkinson, J. Wencel-Delord, F. Glorius, *Angew. Chem. Int. Ed.* **2012**, *51*, 10236-10254; (n) N. Y. S. Lam, Z. Fan, K. Wu, H. S. Park, S. Y. Shim, D. A. Strassfeld, J.-Q. Yu, *J. Am. Chem. Soc.* **2022**, *144*, 2793-2803;

[6] (a) K. Liao, S. Negretti, D. G. Musaev, J. Bacsa, H. M. L. Davies, *Nature* **2016**, *533*, 230-234; (b) Z. Zhang, K. Tanaka, J.-Q. Yu, *Nature* **2017**, *543*, 538-542; (c) O. Daugulis, H.-Q. Do, D. Shabashov, *Acc.*

Chem. Res. **2009**, *42*, 1074-1086; (d) P. Wang, P. Verma, G. Xia, J. Shi, J. X. Qiao, S. Tao, P. T. W. Cheng, M. A. Poss, M. E. Farmer, K.-S. Yeung, J.-Q. Yu, *Nature* **2017**, *551*, 489-493; (e) N. Della Ca, M. Fontana, E. Motti, M. Catellani, *Acc. Chem. Res.* **2016**, *49*, 1389-1400 ; (c) D. Lichosyt, Y. Zhang, K. Hurej, P. Dydio, *Nat. Catal.* **2019**, *2*, 114-122 ; (d) J. F. Hartwig, M. A. Larsen, *ACS Cent. Sci.* **2016**, *2*, 281-292; (e) M. T. Mihai, G. R. Genova, R. J. Phipps, *Chem. Soc. Rev.* **2018**, *47*, 149-171.

[7] (a) I. A. I. Mkhalid, J. H. Barnard, T. B. Marder, J. M. Murphy, J. F. Hartwig, *Chem. Rev.* **2010**, *110*, 890-931; (b) R. Bisht, C. Haldar, M. M. M. Hassan, M. E. Hoque, J. Chaturvedi, B. Chattopadhyay, *Chem. Soc. Rev.* **2022**, *51*, 5042-5100; (c) L. Xu, G. Wang, S. Zhang, H. Wang, L. Wang, L. Liu, J. Jiao, P. Li, *Tetrahedron* **2017**, *73*, 7123-7157; (d) J. S. Wright, P. J. H. Scott, P. G. Steel, *Angew. Chem. Int. Ed.* **2021**, *60*, 2796-2821.

[8] (a) D. G. Hall, *Boronic Acids. Preparation, Applications in Organic Synthesis*, Wiley-VCH, Weinheim, **2011**; (b) E. C. Neeve, S. J. Geier, I. A. I. Mkhalid, S. A. Westcott, T. B. Marder, *Chem. Rev.* **2016**, *116*, 9091-9161.

[9] (a) M. A. Larsen, R. J. Oeschger, J. F. Hartwig, *ACS Catal.* **2020**, *10*, 3415-3424; (b) M. A. Larsen, C. V. Wilson, J. F. Hartwig, *J. Am. Chem. Soc.* **2015**, *137*, 8633-8643; (c) R. Oeschger, B. Su, Y. Yu, C. Ehinger, E. Romero, S. He, J. Hartwig, *Science* **2020**, *368*, 736-741; (d) O. Kuleshova, S. Asako, L. Ilies, *ACS Catal.* **2021**, 11, 5968-5973;

[10] (a) E. Fernandez, *Top. Organomet. Chem.* **2020**, *69*, 207-225; (a) T. Ishiyama, J. Takagi, K. Ishida, N. Miyaura, N. R. Anastasi, J. F. Hartwig, *J. Am. Chem. Soc.* **2002**, 124, 390-391; (b) T. Ishiyama, J. Takagi, J. F. Hartwig, N. Miyaura, *Angew. Chem. Int. Ed.* **2002**, *41*, 3056-3058; (c) T. Ishiyama, Y. Nobuta, J. F. Hartwig, N. Miyaura, *Chem. Commun.* **2003**, 2924-2925; (d) C. W. Liskey, C. S. Wei, D. R. Pahlsa, J. F. Hartwig, *Chem. Commun.* **2009**, 5603-5605; (e) R. J.; Oeschger, M. A. Larsen, A. Bismuto, J. F. Hartwig, *J. Am. Chem. Soc.* **2019**, *141*, 16479-16485; (f) A. Ros, R. Fernandez, J. M.Lassaletta, *Chem. Soc. Rev.* **2014**, *43*, 3229-3243.

[11] (a) W. Chang, Y. Chen, S. Lu, H. Jiao, Y. Wang, T. Zheng, Z. Shi, Y. Han, Y. Lu, Y. Wang, Y. Pan, J.-Q. Yu, K. N. Houk, F. Liu, Y. Liang, *Chem* **2022**, *8*, 1775-1788; (b) S. Pandit, S. Maiti, D. Maiti, *Org. Chem. Front.* **2021**, *8*, 4349-4358. (c) X. Zou, S. Xu, *Chin. J. Org. Chem.* **2021**, **41**, 2610-2620; (d) J. Wang, T. Torigoe, Y. Kuninobu, *Org. Lett.* **2019**, *21*, 1342-1346; (d) X. Lu, Y. Yoshigoe, H. Ida, M. Nishi, M. Kanai, Y. Kuninobu, *ACS Catal.* **2019**, *9*, 1705-1709; (e) H. J. Davis, M. T. Mihai, R. J. Phipps, *J. Am. Chem. Soc.* **2016**, *138*, 12759-12762; (f) B. Lee, M. T. Mihai, V. Stojalnikova, R. J. Phipps, *J. Org. Chem.* **2019**, *84*, 13124-13134; (g) M. T. Mihai, H. J. Davis, G. R. Genov, R. J. Phipps, *ACS Catal.* **2018**, *8*, 3764-3769; (h) M. E. Hoque, R. Bisht, C. Haldar, B. Chattopadhyay, *J. Am. Chem. Soc.* **2017**, *139*, 7745-7748; (i) Y. Wang, W. Chang, S. Qin, H. Ang, J. Ma, S. Lu, Y. Liang, *Angew. Chem. Int. Ed.* **2022**, *61*, e202206797; (j) J. L. Douthwaite, R. J. Phipps, *Tetrahedron* **2022**, *117-118*, 132831.

[12] M. Ditzen, M. Pellegrino, L. B. Vosshall, *Science* **2008**, *319*, 1838-1842.

[13] (a) G. A. Bakken, P. C. Jurs, *J. Med. Chem.* **2000**, *43*, 4534-4541; (b) X. He, A. Alianc, P. R. Ortiz de Montellano, *Bioorg. Med. Chem.* **2007**, *15*, 6649-6658; (c) M. A. Letavic, L. Aluisio, R. Apodaca, M. Bajpai, A. J. Barbier, A. Bonneville, P. Bonaventure, N. I. Carruthers, C. Dugovic, I. C. Fraser, M. L. Kramer, B. Lord, T. W. Lovenberg, L. Y. Li, K. S. Ly, H. Mcallister, N. S. Mani, K. L. Morton, A. Ndifor, S. D. Nepomuceno, C. R. Pandit, S. B. Sands, C. R. Shah, J. E. Shelton, S. S. Snook, D. M. Swanson, W.

Xiao, *ACS Med. Chem. Lett.* **2015**, *6*, 450-454; (d) C. J. Gerry, S. L. Schreiber, *Nat. Rev. Drug Discovery* **2018**, *17*, 333-352.

[14] (a) L. Yang, K. Semba, Y. Nakao, *Angew. Chem. Int. Ed.* **2017**, *56*, 4853-4857; (b) M. E. Hoque, R. Bisht, A. Unnikrishnan, S. Dey, M. M. M. Hassan, S. Guria, R. N. Rai, R. B. Sunoj, B. Chattopadhyay, *Angew. Chem. Int. Ed.* **2022**, *61*, e202203539; (c) R. Bisht, M. E. Hoque, B. Chattopadhyay, *Angew. Chem. Int. Ed.* **2018**, *57*, 15762-15766; (d) Y. Kuninobu, H. Ida, M. Nishi, M. Kanai, *Nat. Chem.* **2015**, *7*, 712-717; (e) S. Lu, T. Zheng, J. Ma, Z. Deng, S. Qin, Y. Chen, Y. Liang, *Angew. Chem. Int. Ed.* **2022**, *61*, e202201285.

[15] (a) S.-T. Bai, C. B. Bheeter, J. N. H. Reek, *Angew. Chem. Int. Ed.* **2019**, *58*, 13039-13043; (b) C. Liu, L. Zhang, L. Li, M. Lei, *J. Org. Chem.* **2021**, *86*, 16858-16866.

[16] (a) J. E. Dannatt, A. Yadav, M. R. Smith III, R. E. Maleczka Jr., *Tetrahedron Lett.* **2022**, *109*, 132578; (b) B. Ghaffari, S. M. Preshlock, D. L. Plattner, R. J. Staples, P. E. Maligres, S. W. Krska, R. E. Maleczka, Jr., M. R. Smith III, *J. Am. Chem. Soc.* **2014**, *136*, 14345-14348; (c) M. E. Hoque, M. M. M. Hassan, B. Chattopadhyay, *J. Am. Chem. Soc.* **2021**, *143*, 5022-5037;(d) G. Wang, L. Liu, H. Wang, Y.-S. Ding, J. Zhou, S. Mao, P. Li, *J. Am. Chem. Soc.* **2017**, *139*, 91-94; (e) J. Jiao, W. Nie, P. Song, P. Li, *Org. Biomol. Chem.* **2021**, *19*, 355-359.

[17] (a) J. Trouvé, P. Zardi, S. Al-Shehimy, T. Roisnel, R. Gramage-Doria, *Angew. Chem. Int. Ed.* **2021**, *60*, 18006-18013.

[18] Deposition Numbers 2216009 contain the supplementary crystallographic data for this paper. These data are provided free of charge by the joint Cambridge Crystallographic Data Centre and Fachinformationszentrum Karlsruhe Access Structures service www.ccdc.cam.ac.uk/structures.

[19] (a) M. M. Williamson, C. M. Prosser-McCartha, S. Mukundan Jr., C. L. Hill, *Inorg. Chem.* **1988**, *27*, 1061-1068; (b) S. Lipstman, S. Muniappan, I. Goldberg, *Acta Cryst.* **2006**, *E62*, m2330-m2332 ; (c) B. Boitrel, V. Baveux-Chambenoît, P. Richard, *Eur. J. Org. Chem.* **2001**, 42132-4221; (d) L. H. Tong, P. Pengo, W. Clegg, J. P. Lowe, P. R. Raithby, J. K. M. Sanders, S. I. Pascu, *Dalton Trans.* **2011**, *40*, 10833-10842.

[20] J.-Y. Cho, C. N. Iverson, M. R. Smith, *J. Am. Chem. Soc.* **2000**, *122*, 12868-12869.

[21] D. W. Robbins, J. F. Hartwig, *Angew. Chem. Int. Ed.* **2013**, *52*, 933-937.

[22] (a) C. J. Barger, R. D. Dicken, V. L. Weidner, A. Motta, T. L. Lohr, T. J. Marks, *J. Am. Chem. Soc.* **2020**, *142*, 8019-8028; (b) M. K. Bisai, K. Gour, T. Das, K. Vanka, S. S. Sen, *Dalton Trans.* **2021**, *50*, 2354-2358; (c) P. Ghosh, A. J. von Wangelin, *Angew. Chem. Int. Ed.* **2021**, *60*, 16035-16043; (d) M.-L. Yuan, J.-H. Xie, S.-F. Zhu, Q.-L. Zhou, *ACS Catal.* **2016**, *6*, 3665-3669.

[23] (a) D. J. Pasto, J. Hickman, *J. Am. Chem. Soc.* **1968**, *90*, 4445-4449; (b) D. J. Pasto, J. Chow, S. K. Arora, Tetrahedron 1969, 25, 1557-1569. (c) J. Niziol, T. Ruman, *Lett. Org. Chem.* **2012**, *9*, 257-262; (d) Y. Yamamoto, R. Fujikawa, T. Umemoto, N. Miyaura, *Tetrahedron* **2004**, *60*, 10695-10700; (e) L. P. Press, A. J. Kosanovich, B. J. McCulloch, O. V. Ozerov, *J. Am. Chem. Soc.* **2016**, *138*, 9487-9497.

[24] (a) H. Tamura, H. Yamazaki, H. Sato, S Sakaki, *J. Am. Chem. Soc.* **2003**, *125*, 16114-16126; (b) M. Tomasini, L. Caporaso, J. Trouvé, J. Poater, R. Gramage-Doria, A. Poater, *Chem. Eur. J.* **2022**, *28*, e202201970.

[25] (a) B. A. Vanchura II, S. M. Preshlock, P. C. Roosen, V. A. Kallepalli, R. J. Staples, R. E. Maleczka, Jr., D. A. Singleton, M. R. Smith, III, *Chem. Commun.* **2010**, *46*, 7724-7726; (b) K. Yamazaki, S. Kawamorita, H. Ohmiya, M. Sawamura, Org. Lett. **2010**, *12*, 3978-3981; (c) B. Chattopadhyay, J. E. Dannatt, I. L. Andujar-De Sanctis, K. A. Gore, R. E. Maleczka, Jr., D. A. Singleton, M. R. Smith, III, *J. Am. Chem. Soc.* **2017**, *139*, 7864-7871.

[26] (a) V. L. Schramm, *Acc. Chem. Res.* **2015**, *48*, 1032-1039; (b) B. Ma, S. Kumar, C. J. Tsai, Z. Hu, R. Nussinov, *J. Theor. Biol.* **2000**, *203*, 383-397; (c) Y. Peng, A. L. Hansen, L. Bruschweiler-Li, O. Davulcu, J. J. Skalicky, M. S. Chapman, R. Brüschweiler, *J. Am. Chem. Soc.* **2017**, 139, 4846-4853.

[27] (a) C. C. C. Johansson Seechurn, V. Sivakumar, D.; Satoskar, T. J. Colacot, *Organometallics* **2014**, *33*, 3514-3522; (b) E. D. Slack, T. J. Colacot, *Org. Lett.* **2021**, *23*, 1561-1565.

[28] Y. Huang, J. Zhang, *Synthesis* **2022**, 54, 3595-3604.

[29] W. Chen, K. Li, Z. Hu, L. Wang, G. Lai, Z. Li, *Organometallics* **2011**, *30*, 2026-2030.

[30] R. Olivera, R. SanMartin, E. Dominguez, X. Solans, M. K. Urtiaga, M. I. Arriortua, *J. Org. Chem.* **2000**, *65*, 6398-6411.

[31] G. H. Chan, D. Y. Ong, Z. Yen, C. Shunsuke, *Helv. Chim. Acta* **2018**, *101*, e1800049.

[32] J. A. Murphy, S. J. Roome, *J. Chem. Soc. Perkin Trans. 1* **1995**, 1349-1358.

[33] H. Tsukamoto, Yoshinori Kondo, *Org. Lett.* **2007**, *9*, 4227-4230.

[34] J. Jiao, W. Nie, P. Song, P. Li, Org. Biomol. Chem. **2021**, 19, 355-359

Chapter 5. Destabilizing predictive copper-catalyzed click reactions by remote interactions with a zinc-porphyrin backbone

5.1 Introduction

In chapter 3, a small library of supramolecular ligands of formula **L** have been synthesized and characterized. The key step is a copper-catalyzed click reaction between a zinc-porphyrin alkyne **1** and the corresponding azidopyridine derivative (**Scheme 1**, top). Such transformation performed well with several 2- and 4-substituted azidopyridines. However, the access to other functionalized azidopyridines starting from the corresponding bromopyridine derivative *via* NaN_3 reaction is not trivial because multi-functionalized bromo- and azido-pyridines can be highly unstable tending to decompose or leading to unpredictable reactivity. As such, we envisioned an alternative route to access supramolecular ligands of formula **L** by means of a key sulfonyl triazole intermediate (**1'**) that should further react with pyridine *N*-oxide derivatives according to literature precedents (**Scheme 1**, bottom).[1] Multifunctionalized pyridine *N*-oxides are straightforward accessible from the corresponding pyridine derivative, thus potentially enabling a new chemical space for accessing novel supramolecular ligands **L**. In the following chapter, we show the unexpected inability to access species **1'** due to an undesired reaction pathway that is favored by the presence of the remotely-located zinc-porphyrin scaffold. Indeed, all attempts led to the formation of zinc-porphyrins of formula **2** that result from a nucleophilic addition of alcohols or water present in trace amounts in the solvent. By a set of control experiments and molecular modelling we postulate that the zinc-porphyrin unit plays a key role in order to stabilize otherwise inaccessible reaction intermediates.

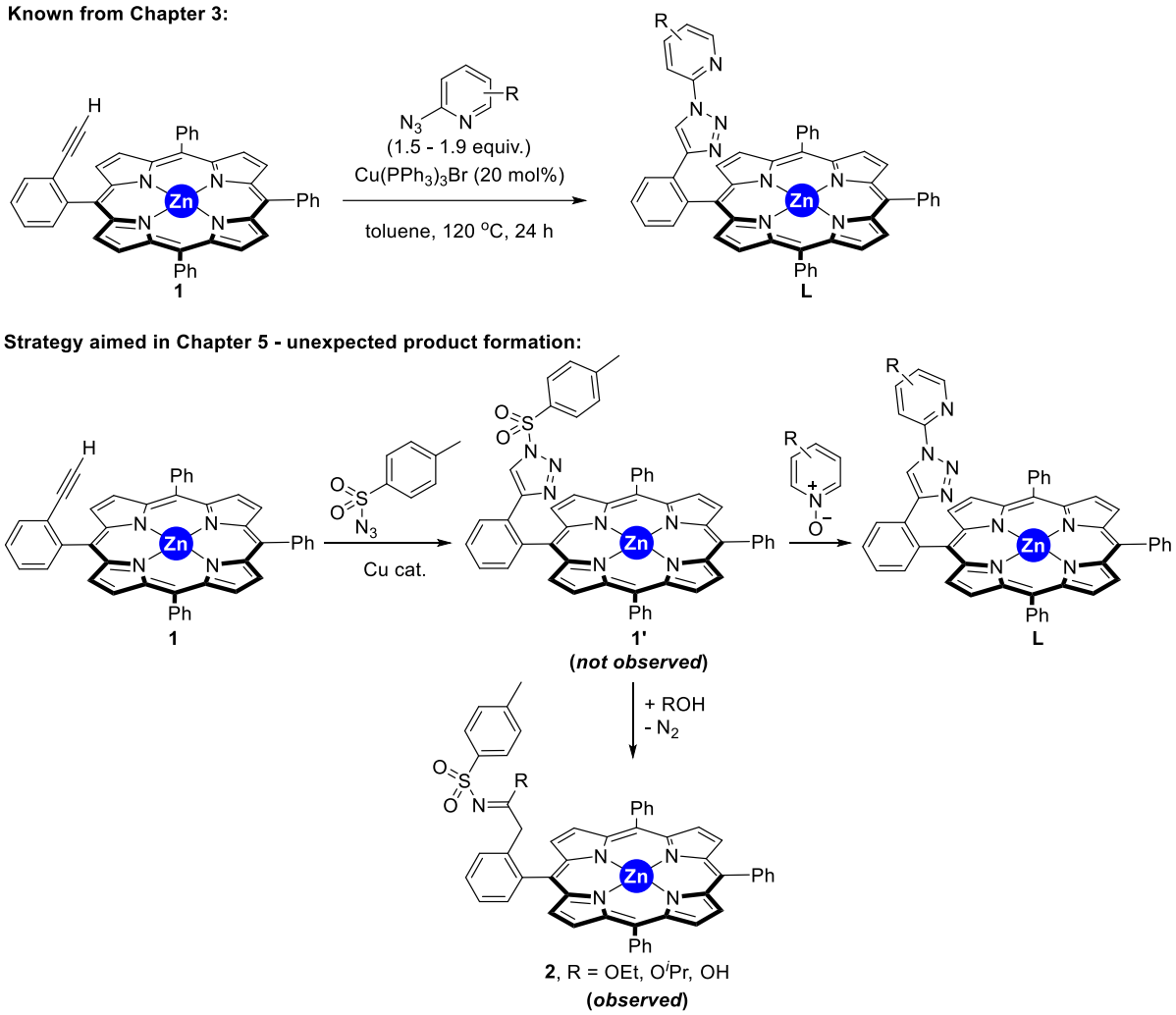

Scheme 1. Previous route to access supramolecular ligands **L** described in chapter 3 (top) and newly-envisioned alternative route showing the unexpected formation of **2** (bottom).

5.2. Results and discussion.

Initially, we verified the attempted strategy presented in **Scheme 1** (bottom) by performing a control experiment with a system lacking a zinc-porphyrin motif (**Scheme 2**). Phenyl acetylene was reacted under known reaction conditions with tosyl azide[2] under copper catalysis[3] affording the expected tosyl triazole compound **A1** in a 73% isolated yield. Next, **A1** efficiently reacted with pyridine *N*-oxide affording the desired triazolopyridine **L1*** in 86% isolated yield, thereby demonstrating the feasibility of such approach for systems lacking a zinc-porphyrin scaffold as similarly known in the literature.[1] The spectral data of **A1** and **L1*** match those reported in the literature.[4,5]

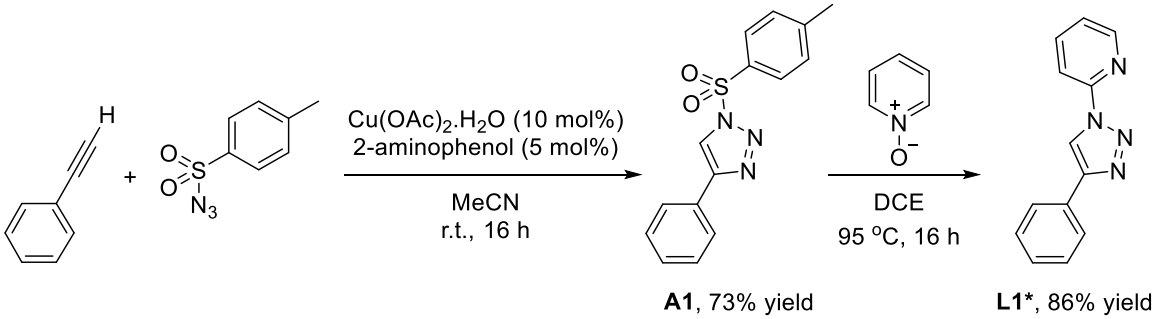

Scheme 2. Synthesis of the triazolopyridine **L1*** following the strategy presented in Scheme 1, bottom. DCE = 1,2-dichloroethane.

With this promising findings in hand and considering the compatibility of *ortho*-substitution patterns in the aromatic ring of phenylacetylene derivatives in copper-catalyzed click chemistry,[6-12] we applied the same copper-catalyzed protocol from **Scheme 2** to the reaction between the alkyne-containing porphyrin **1** and tosyl azide (**Scheme 3**). Unfortunately, the expected porphyrin product **1'** did not form. In fact, the side-product **2-OH** was isolated in 13% isolated yield (**Scheme 3**). **2-OH** likely results from a nucleophilic water attack onto an open-form of a triazole intermediate followed by dinitrogen release and keto-enol tautomerism. Note that water is present in the copper pre-catalyst as well as in the undistilled reagents and/or solvent. This observation is not unprecedented in the area of copper catalyzed click chemistry, especially when there is an excess of water and the reaction is carried out at relatively high temperatures,[13-15] however in most examples it is observed together with the expected sulfonyl triazole compound,[16-18] which is not the case here by using zinc-porphyrins. On the other hand, it must be emphasized that the functionalization of metalloporphyrins by means of click chemistry involving alkyl and aryl azides is well known.[19-23] Intriguingly, no examples of reacting metalloporphyrins with tosyl azides have been reported to the best of our knowledge.

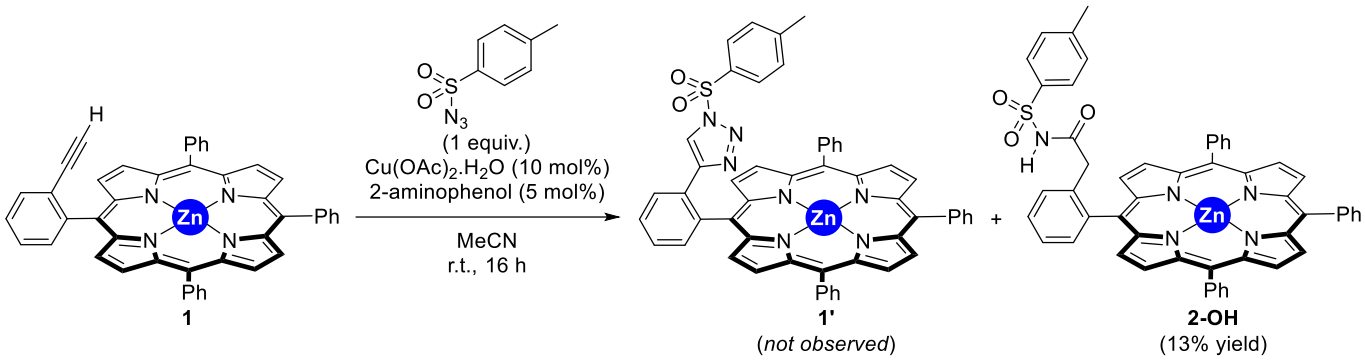

Scheme 3. Attempts to synthesize compound **1'** starting from **1** under copper catalysis and identification of undesired side-product **2-OH**.

In 2007, Fokin, Chang and co-workers reported their seminal work for the preparation of *N*-sulfonyltriazoles similar to **1'** by reacting alkynes with tosyl azides under copper catalysis.[24] The reaction occurred at 0 °C using CuI as the pre-catalyst in the presence of stoichiometric amounts of 2,6-lutidine and chloroform as the solvent. Consequently, we applied such reaction conditions to the alkyne porphyrin **1** (**Table 1**, entry 1). Although full conversion of starting material was observed after 24 hours, the targeted tosyl triazole porphyrin **1'** did not form. However, a major porphyrin compound was formed and isolated in 67% yield corresponding to amidate species **2-OEt** according to HRMS and NMR spectroscopy studies, besides minor formation of **2-OH**. **2-OEt** likely originates in a similar manner as **2-OH** but with ethanol (stabilizer of chloroform) as the nucleophile and release of dinitrogen.[25,26] Performing the reaction at room temperature proceeded with full conversion of **1**, but still affording **2-OEt** in a similar 70% yield whereas the yield of **2-OH** raised to 13% (Table 1, entry 2). Using molecular sieves as well as decreasing the reaction temperature to -20 °C and -70 °C led to 70% and 30% conversions of **1**, respectively, and the yield of **2-OEt** was significantly reduced to 43% and 16%, respectively (**Table 1**, entries 3 and 4). Under these conditions, the side-product **2-OH** was formed only in trace amounts. Replacing chloroform stabilized with ethanol for chloroform stabilized with amylene or THF led to no formation of **2-OEt** (**Table 1**, entries 5 and 6), further demonstrating that the ethanol that reacts is the one found as stabilizer in the chloroform solvent.

Table 1. Attempts to synthesize compound **1'** starting from **1** with CuI pre-catalyst and identification of undesired side-products **2-OEt** and **2-OH**.[a]

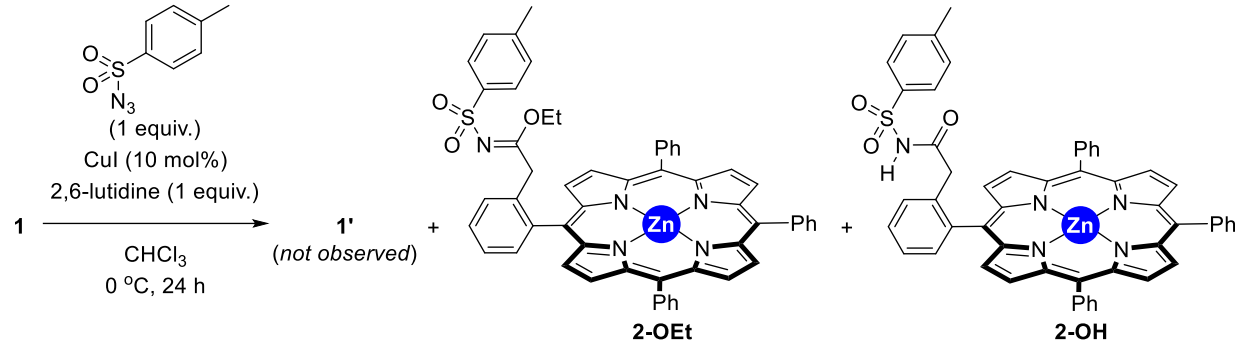

Entry	Deviation from above conditions	Conv. **1** (%)[b]	Yield **2-OEt** (%)[b]	Yield **2-OH** (%)[b]
1	none	>99	67	5
2	20 °C instead of 0 °C	>99	70	13
3[c]	-20 °C instead of 0 °C	70	43	<5
4[c]	-70 °C instead of 0 °C	30	16	<5
5[c]	$CHCl_3$ stabilized with amylene instead of ethanol	30	0	10
6[c]	THF instead of $CHCl_3$	50	0	10

[a] Reaction conditions: **1** (0.100 g, 0.14 mmol), tosyl azide (0.027 g, 0.14 mmol), CuI (0.003 g, 0.014 mmol), 2,6-lutidine (0.015 g, 0.016 mL, 0.14 mmol), chloroform stabilized with ethanol (10 mL), 0 °C, 24 h. [b] Conversion and yields estimated by ^{1}H NMR spectroscopy studies. [c] Reaction performed in the presence of molecular sieves.

Next, and considering the unexpected reactivity of alkyne porphyrin **1** with respect to its counterpart lacking the zinc-porphyrin and with the aim to generalize such reactivity, we envisioned to react **1** with tosyl azide under copper-catalyzed click conditions in the presence of another alcohol. For that, we adapted some reaction conditions from the literature which utilized $CuSO_4 \cdot 5H_2O$ as the pre-catalyst in a mixture of solvents comprising *iso*-propanol and additives such as DABO (DABCO = 1,4-diazabicyclo[2.2.2]octane), AcOH and sodium ascorbate in catalytic amounts (**Table 2**).[27] In this manner, full conversion of **1** and 81% isolated yield of the corresponding amidate product **2-O^{i}Pr** were obtained with trace amounts formation of **2-OH** (**Table 2**, entry 1). Performing the reaction in pure DCM or pure water inhibited the copper-catalyzed process leading to no formation of products (**Table 2**, entries 2 and 3), thereby indicating the key role of *iso*-propanol for enabling the formation of **2-O^{i}Pr** unde copper-catalyzed click chemistry conditions.

Table 2. Attempts to synthesize compound **1'** starting from **1** with $CuSO_4 \cdot 5H_2O$ pre-catalyst and identification of undesired side-products **2-O^{i}Pr** and **2-OH**.[a]

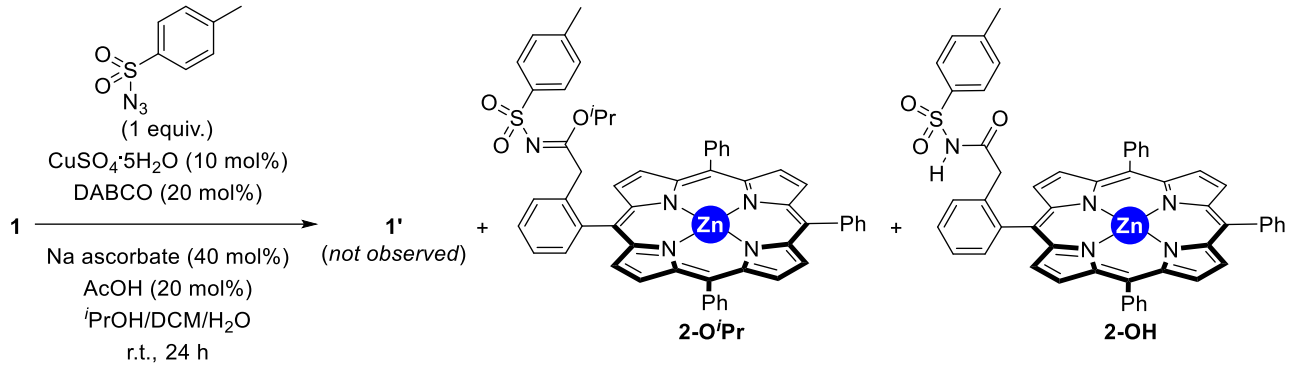

Entry	Deviation from above conditions	Conv. **1** (%)[b]	Yield **2-O^{i}Pr** (%)[b]	Yield **2-OH** (%)[b]
1	none	>99	81	5
2	only DCM as the solvent[c]	<10	0	0
3	only H_2O as the solvent	0	0	0

[a] Reaction conditions: **1** (0.100 g, 0.14 mmol), tosyl azide (0.027 g, 0.14 mmol), $CuSO_4 \cdot 5H_2O$ (0.003 g, 0.014 mmol), DABCO (0.003 g, 0.03 mmol), sodium ascorbate (0.011 g, 0.056 mmol) acetic acid (0.0017 g, 0.0016 mL, 0.028 mmol), ^{i}PrOH/DCM/H_2O (amylene stabilized, 10 mL, v/v 1:1:1,) 20 °C, 24 h. [b] Conversion and yields estimated by ^{1}H NMR spectroscopy studies. [c] DCM stabilized with amylene.

As regards of the previous observations, the copper-catalyzed click reaction with porphyrin alkyne **1** and tosyl azide does not deliver the expected tosyl triazole **1'**, but a series of side-products resulting from nucleophile (alcohol or water) addition towards tosyl amidates (**2-OEt**, **2-O^{i}Pr**) and tosyl amides (**2-OH**). Such findings are in stark contrast with simple phenylacetylene that does deliver the expected tosyl triazole **A1**. As such, the presence of the zinc-porphyrin backbone appears to play an important role to explain the formation of tosyl amidates and tosyl amides products. From a mechanist point of view, and based on previous literature as well,[28-31] we propose the following considerations depicted in **Scheme 4**. The alkyne porphyrin **1** reacts with tosyl azide under copper catalysis affording the well-known cuprated triazole intermediate **A** which is in equilibria towards the formation of intermediate **B**. We anticipate that the equilibria is shifted towards **B** due to intramolecular binding of the diazo fragment to the zinc center of the porphyrin backbone that would promote the release of dinitrogen leading to ketenimine species **C**. Nucleophilic addition of an alcohol reagent leads to the final product **2**. In the case of water addition, a last keto/enol tautomerism is at play to provide the amide product. The nucleophilic attack could be also enhanced by initial coordination of the nucleophile to the zinc center and hydrogen bonding to the sulfone (formation of species **C'**). Although this is unlikely considering that he higher yield is obtained with the less nucleophilic *iso*-propanol reagent, this event cannot be rule out at this stage. Preliminar molecular modelling strongly suggests the feasibility of intermediates **B** and **C'** in which the remotely-located zinc-porphyrin plays an activator role. An

alternative reaction mechanism in which the sulfone in **A** binds to the zinc centre can also be envisaged, thereby destabilizing this intermediate and eventually stabilizing other ones.

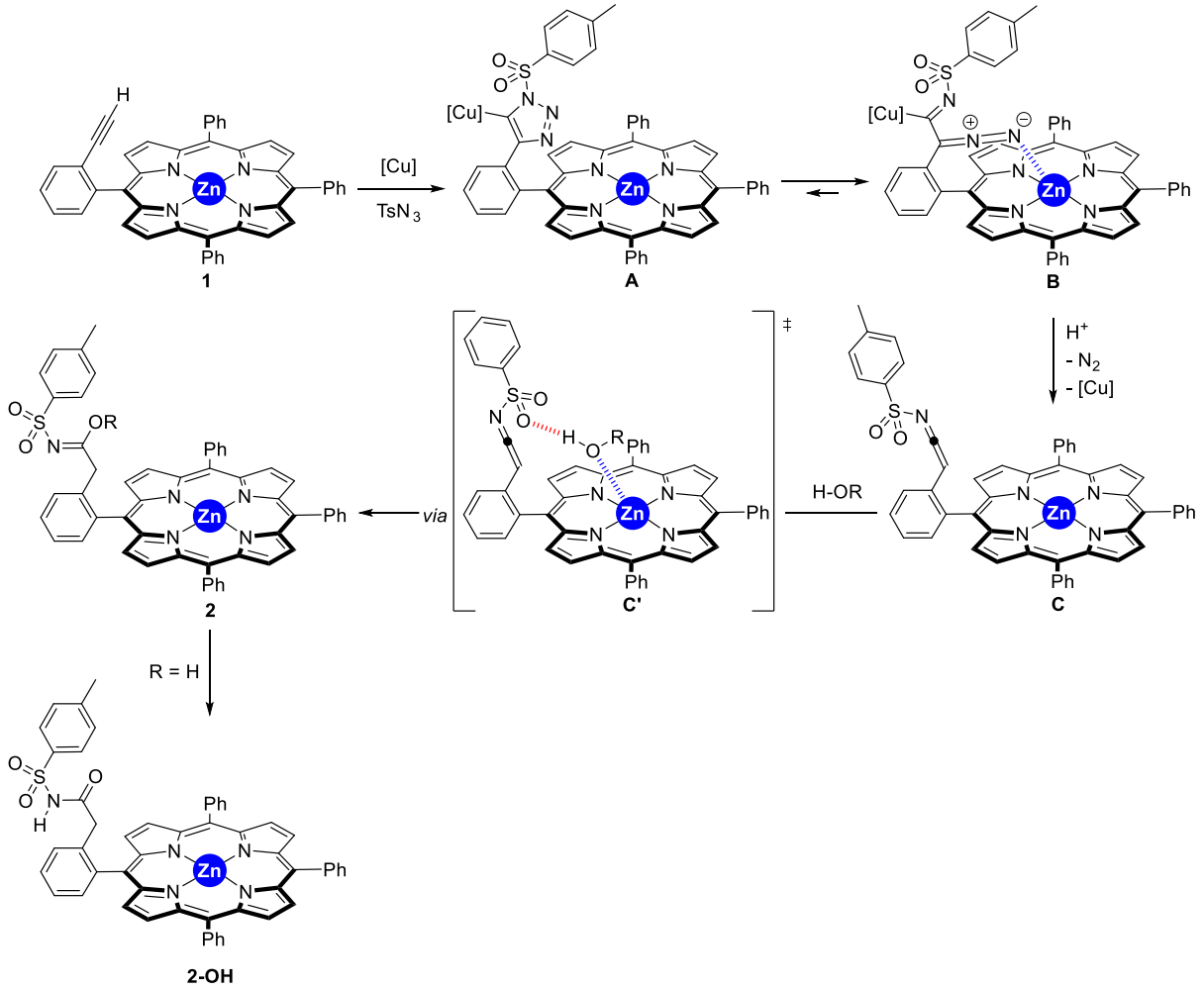

Scheme 4. Postulated reaction mechanism operating for the formation of sulfonyl amidates **2** starting from **1** under copper catalysis highlighting the role of the zinc-porphyrin scaffold in several intermediates.

5.3. Conclusion.

In summary, we have disclosed that the usually highly predictable copper-catalyzed click reaction does not provide the desired tosyl triazole product in the case of zinc-porphyrin compounds upon reaction with tosyl azide under different set of copper catalysts under different reaction conditions. The selectivity is directed towards the formation of sulfonyl amidates in the presence of alcohols or to sulfonyl amide in the presence of water. By means of control experiments, it appears that the zinc-porphyrin motif could play a relevant role by enhancing dinitrogen release and nucleophilic addition, which are key selective-determining steps in the reaction mechanism, *via* remote non-covalent interactions

5.4. Experimental section.

General methods.

Solvents were purified with an MB SPS-800 purification system. Pyrrole was dried with CaH_2 and distilled prior to use. $CDCl_3$ was filtered through alumina and stored under argon over molecular sieves. All the other employed chemicals were purchased from commercial sources and used as received. Unless otherwise specified, reactions were carried out under argon atmosphere by employing standard Schlenk and vacuum-line techniques. ^1H and ^{13}C NMR spectra were recorded with a Bruker GPX (400 MHz) spectrometer. ^1H NMR spectra were referenced to residual protiated solvent (δ = 7.26 ppm for $CDCl_3$). ^{13}C NMR spectra were referenced to $CDCl_3$ δ = 77.16 ppm). Abbreviations for signal couplings are: br, broad; s, singlet; d, doublet; t, triplet; m, multiplet; dd, doublet of doublets; dt, triplet of doublets; td, doublet of triplets; tt, triplet of triplets; tdd, doublet of doublet of triplets. Coupling constants, *J*, were reported in hertz unit (Hz). The reactions were monitored by using a Shimadzu 2014 gas chromatograph equipped with an EquityTM-1 Fused Silica capillary column (30 m x 0.25 mm x 0.25 □m) and an FID detector; conversion and selectivity were determined by using dodecane as internal standard. UV/Vis absorption spectra were recorded with a Specord 205 UV/Vis/NIR spectrophotometer and quartz cuvettes of 1 cm path length. Mass spectroscopy and microanalysis were performed in the laboratories of the Centre Regional de Mesures Physiques de l'Ouest (CRMPO, Université de Rennes 1, Rennes, France). Molecular modeling calculations were performed with the PM3-Spartan molecular modeling program.

Alkyne porphyrin **1** was prepared as discussed in chapter 2 and tosyl azide was prepared according to a literature protocol.[2]

General procedure for the copper-catalyzed reactions: 1 (0.100 g, 0.14 mmol, 1 equiv.), copper catalyst (0.014 mmol, 0.1 equiv.), TsN_3 (0.028 g, 0.14 mmol, 1 equiv.), sodium ascorbate (0 to 0.2 equiv.), 2-aminophenol (0 to 0.05 equiv.), DABCO (0 to 0.2 equiv.), solvent (10 mL), base (0 to 1 equiv.) and AcOH (0 to 0.2 equiv.) were added to an oven dried Schlenk flask. The reaction mixture was stirred at a given temperature under Argon atmosphere for 24 h. Conversion is an estimated value determined by ^1H crude NMR analysis. Isolated yield of **2** was reported after purification of the crude mixture by column chromatography (SiO_2, heptane:DCM, v/v 1:0 to 0:1).

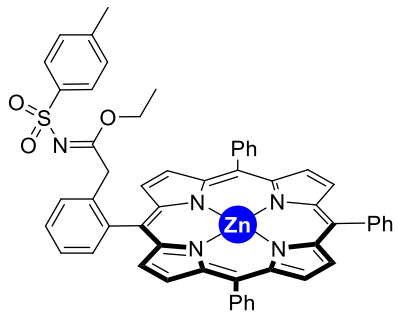

Synthesis and characterization of 2-OEt: Following the general procedure **1** (0.100 g, 0.14 mmol, 1 equiv.), CuI (0.003 g, 0.014 mmol, 0.1 equiv.), TsN_3 (0.027 g, 0.14 mmol, 1 equiv.), DCM (EtOH stabilized, 10 mL) 2,6-lutidine (0.015 g, 0.016 mL, 0.14 mmol, 1 equiv.) were stirred at room temperature under Argon atmosphere during 24 hours. Then, the crude mixture was purified by column chromatography (SiO_2, heptane:DCM, v/v 1:0 to 1:1) affording analytically pure **2-OEt** (90 mg, 70% yield). ^1H NMR (400 MHz, $CDCl_3$): δ = 8.93 (s, 4H), 8.79 (AB, *J* = 56.4, 4H), 8.27-8.14 (m, 7H), 7.81-7.70 (m, 10H), 7.67 (t, *J* = 7.4 Hz, 2H), 6.38 (d, *J* = 0.9 Hz, 4H), 3.91 (s, 2H),

3.70 (q, *J* = 7.1 Hz, 3H), 1.86 (s, 3H), 1.01 (t, *J* = 7.1 Hz, 3H) ppm. $^{13}C\{^{1}H\}$ NMR (101 MHz, $CDCl_3$): δ = 172.64, 150.26, 150.16, 149.78, 143.00, 142.95, 142.67, 142.34, 137.76, 136.18, 134.51, 134.47, 133.67, 132.06, 131.95, 131.89, 131.28, 129.77, 128.52, 128.36, 127.40, 127.38, 126.48, 126.48, 125.58, 125.44, 121.21, 121.01, 117.80, 64.63, 38.88, 20.93, 13.3 ppm. HRMS (ESI, $CHCl_3$) calcd. for $[M]^+$ $C_{55}H_{41}N_5O_3S^{64}Zn$ 915.22161; found: 915.2206 (1 ppm).

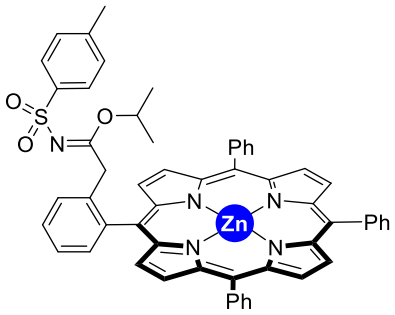

Synthesis and characterization of 2-O^{i}Pr: Following the general procedure **1** (0.100 g, 0.14 mmol, 1 equiv.), $CuSO_4.5H_2O$ (0.004g, 0.014 mmol, 0.1 equiv.), DABCO (0.003 g, 0.03 mmol, 0.2 equiv.), TsN_3 (0.027 g, 0.14 mmol, 1 equiv.), iPrOH/DCM/H_2O (amylene stabilized, 1:1:1, 10 mL), sodium ascorbate (0.011 g, 0.056 mmol, 0.4 equiv.) and AcOH (0.0017g, 0.0016 mL, 0.028 mmol, 0.2 equiv.) were stirred at room temperature under Ar atmosphere during 24 hours. Then, the crude mixture was purified by column chromatography (SiO_2, heptane:DCM, v/v 1:0 to 1:1) affording analytically pure **2-O^{i}Pr** (106 mg, 81% yield). ^1H NMR (400 MHz, $CDCl_3$): δ = 8.94 (s, 4H), 8.83 (AB, *J* = 46.5 Hz, 4H), 8.28-8.12 (m, 8H), 7.81-7.71 (m, 10H), 7.68-7.60 (m, 2H), 6.77 (d, *J* = 8.3 Hz, 2H), 6.51 (d, *J* = 8.3 Hz, 2H), 4.68 (hept, *J* = 6.3 Hz, 1H), 3.90 (s, 2H), 1.89 (s, 3H), 0.98 (d, *J* = 6.3 Hz, 6H) ppm. $^{13}C\{^{1}H\}$ NMR (101 MHz, $CDCl_3$): δ = ^{13}C NMR (101 MHz, Chloroform-*d*) δ 172.42, 150.30, 150.22, 149.93, 142.95, 142.90, 142.53, 142.39, 138.28, 136.18, 134.50, 134.45, 133.94, 132.17, 131.98, 131.93, 131.54, 129.29, 128.58, 128.35, 127.44, 127.42, 126.49, 125.71, 125.32, 121.27, 121.08, 118.06, 72.52, 38.79, 20.98, 20.93. HRMS (MALDI, DCTB) calcd. for $[M]^+$ $C_{56}H_{43}N_5O_3S^{64}Zn$ 929.23726; found: 929.235 (2 ppm) .

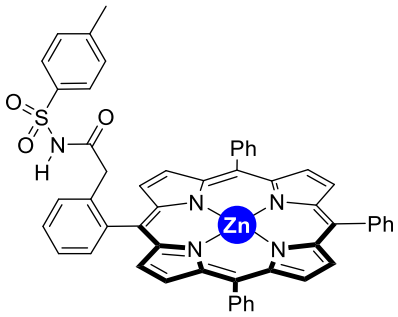

Synthesis and characterization of 2-OH: Following the general procedure **1** (0.100 g, 0.14 mmol, 1 equiv.), CuI (0.003 g, 0.014 mmol, 0.1 equiv.), TsN_3 (0.027 g, 0.14 mmol, 1 equiv.), DCM (EtOH stabilized, 10 mL), 2,6-lutidine (0.015 g, 0.016 mL, 0.14 mmol, 1 equiv.) were stirred at room temperature under Argon atmosphere 24 hours. Then, the crude mixture was purified by column chromatography (SiO_2, heptane:DCM, v/v 1:0 to 0:1) affording analytically pure **2-OH** as a side-product (16 mg, 13% yield). ^1H NMR (400 MHz, $CDCl_3$): δ = 8.94 (s, 4H), 8.78 (AB, *J* = 99.3 Hz, 4H), 8.35-8.13 (m, 7H), 7.83-7.71 (m, 11H), 7.68 (td, *J* = 7.6, 1.4 Hz, 1H), 7.56 (d, *J* = 7.6 Hz, 1H), 7.45 (br, 1H), 7.09 (d, *J* = 8.1 Hz, 2H), 6.65 (d, *J* = 8.1 Hz, 2H), 3.17 (s, 2H), 2.00 (s, 3H) ppm. HRMS (ESI, DCM) calcd. for $[M]^+$ $C_{53}H_{37}N_5O_3S$ ^{64}Zn 887.19031; found: 887.1903 (0 ppm).

5.5. References.

[1] M. B. Harisha, M. Nagaraj, S. Muthusubramanian, N. Bhuvanesh, *RSC Adv*. **2016**, *6*, 58118-58124.

[2] P. Kumar, T. Jiang, S. Li, O. Zainul, S.T. Laughlin, *Org. Biomol. Chem.* **2018**, *16*, 4081-4085.

[3] Y. Liu, X. Wang, J. Xu, Q. Zhang, Y. Zhao, Y. Hu, *Tetrahedron* **2011**, *67*, 6294-6299.

[4] J. Pospech, R. Ferraccioli, H. Neumann, M. Beller, *Chem. Asian J.* **2015**, *10*, 2624–2630.

[5] B. Chattopadhyay, C. I. Rivera Vera, S. Chuprakov, V. Gevorgyan, *Org. Lett.* **2010**, *12*, 2166-2169.

[6] S. T. Jablasone, Jr, Z. Ye, S. Duan, Z.-F. Xu, C.-Y. Li, *Org. Biomol. Chem.* **2021**, *19*, 5758-5761.

[7] Y. Jiang, Q. Wang, R. Sun, X.-Y. Tang, M. Shi, *Org. Chem. Front.* **2016**, *3*, 744-748.

[8] H. J. Jeon, M. S. Kwak, D. J. Jung, J. Bouffard, S.-g. Lee, *Org. Biomol. Chem.* **2016**, *14*, 11238-11243.

[9] T. Miura, T. Nakamuro, K. Hiraga, M. Murakami, *Chem. Commun.* **2014**, *50*, 10474-10477.

[10] Y. Yang, M.-B. Zhou, X.-H. Ouyang, R. Pi, R.-J. Song, J.-H. Li, *Angew. Chem. Int. Ed.* **2015**, *54*, 6595-6599.

[11] W. Zhou, M. Zhang, H. Li, W. Chen, *Org. Lett.* **2017**, *19*, 10-13.

[12] M. Cen, Q. Xiang, Y. Xu, S. Duan, Y. Lv, Z.-F. Xu, C.-Y. Li, *Org. Chem. Front.* **2020**, *7*, 596-601.

[13] S. H. Cho, E. J. Yoo, I. Bae, S. Chang, *J. Am. Chem. Soc.* **2005**, *127*, 16046-16047.

[14] S. H. Cho, S. Chang, *Angew. Chem. Int. Ed.* **2007**, *46*, 1897-1900.

[15] M. P. Cassidy, J. Raushel, V. V. Fokin, *Angew. Chem. Int. Ed.* **2006**, *45*, 3154-3157.

[16] I. Cano, M. C. Nicasio, P. J. Pérez, *Org. Biomol. Chem.* **2010**, *8*, 536-538.

[17] J. Raushel, V. V. Fokin, *Org. Lett.* **2010**, *12*, 4952-4955.

[18] E. J. Yoo, M. Ahlquist, I. Bae, K. B. Sharpless, V. V. Fokin, S. Chang, *J. Org. Chem.* **2008**, *73*, 5520-5528.

[19] K. Ladomenou, V. Nikolaou, G. Charalambidis, A. G. Coutsolelos, *Coord. Chem. Rev.* **2016**, *306*, 1-42.

[20] A. R. L. Araújo, A. C. Tomé, C. I. M. Santos, M. A. F. Faustino, M. G. P. M. S. Neves, M. M. Q. Simões, N. M. M. Moura, S. T. Abu-Orabi, J. A. S. Cavaleiro, *Molecules* **2020**, *25*, 1662.

[21] A. K. Agrahari, P. Bose, M. K. Jaiswal, S. Rajkhowa, A. S. Singh, S. Hotha, N. Mishra, V. K. Tiwari, *Chem. Rev.* **2021**, *121*, 7638-7956.

[22] A. Marrocchi, A. Facchetti, D. Lanari, S. Santoro, L. Vaccaro, *Chem. Sci.* **2016**, *7*, 6298-6308.

[23] S. Hiroto, Y. Miyake, H. Shinokubo, *Chem. Rev.* **2017**, *117*, 2910-3043.

[24] E. J. Yoo, M. Ahlquist, S. H. Kim, I. Bae, V. V. Fokin, K. B. Sharpless, S. Chang, *Angew. Chem. Int. Ed.* **2007**, *46*, 1730-1733.

[25] R. Kranthikumar, R. Chegondi, S. Chandrasekhar, *J. Org. Chem.* **2016**, *81*, 2451-2459.

[26] H. E. Bartrum, S. Carret, J.-F. Poisson, *Synthesis* **2016**, *48*, 3413-3419.

[27] P. B. Sarode, S. P. Bahekar, H. S. Chandak, *Synlett* **2016**, *27*, 2681-2684.

[28] T.-L. Liu, Q.-H. Li, L. Wei, Y. Xiong, C.-J. Wang, *Adv. Synth. Catal.* **2017**, *359*, 1854-1859.

[29] D. J. Jung, H. J. Jeon, J. H. Lee, S.-g. Lee, *Org. Lett.* **2015**, *17*, 3498-3501.

[30] B. Yao, C. Shen, Z. Liang, Y. Zhang, *J. Org. Chem.* **2014**, *79*, 936-942.

[31] W. Song, M. Lei, Y. Shen, S. Cai, W. Lu, P. Lu, Y. Wang, *Adv. Synth. Catal.* **2010**, *352*, 2432-2436.

Chapter 6. A highly sterically congested bis-zinc-porphyrin containing a single buta-1,3-diyne linkage: an adaptable object for supramolecular encapsulation.

6.1. Introduction.

In chapter 3, we have described a general experimental protocol to obtain supramolecular ligands containing a peripheral triazolopyridine backbone in order to place a catalytically active metal site just above the zinc-porphyrin platform that plays the role of molecular recognition towards heterocyclic substrates, typically pyridine derivatives. In fact, during the formation of the supramolecular ligands **L** under copper-catalyzed click reaction conditions starting from the alkyne porphyrin **1**, we identified the formation of dimeric species $\mathbf{1_2}$ in yields that vary depending on the nature of the triazolopyridine reagent being employed (**Table 1**). Notably, when employing the 2-azido-4-*tert*-butyl-pyridine, 26% yield of $\mathbf{1_2}$ was obtained. As regard of the exotic character of this highly sterically demanding species, we decided to explore in detail the origin of this unexpected reactivity and its molecular recognition properties, which is relevant not only in the context of supramolecular chemistry[1] but also for catalysis if the zinc is replaced by a catalytically active metal such as Mn, Fe, Ru or other ones.[2]

Table 1. Synthesis of supramolecular ligands **L** and formation of by-product $\mathbf{1_2}$.[a]

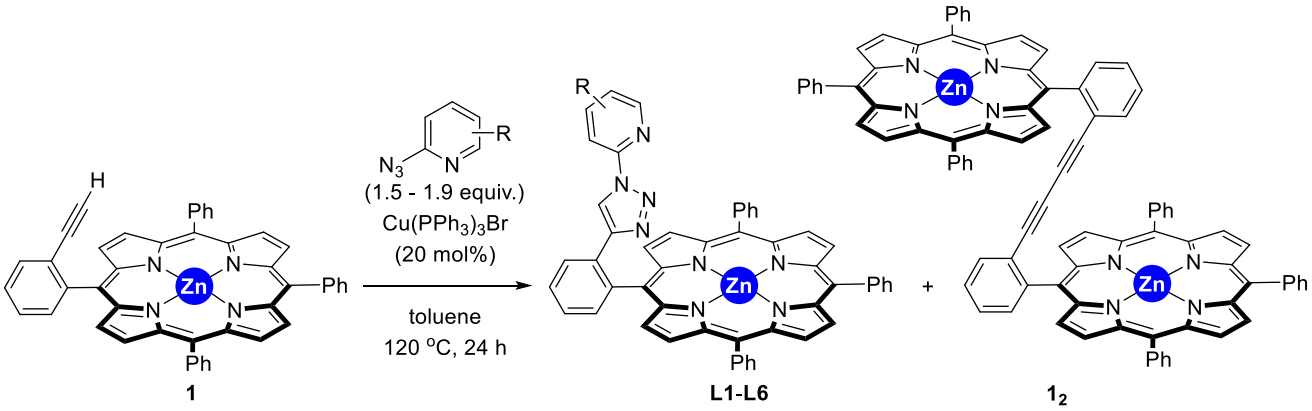

Entry	R	Conv. **1** (%)[b]	Yield **L** (%)[b]	Yield $\mathbf{1_2}$ (%)[b]
1	H (**L1**)	>99	95	<5
2	4-^{t}Bu (**L2**)	>99	74	**26**
3	4-Me (**L3**)	>99	92	**8**
4	6-Me (**L4**)	>99	95	<5
5	4-OMe (**L5**)	>99	90	**10**
6	4-CF_3 (**L6**)	>99	>99	0

[a] Reaction conditions described in chapter 3. [b] Conversion and yields estimated by ^{1}H NMR spectroscopy studies.

6.2. Results and discussion.

Initially, and in view to understand the unexpected formation of dimer **1_2** we wondered whether the copper pre-catalyst $Cu(PPh_3)_3Br$,[3] which is known to outperform state-of-the-art copper catalysts for selective triazole synthesis,[4] is productive enough for the formation of **1_2**. To our surprise, the dimerization reaction of **1** did not proceed in the presence of catalytic amounts of $Cu(PPh_3)_3Br$ and the starting material **1** was fully recovered (**Scheme 1**).

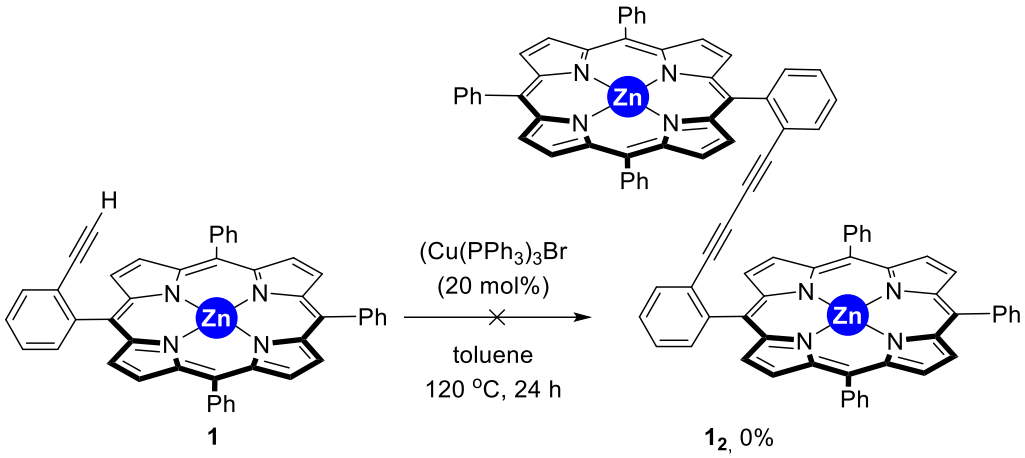

Scheme 1. Attempts to synthesize **1_2** starting from **1** with $Cu(PPh_3)_3Br$ as the pre-catalyst.

This observation indicates that the supramolecular triazolopyridine compound (**L**) formed as a product in **Table 1** could play a role by activating/coordinating the copper species that truly promote the dimerization side-reaction. To address this point, we evaluated a model reaction (**Table 2**), namely the dimerization of phenylacetylene in the presence of $Cu(PPh_3)_3Br$ as the pre-catalyst and an additional ligand **L2*** that corresponds to the triazolopyridine fragment belonging to the supramolecular ligand **L2** that displays the highest yield of dimer **1_2** (**Table 2**, entry 1). Under this reaction condition, the corresponding dimer product 1,4-diphenylbutadiyne formed in 65% isolated yield. Importantly, the reaction in the absence of **L2*** led to no product formation (**Table 2**, entry 2). Replacing the copper salt $Cu(PPh_3)_3Br$ by CuI and addition of PPh_3 ligand to the reaction mixture was completely ineffective (**Table 2**, entries 3-5),

Table 2. Evaluation of dimerization of phenylacetylene under copper catalysis relevant to understand the formation of $\mathbf{1_2}$.[a]

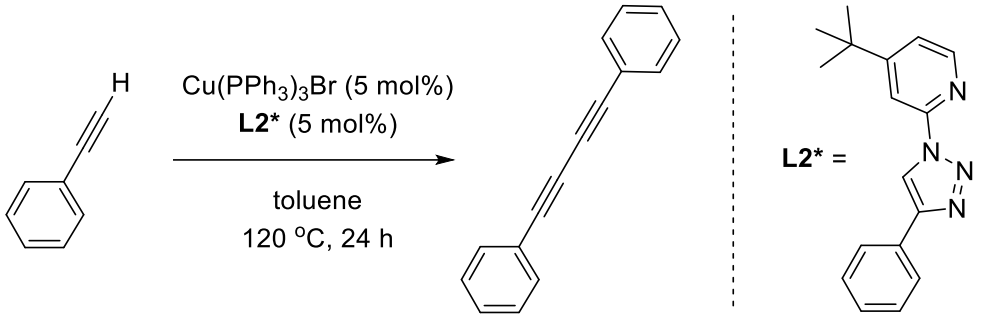

Entry	Deviation from above conditions	Yield 1,4-diphenylbutadiyne product (%)[b]
1	none	65
2	w/o **L2***	<5
3	with CuI instead of $Cu(PPh_3)_3Br$	0
4	with CuI instead of $Cu(PPh_3)_3Br$ and w/o **L2***	0
5	with CuI instead of $Cu(PPh_3)_3Br$ and PPh_3	<5

[a] Reaction conditions: phenylacetylene (0.100 g, 0.98 mmol), $Cu(PPh_3)_3Br$ (0.046 g, 0.049 mmol), **L2*** (0.014 g, 0.049 mmol), toluene (20 mL), 120 °C, 24 h. [b] Isolated yield after purification by column chromatography.

These findings indirectly suggest that the formation of $\mathbf{1_2}$ under copper catalysis in **Table 1** is likely due to the formation of catalytically active triazolopyridine-coordinated copper species (**Cu-L**, **Figure 1**) and that $Cu(PPh_3)_3Br$ is the truly active catalyst for the selective triazole synthesis that yields the supramolecular ligands **L** (**Table 1**). Overall, this is a rare example relevant for the copper-catalyzed click chemistry in which the triazole compound formed behaved as an inhibitor for the triazole synthesis and drives the system towards a side-reaction, in this case a dimerization of alkyne. It is relevant to note that, in general, the triazole compound formed during copper-catalyzed azide-alkyne cycloaddition reactions behaves as a ligand to accelerate the catalysis in an autocatalytic fashion as shown in the early work of Whitesides.[5] Whether formation of monomeric or dimeric copper species are responsible for one product selectivity or the other one remains to be addressed.[6] On another side, the activity of the copper triazolopyridine species (**Cu-L**, **Figure 1**) is dependent on the pyridine electron density, as regards of the yields of $\mathbf{1_2}$ obtained in **Table 1**, indicating a reaction enhancement by electron donating groups. The ability of heteroaromatic *N*,*N*-chelating ligands to coordinate to $[Cu(PPh_3)Br]$ motifs is widely reported.[7]

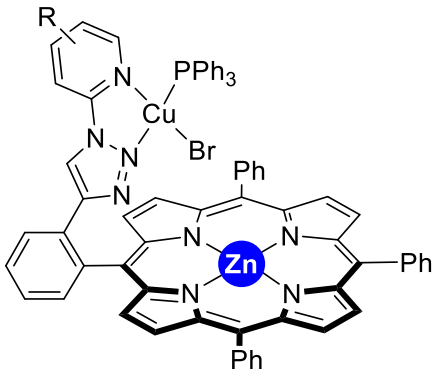

Figure 1. Postulated copper species responsible for the formation of by-product dimer $\mathbf{1_2}$ during the synthesis of the supramolecular ligands **L1**-**L6** in **Table 1**.

Next, we envisioned the high-yielding synthesis of $\mathbf{1_2}$ by performing a copper-catalyzed Glaser-Hay homo-coupling.[8] Indeed, treatment of **1** with catalytic amounts of both CuI and *N*,*N*'-tetramethylethylenediamine (TMEDA) in chloroform solvent at 50 °C during 16 hours afforded the bis-zinc-porphyrin dimer $\mathbf{1_2}$ in 79% isolated yield after purification by column chromatography (**Scheme 2**, top). Alternatively, dimer $\mathbf{1_2}$ was also synthesized by a palladium-catalyzed homo-coupling reaction in the presence of CuI and DABCO in acetonitrile at room temperature.[9] In this case, the isolated yield of $\mathbf{1_2}$ dropped to 61% yield (**Scheme 2**, bottom).

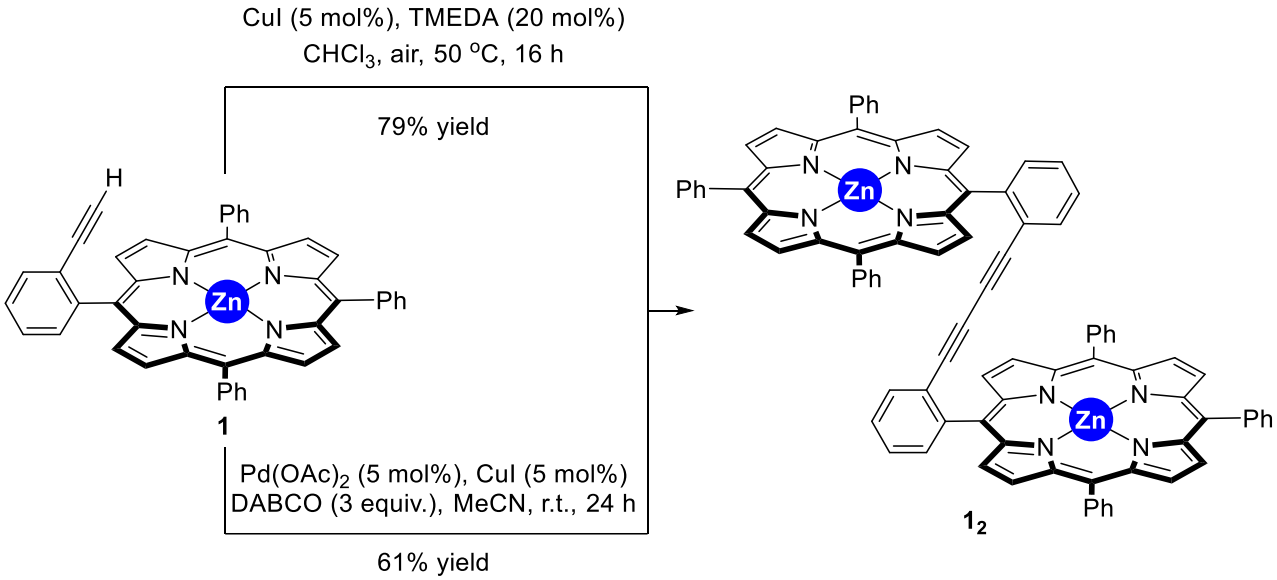

Scheme 2. Synthesis of $\mathbf{1_2}$ starting from **1** under copper catalysis (top) and under palladium/copper catalysis (bottom).

HRMS and multinuclei NMR confirmed the formation of such species. In fact, the relatively simple and symmetric ^{1}H and ^{13}C NMR spectra of $\mathbf{1_2}$ indicate that the two zinc-porphyrin backbones freely rotate along the butadiyne axis besides the highly constrained environment around this doubly triple bond. In other words, dimer $\mathbf{1_2}$ exists as a mixture of two interconverting species, namely a closed form

(**CF**), in which both zinc-porphyrin backbone stuck each other, and an open form (**OF**), in which the zinc-porphyrins reach the maximal distance between both zinc atoms by pointing to opposite directions (**Scheme 3**).

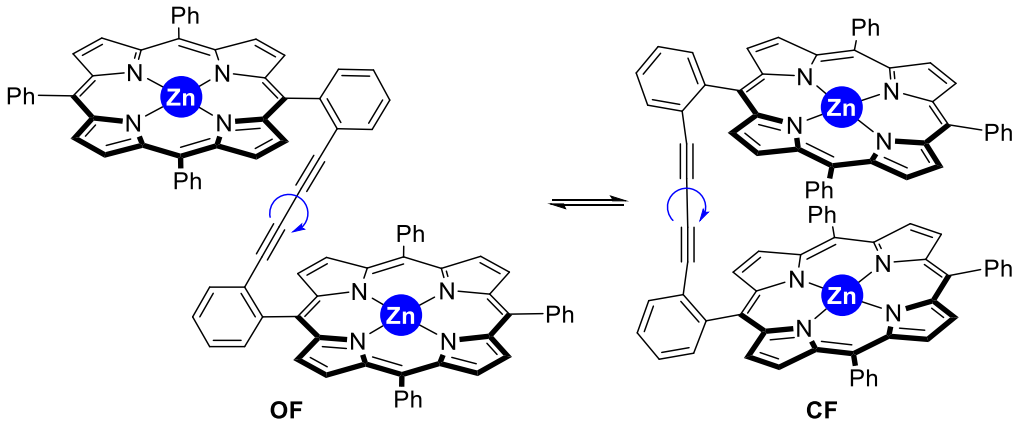

Scheme 3. Extreme cases of an open form (**OF**) and a closed form (**CF**) for dimer $\mathbf{1_2}$.

The postulated equilibria between an open form and a closed form was taken as an advantage for the study of the eventual encapsulation of DABCO between both zinc-porphyrins in the closed form of $\mathbf{1_2}$. We anticipated that each nitrogen atom from DABCO could be involved in a non-covalent Zn···N interaction with each zinc atom from $\mathbf{1_2}$. Indeed, ^{1}H NMR spectroscopy studies comprising a mixture of dimer $\mathbf{1_2}$ and DABCO in a 1:1 ratio featured a strong up-field shift for the proton signals belonging to DABCO that resonate at -4.64 ppm (**Figure 2**),[10] value which is in agreement for the encapsulation of DABCO into highly elaborated (supra)molecular cages containing two zinc-porphyrin units.[11] In addition, DOSY studies revealed that the up-field shifted signal belonging to DABCO are aligned with the proton signals from dimer $\mathbf{1_2}$, thereby indicating formation of a single supramolecular assembly in which both the host ($\mathbf{1_2}$) and the guest (DABCO) diffuse together. In addition, UV-vis titration studies enabled to calculate the binding constant which is in the order of $K_{1.1}$ *ca.* 10^5 M^{-1}, value that compare well with previous systems exhibiting a 1:1 binding stoichiometry. PM3 semi-empirical molecular modeling (Spartan) also indicates the feasibility of the formation of 1:1 assembly between dimer $\mathbf{1_2}$ and DABCO (**Figure 3**).

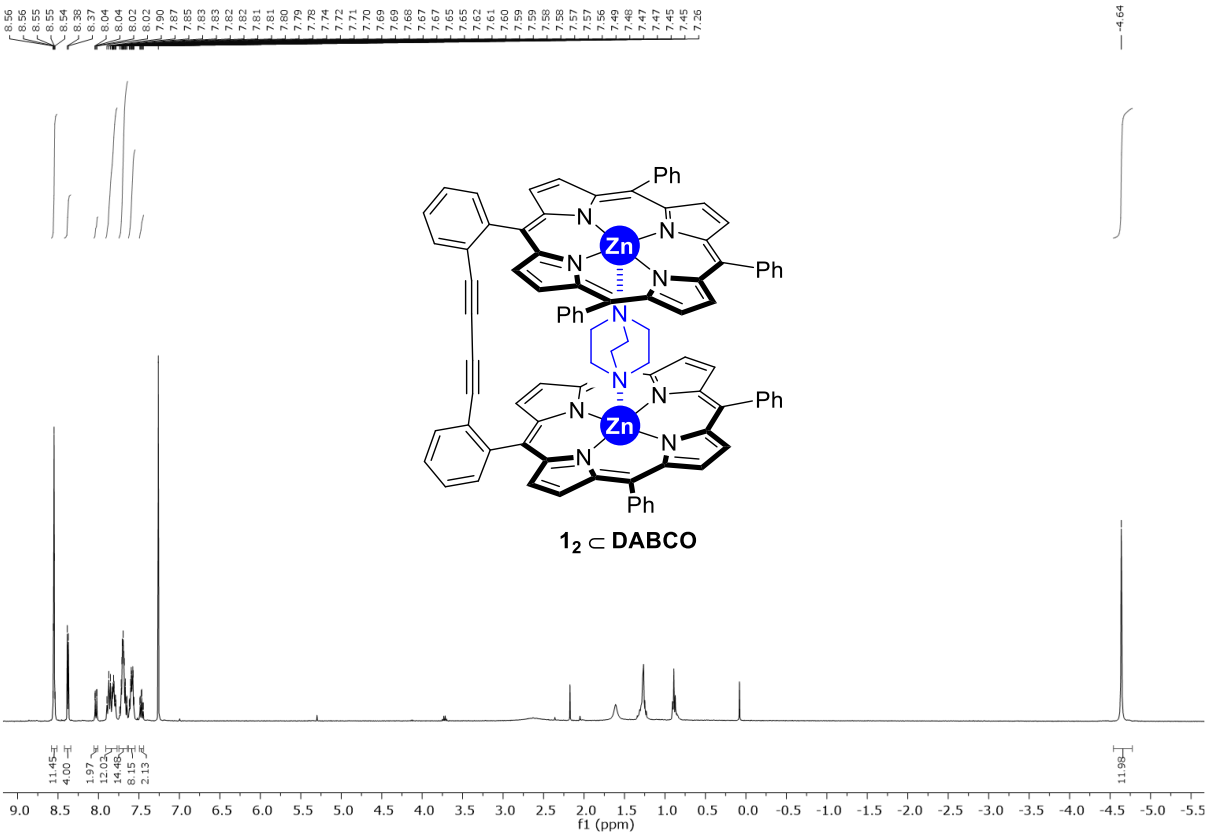

Figure 2. ^{1}H NMR ($CDCl_3$, 400 MHz) spectrum of an equimolar mixture of $\mathbf{1_2}$ and DABCO showing formation of the supramolecular assembly.

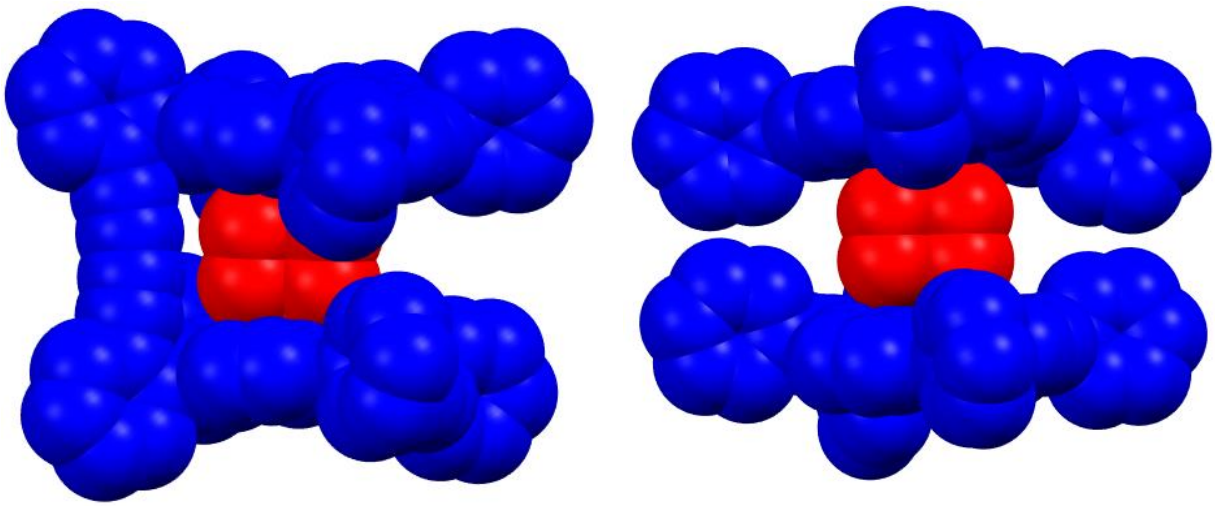

Figure 3. PM3-minimized semi-empirical calculations performed on $\mathbf{1_2} \subset$ DABCO (spacefill representation, two different side views). DABCO guest is shown in red color and the dimeric zinc-porphyrin in blue color.

6.3. Conclusion.

Although the encapsulation of small molecules such as DABCO within (supra)molecular cages made from zinc-porphyrins is known, all examples concern cyclic systems bearing at least two linkers to connect both zinc-porphyrin units.[12] In the present case, we show that such a strong pre-organization is not required for DABCO encapsulation since a simple acyclic bis-zinc-porphyrin system such as $\mathbf{1_2}$ is adaptable enough to drive the self-assembly process to a selective 1:1 encapsulation. In addition, this system provides a significant space available around the encapsulated guest to further explore new physicochemical processes that are less available for the typical cases in which the highly sophisticated (supra)molecular cages impose little access to additional events. Overall, by rational understanding the formation of an unexpected side-product in a copper-catalyzed click reaction, we have discovered the unique supramolecular properties found in a sterically congested bis-zinc-porphyhrin scaffold. Metalloporphyrins based on this chemical design might be ideal constituents for catalytic molecular machines and/or switchable catalysts.[13]

6.4. Experimental section.

General methods.

Solvents were purified with an MB SPS-800 purification system. Pyrrole was dried with CaH_2 and distilled prior to use. $CDCl_3$ was filtered through alumina and stored under argon over molecular sieves. All the other employed chemicals were purchased from commercial sources and used as received. Unless otherwise specified, reactions were carried out under argon atmosphere by employing standard Schlenk and vacuum-line techniques. ^1H and ^{13}C NMR spectra were recorded with a Bruker GPX (400 MHz) spectrometer. ^1H NMR spectra were referenced to residual protiated solvent (δ = 7.26 ppm for $CDCl_3$). ^{13}C NMR spectra were referenced to $CDCl_3$ δ = 77.16 ppm). Abbreviations for signal couplings are: br, broad; s, singlet; d, doublet; t, triplet; m, multiplet; dd, doublet of doublets; dt, triplet of doublets; td, doublet of triplets; tt, triplet of triplets; tdd, doublet of doublet of triplets. Coupling constants, *J*, were reported in hertz unit (Hz). The reactions were monitored by using a Shimadzu 2014 gas chromatograph equipped with an EquityTM-1 Fused Silica capillary column (30 m x 0.25 mm x 0.25 µm) and an FID detector; conversion and selectivity were determined by using dodecane as internal standard. UV/Vis absorption spectra were recorded with a Specord 205 UV/Vis/NIR spectrophotometer and quartz cuvettes of 1 cm path length. Mass spectroscopy and microanalysis were performed in the laboratories of the Centre Regional de Mesures Physiques de l'Ouest (CRMPO, Université de Rennes 1, Rennes, France). Molecular modeling calculations were performed with the PM3-Spartan molecular modeling program.

Alkyne porphyrin **1** was prepared as discussed in chapter 2 and ligand **L2*** was prepared as discussed in chapter 3.

General protocol for the homo-coupling of phenylacetylene: Into a dried Schlenk tube charged with a stirring bar, phenylacetylene (0.100 g, 0.107 mL 9.8 x 10^{-4} mol, 1 equiv.), $Cu(PPh_3)Br$ (0.046 g, 4.9 x 10^{-5}, 0.05 equiv.), **L2*** (0.014 g, 4.9 x 10^{-5}, 0.05 equiv.) and dry toluene (20 mL) were added. The reaction mixture was stirred for 24 hours at 120°C. GC-MS and GC-FID analysis showed a conversion of 65% and an estimated yield of 54%. Back at room temperature, the solvents were evaporated. The crude mixture was further purified by column chromatography (SiO_2, *n*-heptane:EtOAc, v/v 1:0 to 9:1) affording the homocoupling product as a colourless oil (0.047g, 47% yield.). ^1H NMR (400 MHz, $CDCl_3$): δ = 7.54 (dd, *J* = 7.9, 1.8 Hz, 2H), 7.41-7.28 (m, 8H) ppm. $^{13}C\{^1H\}$ NMR (101 MHz, $CDCl_3$): δ = 133.84, 133.65, 132.50, 129.20, 128.73, 128.52, 128.44, 121.82, 81.56, 73.92 ppm. The spectral data match those find in the litterature.[14]

Glaser-Hay cross coupling procedure for the synthesis of dimer $\mathbf{1_2}$: Into a dried Schlenk tube charged with a stirring bar, **1** (0.100 g, 0.14 mmol, 1 equiv.), CuI (0.001 g, 0.007 mmol, 0.05 equiv.), dry $CHCl_3$ (5 mL) and N,N'-tetramethylethylenediamine (0.003 g, 4µL, 0.025 mmol, 0.02 equiv.) were added and the reaction mixture was stirred for 16 hours at 50 °C under air atmosphere. Then the solvents were evaporated and the crude mixture was purified by column chromatography (SiO_2, *n*-heptane:DCM, v/v 1:0 to 7:3) affording analytically pure bis-alkyne zinc porphyrin $\mathbf{1_2}$ as a purple powder (0.079 g, 79% yield.). ^1H NMR (400 MHz, $CDCl_3$): δ = 8.92 (AB, *J* = 16 Hz 8H), 8.69-8.51 (AB, *J* = 120 Hz, 8H), 8.26-8.19 (m, 4H), 8.13-7.99 (m, 8H), 7.85-7.59 (m, 20H), 7.38 (td, *J* = 7.6, 1.4 Hz, 2H), 7.24 (d, *J* = 7.6 Hz, 2H), 6.99

(d, J = 7.6 Hz, 2H) ppm. $^{13}C\{^{1}H\}$ NMR (101 MHz, $CDCl_3$): δ = 150.17, 149.97, 149.94, 149.74, 145.19, 142.92, 142.68, 134.51, 134.39, 134.35, 134.08, 132.14, 132.03, 131.95, 131.79, 131.06, 127.50, 127.43, 127.37, 126.67, 126.54, 126.50, 126.41, 125.16, 121.38, 120.91, 117.84, 81.52 ppm. HRMS (ESI): *m/z* calcd for $C_{92}H_{54}N_8{}^{64}Zn_2$: 1398.30489 $[M]^{+\cdot}$; 1398.3055 (0 ppm).

Palladium/Copper co-catalyzed synthesis of 1_2: Into a dried Schlenk tube charged with a stirring bar, **1** (0.100 g, 0.14 mmol, 1 equiv.), CuI (0.001 g, 0.007 mmol, 0.05 equiv.), $Pd(OAc)_2$ (0.002 g, 0.007 mmol, 0.05), DABCO (0.478 g ,0.426 mmol, 3 equiv.) and dry acetonitrile (5 mL) were added and the reaction mixture was stirred for 16 hours at room temperature under air atmosphere. Then the solvents were evaporated and the crude mixture was purified by column chromatography (SiO_2, *n*-heptane:DCM, v/v 1:0 to 7:3) affording analytically pure bis-alkyne zinc porphyrin **1_2** as a purple powder (0.061 g, 61% yield.).

NMR binding experiment between bis alkyne porphyrin 1_2 and DABCO (1:1 ratio): 1_2 (5 mg, 3.57 x 10^{-3} mmol, 1 equiv.) was placed in an NMR tube and dried under vacuum for few minutes. Then, dry $CDCl_3$ (0.75 mL) was added and the corresponding ^{1}H NMR spectrum was recorded. Then, 1 equiv. of a diluted solution of DABCO (0.4 mg, 3.57 x 10^{-3} mmol, 1 equiv.) was added to the NMR tube containing the host **1_2** and the corresponding ^{1}H NMR spectrum was recorded showing strong up-field shifts for the DABCO proton signals. DOSY NMR also shows that both DABCO and **1_2** diffuse as one species.

UV titration

A solution of bis alkyne porphyrin 1_2 (Solution A) was prepared by dissolving 1_2 (5.6 mg, 4 x 10^{-6} mol) in 100 mL of DCM (4 x 10^{-4} mol.L^{-1}). A solution of DABCO (Solution B) was prepared by dissolving DABCO (22.6 mg, 2 x 10^{-4} mol) in 5 mL of DCM (4 x 10^{-2} mol.L^{-1}). A solution of a mixture of DABCO and 1_2 was prepared by taking 1 mL of (B) and by addition of (A) to 20 mL (Solution C) of DCM (2 x 10^{-3} mol.L^{-1}).

UV titration was done by addition of 30 small aliquot of C (10 µL) into a solution of A (2mL). The binding constant value was determined by Bindfit software using Nelder-Mead method. K = 1.34 x 10^{5} ± 0.3 M^{-1}.

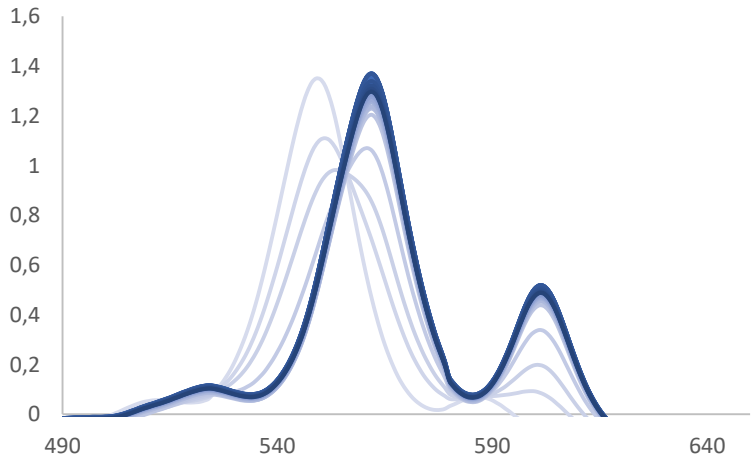

Figure 4. UV-titration spectrum.

6.5. References.

[1] (a) J.-M. Lehn, *Angew. Chem. Int. Ed.* **1988**, *27*, 89-112; (b) G. T. Williams, C. J. E. Haynes, M. Fares, C. Caltagirone, J. R. Hiscock, P. A. Gale, *Chem. Soc. Rev.* **2021**, *50*, 2737-2763.

[2] (a) B. Meunier, *Chem. Rev.* **1992**, *92*, 1411-1456; (b) M. M. Pereira, L. D. Dias, M. J. F. Calvete, *ACS Catal.* **2018**, *8*, 10784-10808; (c) H. Lua, X. P. Zhang, *Chem. Soc. Rev.* **2011**, *40*, 1899-1909.

[3] S. Lal, S. Díez-González, *J. Org. Chem.* **2011**, *76*, 2367-2373.

[4] (a) S. Díez-González, *Catal. Sci. Technol.* **2011**, *1*, 166-178; (b) H. C. Kolb, M. G. Finn, K. B. Sharpless, *Angew. Chem. Int. Ed.* **2001**, 40, 2004-2021.

[5] S. N. Semenov, L. Belding, B. J. Cafferty, M. P. S. Mousavi, A. M. Finogenova, R. S. Cruz, E. V. Skorb, G. M. Whitesides, *J. Am. Chem. Soc.* **2018**, *140*, 10221-10232.

[6] B. T. Worrell, J. A. Malik, V. V. Fokin, *Science* **2013**, *340*, 457-460.

[7] (a) R. K. Gujadhur, C. G. Bates, D. Venkataraman, *Org. Lett.* **2001**, *3*, 4315-4317; (b) P. F. Barron, L. M. Engelhardt, P. C. Healy, J. D. Kildea, A. H. White, *Inorg. Chem.* **1988**, *27*, 1829-1834; (c) A. Mitrofanov, M. Manowong, Y. Rousselin, S. Brandès, R. Guilard, A. Bessmertnykh-Lemeune, P. Chen, K. M. Kadish, N. Goulioukina, I. Beletskaya, *Eur. J. Inorg. Chem.* **2014**, 3370-3386; (d) J.-L. Chen, X.-F. Cao, J.-Y. Wang, L.-H. He, Z.-Y. Liu, H.-R. Wen, Z.-N. Chen, *Inorg. Chem.* **2013**, *52*, 9727-9740; (e) K. A. Vinogradova, V. F. Plyusnin, A. S. Kupryakov, M. I. Rakhmanova, N. V. Pervukhina, D. Y. Naumov, L. A. Sheludyakova, E. B. Nikolaenkova, V. P. Krivopalov, M. B. Bushuev, *Dalton Trans.* **2014**, *43*, 2953-2960; (f) D. H. Jara, L. Lemus, L. Farías, E. Freire, R. Baggio, J. Guerrero, *Eur. J. Inorg. Chem.* **2012**, 1579-1583.

[8] (a) C. Glaser, *Ber. Dtsch. Chem. Ges.* **1869**, *2*, 422-424; (b) C. Glaser, *Justus Liebigs Ann. Chem.* **1870**, *154*, 137-171; (c) A. Hay, *J. Org. Chem.* **1960**, 25, 1275-1276; (d) A. S. Hay, *J. Org. Chem.* **1962**, *27*, 3320-3321; (e) P. Siemsen, R. C. Livingston, F. Diederich, *Angew. Chem. Int. Ed.* 2000, *39*, 2632-22657; (f) L. Su, J. Dong, L. Liu, M. Sun, R. Qiu, Y. Zhou, S.-F. Yin, *J. Am. Chem. Soc.*, **2016**, *138*, 12348-12351.

[9] (a) J.-H. Li, Y. Liang, Y.-X. Xie, *J. Org. Chem.* **2005**, *70*, 4393-4396; (b) R. Rossi, A. Carpita, C. Bigelli, *Tetrahedron Lett.* **1985**, *26*, 523-526; (c) A. Toledo, I. Funes-Ardoiz, F. Maseras, A. C. Albéniz, *ACS Catal.* **2018**, *8*, 7495-7506.

[10] The addition of excess of DABCO resulted in the disappearance of the chemical shift ascribed to the encapsulation and the merger of a new one at a chemical shifts in which free DABCO is in exchange with higher aggregates involving eventual binding to the zinc-porphyrin.

[11] L. Poyac, C. Rose, M. Wahiduzzaman, A. Lebrun, G. Cazals, C. H. Devillers, P. G. Yot, S. Clément, S. Richeter, *Inorg. Chem.* **2021**, *60*, 19009-19021.

[12] (a) R. S. Wylie, E. G. Levy, J. K. M. Sanders, *Chem. Commun.* **1997**, 1611-1612; (b) R. Djemili, L. Kocher, S. Durot, A. Peuronen, K. Rissanen, V. Heitz, *Chem. Eur. J.* **2019**, *25*, 1481-1487; (c) M.

Nakash, J. K. M. Sanders, *J. Org. Chem.* **2000**, *65*, 7266-7271; (d) P. Mondal, S. Banerjee, S. P. Rath, S. Prasad, *Eur. J. Inorg. Chem.* **2019**, 3629-3637; (e) L. Schoepff, L. Kocher, S. Durot, V. Heitz, *J. Org. Chem.* **2017**, *82*, 5845-5851; (f) A. L. Kieran, A. D. Bond, A. M. Belenguer, J. K. M. Sanders, *Chem. Commun.* **2003**, 2674-2675; (g) H. Ding, X. Meng, X. Cui, Y. Yang, T. Zhou, C. Wang, M. Zeller, C. Wang, *Chem. Commun.* **2014**, 50, 11162-11164; (h) J. Taesch, V. Heitz, F. Topić, K. Rissanen, *Chem. Commun.* **2012**, *48*, 5118-5120; (i) C. G. Oliveri, N. C. Gianneschi, S. B. T. Nguyen, C. A. Mirkin, C. L. Stern, Z. Wawrzak, M. Pink, *J. Am. Chem. Soc.* **2006**, *128*, 16286–16296

[13] (a) V. Blanco, D. A. Leigh, V. Marcos, *Chem. Soc. Rev.* **2015**, *44*, 5341-5370; (b) L. van Dijk, M. J. Tilby, R. Szpera, O. A. Smith, H. A. P. Bunce, S. P. Fletcher, *Nature Rev. Chem.* **2018**, *2*, 0117; (c) A. Goswami, S. Saha, P. K. Biswas, M. Schmittel, *Chem. Rev.* **2020**, *120*, 125-199.

[14] A. S. Batsanov, J. C. Collings, I. J. S. Fairlamb, J. P. Holland, J. A. K. Howard, Z. Lin, T. B. Marder, A. C. Parsons, R. M. Ward, J. Zhu, *J. Org. Chem.* **2005**, *70*, 703-706.

Chapter 7. Catalyst complexity in a bio-inspired iron complex that displays Markovnikov selectivity for the Wacker-type oxidation of olefins

7.1 Introduction

Since the seminal contribution by Smidt and co-workers in 1959 demonstrating the ability of palladium catalysts to oxidize olefins into carbonyl-containing products,[1] tremendous efforts have been devoted to understand, apply and improve the efficiency of this reaction.[2] In this respect, the development of the palladium-catalyzed production of acetaldehyde from ethylene by the Wacker company in the 1960's remains a major breakthrough in view of the industrial implementation.[3] The last decades have witnessed impressive research aiming at (1) circumventing the issues associated to the harsh reaction conditions that make functional groups incompatible (searching for milder reaction conditions by avoiding chlorides, copper salts and acids)[4] as well as (2) disclosing palladium catalysts by ligand design to selectively control the Markovnikov or anti-Markovnikov products, that is, the ketone or the aldehyde when starting from a terminal olefin (**Equation 1**).[5]

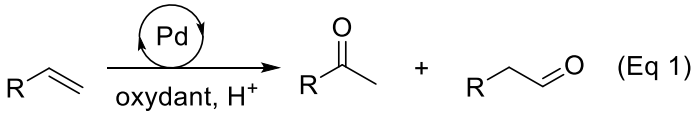

Alternatively, developing oxidation methodologies with metal catalysts derived from the first row appear promising from a sustainable point of view.[6] Owing to the almost perfect atom-economy, Wacker-type reactions have been the subject of study in order to replace the scarce palladium catalyst by more abundant and less toxic metal complexes.[7] From the many ones studied, iron complexes were found efficient for the anti-Markovnikov selective production of aldehydes starting from olefins as pioneered by Che using highly-sophisticated iron(III)-porphyrin catalysts.[8] Recently, Arnold and co-workers engineered by directed evolution a remarkable heme-containing enzyme that affords anti-Markovnikov products under ambient pressure and thousands of turnover numbers (TONs).[9] Methodologies leading to Markovnikov ketone products have been pioneered by the groups of Han and Knölker, independently, in the presence of hydrosilanes as the hydrogen source (**Figure 1**, top).[10] Notably, Knölker and co-workers demonstrated the ability of iron(III) catalysts to operate under air at room temperature provided that dibenzoylmethanato (dbm) or neoucuproine ligands were employed.[10e] However, variable amounts of alcohols or aldehydes are still formed depending on the nature of the starting olefin substrates and the reaction conditions (**Figure 1**, top).[10]

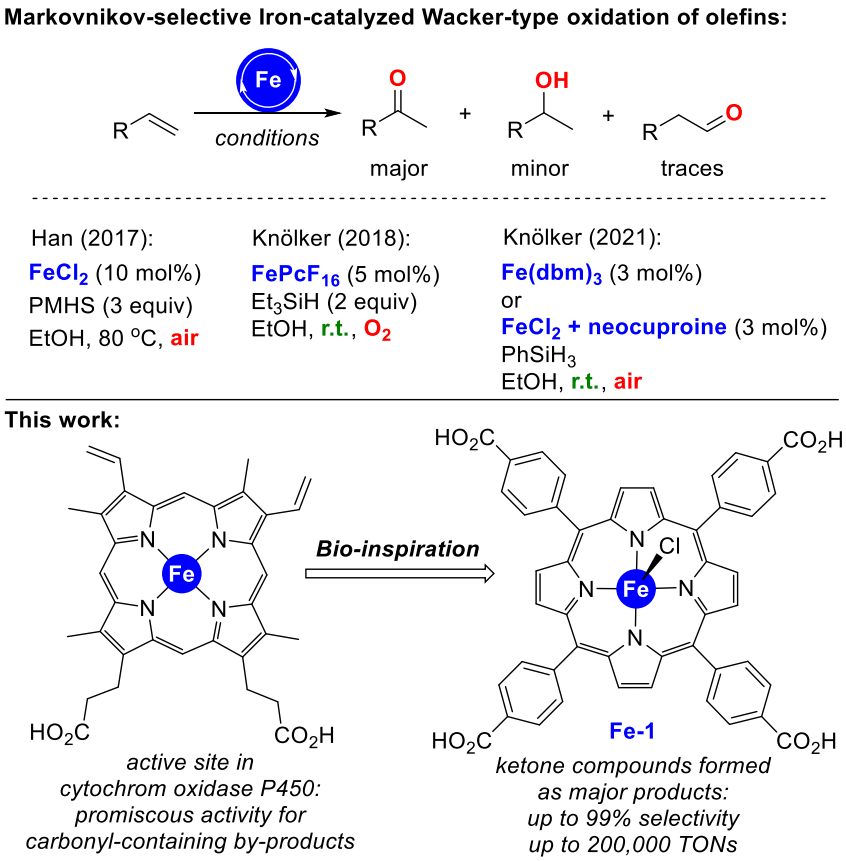

Figure 1. State-of-the-art of the Markovnikov-selective iron-catalyzed Wacker-type oxidation of olefins (top) and current bio-inspired approach (bottom). PMHS = polymethylhydrosiloxane, $FePcF_{16}$ = hexadecafluorinated iron-phthalocyanine, dbm = dibenzoylmethanato.

Interestingly, some contributions dealing with the use of heme-containing cytochromes P-450 for oxidation chemistry reported the trace formation of carbonyl-containing by-products besides the more common and expected hydroxylated products.[11] The promiscuous activity of these enzymes inspired us to study a series of iron(III)-porphyrin complexes containing peripheral carboxylic acid groups, similar to the enzymatic heme active site,[12] as catalysts for Wacker-type reactions (**Figure 1**, bottom). We found that the iron(III) complex **Fe-1** containing the carboxylic acid functionalities located in *para* position of the *meso* phenyl groups[13] behave as a highly active catalyst for the Markovnikov-selective production of ketones from olefins in the presence of hydrosilanes as reagents and an oxygen source (air or dioxygen) with up to *c.a* 200,000 TONs (**Figure 1**, bottom). Moreover, kinetic studies and unexpected identification of by-products for some types of unbiased olefins revealed the complexity of the catalysis with multiple catalytic cycles being operative to some extent. In addition, we herein provide for the first time spectroscopic evidences for the formation of the so far elusive iron-hydride species, which has been postulated as key intermediate previously.[10]

7.2. Results and discussion.

7.2.1 Initial catalytic assessment.

Firstly, the oxidation of 4-*tert*-butylstyrene (**1a**) was evaluated as a model reaction under a set of reaction conditions similar to those reported by Han and Knölker,[10] that is, in the presence of Et_3SiH and an oxidating atmosphere in ethanol solvent (**Table 1**).[14] By using the iron(III)-porphyrin complex **Fe-1** in 7.5 mol% catalyst loading under O_2 atmosphere, full conversion of starting material was reached after 18 hours with 98% selectivity towards the formation of the ketone product **2a** resulting from Markovnikov selectivity (**Table 1**, entry 1). The remaining 2% corresponded to the alcohol by-product **3a** and no aldehyde was detected. The influence of the ligand is remarkable for this type of reaction since bearing the carboxylic acid group in *meta* or *ortho* position of the *meso*-substituted phenyl groups decreased the conversion to 90% and 29%, respectively, while keeping similar levels of alcohol by-products.[14] When using the carboxylic ester version of **Fe-1**, that is replacing all four CO_2H groups by CO_2Me groups, no activity was encountered (**Table S1** in the Experimental section).[14]

Importantly, we noted that the water content in the ethanol solvent has a major impact on the outcome of the catalysis (**Table S2** in the Experimental section).[14] In the range from 0 to 10% volume content, we identified 4% as the suitable amount of water, which corresponds to the commercially supplied ethanol. Higher content of water increased the amount of alcohol by-product (**Table 1**, entry 2-3), whereas lower amounts affected the overall conversion (**Table 1**, entries 4-5). Other solvents were not successful (**Table S3** in the Experimental section).[14] As such, the influence of water has a clear effect on the formation of alcohol by-product as well as on the solubility of the iron catalyst in the reaction media. Interestingly, it was possible to reduce the loading of both the iron catalyst to 2.5 mol% and the hydrosilane reagent to 2 equivalents while keeping an excellent reactivity and selectivity (**Table 1**, entry 6). Decreasing even lower the catalyst loading to 1.5 mol% led to a modest 73% conversion (**Table 1**, entry 7). The catalysis was similarly efficient when switching O_2 by air (**Table 1**, entries 8-9) and a kinetic experiment revealed a direct correlation between product formed and substrate consumed (**Figures S1-S2** in the Experimental section).[14] For comparison purposes, a reaction was carried out by replacing **Fe-1** by **FeClTPP** (TPP = tetraphenylporphyrin) (**Table 1**, entry 10) and by a combination of **FeClTPP** and benzoic acid (**Table 1**, entry 11). In both cases, a very poor reactivity was found and the starting material **1a** was almost unconsumed, thus highlighting the relevance of covalently-linking the carboxylic acid groups to the iron-porphyrin backbone in **Fe-1**. To verify whether the reaction involved formation of transient radical species as known for similar iron catalysts,[10] we performed a catalytic reaction in the presence of TEMPO [TEMPO = (2,2,6,6-tetramethylpiperidin-1-yl)oxyl] as a radical trapping agent (**Table 1**, entry 12). In this case, the reactivity was suppressed, thereby supporting the formation of radicals in the catalytic cycle.

Table 1. Evaluation of the reaction conditions for the **Fe-1**-catalyzed oxidation of 4-*tert*-butylstyrene.[a]

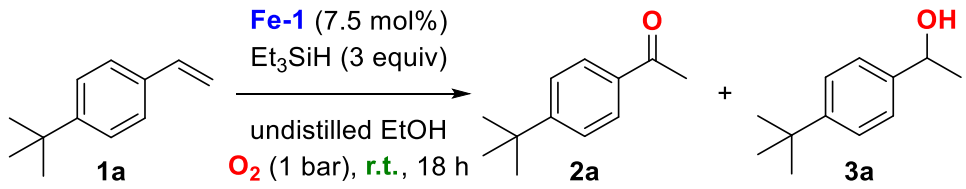

Entry	Deviation from above reaction conditions	Conv. (%)[b]	Yield **2a** (%)[b]	Yield **3a** (%)[b]
1[c]	none	>99	98	2
2	10% water content	>99	92	8
3	6% water content	>99	91	9
4	2% water content	86	82	4
5	0.2% water content	60	57	3
6[d]	**Fe-1** (2.5 mol%), Et_3SiH (2 equiv)	>99	98	2
7[d]	**Fe-1** (1.5 mol%), Et_3SiH (2 equiv)	73	64	9
8[d]	as entry 6 and air instead of O_2	95	90	5
9	as entry 8 and 48 hours	>99	93	7
10[e]	**FeClTPP** instead of Fe-1	<5	<5	n.d.
11	as entry 10 with $PhCO_2H$ (20 mol%)	<10	<10	n.d.
12	with TEMPO (1 equiv)	0	0	0
13	with K_2CO_3 or NEt_3 (30 mol%)	0	0	0

[a] Reaction conditions: **1a** (0.325 mmol), Et_3SiH (0.975 mmol), **Fe-1** (7.5 mol%), undistilled EtOH (3 mL), O_2 (1 bar, balloon), r.t., 18 hours. [b] Conversion and yields determined by GC and GC-MS using dodecane as internal standard. [c] Water content in commercial EtOH is 4% in volume. [d] 24 hours instead of 18 hours. [e] Reaction conditions: 1a (0.325 mmol), Et_3SiH (0.975 mmol), **FeClTPP** (5 mol%), EtOH (3 mL), air, r.t., 24 hours. **TPP** = tetraphenylporphyrin. n.d. = not determined.

Furthermore, the reaction was found to not proceed in the presence of a inorganic or organic bases such as potassium carbonate (K_2CO_3) or triethylamine (NEt_3) that can deprotonate the carboxylic acid groups from the iron catalyst (**Table 1**, entry 13). Indeed, the presence of a purple precipitate under these reaction conditions additionally indicates, in an indirect way, that the iron-catalyzed Wacker-type reaction occurs under a homogeneous regime in the present case of study. Such observation was taken as an advantage to explore a proof-of-concept temporal control of reactivity by sequential addition of base and acid (**Figure 2**). The catalysis was executed under standard conditions and after one hour, triethylamine (NEt_3) was added to shut down the activity because the iron complex appears as insoluble

tetracarboxylate species. Addition of trifluoroacetic acid (TFA) after two hours enabled to solubilize again the iron catalyst, thereby restoring the activity of the catalyst with the same levels of ketone selectivity. The careful and precise addition of both organic base (30 mol%) and organic acid (50 mol%), respectively, is critical for the observed temporal control of reactivity.[14]

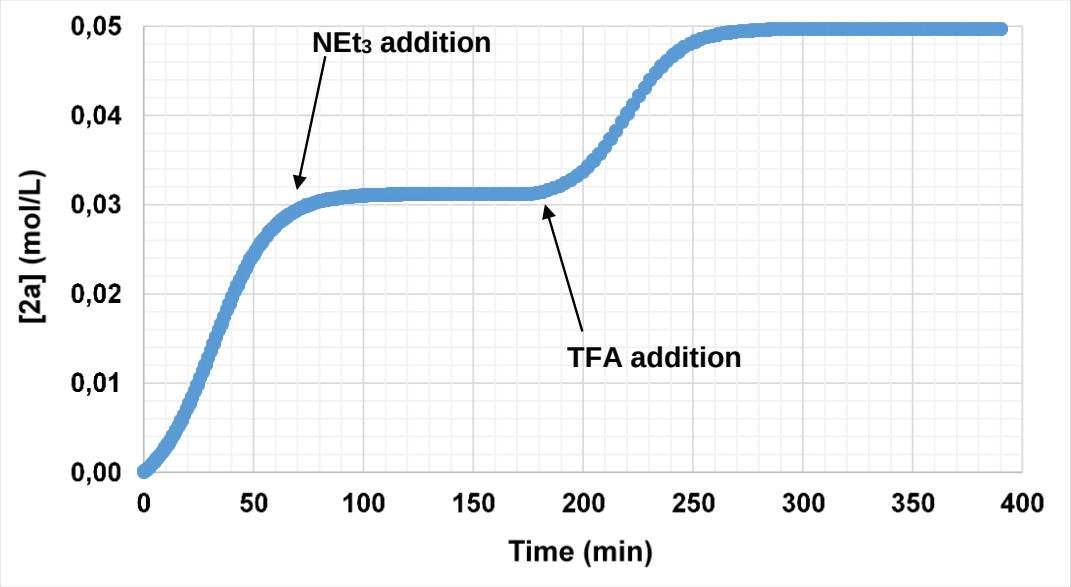

Figure 2. Temporal control of the reactivity in the iron-catalyzed Wacker-type oxidation of olefin **1a** by *in situ* addition of NEt_3 base and TFA acid. Reaction conditions derived from Table 3, entry 1 (*vide infra*).

7.2.2. From catalyst deactivation to catalyst outperformance.

Unexpectedly, we realized that samples of **Fe-1** that were stored under air atmosphere were inactive in catalysis when applying the optimal reaction conditions (**Table 1**, entries 1, 6, 8 and 9) after some time. Indeed, HRMS (MALDI) studies unambiguously revealed the presence of a μ-oxo-bridged diiron species **Fe-2** (*m/z* for $C_{96}H_{56}N_8O_{17}{}^{56}Fe_2$ 1704.263 with 12 ppm error measurement) derived from **Fe-1** that was formed upon prolonged standing under ambient air (**Scheme 1** and **Figure S3** in the exprimental section).[14] The formation of similar dimeric species from H_2O and/or O_2 with iron-porphyrins is well-known.[15,16] It is worthy to note at this stage, that Knölker and co-workers did identify μ-oxo-bridged diiron species with phthalocyanine ligand around iron as active and selective catalysts for Markvonikov-selective oxidation of olefins in the presence of Et_3SiH as hydrogen source.[10c,d] In stark contrast, **Fe-1** does form thermodynamically stable dimeric species that cannot be cleaved by Et_3SiH, strongly suggesting that dimers are not involved in the catalytic cycle for the oxidation of olefins into ketones using the bio-inspired **Fe-1** catalyst. In fact, the formation of dimeric species might be considered as an off cycle intermediate for the current case of study.

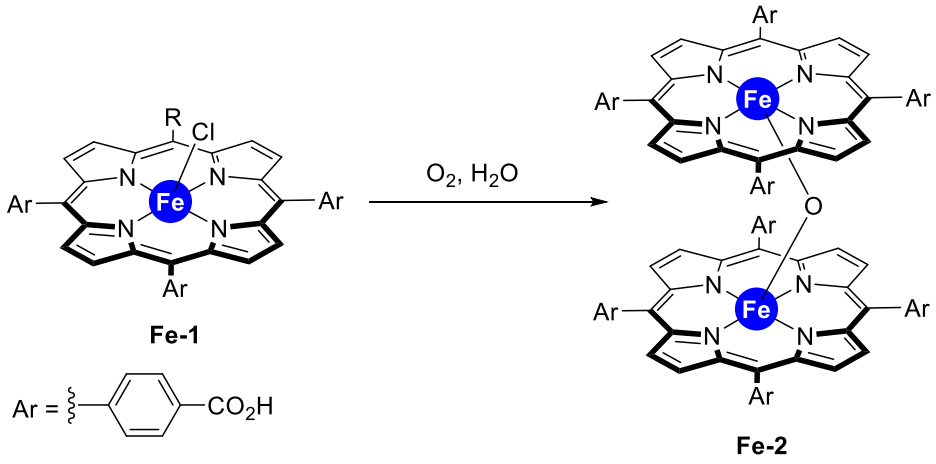

Scheme 1. Formation of μ-oxo-bridged diiron species **Fe-2** from **Fe-1** upon prolonged standing under ambient conditions.

In order to avoid undesired catalyst inhibition pathways *via* formation of μ-oxo-bridged dimeric species, we evaluated the influence of the nature of the hydrosilane reagent in the catalytic outcome when using **Fe-2** as a precatalyst under air atmosphere (**Table 2**). As above stated, the oxidation reaction using Et_3SiH with the dimer **Fe-2** led to negligible conversion of substrate **1a** and formation of traces of ketone **2a** (**Table 2**, entry 1). Similar poor results were found by employing Ph_3SiH and PMHS (**Table 2**, entires 2-3). However, the reactivity and selectivity was fully recovered when using Ph_2SiH_2 or $PhSiH_3$ as reagents, respectively (**Table 2**, entries 4-5). Interestingly, the reactions were shortened to 5 hours whereas alcohols by-products raised to 8-9%, values that compare well with state-of-the-art Knölker's systems.[10e] In order to better understand this unexpected catalyst deactivation *via* dimer formation, we studied the feasibility of *in situ* catalyst activation starting from **Fe-2** as the catalyst in the presence of unreactive Et_3SiH (**Table 2**, entry 1) provided that catalytic quantities of $PhSiH_3$ are present to cleave the dimer (**Table 2**, entry 6-7). In fact, under unreactive conditions, the addition of 10 mol% of $PhSiH_3$ led 43% conversion of olefin **1a** into ketone **2a** in a selective manner (**Table 2**, entry 6). As expected, raising the $PhSiH_3$ loading to 20 mol% in the presence of 2 equivalents of Et_3SiH afforded the ketone product in 98% yield (**Table 2**, entry 7), thereby demonstrating that the catalysis at play with Et_3SiH does not involve formation of dimeric iron species. Other additives were evaluated in order to cleave the dimeric iron structure **Fe-2** into the catalytically active monomeric **Fe-1**. For instance, HCl as additive proved successful for this purpose although leading to a modest yield of *ca.* 50% of ketone **2a** (**Table 2**, entries 8-9). This finding indicate that fine-tuning reaction conditions may lead to the formation of the active **Fe-1** species with a rather cheap and affordable Brønsted acid in catalytic amounts.

Table 2. Optimization of the reaction conditions for the **Fe-2**-catalyzed oxidation of 4-*tert*-butylstyrene.[a]

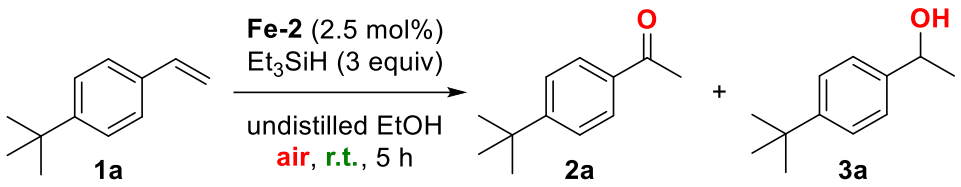

Entry	Deviation from above reaction conditions	Conv. (%)[b]	Yield **2a** (%)[b]	Yield **3a** (%)[b]
1[c]	none	<5	<5	n.d.
2	with Ph_3SiH instead of Et_3SiH	<5	<5	n.d.
3	with PMHS instead of Et_3SiH	<5	<5	n.d.
4	with Ph_2SiH_2 instead of Et_3SiH	>99	91	9
5	with $PhSiH_3$ instead of Et_3SiH	>99	92	8
6	with $PhSiH_3$ (10 mol%)	43	43	n.d.
7	with $PhSiH_3$ (20 mol%)	>99	98	2
8	with HCl (10 mol%)	60	48	12
9	with HCl (20 mol%)	62	49	13

[a] Reaction conditions: **1a** (0.325 mmol), Et_3SiH (0.975 mmol), **Fe-2** (2.5 mol%), EtOH (3 mL), air, r.t., 5 hours. [b] Conversion and yields determined by GC and GC-MS using dodecane as internal standard. [c] Water content in commercial EtOH is 4% in volume. n.d. = not determined.

Having established the unique activation mode of the iron pre-catalyst **Fe-2** in the presence of $PhSiH_3$ as the reductant (**Table 2**, entry 5), we further studied the potential of the present catalyst regarding catalyst stability, reactivity, selectivity and recyclability. In fact, by reducing the catalyst loading to 1.25 mol%, still full conversion of **1a** and 92% yield of ketone **2a** was obtained (**Table 3**, entries 1-2). However, decreasing the number of equivalents of $PhSiH_3$ by half led to 10% remaining of starting material while keeping an excellent Markovnikov selectivity (**Table 3**, entry 3). As it was observed for the pre-catalyst **Fe-1** (**Table 1**, entries 1-5), the amount of water also influenced the catalytic outcome observed when employing the pre-catalyst **Fe-2**. For instance, by reducing the water content in the media from 4% to 0.2% in volume, the conversion of **1a** and yield of ketone **2a** dropped by half after 12 hours (**Table 3**, entry 4). Additional kinetic experiments revealed that the substrate (**1a**) consumption is directly related to the formation of the Markovnikov ketone product **2a** at different catalyst concentrations (see **Figures S4-S8** in the Experimental section).[14] The first order in catalyst strongly supports formation of monomeric specie throughout the whole catalytic cycle. As observed by Knolker for other iron-catalyzed Wacker-type oxidation of olefins,[10c-10e] alcohol **3a** is not here an intermediate

because using **3a** as the substrate led to no ketone formation with full recovery of the starting material (**Table 3**, entry 5). The temperature range was assessed and the reaction was found operative even at challenging 0 °C with 40% yield of ketone **2a** after 5 hours (**Table 3**, entry 6). Nevertheless, to the best of knowledge, this is the first example in which a transition metal catalyzed Wacker-type oxidation of olefins is reported to work at such low temperature. On the other hand, the catalysis performed at 50 °C was found detrimental for the catalysis with 70% yield of **2a** (**Table 3**, entry 7) although a more than six-fold rate acceleration was reached when compared to the reaction at 0 °C (see **Figure S17** and **Table S9** in the Experimental section).[14,17] Kinetic studies following on time both substrate and silane consumption as well as ketone formation established that the reaction at 50 °C reached a plateau at one hour with complete silane consumption (see **Figures S10**-**S12** in the Experimental section).[14] This unexpected silane degradation was catalyzed by the iron catalyst since no silence consumption was observed in the absence of **Fe-2** or **Fe-1** under catalytically relevant conditions.[14] Interestingly, we disclosed an intriguing dilution effect since the catalysis was faster (3 hours) when performed in a two times more diluted media (**Table 3**, entry 8). Under this reaction condition, decreasing the catalyst loading to 1.25 mol% did not influence the selectivity although the reaction required 8 hours for completion (**Table 3**, entry 9). Additional control experiments highlight the need of all reagents for the success of the transformation (**Table 3**, entries 10-11) and that the O_2 from air is the oxidant for this transformation (**Table 3**, entry 12).

Table 3. Evaluation of the reaction conditions for the **Fe-2**-catalyzed oxidation of *tert*-butylstyrene in the presence of $PhSiH_3$.[a]

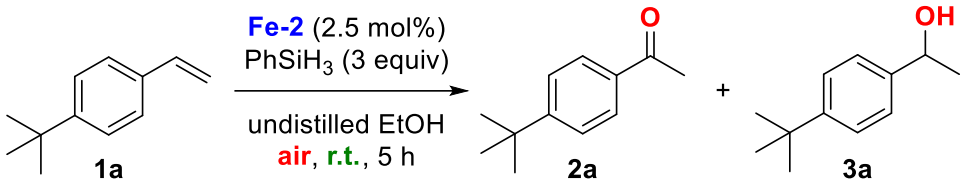

Entry	Deviation from above reaction conditions	Conv. (%)[b]	Yield **2a** (%)[b]	Yield **3a** (%)[b]
1[c]	none	<99	92	8
2[d]	with **Fe-2** (1.25 mol%)	<99	92	8
3[e]	as entry 2, with Et_3SiH (1.5 equiv)	90	85	5
4[e]	with dry EtOH (0.2% water content)	51	47	4
5	**3a** as substrate instead of **1a**	0	0	0
6	0 °C instead of r.t.	40	40	n.d.
7	50 °C instead of r.t.	75	70	5
8	with undistilled EtOH (6 mL), 3 h	<99	92	8
9[d]	as entry 8 with **Fe-2** (1.25 mol%)	<99	92	8
10	absence of $PhSiH_3$	0	0	0
11	absence of **Fe-2**	0	0	0
12	Argon instead of air	0	0	0

[a] Reaction conditions: **1a** (0.325 mmol), Et_3SiH (0.975 mmol), **Fe-2** (2.5 mol%), EtOH (3 mL), air, r.t., 5 hours. [b] Conversion and yields determined by GC and GC-MS using dodecane as internal standard. [c] Water content in commercial EtOH is 4% in volume. [d] 8 hours of reaction time. [e] 12 hours of reaction time. n.d. = not determined.

Moreover, the **Fe-2** pre-catalyst is a platform compatible to study temporal control of catalysis by *in situ* switching the atmosphere of the reaction as a chemical stimuli (**Figure 3**).

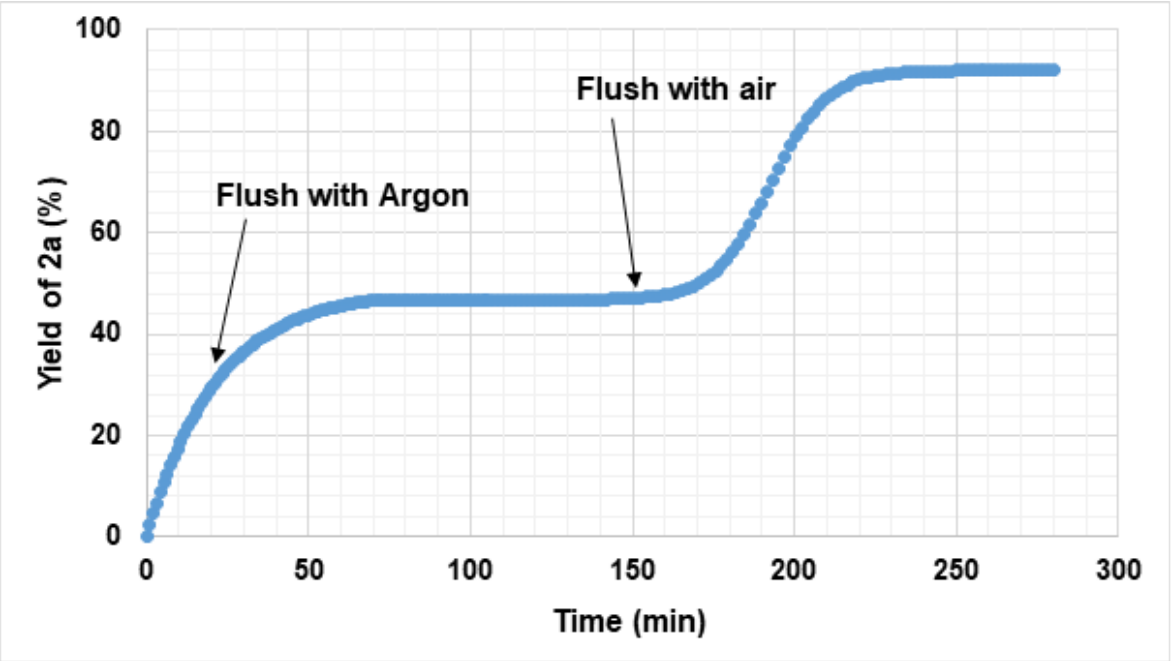

Figure 3. Temporal control of the reactivity in the iron-catalyzed Wacker-type oxidation of olefin **1a** by switching the atmosphere from air to argon under two cycles. Reaction conditions derived from **Table 3**, entry 1.

In addition, the robustness of such catalysis was exemplified by using as low as 1 ppm catalyst loading of **Fe-2** (**Scheme 2**). At room temperature, after 48 hours a TON value of 32,500 was reached and it increased to 190,000 when the reaction was carried out at 50 ºC. Because of the carboxylic acid functional groups present in the iron catalyst, we tested, as a proof of concept, the possibility to recover the iron catalyst by trivial acid/base treatment and precipitation (see **Table S13** in the Experimental section).[14] Indeed, it was possible to perform up to 2 runs with the recycled iron catalyst while keeping similar levels of reactivity (full conversion of olefin **1a** in less than 5 hours) and selectivity (>92% yield of ketone **2a**).[14]

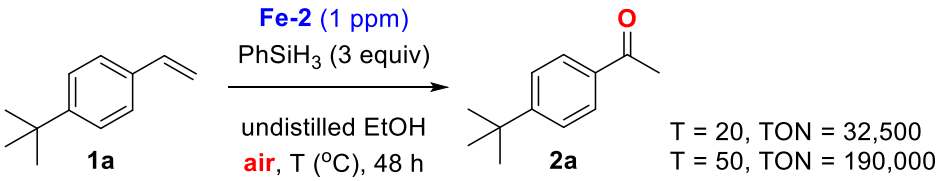

Scheme 2. Search for the highest TON in the iron-catalyzed Wacker-type oxidation of 4-*tert*-butylstyrene.

7.2.3 Circumventing unexpected side-reactions and substrate scope evaluation.

The formation of alcohol side-product **3a** for the oxidation of 4-*tert*-butylstyrene (**1a**) was reduced to a residual 2% (**Table 1**, entry 1 and 6; and **Table 2**, entry 7), which is remarkable as regards of literature precedents.[10] Intriguingly, we noted that the order of addition of reagents plays a key role in the product selectivity as illustrated for the case of the olefin **1b** (**Scheme 3**). Besides the formation of the desired ketone (**2b**) and alcohol (**3b**) side-product, compounds such as **4b** resulting from a

reductive homo-coupling were formed in significant quantities (up to 55%) when the olefin substrate was introduced as the last component in the reaction mixture (**Scheme 3**, top). In this case, the formation of **4b** may follow a mechanism involving radical hydrogen atom transfer[18] as discussed by the breakthrough contributions by Baran on iron-catalyzed olefin functionalization,[19a-d] and by others later.[19e-k] Importantly, by adding the silane $PhSiH_3$ reagent as the last component to the reaction mixture, the side-product **4b** was reduced to trace amounts with the desired ketone formed in 71% yield (**Scheme 3**, bottom), which is notable considering the steric and electronics effects that make substrate **1b** prone to stabilize different benzylic radical intermediates (*vide infra*).[10e]

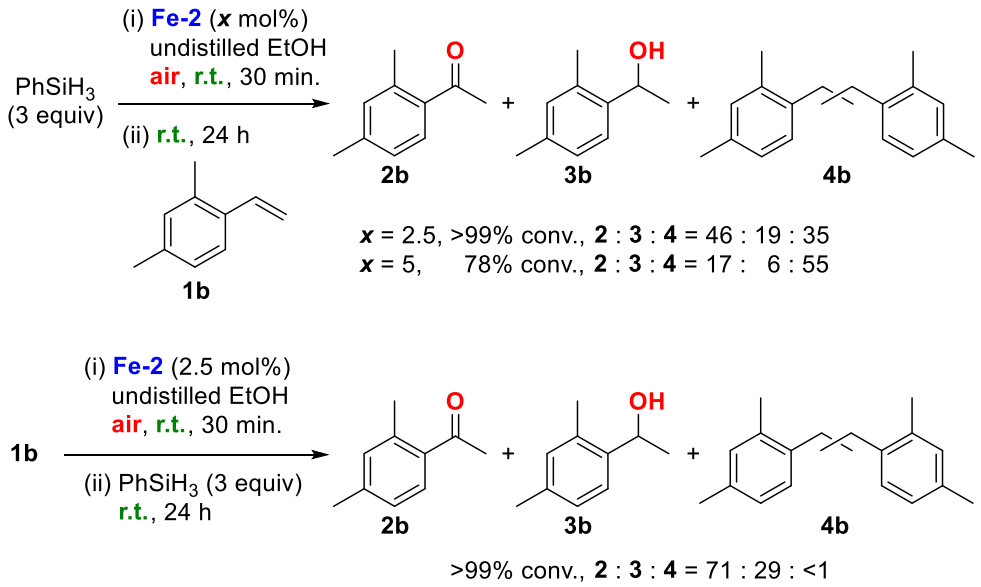

Scheme 3. Experiments highlighting the impact of the order of addition of the reagents in the product selectivity of the **Fe-2**-catalyzed Wacker-type oxidation of 2,4-dimethylstyrene. Product **4b** exists as a mixture of branched isomers.

The variation of product selectivity depending on the order of addition of reagents was a general trend found for most of the aryl olefins tested in this study (see **Figure S18** in the Experimental section).[14]

After a detailed analysis for the search of the optimal reaction conditions, we evaluated the olefin scope of the **Fe-2**-catalyzed Wacker-type oxidation. In the case of aryl olefins as the substrates, the reactions were completed in less than 5 hours and the tolerance of the catalytic system made possible the use of different functional groups including aryl, alkyl, halides such as fluoride, chloride and bromide, ethers, and carboxylic acids (**2c-h**).[20] In all cases, the alcohol side-products did not reach more than 5%, which is acknowledgeable as regards of literature precedents.[10] Importantly, the reaction was compatible with ester groups affording exclusively (99% selectivity) the ketone product **2i** with no detectable formation of alcohol side-product this time. The catalysis was also compatible with pyridine heterocycles affording the corresponding ketone product **2j** in 91% yield. These observations

outperform current state-of-the-art iron catalysts in terms of activity and selectivity. For instance, it should be noted that the challenging heterocyclic-containing product **2j** was prepared elsewhere in 85% yield under harsher reaction conditions of temperature (80 °C) and longer time (12 hours).[10a]

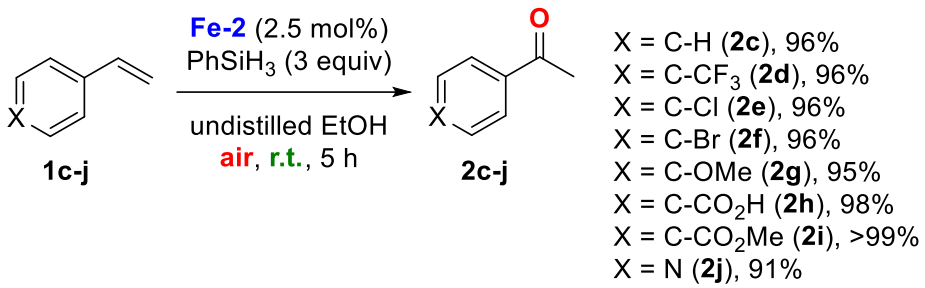

Scheme 4. Evaluation of (hetero)aryl olefins in the **Fe-2**-catalyzed Wacker-type oxidation. Reaction conditions: (i) **1** (0.325 mmol), **Fe-2** (2.5 mol%), EtOH (3 mL), air, r.t., 30 min (ii) $PhSiH_3$ (0.975 mmol), air, r.t. 4.5 hours. GC yields reported after performing at least 3 experiments for each substrate.

Next, we enlarged the substrate scope to purely aliphatic olefins (**Scheme 5**), which are much less reactive that the aryl ones.[20] For instance, terminal as well as internal olefins are typically reactive using a high iron catalyst loading (20 mol%),[10a] if not, the yields did not exceed 60%.[10e] In the present case, using **Fe-2** at 2.5 mol% catalyst loading under ambient conditions of pressure and temperature, 1-octene and *cis*-cyclooctene substrates afforded the ketone products **2k** and **2l** resulting from Markovnikov selectivity in an unprecedented 82% and 85% yield, respectively, whereas the alcohol side-products formed in 12-13% range (**3k**-**3l**). Unexpectedly, side-products resulting from hydrogenation of the starting material formed in 3-5% (**5k**-**5l**). Such findings were also observed when using bio-sourced methyl oleate and the highly sterically congested norbornene as the substrates, in which, besides the major formation of ketone product (77% of **2m** and 67% of **2n**), the hydrogenated side-products raised to 10% (**5m** and **5n**). As such, careful analysis of the reaction mixtures revealed that, for the case of aliphatic olefins, iron-catalyzed hydrogenation pathways compete with alcohol formation as the side-products. In the case of the sterically constrained norbornene, epoxyde side-product **6n** formed in 20% yield.[21]

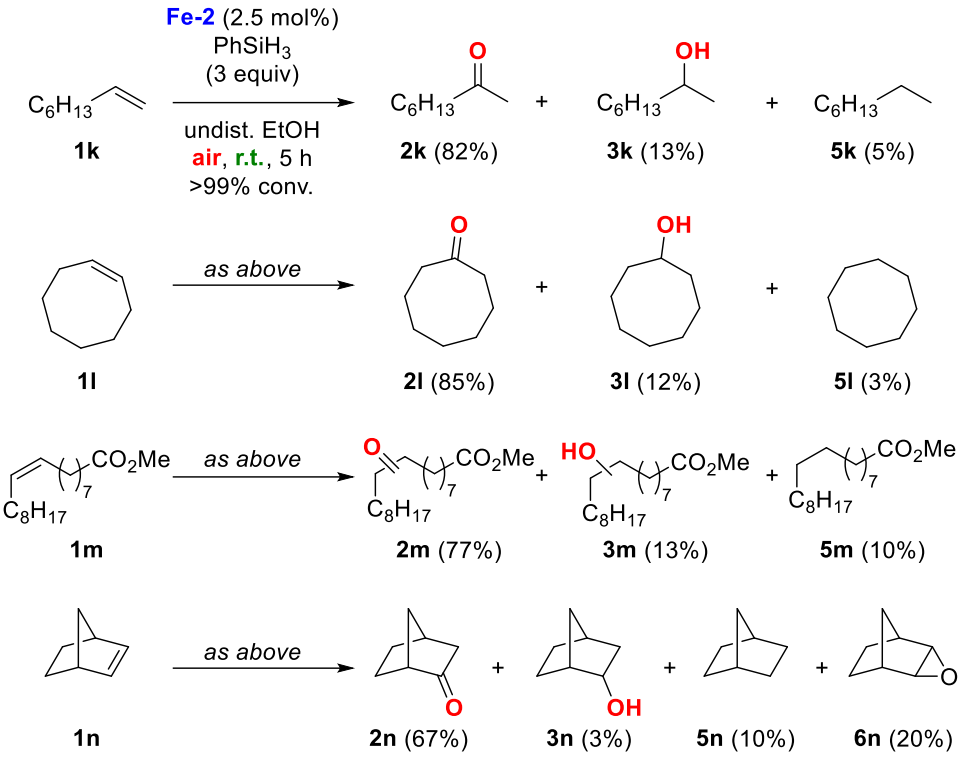

Scheme 5. Evaluation of aliphatic olefins in the **Fe-2**-catalyzed Wacker-type oxidation. Reaction conditions: (i) **1** (0.325 mmol), **Fe-2** (2.5 mol%), EtOH (3 mL), air, r.t., 30 min (ii) $PhSiH_3$ (0.975 mmol), air, r.t. 4.5 hours. GC yields reported after performing at least 3 experiments for each substrate.

As a follow-up series of substrates, we evaluated the reaction outcome for allyl-containing derivatives (**1o**-**1r**, **Table 4**),[20] which are known to undergo predominantly oxidative C=C bond cleavage to aldehydes under iron catalysis (**7**),[10a,22] or isomerization/oxidation tandem sequence under nickel catalysis.[23] For allyl-benzene derivatives **1o** and **1p**, the current **Fe-2**-catalyzed methodology provides the major ketone products **2o**-**2p** resulting from a formal Markovnikov selectivity in an unprecedented range of 44-52% yield (**Table 4**, entries 1-2). Besides the expected formation of alcohol side-products (**3o**-**3p**), the benzylic alcohols **8o**-**8p** resulting from the hydrogenation of aldehydes (**7o**-**7p**) were also detected (**Table 4**, entries 1-2), emphasizing the relevance of hydrogenation side-reactions for this particular type of substrates under iron catalysis. In the case of the trifluoromethoxy-substituted derivative (**1q**), the catalysis was less selective with the ketone **2q** formed in 38% yield (**Table 4**, entry 3). For this substrate, hydrogenation of the olefin double bond was observed in a non-negligible 14% yield. On the other hand, a more chemically-robust allylcyclohexane (**1r**) did not undergo any C=C bond cleavage and the ketone product **2r** was obtained in a handful 70% yield with 29% of alcohol **3r** and 1% of hydrogenated **5r** as side-products (**Table 4**, entry 4).

Table 4. Evaluation of allyl-containing derivatives in the **Fe-2**-catalyzed Wacker-type oxidation.[a,b]

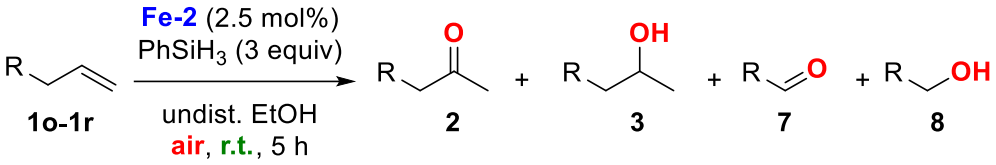

1	R	Conv. (%)[c]	Yield **2** (%)[c]	Yield **3** (%)[c]	Yield **7** (%)[c]	Yield **8** (%)[c]
1o	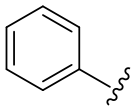	>99	**52**	2	11	25
1p	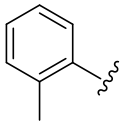	>99	**44**	10	12	27
1q	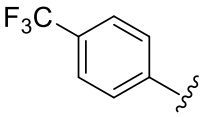	>99[d]	**38**	18	0	28
1r	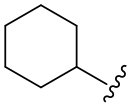	>99[e]	**70**	29	0	0

[a] Reaction conditions: (i) **1** (0.325 mmol), **Fe-2** (2.5 mol%), EtOH (3 mL), air, r.t., 30 min (ii) $PhSiH_3$ (0.975 mmol), air, r.t. 4.5 hours. [b] Water content in commercial EtOH is 4% in volume. [c] Conversion and yields determined by GC and GC-MS using dodecane as internal standard after performing at least 3 experiments for each substrate. [d] 14% of product resulting from olefin hydrogenation of **1q** was detected. [e] 1% of product resulting from olefin hydrogenation of **1r** was detected.

Finally, inspired by recent discoveries regarding the oxidation chemistry of indole heterocycles by heme-enzymes[24] and in view to replace the highly acidic and oxidizing reagents (HCl, hypervalent halides, peroxy acids, oxone) typically employed with state-of-the-art methodologies[25] by more sustainable and benign protocols, we applied our iron-catalyzed methodology to indole **1s** (**Scheme 6**). Under the developed reaction conditions, full conversion was observed in only 30 minutes and the 2-oxindole product **2s** was isolated in a non-optimized 71% yield. The reaction required H_2O_2 as the oxidant and the absence of silane, thereby suggesting that reaction mechanism taking place here is different than that operating for aromatic and aliphatic olefins. To the best of our knowledge, this is the first use of an abiological catalyst enabling formation of 2-oxindole from indole. Note that this type of heterocycles are privileged motifs in chemicals that display important pharmacological properties.[26]

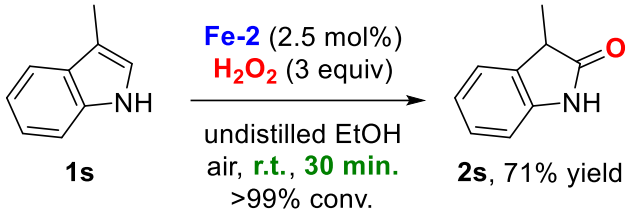

Scheme 6. Fe-2-catalyzed Wacker-type oxidation of an indole derivative. Reaction conditions: (i) **1s** (0.325 mmol), **Fe-2** (2.5 mol%), $PhSiH_3$ (0.975 mmol), EtOH (3 mL), air, r.t., 30 min.

7.2.4. Mechanistic insights.

All the above mentioned experiments together with previous contributions point out to the eventual formation of an iron-hydride intermediate as key species that drives the reaction either to ketone formation or to the other side-products depending on the reaction conditions as well as the nature of the olefin substrate.[10,19] To the best of our knowledge, no iron-hydride species have been spectroscopically characterized in the context of Wacker-type oxidation of olefins nor iron-catalyzed reductive olefin functionalization.[10,19] As such, we pursued the synthesis of such elusive iron-hydride species.[27] In fact, by simple mixing a combination of **Fe-1** and **Fe-2** with $PhSiH_3$ in DMSO-d_6 (DMSO = dimethylsulfoxide) under air atmosphere, a single species **Fe-H** was formed according to ^{1}H NMR spectroscopy studies (**Scheme 7**).

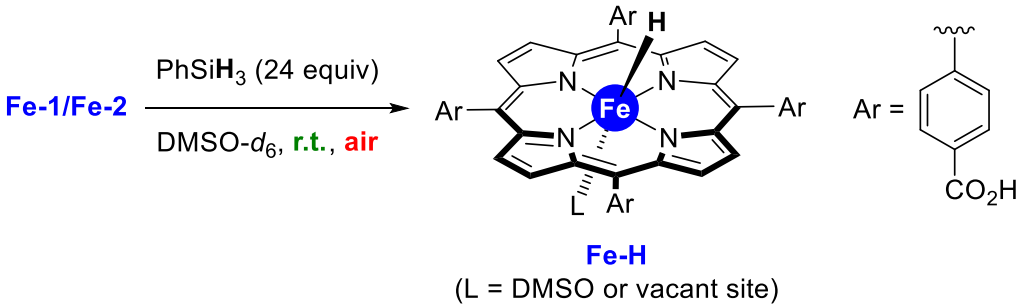

Scheme 7. Synthesis of **Fe-H** species starting from **Fe-1** and **Fe-2** in the presence of $PhSiH_3$ as hydride source.

A broad signal at δ = -20.1 ppm was unambiguously evidenced indicating the formation of iron-hydride species (**Figure 4**).[27] The integrity of the overall ligand backbone was confirmed as well (see **Figure S21** in the Experimental section).[14] For instance, the proton signals from the carboxylic acid groups resonate at 11.7 ppm as similarly observed in the **Fe-1** complex (**Figure 4**).[13] In the absence of iron species, the hydride signal was not observed.[28] In contrast to previous reports, the formation of iron-hydride species with this bio-inspired ligand is facile and does not require the presence of EtOH as it was postulated.[10] Unfortunately attempts to perform HRMS and obtaining single crystals suitable for X-ray diffraction studies failed so far. Consequently, the eventual coordination of DMSO to stabilize the iron-hydride species **Fe-H** remains to be addressed.

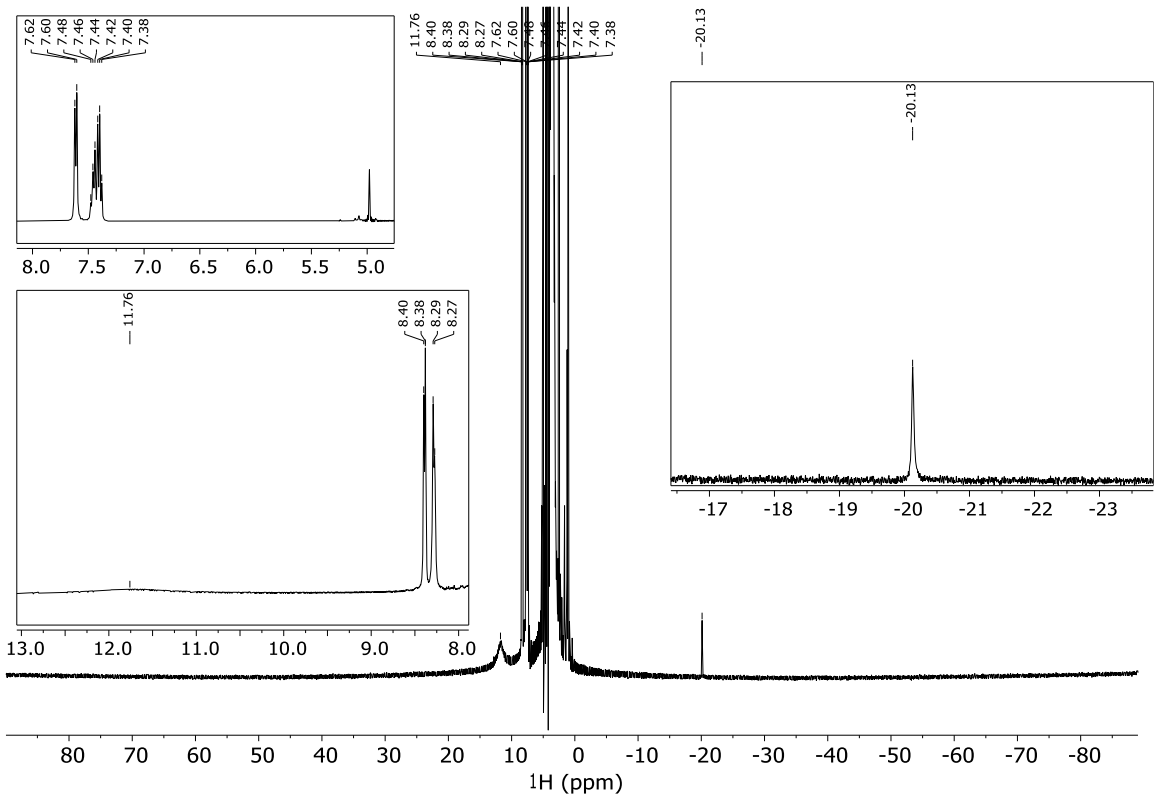

Figure 4. ^{1}H NMR (DMSO-d_6, 298 K) spectrum of the **Fe-H** species. Zoom areas indicating the presence of the phenyl groups (left, top, framed), of the carboxylic acid and pyrrole groups (left, bottom, framed) and of a hydride signal (right, framed).

Considering the experimentally demonstrated formation of iron-hydride species with a ligand comprising a bio-inspired scaffold as well as previous observations discussed in detail above and precedents in the literature,[10] we propose a general mechanistic overview for this Wacker-type transformation in which monomeric iron species are present throughout the whole catalytic cycle with dimeric iron formation as an off cycle pathway (**Scheme 8**). The main catalytic cycle that operates when adding the silane as the last reagent is the one responsible for forming the ketone product **2** starting from olefin starting material **1** (light blue color, **Scheme 8**). On the other hand, adding the olefin starting material as the last reagent favors the reductive homo-coupling pathway towards products **4** in which both silane and ethanol are source of hydrogen atoms (light red color, **Scheme 8**), which is analogous to the iron-catalyzed reductive olefin functionalization chemistry.[19] In addition, taking into account the role of iron-hydride species in the reduction of both ketones and olefins,[6,27,29] and the slight increase of alcohols and alkanes side-products for aliphatic olefin substrates, we propose that the **Fe-H** intermediate is the active species for the formation of alcohol side-products **3** (light grey color, **Scheme 8**) as well as for the hydrogenation of the olefin to the alkane side-products **5** (light green color, **Scheme 8**). Note that the role of silane as hydride source has been elegantly demonstrated by Knölker in thorough mechanistic studies of iron-catalyzed Wacker-type oxidation of olefins.[10c-e]

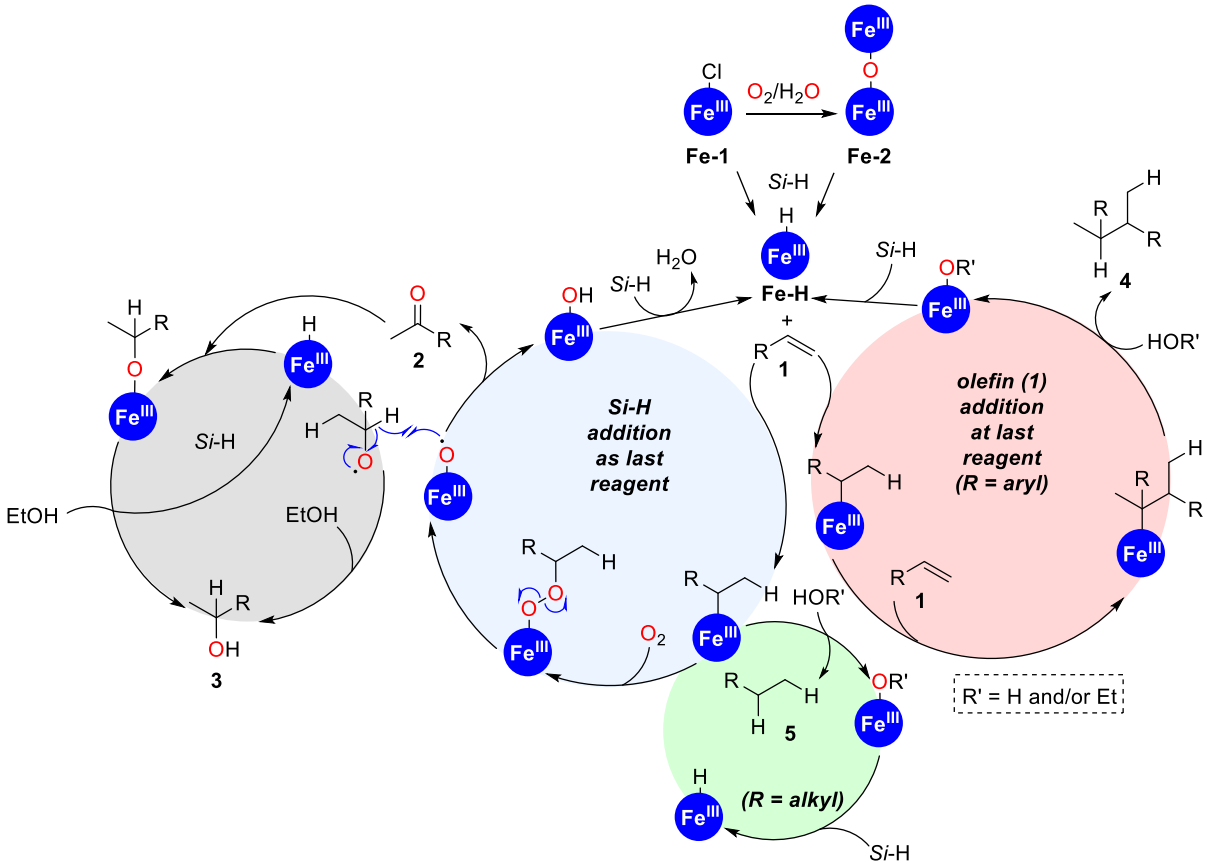

Scheme 8. Postulated, simplified reaction mechanism for the iron-catalyzed Wacker-type oxidation of olefins **1** into **2** (light blue color circle) and mechanistic proposal for the formation of side-products **3** (light grey color circle**)**, **4** (light red color circle) and **5** (light red color circle). The mechanistic blue half-arrows (one-electron move) apply only to the iron-catalyzed Wacker-type oxidation of olefins **1** into **2** (light blue color circle). The heme-like porphyrin ligand around the iron center is not depicted for the sake of clarity. *Si*-H stands for any silane.

7.2.5. Conclusion.

In summary, we have introduced an iron(III) catalyst that is highly active (*ca.* 200,000 TONs) and highly selective (up to 99% ketone selectivity for linear olefins) for the Wacker-type oxidation of olefins. The catalyst, which is based on the promiscuous activity encountered in several cytochromes from the P450 family, is built around a trivial porphyrin backbone containing carboxylic acid groups in the periphery. Whereas the remote carboxylic acid groups belonging to heme-containing porphyrins are relevant for several biological purposes,[30] the role of these functional groups in the present bio-inspired iron catalyst is to facilitate the stabilization of a key iron-hydride intermediate species (**Fe-H**, **Scheme 7**) in the catalytic cycle and increasing the solubility of the catalytic system in ethanol media. In-depth substrate scope evaluation and mechanistic studies indicate the paramount importance of precisely fine-tuning the reaction conditions to control catalyst reactivity for selective product formation. For instance, styrene derivatives lead to acetophenone derivatives (91-99%) when silanes were added as last reagents to the reaction mixture. If not, side-products resulting from ketone hydrogenation (alcohol formation) and unprecedented reductive olefin homo-coupling were significantly obtained. In the case of aliphatic olefins, minor formation of hydrogenated olefins were observed for challenging substrates besides major formation of ketone products (67-85%). Moreover, allyl-containing derivatives that are known to undergo oxidative C=C scission under similar reaction conditions, still afforded in the present case promising yields of ketone products (38-70%). The applicability of this protocol is demonstrated with the selective oxidation of a biologically-relevant indole to 2-oxindole without the requirements to use highly oxidizing agents but just air. In addition, this iron catalyst exhibits temporal control of reactivity by switching the atmosphere or by sequential addition of bases and acids as well as promising recyclability and reusability properties. Overall, the presented contribution points out that the rational design of iron catalysts is of relevance for disclosing highly selective transformations even if multiple catalytic cycles operate simultaneously. We anticipate that the unique iron-based catalyst studied here should found new applications in olefin functionalization [31] and as a building block for incorporation in solid supports or metal-organic frameworks[32] in view to disclose heterogeneous versions of the Wacker-type oxidation of olefins.

7.3. Experimental section.

7.3.1. General methods.

Solvents were purified with an MB SPS-800 purification system. Pyrrole was dried with CaH_2 and distilled prior to use. All solvent used for catalytic experiment were dried with CaH_2 and distillated prior to use. $CDCl_3$ was filtered through alumina and stored under argon over molecular sieves. All the other employed chemicals were purchased from commercial sources and used as received. Unless otherwise specified, reactions were carried out under argon atmosphere by employing standard Schlenk and vacuum-line techniques. ^{1}H and ^{13}C NMR spectra were recorded with a Bruker GPX (400 MHz) spectrometer. ^{1}H NMR spectra were referenced to residual protiated solvent (δ = 7.26 ppm for $CDCl_3$). ^{13}C NMR spectra were referenced to $CDCl_3$ δ = 77.16 ppm). Abbreviations for signal couplings are: br, broad; s, singlet; d, doublet; t, triplet; q, quadruplet; hept, heptuplet; m, multiplet; dd, doublet of doublets; dt, triplet of doublets; td, doublet of triplets; tt, triplet of triplets; tdd, doublet of doublet of triplets. Coupling constants, *J*, were reported in hertz unit (Hz). The reactions were monitored by using a Shimadzu 2014 gas chromatograph equipped with an EquityTM-1 Fused Silica capillary column (30 m x 0.25 mm x 0.25 µm) and an FID detector; conversion and selectivity were determined by using dodecane as internal standard. UV/Vis absorption spectra were recorded with a Specord 205 UV/Vis/NIR spectrophotometer and quartz cuvettes of 1 cm path length. Mass spectroscopy were performed in the laboratories of the Centre Regional de Mesures Physiques de l'Ouest (CRMPO, Université de Rennes 1, Rennes, France).

7.3.2. Synthesis and characterization of iron complexes.

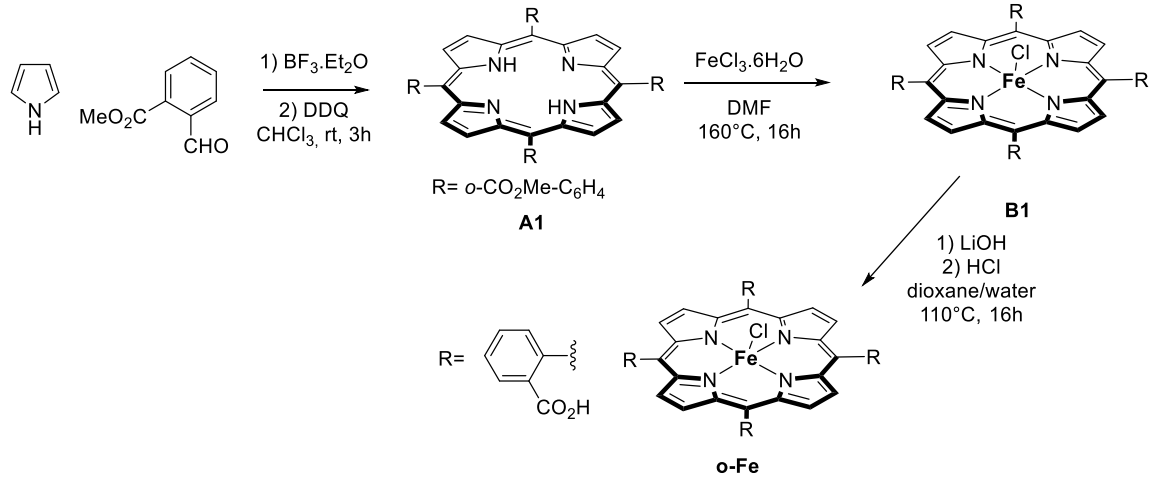

Scheme S1. Synthesis of the iron complex **o-Fe**.

Synthesis and characterization of A1: Distilled pyrrole (0.34 g, 0.35 mL, 5.0 mmol 1 equiv.) and methyl 2-formylbenzoate (0.83 mg, 0.7 mL, 5.0 mmol, 1 equiv.) were added to a pre-dried round bottom flask under argon atmosphere. DCM (500 mL) was added and the reaction mixture was covered with aluminum foil followed by addition of $BF_3{\cdot}Et_2O$ (0.31 mL, 2.5 mmol, 0.5 equiv.). The reaction mixture was stirred for 2.5 hours at room temperature protected from light, then, DDQ (1.13 g, 5.0 mmol, 1 equiv.) was added and the reaction mixture was stirred for another 16 hours. Then, Et_3N was added to quench the reaction and after 5 minutes, the solvent was evaporated under vacuum. The crude mixture was purified by SiO_2 column chromatography (heptane:DCM, 9:1 to 1:9, v/v) affording **A1** as a purple powder. The fractions containing the four atropoisomers were collected and evaporated yielding the product **A1** as purple crystals (0.4 g, 38% yield). ^{1}H NMR (400 MHz, $CDCl_3$): δ = 8.65–7.59 (m, 24H), 2.89 (s, 3H), 2.78 (s, 3H), 2.73 (s, 3H), 2.61 (s, 3H), −2.42 (s, 2H) ppm. The data match those found in the literature.[1]

Synthesis and characterization of B1: **A1** (0.16 g, 0.19 mmol, 1 equiv.), $FeCl_2{\cdot}4H_2O$ (0.47 g, 2.4 mmol, 13 equiv.) and DMF (20 mL) were introduced in a round bottom flask equipped with a stirring bar. The reaction mixture was refluxed for 16 hours at 160 °C, then, the solvent was slowly evaporated at 80 °C under vacuum until all residual DMF was removed from the reaction mixture. Back at room temperature, the crude was washed with HCl (1M) and water until the aqueous phase became colorless, then the solid was dissolved in dichloromethane. The organic layer was dried with $MgSO_4$, filtered and the solvent was evaporated under vacuum yielding the pure product **B1** (0.18 g, 99% yield). ^{1}H NMR (400 MHz, $CDCl_3$): δ = 80.4, 14.4, 13.7, 13.5, 12.4 ppm. λ_{abs}/nm (DMF), ($\varepsilon/10^3$ M^{-1} cm^{-1}): 421 (78.1), 519 (7.25), 577 (6.62). The data match those found in the literature.[1]

Synthesis and characterization of o-Fe: B1 (1.450 g, 1.55 mmol, 1 equiv.), LiOH (3,72 g, 155 mmol, 100 equiv.) and dioxane/water (150 mL, 7/1, v/v) were introduced in a round bottom flask equipped with a stirring bar. The reaction mixture was refluxed for 16 hours at 110 °C, then, the solvent was evaporated and the product was precipitated with HCl (1M) at pH = 1 (followed by pH paper). The solution was filtrated and the solid was washed with HCl (1M), water, heptane and dichloromethane and then dried under vacuum yielding the pure product

o-Fe (1.38 g, 99% yield). ^{1}H NMR (400 MHz, DMSO-d_6): δ = 73.4, 10.1, 9.7, 9.3 ppm. λ_{abs}/nm (DMF), ($\varepsilon/10^3$ M^{-1} cm^{-1}): 426 (17.5), 515 (2.64), 573 (1.42). HRMS (ESI) calcd. for [M–Cl]$^+$ $C_{48}H_{28}N_4O_8{}^{56}Fe$ 844.1251, found 844.1249 (0 ppm). The data match those found in the literature.[1]

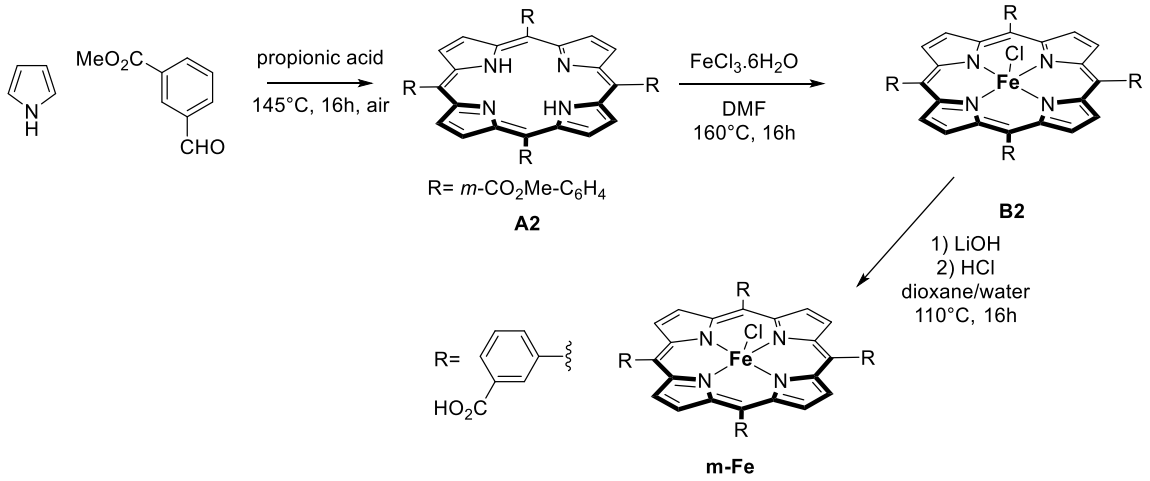

Scheme S2. Synthesis of the iron complex **m-Fe**.

Synthesis and characterization of A2: Distilled pyrrole (2 g, 2.07 mL, 30 mmol, 1 equiv.) and methyl 3-formylbenzoate (5 g, 30 mmol, 1 equiv.) were added to a pre-dried round bottom flask containing propionic acid (150 mL). The reaction mixture was covered with aluminum foil and refluxed for 16 hours at 145 °C. After cooling to room temperature, the resulting purple crystals were filtered and washed with water and then dissolved in dichloromethane. The organic layer was dried with $MgSO_4$, filtered and the solvent was evaporated affording a crude mixture that was purified by SiO_2 column chromatography (heptane:DCM, 9:1 to 1:9, v/v). The filtrate was then evaporated under vacuum yielding the pure product **A2** (1.21 g, 19% yield). ^{1}H NMR (400 MHz, $CDCl_3$): δ = 8.92 (s, 4H), 8.82 (s, 8H), 8.52 (d, J = 8 Hz, 4H), 8.43 (d, J = 8 Hz, 4H), 7.88 (t, J = 7.6 Hz, 4H), 4.02 (s, 12H), −2.77 (s, 2H) ppm. The data match those found in the literature.[1]

Synthesis and characterization of B2: A2 (0.43 g, 0.5 mmol, 1 equiv.), $FeCl_2{\cdot}6H_2O$ (1.24 g, 6.5 mmol, 13 equiv.) and DMF (30 mL) were introduced in a round bottom flask equipped with a stirring bar. The reaction mixture was refluxed for 16 hours at 160 °C, then the solvent was slowly evaporated at 80°C under vacuum until all residual DMF was removed from the reaction mixture. Back at room temperature, the crude was washed with HCl (1M) and water until the aqueous phase became colorless, then the solid was dissolved in dichloromethane. The organic layer was dried with $MgSO_4$, filtered and the solvent was evaporated under vacuum yielding the pure product **B2** (0.42 g, 99% yield). ^{1}H NMR (400 MHz, $CDCl_3$): δ = 80.3, 13.3, 12.2, 8.39, 7.72 ppm. λ_{abs}/nm (DMF), ($\varepsilon/10^3$ M^{-1} cm^{-1}): 424 (92.6), 520 (7.59), 569 (11.2). The data match those found in the literature.[1]

Synthesis and characterization of m-Fe: B2 (0.26 g, 0.28 mmol, 1 equiv.), LiOH (1,32 g, 55 mmol, 200 equiv.) and dioxane/water (68 mL, 7/1, v/v) were introduced in a round bottom flask equipped with a stirring bar. The reaction mixture was refluxed for 16 hours at 105 °C,

then, the solvent was evaporated and the product was precipitated with HCl (1M) at pH = 1 (followed by pH paper). The solution was filtrated and the solid was washed with HCl (1M), water, heptane and dichloromethane and then dried under vacuum yielding the pure product **m-Fe** (0.24 g, 99% yield). ^{1}H NMR (400 MHz, DMSO-d_6): δ = 80.3, 13.6, 13.3, 12.2 ppm. λ_{abs}/nm (DMF), ($\varepsilon/10^3$ M^{-1} cm^{-1}): 416 (62.4), 522 (5.51), 573 (5.26). HRMS (ESI) calcd. for $[M–Cl]^+$ $C_{48}H_{28}N_4O_8{}^{56}Fe$ 844.1251, found 844.1249 (0 ppm). The data match those found in the literature.[1]

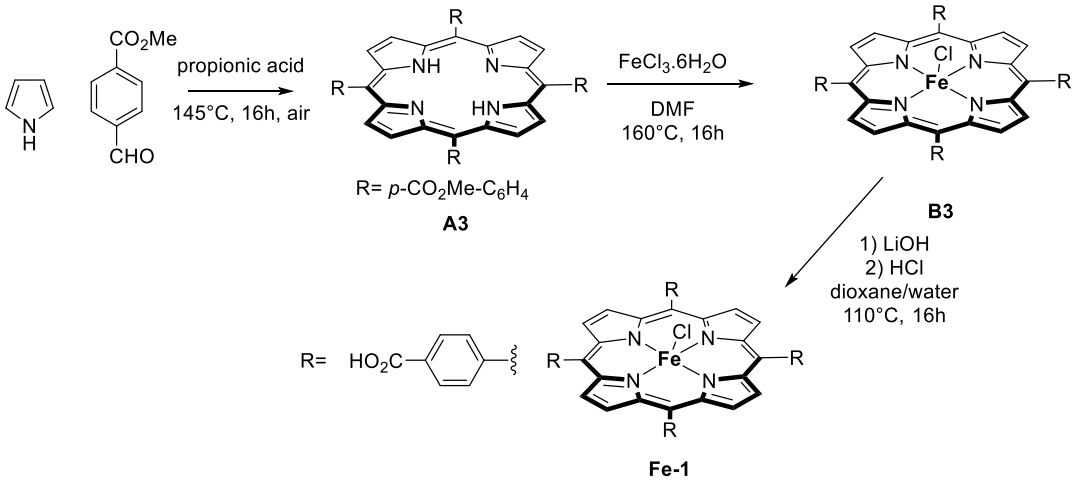

Scheme S3. Synthesis of the iron complex **Fe-1**.

Synthesis and characterization of A3: Distilled pyrrole (1 g, 1.04 mL, 15 mmol, 1 equiv.) and methyl 4-formylbenzoate (2.48 g, 15 mmol, 1 equiv.) were added to a pre-dried round bottom flask containing propionic acid (75 mL). The reaction mixture was covered with aluminum foil and the reaction mixture was refluxed for 16 hours at 145 °C. After cooling to room temperature, the resulting purple crystals were filtered and washed with water and then dissolved in dichloromethane. The organic layer was dried with $MgSO_4$, filtered and the solvent was evaporated affording a crude mixture that was purified by filtration on neutral alumina with dichloromethane as the eluent. The filtrate was then evaporated under vacuum yielding the pure product **A3** (1.14 g, 34% yield). ^{1}H NMR (400 MHz, $CDCl_3$): δ = 8.82 (s, 8H), 8.51–8.25 (AB system, J = 6.3 Hz, 8H), 4.12 (s, 12H), −2.80 (s, 2H). The data match those found in the literature.[1]

Synthesis and characterization of B3: A3 (1.14 g, 5.1 mmol, 1 equiv.), $FeCl_2{\cdot}4H_2O$ (13.1 g, 66 mmol, 13 equiv.) and DMF (150 mL) were introduced in a round bottom flask equipped with a stirring bar. The reaction mixture was refluxed for 16 hours at 160 °C, then, the solvent was slowly evaporated at 80°C under vacuum until all residual DMF was removed from the reaction mixture. Back at room temperature, the crude was washed with HCl (1M) and water until the aqueous phase became colorless, then, the solid was dissolved in dichloromethane. The organic layer was dried with $MgSO_4$, filtered and the solvent was evaporated under vacuum yielding the pure product **B3** (0.870, g, 87% yield). ^{1}H NMR (400 MHz, $CDCl_3$): δ = 80.65, 14.07, 12.96, 8.44, 7.72, 7.31, 5.36, 4.84, 4.34 ppm. λ_{abs}/nm (DMF), ($\varepsilon/10^3$ M^{-1} cm^{-1}): 428 (109), 520 (7.25), 571 (8.47). The data match those found in the literature.[1]

Synthesis and characterization of Fe-1: B3 (0.870 g, 4.44 mmol, 1 equiv.), LiOH (32 g, 1.33 mol, 300 equiv.) and dioxane/water (250 mL, 7/1, v/v) were introduced in a round bottom flask equipped with a stirring bar. The reaction mixture was refluxed for 16 hours at 110 °C, then, the solvent was evaporated and the product was precipitated with HCl (1M) at pH = 1 (followed by pH paper). The solution was filtrated and the solid was washed with HCl (1M), water, heptane and dichloromethane and then dried under vacuum yielding the pure product **Fe-1** (0.745 g, 90% yield). ^{1}H NMR (400 MHz, DMSO-d_6): δ = 80, 74.1, 13.8, 10.0 ppm. λ_{abs}/nm (DMF), ($\varepsilon/10^3$ M^{-1} cm^{-1}): 415 (28.8), 522 (6.52), 571 (4.55). HRMS (ESI) calcd. for $[M–Cl]^+$ $C_{48}H_{28}N_4O_8{}^{56}Fe$ 844.1251, found 844.1249 (0 ppm). The data match those found in the literature.[1]

7.3.3. Catalysis and kinetic studies.

7.3.3.1. Wacker type oxidation: catalyst evaluation.

Alkene oxidation reaction: An iron porphyrin complex (0.024 mmol, 0,075 equiv.), EtOH/H_2O (3 mL, 96/4, v/v), *tert*-butylstyrene (52 mg, 60 µL, 0.325 mmol, 1 equiv.), Et_3SiH (113 mg, 156 µL, 0.975 mmol, 3 equiv.) and dodecane (0.081 mmol, 0.25 equiv.) were added to an oven-dried Schlenk flask. A balloon filled with pure oxygen was placed onto the Schlenk tube and the reaction mixture was stirred at room temperature for 18 hours.

Table S1. Catalyst evaluation in the oxidation of *tert*-butylstyrene.

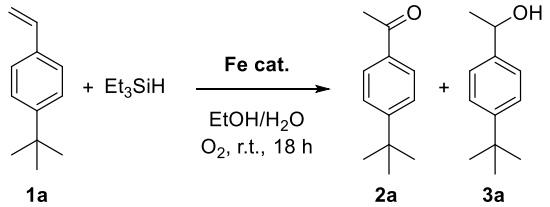

1a 2a 3a

Entry	Cat loading (mol%)	Conversion (%)	Ketone (%)	Alcohol (%)
1	**B1** (7.5)	0	0	0
2	**B2** (7.5)	0	0	0
3	**B3** (7.5)	0	0	0
4	**o-Fe** (7.5)	29	27	2
5	**m-Fe** (7.5)	93	90	3
6	**Fe-1** (7.5)	>99	98	2

7.3.3.2. Wacker type oxidation: influence of water.

Alkene oxidation reaction: Fe-1 (21.4 mg, 0.024 mmol, 0,075 equiv.), solvent (3 mL), *tert*-butylstyrene (52 mg, 60 µL, 0.325 mmol, 1 equiv.), Et_3SiH (113 mg, 156 µL, 0.975 mmol, 3 equiv.) and dodecane (0.081 mmol, 0.25 equiv.) were added to an oven-dried Schlenk flask. A balloon filled with pure oxygen was placed onto the Schlenk tube and the reaction mixture was stirred at room temperature for 16 hours.

Table S2. Water content evaluation in the oxidation of *tert*-butylstyrene

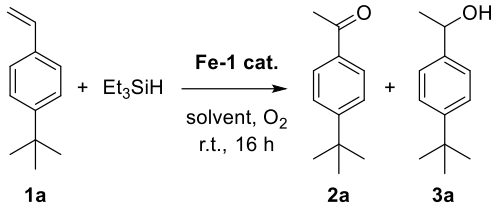

Entry	Water (%) in Ethanol	Conversion (%)	Ketone (%)	Alcohol (%)
1	0.2	60	57	3
2	2	86	82	4
3	4	>99	98	2
4	6	>99	91	9
5	10	>99	92	8

7.3.3.3. Wacker type oxidation: influence of solvent.

- Alkene oxidation reaction: Fe-1 (21.4 mg, 0.024 mmol, 0.075 equiv.), solvent (3 mL), *tert*-butylstyrene (52 mg, 60 µL, 0.325 mmol, 1 equiv.), Et_3SiH (113 mg, 156 µL, 0.975 mmol, 3 equiv.) and dodecane (0.081 mmol, 0.25 equiv.) were added to an oven-dried Schlenk flask. A balloon filled with pure oxygen was placed onto the Schlenk tube and the reaction mixture was stirred at room temperature for 16 hours.

Table S3. Solvent evaluation in the oxidation of *tert*-butylstyrene.

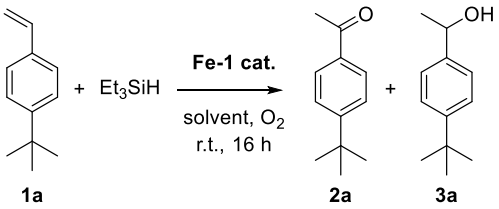

Entry	Solvent	Conversion	Ketone	alcool
1	EtOH/H_2O (96/4)	>99	98	2
2	EtOH (99.8%)	60	57	3
3	MeOH	57	51	6
4	^{i}PrOH	<5	<5	0
5	1-pentanol	<5	<5	0
6	3-Me-1-butanol	5	<5	0
7	Diethylcarbonate	0	0	0
8	Furfuryl alcohol	19	0	17

7.3.3.4. Wacker type oxidation: optimization of experimental conditions.

- Alkene oxidation reaction: Fe-1, EtOH/H_2O (3 mL, 96/4, v/v), *tert*-butylstyrene (52 mg, 60 µL, 0.325 mmol, 1 equiv.), Et_3SiH, and dodecane (0.081 mmol, 0.25 equiv.) were added to an

oven-dried Schlenk flask. A balloon filled with pure oxygen or air was placed onto the Schlenk tube and the reaction mixture was stirred at room temperature for a given time.

Table S4. Optimization of reaction conditions in the **Fe-1**-catalyzed oxidation of *tert*-butylstyrene.

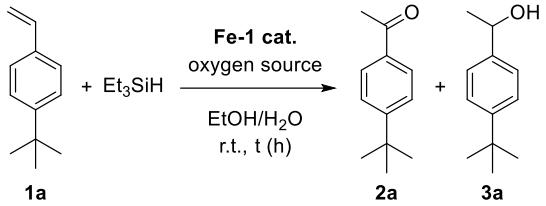

1a 2a 3a

Entry	Cat loading (%)	Source of oxygen	Silane loading (%)	Time (h)	Conversion (%)	Ketone (%)	Alcool (%)
1	7.5	O_2	300	18	>99	98	2
2	5	O_2	300	18	>99	98	2
3	2.5	O_2	200	24	>99	98	2
4	1.5	O_2	200	24	73	64	9
5	5	air	200	24	95	89	6
6	5	air	200	48	>99	94	6
7	2.5	air	200	24	95	90	5
8	2.5	air	200	48	>99	93	7

7.3.3.5. Wacker type oxidation kinetic.

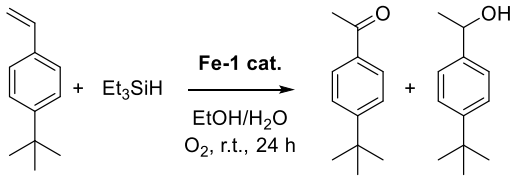

1a 2a 3a

- Alkene oxidation reaction: Fe-1 (7.1 mg, 0.08 mmol, 0,025 equiv.), EtOH/H_2O (3 mL, 96/4, v/v), *tert*-butylstyrene (52 mg, 60 µL, 0.325 mmol, 1 equiv.), Et_3SiH (76 mg, 104 µL, 0.650 mmol, 2 equiv.) and dodecane (0.081 mmol, 0.25 equiv.) were added to an oven-dried Schlenk flask. A balloon filled with pure oxygen was placed onto the Schlenk tube and the reaction mixture was stirred at room temperature for 24 hours. Yield (%) was monitored by GC analysis using dodecane as the internal standard. Formation of ketone product **[2a]** and conversion of alkene **[1a]** *versus* time (h) are plotted in **Figure S1-S2** (fitted values are shown in bleu, and experimental values are shown in orange dots).

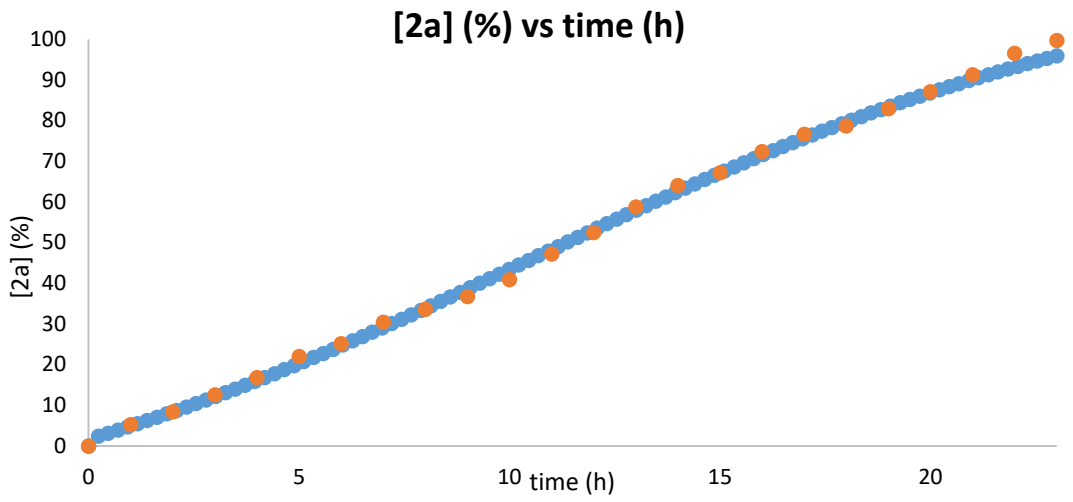

Figure S1. Ketone production **[2a]** *versus* time at 2.5 mol% of catalyst **Fe-1**.

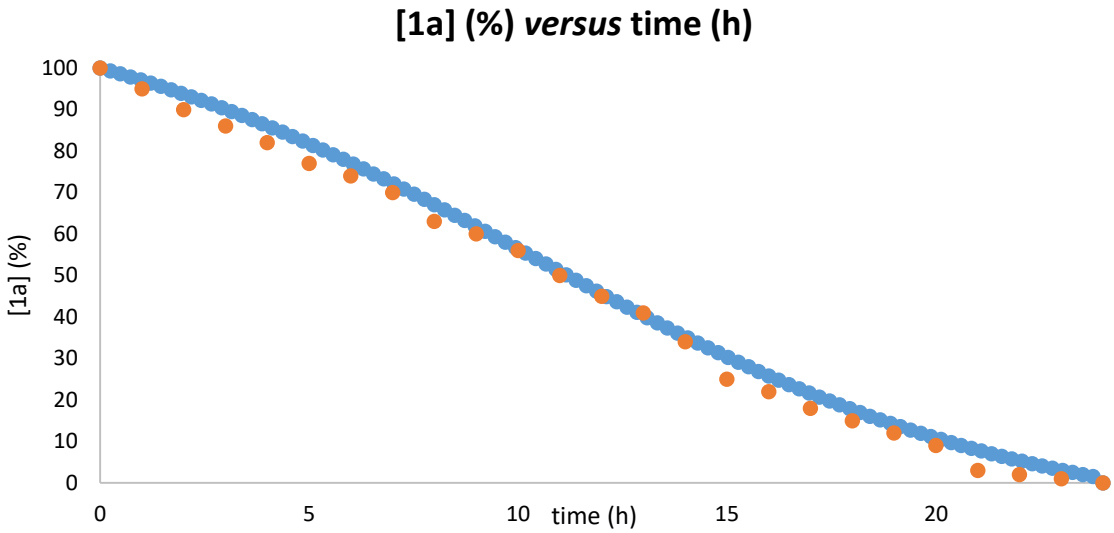

Figure S2. Olefin consumption **[1a]** *versus* time at 2.5 mol% of catalyst **Fe-1**.

7.3.3.6. Wacker type oxidation: deactivation of the catalyst study.

- Catalyst deactivation evidence: A previously active catalyst (**Fe-1**) was stored under air for 3 months at room temperature and was added (14.2 mg, 0.016 mmol, 0.05 equiv.) to oven-dried Schlenk flask with EtOH/H_2O (3 mL, 96/4, v/v), *tert*-butylstyrene (52 mg, 60 µL, 0.325 mmol, 1 equiv.), Et_3SiH (76 mg, 104 µL, 0.650 mmol, 2 equiv.) and dodecane (0.081 mmol, 0.25 equiv.). A balloon filled with pure oxygen was placed onto the Schlenk tube and the reaction mixture was stirred at room temperature for 24 hours. This experiment was conducted 3 times and only trace amounts of ketone **2** (<5%) were detected by GC-MS analysis.

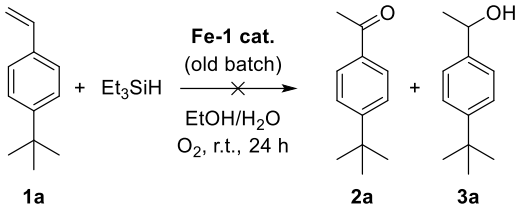

This catalyst deactivation was ascribed to the formation of a μ-oxo-bridged diiron complex according to a characterization by mass spectroscopy.^{1}H NMR spectroscopy studies show a mixture of two iron porphyrin species, but due to the paramagnetic effect of the iron nucleus, further characterization using this spectroscopic method is no feasible because hydrogen signals are broad and overlap each other. The deactivation is ascribed to the atmospheric oxygen/water stored kept together with the catalyst that slowly oxidize the pure **Fe-1** iron porphyrin to yield the μ-oxo-bridged complex **Fe-2**.

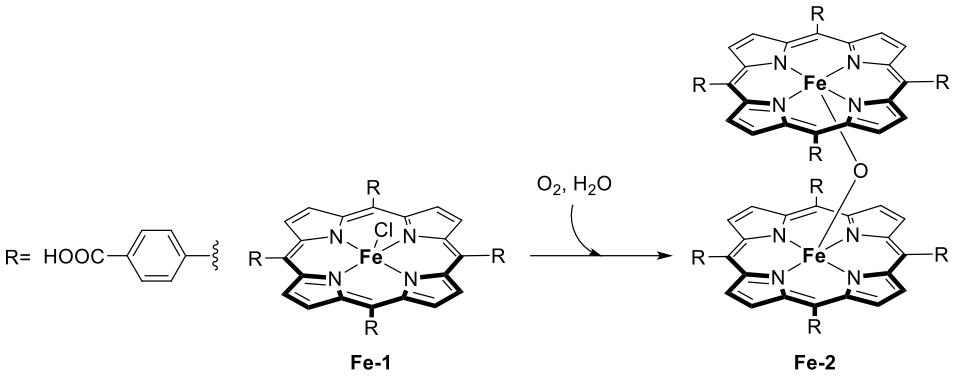

Scheme S4. Dimerization of **Fe-1** leading to a μ-oxo-bridged iron species **Fe-2**.

Characterization of the complex Fe-2: ^{1}H NMR (400 MHz, DMSO-d_6): δ = 79.63, 73.92, 13.66, 12.77, 11.23, 10.39, 9.97, 8.38, 7.67 ppm. HRMS (MALDI): *m/z* calcd for $C_{96}H_{56}N_8O_{17}{}^{56}Fe_2$ 1704.24567 $[M]^{+\cdot}$; found: 1704.263 (12 ppm). Other species detected that originate from the fragmentation of the μ-oxo-bridged iron complex: *m/z* calcd for $C_{48}H_{28}N_4O_8{}^{56}Fe$ 844.1251 $[M]^{+}$; found: 844.126 (1 ppm); m/z calcd for $C_{48}H_{28}N_4O_8{}^{35}Cl^{56}Fe$ 879.09396 $[M]^{+}$; found: 879.095 (1 ppm).

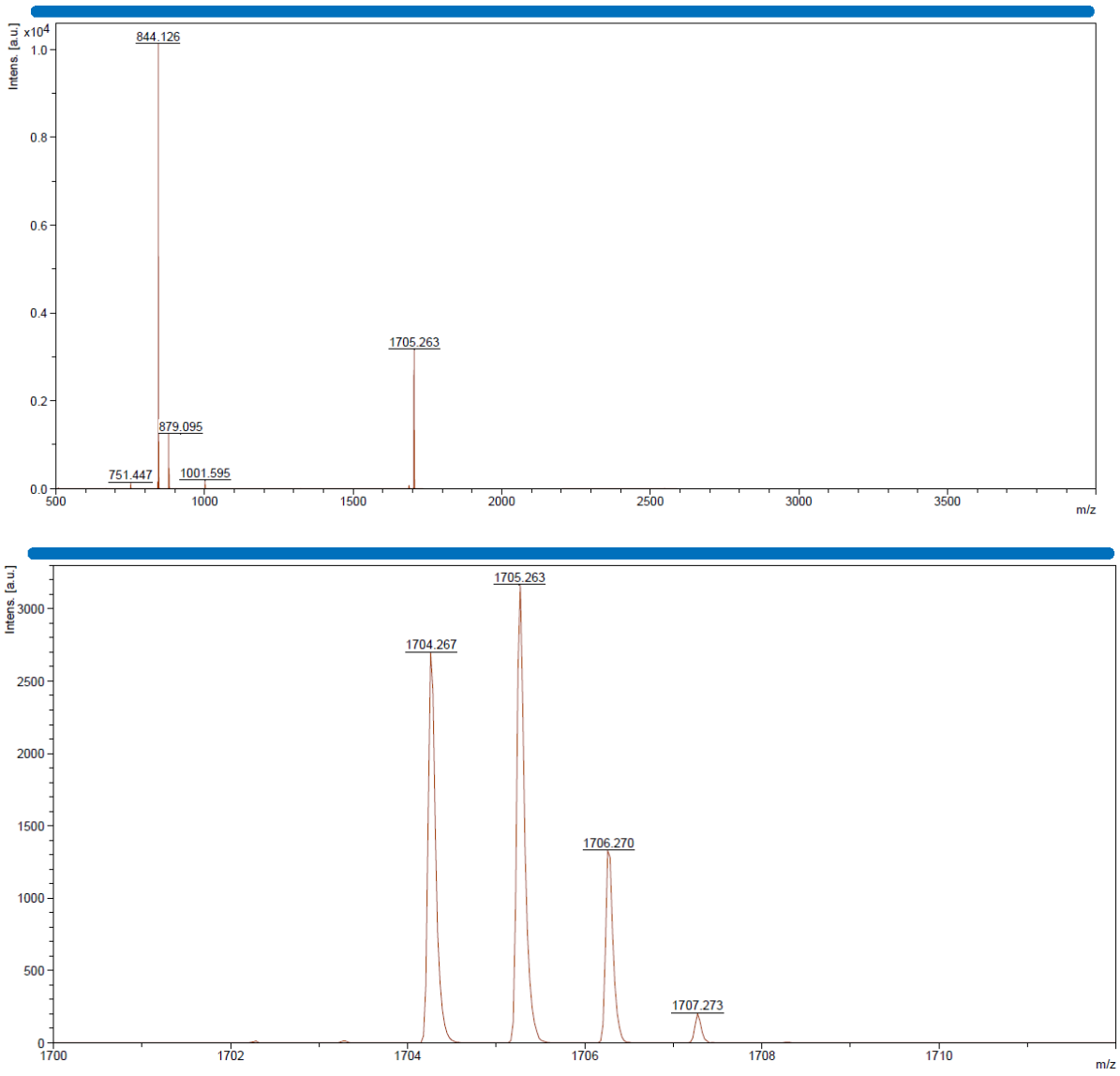

Figure S3. HRMS (MALDI) study on iron complex **Fe-2**.

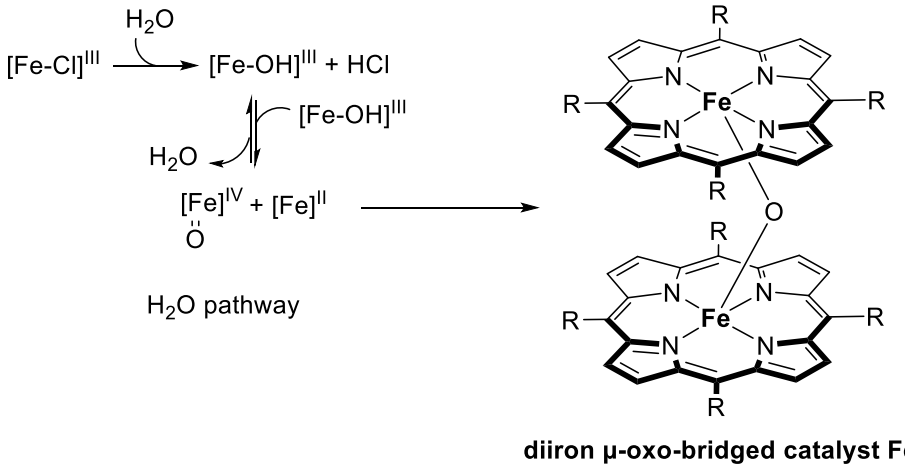

diiron μ-oxo-bridged catalyst Fe-2

Scheme S5. Mechanism proposal for aerobic iron porphyrin dimerization according to reference [2].

7.3.3.7. Wacker type oxidation using diiron oxo-bridged catalyst Fe-2.

Alkene oxidation reaction: Fe-2 (14.2 mg, 0.016 mmol, 0.025 equiv.), EtOH/H_2O (3 mL, 96/4, v/v), *tert*-butylstyrene (52 mg, 60 µL, 0.325 mmol, 1 equiv.), silane (0.975 mmol, 3 equiv.) and dodecane (0.081 mmol, 0.25 equiv.) were added to an oven-dried Schlenk flask. A balloon filled with air was placed onto the Schlenk tube and the reaction mixture was stirred at room temperature for a given time. Yield (%) was monitored by GC analysis using dodecane as the internal standard.

Table S5. Silane evaluation in the **Fe-2**-catalyzed oxidation of *tert*-butylstyrene.

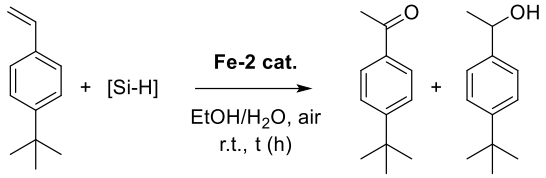

Entry	Silane	Time (h)	Conversion	Ketone	Alcohol
1	Et_3SiH	24	<5	<5	0
2	$PhSiH_3$	5	>99	92	8
3	Ph_2SiH_2	5	>99	91	9
4	Ph_3SiH*	24	<5	<5	0
5	PMHS	24	<5	<5	0

*Ph_3SiH wasn't soluble in the reaction media.

7.3.3.8. Wacker type oxidation using Et_3SiH and an additive to activate the catalyst.

Alkene oxidation reaction: Fe-2 (14.2 mg, 0.016 mmol, 0.025 equiv.), EtOH/H_2O (3 mL, 96/4, v/v), *tert*-butylstyrene (52 mg, 60 µL, 0.325 mmol, 1 equiv.), Et_3SiH (113 mg, 156 µL, 0.975 mmol, 3 equiv.) dodecane (0.081 mmol, 0.25 equiv.) and an additive were added to an oven-dried Schlenk flask. A balloon filled with air was placed onto the Schlenk tube and the reaction mixture was stirred at room temperature for 24 hours. Conversion and yield were monitored by GC-MS using dodecane as the internal standard.

Table S6. Additive evaluation for the oxidation of *tert*-butylstyrene in the presence of Et_3SiH.

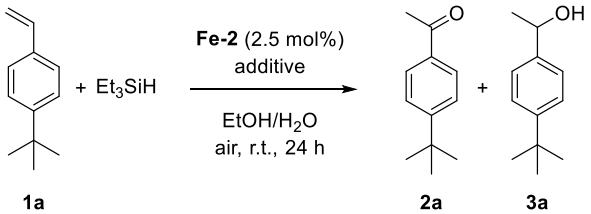

Entry	Additive	Conversion	Ketone	alcool
1	-	<5	<5	0
2	HCl (10 mol%)	60	48	12
3	HCl (20 mol%)	62	49	13
4	$PhSiH_3$ (10 mol%)	43	42	traces
5	$PhSiH_3$ (20 mol%)	>99	98	2

Consideration: In situ activation of the **Fe-2** catalyst can be done by either adding hydrochloric acid or $PhSiH_3$. It is important to note that $PhSiH_3$ play multiple roles in this case, both as an activator for the catalyst and as a reductant involved in the catalytic cycle. However, the results from Table S6 (entry 5) demonstrate that even if all $PhSiH_3$ are able to yield 3 equivalents of hydrogen and thus of ketone product, 40% of the ketone should be missing at the end of the reaction. In this case, full conversion is reached, demonstrating that $PhSiH_3$ unambiguously plays the role of catalyst activator.

Mechanistic discussion: A mechanistic proposal for additive activation of the catalyst is proposed in **Scheme S6**. Regarding the pathway 1) both ethanol and water contained from the solvent can potentially play the role of nucleophile yielding monomeric iron oxo derivative, that are transformed in situ by phenylsilane to yield the iron hydride active intermediate. Activation via pathway 2) can process by either an ionic (A) or a radical route (B). Both mechanism can be envisaged yielding the same monomeric iron porphyrin product.

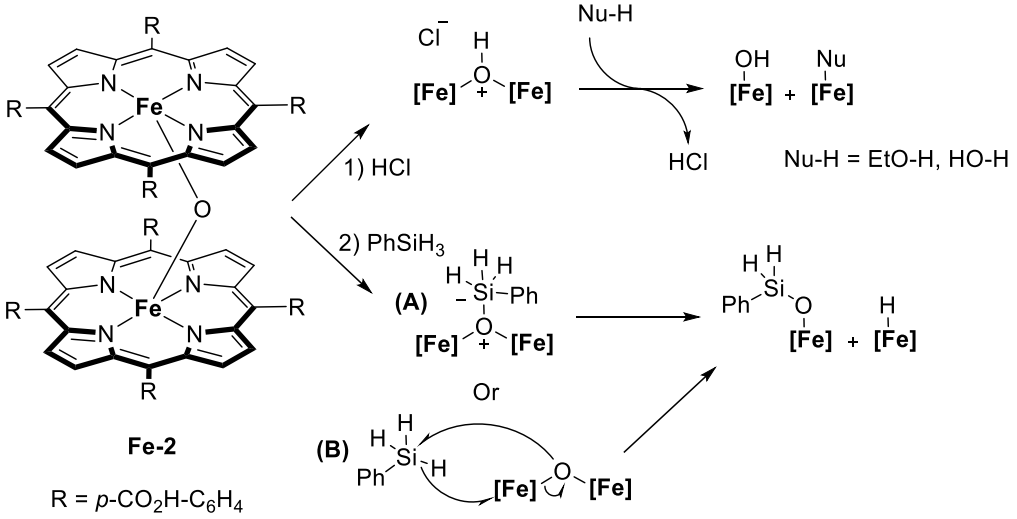

Scheme S6. Mechanism proposal for iron porphyrin dimer **Fe-2** catalyst activation.

7.3.3.9. Evaluation of reaction conditions of Wacker-type oxidation using $PhSiH_3$.

Alkene oxidation reaction (influence of water content): The diiron catalyst **Fe-2** (14.2 mg, 0.016 mmol, 0.025 equiv.), EtOH/H_2O (3 mL, 96/4, v/v), *tert*-butylstyrene (52 mg, 60 µL, 0.325 mmol, 1 equiv.), $PhSiH_3$ (102 mg, 117 µL, 0.975 mmol, 3 equiv.) and dodecane (0.081 mmol, 0.25 equiv.) were added to an oven-dried Schlenk flask. A balloon filled with air was placed onto the Schlenk tube and the reaction mixture was stirred at room temperature for a given time. Conversions and yields were monitored by GC-MS using dodecane as the internal standard.

Table S7. Influence of water content in the oxidation of *tert*-butylstyrene.

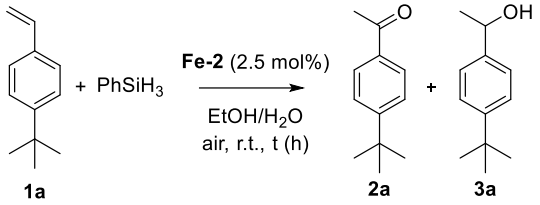

Entry	Water (%) in Ethanol	Time (h)	Conversion (%)	Ketone (%)	Alcool (%)
1	0.2	24	51	47	4
2	4	5	>99	92	8

Alkene oxidation reaction (final optimization): The diiron catalyst **Fe-2** (14.2 mg, 0.016 mmol, 0.025 equiv.), EtOH/H_2O (3 mL, 96/4, v/v), *tert*-butylstyrene (52 mg, 60 µL, 0.325 mmol, 1 equiv.), $PhSiH_3$ and dodecane (0.081 mmol, 0.25 equiv.) were added to an oven-dried Schlenk flask. A balloon filled with air was placed onto the Schlenk tube and the reaction mixture was stirred at room temperature for 24 hours. Conversions and yields were monitored by GC-MS using dodecane as the internal standard.

Table S8. Evaluation of catalyst and silane loading in the oxidation of *tert*-butylstyrene.

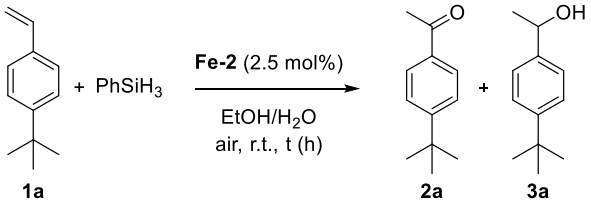

Entry	Cat loading (%)	$PhSiH_3$ loading (%)	Time (h)	Conversion (%)	Ketone (%)	Alcohol (%)
1	5	300	4.5	100	92	8
2	2.5	300	8	100	92	8
3	2.5	150	12	90	85	4

7.3.3.10. Wacker-type oxidation kinetic studies.

Catalysis at 2.5 mol% of iron catalyst.

Alkene oxidation reaction: The diiron catalyst **Fe-2** (14.2 mg, 0.016 mmol, 0.025 equiv.), EtOH/H_2O (3 mL, 96/4, v/v), *tert*-butylstyrene (52 mg, 60 µL, 0.325 mmol, 1 equiv.), $PhSiH_3$ (102 mg, 117 µL, 0.975 mmol, 3 equiv.) and dodecane (0.081 mmol, 0.25 equiv.) were added to an oven-dried Schlenk flask. A balloon filled with air was placed onto the Schlenk tube and the reaction mixture was stirred at room temperature for 5 hours. Conversion and yield were monitored by GC using dodecane as the internal standard. Formation of ketone product [**2a**] and conversion of alkene [**1a**] *versus* time (h) are plotted in **Figures S4-S5** (fitted values are shown in bleu, and experimental values are shown in orange dots).

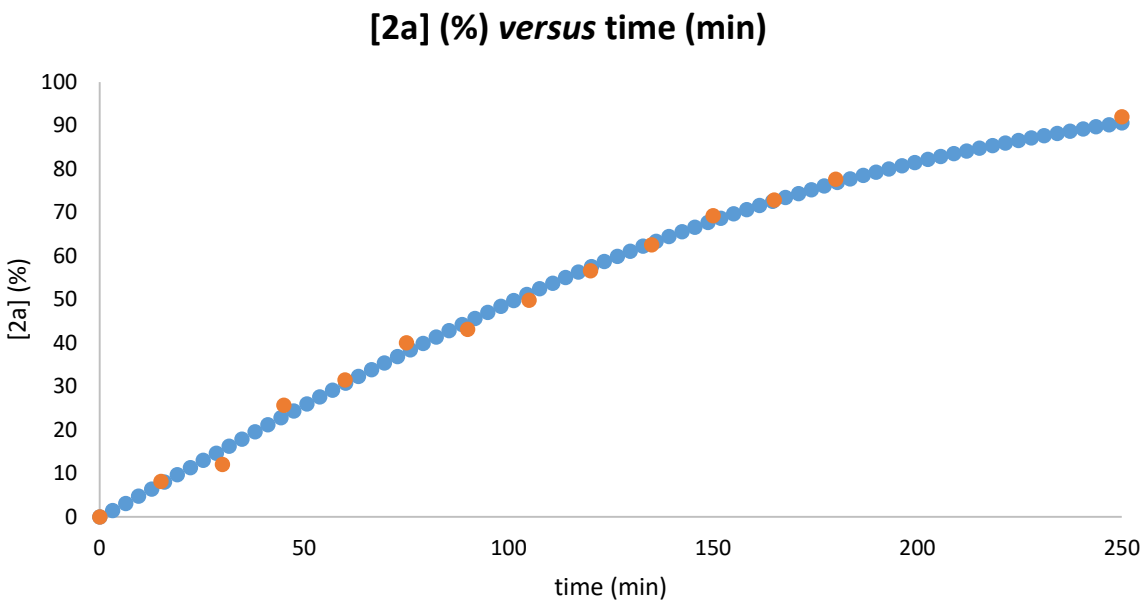

Figure S4. Ketone production **[2a]** *versus* time at 2.5 mol% of catalyst **Fe-2**.

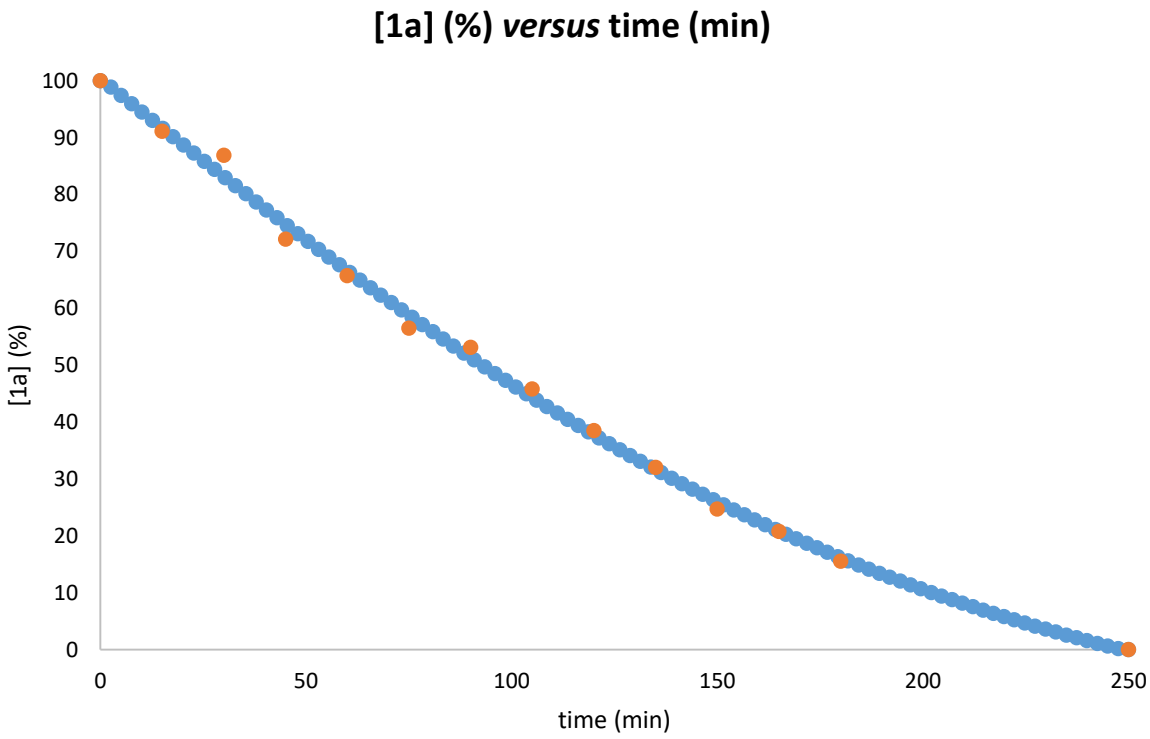

Figure S5. Olefin consumption **[1a]** *versus* time at 2.5 mol% of catalyst **Fe-2**.

Catalysis at 1.25 mol% of iron catalyst.

Alkene oxidation reaction: The diiron catalyst **Fe-2** (7.1 mg, 0.008 mmol, 0.0125 equiv.), EtOH/H_2O (3 mL, 96/4, v/v), *tert*-butylstyrene (52 mg, 60 µL, 0.325 mmol, 1 equiv.), $PhSiH_3$ (102 mg, 117 µL, 0.975 mmol, 3 equiv.) and dodecane (0.081 mmol, 0.25 equiv.) were added to an oven-dried Schlenk flask. A balloon filled with air was placed onto the Schlenk tub and the reaction mixture was stirred at room temperature for 8 hours. Conversion and yield were monitored by GC using dodecane as the internal standard. Formation of ketone product [**2a**] and conversion of alkene [**1a**] *versus* time (h) are plotted in **Figures S6-S7** (fitted values are shown in bleu, and experimental values are shown in orange dots.

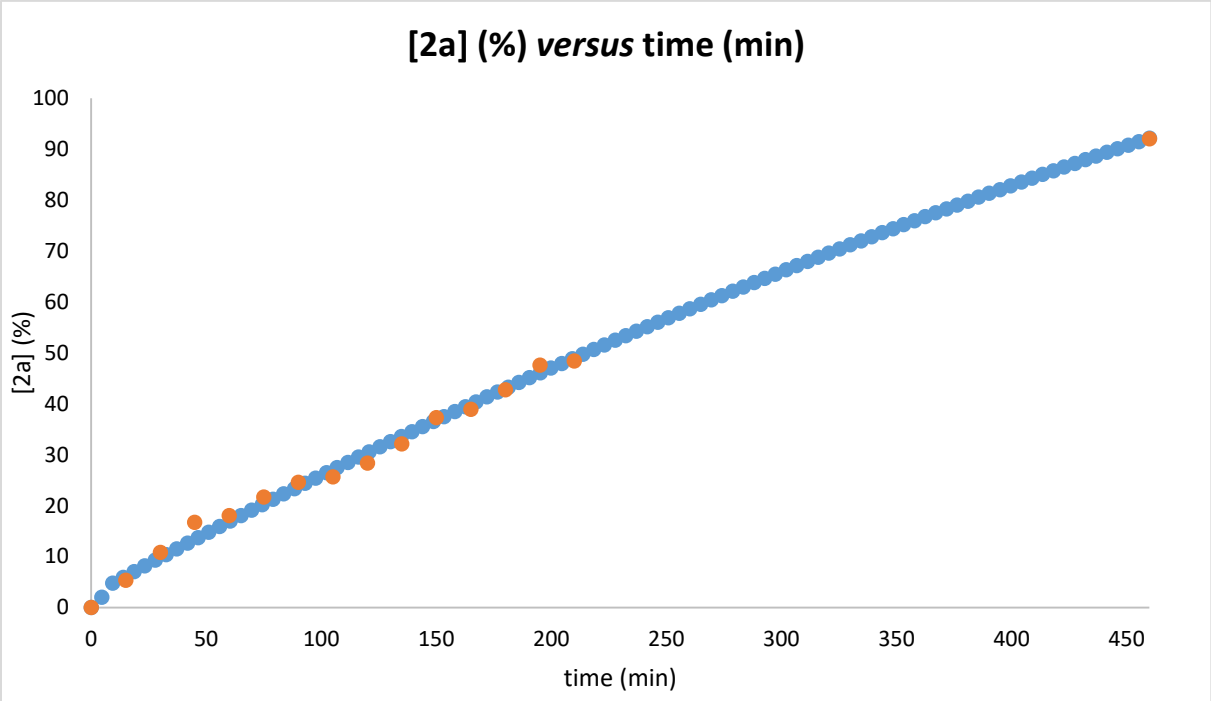

Figure S6. Ketone production **[2a]** *versus* time at 1.25 mol% of catalyst **Fe-2**.

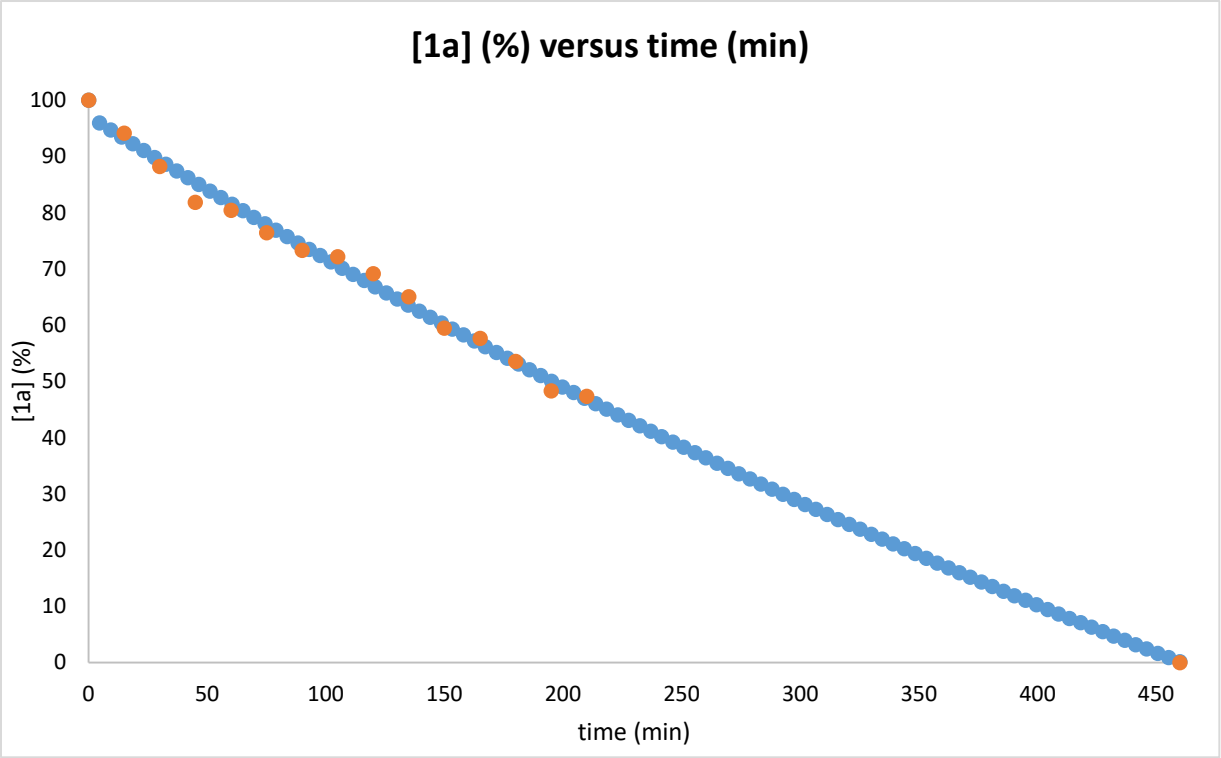

Figure S7. Olefin consumption **[1a]** *versus* time at 1.25 mol% of catalyst **Fe-2**.

7.3.3.11. Determination of the catalyst order.

Reaction kinetic: rate = k x [catalyst]

If the reaction kinetic is first order in catalyst, then for two different reaction (1 and 2) conducted at different catalyst concentration :

Rate 1 = Rate 2 x $[catalyst]_2/[catalyst]_1$

Regarding the oxidation reaction investigated, following conversion instead of product formation is more precise because two products are formed during the course of the reaction, therefore increasing measurement bias.

Conversion of the [alkene] starting material follow the same rule :

Rate x t = $[alcohol + ketone]_t$; therefore : Rate x t = $[conversion\ of\ alkene]_t$, then

$Conversion_1/t = Conversion_2/t \times [catalyst]_2/[catalyst]_1$

If the reaction kinetic is first order in catalyst :

Conversion (1.25 mol %)/t = (Conversion (2.5 mol%)/t)/2

In this case curve 1 (1.25 mol%) almost fully overlap curve 2 (2.5mol%) when conversion of 2 (2.5 mol%) is divided by 2 at the same time of reaction indicating that the kinetic reaction is order 1 in catalyst (**Figure S8**).

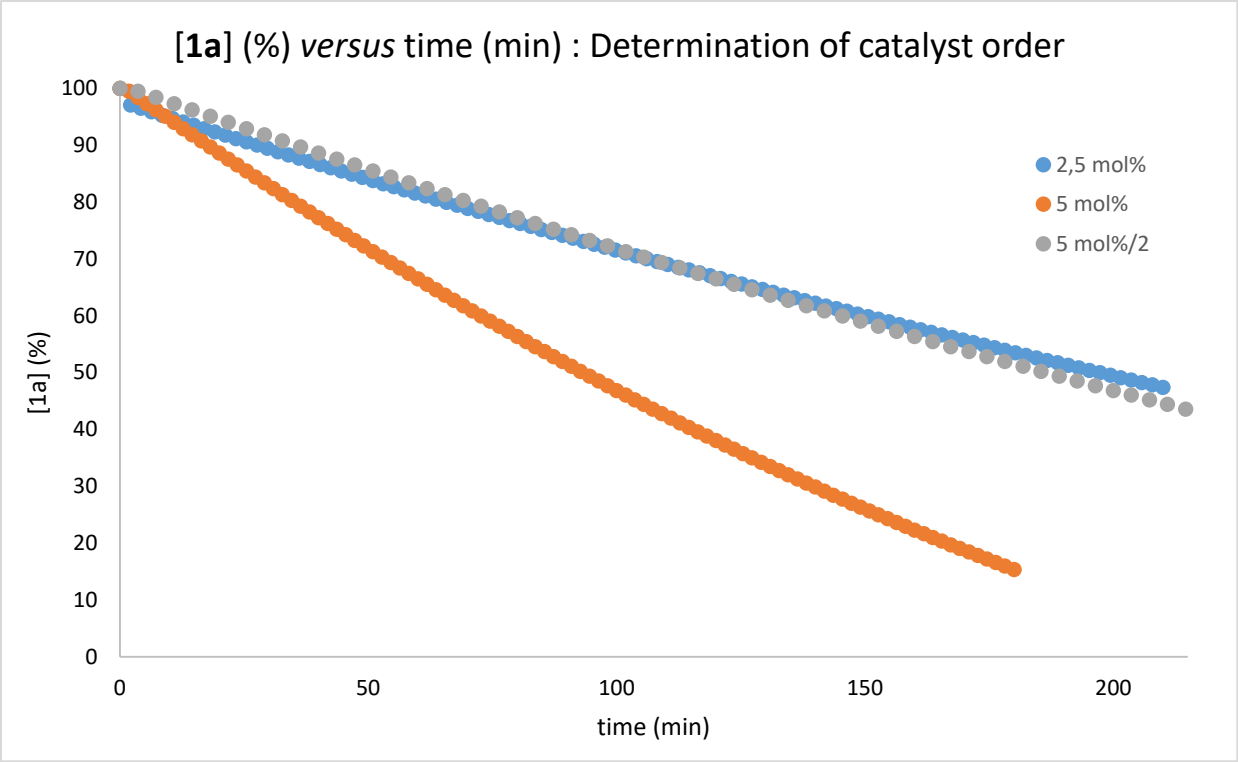

Figure S8. Iron-catalyzed Wacker-type oxidation studies for the determination of iron catalyst order. Reaction performed at 1.25 mol% iron catalyst (blue line), at 2.5 mol% iron catalyst (orange line) and result from dividing the orange line by 2 (grey line).

7.3.3.12. Wacker-type oxidation at 0 °C.

Alkene oxidation reaction at 0°C: The diiron catalyst **Fe-2** (14.2 mg, 0.016 mmol, 0.025 equiv.), EtOH/H_2O (3 mL, 96/4, v/v), *tert*-butylstyrene (52 mg, 60 µL, 0.325 mmol, 1 equiv.), dodecane (0.081 mmol, 0.25 equiv.) were added to an oven-dried Schlenk flask. The reaction mixture was cooled down to 0°C using an ice bath and $PhSiH_3$ (102 mg, 117 µL, 0.975 mmol, 3 equiv.) was added. A balloon filled with air was placed onto the Schlenk tube and the reaction mixture was stirred and maintained at 0°C for 5 hours. Conversion and yield were monitored by GC using dodecane as the internal standard. Formation of ketone product [**2a**] and conversion of alkene [**1a**] *versus* time (h) are plotted in **Figures S9-S10** (fitted values are shown in bleu, and experimental values are shown in orange dots.

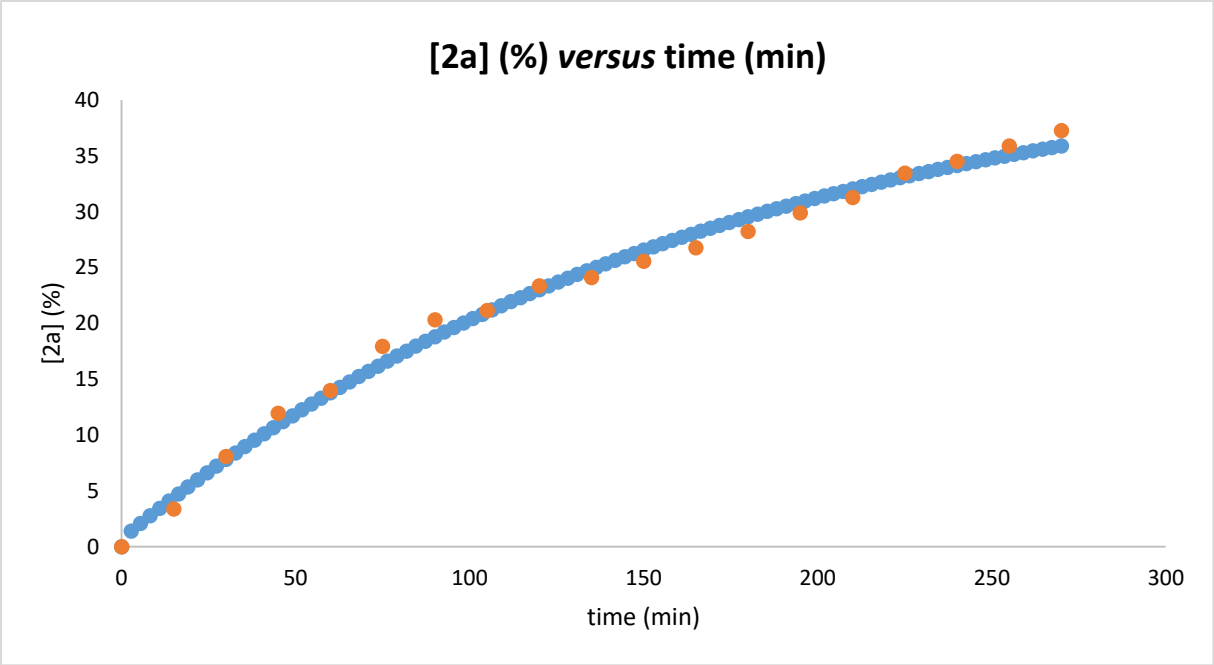

Figure S9. Ketone production **[2a]** *versus* time at 2.5 mol% of catalyst **Fe-2** and 0°C.

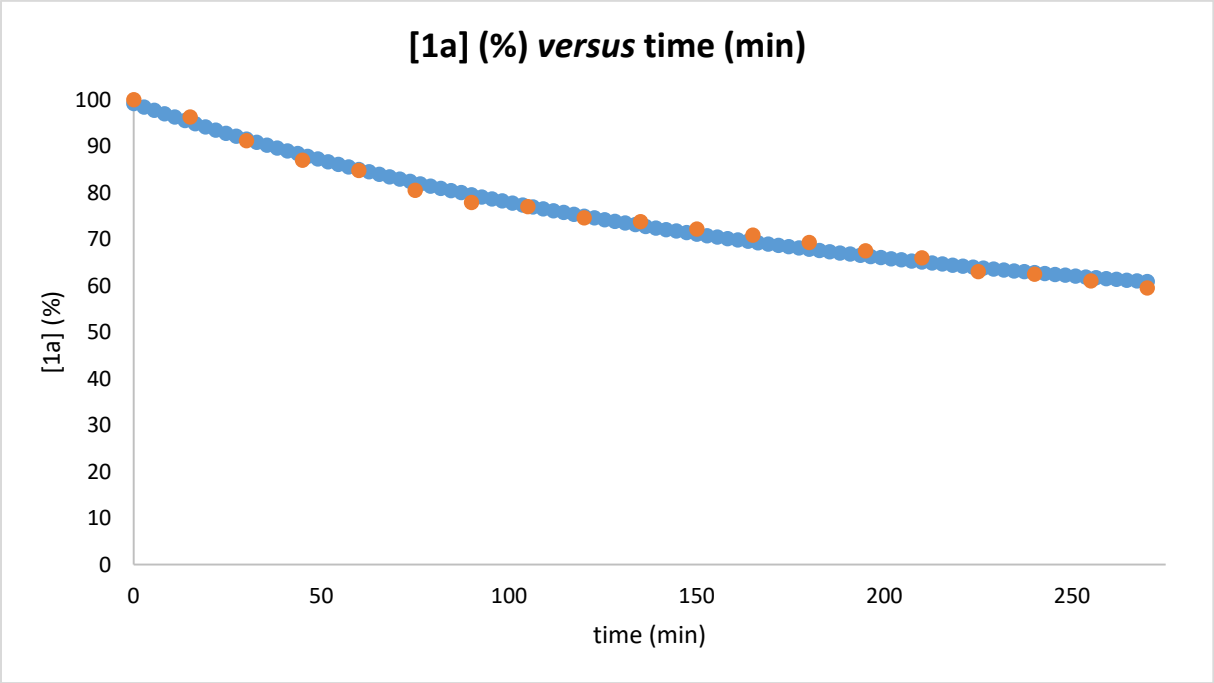

Figure S10. Olefin consumption **[1a]** *versus* time at 2.5 mol% of catalyst **Fe-2** and 0°C.

7.3.3.13. Wacker-type oxidation at 50 °C.

Alkene oxidation reaction at 50 °C: The diiron catalyst **Fe-2** (14.2 mg, 0.016 mmol, 0.025 equiv.), EtOH/H_2O (3 mL, 96/4, v/v), *tert*-butylstyrene (52 mg, 60 µL, 0.325 mmol, 1 equiv.) and dodecane (0.081 mmol, 0.25 equiv.) were added to an oven-dried Schlenk flask. The reaction mixture was heated up to 50 °C and $PhSiH_3$ (102 mg, 117 µL, 0.975 mmol, 3 equiv.) was added. A balloon filled with air was placed onto the Schlenk tube and the reaction mixture was stirred for 2.5 hours. Conversion and yield were monitored by GC using dodecane as the internal standard. Formation of ketone product [**2a**] and conversion of both alkene [**1a**] and silane [**Si-H**] *versus* time (h) are plotted in **Figures S11-S13** (fitted values are shown in bleu, and experimental values are shown in orange dots.

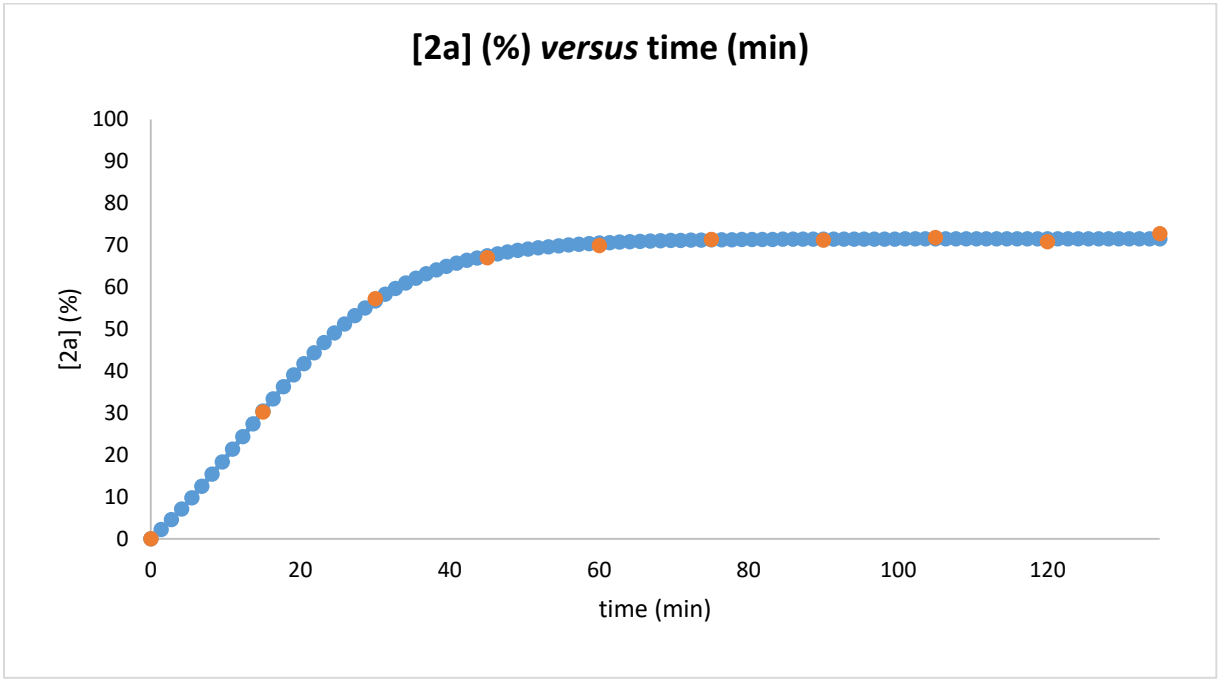

Figure S10. Ketone production **[2a]** *versus* time at 2.5 mol% of catalyst **Fe-2** and 50°C.

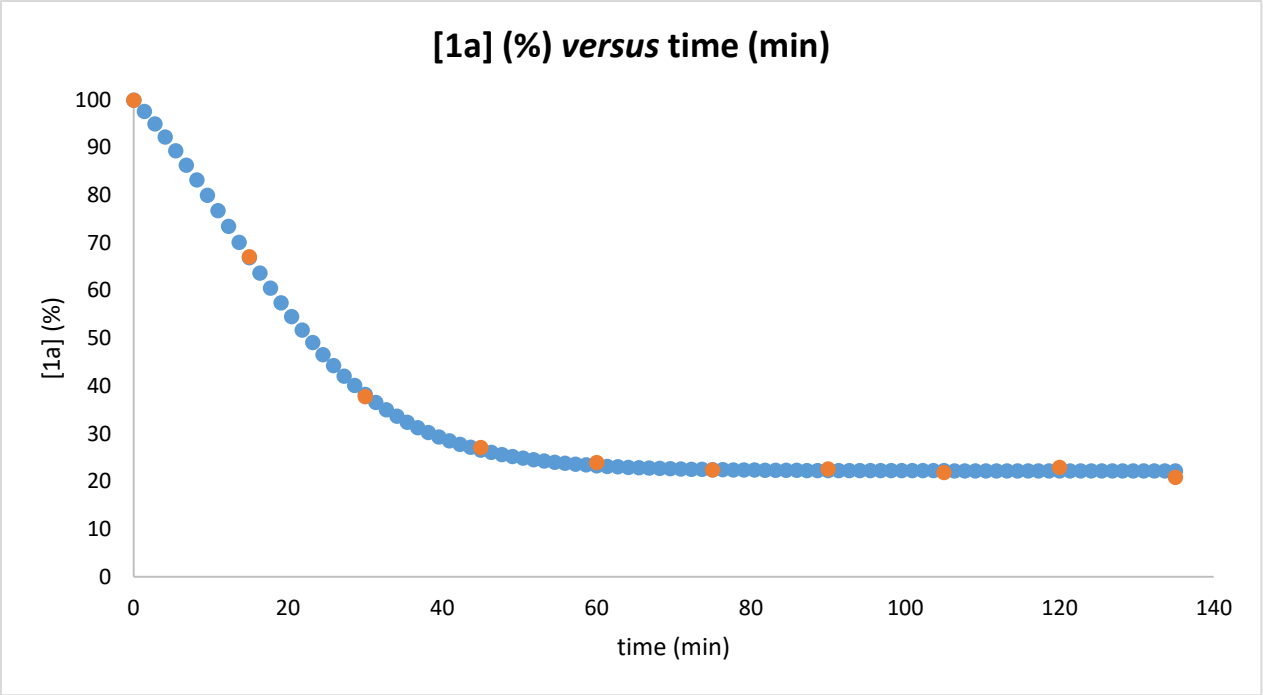

Figure S11. Olefin consumption **[1a]** *versus* time at 2.5 mol% of catalyst **Fe-2** and 50°C.

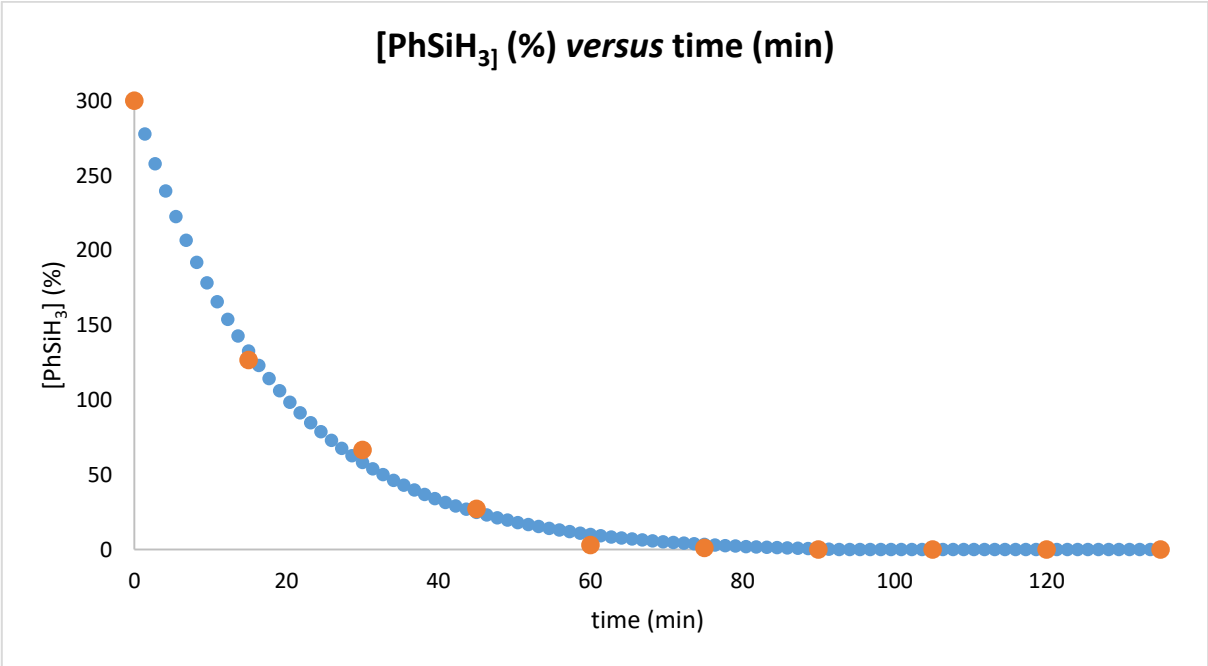

Figure S12. Silane consumption **[Si-H]** *versus* time at 2.5 mol% of catalyst **Fe-2** and 50°C.

Comment: The oxidation reaction is faster at higher temperature. However, after 1 hour all $PhSiH_3$ reductant is consumed, therefore, the catalytic cycle is stopped. In fact, the maximum estimated yield for product and the maximum alkene conversion were reached after full conversion of $PhSiH_3$.

Alkene oxidation reaction at 50°C without catalyst: EtOH/H_2O (3 mL, 96/4, v/v), *tert*-butylstyrene (52 mg, 60 µL, 0.325 mmol, 1 equiv.) and dodecane (0.081 mmol, 0.25 equiv.) were added to an oven-dried Schlenk flask. The reaction mixture was heated up to 50°C and $PhSiH_3$ (102 mg, 117 µL, 0.975 mmol, 3 equiv.) was added. A balloon filled with air was placed onto the Schlenk tube and the reaction mixture was stirred for 24 hours. Conversion and yield were monitored by GC using dodecane as the internal standard.

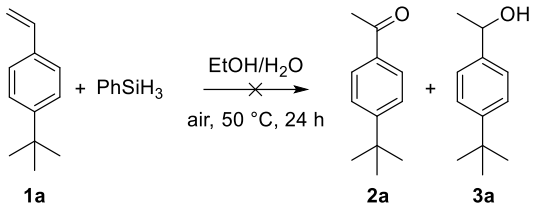

Comment: After 24 hours of reaction, no product, nor conversion of both alkene and $PhSiH_3$ (less than 5% conversion) were detected clearly showing that the catalyst is responsible for the fast degradation of $PhSiH_3$ as well as the formation of oxidated product at this temperature.

7.3.3.14. Wacker-type oxidation reaction at different concentrations.

Alkene oxidation reaction at 6 mL of solvent instead of 3 mL: The diiron catalyst **Fe-2** (14.2 mg, 0.016 mmol, 0.025 equiv.), EtOH/H_2O (6 mL, 96/4, v/v), *tert*-butylstyrene (52 mg, 60 µL, 0.325 mmol, 1 equiv.), $PhSiH_3$ (102 mg, 117 µL, 0.975 mmol, 3 equiv.) and dodecane (0.081 mmol, 0.25 equiv.) were added to an oven-dried Schlenk flask. A balloon filled with air was placed onto the Schlenk tube and the reaction mixture was stirred at room temperature for 5 hours. Conversion and yield were monitored by GC using dodecane as the internal standard. Conversion and yield were monitored by GC using dodecane as the internal standard. Formation of ketone product [**2a**] and conversion of alkene [**1a**] *versus* time (h) are plotted in **Figures S13-S14** (fitted values are shown in bleu, and experimental values are shown in orange dots.

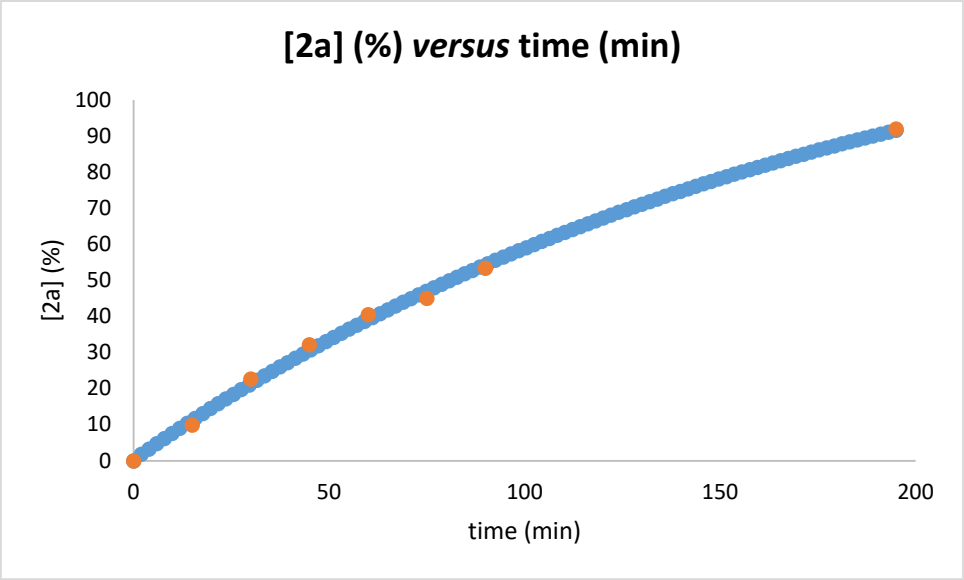

Figure S13. Ketone production **[2a]** *versus* time at 2.5 mol% of catalyst **Fe-2** and room temperature under diluted conditions.

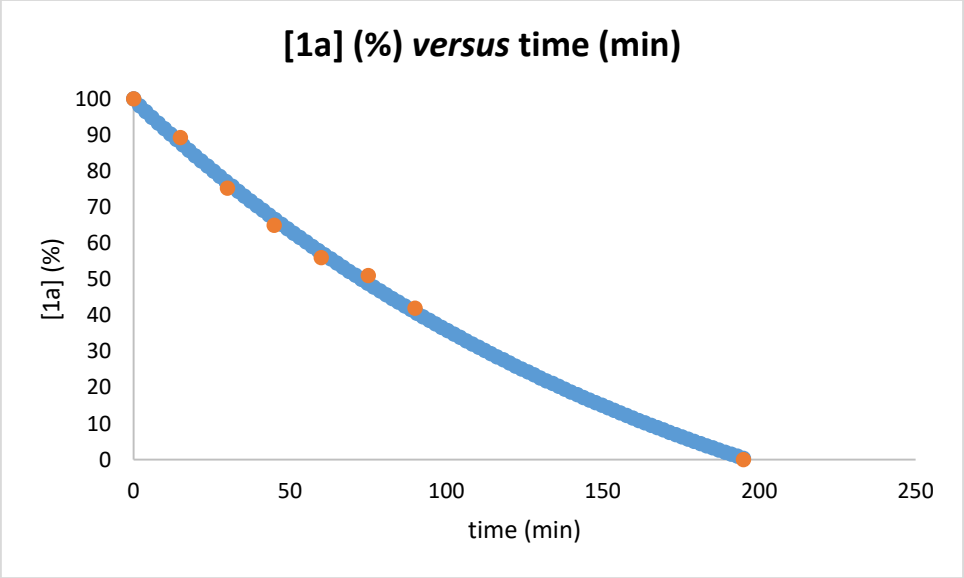

Figure S14. Olefin consumption **[1a]** *versus* time at 2.5 mol% of catalyst **Fe-2** and room temperature under diluted conditions.

Alkene oxidation reaction at 1.25 mol% of iron catalyst under diluted conditions: The diiron catalyst **Fe-2** (7.1 mg, 0.004 mmol, 0.0125 equiv.), EtOH/H_2O (6 mL, 96/4, v/v), *tert*-butylstyrene (52 mg, 60 µL, 0.325 mmol, 1 equiv.), $PhSiH_3$ (102 mg, 117 µL, 0.975 mmol, 3 equiv.) and dodecane (0.081 mmol, 0.25 equiv.) were added to an oven-dried Schlenk flask. A balloon filled with air was placed onto the Schlenk tube and the reaction mixture was stirred at room temperature for 5 hours. Conversion and yield were monitored by GC using dodecane as the internal standard. Formation of ketone product [**2a**] and conversion of alkene [**1a**] *versus* time (h) are plotted in **Figures S15-S16** (fitted values are shown in bleu, and experimental values are shown in orange dots.

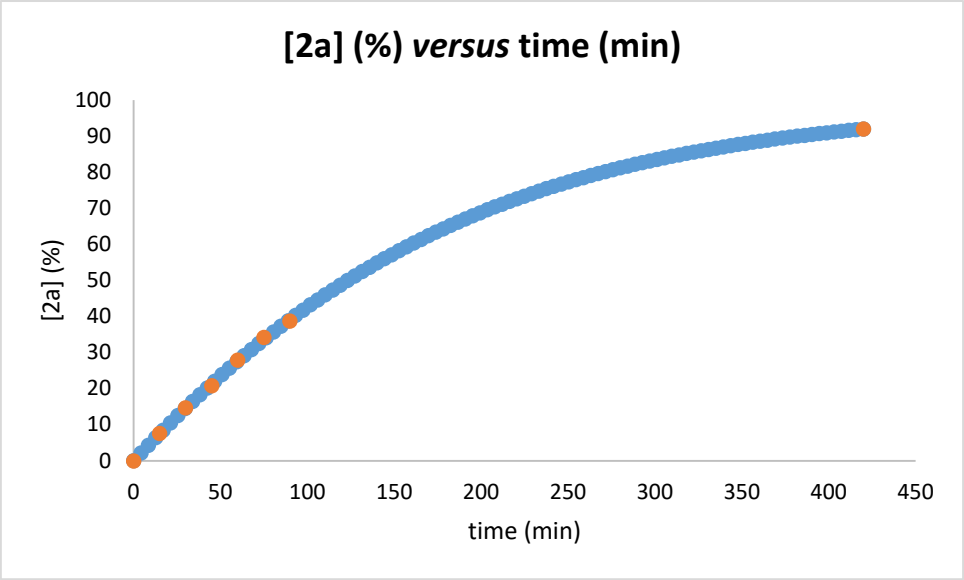

Figure S15. Ketone production **[2a]** *versus* time at 1.25 mol% of catalyst **Fe-2** and room temperature under diluted conditions.

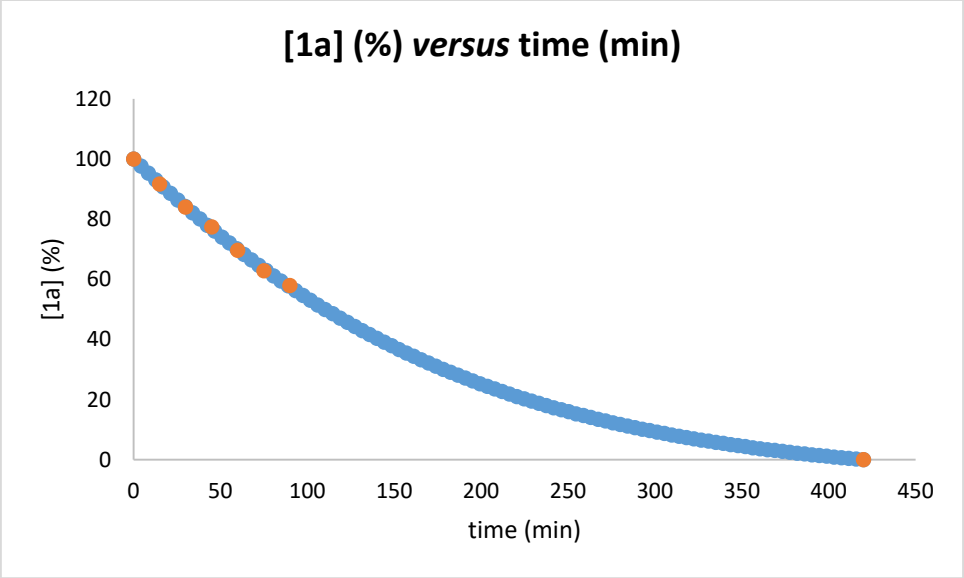

Figure S16. Olefin consumption **[1a]** *versus* time at 1.25 mol% of catalyst **Fe-2** and room temperature under diluted conditions.

7.3.3.15. Summary of all kinetic profiles.

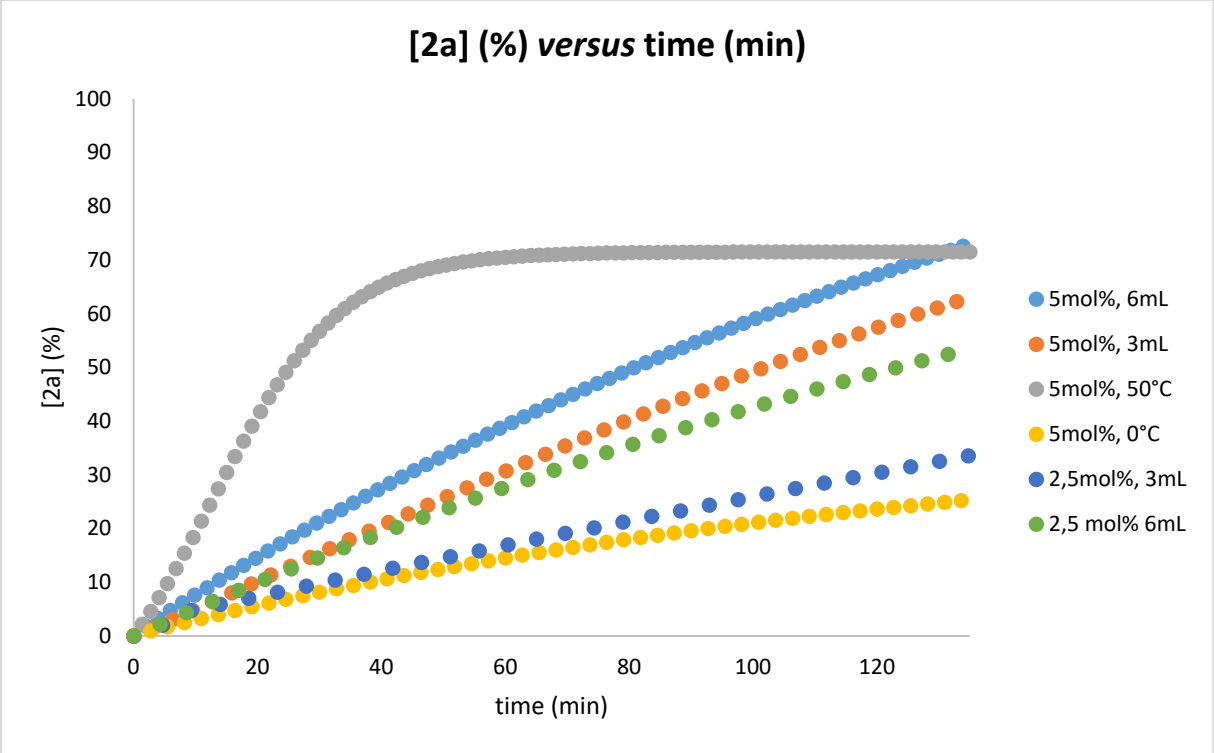

Figure S17. Summary of all kinetic profiles.

- TOF determination of the oxidation reaction

TOF values (rate: mol/s) were determined after 30 min of reaction thanks to the kinetic profiles obtained.

Table S9. Summary of all reaction rates (mol/s) calculated by kinetic analysis.

conditons	catalyst loading	Observed rate at 30 min (mol/s)
3 mL, 50 °C	5 mol%	1.02182×10^{-7}
6 mL, r.t.	5 mol%	3.84218×10^{-8}
3 mL, r.t.	5 mol%	3.01777×10^{-8}
6 mL, r.t.	2.5 mol%	2.48×10^{-8}
3 mL, r.t.	2.5 mol%	$1.93\ E \times 10^{-8}$
3 mL, 0 °C	5 mol%	1.59×10^{-8}

7.3.3.16. Turnover number (TON) calculations.

Preliminary saturated solution calculations:

Experiment 1: The diiron catalyst **Fe-2** (25.2 mg, 1.43 x 10^{-5} mol) was added in a round bottom flask equipped with a stirring magnet and slowly diluted in a solution of ethanol/water (96/4, v/v) by 5 mL step. Full solubility of **Fe-2** was reached after addition of 100 mL of solvent while stirring. No precipitation was observed after the stirring was stopped.

Experiment 2: The diiron catalyst **Fe-2** (5.3 mg, 3 x 10^{-6} mol) was added in a round bottom flask equipped with a stirring magnet and a solution of ethanol/water (6 mL, 96/4, v/v) was added. After stirring 15 min at room temperature, the mixture was filtrated and 3 mL of the homogeneous solution filtrated were evaporated giving 0.7 mg of the **Fe-2** catalyst.

With these two experiment in hand, we can approximate the solubility of the **Fe-2** catalyst to be = (0.7/3 + 25.2/100)/2 = 0.24 $mg.mL^{-1}$.

TON determination experiment: To an oven dried schlenk flask was added mL of a saturated solution of the diiron catalyst **Fe-2** (11 µL, 2.64 x 10^{-6} mg, 1.5 x 10^{-9} mol, 1 x 10^{-6} equiv.), EtOH/H_2O (96/4) (27 mL), tert-butylstyrène (0.480 g, 0.549 mL, 3 x 10^{-3} mol, 1 equiv.), $PhSiH_3$ (0.974 g, 1.11 mL, 9 x 10^{-3} mol, 3 equiv.). A ballon filled with air was added onto the schlenk and the reaction mixture was stirred at room temperature or at 50°C for 1 week. Conversion and estimated yield were monitored by GC-MS. Small aliquots of the solution were taken every 24h for 120h. No conversion of alkene was detected after 48h of reaction. The final TON calculated is an average value of 4 different estimated yield taken after 48, 72, 96 and 120h of reaction respectively.

Entry	temperature	TON	Yield (%)
1	20°C	32 500	3.25
2	50°C	190 000	19

Table 10: TON observed at different temperature

7.3.3.17. Control experiments.

Alkene oxidation reaction without silane reductant: The diiron catalyst **Fe-2** (14.2 mg, 0.008 mmol, 0.025 equiv.), EtOH/H_2O (3 mL, 96/4, v/v), *tert*-butylstyrene (52 mg, 60 µL, 0.325 mmol, 1 equiv.) and dodecane (0.081 mmol, 0.25 equiv.) were added to an oven-dried Schlenk flask. A balloon filled with air was placed onto the Schlenk tube and the reaction mixture was stirred at room temperature for 24 hours. Traces of starting material conversion and product formation were detected (<5%).

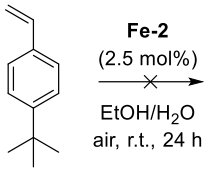

Alkene oxidation reaction without catalyst: EtOH/H_2O (3 mL, 96/4, v/v), *tert*-butylstyrene (52 mg, 60 µL, 0.325 mmol, 1 equiv.), $PhSiH_3$ (102 mg, 117 µL, 0.975 mmol, 3 equiv.) and dodecane (0.081 mmol, 0.25 equiv.) were added to an oven-dried Schlenk flask. A balloon filled with air was placed onto the Schlenk tube and the reaction mixture was stirred at room temperature for 24 hours. No traces of starting material conversion nor product formation were detected.

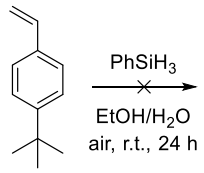

Alkene oxidation reaction under argon atmosphere: The diiron catalyst **Fe-2** (14.2 mg, 0.016 mmol, 0.025 equiv.), EtOH/H_2O (3 mL, 96/4, v/v), *tert*-butylstyrene (52 mg, 60 µL, 0.325 mmol, 1 equiv.), $PhSiH_3$ (102 mg, 117 µL, 0.975 mmol, 3 equiv.) and dodecane (0.081 mmol, 0.25 equiv.) were added to an oven-dried Schlenk flask. The schlenk was flushed 4 times using argon and kept under 1 argon atmosphere. The reaction mixture was stirred at room temperature for 24 hours. No traces of starting material conversion nor product formation were detected.

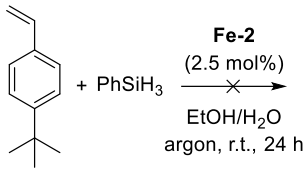

Comment: This reaction clearly demonstrate that oxygen coming from the air atmosphere is the source of oxygen in the observed product (as described elsewhere).[3]

Alcohol oxidation reaction: The diiron catalyst **Fe-2** (14.2 mg, 0.008 mmol, 0.025 equiv.), EtOH/H_2O (3 mL, 96/4, v/v), racemic phenylethanol (40 mg, 40 µL, 0.325 mmol, 1 equiv.), $PhSiH_3$ (102 mg, 117 µL, 0.975 mmol, 3 equiv.) and dodecane (0.081 mmol, 0.25 equiv.) were added to an oven-dried Schlenk flask. A balloon filled with air was placed onto the Schlenk

tube and the reaction mixture was stirred at room temperature for 24 hours. No traces of starting material conversion nor product formation were detected.

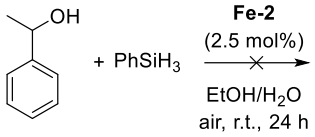

Comment: The absence of alcohol reactivity indicate that its formation during the course of reaction is due to an irreversible side reaction rather than an intermediate species produced in situ.

Alkene oxidation reaction with FeClTPP as pre-catalyst: The iron pre-catalyst **FeClTPP** (11.2 mg, 0.016 mmol, 0.05 equiv.), EtOH/H_2O (6 mL, 96/4, v/v), *tert*-butylstyrene (52 mg, 60 µL, 0.325 mmol, 1 equiv.), a silane and dodecane (0.081 mmol, 0.25 equiv.) were added to an oven-dried Schlenk flask. A balloon filled with air was placed onto the Schlenk tube and the reaction mixture was stirred at room temperature for 24 hours. Conversion and yield were monitored by GC using dodecane as the internal standard.

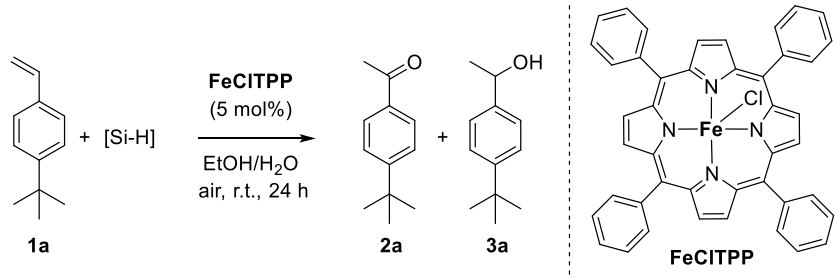

Table S11. Wacker-type oxidation using **FeClTPP** and silane derivatives.

Entry	Silane	Time (h)	Conv. (%)	Ketone (%)	Alcohol (%)	other side-products (%)
1	Et_3SiH	24	0	0	0	0
2	$PhSiH_3$	4	>99	81	8	11

Comment: FeClTPP is a reactive catalyst for Wacker-type oxidation using $PhSiH_3$ and not reactive at all using Et_3SiH as it was reported elsewhere.[3] The selectivity between ketone and alcohol product is worse than with **Fe-2**. The quantity of hydrogenated and dimer side-products increase to reach 11% of the total product. Moreover, no efficient protocol beyond SiO_2 column chromatography process was effective to recover the catalyst, in sharp contrast with **Fe-2** tetracarboxylic porphyrin.

Alkene oxidation reaction using FeTPP(Cl) and benzoic acid: The iron pre-catalyst FeClTPP (11.2 mg, 0.016 mmol, 0.05 equiv.), benzoic acid (8 mg, 0.065 mmol, 0.20 equiv.), EtOH/H_2O (6 mL, 96/4, v/v), *tert*-butylstyrene (52 mg, 60 µL, 0.325 mmol, 1 equiv.), $PhSiH_3$ (102 mg, 117 µL, 0.975 mmol, 3 equiv.) and dodecane (0.081 mmol, 0.25 equiv.) were added to an oven-dried Schlenk flask. A balloon filled with air was placed onto the Schlenk tube and the reaction

mixture was stirred at room temperature. A conversion of 10% and 9% of ketone product was estimated by GC-MS and GC-FID.

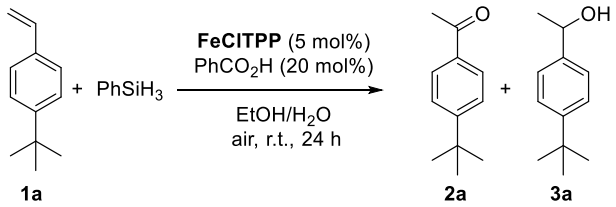

Alkene oxidation reaction with addition of base: The diiron catalyst **Fe-2** (14.2 mg, 0.008 mmol, 0.025 equiv.), K_2CO_3 (9 mg, 0.065 mmol, 0.20 equiv.), EtOH/H_2O (6 mL, 96/4, v/v), *tert*-butylstyrene (52 mg, 60 µL, 0.325 mmol, 1 equiv.), $PhSiH_3$ (102 mg, 117 µL, 0.975 mmol, 3 equiv.) and dodecane (0.081 mmol, 0.25 equiv.) were added to an oven-dried Schlenk flask. A balloon filled with air was placed onto the Schlenk tube and the reaction mixture was stirred at room temperature. No conversion was detected by GC-MS and GC-FID analysis.

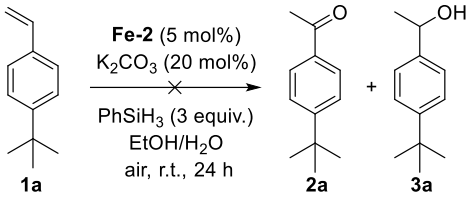

Comment: The lack of reactivity can be ascribed to the importance of the carboxylic acid group or to the poor solubility of the catalyst upon full deprotonation in the reaction media.

Alkene oxidation reaction in the presence of a radical scavenger: The diiron catalyst **Fe-2** (14.2 mg, 0.016 mmol, 0.025 equiv.), TEMPO (51 mg, 0.325 mmol, 1 equiv.), EtOH/H_2O (6 mL, 96/4, v/v), *tert*-butylstyrene (52 mg, 60 µL, 0.325 mmol, 1 equiv.), $PhSiH_3$ (102 mg, 117 µL, 0.975 mmol, 3 equiv.) and dodecane (0.081 mmol, 0.25 equiv.) were added to an oven-dried Schlenk flask. A balloon filled with air was placed onto the Schlenk tube and the reaction mixture was stirred at room temperature. No conversion as well as no product formation was detected by GC-MS analysis strongly suggesting that the iron Wacker oxidation process via a radical pathway.

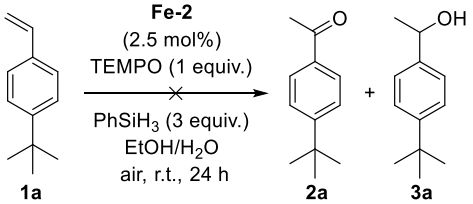

7.3.3.18. Study of the catalytic outcome depending on the order of addition of the reagents.

Addition of olefin in the last step.

Alkene oxidation reaction: The diiron catalyst **Fe-2**, EtOH/H_2O (3 mL, 96/4, v/v), $PhSiH_3$ (102 mg, 117 µL, 0.975 mmol, 3 equiv.) and dodecane (0.081 mmol, 0.25 equiv.) were added to an oven-dried Schlenk flask. The reaction mixture was stirred at room temperature for 30 minutes and 2,4-dimethylstyrene (43 mg, 47 µL, 0.325 mmol, 1 equiv.) was added. A balloon filled with air was placed onto the Schlenk tube and the reaction mixture was kept stirring for 24 hours. Conversion and yield were monitored by GC using dodecane as the internal standard.

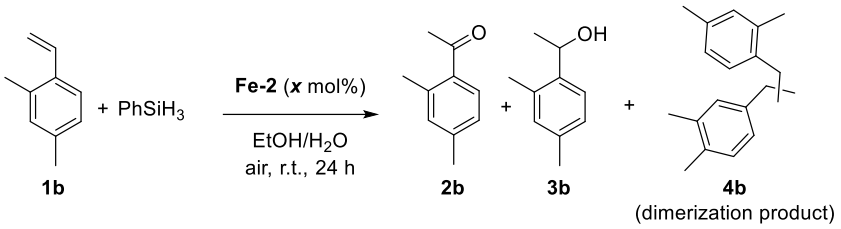

Table S12. Iron-catalyzed reductive dimerization of olefin **1b**.

Entry	***x***	Conv. (%)	Ketone (%)	Alcohol (%)	Dimer (%)
1	5	>99	46	19	35
2	10	78	17	6	55

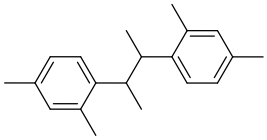

Bibenzyl-α,α',2,2',4,4'-tetramethyl (4b): The dimer product **4b** was isolated following the general procedure described above and it was purified (10 mg, 22% yield) by column chromatography (SiO_2, EtOAc/heptane (0:1 to 1:9, v/v). ^1H NMR (400 MHz, $CDCl_3$): δ = 7.19 (d, *J* = 7.9 Hz, 1H), 7.07 (d, *J* = 7.9 Hz, 2H),7.06 (s, 1H), 7.05 – 6.99 (m, 2H), 6.87 (dd, *J* = 7.1, 1.7 Hz, 1H), 6.80 (d, *J* = 1.7 Hz, 1H), 3.25 (tdd, *J* = 6.9, 4.8, 2.8 Hz, 1H), 3.2 –3.16 (m, 1H), 2.36 (s, 3H), 2.33 (s, 3H), 2.21 (s, 3H), 2.16 (s, 3H), 1.32–1.22 (m, 3H), 1.03 – 0.87 (m, 3H) ppm. $^{13}C\{^1H\}$ NMR (101 MHz, $CDCl_3$): δ = 142.30, 142.01, 135.68, 134.80, 134.75, 134.43, 130.95, 130.76, 126.97, 126.39, 126.15, 39.64, 20.93, 20.83, 20.42, 20.09, 19.99, 19.63 ppm. HRMS (ESI): *m/z* calcd for $C_{24}H_{35}$: 323.27333 $[M+H]^+$; found: 323.2737 (1 ppm).

Comment: Using GC-MS spectroscopy two picks corresponding to different dimerization product were detected at the end of reaction. The mass fragmentation suggests that only branched:linear or branched:branched dimer product may correspond to the two fragmentation pick observed. The product structure detected by GC-MS and the increased quantity formed following catalyst loading increase indicate that the dimerization step is probably made possible after hydrometalation/hydrogen radical addition of the C-C styrene double bond (Scheme S7). Integration of the two dimer picks by GC and GC-MS shows that they are produced approximatively in the same amount (± 2%), for every substrate tested. The hydrogen required to quench the reaction to yield the fully hydrogenated dimer product can originate from iron hydride formed in situ, $PhSiH_3$ starting material or byproduct or both protic solvent used (EtOH or H_2O). On the other hand, no dimerization product were detected for aliphatic C-C double bond using these experimental conditions.

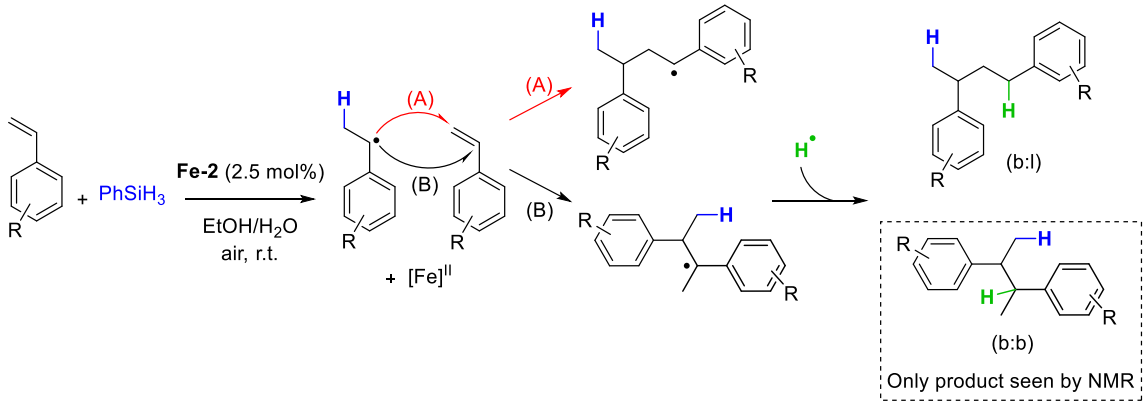

Scheme S7. Proposed mechanism for iron-catalyzed reductive styrene dimerization.

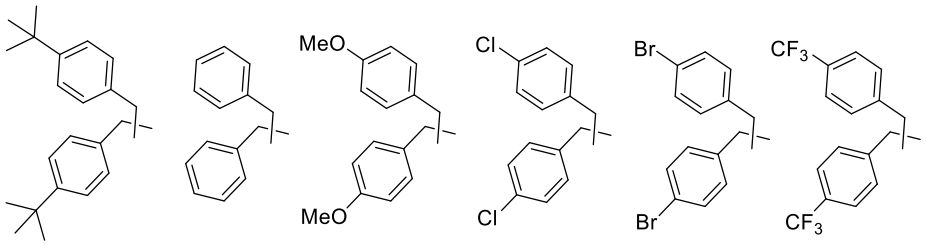

Figure S18. Other dimerization products derived from the iron-catalyzed reductive homo-coupling detected by GC-MS.

The GC-MS retention and fragmentation of all dimer product detected are listed below. In every case, two pick having the same molar mass, corresponding to dimer products were detected in a 1:1 ratio.

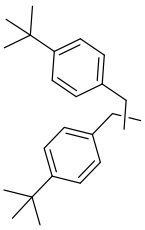

Bibenzyl, α,α′,4,4′-ditertbutyl: GC: t_R = 12.5; 13.0 min; MS (EI): *m/z* = 322 (M^+, 1), 207 (3), 161 (100), 146 (10), 131 (10), 117 (5), 105 (5), 91 (5), 57 (15).

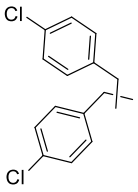

Bibenzyl, α,α′,4,4′-dichloro: GC: t_R = 11.9; 12.2 min; MS (EI): *m/z* = 278 (M^+, 1), 139 (100), 103 (40), 77 (20).

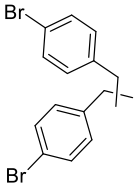

Bibenzyl, α,α′,4,4′-dibromo: GC: t_R = 23.5; 24.2 min; MS (EI): *m/z* = 368 (M^+, 1), 183 (100), 104 (100), 77 (20).

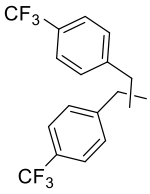

Bibenzyl, α,α′,4,4′-di-trifluoromethyl: GC: t_R = 14.2; 14.8 min; MS (EI): *m/z* = 346 (M^+, 1), 327 (3), 173 (100), 153 (25), 133 (30), 127 (10), 77 (2).

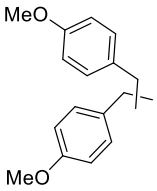

Bibenzyl, α,α′,4,4′-dimethoxy: GC: t_R = 25.8; 27.3 min; MS (EI): *m/z* = 270 (M^+, 1), 135 (100), 105 (10), 91 (6), 79 (5).

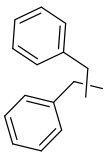

Bibenzyl, α,α′,: GC: t_R = 15.1; 15.4 min; MS (EI): *m/z* = 210 (M^+, 1), 105 (100), 91 (5), 77 (15).

Addition of silane in the last step.

Alkene oxidation reaction: The diiron catalyst **Fe-2** (14.2 mg, 0.008 mmol, 0.025 equiv.), EtOH/H_2O (6 mL, 96/4, v/v), 2,4 dimethylstyrene (43 mg, 47µL, 0.325 mmol, 1 equiv.) and dodecane (0.081 mmol, 0.25 equiv.) were added to an oven-dried Schlenk flask. The reaction mixture was stirred at room temperature for 30 minutes and $PhSiH_3$ (102 mg, 117 µL, 0.975 mmol, 3 equiv.) was added. A balloon filled with air was placed onto the Schlenk tube and the reaction mixture was kept stirring for 24 hours. Conversion and yield were monitored by GC using dodecane as the internal standard. This experiment was run two times showing only traces amount (< 1%) of the dimeric species **4b**.

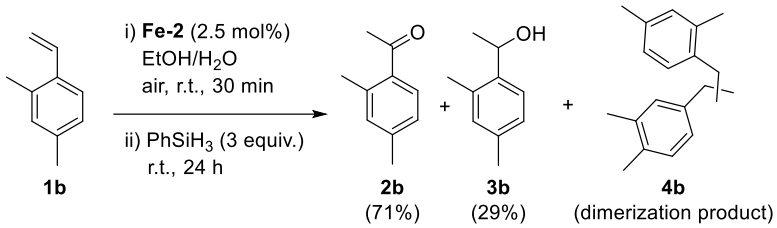

Comment: The order of addition is of high importance since the dimer byproduct **4** can become the major compound produced or can only be detected as traces amount (<1%) depending on the experimental procedure.

7.3.3.19. Wacker-type oxidation of allyl derivatives: unexpected reactivity investigation.

Allyl alkene oxidation reaction: The diiron catalyst **Fe-2** (14 mg, 0.008 mmol, 0.025 equiv.), EtOH/H_2O (6 mL, 96/4, v/v), an allyl derivative (0.325 mmol, 1 equiv.), dodecane (0.081 mmol, 18.4 µL, 0.25 equiv.) and, lastly, $PhSiH_3$ (102 mg, 117 µL, 0.975 mmol, 3 equiv.) were added to an oven-dried Schlenk flask. A balloon filled with air was placed onto the Schlenk tube and the reaction mixture was stirred at room temperature until completion of the reaction as monitored by GC-MS and TLC chromatography.

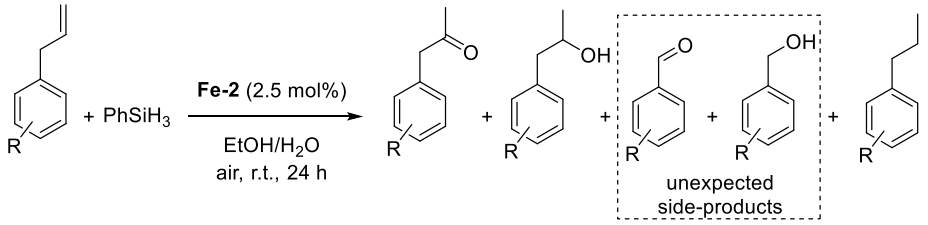

Benzaldehyde and benzyl alcohols (framed in the scheme above) were produced in low to moderate yield. It can be explain by an iron-catalyzed O_2-mediated fragmentation of an iron-peroxy intermediate (Scheme S8). The rearrangement is favored at the benzylic position. Aldehyde formation can be explained by β elimination of intermediate **A**. Simple quench of intermediate **A** by a hydrogen radical may produce the benzylic alcohol observed by GC-MS. Acetaldehyde side-product was not detected by GC-MS analysis due to its low boiling point.

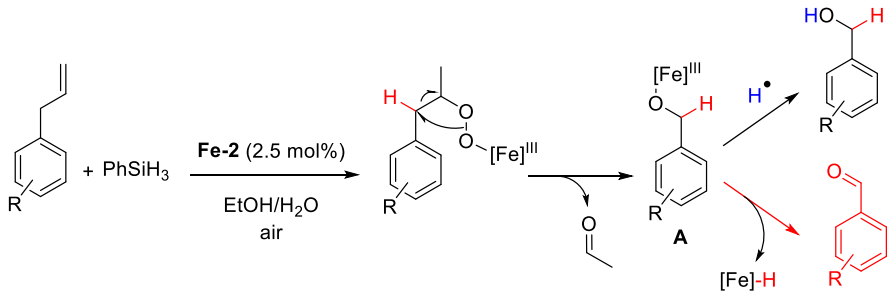

Scheme S8. Proposed mechanism for the iron-catalyzed benzallylic rearrangement

Interestingly, no fragmentation/rearrangement was detected for cyclohexane allyl, indicating that the benzyl group plays a critical role to yield benzaldehyde and benzyl alcohol (see below).

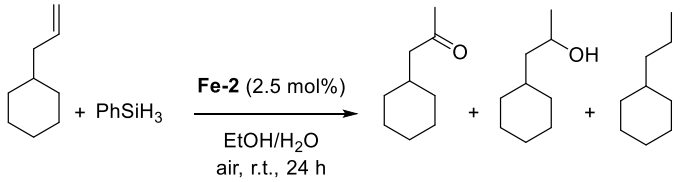

7.3.3.19. Recyclability of the iron catalyst.

Acid-base work-up recovery of the iron catalyst: The diiron catalyst **Fe-2** (14.2 mg, 0.008 mmol, 0.025 equiv.), EtOH/H_2O (6 mL, 96/4, v/v), *tert*-butylstyrene (52 mg, 60 µL, 0.325 mmol, 1 equiv.), $PhSiH_3$ (102 mg, 117 µL, 0.975 mmol, 3 equiv.) and dodecane (0.081 mmol, 0.25 equiv.) were added to an oven-dried Schlenk flask. A balloon filled with air was placed onto the Schlenk tube and the reaction mixture was stirred at room temperature for 3 hours. The reaction mixture was evaporated and DCM (or EtOAc) and NaOH (1M) (1:1) was added. The organic phase was extracted 3 times and further purified by SiO_2 column chromatography to yield the pure product. The aqueous phase was acidified with HCl (1M) in order to reach approximatively pH = 1 (paper pH test). Precipitation of the catalyst was observed and it was recovered by filtration. The catalyst was dissolved in EtOH (99.95%) and added into an oven-dried Schlenk flask. After evaporation of the solvent, EtOH/H_2O (6 mL, 96/4, v/v), *tert*-butylstyrene (52 mg, 60 µL, 0.325 mmol, 1 equiv.), $PhSiH_3$ (102 mg, 117 µL, 0.975 mmol, 3 equiv.) and dodecane (0.081 mmol, 0.25 equiv.) were added. A balloon filled with air was placed onto the Schlenk tube and the reaction mixture was stirred at room temperature for 4 hours. Conversion and yield were monitored by GC using dodecane as the internal standard (Table S13). The longer reaction time required for the second run (Table S13, entry 2) was ascribed to the small loss of catalyst loading during the filtration process. It is important to note that the reaction mixture should be quenched/evaporated after full conversion of the styrene starting material as it was found that the catalyst partially decompose itself upon unnecessary long exposure time.

Table S13. Recyclability and reusability of the iron catalyst.

Entry	run	Time (h)	Conversion (%)	Ketone (%)	Alcohol (%)
1	1	4	>99	92	8
2	2	4.5	>99	93	7

Recovery of the iron catalyst by precipitation in a non-polar organic solvent: The diiron catalyst **Fe-2** (14.2 mg, 0.008 mmol, 0,025 equiv.), EtOH/H_2O (6 mL, 96/4, v/v), *tert*-butylstyrene (52 mg, 60 µL, 0.325 mmol, 1 equiv.), $PhSiH_3$ (102 mg, 117 µL, 0.975 mmol, 3 equiv.) and dodecane (0.081 mmol, 0.25 equiv.) were added to an oven-dried Schlenk flask. A balloon filled with air was placed onto the Schlenk tube and the reaction mixture was stirred at room temperature for 3 hours. The reaction mixture was evaporated, and then DCM (or EtOAc) was added. Filtration of the crude mixture and washing with DCM (or EtOAc) allows the recovery of catalyst from the organic mixture. The pure ketone product was further purified by SiO_2 column chromatography. In parallel the catalyst was dissolved in EtOH

(99.95%) and the mixture was evaporated in a previously weighted round bottom flask (12 mg, 85% recovered yield).

7.3.3.20. Temporal control of the oxidation reaction.

Temporal control of the oxidation reaction by *in situ* switch of the atmosphere: The diiron catalyst **Fe-2** (28.4 mg, 0.016 mmol, 0.025 equiv.), EtOH/H_2O (12 mL, 96/4, v/v), *tert*-butylstyrene (104 mg, 120 µL, 0.650 mmol, 1 equiv.), $PhSiH_3$ (204 mg, 234 µL, 1.950 mmol, 3 equiv.) and dodecane (0.162 mmol, 0.25 equiv.) were added to an oven-dried Schlenk flask. A balloon filled with air was placed onto the Schlenk tube and the reaction mixture was stirred at room temperature. After 30 minutes, the reaction mixture was flushed with argon for 5 minutes and stirred under argon (1 bar). After 150 minutes, the reaction mixture was flushed with air for 5 minutes and stirred under air (1 atm) for 300 additional minutes. During the course of this study, small aliquots were taken every 15 min up to full conversion of the starting material (monitored by TLC) at 300 min of reaction. Fitted values are shown in Figure S19.

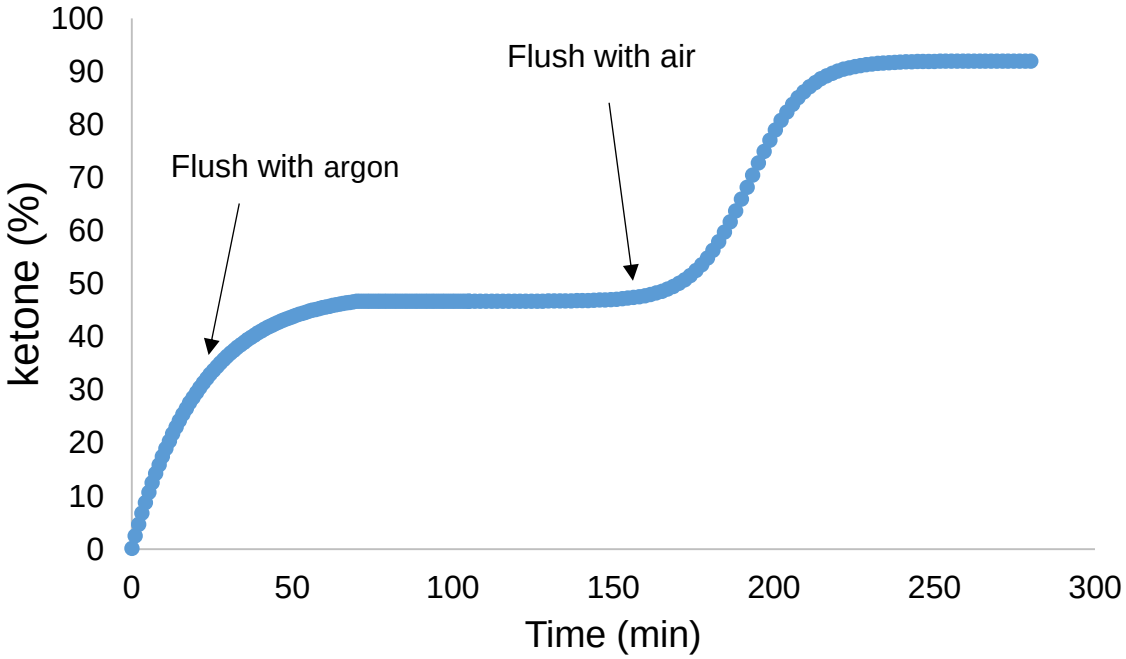

Figure S19. Temporal control of the Fe-catalyzed Wacker-type oxidation by switching the atmosphere.

Temporal control of the oxidation reaction by *in situ* switch of acid/base reaction conditions: The diiron catalyst **Fe-2** (28.4 mg, 0.016 mmol, 0.025 equiv.), EtOH/H_2O (12 mL, 96/4, v/v), *tert*-butylstyrene (104 mg, 120 µL, 0.650 mmol, 1 equiv.), $PhSiH_3$ (204 mg, 234 µL, 1.950 mmol, 3 equiv.) and dodecane (0.162 mmol, 0.25 equiv.) were added to an oven-dried Schlenk flask. A balloon filled with air was placed onto the Schlenk tube and the reaction mixture was stirred at room temperature. After 60 minutes, NEt_3 (19.7 mg, 27 µL, 0.195 mmol, 0.3 equiv.) was added to the reaction mixture. After additional 120 minutes, TFA (37 mg, 25 µL, 0.325 mmol,

0.5 equiv.) was added to the reaction mixture. During the course of this study, small aliquots were taken every 15 min (and analyzed by GC-MS and GC-FID) up to full conversion of the starting material (monitored by TLC) at 400 min of reaction. Fitted values are shown in **Figure 2** in the main text of the manuscript.

7.3.4. Synthesis and characterization of the iron hydride species.

Fe-2 complex characterization: The diiron catalyst **Fe-2** (8 mg, 0.0045 mmol) and DMSO-d_6 (0.5 mL) were added to an oven-dried NMR tube. The NMR tube was vigorously shaken and set for ^{1}H NMR analysis (Figure S20).

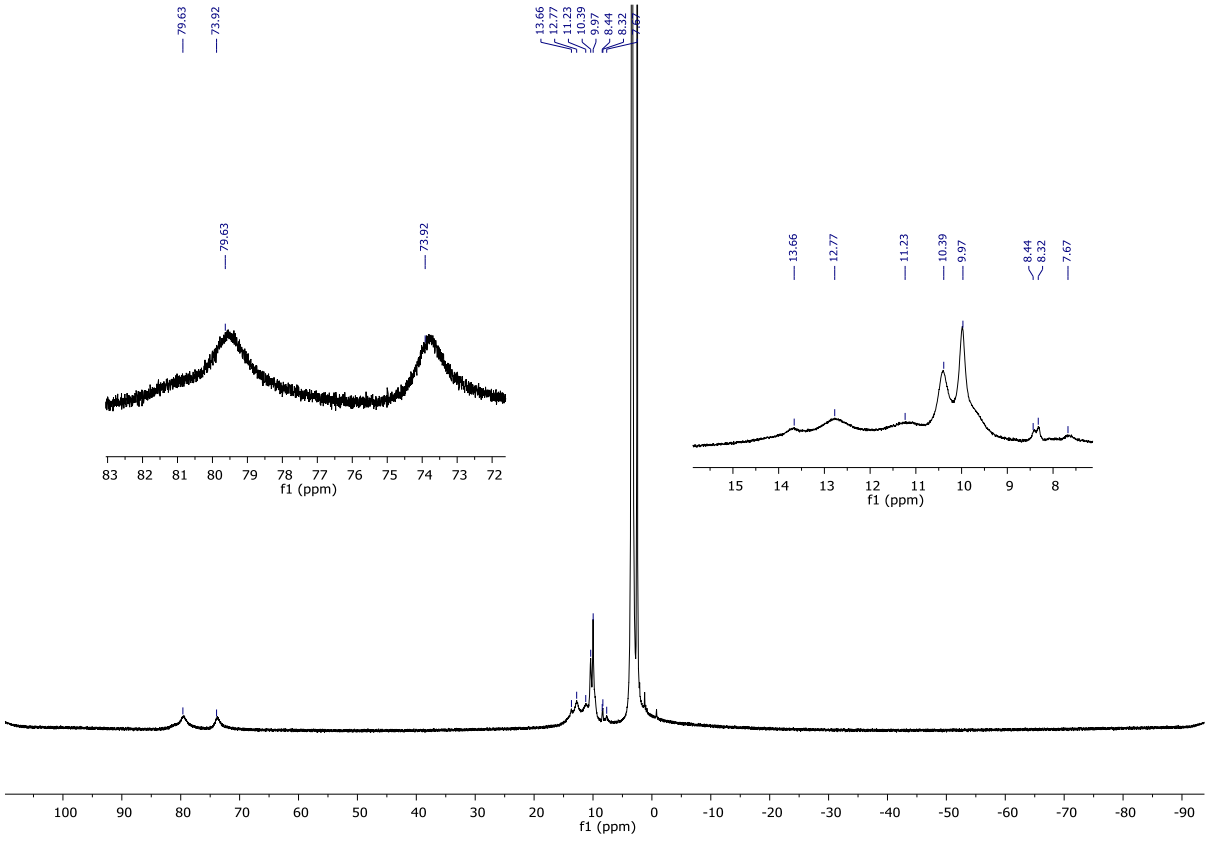

Figure S20. ^{1}H NMR (DMSO-d_6, 400 MHz) spectrum of **Fe-2**.

Fe-H synthesis and characterization: The diiron catalyst **Fe-2** (same batch as used above, 8 mg, 0.0045 mmol, 1 equiv.), $PhSiH_3$ (1.1 mg, 1.3 µL, 0.11 mmol, 24 equiv.), and DMSO-d_6 (0.5 mL) were added to an oven-dried NMR tube. The NMR tube was vigorously shaken and set for ^{1}H NMR analysis (Figure S21). The pyrrole β hydrogen signals were shifted from δ = 75-80 ppm to δ = 8.27-8.40 ppm, a clear evidence of the carboxylic acid group at δ = 11.7 ppm and the apparition of a signal at δ = –20.1 ppm that was abscribed to the metal hydride produced in situ. The ^{1}H *meso*-phenyl hydrogen atoms are overlapping with the aromatic phenylsilane hydrogens (note that $PhSiH_3$ is in large excess in the reaction mixture).

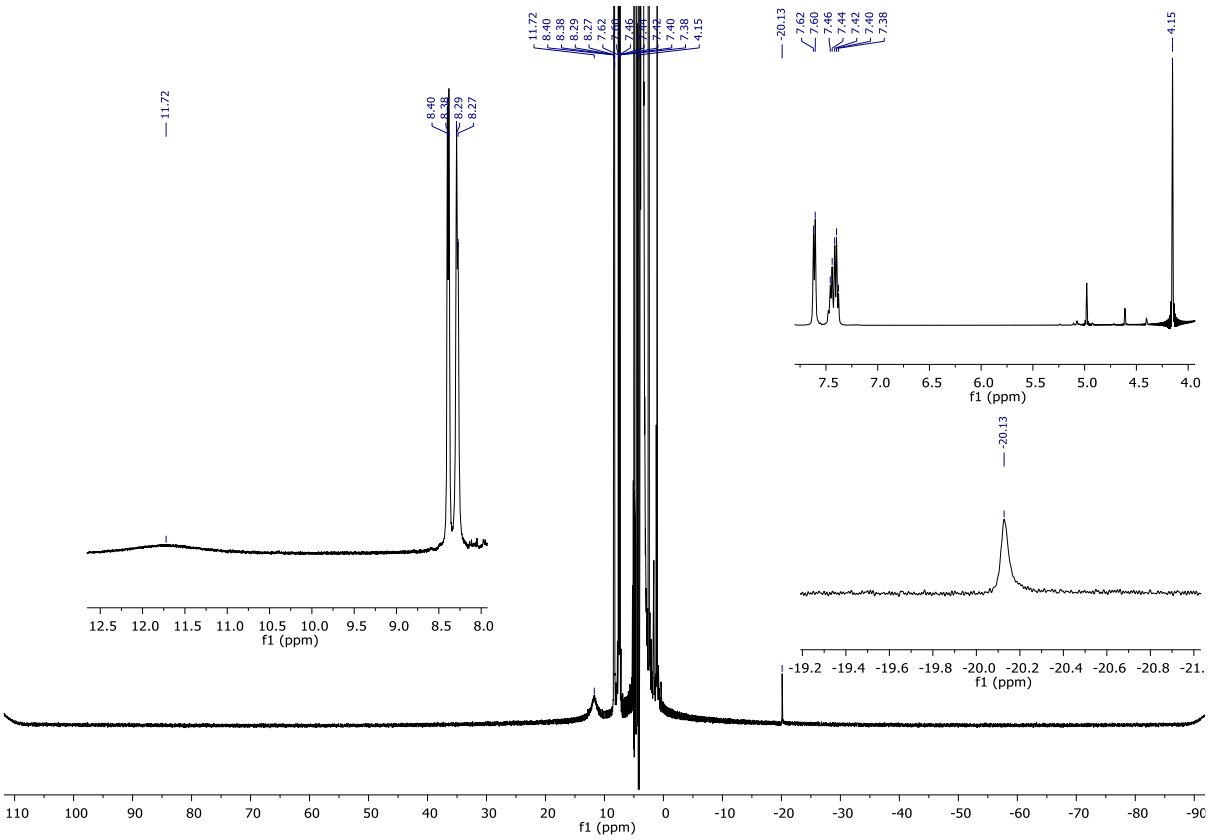

Figure S21. ^{1}H NMR (DMSO-d_6, 400 MHz) spectrum of **Fe-2** upon addition of $PhSiH_3$: Fe-H evidence.

7.3.5. Substrate scope of the iron-catalyzed Wacker-type oxidation reaction and product characterization.

General procedure of the catalysis: The diiron catalyst **Fe-2** (14 mg, 0.008 mmol, 0.025 equiv.), an alkene derivative **1** (0.325 mmol, 1 equiv.), EtOH/H_2O (12 mL, 96/4, v/v), dodecane (0.081 mmol, 18.4 µL, 0.25 equiv.) and, lastly, $PhSiH_3$ (102 mg, 117 µL, 0.975 mmol, 3 equiv.) were added to an oven-dried Schlenk flask. A balloon filled with air was placed onto the Schlenk tube and the reaction mixture was stirred at room temperature until completion of the reaction monitored by GC-MS and TLC chromatography. Then, the reaction mixture was evaporated and the pure ketone product **2** was isolated by SiO_2 column chromatography using EtOAc/heptane as the eluent. Note that in some cases, notably with styrene derivatives, long exposure to vacuum under the Schlenk line may sublimate the final ketone product. In this case, the reaction was purified by SiO_2 column chromatography using EtOAc/pentane as the eluent (same ratio) and the product fraction was kept for 30 min under Schlenk line vacuum.

Each substrate was evaluated at least 3 times and the given data is an average value of 2 to 3 catalysis reaction.

Derivatization procedure for aliphatic olefins: After completion of the reaction, the volatiles were evaporated under reduced pressure and EtOAc and NaOH (1M) were added. The aqueous phase was extracted with EtOAc (x 3) and the combined organic layer was washed with brine solution. After drying over $MgSO_4$ and filtration, the solvents were evaporated under reduced pressure. Then, EtOH (3 mL) and a solution of previously prepared 2,4-dinitrophenylhydrazine (DNPH) solution (8 mL) was added. The reaction mixture was stirred overnight and then evaporated under reduced pressure. EtOAc and a saturated solution of $NaHCO_3$ were added. The organic layer was separated and the aqueous layer was extracted with EtOAc (x 3). The combined organic layer was washed with brine solution. After drying over $MgSO_4$ and filtration, the solvents were evaporated under reduced pressure. The derivatized ketone product was purified by SiO_2 column chromatography using EtOAc/heptane as the eluent.

DNPH solution preparation: 2,4-Dinitrophenylhydrazine (3 g, 1.51 x10 $^{-2}$ mol) was solubilized in 30 mL of H_2SO_4. Then, it was slowly dissolved (exothermic reaction) in a EtOH/H_2O solution (90 mL, 7:2, v/v). The mixture was stirred at room temperature for 5 minutes and kept at 4°C until it was used. Experimental procedure adapter from reference [4].

For styrene derivatives as the substrates:

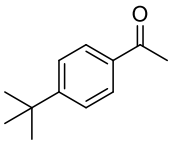

4-*tert*-Butylacetophenone (2a): Starting from 4-*tert*-butylstyrene (**1a**) and following the general procedure, the reaction mixture was stirred for 3 hours. Quantitative conversion was estimated by GC-MS and GC (FID) analysis showing the formation of 92% of ketone product **2a**, 8% of alcohol **3a** (not isolated) and traces of hydrogenated and dimerized side-products. Purification by SiO_2 column chromatography using EtOAc/heptane (0/1 to 1/5, v/v) eluent afforded the analytically pure ketone product **2a** (50 mg, 87% yield). ^{1}H NMR (400 MHz, $CDCl_3$): δ = 7.90 (d, *J* = 8.6 Hz, 1H), 7.48 (d, *J* = 8.6 Hz, 2H), 2.58 (s, 3H), 1.34 (s, 9H) ppm. $^{13}C\{^1H\}$ NMR (101 MHz, $CDCl_3$): δ = 197.82, 156.81, 134.64, 128.29, 125.50, 35.11, 31.10, 26.54 ppm. The spectral data match those found in literature.[5]

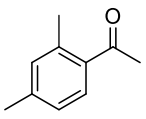

2-4-Dimethylacetophenone (2b): Starting from 2,4-dimethylstyrene (**1b**) and following the general procedure, the reaction mixture was stirred for 4 hours. Quantitative conversion was estimated by GC-MS and GC (FID) analysis showing the formation of 71% of ketone product **2b**, 29% of alcohol **3b** (not isolated) and traces of hydrogenated and dimerized side-products. Purification by SiO_2 column chromatography using EtOAc/heptane (0/1 to 1/5, v/v) eluent afforded the analytically pure ketone product **2b** (32 mg, 67 % yield.). ^{1}H NMR (400 MHz, $CDCl_3$): δ = 7.63 (d, *J* = 8.0 Hz, 1H), 7.06 (d, *J* = 8.0 Hz, 1H), 7.06 (s, 1H) 2.56 (s, 3H), 2.52 (s, 3H), 2.35 (s, 3H) ppm. $^{13}C\{^1H\}$ NMR (101 MHz, $CDCl_3$): δ = 201.00, 142.13, 138.92, 134.72, 132.92, 129.96, 126.29, 29.33, 21.78, 21.34 ppm. The spectral data match those found in literature.[6]

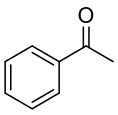

Acetophenone (2c): Starting from styrene (**1c**) and following the general procedure, the reaction mixture was stirred for 4 hours. Quantitative conversion was estimated by GC-MS and GC (FID) analysis showing the formation of 96% of ketone product **2c**, 4% of alcohol **3c** (not isolated) and traces of hydrogenated and dimerized side-products. Purification by SiO_2 column chromatography using EtOAc/heptane (0/1 to 1/5, v/v) eluent afforded the analytically pure ketone product **2c** (32 mg, 82% yield.). ^{1}H NMR (400 MHz, $CDCl_3$): δ = 7.94 (dd, *J* = 7.1, 1.5 Hz, 2H), 7.54 (td, *J* = 7.1, 1.5 Hz, 1H), 7.44 (t, *J* = 7.1 Hz, 2H), 2.58 (s, 3H) ppm. $^{13}C\{^1H\}$ NMR (101 MHz, $CDCl_3$): δ = 198.09, 137.12, 133.08, 128.55, 128.28, 26.58 ppm. The spectral data match those found in literature.[7]

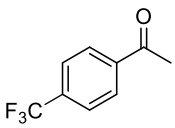

4-Trifluoromethyl-acetophenone (2d): Starting from 4-trifluoromethylstyrene (**1d**) and following the general procedure, the reaction mixture was stirred for 4 hours. Quantitative conversion was estimated by GC-MS and GC (FID) analysis showing the formation of 96% of ketone product **2d**, 4% of alcohol **3d** (not isolated) and traces of hydrogenated and dimerized side-products. Purification by SiO_2 column chromatography using EtOAc/heptane (0/1 to 1/5, v/v) eluent afforded the analytically pure ketone product **2d** (53 mg, 86% yield.). ^{1}H NMR (400 MHz, $CDCl_3$): δ = 8.06 (d, *J* = 8.0 Hz, 1H), 7.73 (d, *J* = 8.0 Hz, 1H), 2.64 (s, 3H) ppm. $^{13}C\{^1H\}$ NMR (101 MHz, $CDCl_3$): δ = 196.92, 139.68, 134.41 (q, *J* = 32.7 Hz), 128.60, 125.65 (q, *J* = 3.8 Hz), 123.59 (d, *J* = 272.5 Hz), 26.73 ppm. $^{19}F\{^1H\}$ NMR (376 MHz, $CDCl_3$): δ = -63.18 ppm. The spectral data match those found in literature.[8]

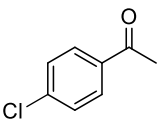

4-Chloroacetophenone (2e): Starting from 4-chlorostyrene (**1e**) and following the general procedure, the reaction mixture was stirred for 4 hours. Quantitative conversion was estimated by GC-MS and GC (FID) analysis showing the formation of 96% of ketone product **2e**, 4% of alcohol **3e** (not isolated) and traces of hydrogenated and dimerized side-products. Purification by SiO_2 column chromatography using EtOAc/heptane (0/1 to 1/5, v/v) eluent afforded the analytically pure ketone product **2e** (36 mg, 71% yield.). ^{1}H NMR (400 MHz, $CDCl_3$): δ = 7.89 (d, *J* = 8.6 Hz, 2H), 7.44 (d, *J* = 8.6 Hz, 2H), 2.59 (s, 3H) ppm. $^{13}C\{^1H\}$ NMR (101 MHz, $CDCl_3$): δ = 196.81, 139.58, 135.45, 129.73, 128.90, 26.56 ppm. The spectral data match those found in literature.[9]

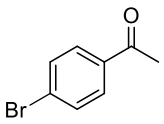

4-Bromoacetophenone (2f): Starting from 4-bromostyrene (**1f**) and following the general procedure, the reaction mixture was stirred for 4 hours. Quantitative conversion was estimated by GC-MS and GC (FID) analysis showing the formation of 96% of ketone product **2f**, 4% of alcohol **3f** (not isolated) and traces of hydrogenated and dimerized side-products. Purification by SiO_2 column chromatography using EtOAc/heptane (0/1 to 1/5, v/v) eluent afforded the analytically pure ketone product **2f** (54 mg, 83% yield.). ^{1}H NMR (400 MHz, $CDCl_3$): δ = 7.81 (d, *J* = 8.6 Hz, 2H), 7.59 (d, *J* = 8.6 Hz, 2H), 2.57 (s, 3H) ppm. $^{13}C\{^1H\}$ NMR (101 MHz, $CDCl_3$): δ = 196.94, 135.84, 131.88, 129.83, 128.29, 26.52 ppm. The spectral data match those found in literature.[10]

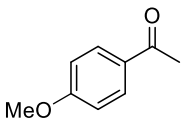

4-Methoxyacetophenone (2g): Starting from 4-methoxystyrene (**1g**) and following the general procedure, the reaction mixture was stirred for 4 hours. Quantitative conversion was estimated by GC-MS and GC (FID) analysis showing the formation of 95% of ketone product **2g**, 5% of alcohol **3g** (not

isolated) and traces of hydrogenated and dimerized side-products. Purification by SiO_2 column chromatography using EtOAc/heptane (0/1 to 1/5, v/v) eluent afforded the analytically pure ketone product **2g** (37 mg, 75% yield.). ^{1}H NMR (400 MHz, $CDCl_3$): δ = 7.91 (d, J = 8.9 Hz, 1H), 6.91 (d, J = 8.9 Hz, 2H), 3.85 (s, 3H), 2.53 (s, 3H) ppm. $^{13}C\{^1H\}$ NMR (101 MHz, $CDCl_3$): δ = 196.69, 163.48, 130.56, 130.36, 113.67, 55.44, 26.29 ppm. The spectral data match those found in literature.[11]

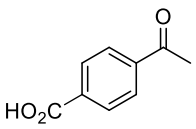

4-Carboxyacetophenone (2h): Starting from 4-vinylbenzoic acid (**1h**) and following the general procedure, the reaction mixture was stirred for 4 hours. Purification by SiO_2 column chromatography using EtOAc/heptane (0/1 to 1/0, v/v) eluent afforded the analytically pure ketone product **2h** (42 mg, 78 % yield).^{1}H NMR (400 MHz, acetone-d_6): δ = 11.52 (br, 1H), 8.11 (AB, 4H, J = 22 Hz), 2.65 (s, 3H) ppm. $^{13}C\{^1H\}$ NMR (101 MHz, acetone-d_6): δ = 198.27, 167.46, 141.94, 135.63, 131.20, 129.64, 27.53 ppm. The spectral data match those found in literature.[12]

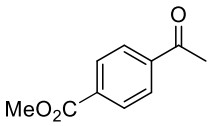

4-Methoxycarbonylacetophenone (2i): Starting from methyl 4-vinylbenzoate (**1i**) and following the general procedure, the reaction mixture was stirred for 4 hours. Quantitative conversion was estimated by GC-MS and GC (FID) analysis showing the formation of >99% of ketone product **2i**, and traces of hydrogenated and dimerized side-products. Purification by SiO_2 column chromatography using EtOAc/heptane (0/1 to 3/5, v/v) eluent afforded the analytically pure ketone product **2i** (54 mg, 94 % yield). ^{1}H NMR (400 MHz, $CDCl_3$): δ = 8.12 (d, J = 8.5 Hz, 2H), 8.00 (d, J = 8.5 Hz, 2H), 3.95 (s, 3H), 2.64 (s, 3H) ppm. $^{13}C\{^1H\}$ NMR (101 MHz, $CDCl_3$): δ = 197.48, 166.20, 140.25, 133.90, 129.81, 128.18, 52.43, 26.84 ppm. The spectral data match those found in literature.[13]

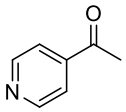

4-Acetylpyridine (2j): Starting from 4-vinylpyridine (**1j**) and following the general procedure, the reaction mixture was stirred for 16 hours. Quantitative conversion was estimated by GC-MS and GC (FID) analysis showing the formation of 91% of ketone product **2j**, 9% of alcohol **3j** (not isolated) and traces of hydrogenated side-products. Purification by SiO_2 column chromatography using EtOAc/heptane (0/1 to 4/5, v/v) eluent afforded the analytically pure ketone product **2j** (22 mg, 56 % yield). ^{1}H NMR (400 MHz, $CDCl_3$): δ = 8.83 (s, 1H), 7.73 (d, J = 5.0 Hz, 1H), 2.64 (s, 1H) ppm. The spectral data match those found in literature.[14]

For aliphatic olefin derivatives as the substrates:

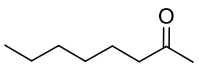

2-Octanone (2k): Starting from methyl 1-octene (**1k**) and following the general procedure, the reaction mixture was stirred for 16 hours. Quantitative conversion was estimated by GC-MS and GC (FID) analysis showing the formation of 82% of ketone product **2k**, 13% of alcohol **3k** (not isolated) and 5% of hydrogenated side-products. Purification by SiO_2 column chromatography using EtOAc/heptane (0/1 to 1/5, v/v) eluent afforded the analytically pure ketone product **2k** (33 mg, 80% yield.). ^{1}H NMR (400 MHz, $CDCl_3$): δ = 2.41 (t, J = 7.5 Hz, 2H), 2.13 (s, 3H), 1.62–1.51 (m, 2H), 1.36–1.23 (m, 7H), 0.93–0.82 (m, 3H) ppm. $^{13}C\{^1H\}$ NMR (101 MHz, $CDCl_3$): δ = 209.29, 43.82, 31.58, 29.81, 28.85, 23.84, 22.48, 14.00 ppm. The spectral data match those found in literature.[10]

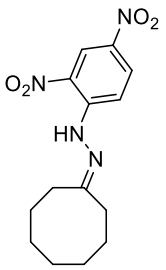

1-Cyclooctylidene-2-(2,4-dinitrophenyl)hydrazine derived from cyclooctanone (2l): Starting from cis-cyclooctene (**1l**) and following the general procedure, the reaction mixture was stirred for 16 hours. Quantitative conversion was estimated by GC-MS and GC (FID) analysis showing the formation of 85% of ketone product **2l**, 12% of alcohol **3l** (not isolated) and 3% of hydrogenated side-products. The final product was isolated as a 2,4-dinitrophenylhydrazine derivative following the general derivatization procedure (44 mg, 44% yield). ^{1}H NMR (400 MHz, $CDCl_3$): δ = 11.22 (s, 1H), 9.12 (d, J = 2.6 Hz, 1H), 8.28 (dd, J = 9.6, 2.6 Hz, 1H), 7.98 (d, J = 9.6 Hz, 1H), 2.57–2.50 (m, 4H), 1.96–1.82 (m, 4H), 1.64–1.53 (m, 4H), 1.48–1.42 (m, 2H) ppm. ^{13}C NMR (101 MHz, $CDCl_3$): δ = 164.76, 145.12, 137.52, 129.89, 128.92, 123.56, 116.37, 36.81, 28.55, 27.37, 26.28, 25.49, 24.70, 24.27 ppm. HRMS (ESI): *m/z* calcd for ($C_{14}H_{18}N_4O_4$) $[M+Na]^+$ 329.1220; found: 329.1219 (0 ppm).

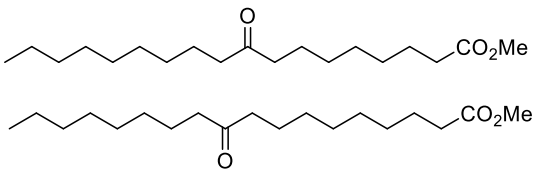

Methyl 9 (and/or 10)-oxooctadecanoate (2m): Starting from methyl oleate (**1m**) and following the general procedure, the reaction mixture was stirred for 16 hours. Quantitative conversion was estimated by GC-MS and GC (FID) analysis showing the formation of 77% of ketone products **2m**, 13% of alcohol **3m** (not isolated) and 10 % of hydrogenated side-products. Purification by SiO_2 column chromatography using EtOAc/heptane (0/1 to 1/5, v/v) eluent afforded the ketone product **2m** (65 mg, 63% yield.) with traces of phenylsilane derivative as contaminant. ^{1}H NMR (300 MHz, $CDCl_3$): δ = 3.65 (s, 3H), 2.37 (t, J = 7.4 Hz, 4H), 2.29 (t, J = 7.5 Hz, 2H), 1.68–1.48 (m, 7H), 1.35–1.19 (m, 21H), 0.90–0.83 (m, 3H) ppm. ^{13}C{^{1}H} NMR (75 MHz, $CDCl_3$): δ = 211.69, 174.29, 51.45, 42.84, 42.76, 42.71, 34.07, 34.04, 31.86, 31.82, 29.43, 29.42, 29.38, 29.27, 29.20, 29.18, 29.14, 29.07, 29.04, 28.94, 24.90, 24.86, 23.89, 23.81, 23.75, 22.66, 22.64, 14.10 ppm. The spectral data match those found in literature.[15]

For allyl-containing derivatives as the substrates:

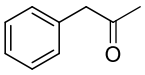

Phenylacetone (2o): Starting from allylbenzene (**1o**) and following the general procedure, the reaction mixture was stirred for 16 hours. Quantitative conversion was estimated by GC-MS and GC (FID) analysis showing the formation of 52% of the ketone product **2o**, 2% of the alcohol **3o**, 11% of aldehyde **7o**, 25% of benzyl alcohol **8o** and 10% of hydrogenated side-products. Purification by SiO_2 column chromatography using EtOAc/heptane (0/1 to 1/5, v/v) eluent afforded the analytically pure ketone product **2o** (23 mg, 52% yield). ^{1}H NMR (400 MHz, $CDCl_3$): δ = 7.37–7.31 (m, 2H), 7.31–7.24 (m, 1H), 7.23–7.18 (m, 2H), 3.70 (s, 2H), 2.15 (s, 3H) ppm. The spectral data match those found in literature.[16]

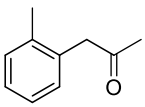

2-Methylphenylacetone (2p): Starting from 1-allyl-2-methylbenzene (**1p**) and following the general procedure, the reaction mixture was stirred for 16 hours. Quantitative conversion was estimated by GC-MS and GC (FID) analysis showing the formation of 44% of ketone product **2p**, 10% of alcohol **3p**, 12% of aldehyde **7p**, 27% of benzyl alcohol **8p** and 5% of hydrogenated side-products. Purification by SiO_2 column chromatography using EtOAc/heptane (0/1 to 1/5, v/v) eluent afforded the analytically pure ketone product **2p** (19 mg, 40% yield). ^{1}H NMR (400 MHz, $CDCl_3$): δ = 7.22–7.10 (m, 4H), 3.71

(s, 2H), 2.25 (s, 3H), 2.14 (s, 3H) ppm. $^{13}C\{^{1}H\}$ NMR (101 MHz, $CDCl_3$): δ = 206.32, 136.83, 133.16, 130.49, 130.35, 127.39, 126.28, 49.15, 29.22, 19.60 ppm. The spectral data match those found in literature.[17]

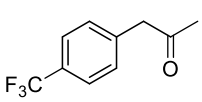

4-Trifluorophenylacetone (2q): Starting from 1-allyl-4-trifluoromethylbenzene (**1q**) and following the general procedure, the reaction mixture was stirred for 16 hours. Quantitative conversion was estimated by GC-MS and GC (FID) analysis showing the formation of 38% of ketone product **2q**, 18% of alcohol **3q**, 28% of benzyl alcohol **8q** and 14% of hydrogenated side-products. Purification by SiO_2 column chromatography using EtOAc/heptane (0/1 to 1/5, v/v) eluent afforded the analytically pure ketone product **2q** (23 mg, 35 % yield). ^{1}H NMR (400 MHz, $CDCl_3$): δ = 7.59 (d, *J* = 8.0 Hz, 1H), 7.31 (d, *J* = 8.0 Hz, 1H), 3.78 (s, 1H), 2.20 (s, 1H) ppm. $^{13}C\{^{1}H\}$ NMR (101 MHz, $CDCl_3$): δ = 204.95, 138.09 (d, *J* = 1.6 Hz), 129.82, 129.43 (q, *J* = 32.5 Hz), 125.59 (q, *J* = 3.8 Hz), 124.12 (d, *J* = 272.0 Hz), 50.36, 29.58 ppm. $^{19}F\{^{1}H\}$ NMR (376 MHz, $CDCl_3$): δ = -62.58 ppm. The spectral data match those found in literature.[18]

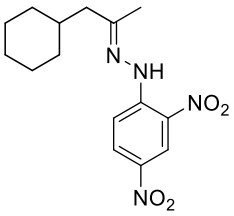

1-(1-cyclohexylpropan-2-ylidene)-2-(2,4-dinitrophenyl)hydrazine derived from cyclohexylacetone (2r): Starting from allylcyclohexane (**1r**) and following the general procedure, the reaction mixture was stirred for 16 hours. Quantitative conversion was estimated by GC-MS and GC (FID) analysis showing the formation of 70% of ketone **2r** product, 29% of alcohol **3r** and 1% of hydrogenated side-products. The final product was isolated as a 2,4-dinitrophenylhydrazine derivative following the general derivatization procedure (12 mg, 12% yield). ^{1}H NMR (400 MHz, $CDCl_3$): δ = 11.37 (s, 1H), 9.47 (d, *J* = 2.6 Hz, 1H), 8.64 (ddd, *J* = 9.6, 2.6, 0.8 Hz, 1H), 8.30 (d, *J* = 9.6 Hz, 1H), 2.65 (d, *J* = 6.8 Hz, 2H), 2.39 (s, 3H), 2.16–1.98 (m, 5H), 1.70–1.49 (m, 4H), 1.35 (q, *J* = 14.2, 12.6 Hz, 2H) ppm. $^{13}C\{^{1}H\}$ NMR (101 MHz, $CDCl_3$): δ = 157.57, 145.21, 137.65, 130.00, 129.02, 123.55, 116.50, 46.67, 35.57, 33.22, 26.28, 26.14, 16.13 ppm. HRMS (ESI): *m/z* calcd for ($C_{15}H_{20}N_4O_4$) $[M+Na]^+$ 343.1374; found: 343.1377 (1 ppm).

Indole oxidation procedure: The diiron **Fe-2** catalyst (14 mg, 0.016 mmol, 0.025 equiv.), EtOH/H_2O (3 mL, 96/4, v/v), 3-methylindole **1s** (0.325 mmol, 1 equiv.), dodecane (0.081 mmol, 18.4 µL, 0.25 equiv.) and lastly H_2O_2 (30% w/v, 33 mg, 111 µL, 0.975 mmol, 3 equiv.). The reaction mixture was stirred at room temperature until completion of the reaction monitored by GC-MS and TLC chromatography. Then, the reaction mixture was evaporated and the pure product was isolated by SiO_2 column chromatography using EtOAc/Heptane as the eluent. All experiments were run 3 times and the given data are an average value.

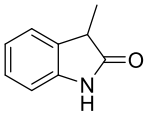

3-Methyloxindole (2s): Following the general procedure, the reaction mixture was stirred for 30 min. Quantitative conversion was estimated by GC-MS and GC (FID) analysis. Purification by SiO_2 column chromatography using EtOAc/heptane (0/1 to 1/1, v/v) eluent afforded the analytically pure 3-methyloxindole product **2s** (34 mg, 71% yield). ^{1}H NMR (400 MHz, $CDCl_3$): δ = 8.39 (s, 1H), 7.21 (td, *J* = 7.5, 1.0 Hz, 2H), 7.03 (td, *J* = 7.5, 1.0 Hz, 1H), 6.90 (d, *J* = 7.5 Hz, 1H), 3.47 (q, *J* = 7.7 Hz, 1H), 1.50 (d, *J* = 7.7 Hz, 3H) ppm. $^{13}C\{^{1}H\}$ NMR (101 MHz, $CDCl_3$): δ = 181.10, 141.10, 131.25, 127.87, 123.83, 122.37, 109.62, 41.00, 15.23 ppm. The spectral data match those found in literature.[19]

7.4. References.

[1] J. Smidt, W. Hafner, R. Jira, J. Sedlmeier, R. Sieber, R. Rüttinger, H. Kojer, *Angew. Chem.* **1959**, *71*, 176-182.

[2] (a) J. A. Keith, R. J. Nielsen, J. Oxgaard, W. A. Goddard, *J. Am. Chem. Soc.* **2007**, *129*, 12342-12343; (b) J. A. Keith, P. M. Henry, *Angew. Chem. Int. Ed.* **2009**, *48*, 9038-9049; (c) P. Kocovsky, J.- E. Backvall, *Chem Eur. J.* **2015**, *21*, 36-56; (d) J. J. Dong, W. R. Browne, B. L. Feringa, *Angew. Chem. Int. Ed.* **2015**, *54*, 734-744; (e) T. V. Baiju, E. Gravel, E. Doris, I. N. N. Namboothiri, *Tetrahedron Lett.* **2016**, *57*, 3993-4000; (f) X. Qi, D. G. Kohler, K. L. Hull, P. Liu, *J. Am. Chem. Soc.* **2019**, *141*, 11892-11904; (g) J. Muzart, *Tetrahedron* **2021**, *87*, 132024.

[3] (a) W. Hafner, R. Jira, J. Sedlmeier, J. Smidt, *Chem. Ber.* **1962**, *95*, 1575-1581; (b) J. Smidt, W. Hafner, R. Jira, R. Sieber, J. Sedlmeier, A. Sabel, *Angew. Chem. Int. Ed.* **1962**, *1*, 80-88; (c) R. Jira, *Angew. Chem. Int. Ed.* **2009**, *48*, 9034-9037.

[4] (a) A. Comas-Vives, A. Stirling, A. Lledós, G. Ujaque, *Chem. Eur. J.* **2010**, *16*, 8738-8747; (b) M. S. Sigman, E. W. Werner, *Acc. Chem. Res.* **2012**, *45*, 874-884; (c) A. Stirling, N. N. Nair, A. Lledo, G. Ujaque, *Chem. Soc. Rev.* **2014**, *43*, 4940-4952; (d) Y. Ura, *Synthesis* **2021**, *53*, 848-860; (e) B. Morandi, Z. K. Wickens, R. H. Grubbs, *Angew. Chem. Int. Ed.* **2013**, *52*, 2944-2948; (f) B. Morandi, Z. K. Wickens, R. H. Grubbs, *Angew. Chem. Int. Ed.* **2013**, *52*, 9751-9754; (g) Z. K. Wickens, B. Morandi, R. H. Grubbs, *Angew. Chem. Int. Ed.* **2013**, *52*, 11257-11260; (h) M. Hu, W. Wu, H. Jiang, *ChemSusChem* **2019**, *12*, 2911-2935.

[5] (a) W. H. Clement, C. M. Selwitz, *J. Org. Chem.* **1964**, *29*, 241-243; (b) J. Tsuji, *Synthesis* 1984, 369-384; (c) J. Tsuji, H. Nagashima, H. A. Nemoto, *Org. Synth.* **1984**, *62*, 9-13; (d) J. M. Takacs, X.-t. Jiang, *Curr. Org. Chem.* **2003**, *7*, 369-396; (e) C. N. Cornell, M. S. Sigman, *Inorg. Chem.* **2007**, *46*, 1903-1909; (f) D. Wang, A. B. Weinstein, P. B. White, S. S. Stahl, *Chem. Rev.* **2018**, *118*, 2636-2679; (g) J. Muzart, *Tetrahedron* **2021**, *87*, 132024; (h) Y. Ura, *Chem. Rec.* **2021**, *21*, 3458-3469.

[6] (a) C. Bolm, J. Legros, J. Le Paih, L. Zani, *Chem. Rev.* **2004**, *104*, 6217-6254; (b) *Catalysis without Precious Metals* (Ed.: R. M. Bullock), Wiley-VCH, Weinheim, **2010**; (c) I. Bauer, H.-J. Knölker, *Chem. Rev.* **2015**, *115*, 3170-3387; (d) K. S. Egorova, V. P. Ananikov, *Angew. Chem. Int. Ed.* **2016**, *55*, 12150-12162; (e) A. Fürstner, *ACS Cent. Sci.* **2016**, *2*, 778-789; (f) E. B. Bauer, *Isr. J. Chem.* **2017**, *57*, 1131-1150; (g) S. Rana, J. P. Biswas, S. Paul, A. Paik, D. Maiti, *Chem. Soc. Rev.* **2021**, *50*, 243-472.

[7] (a) R. A. Fernandes, A. K. Jha, P. Kumar, *Catal. Sci. Technol.* **2020**, *10*, 7448-7470; (b) P. Rajeshwaran, J. Trouvé, K. Youssef, R. Gramage-Doria, *Angew. Chem. Int. Ed.* doi: 10.1002/anie.202211016.

[8] (a) G.-Q. Chen, Z.-J. Xu, C.-Y. Zhou, C.-M. Che, *Chem. Commun.* **2011**, *47*, 10963-10965; (b) Y.-D. Du, C.-W. Tse, Z.-J. Xu, Y. Liu, C.-M. Che, *Chem. Commun.* **2014**, *50*, 12669-12672.

[9] S. C. Hammer, G. Kubik, E. Watkins, S. Huang, H. Minges, F. H. Arnold, *Science* **2017**, *358*, 215-218; (b) J. Soler, S. Gergel, C. Klaus, S. C. Hammer, M. Garcia-Borràs, *J. Am. Chem. Soc.* **2022**, *144*, 15954-15968.

[10] (a) B. Liu, F. Jin, T. Wang, X. Yuan, W. Han, *Angew. Chem. Int. Ed.* **2017**, *56*, 12712-12717; (b) B. Liu, W. Han, *Synlett* 2018, 29, 383-387; (c) F. Puls, H.-J. Knölker, *Angew. Chem. Int. Ed.* **2018**, *57*, 1222-1226; (d) F. Puls, F. Seewald, V. Grinenko, H.-H. Klauß, H.-J. Knölker, *Chem. Eur. J.* **2021**, *27*, 16776-16787; (e) F. Puls, P. Linke, O. Kataeva, H.-J. Knölker, *Angew. Chem. Int. Ed.* **2021**, *60*, 14083-14090.

[11] (a) D. Mansuy, J. Leclaire, M. Fontcave, M. Momenteau, *Biochem. Biophys. Res. Commun.* **1984**, *119*, 319-325; (b) S. P. de Visser, D. Kumar, S. Shaik, *J. Inorg. Biochem.* **2004**, *98*, 1183-1193; (c) Y.-C. Yin, H.-L. Yu, Z.-J. Luan, R.-J. Li, P.-F. Ouyang, J. Liu, J.-H. Xu, *ChemBioChem.* **2014**, *15*, 2443-2449 ; (d) F. P. Guengerich, A. W. Munro, *J. Biol. Chem.* **2013**, *288*, 17065-17073; (e) R. J. Kazlauskas, *Curr. Opin. Chem. Biol.* **2005**, *9*, 195-201.

[12] (a) T. Shimizu, A. Lengalova, V. Martinek, M. Martinkova, *Chem. Soc. Rev.* **2019**, *48*, 5624-5657; (b) J. Dong, E. Fernandez-Fueyo, F. Hollmann, C. E. Paul, M. Pesic, S. Schmidt, Y. Wang, S. Younes, W. Zhang, *Angew. Chem. Int. Ed.* **2018**, *57*, 9238-9261; (c) S. Wu, Y. Zhou, Z. Li, *Chem. Commun.* **2019**, *55*, 883-896; (d) X. Huang, J. T. Groves, *Chem. Rev.* **2018**, *118*, 2491-2553; (e) F. P. Guengerich, *ACS Catal.* **2018**, *8*, 10964-10976; (f) A. Ciaramella, G. Catucci, G. Gilardi, G. Di Nardo, *Int. J. Biol. Macromol.* **2019**, *140*, 577-587; (g) I. G. Denisov, T. M. Makris, S. G. Sligar, I. Schlichting, *Chem. Rev.* **2005**, *105*, 2253-2277; (h) J. Liu, S. Chakraborty, P. Hosseinzadeh, Y. Yu, S. Tian, I. Petrik, A. Bhagi, Y. Lu, *Chem. Rev.* **2014**, *114*, 4366-4469; (i) C. M. Krest, E. L. Onderko, T. H. Yosca, J. C. Calixto, R. F. Karp, J. Livada, J. Rittle, M. T. Green, *J. Biol. Chem.* **2013**, *288*, 17074-17081.

[13] S. Kasemthaveechok, B. Fabre, G. Loget, R. Gramage-Doria, *Catal. Sci. Technol.* **2019**, *9*, 1301-1308

[14] See details in the Experimental section.

[15] D. M. Kurtz, Jr., *Chem. Rev.* **1990**, *90*, 585-606.

[16] A mechanism for the formation of **Fe-2** from **Fe-1** is proposed in **Scheme S5** in the Experimental section.

[17] The reaction rate at 50 ^{o}C is 1.02 x 10^{-7} mol.s^{-1} while the reaction rate at 0 ^{oC} is 1.59 x 10^{-8} mol.s^{-1}, see reference [14].

[18] A mechanism for the formation of **4b** is proposed in **Scheme S7** in the Experimental section in agreement with reference [19].

[19] (a) J. C. Lo, J. Gui, Y. Yabe, C.-M. Pan, P. S. Baran, *Nature* **2014**, *516*, 343-348; (b) J. C. Lo, Y. Yabe, P. S. Baran, *J. Am. Chem. Soc.* **2014**, *136*, 1304-1307; (c) H. T. Dao, C. Li, Q. Michaudel, B. D. Maxwell, P. S. Baran, *J. Am. Chem. Soc.* **2015**, *137*, 8046-8049; (d) J. C. Lo, D. Y. Kim, C.-M. Pan, J. T. Edwards, Y. Yabe, J. H. Gui, T. Qin, S. Gutierrez, J. Giacoboni, M. W. Smith, P. L. Holland, P. S. Baran, *J. Am. Chem. Soc.* **2017**, *139*, 2484-2503; (e) D. Kim, S. M. Wahidur Rahaman, B. Q. Mercado, R. Poli, P. L. Holland, *J. Am. Chem. Soc.* **2019**, *141*, 7473-7485; (f) e) S. A. Green, S. W. M. Crossley, J. L. M. Matos, S. Vásquez-Céspedes, S. L. Shevick, R. A. Shenvi, *Acc. Chem. Res.* **2018**, *51*, 2628-2640; (g) H. Jiang, W. Lai, H. Chen, *ACS Catal.* **2019**, *9*, 6080-6086; (h) S. L. Shevick, C. V. Wilson, S. Kotesova, D. Kim, P. L. Holland, R. A. Shenvi, *Chem. Sci.* **2020**, *11*, 12401-12422; (i) S. Sarkar, K. P. S. Cheung, V. Gevorgyan, *Chem. Sci.* **2020**, *11*, 12974-12993; (j) P. V. Kattamuri, J. G. West, *J. Am. Chem.*

Soc. **2020**, *142*, 19316-19326; (k) W. P. Thomas, S. V. Pronin, *Acc. Chem. Res.* **2021**, *54*, 1347-1359.

[20] Note that the isolated yields of **2** were lower than the reported GC yields (using dodecane as internal standard) due to the low boiling point of the compounds, see reference [14].

[21] For examples of selective iron-catalyzed epoxidation of olefins, see: R. Mas-Ballesté, L. Que, *J. Am. Chem. Soc.* **2007**, *129*, 15964-15972; (b) K. Hasan, N. Brown, C. M. Kozak, *Green Chem.* **2011**, *13*, 1230-1237.

[22] A. Gonzalez-de-Castro, J. L. Xiao, *J. Am. Chem. Soc.* **2015**, *137*, 8206-8218.

[23] B. Liu, P. Hu, F. Xu, L. Cheng, M. Tan, W. Han, *Commun. Chem.* **2019**, *2*, 5.

[24] (a) L. Leone, D. D'Alonzo, O. Maglio, V. Pavone, F. Nastri, A. Lombardi, *ACS Catal.* **2021**, *11*, 9407-9417; (b) P. Mondal, S. Rajapakse, G. B. Wijeratne, *J. Am. Chem. Soc.* **2022**, *144*, 3843-3854.

[25] (a) C. E. Dalgliesh, W. Kelly, *J. Chem. Soc.* **1958**, 3726-3727; (b) X. Jiang, C. Zheng, L, Lei, K. Lin, C. Yu, *Eur. J. Org. Chem.* **2018**, 1437-1442; (c) S. V. Shelar, N. P. Argade, *Org. Biomol. Chem.* **2019**, *17*, 6671-6677; (d) J. Xu, L. Lian, H. Zheng, Y. R. Chi, R. Tong, *Nature Commun.* **2019**, *10*, 4754; (e) G. Zhao, L. Liang, E. Wang, S. Lou, R. Qi, R. Tong, *Green Chem.* **2021**, *23*, 2300-2307; (f) P. Liang, H. Zhao, T. Zhou, K. Zeng, W. Jiao, Y. Pan, Y. Liu, D. Fang, X. Ma, H. Shao, *Adv. Synth. Catal.* **2021**, *363*, 3532-3538; (f) T. Mintz, N. Y. More, E. Gaster, D. Pappo, *J. Org. Chem.* **2021**, *86*, 18164-18178.

[26] (a) M. Kaur, *Key Heterocycle Cores for Designing Multitargeting Molecules* (Ed.: O. Silakari), Elsevier, **2018**; pp 211-246; (b) M. Kaur, M. Singh, N. Chadha, O. Silakari, *Eur. J. Med. Chem.* **2016**, *123*, 858-894; (c) S. Peddibhotla, *Curr. Bioact. Compd.* **2009**, *5*, 20-38; (d) Y. M. Khetmalis, M. Shivani, S. Murugesan, K. V. G. C. Sekhar, *Biomed. Pharmacother.* **2021**, *141*, 111842.

[27] For the synthesis and spectroscopic characterization of iron-hydride species in the context of other type of catalysis, see: (a) R. J. Kazlauskas, M. S. Wrighton, *Organometallics* **1982**, *1*, 602-611; (b) H.-J. Knölker, E. Baum, H. Goesmann, R. Klauss, *Angew. Chem. Int. Ed.* **1999**, *38*, 2064-2066; (c) N. Gorgas, B.Stöger, E. Pittenauer, G. Allmaier, L. F. Veiros, K. Kirchner, *Organometallics* **2014**, *33*, 6905-6914; (d) M. Mastalir, M. Glatz, N. Gorgas, B. Stöger, E. Pittenauer, G. Allmaier, L. F. Veiros, K. Kirchner, *Chem. Eur. J.* **2016**, *22*, 12316-12320; (e) N. Gorgas, B. Stöger, L. F. Veiros, K. Kirchner, *ACS Catal.* **2016**, *6*, 2664-2672; (f) F. Bertini, N. Gorgas, B. Stöger, M. Peruzzini, L. F. Veiros, K. Kirchner, L. Gonsalvi, *ACS Catal.* **2016**, *6*, 2889-2893; (g) S. Jiang, S. Quintero-Duque, T. Roisnel, V. Dorcet, M. Grellier, S. Sabo-Etienne, C. Darcel, J.-B. Sortais, *Dalton Trans.* **2016**, *45*, 11101-11108.

[28] The chemical shift of the non-aromatic hydrogen atoms from $PhSiH_3$ appear at *ca.* δ = 4.20 ppm values, see: J. John, E. Gravel, A. Hagège, H. Li, T. Gacoin, E. Doris, *Angew. Chem. Int. Ed.* **2011**, *50*, 7533-7536.

[29] (a) C. P. Casey, H. Guan, *J. Am. Chem. Soc.* **2007**, *129*, 5816-5817; (b) T. G. Linford-Wood, N. T. Coles, R. L. Webster, *Green Chem.* **2021**, *23*, 2703-2709; (c) Y. Li, S. Yu, X. Wu, J. Xiao, W. Shen, Z. Dong, J. Gao, *J. Am. Chem. Soc.* **2014**, *136*, 4031-4039; (d) T. N. Gieshoff, M. Villa, A. Welther, M. Plois, U. Chakraborty, R. Wolf, A. J. von Wangelin, *Green Chem.* **2015**,

17, 1408-1413; (e) R. Xu, S. Chakraborty, S. M. Bellows, H. Yuan, T. R. Cundari, W. D. Jones, *ACS Catal.* **2016**, *6*, 2127-2135; (f) S. Fleischer, S. Zhou, K. Junge, M. Beller, *Angew. Chem. Int. Ed.* **2013**, *52*, 5120-5124; (g) D. Wei, C. Darcel, *Chem. Rev.* **2019**, *119*, 2550-2610.

[30] (a) L. S. Reid, Marcia, R. Mauk, A. G. Mauk, *J. Am. Chem. Soc.* **1984**, *106*, 2182-2185; (b) L. S. Reid, A. R. Lim, A. G. Mauk, *J. Am. Chem. Soc.* **1986**, *108*, 8197-8201; (c) K.-B. Lee, G. N. La Mar, R. K. Pandey, I. N. Rezzano, K. E. Mansfield, K. M. Smith, *Biochemistry* **1991**, *30*, 1878-1887; (d) J. J. Warren, J. M. Mayer, *J. Am. Chem. Soc.* **2011**, *133*, 8544-8551; (e) Y. Deng, M. L. Weaver, K. R. Hoke, E. V. Pletneva, *Inorg. Chem.* **2019**, *58*, 14085-14106.

[31] S. Tang, K. Liu, C. Liu, A. Lei, *Chem. Soc. Rev.* **2015**, *44*, 1070-1082; (b) S. W. M. Crossley, C. Obradors, R. M. Martinez, R. A. Shenvi, *Chem. Rev.* **2016**, *116*, 8912-9000; (c) Z. Dong, Z. Ren, S. J. Thompson, Y. Xu, G. Dong, *Chem. Rev.* **2017**, *117*, 9333-9403; (d) X.-W. Lan, N.-X. Wang, Y. Xing, *Eur. J. Org. Chem.* **2017**, 5821-5851; (e) H. Jiang, A. Studer, *Chem. Soc. Rev.* **2020**, *49*, 1790-1811; (f) M. Patel, B. Desai, A. Sheth, B. Z. Dholakiya, T. Naveen, *Asian J. Org. Chem.* 2021, 3201-3232.

[32] (a) S. Durot, J. Taesch, V. Heitz, *Chem. Rev.* **2014**, *114*, 8542-8585; (b) X. Zhang, M. C. Wasson, M. Shayan, E. K. Berdichevsky, J. Ricardo-Noordberg, Z. Singh, E. K. Papazyan, A. J. Castro, P. Marino, Z. Ajoyan, Z. Chen, T. Islamoglu, A. J. Howarth, Y. Liu, M. B. Majewski, M. J. Katz, Joseph E. Mondloch, Omar K. Farhaa, *Coord. Chem. Rev.* **2021**, *429*, 213615.

Conclusion and perspectives

During the course of this PhD thesis, we successfully developed a sustainable bioinspired iron catalyst for alkene oxidation based on the promiscuous activity encountered in the family of cytochromes P-450 as well as the synthesis of new zinc-porphyrin based supramolecular ligands that feature substrate pre-organization features, making them highly active and selective in challenging iridium-catalyzed C-H borylations. On the other hand, careful investigation of side-products during the synthesis of the zinc-porphyrin supramolecular ligands showcased a unique reactivity for the copper-catalyzed click 1,3-dipolar cycloaddition reaction. One of these molecules turned out to be very appropriate for molecular encapsulation.

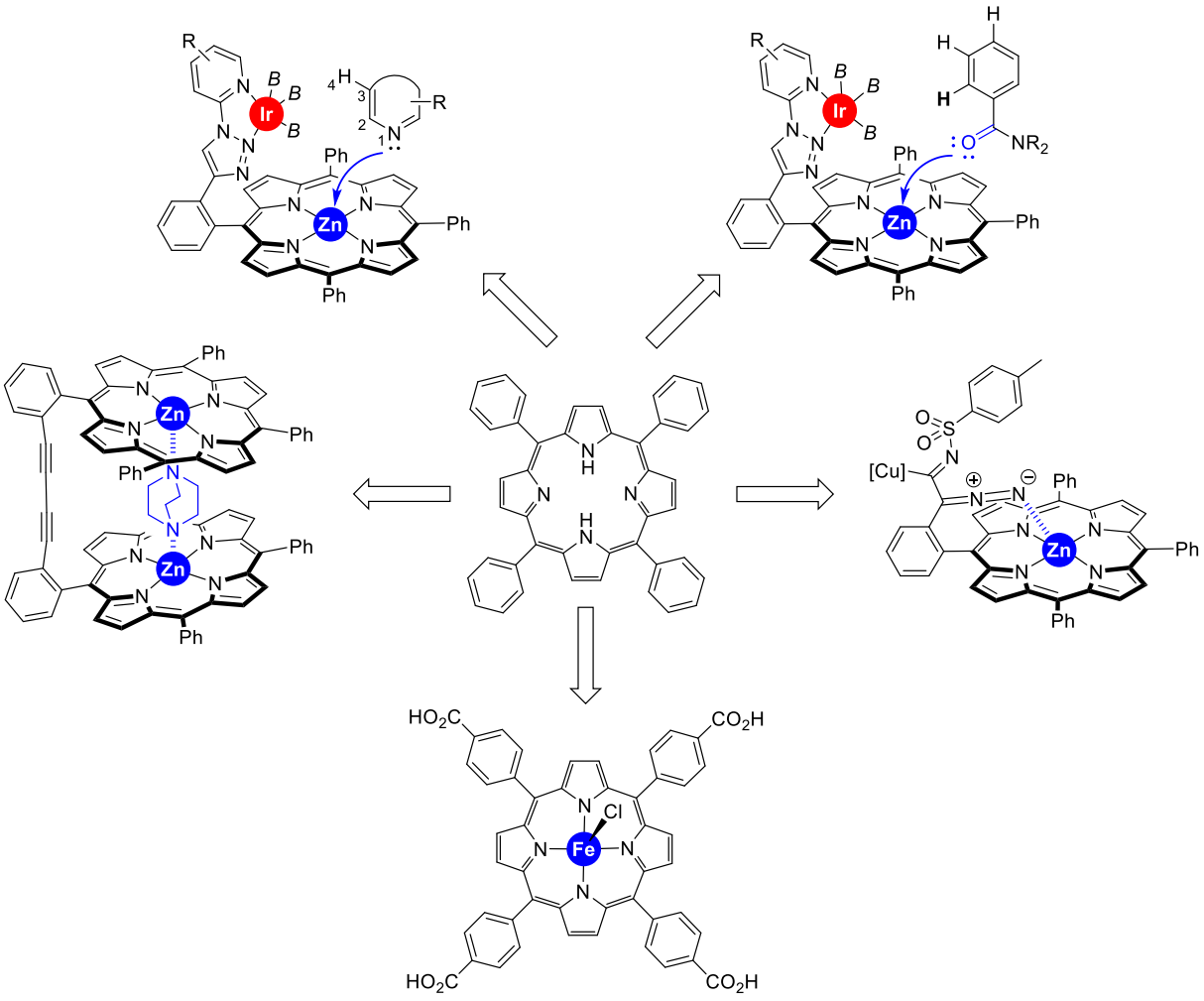

The **first chapter** of this work was dedicated to the in-depth study and summary of the state-of-the-art supramolecular metal catalysts exploiting remote non-covalent interactions in the second coordination sphere beyond hydrogen bonding.

In the **second chapter**, a supramolecular iridium catalyst enabling selective *meta*-C-H borylation of challenging pyridines derivatives exploiting Zn···N non-covalent interaction between the substrate and the catalyst was developed. Control experiment demonstrated the importance of substrate preorganization around the active metal center for both the activity

of the iridium catalyst as well as the selectivity observed. Mechanistic insights and kinetic investigation showed that the system display enzyme-like behaviours. The control of the second coordination sphere of the catalyst enabled interesting features like substrate selectivity and dormant reactivity. In particular, the steric patterns on the substrate were found to have a dramatic impact on the catalytic outcome as *ortho* and *para* substituent on the pyridine aromatic ring completely inhibited the reaction. In addition, multiple functional group such as electron rich, electron poor and weakly directing group substituent were tolerated. Moreover, the reaction was also applicable toward the functionalization of N-alkylated imidazoles.

The **chapter 3** was dedicated to the careful investigation of the *meta*-selective supramolecular iridium catalysis developed in the previous chapter by analyzing the limitations and deactivation pathways at the catalyst. This fundamental understanding led to find a new supramolecular version that outperforms the previously-developed one by significantly reducing the reaction time to a couple of hours. In particular, the commonly used and most active $[Ir(COD)(OMe)]_2$ precatalyst was found to inhibit to some extent the coordination of the pyridine substrate to the zinc-porphyrin molecular recognition site. Unexpectedly, the most electron rich 4-tert-butyl substituted supramolecular ligand was almost completely inactive for C-H borylation reaction, which strikingly contrasts with literature precedents. This unusual inactivity compared to the state-of-the-art iridium C-H borylation reactions using *N*,*N*-chelating ligands was ascribed to the poisoning of the zinc recognition site by the ligand itself in an intermolecular fashion manifold. By careful fine-tuning of the reaction conditions (addition of HBpin catalytic additive amongst other parameters) and taking the previously limitations into account, we found that the supramolecular ligand featuring a 4-methyl substitution pattern as the most suitable one affording *meta* selective C-H borylation of pyridines with high activity (up to 90%) while keeping an exquisite level of selectivity (>99%).

The **chapter 4** shows that the well-known and largely considered “predictable” copper catalyzed tosyl azide click chemistry did not work as expected in the presence of zinc-porphyrins containing an alkyne group located just above the zinc center. Dinitrogen release of an intermediate and nucleophile addition of protic solvents led to an undesired reaction pathway. Preliminar mechanistic investigations by means of control experiments suggest that the equilibrium between ring opening and cyclisation may be shifted towards the open form and subsequent loss of N_2 via Zn···N stabilization of the nitrogen anion. This unique reactivity appears to be in sharp contrast with published literature with substrates lacking the zinc-porphyrin backbone.

The **chapter 5** describes the synthesis of a supramolecular “cage like” bis zinc-porphyrin for molecular encapsulation. The sterically congested bis-zinc-porphyrin comprise a rigid linker: butadiyne. It represents a promising example in which the encapsulation of a small molecule guset takes place in host rather flexible that contains only a simple connector between both coordination sites. Its formation was a result of an unexpected reactivity of the in situ produced triazolo-pyridine ligand synthesis from chapter 3 as shown by a series of control experiments.

The **sixth chapter** is focused to the application of the chapter-2-reported supramolecular strategy in the kinetic enhancement of the *ortho*-selective C-H borylation of tertiary benzamides and other carbonyl-containing derivatives by the exploitation of a single

and weak Zn···O=C non-covalent interaction between the catalsyt and the substrate. The catalyst design was applied to the C-H borylation of multiple substrates showing that steric hindrance plays a key role for the reaction selectivity and activity. Moreover, formation of deoxygenated side-products were avoided by addition of a cyclohexene that was anticipated to act as a pinacolborane scavenger. The present work spans the scope of selective catalysts for C-H borylation of unbaised arene and it is a unique case in which Zn···O=C non-covalent interactions do enhance the overall catalyst activity.

The **last chapter** of this thesis showcased the use of a bio-inspired iron porphyrin catalyst for the sustainable Wacker-type oxidation of alkene derivatives using hydrosilane as the reductant. The reaction was selective towards the Markovnikov product (ketone formation) using triethylsilane as the reductant (99% yield in 24 hours) under air atmosphere as the sole oxidant at room temperature. The deactivation of the catalyst was characterized and it was ascribed to the slow oxidation of iron porphyrin to a μ-oxo bridged diiron inactive form. Mechanism investigations showed that catalytic amounts of simple Lewis acid such as hydrochloric acid, or of more reactive hydrosilane such as phenylsilane could activate the μ-oxo catalyst. Moreover, phenylsilane was found to be the most effective hydrosilane for the iron-catalyzed Wacker-type oxidation of styrene and aliphatic alkene derivatives in isolated yields up to 94% in short reaction time (less than 3 hours). On another side, we also successfully identify the yet elusive Fe-H postulated active intermediate by NMR spectroscopy. Further identification of side-products and careful fine-tuning of the reaction conditions gave evidence for the complex multiple catalytic cycles at play in this catalysis. By taking into advantage the carboxylic acid groups present onto the catalyst as well as the poor solubility of the iron catalyst in organic solvent, two simple experimental procedure made the recyclability of the catalyst possible. Furthermore, the first example of an iron catalyzed oxidation of indole derivative was disclosed using H_2O_2 as the oxidant this time.

Enzyme, nature's catalyst are a source of inspiration for chemists since ever. In this regard, multiple supramolecular strategies have been developed and successfully managed to merge supramolecular chemistry with transition metal catalysis in order to produce efficient and selective chemical transformations. The work described in this thesis is dedicated to the development of uncommon Zn···N and Zn···O=C weak interactions for direct the activity and selectivity of challenging C-H borylation reactions. In particular, we demonstrated the unique properties of a bifunctional supramolecular catalysts featuring a zinc-based molecular recognition site and a peripherally located iridium active site bound to the triazolo-pyridine coordinating arm. In parallel, bio-inspiration of the promiscuous activity of P-450 enzymes motivated us to search for a sustainable iron-catalyzed Wacker-type oxidation of olefins. Importantly, an important body of this work is devoted to the mechanistic understanding of the catalysis and how this rational can be used to further develop more powerful catalysts.

Future work regarding the study disclosed in this PhD thesis could be the following:

(1) Replacing the iridium active site for other noble metals such as Pd or Ru to tackle existing reactivity issues on C-H functionalizations, in particular those associated to the poor reactivity found in unbiased substrates such as heterocycles or carbonyl-containing substrates that are compatible with the supramolecular strategy developed in this thesis.

(2) Replacing the iridium active site for first row transition metals such as Fe, Ni, Cu, Co, etc. that are known to chelate to *N*,*N*-containing ligands similar to the ones developed in this thesis.

(3) Application of new supramolecular catalysts in copper and iridium hydroboration of vinyl-pyridines, iridium-catalyzed C-H bond silylation of pyridines, nickel-catalyzed C-H alkenylations, iridium-catalyzed C-H deuteriations, and iridium-catalyzed borylation via nitrile cleavage. Some preliminary results have been found for a few of these reactions and should be further studied in the future.

(4) The *N*,*N*-chelating triazolopyridine unit of the supramolecular catalysts could be replaced by other type of metal-coordinating groups in order to further exploit Zn···N and Zn···O=C weak interactions.

(5) Because the triazolopyridine ligands L* were efficient ligands in the iridium-catalyzed *ortho*-selective C-H borylation of carbonyl derivatives (chapter 6), future work coud be devoted to the optimization of the triazolopyridine backbone structure in order to introduce a new non-supramolecular ligand family to the very challenging iridium C-H borylation of arenes. Reaction at very high temperature (>120°C) could be investigated switching from the borylation candidate p-xylene solvent to highly sterically hindered mesitylene. Mechanism investigation needs to be addressed in order to determine the key intermediate species involved in the reactions.

(6) The work carried out in chapter 5 tend to indicate that triazolopyridine could be a suitable ligand for Glaser-Hay homocoupling reaction. Further optimization and mechanistic investigation will need to be addressed in order to understand the key intermediate at play and to search for a ligand that outperforms state-of-the-art Glaser-Hay homocoupling catalysts.

(7) Using the supramolecular “cage like” bis zinc-porphyrin scaffold as a nano-reactor for selective guest functionalization. Other metallo-porphyrin containing Mn, Fe or Ru could be synthesized and used for catalytic application in confined space.

(8) The Wacker-type oxidation reaction using other first row transition metal catalysts is highly attractive. Future work could be dedicated to the search of a metal catalyst compatible with the commercially available PHMS hydrosilane reductant, which is an industrial waste and its recyclability/reutilization is highly encouraged. Alternatively, replacing olefins by alkynes could be promising, for instance, the study of acetylene oxidation for acetaldehyde production. Furthermore, the metal electronic density modification by implementation of electron donating or withdrawing group on the pyrrole backbone could lead to dramatic reactivity modification. Regarding the huge turnover number (TON) observed, heterogeneous industrial application for sustainable Wacker type oxidation could be investigated

UNIVERSITÉ DE RENNES 1

Titre : Contrôle de la réactivité chimique avec des porphyrines metallés comme catalyseurs supramoléculaires et bio-inspirés

Mots clés : iridium ; fonctionnalisation C-H ; fer ; oxydation ; catalyse homogène ; cuivre

Résumé : Ces dernières décennies, et inspirés des enzymes, les catalyseurs métalliques supramoléculaires permettant la reconnaissance moléculaire par liaison hydrogène ou appariement d'ions ont été explorés afin de contrôler d'importantes transformations organiques. Dans cette thèse, les interactions non covalentes cinétiquement labiles Zn···N et Zn···O=C ont été exploitées par la première fois dans la deuxième sphère de coordination des catalyseurs métalliques. Ils se sont avérés utiles pour contrôler l'activité et la sélectivité des fonctionnalisations difficiles des liaisons C-H catalysées par l'iridium, qui sont pertinentes dans un contexte de chimie durable. Des borylations C-H sélectives ont été réalisées sur un site spécifique situé à quatre liaisons de distance du site de reconnaissance moléculaire pour des azines et benzamides comme substrats. Une telle précision a été prédite par la modélisation et les études mécanistiques ont révélé des propriétés enzymatiques intéressantes. Des produits inattendus se sont formés sous catalyse au cuivre lors de la synthèse des ligands supramoléculaires. Cela a été pris comme un avantage pour concevoir un récepteur supramoléculaire de petites molécules organiques. Enfin, un catalyseur artificiel au fer inspiré de la promiscuité de certains cytochromes de la famille P-450 en réactions d'oxydations a été développé. Ce catalyseur de fer est sélectif pour former de cétones à partir d'oléfines à l'air et à température ambiante avec une activité et sélectivité sans précédent en raison de la formation d'espèces d'hydrure de fer.

Title : Control of Chemical Reactivity with Metallated Porphyrins as Supramolecular and Bio-Inspired Catalysts

Keywords : iridium ; C-H functionalization ; iron ; oxidation ; homogeneous catalysis ; copper

Abstract : The last decades, and much inspired by enzymes, supramolecular metal catalysts enabling molecular recognition via weak hydrogen bonding or ion pairing have been largely explored in order to control important organic transformations. In this PhD thesis, kinetically labile Zn···N and Zn···O=C non-covalent interactions have been exploited in the second coordination sphere of metal catalysts for the first time. They turned out to be useful tools to control the activity and selectivity of challenging iridium-catalyzed C-H bond functionalizations, which are relevant in the context of sustainability. Selective C-H borylations have been achieved at a specific site located four chemical bonds apart from the molecular recognitions site for azines and benzamides as substrates. Such atom-precise catalysis was predicted by molecular modelling and the mechanistic studies revealed unique enzymatic features. Unexpected products formed under copper catalysis during the synthesis of the supramolecular ligands, highlighting the non-trival reactivity found in these species. This was taken as an advantage to design a supramolecular receptor for small organic guests. Lastly, an abiological iron catalyst inspired by the promiscuous oxidase activity encountered in several cytochromes from the P-450 family was developed. This iron catalyst is selective for the formation of ketones products starting from olefins under aerobic conditions at room temperature with unprecedented levels of activity and selectivity due to the spectroscopically characterized formation of so far elusive iron-hydride species.